Synthesis of annulated π-systems based on a tribenzotriquinacene core

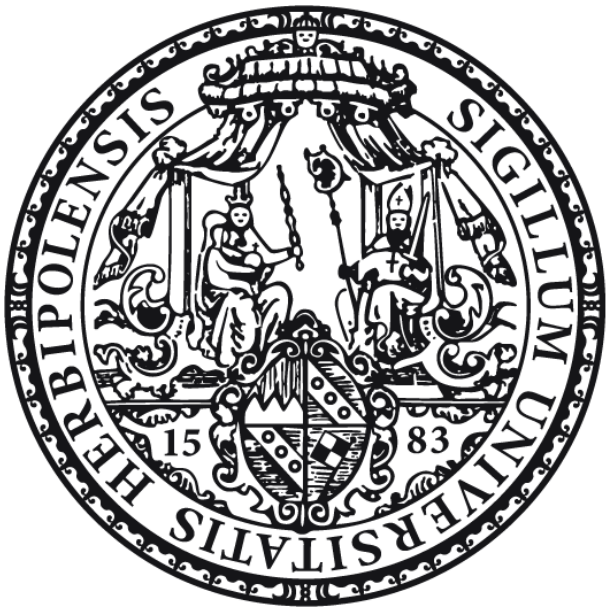

Dissertation zur Erlangung des naturwissenschaftlichen Doktorgrades
der Julius-Maximilians-Universität Würzburg

vorgelegt von

Rachel Abigail Buschmann

aus Derby, Großbritannien

Würzburg 2019

Eingereicht bei der Fakultät für Chemie und Pharmazie am

_____

Gutachter der schriftlichen Arbeit

1. Gutachter: _____

2. Gutachter: _____

Prüfer des öffentlichen Promotionskolloquiums

1. Prüfer: _____

2. Prüfer: _____

3. Prüfer: _____

Datum des öffentlichen Promotionskolloquiums

_____

Doktorurkunde ausgehändigt am

_____

For my family

Don't let anyone rob you of your imagination, your creativity or your curiosity. **Mae Jemison**

Die vorliegende Arbeit wurde im Zeitraum von August 2013 bis September 2018 am Institut für Organische Chemie der Julius-Maximilians-Universität Würzburg angefertigt.

Teile dieser Arbeit wurden bereits veröffentlicht in:

M. Vogt, R. Buschmann, S. Toksabay, M. Schmitt, M. Schwab, M. Bode, A. Krueger, „Self-Assembly and Electronic Structure of Tribenzotriquinacenes on Ag (111),“ *J. Phys. Chem. C* **2019**, *123*, 5469–5478.”

Weitere Veröffentlichung:

E. Reusch, D. Kaiser, D. Schleier, R. Buschmann, A. Krüger, T. Hermann, B. Engels, I. Fischer, P. Hemberger, „Pentadiynylidene and its Methyl-Substituted Derivates: Threshold Photoelectron Spectroscopy of R1-C5-R2 Triplet Carbon Chains,“ *J. Phys. Chem. A* **2019**, *123*, 2008–2017.”

Acknowledgements

First and foremost I would like to thank my supervisor Prof. Anke Krüger for the opportunity to complete this research in her group. Her knowledge, guidance and enthusiasm for science was invaluable.

I would also like to express my sincere gratitude to the employees of the Organic Chemistry institute: I am indebted to Dr Matthias Grüne, Dr Ann-Christin Pöppler, Patricia Altenberger and Elfriede Ruckdeschel for advice when measuring and interpreting NMR spectra, as well as Dr Michael Büchner, Juliane Adelmann, Fritz Dadrich and Antje Heckmann for mass measurements. I would especially like to thank Liselotte Michels and Sabine Timmroth for the elemental analysis measurements, Matthias Fromm for the support in the teaching lab, Jonathan Landeck for his glassblowing expertise, Michael Ramold and Markus Braun for their help with repairs and the steady dry ice supply, Bernd Brunner for his help with IT issues and everyone at the chemical store.

The members of the Krueger group deserve a special mention, for the enjoyable working environment and their intellectual and emotional support. Thanks to Stefan Wachtler and Julia Puck, for being very pleasant fume hood partners and to Dr Yvonne Kirchwehm, from whom I learnt a lot about tribenzotriquinacene research. Dr Sarah Schweeberg and Julia Puck shared my enthusiasm for baking and I am grateful for the regular supply of cake! Thanks to all group members, past and present: Dr Johannes Auerswald, Dr Patrick Betz, Christian Bauer, Dr Peter Buschmann, Dr Steffen Heyer, Dr Benjamin Kiendl, Stefan Kupka, Dr Daniel Lang, Viktor Merz, Andreas Muzha, Dr Sara Ranjbar, Lena Roos, Dr Sarah Schweeberg, Sinem Toksabay, Sebastian Vettermann, Dr Thilo Waag and Stefan Wachtler.

I'm very grateful for the financial support from the DFG GRKs 1221 and 2112, as well as the members for the stimulating disscusions and providing fresh perspective on my work. I would like to thank Julia Merz from the group of Prof. Marder for her support with borylation and SUZUKI coupling reactions, as well as Dr Alexandra Friedrich, Carsten Paulmann (PETRA III synchotron), Dr Krzysztof Radacki and Johannes Krebs for the x-ray crystal structure determination.

Collaborating with Prof. Matthias Bode, Matthias Vogt, Martin Schmitt and Markus Schwab was a rewarding experience and I am grateful for their expertise in producing high quality STM images and the many fruitful discussions about the orientation of molecules on a metal

surface. Thanks to Astrid Kudzus from the group of Prof. Würthner for gradient sublimation in the preparation of samples for STM analysis.

I had the pleasure of supervising many students and I would like to take the opportunity to mention the valuable contributions of the apprentices Maria Son, Felix Mitesser and Julian Herbert, as well as the students Iris Bodenschlägel, Marian Deutsch, Thomas Hertle, Michael Hofmann, Lena Roos and Markus Voelckel.

Outside of the lab I would like to thank my church family, particularly the small groups I was part of, whose prayers and encouragement helped when I most needed it. Rowing also provided a valuable break from lab work and I enjoyed the company of the students at ARCW, both off and on the water.

Lastly, I am grateful for the support of my parents Peter and Stella and brother Matthew, without whom I would not be where I am today. Last but definitely not least, I would like to thank my loving, supportive, encouraging and patient husband Peter, who often helped me put things into perspective.

Table of Contents

1 Introduction

1.1 Carbon – a plethora of allotropes

Carbon is not only the basis of organic chemistry, but is capable of forming many allotropes due to its valency. The properties of these different allotropes are astounding, considering that by changing only the hybridisation state and atomic arrangement provide us with the conducting and lubricating properties of graphite, the unrivalled hardness of diamond or the electronic and optoelectronic properties of newer carbon materials such as fullerenes, nanotubes and graphene.[1-3]

1.2 Graphene

As one of the more recent carbon allotropes, there is no doubt that graphene has taken the world by storm since the mechanical exfoliation of graphite was presented by GEIM and NOVOSELOV in 2004, who later won the Nobel prize for their work on the isolation of single-layer graphene.[4] This contradicted LANDAU and PEIERLS, who calculated in the 1930s that 2D crystals are thermodynamically unstable and cannot exist,[5,6] a viewpoint, which was also supported by MERMIN.[7] Despite this, scientists such as WALLACE,[8] MCCLURE,[9] SLONCZEWSKI[10] and SEMENOFF[11] studied and predicted the properties of a 2D crystal of graphite. Oxidation of graphite and the subsequent exfoliation and reduction of graphite oxide was recorded as early as 1859 by BRODIE.[12] HUMMERS'[13] oxidation method offered an efficient alternative in 1958 and the first single graphene sheets were identified with transmission electron microscopy in 1961 by BOEHM *et al*.[14]

Other attempts to isolate graphene before 2004 included the preparation of intercalation compounds from graphite, from which layers were exfoliated,[14-16] as well as mechanical manipulation of highly orientated pyrolytic graphite (HOPG).[17,18] However, the isolation of single-layer samples was not possible with these methods; this was achieved for the first time by GEIM and NOVOSOLEV.[4]

Graphene consists of sp^2-hybridised carbon atoms in a planar honeycomb lattice. Pristine graphene boasts extraordinary properties: structural flexibility, the highest tensile strength ever recorded,[19] plus high electrical and thermal conductivity as a zero-bandgap semiconductor[20,21] and a large theoretical surface area.[22] Mechanical exfoliation with tape produces the highest quality samples and graphene prepared using other techniques does not always display equivalent characteristics, however this method cannot be scaled up for mass

production.[23] Other production and isolation methods include the exfoliation and stabilisation of individual sheets in solution (a top-down method),[24-28] catalysed growth *in situ* on a substrate[29] and bottom-up methods from organic precursors.[30,31]

The quality of the graphene directly affects the electrical and optical properties, therefore the presence of structural disorders such as defects and impurities have an adverse effect.[32,33] Graphene samples usually contain distortions and holes in their structure. These defects can be used to create a bandgap and introduce local semi-conducting areas, which is a prerequisite for electrical applications such as transistors.[20] Most electronic applications require a band gap between the valence and conduction bands, therefore there is great interest in inducing and controlling such a gap in graphene.

1.3 Molecular electronics

Electronic devices based on organic molecules ("molecular-scale electronics") have the potential to compete with current silicon technologies due to the reduced size of single molecules, tunable properties derived from designable structures and relatively low-cost bulk synthesis methods.[34] For high-performance devices, understanding the movement of electrons to and through single molecules is crucial, for which accurate conductance values are required.[35]

Scanning tunnelling microscopy (STM) is a valuable tool for visualising organic molecules on metal substrates, as the tunnelling current is proportional to the local density of states (LDOS) of the surface at the position of the tip.[36] In addition, the current-voltage characteristics of single molecules can be determined with scanning tunnelling spectroscopy (STS). For this, the molecule is positioned between two electrodes: the freely moveable STM tip and the conducting solid substrate.[37]

Molecular manipulation and translation can also be induced by the STM tip,[38,39] which can be used to stitch molecules together by moving the reactants mechanically towards each other and then mediating a chemical reaction by excitation with tunnelling electrons.[40] The surface assisted chemical syntheses of graphene-like molecules on metal substrates is described in more detail in section 1.3.2.

Investigating the strength of non-covalent interactions between a substrate and its adsorbed organic molecule is of great importance,[41] as this directly affects the electronic properties of the resulting interface.[42,43] Atomically flat noble metal surfaces in ultrahigh vacuum are ideal

substrates for probing the intramolecular interactions, as their high diffusivity allows the organic molecules to freely interact and aggregate upon cooling.[44] Furthermore, STM images provide valuable insights into the relative alignment of molecules, which differs to that in solution.

1.3.1 Tuning the electronic properties of graphene

Graphene nanoribbons (GNRs), which are nanometre-wide strips of graphene, are promising model-systems for investigating the properties of graphene itself.[45] In addition, reducing the width of GNRs leads to the opening of a band gap, the size of which is inversely proportional to the width according to theoretical studies.[46,47] A stepwise bottom-up strategy is preferred for the synthesis of GNRs to ensure structural precision and defined edges. In the following sections, other strategies for tuning the electronic properties of graphene are described: the introduction of holes and defects, as well as fluorine functionalisation.

1.3.2 Holey graphene

Introducing nanosized pores results in holey graphene, which alters the electronic properties and makes the material more favourable for transistor applications. In addition the material can be used as a molecular sieve. MORENO and colleagues synthesised dibromo-substituted diphenylbianthracene **1**, which was polymerised on a Au(111) surface under ultrahigh vacuum by annealing to 200°C.[48] On increasing the temperature to 400°C, cyclo-dehydrogenation took place and finally an intramolecular cyclodehydrogenation at 450°C (see Figure 1.1). The resulting nanoporous graphene has an electronic structure where semi-conductor bands with an energy gap of 1 eV coexist with defined localised states created by the pores.[48] Controlling the pore size of covalent nanostructures is an expanding field of work,[50-53] building on the foundation of previously reported surface-assisted synthesis strategies for GNRs.[54-56] The regioselectivity of surface assisted cyclohydrogenation can afford different products when compared to solution synthesis routes, as demonstrated by NARITA, MÜLLEN, CHI and colleagues, who subjected a precursor molecule to both routes.[57]

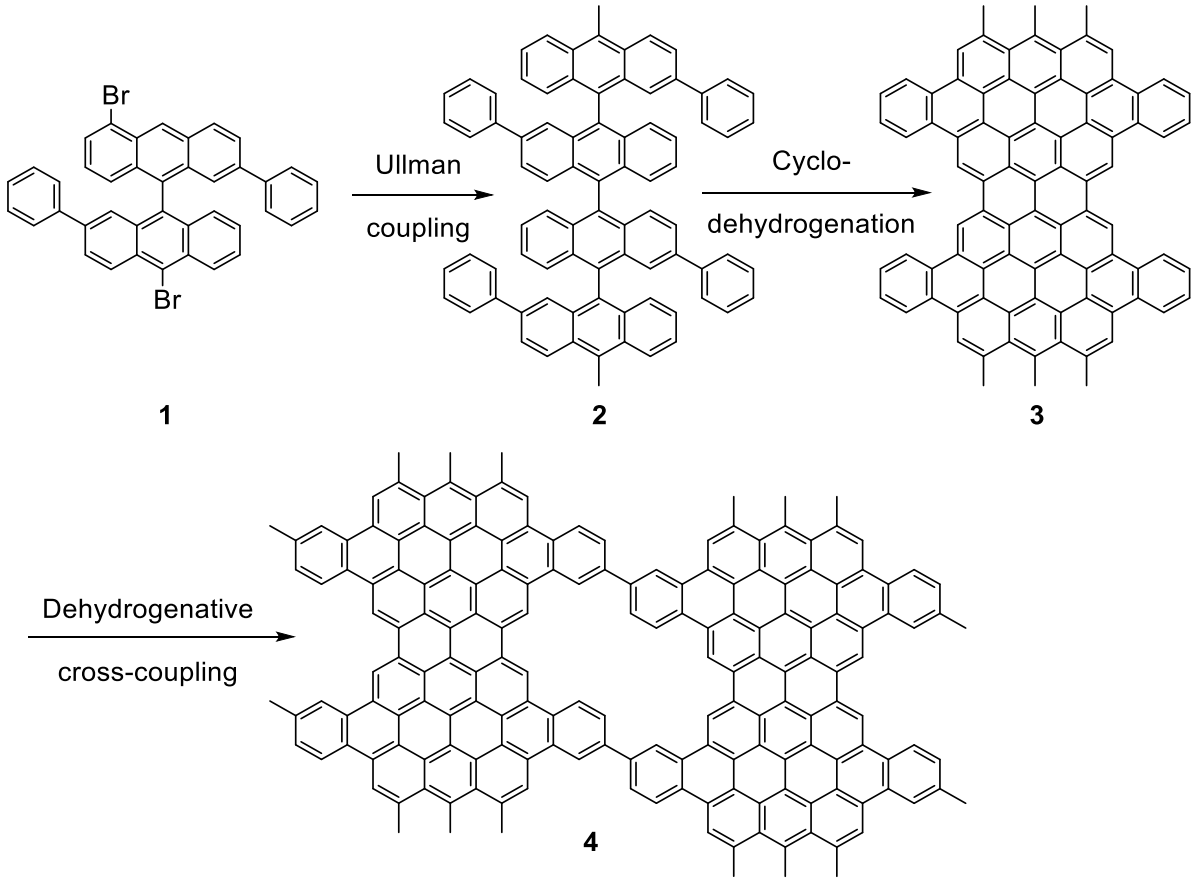

Figure 1.1 Synthesis of nanoporous graphene by MORENO *et al.* on Au(111).[48] ULLMAN coupling: 200°C, cyclodeydrogenation: 400°C, intramolecular cyclodehydrogenation: 450°C.

1.3.3 Defective graphene

Lattice imperfections occur naturally in graphene during growth and processing and these defects are able to migrate through the lattice.[21,49] The simplest defect is a single vacancy, where one atom is removed. As a result, a five- membered ring and a nine-membered ring are formed (see Figure 1.2). This is a topological defect: reconstruction of the hexagonal carbon lattice after removal of an atom is not possible, therefore non-hexagonal rings are formed.

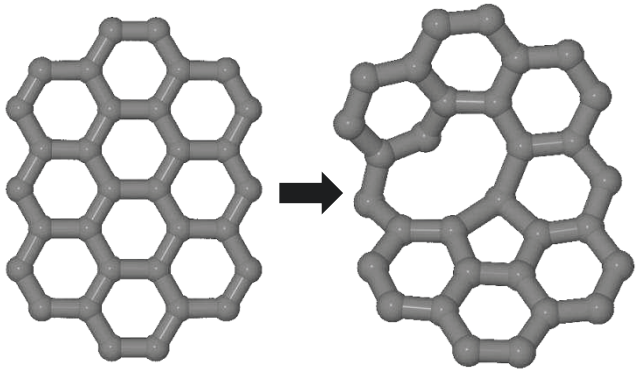

Figure 1.2 Single vacancy defect (right).[21,49] Hydrogen atoms have been omitted for clarity.

Another point defect is the STONE-WALES defect,[58] which does not involve any removed or added atoms (see Figure 1.3). By "rotating" one of the C-C bonds by 90°, four hexagons are transformed into two pentagons and two heptagons. Although the STONE-WALES defect is assumed to only be a local topological defect, computational studies from MA *et al.* reveal that these imperfections led to large out-of-plane displacements of the atoms.[59] The removal of multiple atoms may lead to larger and more complex defect configurations, as the reconstruction of the resulting dangling bonds introduces curvature and a warped structure.[21,60]

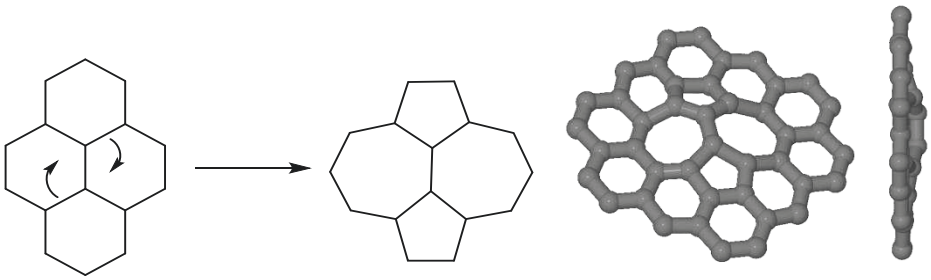

Figure 1.3 Formation of the Stone-Wales defect (5577),[21,49] and 3D models in an extended carbon network to demonstrate the curvature.

Recent examples of azulene embedded nanographenes demonstrate the effect of a 5-7 motif on their structures and properties. PEÑA, PASCUAL and coworkers described the on-surface cyclodehydrogenation of cojoined cove regions in a heavily distorted precursor, generating azulene fragments and increasing planarity and flexibility of the molecule.[61] MÜLLEN, FASEL, FENG *et al*. synthesised azuelene embedded nanographenes in solution and on a Au(111) surface, observing a narrow energy gap of 0.27 eV and pronounced open shell character.[62]

Defects strongly affect the electronic properties of graphene because the DIRAC equation (which replaces the SCHRÖDINGER equation for electrons in graphene) has to be modified to account for the structural changes.[21] Furthermore, altering the overlap of p_z-orbitals and the bond lengths within and surrounding defects has a significant impact on the electronic structure, as does the local rehybridsation of σ- and π-orbitals.[21] Defects are scattering centres for electron waves,[21] which theoretical studies indicate decreases the conductance of the material in graphene nanoribbons. For graphene nanoribbons this effect is position dependent, as the greatest decrease in conductance is obseved in the middle of the nanoribbon and the smallest decrease at the edge.[63]

1.3.4 Fluorinated graphene

Graphene halides contain covalently bonded halogen atoms and have different electronic properties compared to graphene, as the attachment of these atoms to sp^2 carbons changes the hybridisation state to sp^3. Stoichiometric graphene fluoride, (refered to as fluorographene: C_1F_1) is prepared either by fluorination of graphene or exfoliation of graphite fluoride and is stable under ambient conditions.[64] Fluorographene is an insulator,[65] but partially fluorinated graphene materials are semiconductors, whose band-gap size depends on the extent of fluorination.[66-68]

The possibility of a bottom-up synthesis from organic precursors has attracted a lot of attention, as the size, functionality and defects of nano(graphenes) produced can be controlled.

1.4 Nanographenes

Nanographenes can be defined as graphene sheets with the size of 1–100 nm and "nanographene molecules" as polycyclic aromatic hydrocarbons (PAHs) with defined chemical structures and sizes between 1–5 nm.[69] Nanographene molecules are extended by applying oxidative cyclohedrogenation to yield highly defined graphene nanoribbons.

1.4.1 Extension of polyaromatic hydrocarbons

The formation of new C-C bonds is the key to constructing and extending polyaromatic hydrocarbons (PAHs). There is an ever increasing number of transformations which can be employed, a selection of which are described in more detail below: 1) oxidative coupling and the SCHOLL reaction, 2) alkyne benzannulation, 3) one-shot annulative π-extension (APEX), 4) C-H arylation, 5) cross-coupling, 6) photocyclisation, 7) photochemical cyclodehydro-

chlorination (CDHC) and cyclodehydrogenofluorination (CDFC) as well as 8) Al_2O_3-mediated hydrogen fluoride elimination.

1) Oxidative coupling and the SCHOLL reaction

The first oxidative dimerisation of aromatic compounds was reported by LÖWE in 1871.[70] A similar effect was observed by SCHOLL in 1910, upon heating a quinone with $AlCl_3$ at 140–145°C.[71] It is important to differentiate between the two reactions: oxidative aromatic coupling refers to the reaction of electron rich aromatic compounds exclusively, such as phenols and alkyl aryl ethers. The mechanism involves the formation of radical cations of the substrate during the reaction.[72] A reaction only takes place when the overall electron density of the molecule is relatively high and only at the position of highest electron density.

In contrast, the SCHOLL reaction is not as sensitive to the distribution of electron density and requires a strong acid (often a LEWIS acid) and an oxidant. It is possible to achieve this with a single reagent. There are two different proposed mechanisms for the SCHOLL reaction, one of which is the arenium cation mechanism (shown for the synthesis of perylene 6 in Figure 1.4 below).[73] The aryl species is protonated to form an electrophilic σ complex, where H^+ can also represent a LEWIS acid. Attack at the second aromatic ring forms a new C-C bond and hydrogen elimination restores aromaticity.

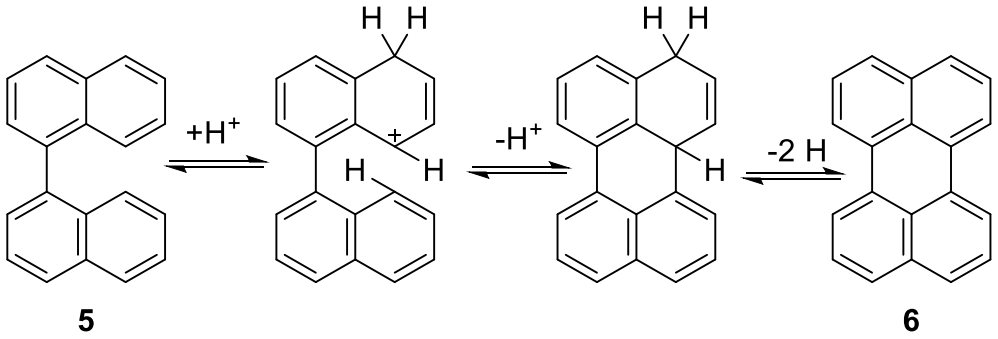

Figure 1.4 Proposed arenium cation mechanism.[72]

The second suggested mechanism is the radical cation mechanism, which is shown in Figure 1.5.[74] Differentiating between the two mechanisms is however challenging, as most of the LEWIS acids used in the SCHOLL reaction are also milder or stronger oxidants and are therefore able to catalyse a variety of reactions. Over the years interest in this transformation increased and many different reagent systems have been proposed.[75-91] Commonly used reagents include $FeCl_3$,[75-77] $AlCl_3$,[78-80] (bis(trifluoroacetoxy)iodo)benzene (PIFA) / $BF_3{\cdot}Et_2O$,[83] $MoCl_5$,[81-82] and 2,3-dichloro-5,6-dicyano-1,4-benzoquinone (DDQ).[86-88]

The choice of oxidant and the reaction conditions could also affect the mechanism, for example GRYZBOWSKI and colleagues analysed the literature in their review and concluded that reactions taking place at room temperature with a mild one-electron oxidant such as iron(III) chloride or molybdenum(V) chloride probably undergo a radical cation mechanism. In contrast, transformations which proceed at 120–160°C in the presence of a strong LEWIS acid follow the arenium cation mechanism.[72] WALDVOGEL and coworkers have studied the $MoCl_5$ mediated SCHOLL reaction extenstively, and confirmed that the radical cationic mechanism seems to be followed. Furthermore, they reported that a minimum of 0.75 eq. of $MoCl_5$ per bond are required.[82,92] DDQ has also been thoroughly investigated, and the results from RATHORE *et al.* strongly favour the cation-radical pathway for the SCHOLL reaction. The involvement of a parallel arenium ion mechanism however cannot be ruled out completely, as arenium ions and cation radicals can coexist and interchange under SCHOLL reaction conditions.[93]

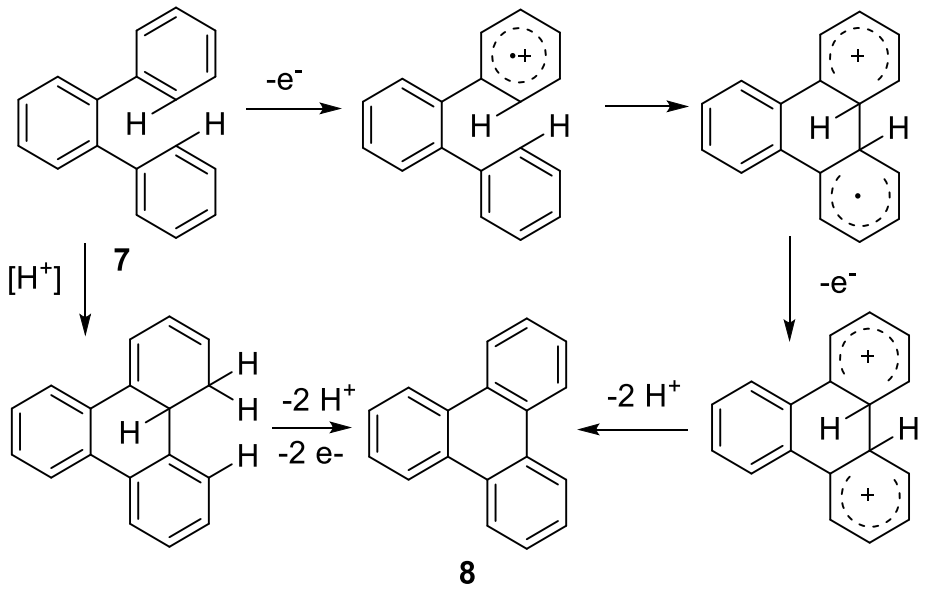

Figure 1.5 Proposed radical cation mechanism.[72]

MÜLLEN *et al.* published many protocols for the SCHOLL reaction of hexabenzocoronene derivatives,[94-105] forming up to 54 new C-C bonds during one reaction.[78] A solvent-free procedure has been published recently, using $FeCl_3$ and a planetary ball mill, which was also able to reproduce the formation of 54 new C-C bonds in one transformation.[106]

With a variety of reagent systems available, the mechanism of the SCHOLL reaction is not fully understood and often systematic testing of many different conditions is necessary for each precursor.

2) Alkyne Benzannulation

Multiple benzannulation reactions promoted by a BRØNSTED acid can provide an alternative to the SCHOLL reaction, as demonstrated by researchers in the CHALIFOUX group who synthesised functionalised pyrenes (see Figure 1.6). Using trifluoroacetic acid (TFA) only yielded the monocyclised product, but switching to a stronger acid like trifluoromethane-sulfonic acid (TfOH) the second cyclisation reaction took place.[107] Adjusting this protocol enabled the synthesis of narrow graphene nanoribbons.[108]

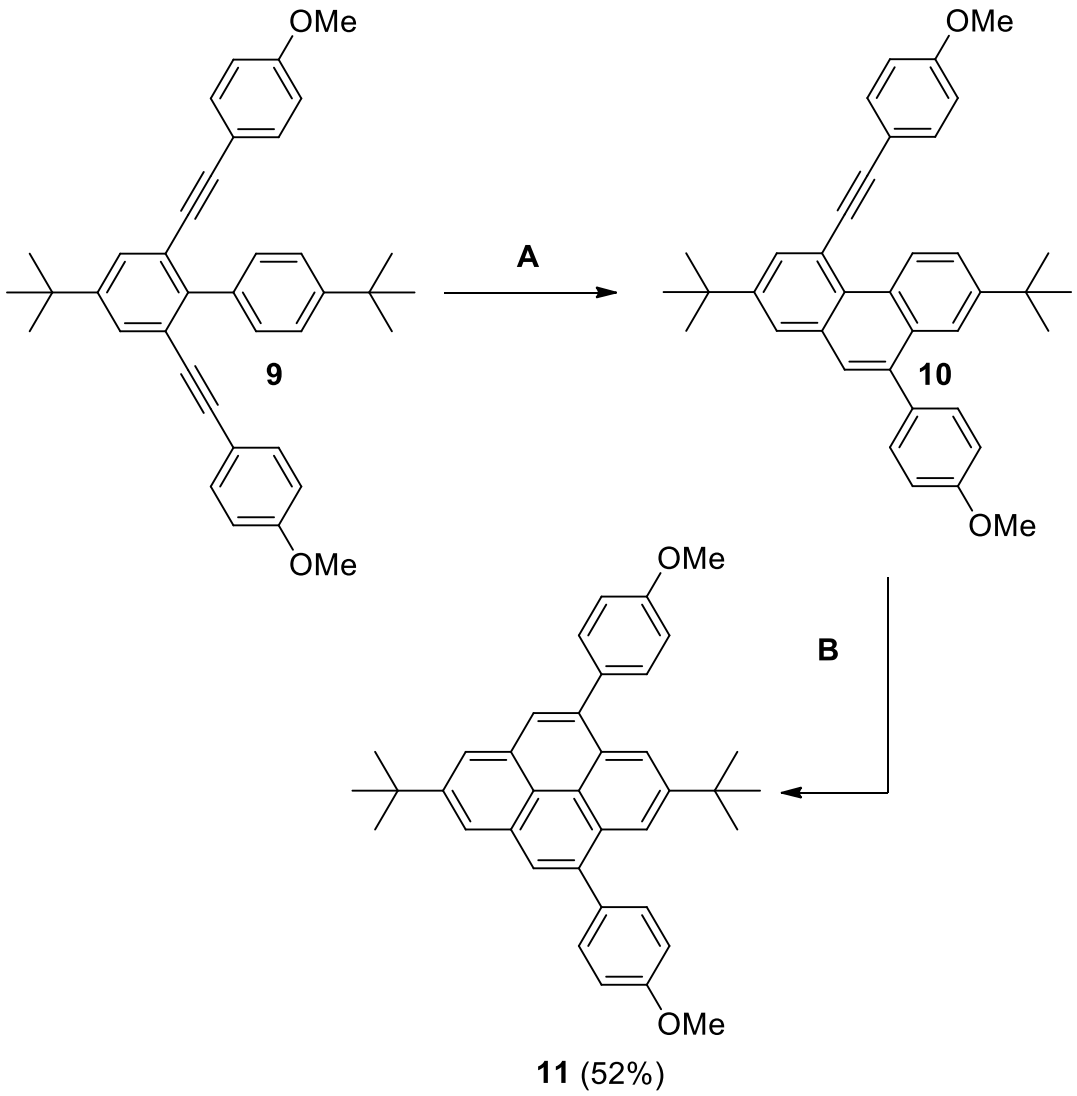

Figure 1.6 Synthesis of functionalised pyrene **11** via alkyne benzannulation.[107]
A: TFA, CH_2Cl_2, RT; **B**:TfOH, CH_2Cl_2, 0°C.

3) One-shot annulative π-extension (APEX)

Selective reactions offer the opportunity to construct nanographene molecules in a programmable manner. When describing the edges of graphene nanoribbons, it is possible to

differentiate between two different achiral edges: armchair and zig-zag edges, the classifcation of which depends on the relative orientation of the hexagons relative to the length of the GNR.[109] When applying this nomenclature to PAHs, three different regions can be identified at which extension is possible: the bay region (concave armchair edge), K region (convex armchair edge) and the L-region (zig-zag edge), which are shown below in Figure 1.7.

ITAMI and cowokers presented the K-selective one-shot annulative π-extension, which employs a $Pd(CH_3CN)_4(SbF_6)_2$ / *o*-chloranil catalytic system with silicon-bridged aromatics as π-extending agents, which react selectively at the convex armchair edge.[110] Another advantage is that pre-functionalised starting materials are not necessary, as the reaction is based on a double C-H activation.

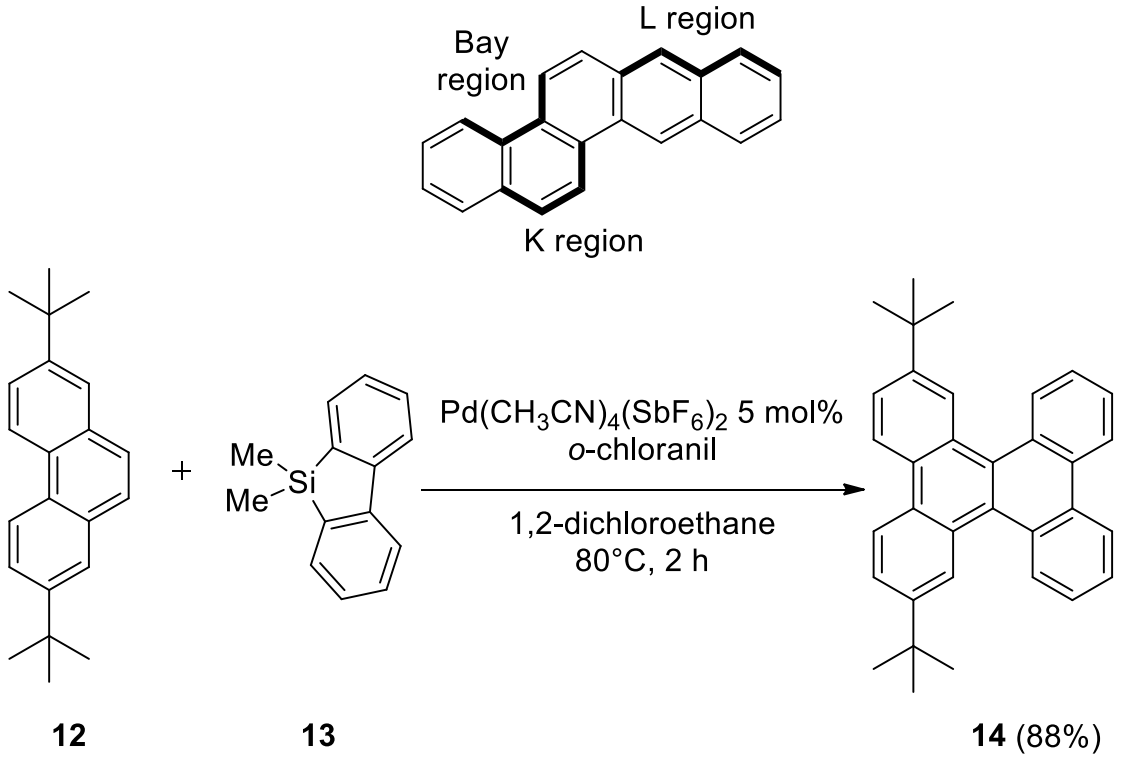

Figure 1.7 Regions of PAHs and an example of APEX reaction conditions.[110]

Adapted protocols have described the extension of corannulene,[111] pyrene,[112] heteroaromatics[113] and a π-extension reaction of alkynes to form diarylphenanthrenes.[114]

4) C-H arylation

The palladium catalysed intermolecular C-H arylation transformation can be carried out with arylhalides (bromides and iodides) or aryltriflates in the presence of Pd(II) catalysts.[116] A

stoichiometric amount of a base such as 1,8-diazabicyclo(5.4.0)undec-7-ene (DBU) is added to trap the acid that is formed during HX-elimination (see Figure 1.8).

Non-planar examples include the extension of corannulene and elimination of chloride to form new five-membered rings.[117] The synthesis of other bowl-shaped PAHs has also been reported.[118] The formation of six-membered rings in picenes and helicenes are also well-known.[119-121]

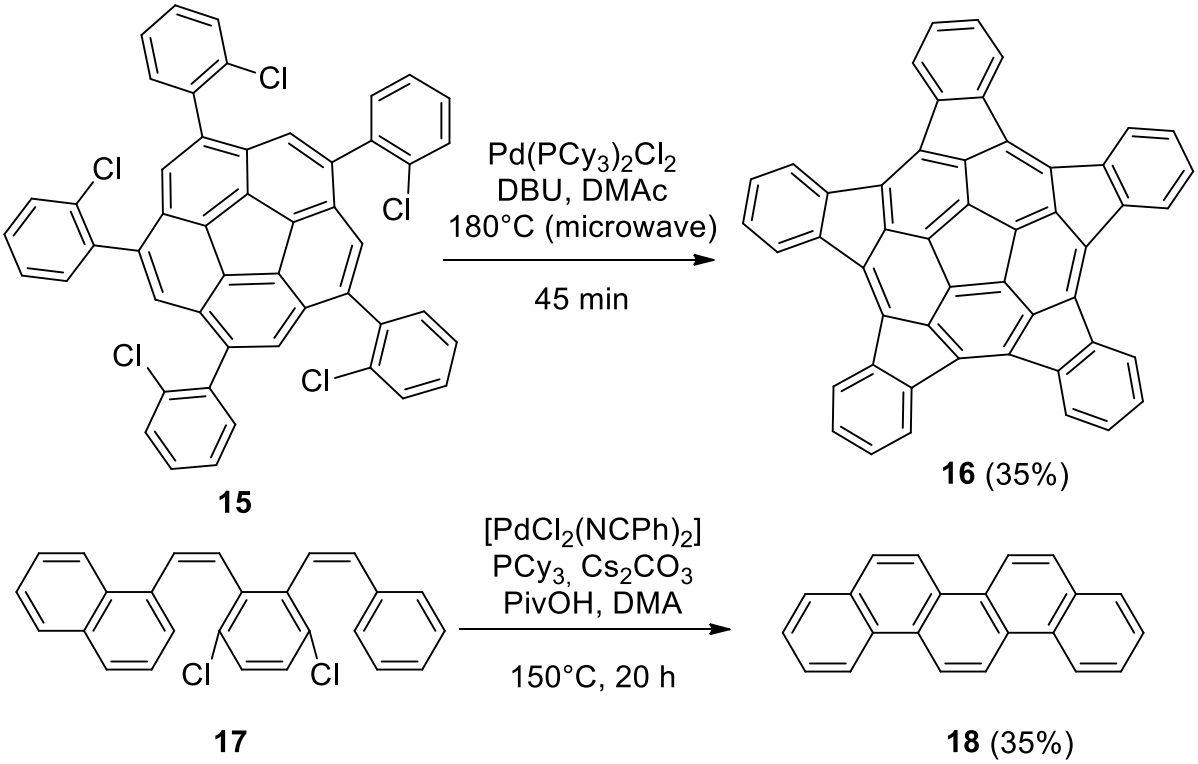

Figure 1.8 Non-planar and planar examples of C-H arylation.[117,119]

Recent findings from KOGA *et al.* detail a Pd(II) catalysed annulative dimerisation of chlorophenylenes through double C-H activation, which is unsual because the C-Cl bonds are activated and attack nearby aromatic C-H bonds within a terphenyl molecular framework.[122]

5) Cross coupling reactions

Cross coupling reactions are another class of Pd catalysed coupling method. The reactions reported by HIYAMA,[123] KUMADA,[124] NEGISHI,[125] STILLE,[126] and SUZUKI[127] have defined this field and are often employed in the stepwise synthesis of PAHs.[128] The SUZUKI coupling, which is the Pd(0) catalysed reaction between a boronic acid and an organohalide (see Figure 1.9) is of particular interest for many reasons: mild reaction conditions with non-toxic reagents, high product yields, toleration of a wide range of functional groups, high regioselectivity and easy separation of the inorganic boron compounds.[129] For the extension

of polyaromatic hydrocarbons, the introduction of pinacol boronic esters via borylation, can be employed for late-stage SUZUKI couplings.[130]

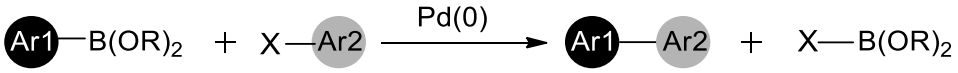

Figure 1.9 General scheme for SUZUKI coupling.

Introduction of boronic ester groups can be achieved either directly via a iridium-catalysed direct C–H borylation or a palladium-catalysed borylation of halogenated precursors.[130] The direct borylation method has already been implemented to functionalise many PAHs, such as pyrene,[131] corannulene[132] and helicenes (nonplanar screw-shaped PAHs).[133,134] Although subsequent SCHOLL reactions are often needed to anneal the nanographene precursors, it is possible to combine a SUZUKI coupling and a C-H arylation in a one-pot annulation cascade reaction, as demonstatrated by the groups of SCOTT, DE MEIJERE and WÜRTHNER and visualised below in Figure 1.10.[135-141]

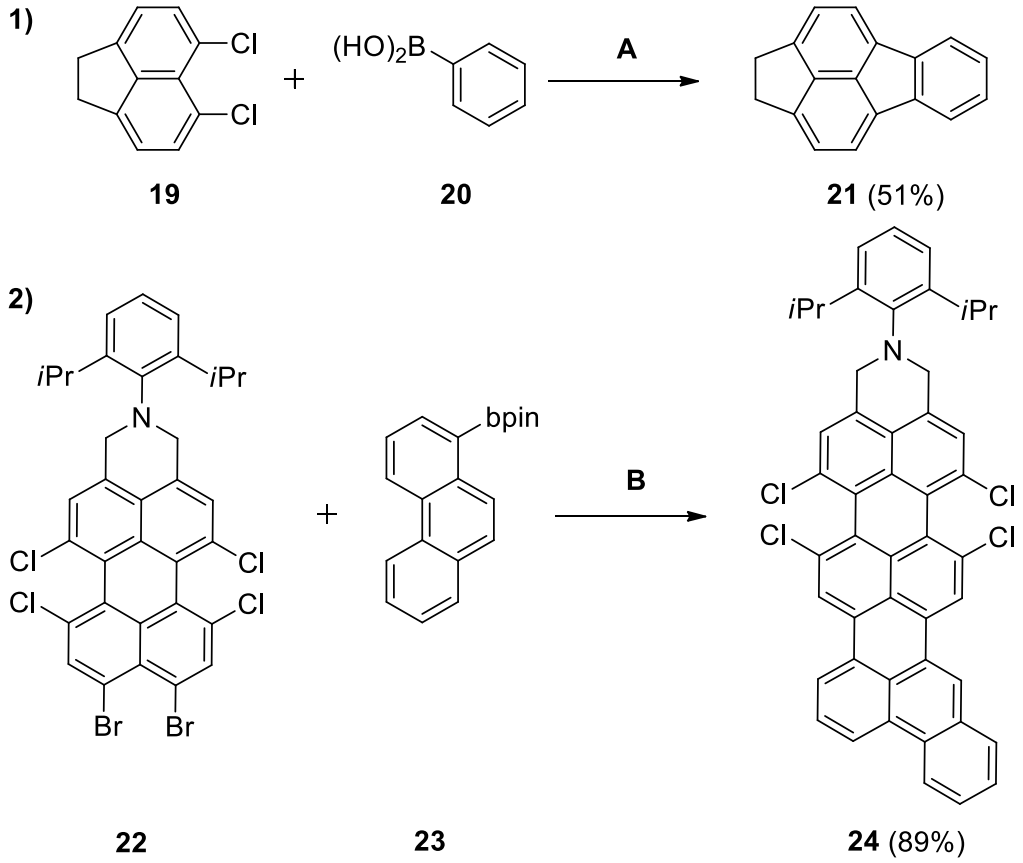

Figure 1.10 Examples of SUZUKI coupling cascade reactions from 1) SCOTT[135] and 2) WÜRTHNER.[141] **A**: 20% $Pd_2(dba)_3$, 50% $(t\text{-}Bu)_3P{\cdot}HBF_4$,excess DBU, DMAc,

microwave, 175°C, 40 min. **B**: $[Pd_2(dba)_3]$ $CHCl_3$ (10 mol%), $PCy_3 \cdot HBF_4$ (40 mol%), Cs_2CO_3 (3.0 eq.), 200°C, 20 h.

6) Photocyclisation

MALLORY and colleagues systematically explored the iodine catalysed photocyclisation of *cis*-stilbenes to phenanthrenes.[142,143] In recent years, this method has been extensively used for the synthesis of helicenes,[144,145] which contain the phenanthrene substructures, such as helicene **29** in Figure 1.11 below. KATZ proposed an improved methodology, where a stoichiometric amount of iodine and an excess of propylene oxide under argon lead to higher yields.[146] Propylene oxide acts as a scavenger for hydrogen iodide, which can otherwise photoreduce double bonds and generate multiple side-products.[147]

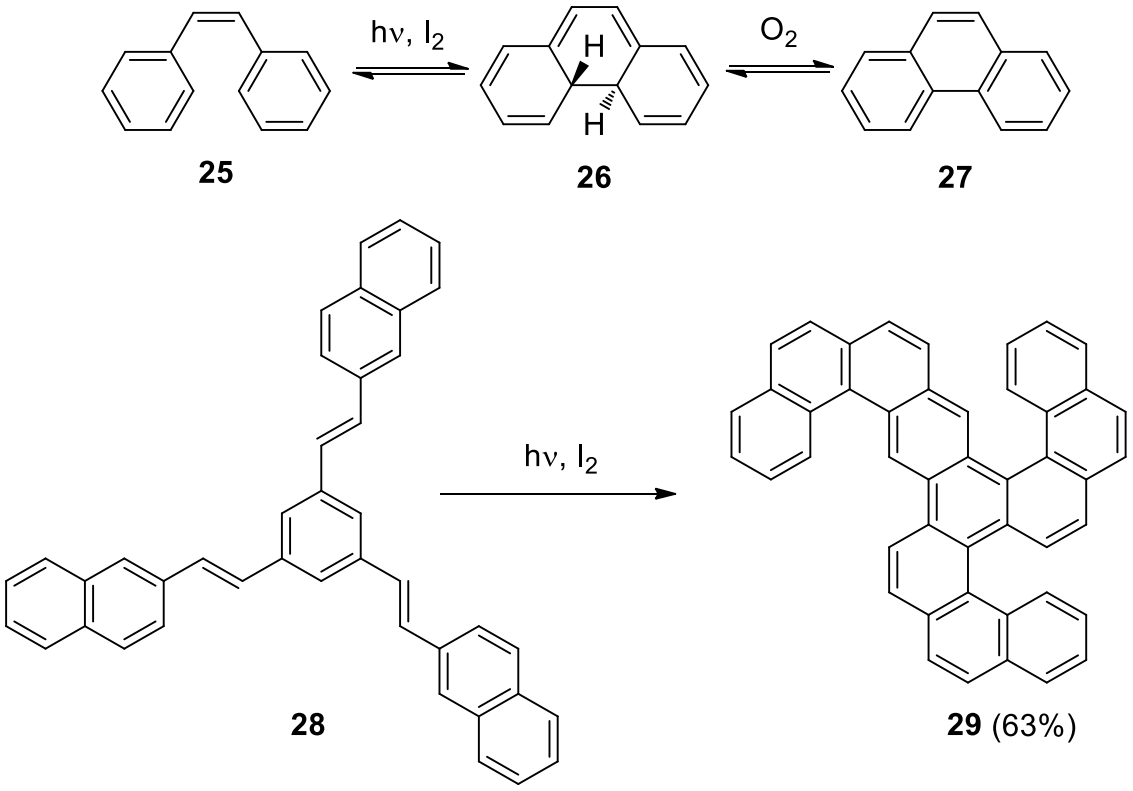

Figure 1.11 Formation of phenanthrene **27** and helicene **29** by photocyclisation.[142,145]

7) Photochemical cyclodehydrochlorination and cyclodehydrofluorination

This transformation, although also catalysed by UV light, differs from photocylocylisation as an additional oxidant is not required and HCl is eliminated. The photochemical cyclodehydrochlorination (CDHC), first described by SATO *et al.*,[148,149] and more recently investigated by MORIN and coworkers, is a regioselective reaction which utilises chlorinated precursors to access polyarenes, which are not possible to synthesise using the SCHOLL

reaction.[150] The regioselectivity originates from the placement of chlorine atoms at the desired positions beforehand and as a result the reaction conditions are milder than those of oxidative couplings. In MORIN's protocol, sodium carbonate is added to neutralise the solution, as HCl is generated upon cyclodehydrochlorination. This method has also been used for the synthesis of helical graphene nanoribbons, which confirms the success of this method for multiple bond formation.[151]

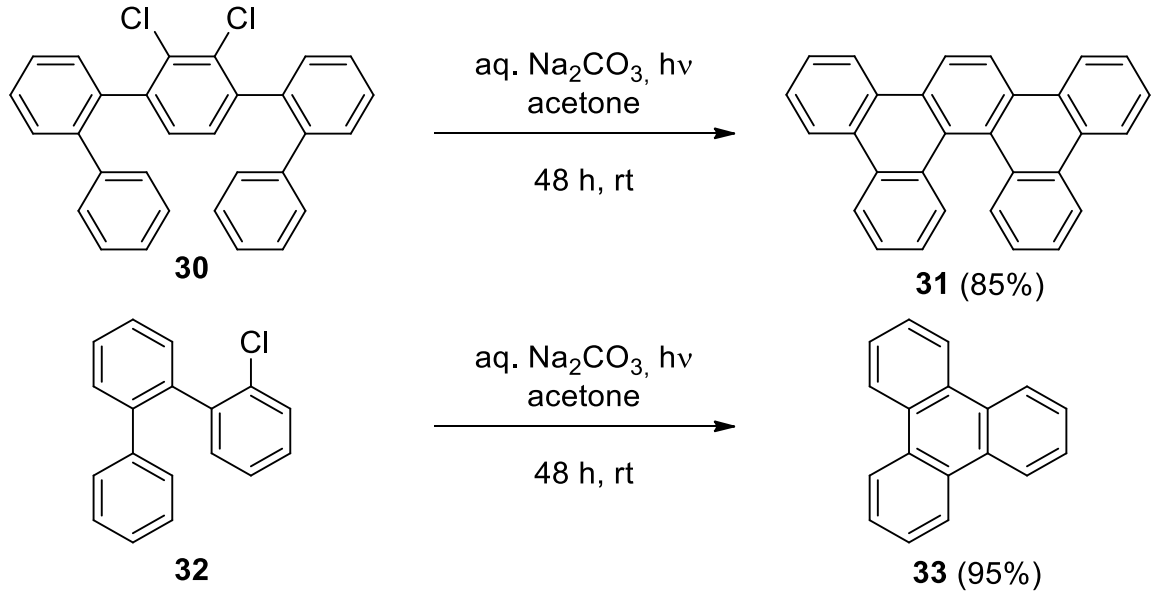

Figure 1.12 Photochemical cyclodehydrochlorination reaction conditions.[150]

Photocyclodehydrofluorination (PCDHF) is also literature known, but limited to the synthesis of terphenyls and phenanthrenes such as the trifluorophenanthrene derivative **35** in Figure 1.13 below.[152] Although this reaction is catalysed by UV light, it differs from the MALLORY type photocyclisation as oxdiants (including oxygen and iodine) are excluded: stilbenes undergo ring closure and HF is eliminated. The use of oxdiants promotes the classical photocyclisation, however eliminative loss of HF and even fluorine atom migration have been observed as a side-reactions.[153,154]

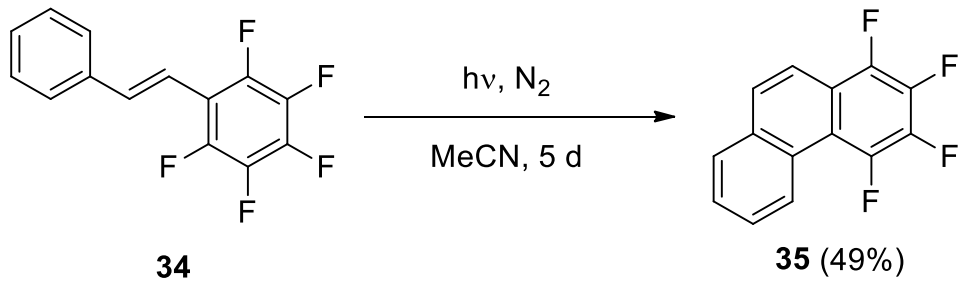

Figure 1.13 Photocyclodehydrofluorination (PCDHF).[152]

8) Al_2O_3 mediated hydrogen fluoride elimination

AMSHAROV and coworkers have systematically explored the intramolecular Aryl-Aryl coupling of fluoroarenes through Al_2O_3-mediated HF elimination.[155,156] The advantage of this method is that chlorine and bromine atoms in the molecule are tolerated. In addition, the C-F bond can only be activated if the fluorine atom is in the cove or fjord region (see Figure 1.14), whereas C-F bonds in the periphery do not react. Moreover, this regioselective strategy can construct five-membered rings in curved aromatic systems,[160-162] as well as planar nanographenes which are not accessible via oxidative coupling reactions (see Figure 1.14).[163]

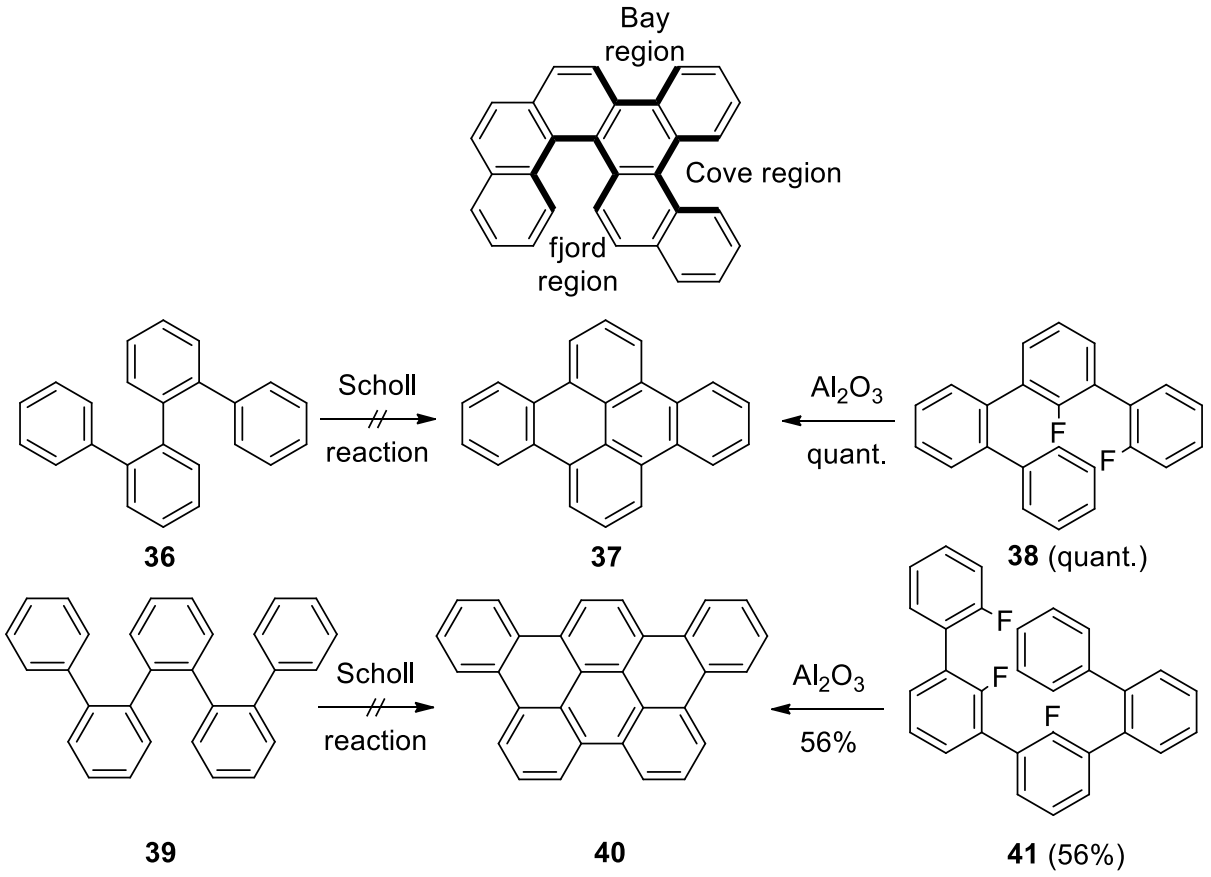

Figure 1.14 Molecular regions in PAHs and examples of nanographenes synthesised with AMSHAROV's H-F zipping approach.[163]

1.4.2 Fluorinated polyaromatic hydrocarbons

Regioselectively fluorinated PAHs are a promising class of organic semiconducting materials because of the unique properties of the fluorine substituents, as demonstrated by the fluoropicenes.[164] Introducing two fluorine atoms into PAHs increases their solubility and reduces the HOMO-LUMO energy gaps compared to non-fluorinated PAHs by 0.02–0.26 eV.[164] The low steric demand of fluorine results in the preservation of planarity in the

π-system and therefore has little effect on their π-π stacking in the solid state. The synthesis of many singly fluorinated chrysenes, picenes and phenanthrenes has been reported by FUCHIBE and colleagues,[164-166] an example of which is shown below in Figure 1.15.

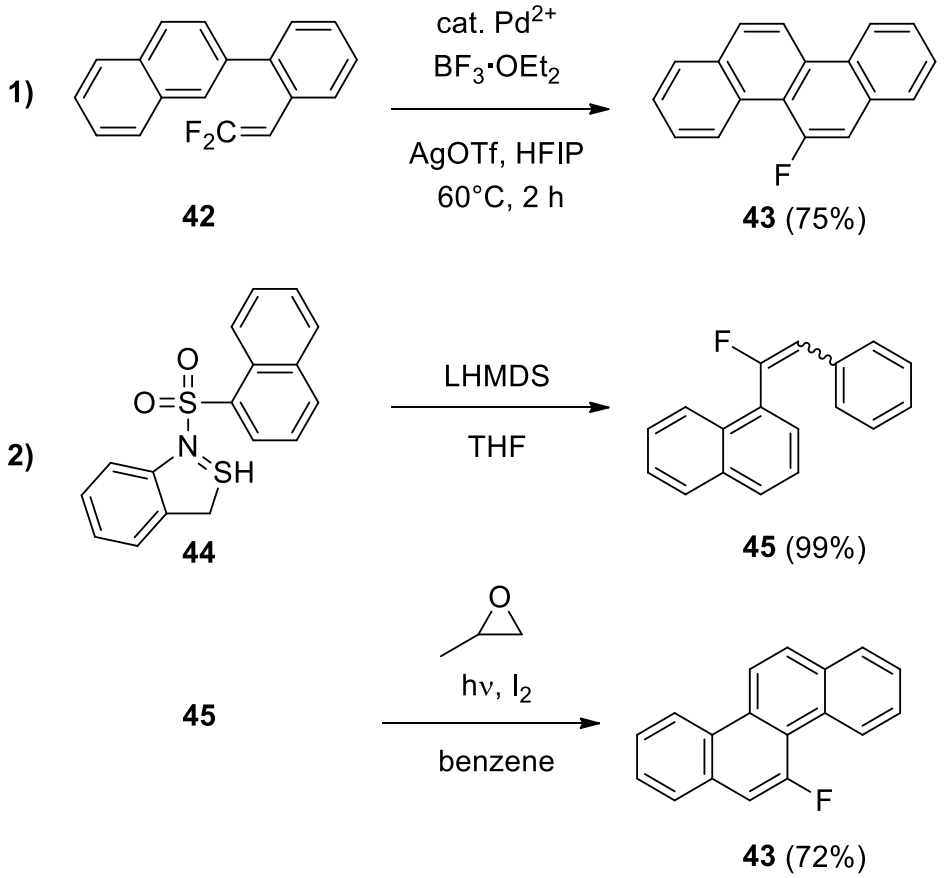

Figure 1.15 Synthesis of fluorinated PAH **43** according to 1) FUCHIBE *et al.*[164] and 2) BANERJEE *et al.*[167]

Regiospecifically fluorinated PAHs, such as 5-fluorochrysene **42**, can be synthesised using an alternative route, which involves diarylfluoroalkene precursors such as **45** (see Figure 1.15).[167] These precursors are synthesised via JULIA-KOCIENSKI olefination, followed by an oxidative photocylisation to afford fluorinated chrysenes. Contrary to FUCHIBE's findings, a small deviation from planarity was observed for the fluorinated chrysenes.[167] The ^{1}H and ^{13}C nuclear magnetic resonance (NMR) spectral features for PAHs containing a bay-region fluorine atom were also commented upon, as a new coupling between the bay-region fluorine atom and the nearest hydrogen atom on the adjacent ring is observed. These through-space H-F coupling interactions due to direct overlap between fluorine and C-H bond orbitals, plus C-F couplings have also been described by other groups.[168,169]

1.4.3 Introducing strain in nanographenes

This section describes reactions which lead to the formation of five- and seven-membered rings, as their introduction into nanographenes provides model systems for studying defective graphene. In addition, induced curvature as a result of non-hexagonal rings opens up the possibility of (opto)electronic applications.

Five-membered rings

Strain is induced in a molecule upon introduction of five-membered rings, which leads to contortion and ultimately to non-planar structures. Flash vacuum pyrolysis (FVP), which involves heating molecules in the gas phase to very high temperatures (500–1100°C) for a very short period time, was the method of choice for synthesising corannulenes before solution based syntheses were developed. Two examples of the formation of five-membered rings are shown below in Figure 1.16. The advantage of FVP is that molecules can be synthesised, which are not easy to access using other methods, but it is restricted to batch sizes of 1 g or less and yields rarely exceed 35%.[170]

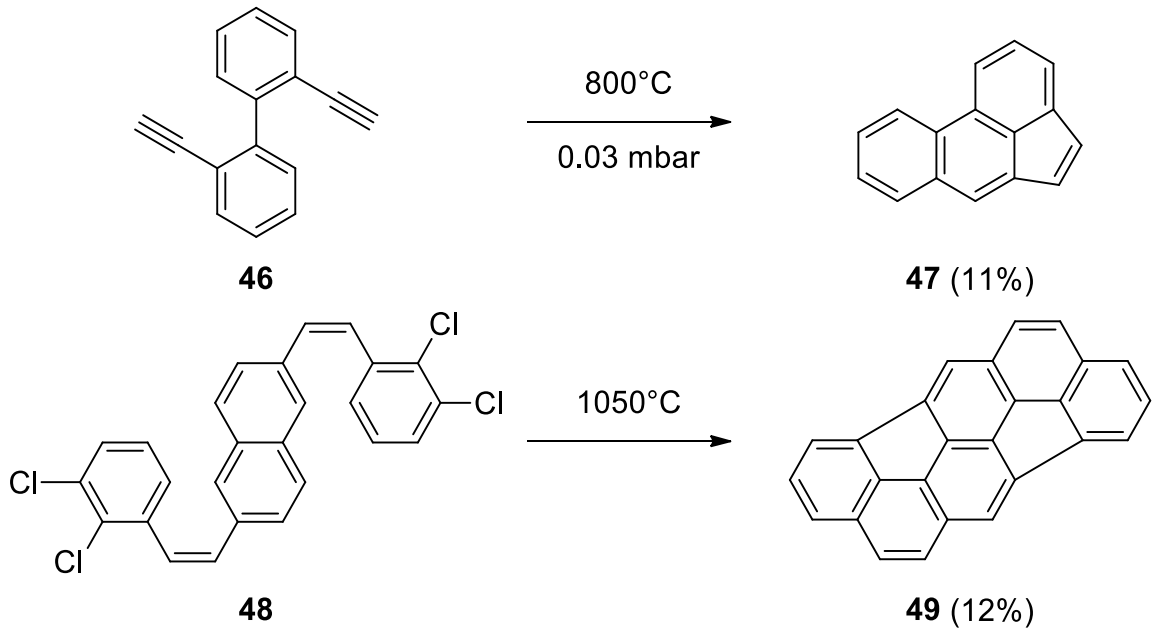

Figure 1.16 Formation of five-membered rings via FVP.[170,171]

The unexpected formation of five-membered rings when applying SCHOLL reaction conditions has been observed on several occasions, two examples of which are shown below in Figure 1.17.[75,79,172-176] As the mechanism of the SCHOLL reaction is still not fully understood and MÜLLEN oberserved that the prescence of both radical cations and arenium ions can contribute to a cyclisation, the regioselectivity of such reactions cannot easily be predicted.[172]

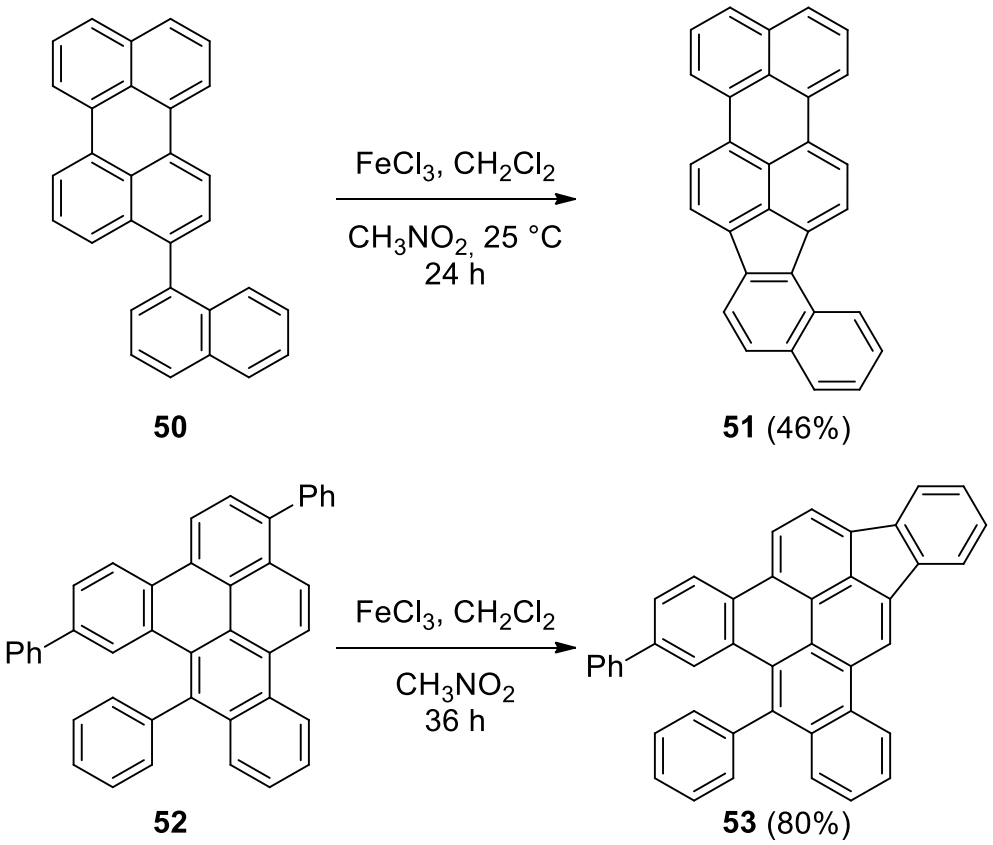

Figure 1.17 Formation of five-membered rings via the SCHOLL reaction.[79,176]

Cylopentannulation, which is a palladium(0) catalysed carbannulation with substituted acetylenes, is another transformation which forms five-membered rings. This method has been applied to the extension and contortion of many molecules, including bromo-functionalised pyrenes,[177,178] anthracenes[177,178] (Figure 1.18), phenanthrenes[179] and helicenes.[179] The formation of two neighbouring five-membered rings is also achievable with suitably adapted protocols.[180,181]

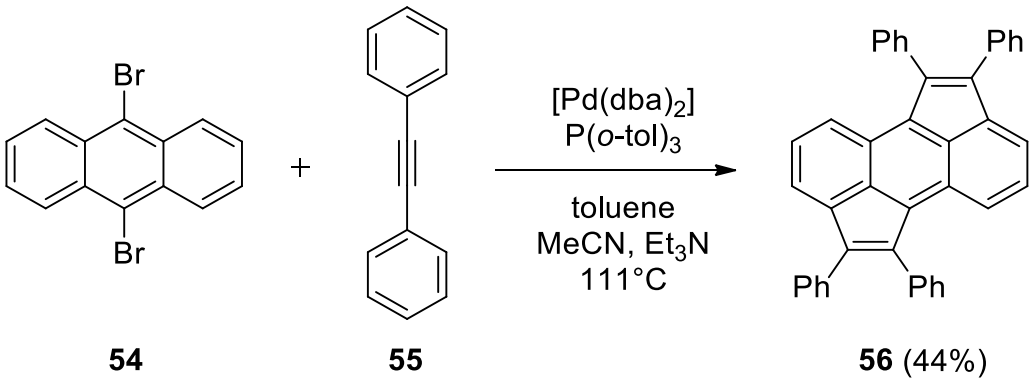

Figure 1.18 Synthesis of cyclpentannulated anthracene **56**.[177]

Finally, indenofluorenes (PAHs containing alternating six- and five-membered rings) have received considerable attention due to the anti-aromatic character of their fully conjugated systems and the potential application as organic semiconductors.[182] The multi-step synthesis of molecules such as **57** and **58** features FRIEDEL-CRAFTS acylation to form a five-membered ring with a ketone attached, which undergos subsequent GRIGNARD and reduction reactions.

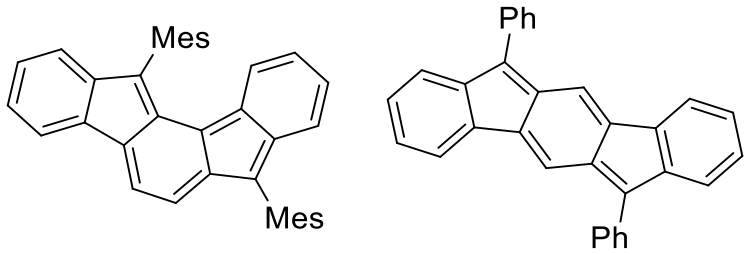

57 **58**

Figure 1.19 Indenofluorenes **57** and **58**.[183,184]

Seven-membered rings

Embedding seven-membered carbocycles into nanographenes is a desirable goal as by forming the aromatic cycloheptatrienyl cation, holes injected into p-type organic semi-conductors are stabilised. The resulting molecules are saddle shaped with negative curvature. The formation of seven-membered rings is quite rare in nanographenes, the first example is the SCHOLL reaction of a sterically overcrowded but flexible precursor **59** from DUROLA (see Figure 1.20).[185]

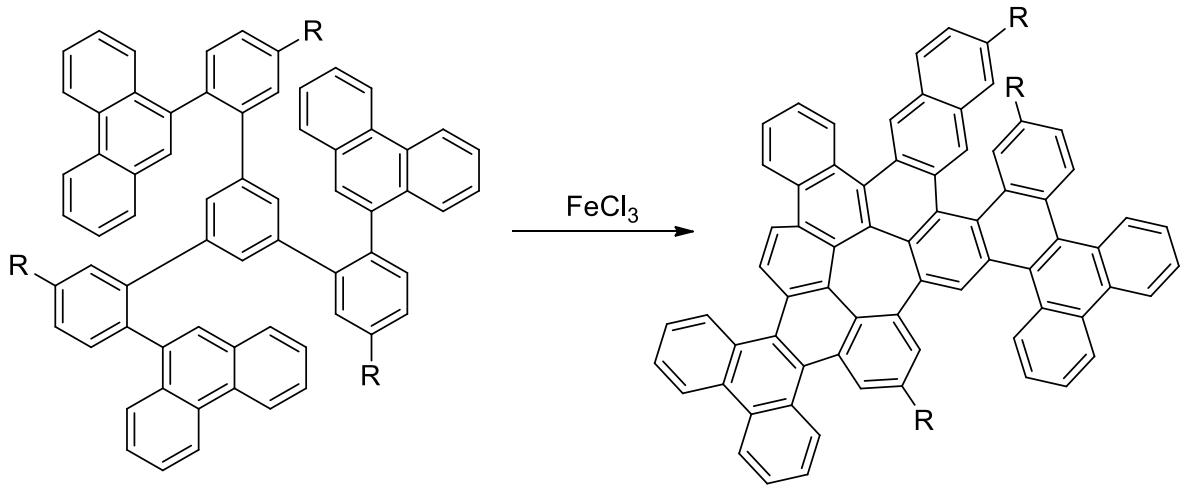

59 **60** (73%)

Figure 1.20 Synthesis of PAH **60**.[185] R: *tert*-butyl.

Palladium catalysed intramolecular C-H arylation can also lead to seven-membered rings, as demonstrated by SEGAWA, ITAMI and coworkers and shown below in Figure 1.21. The unexpected formation of four seven-membered rings instead of six-membered rings is thought to be due to steric repulsion exerted in the intermediates.[186]

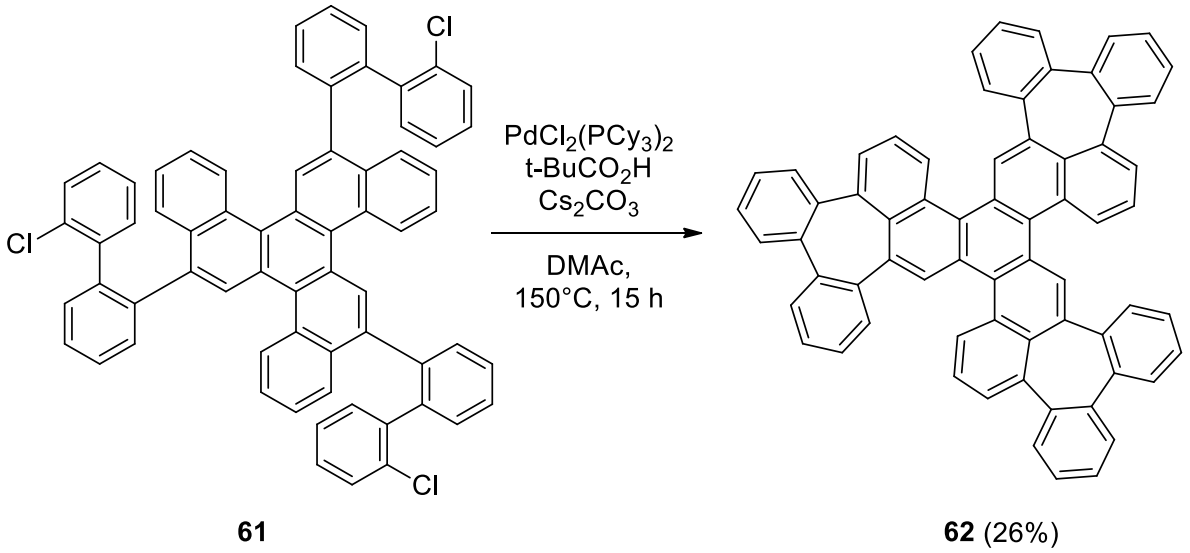

Figure 1.21 Formation of seven-membered rings.[186]

Arguably the most impressive examples of a curved nanographenes to-date come from ITAMI, SCOTT *et al*., who synthesised $C_{80}H_{30}$ and a *tert*-butylated analogue in two or three steps from corannulene.[187] Five seven-membered rings were formed through C-H activation and subsequent cyclodedrogenation, which warps the molecule and leads to significant changes in the solubility, optical and electronic properties. Two of the precursors are shown below in Figure 1.22.

[7]-circulene, which consists of a central heptagon surrounded by seven six-membered rings has been synthesised by YAMAMOTO according to two different methods, the former forming a seven-membered ring via photocyclisation and the latter via FVP.[188,189] MIAO recently published a synthesis of heptabenzo[7]circulene, where the central heptagon was formed by a the expansion of a cyclohexanone moeity. An extended saddle shaped [7]-helicene could be realised by CRUZ *et al*., featuring alkyne cycloisomerisation to introduce seven-membered rings.[191]

Seven-membered versions of indenofluorenes have also been reported by MIAO, which are synthesised using a similar strategy and are p-type organic semiconductors.[192] This research group also described the preparation of several molecules, where pre-formed seven-membered rings are introduced and the surrounding scaffold extended.[193-196]

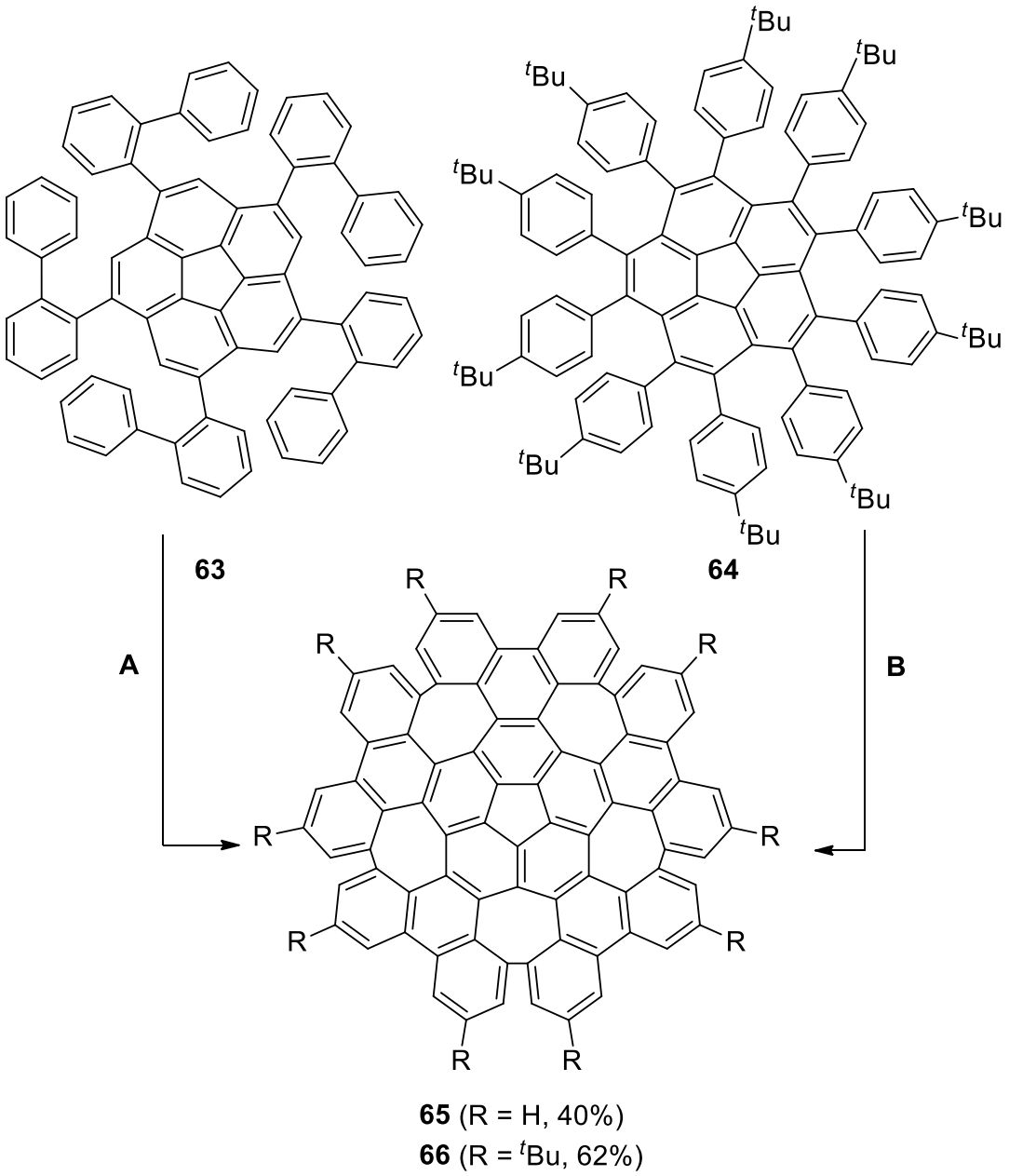

Figure 1.22 Synthesis of grossly warped nanographenes **65** and **66**.[187]
A: DDQ (10 eq.), TfOH/CH_2Cl_2 (5:95), 0°C, 30 min;
B: $FeCl_3$ (31 eq.), CH_2Cl_2/nitromethane (115:1), 25°C, 1 h.

To conclude, the formation of five- and seven-membered rings is not always predictable, but leads to the formation of interesting curved nanographenes.

1.4.4 Tribenzotriquinacene as a defective core

The introduction of a rigid, curved defect centre into graphene is desirable in order to alter the properties in a controlled manner. Holes are considered to be more more problematic than

defects composed of non-hexagonal rings, due to the reactive dangling bonds at their rim and the increased flexibility of the material.

Naturally occurring defects in graphene can migrate through the lattice and do not provide the necessary curvature, so a bottom-up strategy is required. Tribenzotriquinacene (TBTQ, **68**) is a bowl-shaped aromatic hydrocarbon, whose curved structure derives from the three fused five-membered rings at its centre, and is hypothesised be a suitable defect centre for a nanographene by KUCK and colleagues.[197]

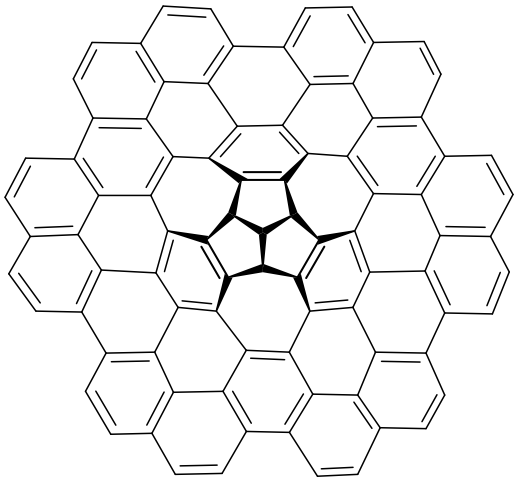

Figure 1.23 Hypothesised structure of a defective nanographene with a TBTQ core.[197]

The triquinacene core of TBTQ provides it with its conformationally rigid structure, and the first reported synthesis is from WOODWORD and colleagues in 1964.[198] Compared to the highly reactive and instable triquinacene (**67**), TBTQ is stabilsed by the three benzene rings and is therefore a suitable candidate for the simulation of a graphene defect centre.[199]

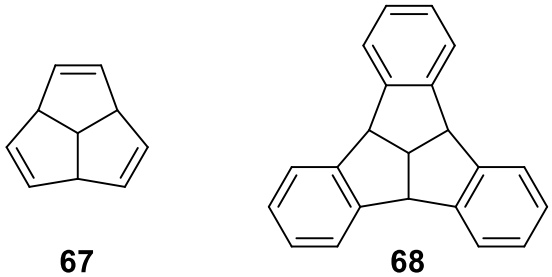

Figure 1.24 Triquinacene (**67**), TBTQ **68**.

1.5 Tribenzotriquinacene crystal structure

The crystal structures of TBTQ **68** and the methyl derivative **69** can be seen below in Figure 1.25.[200,201] Both molecules adopt a perfect C_{3v} conformation in the solid state, and the three

indane wings adopt mutually orthogonal orientations (87.2° for Me-TBTQ **69**, 87.7° for H-TBTQ **68** as shown in Figure 1.25).

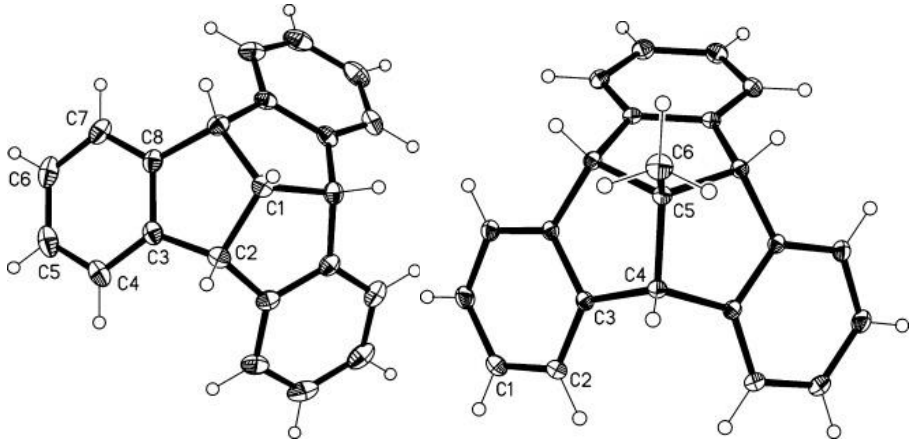

Figure 1.25 Crystal structures of H-TBTQ **68** (left) and Me-TBTQ **69** (right). The figures are taken from ref [200] and reproduced with permission Copyright 2013, Wiley-VCH Verlag GmbH & Co. KgaA, Weinheim.

Me-TBTQ **69** crystallises in the rhombohedral space group R*3m* and is packed in parallel columnar stacks, with perfectly axial convex-concave packing.[201-203] The packing behaviour of H-TBTQ **68** is reported to be similar, but the space group is R*3c* and the molecules in the stack are not perfectly parallel, rather rotated relatively to each other by +6° and -6°. Functionalisation at the *centro* group does not drastically change the structure, but **68** displays a tighter crystal packing, as the apical methyl group is not present (distance between the central carbon atoms in adjacent molecules: 4.75 Å for H-TBTQ **68**; 5.95 Å for Me-TBTQ **69**).[200]

1.6 Tribenzotriquinacene synthesis

KUCK documented the first synthesis of Me-TBTQ **69** in 1984,[204] which is referred to as the double cyclodehydration strategy (see Figure 1.26).[111,112] Starting with a condensation reaction between an indanedione derivative and diphenylmethanol, the isolated diketone is reduced and cyclised. The synthesis of unsubstituted TBTQ **68** was reported using similar conditions in 1992.[205] Functionalisation at the *centro* position is possible if the functional

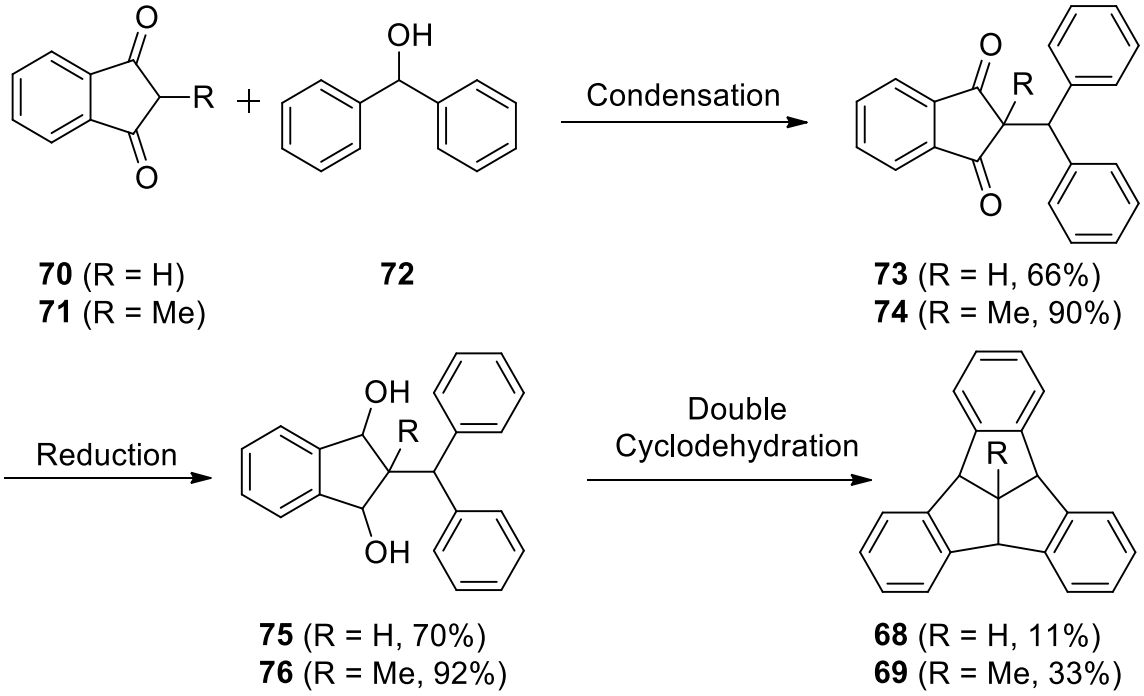

Figure 1.26 Outline of the double cyclodehydration strategy by KUCK *et al.*[204,205]

group is introduced into the starting materials.

The overall yield for H-TBTQ **68** is very low at only 5% (compared to Me-TBTQ **69**: 27%), which could only be marginally improved upon by KUCK in 1994 to yield 4–19%.[206] HOPF and coworkers presented an alternative synthesis pathway for TBTQ **68** in 2012, which offers a 19% overall yield in only three steps and a 32% yield for the final cyclisation step as shown in Figure 1.27.[207]

In addition, the triple cyclisation pathway from HOPF can be used to functionalise TBTQs with methyl, bromo and methoxy groups at the "*ortho*" positions of the aromatic periphery to give C_1- and C_3-chiral derivatives.[207]

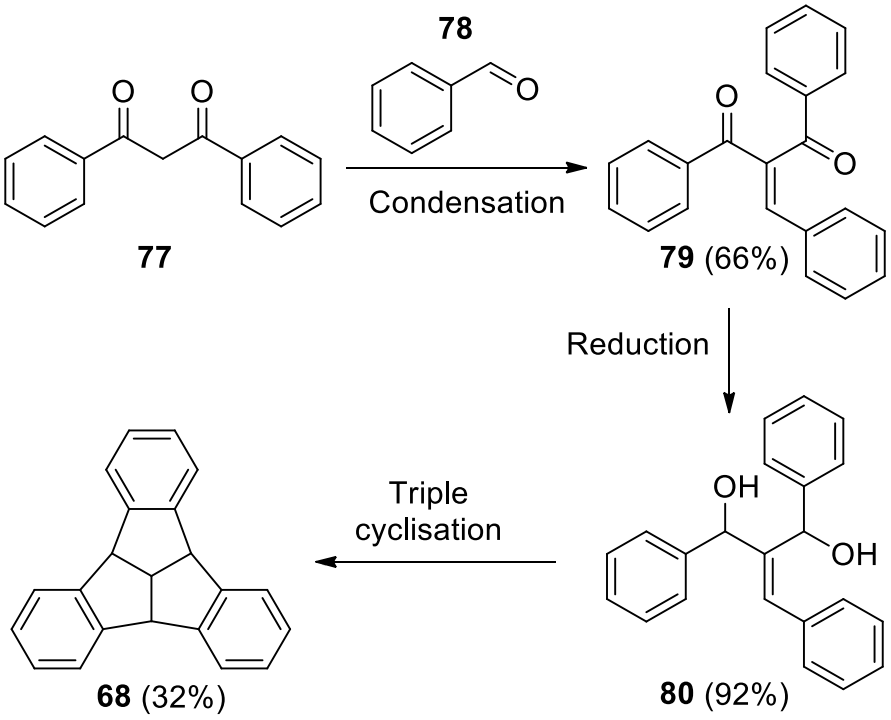

Figure 1.27 Overview of the triple cyclisation pathway by HOPF *et al.*[207]

1.7 Tribenzotriquinacene functionalisation

There are four different positions on the TBTQ scaffold, which are highlighted in Figure 1.28. As already mentioned, KUCK's TBTQ synthesis can be used to introduce groups at the *centro* position, which is however restricted to pre-functionalised indanediones with alkyl substituents such as methyl, ethyl, benzyl, *n*-butyl and iso-propyl, which increase the solubility.[208-210] Post-functionalisation at this position is also possible, but only takes place via a tribenzodihydroacepentalene derivative.

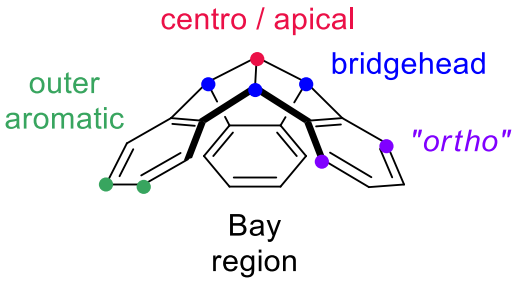

Figure 1.28 3D depiction of tribenzotriquinacene indicating the different positions.

In 2016, DHARA *et al.* reported the introduction of a terminal alkyne at the *centro* position, which could undergo further transformations such as azide-alkyne HUISGEN cycloaddition and a SONOGASHIRA cross coupling.[211] A recent short review from BEUERLE *et al.* summarises

the most important transformations and strategies for the functionalisation of TBTQs,[212] of which the most relevant examples are described in more detail here.

The benzhydrilic bridgehead positions are by far the most reactive positions and the advantage of functionalisation at this position is increased solubility upon introduction of alkyl groups.[213] Radical bromination[201,214] followed by S_N1-type substitution reactions lead to a variety of products,[199,213,215-217] some examples are summarised below in

Figure **1.29**.

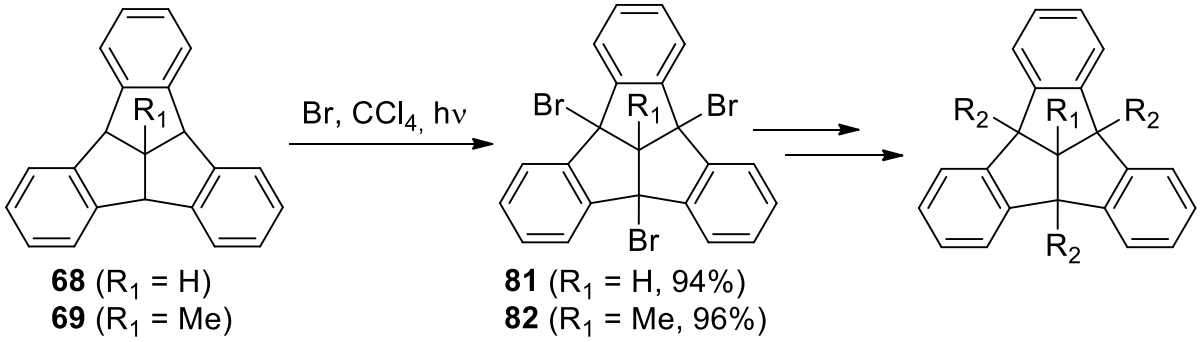

Figure 1.29 Functionalisation of the TBTQ bridgehead positions.[199,201,213-217]

R_2 = Me, Et, Allyl, Cl, OH, OMe, N_3, NH_2, NMe_2, Phenyl, C_6H_4OMe.

Polymetalation of tribenzotriquinacene and formation of the tribenzacepentalene dianion can be realised upon reacting with a mixture of *n*-butyllithium and potassium-*tert*-pentoxide (LOCHMANN-SCHLOSSER base)[218] In addition to the interest surrounding the properties of such dianions, using electrophiles to trap these reactive compounds can lead to trisubstituted TBTQs, where three different functional groups occupy the bridgehead positions.[218] Monometalation with sodium and potassium metal bases has also been reported by KLETT and colleagues, who observed configurationally stable ineractions of the metal ions with the convex or concave face of the bowl, in the absence of bowl-to-bowl conversion.[219]

Methyl groups can also be used to block the reactive bridgehead positions in order to functionalise the outer aromatic positions. Although these reactions are not regioselective, bromination and iodination at these positions are useful transformations, as they pave the way for further substitution or coupling reactions.[197,201,220-224]

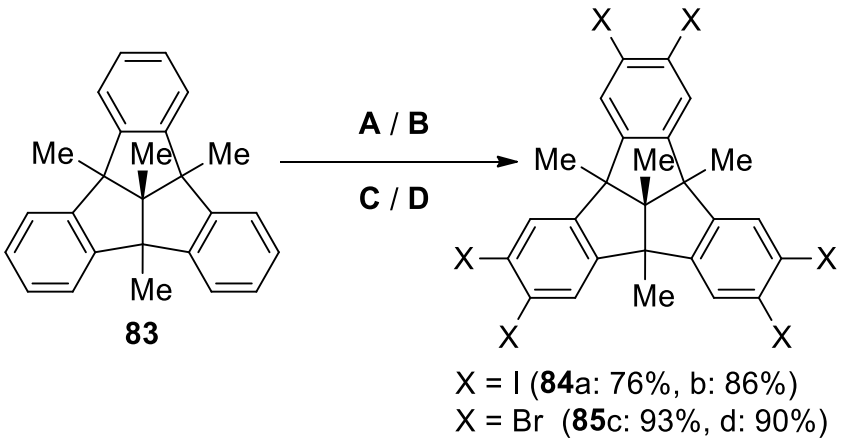

Figure 1.30 Examples of bromination and iodination of the outer aromatic positions.[197,223] **A**: H_5IO_6 / H_2SO_4 / KI, 0→20°C, 20 h. **B**: *N*-iodosuccinimide, TFA, microwave, 70°C, 1 h. **C**: Fe / I_2 / CCl_4; Br_2, 60°C, 24 h. **D**: *N*-bromosuccinimide, TFA, microwave, 70°C, 3 h.

Alternatively, pre-functionalised starting materials can introduce moieties at the aromatic periphery, so that blocking the bridgehead positions in advance is not necessary.[225,226] Chloromethylation can be carried out at the *meta* positions once the triquinacene core has been formed, eliminating the need to block the bridgehead positions.[227]

Extension of the indane wings can be realised from the outer aromatic positions,[228-230] which is important for the construction of supramolecular assemblies such as organic cages[231,232] supramolecular nanotubes,[233] host-guest complexes,[222,234-236] chemosensors,[237] metallo-squares,[238-239] and cavitands.[240] For these applications, the synthesis of enantiopure TBTQs has been explored fully.[233,238-242]

Finally, funtionalisation at the *meta* positions can lead to the formation of an extended TBTQ containing macrocyclic pores, as KUCK *et al*. recently demonstrated.[243] Starting from hexamethoxy TBTQ **86**, the key steps were repeated conversion from methoxy to triflate, followed by SUZUKI coupling and SCHOLL reactions to yield TBTQ **88** (Figure 1.31). The radii of pores in this TBTQ based macrocycle are between 2.9 and 3.0 Å and the binding of a chloride atom was investigated.

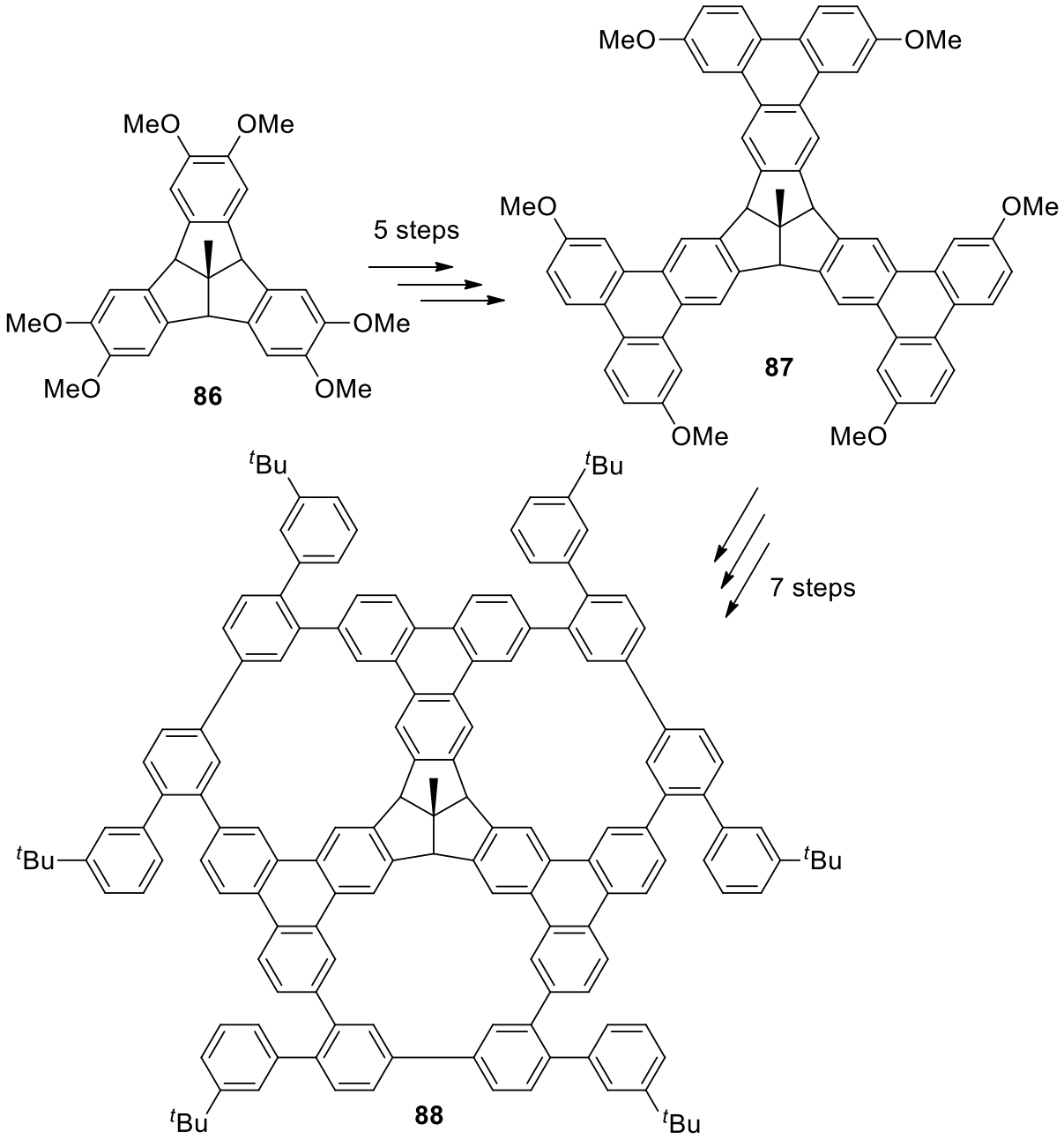

Figure 1.31 Synthesis of TBTQ **88**.[243]

The *ortho* positions are considered the most challenging to functionalise, and are not possible to post-functionalise with electrophilic aromatic substitution due to steric factors. Aside from HOPF's triple cyclisation method (see section 1.6), KIRCHWEHM *et al.* reported the synthesis of a TBTQ bearing methyl groups at all six *ortho* positions.[244] The addition of a nucleophile was also achieved at the *ortho* position of the electrophilically activated Mn carbonyl complex of a methylated TBTQ, but is unlikely to survive removal of the metal complex and re-aromatisation.[245]

KUCK published the first example of direct *ortho* functionalisation in 2016.[246] 2-Hydroxy-substituted tribenzotriquinacenes were reduced with *o*-iodoxybenzoic acid, to afford the C_s- and C_1-symmetrical TBTQ-*o*-quinones **90** and **91** in a 1:1 ratio. Chromatographic separation of the two quinones was possible and further functionalisation of the aromatic ring was explored.

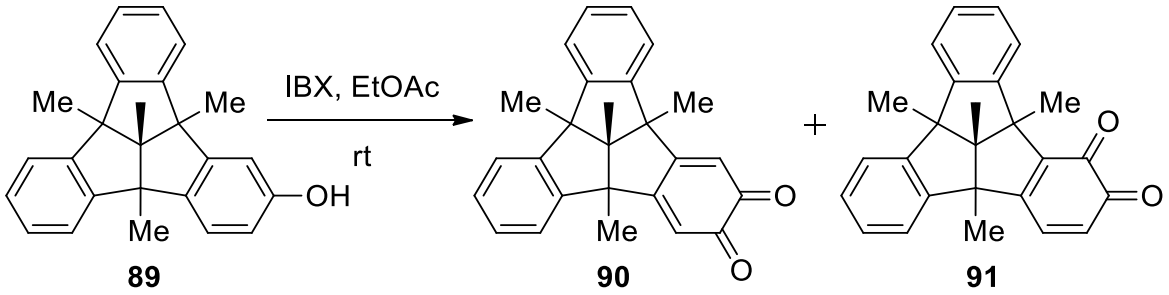

Figure 1.32 Preparation of an unexpected TBTQ-*o*-quinone **91**.[246]

1.8 Extended TBTQs

Ortho-functionalised TBTQs are promising building blocks for bridging the bay region and extending the carbon network, working towards a defective nanographene. KUCK and MUGHAL reported the formation of one cycloheptatriene ring,[247] but adapting this method to accommodate the formation of three seven-membered rings was not successful.[248] Potential explanations for this are unfavourable crowding and poorly soluble reaction intermediates.

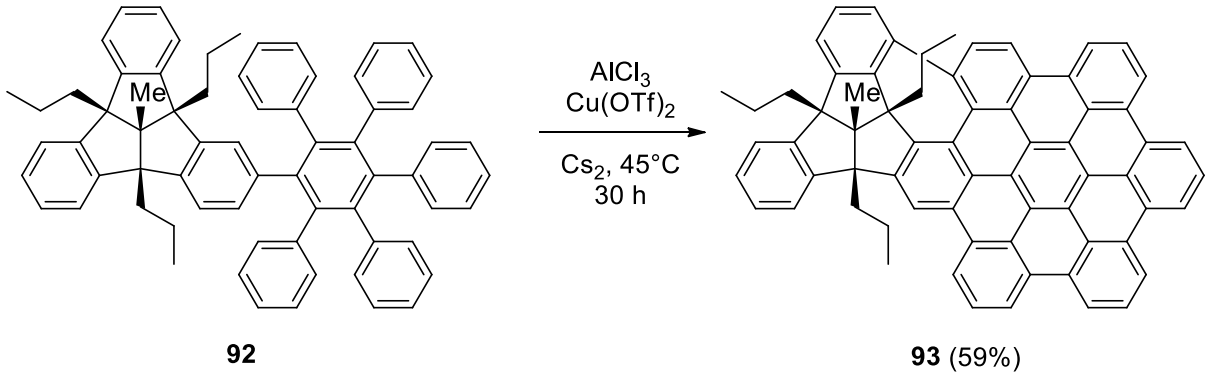

Figure 1.33 Synthesis of TBTQ **93**.[247]

Adopting a different approach, the three-fold SCHOLL-type cycloheptatriene ring formation was achieved by KUCK *et al.* in 2016[249] Methoxy functionalised TBTQ **94** was subjected to boron tribromide to give the corresponding trihydroxy-TBTQ **95** and a subsequent reaction of this molecule with triflic anhydride afforded the TBTQ triflate **96**. A SUZUKI coupling with

methoxy functionalised boronic acids yielded precursor TBTQ **98**, which under SCHOLL reaction conditions gave the "wizard hat" TBTQ **99**.

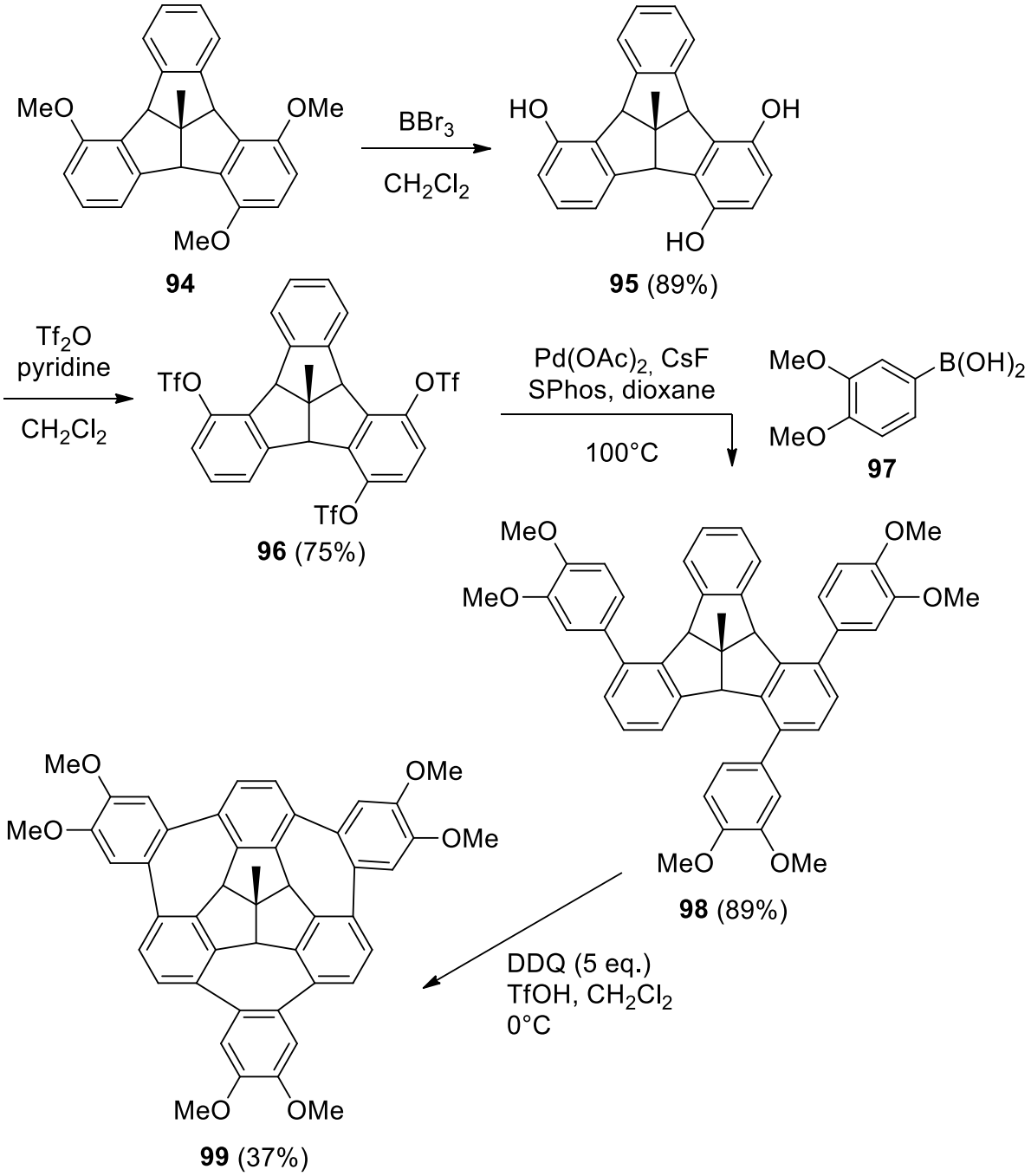

Figure 1.34 Synthesis of TBTQ **99**.[249]

2 Aims

Based on the literature summary in the previous section, it is clear that defect engineering of (nano)graphenes is a fascinating topic of research, as the deliberate introduction of rigid, curved deformations is likely to result in interesting electronic properties. TBTQ, if embedded in a nanographene, can be considered as a rigid defect centre: rigidity originates from the strain induced by its three five-membered rings and this core does not contribute to the conjugated π-system. Owing to the multitude of transformations available to achieve aryl-aryl coupling, combined with the unique reactivities of the different positions in TBTQ, there remains a substantial number of topics for further study. In addition, further investigations into the interaction of TBTQ molecules with a metal substrate and the effect of phenanthrene moeities on the stacking arrangements of TBTQ crystal structures would complement previous research and extend the π-system.

This work is split into four individual projects, which are ordered in increasing complexity and according to the position of TBTQ that is functionalised, as described below in more detail and summarised in Figure 2.1.

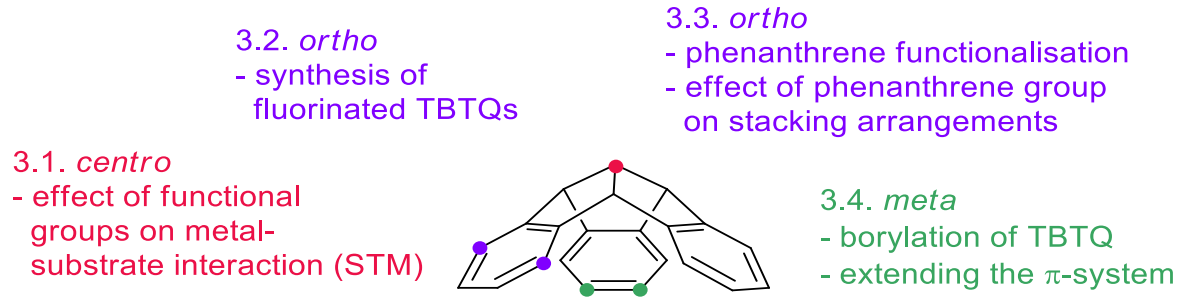

Figure 2.1 Positions of TBTQ, indicated in red (centro), purple (*ortho*) and green (*meta*)and a concise summary of the main aims of the individual chapters.

Influence of the functionalisation of the centro position – STM investgation of TBTQ

Although the crystal structure and packing behaviour of literature known H-TBTQ **68** and *centro*-functionalised Me-TBTQ **69** are well documented[200] the arrangement of these molecules on a metal surface has not yet been explored. For this project, a cooperation with the group of Prof. M. BODE (Dept. of Physics, Universität Würzburg) aims to investigate the different arrangements of TBTQs **68** and **69** on a Ag(111) surface, using scanning tunneling microscopy (STM).

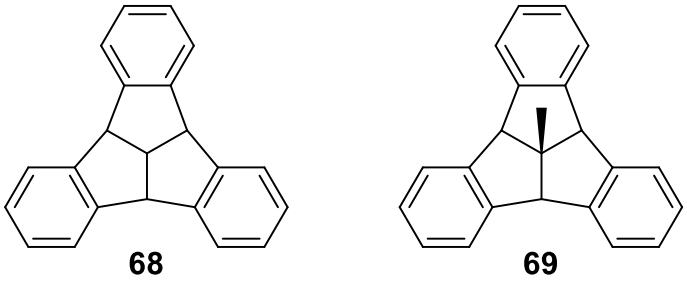

Figure 2.2 TBTQs **68** and **69**.

Functionalisation of the ortho position – synthesis of fluorinated TBTQs

Fluorinated TBTQs are desirable molecules to synthesise as the presence of one or multiple fluorine atoms is likely to give rise to interesting electronic properties. In addition, photo-cyclodehydrofluorination or Al_2O_3 HF elimination reactions could be used to extend the scaffold in regioselective manner as a viable alternative to the SCHOLL reaction. AMSHAROV predicts that the surface assisted construction of nanoscale electrical devices could be realised via C-C coupling on insulating metal oxides, for which suitably fluorinated precursors are required.[159] For initial investigations into the viability of fluorinated TBTQs, synthetic aims TBTQ **100** and **101** are chosen.

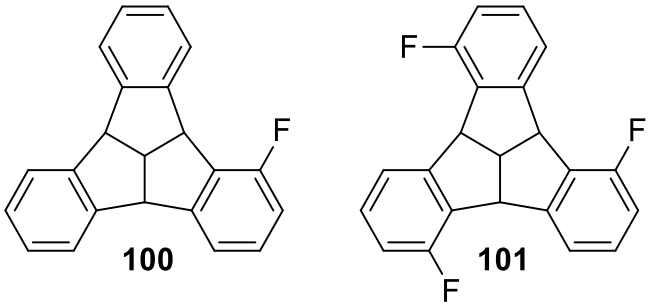

Figure 2.3 Synthetic aims TBTQs **100** and **101**.

Funtionalisation of the ortho position – synthesis of phenanthreno-TBTQs and study of their stacking arrangements

The aim of this project is to extend TBTQ, in order to generate a defective nanographene with a TBTQ core. KIRCHWEHM's strategy focused on functionalisation at the *ortho*-positions, by introducing phenanthrene groups with a view to bridge the bay region[250] and this work will build upon her findings. In addition, crystal structures of phenenathrene-containing TBTQs would provide a valuable insight into their stacking arrangements in the solid-state.

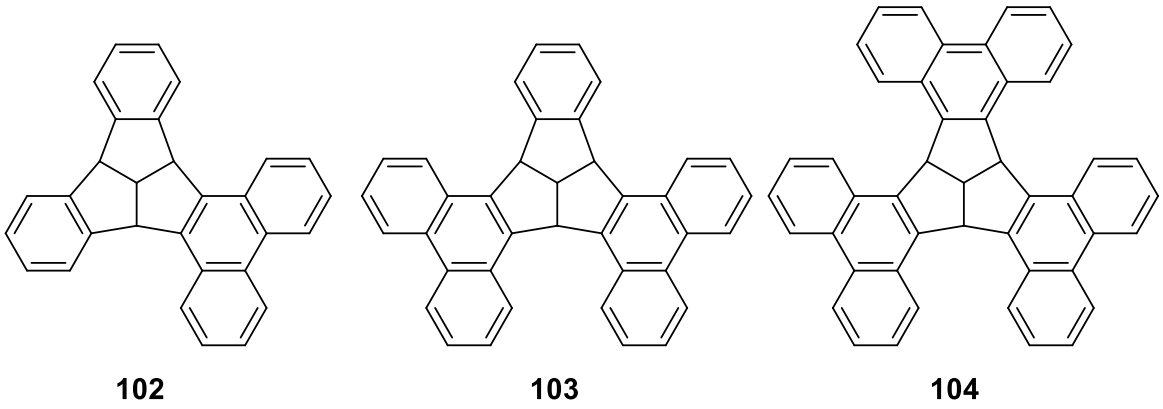

Figure 2.4 Synthetic aims: phenanthrene functionalised TBTQs **102**–**104**.

Functionalisaion of the meta position – Borylation and extension of TBTQ with pheanthrene moeities

Introducing functional groups in the starting materials often leads to extra steps and ultimately long syntheses pathways. This project aims to explore borylation of the outer aromatic positions of Me-TBTQ **69**, with the aim of synthesising extended TBTQs such as TBTQ **106**, that posess a "snowflake"-like geometry.

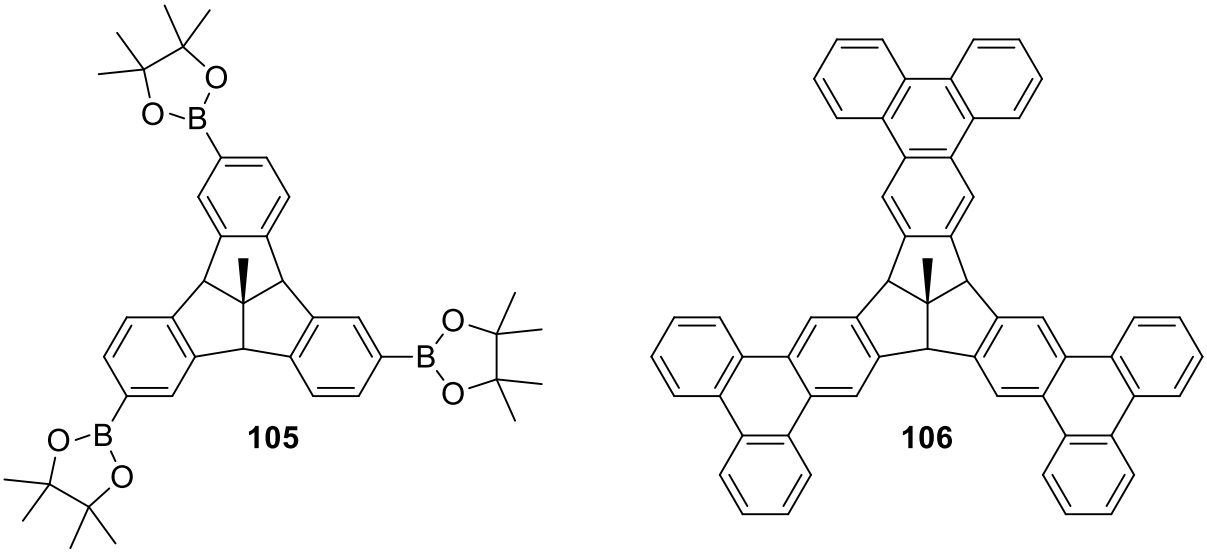

Figure 2.5 Synthetic aims: borylated TBTQ **105** and extended TBTQ **106**.

3 Results and Discussion

3.1 Influence of the functionalisation of the *centro*-position – STM investgation of TBTQ

As already mentioned in the introduction, investigating the strength of non-covalent interactions between a substrate and an adsorbed organic molecule is of great importance for the field of molecular electronics,[41] as this directly affects the electronic properties of the resulting interface.[42,43] Atomically flat noble metal surfaces in ultrahigh vacuum are ideal substrates for probing the intramolecular interactions.[257] STM images provide valuable insights into the relative alignment of molecules, which differs to those observed in solution.

Until now the only example of STM investigations of TBTQs focused on the attachment of three di-*n*-alkyl sulfide anchor groups at the bridgehead positions, which were able to attach to a Au(111) surface and formed self-assembled monolayers on a matrix of decanethiol.[251,257] In this example, TBTQ molecules do not form a continuous layer but are embedded as individual molecules in an alkylthiol matrix, with the TBTQ moiety residing with its concave side pointing outwards on top of a densely packed alkyl chain layer.[251,257] Furthermore, their interaction with the metal surface is governed by the adhesion of the thioether anchor groups.[251,257] It is expected that TBTQs without anchor groups will interact and orient themselves in a different way, as the the π-system of the molecules can directly interact with the electronic states at the metal surface, thus providing valuable insights in the electronic structure of the adsorbates.[257] Previous work from KUCK, HOPF *et al*. described the crystal structures and packing behaviour of TBTQs **68** and **69**,[200] but the aggregation and alignment TBTQs is expected to be altered when adsorbed to a metal surface.[257] Additionally, the relative alignment of TBTQ molecules could provide an insight into π-π and π-H intermolecular interactions.

The arrangement of bowl-shaped corannulene **107** on a Cu(111) surface is literature-known: the bowl is tilted and its opening points away from the surface, so that a single bond in the five-membered ring is closest to the surface, owing to a charge redistribution between the substrate and molecule.[253,257] Extending corannulene with aromatic moieties led to a significant change in the adsorption mode, so that the molecule "stood" on its rim.[252,257] Several other publications detail STM investigations of other extended coranulenes,[254] as well as of aggregates of a C_{70}-fragment buckybowl[255] and hemifullerenes.[256]

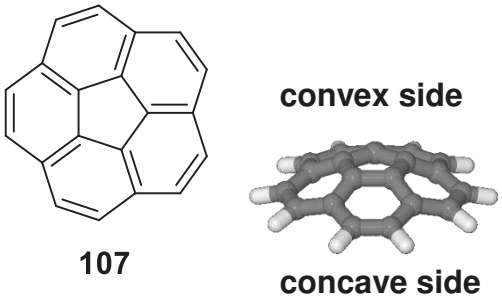

Figure 3.1 Structure of corannulene (**107**) and 3D-model indicating concave and covex sides.

H-TBTQ **68** and Me-TBTQ **69** (see Figure 2.2) were chosen for the STM investigations, as their crystal structures and syntheses are literature known.[200] H-TBTQ **68** was synthesised according to the HOPF triple cyclisation pathway, as can be seen below in Figure 3.2. The KNOEVENAGEL step afforded diketone **77** in 65% yield, which is comparable with the literature yield of 66%.[207] Traces of ethyl acetate were removed via Kugelrohr distillation, but the viscous yellow did not solidify upon standing. As the spectroscopic data was in accordance with the literature values, it was therefore decided to continue with the LUCHE reduction, which gave a combined yield of the two diastereoisomers of 82%. The final cyclisation step afforded the desired product in an 18% yield, which is lower than the literature value: 32%. After gradient sublimation, as carried out by A. KUDZUS from the research group of Prof. F. WÜRTHNER, a satisfactory amount of product was purified for STM investigations.

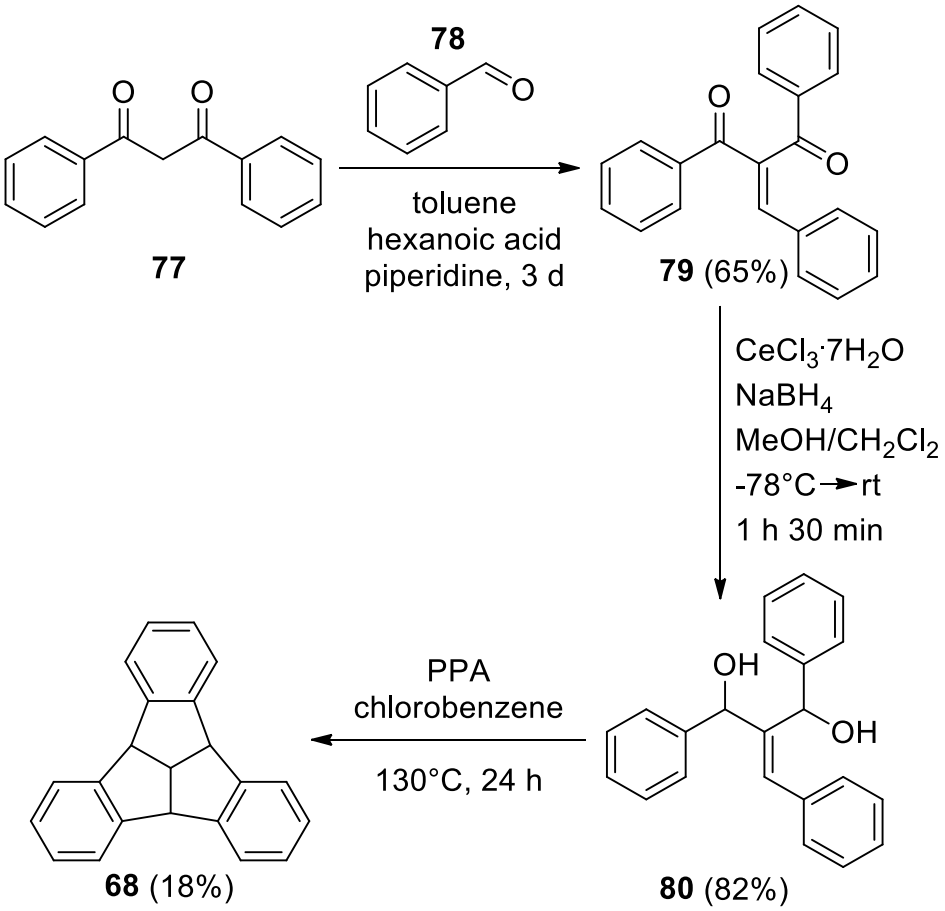

Figure 3.2 Synthesis of TBTQ **68**, according to the HOPF triple cyclisation pathway.[207]

Me-TBTQ **69** was synthesised according to KUCK's protocol, as summarised below in Figure 3.3. The lower yield of 57% for the first step can be explained by the readily air-oxidisable product. Despite following the protocol of KUCK, ensuring a quick work-up and storing the product below 0°C, a higher yield could not be achieved. For the acid catalysed alkylation step, a yield of 76% was achieved. The reduction reaction with $LiAlH_4$ afforded two isomers, which were separated by fractional recrystallisation from MeOH, and the lower yield of 45% was due to difficulties in isolating the two isomers completely from the oily residue. Finally, the cyclisation step gave the desired product in a 12% yield, as after many repeated recrystallisations of the raw product in xylene, it was not possible to isolate more of the product. TBTQ **68** was purified prior to STM investigations by sublimation.

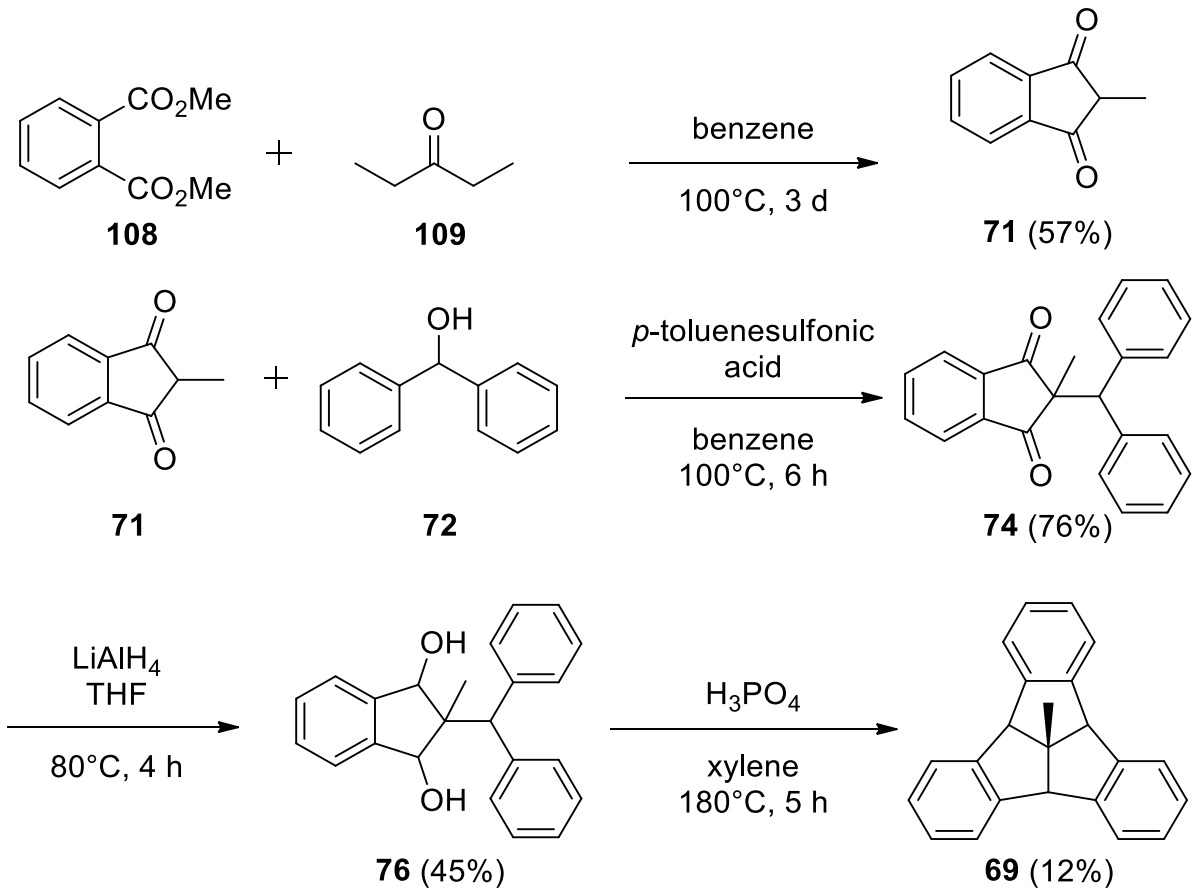

Figure 3.3 Synthesis of TBTQ **69** according to KUCK's protocol.[205]

Both TBTQs were investigated by Prof. M. BODE and his coworkers M. VOGT, M. SCHMITT and M. SCHWAB on Ag(111) using STM. It was observed during initial experiments with Me-TBTQ **69** at room temperature on Ag(111) and Au(111) that the molecules vanished over time, which indicates that they did not adsorb strongly on the surface.

Cooling to 5.5 K gave more promising results with Ag(111), and defined islands of Me-TBTQ **69** were observed, which formed on the atomically flat terraces of the Ag(111) substrate, as shown below in Figure 3.4.[257] The shape, length and height of these islands depends on the amount of coverage.[257] Narrow "zig-zag" islands which change direction by increments of 60° (Figure 3.4a) are formed in the case of low coverage with Me-TBTQ **69** and the width of these strips increases with increasing coverage (Figure 3.4b).[257] On increasing the coverage, the island-island separation distance decreases and double-layer (DL) islands appear upon continued increased coverage, which eventually cover the whole surface. (Figure 3.4d).[257]

Two orientations of A-type ("zig-zag") islands exist for Me-TBTQ **69** (see Figure 3.4), with their edges and nearest neighbour molecular rows rotated by about (14 ± 1)° with respect to

the direction of the substrate.[257] When considering the top layer atoms of Ag(111), a higher number of orientations should be possible, as the C_6 symmetry of the surface layer would allow for rotation of the molecules by 180°, but other orientations were not observed in STM images.[257]

A possible reason for this can be provided when taking the second layer of atoms in silver. Ag(111) adopts a face centred cubic (fcc) crystal structure with, in theory, three high-symmetry adsorption sites: "top sites" on top of Ag atoms, "bridging sites" between two atoms, and "hollow sites" between three atoms.[257] The hollow sites can be further categorised as hexagonal close-packed (hcp) sites and face centered cubic (fcc) sites, depending on whether a silver atom can be found in the first subsurface Ag layer beneath the hollow site.[257] Models from M. VOGT displaying the epitaxial relationship between TBTQ molecules and the Ag(111) suggested that the centre of the TBTQ for one of the orientations is above an hcp hollow site with a second layer silver atom beneath it, whereas the centre of the TBTQs is above an fcc hollow site for the second orientation.[257] Although the STM images provide an explaination for the relative orientation and the spacing of the molecule, the exact position of a TBTQ molecule with respect to the Ag unit cell cannot be determined.[257]

Previously, the adsorption of a selection of organic molecules on a Ag(111) surface was simulated by JALKANEN *et al.*,[258] who concluded that for benzene the the fcc hollow site is preferred.[257] In addition, earlier calculations were confirmed that the molecules lie 2.4 Å above the surface, with their hydrogen atoms slightly bent away from the surface.[259,257] Density functional theory (DFT) calculations carried out by ZUREK and colleagues on subsituted benzenes concluded that weak activating groups such as methyl and fluorine do not have preference for adsorbing to a particular site, unlike strong activating and deactivating functional groups.[260]

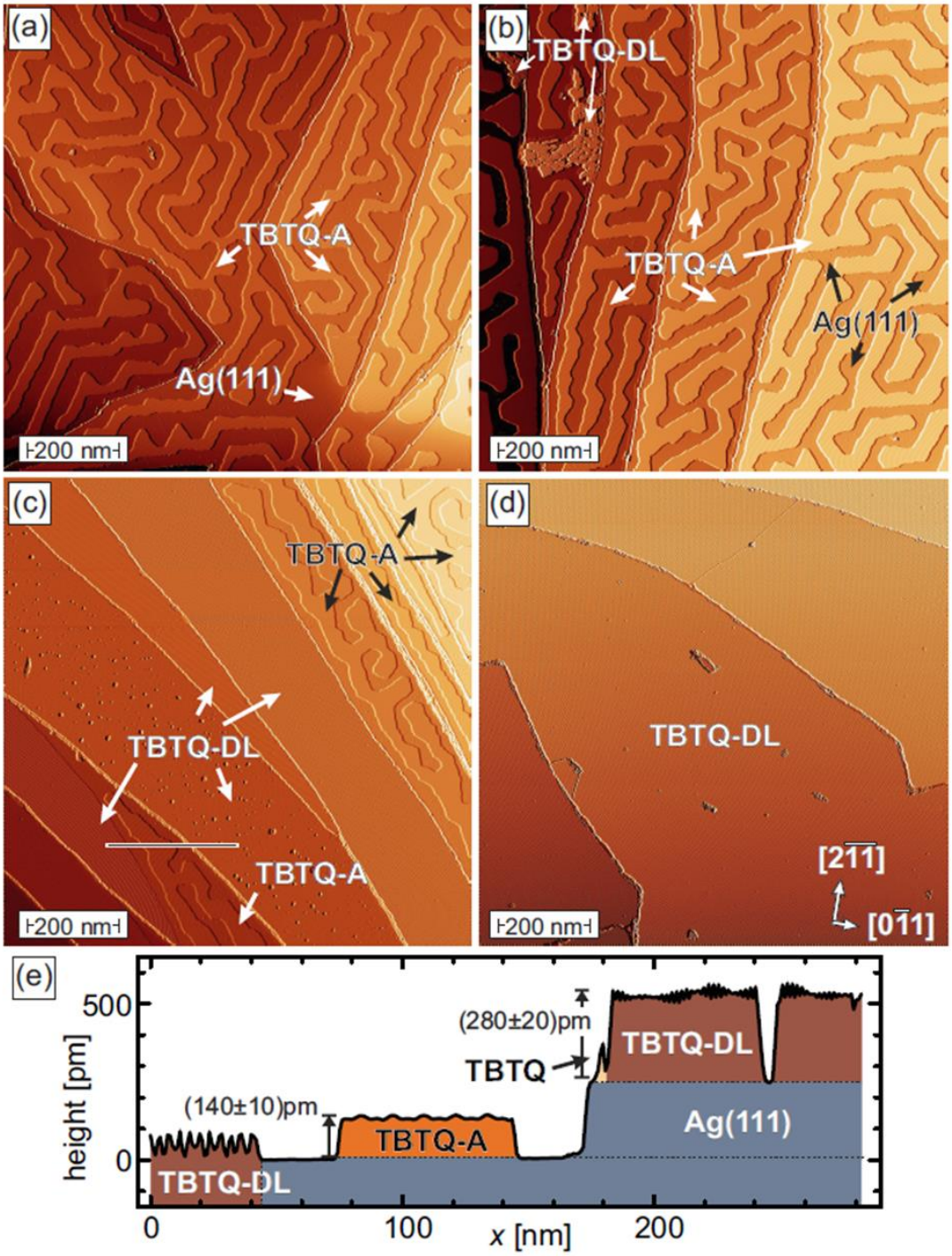

Figure 3.4 Topography of Me-TBTQ **69** molecules on Ag(111) at deposition times of (a) 2 min, (b) 4 min, (c) 6 min, and (d) 8 min. Panel (e) shows a line profile taken along the grey line in (c). At low coverage, islands of Me-TBTQ **69**-A are visible with an apparent height of (140 ± 10) pm. At higher coverage, double-layer regions (TBTQ-DL) are formed, with an apparent height of (280 ± 20) pm. Imaging parameters: U = 1 V; I = 100 pA. STM images and line profile are the work of M. VOGT, M. SCHMITT, and M. BODE.[257] Reprinted with permission from M. Vogt, R. Buschmann, S. Toksabay, M. Schmitt, M. Schwab, M. Bode,

A. Krueger, **2019**, *123*, 5469–5478. Copyright 2019 American Chemical Society.

It is reasonable to assume that the protrusion extending by approx 50 pm from the centre of the TBTQ (visible as a light area in Figure 3.5) originates from the methyl group bound to *centro*-position.[257] The contrast between this methyl group and the rest of the TBTQ molecule in STM images in Figure 3.5 indicates the clear identification of this *centro*-position.

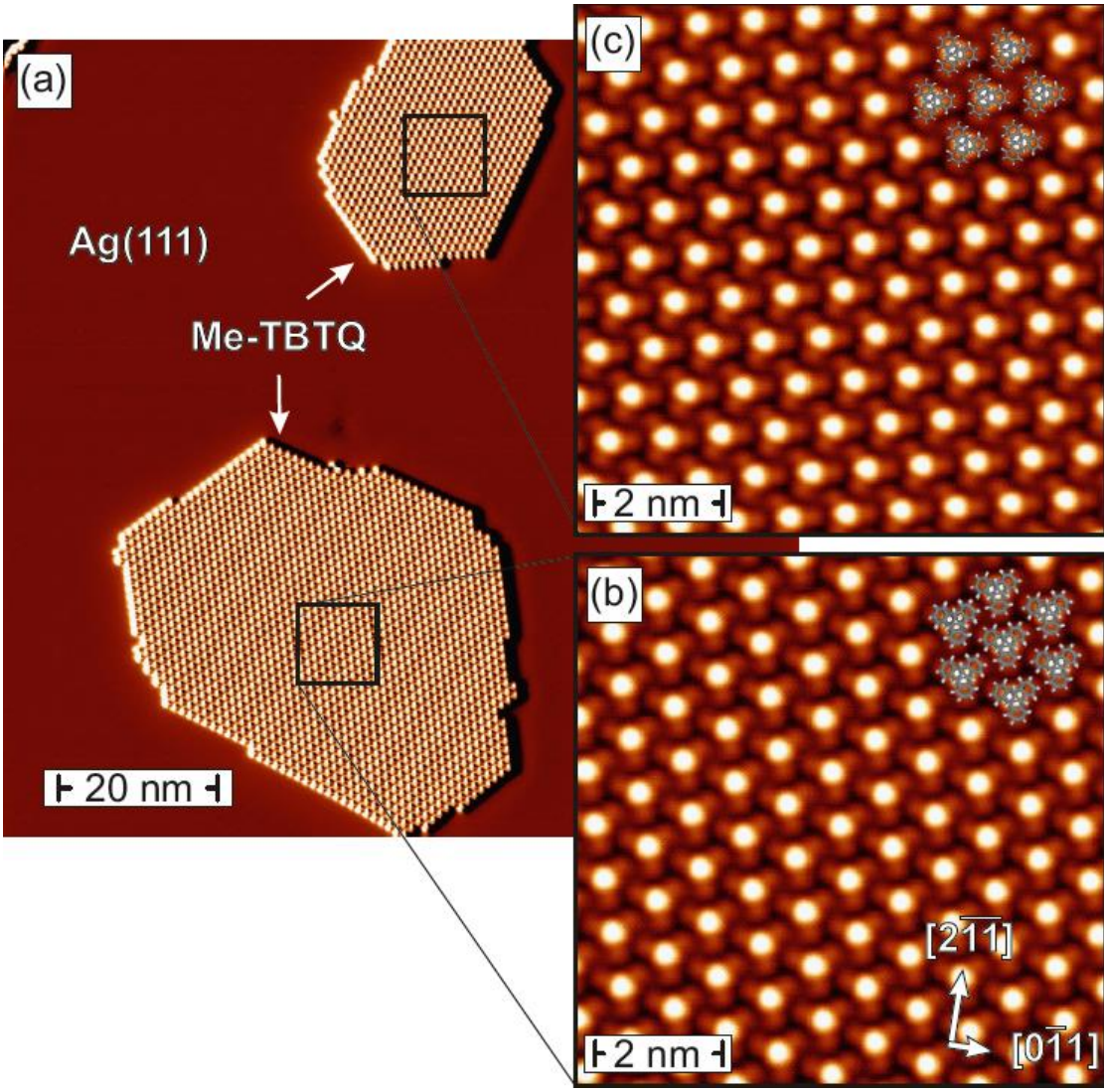

Figure 3.5 Two different islands of Me-TBTQ **69** (a) on Ag(111) at sub-monolayer coverage, with STM images (b) and (c) at higher magnification displaying a hexagonal lattice with two orientations, with nearest neighbours aligned to the direction of the island edge in both examples. Imaging parameters: in (a): U = 1 V, in (b) and (c): U = -500 mV; I = 100 pA. STM images are the work of M. VOGT, M. SCHMITT, and M. BODE.[257] Reprinted with permission from M.

This poition has the potential to be exploited for the controlled positioning of other functional groups in a highly ordered lattice, where the TBTQ scaffold acts as an anchor group to the metal surface.[257] BEUERLE and coworkers have recently reported on the efficient and flexible functionalization of the *centro*-position (also referred to as apical) position of TBTQs.[211,257]

Worthy of note is that the lattice parameters a and b of the two-dimensional hexagonal lattice on Ag(111) differ largely from the values in a bulk single crystal of Me-TBTQ **69**. Whereas a = b = 14.96 Å have been measured by single crystal x-ray crystallography,[200] when TBTQ **69** is deposited on Ag(111), a and b have a value of (18.0 ± 1.1) Å indicating a lattice expansion.[257] In addition, the apparent height of the molecule in A-type islands is (140 ± 10) pm, which is in agreement with the value of 142 pm (1.42 Å) measured for the triquinacene moeity from the crystal structure data, as displayed in Figure 3.6(b) below.[200,257] This suggests that the strong dispersion or charge transfer interaction between the benzene rings and the surface leads to an almost parallel orientation of the benzene rings on the surface, resulting in a lattice expansion as these benzene rings stretch away from the triquinacene core.[257]

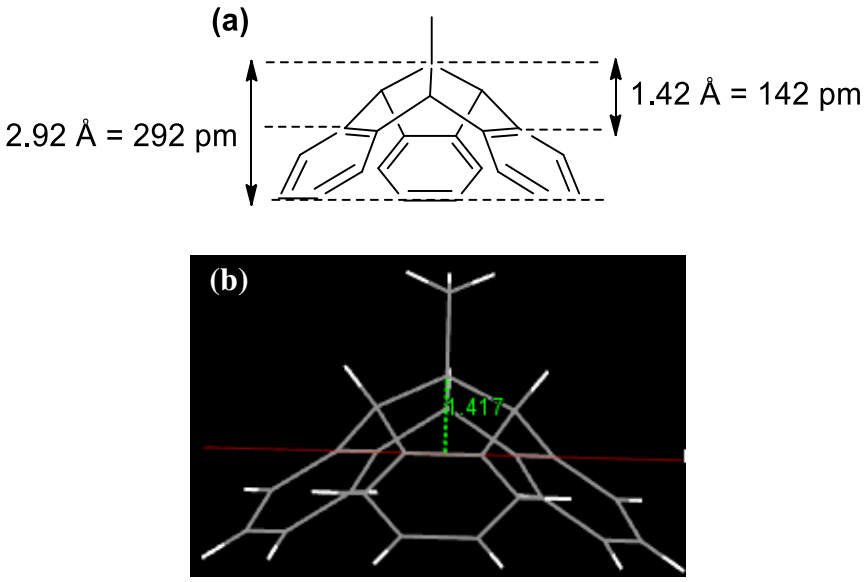

Figure 3.6 (a) Pictoral representation of TBTQ **69**, with the height of the triquinacene moiety and the TBTQ moeity indicated. These values are taken from the cif file of CCDC-907601, accessed from the Cambridge Data Centre (CCDC).[200] (b) TBTQ **69** structure as viewed in the crystal structure visualisation programme Mercury,[261,262] indicating the height of the triquinacene moeity. This image was generated from the cif file of CCDC-907601.[200]

For TBTQ **68**, the TBTQ molecules predominantly form narrow 50 nm wide "zig-zag"islands with straight edges at a very low coverage (significantly less than a single molecular layer).[257] These islands often change direction by about 60° and vary in length from 10 nm to 100 nm, as shown in STM image of Figure 3.7(a), [257] The island edges are not oriented along a high symmetry axis of the substrate but tilted by (14 ± 1)° with respect to the direction of the ⟨011⟩ Ag(111) surface.[257] The apparent height of these islands, named TBTQ-A (Figure 3.7), amounts to (180 ± 20) pm at a bias voltage of U = 500 mV, as revealed by the line profile measured along the grey line in the centre of Figure 3.7(a) which is plotted in the bottom panel.[257]

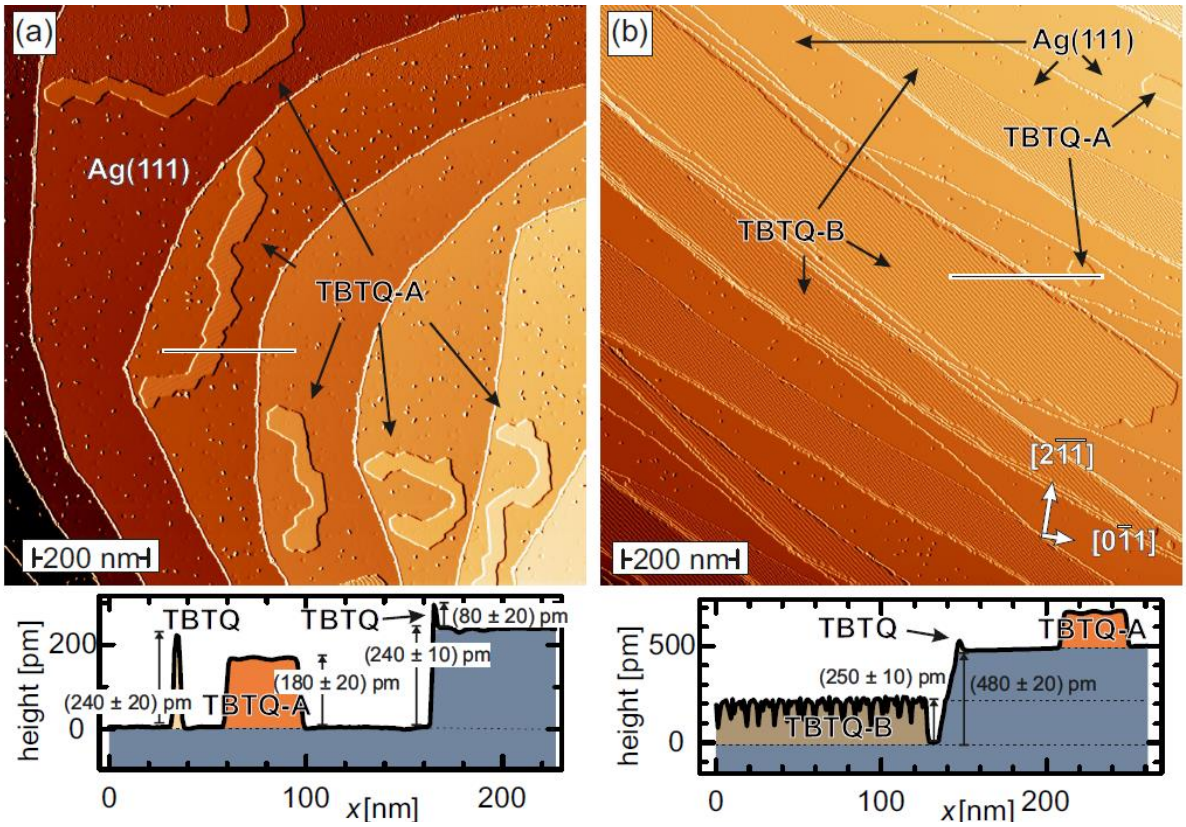

Figure 3.7 Topography of TBTQ (**69**) molecules deposited on Ag(111) at (a) low and (b) high coverage. The bottom panels show line profiles taken along the grey horizontal lines, from the respective panels above. Whereas narrow islands with an apparent height of (180 ± 20) pm appear at low coverage (a) (TBTQ-A), the TBTQ islands at high coverage are more rough, about (250 ± 10) pm high, and usually extend over the entire terrace of the substrate (TBTQ-B). Imaging parameters: U = 500 mV, 1 V; I = 300 pA. STM images and line profile are the work of M. VOGT, M. SCHMITT, and M. BODE.[257] Reprinted with permission from M. Vogt, R. Buschmann, S. Toksabay, M. Schmitt, M. Schwab, M. Bode, A. Krueger, **2019**, *123*, 5469–5478. Copyright 2019 American Chemical Society.

A second type of island, called TBTQ-B and also shown in Figure 3.7, are observed at higher coverage (almost at completion of a monolayer).[257] As can be seen in Figure 3.7(b) these islands are typically extended along the terraces of the Ag(111) substrate with length up to several µm.[257] The TBTQ-B structure covers the full width of most terraces, with narrow trenches remaining uncovered along the step edges.[257] A few Ag(111) terraces remain largely uncovered with just a few relatively small TBTQ-A islands. However, the particular stripe pattern visible for TBTQ-B in Figure 3.7(b) is an artifact caused by the pixel resolution

(1024 × 1024) which, in superposition with the TBTQ-B corrugation across the unit cell, results in a moiré pattern.[257] This moiré pattern is also visible in the line profile drawn along the line, which is displayed in the lower panel of. Figure 3.7(b) and reveals an apparent island height of (250 ± 10) pm.[257]

The relatively large lateral extension of both, TBTQ-A islands and larger TBTQ-B strips, can only insufficiently be captured by the scanning tunneling microscope, since the maximal scan range is limited to a maximal value of 2.5 µm × 2.5 µm. per STM image.[257] As some terraces exhibit a width of at least 400 nm, room temperature surface diffusion of TBTQ on Ag(111) is clearly strong enough to enable the resulting island structure to order on length scales much longer than what is known from metal epitaxy.[257]

As for Me-TBTQ **69**, there are two separate orientations of TBTQ-**68** islands. Both islands exhibit straight island edges which often turn direction by 60° and none of the edges are aligned with the high-symmetry directions of the Ag(111) surface layer: ⟨011⟩, ⟨211⟩.[257] A hexagonal pattern of triangular shaped TBTQ molecules is recognisable and the nearest neighbour intermolecular distance of (1.05 ± 0.05) nm.[257] The nearest neighbour rows are oriented in the same direction as the island edges and rotated by +(14 ± 1)° and –(14 ± 1)° relative to the Ag(111) direction, as shown in Figure 3.8(b) and Figure 3.8(c), respectively.[257]

Interestingly, the lattice parameters a and b of the two-dimensional hexagonal lattice of TBTQ **68** on Ag(111) differ largely from the values in a bulk single crystal.[257] Whereas a = b = 15.89 Å have been measured by single crystal x-ray crystallography,[200] the same lattice vectors have a value of (18.1 ± 1.0) Å when TBTQ **68** is deposited on Ag(111).[257] This significant lattice expansion indicates a strong influence of the substrate on the two-dimensional packing of the molecules as also observed for Me-TBTQ **69**.[257]

In the TBTQ A islands, the molecules arrange themselves with the opening of the bowl towards the substrate,[257] contrasting to what is observed e.g. for bridgehead–functionalised TBTQ[251] or corannulene.[253] In the latter, the electron density is largest above the central pentagon atom on the convex face, resulting in a strong electrostatic interaction between the convex face and the metal surface.[253,257] In contrast, the terminal hydrogen atoms at the outer edge experience only weak adsorption interactions with the surface. [253,257] Consequently, the concave side and the bowl-opening point away from the surface.[253,257] This strong electrostatic interaction arises from PAULI repulsion induced in the substrate by the high

electron density of the convex side, which in turn induces a large dipole moment across the adsorbate complex.[263,264] For TBTQs **68** and **69** on the other hand, the electron density is highest at the centre of of the three benzene rings, which, although attached to the triquinacene core, are spatially separated from each other.[257] Therefore, the π-electron density is not distributed over the whole molecule, which explains why this molecule prefers to attach to silver with the opening faced downwards, via the electron-rich benzene rings.[257]

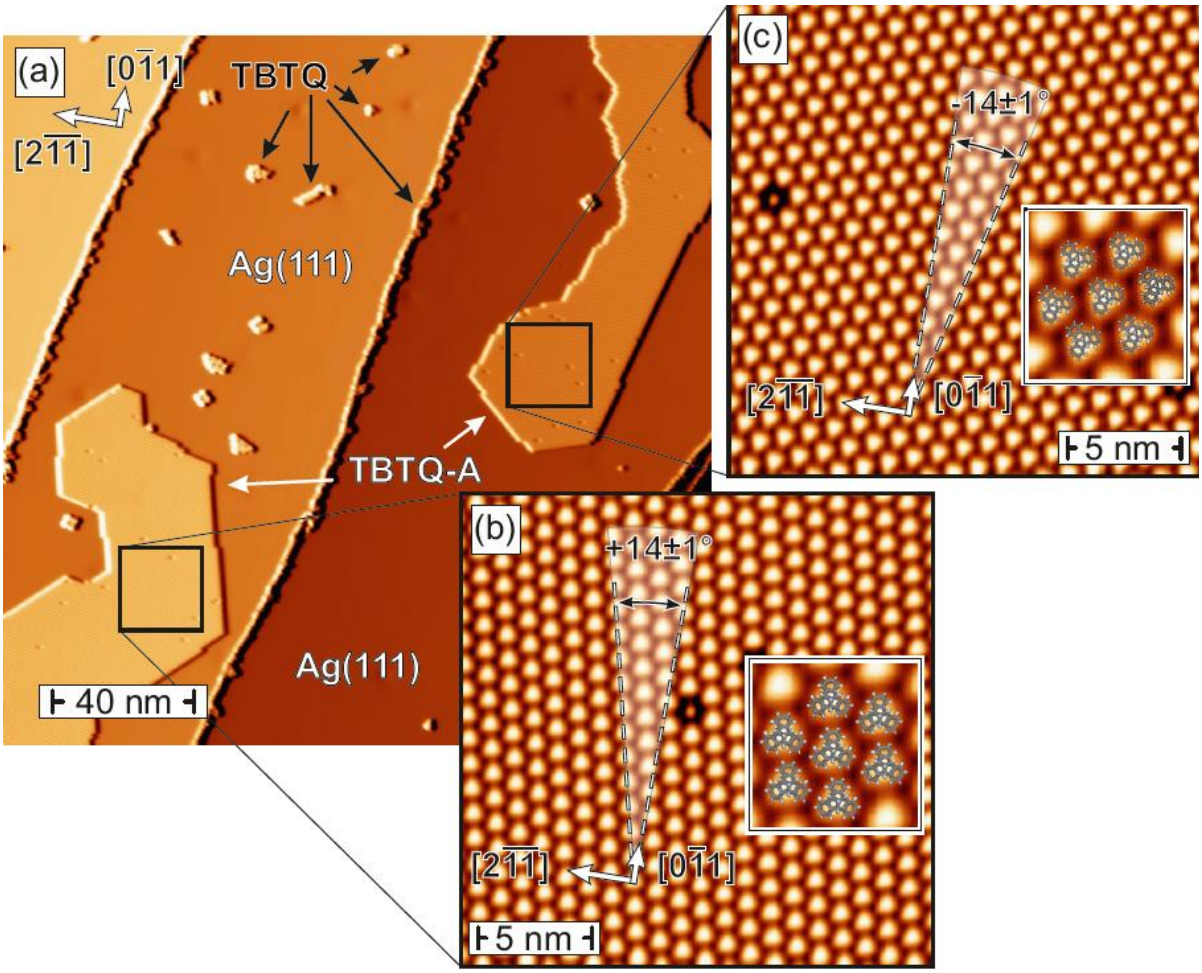

Figure 3.8 (a) STM topographic image of TBTQ **68** on Ag(111) at low submonolayer coverage. Small islands are indicated by black arrows; the vast majority of molecules form TBTQ-A islands on Ag(111), whereby two orientations, magnified in in (b) and (c), can be distinguished. Imaging parameters: U = 1 V for overview scan, U = -500 mV for zoom-ins; I = 300 pA. STM images are the work of M. VOGT, M. SCHMITT, and M. BODE.[257] Reprinted with permission from M. Vogt, R. Buschmann, S. Toksabay, M. Schmitt, M. Schwab, M. Bode, A. Krueger, **2019**, *123*, 5469–5478. Copyright 2019 American Chemical Society.

On increasing the coverage, the arragement of molecules and epitaxial relationship changes significantly, leading to a windmill-like structure, which can be seen in Figure 3.9.[257] TBTQ-B islands do not cover the substrate homogeneously, but exhibit a hexagonal hole lattice with a nearest neighbor distance of (2.72 ± 0.10) nm.[257] The holes possess a diameter of about 1 nm and extend all the way down to the Ag(111) substrate.[257] Each hole is tangentially surrounded by six protruding lines which "connect" the hole with its neighbours.[257]

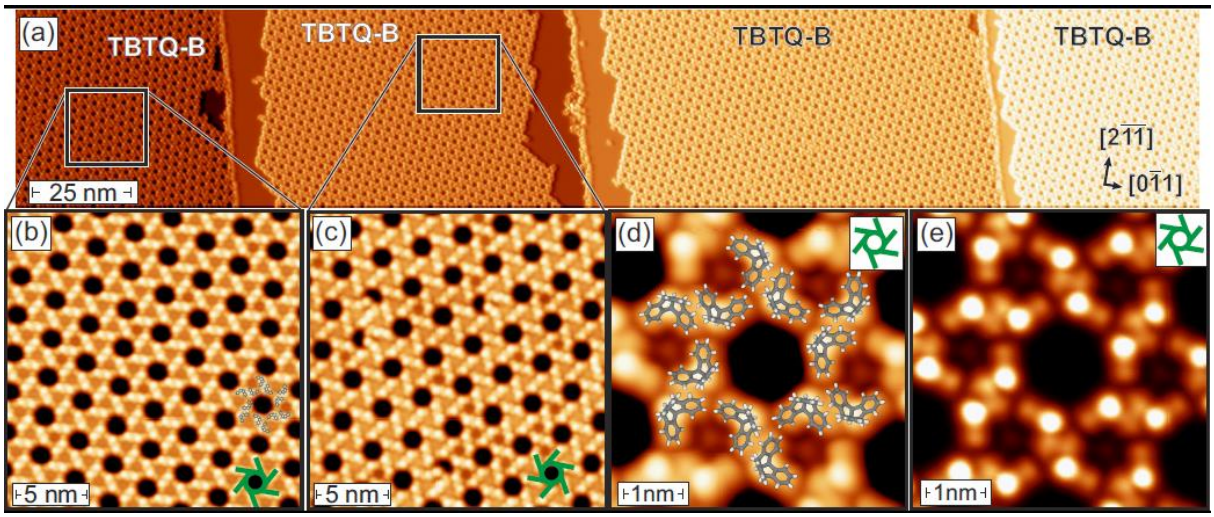

Figure 3.9 Large scale STM topographic image of four atomically flat Ag(111) terraces, each covered with a high submonolayer coverage of TBTQ **68** molecules, resulting in a holey hexagonal lattice (TBTQ-B islands). The holes are surrounded by windmill-like structures which occur in two rotational senses, (b) clockwise and (c) anti-clockwise (shown by green indicator scheme).(d) Constant-current and I constant-height STM images showing the molecular structure of the clockwise rotating windmill structure shown in (b). Imaging parameters: I = 100 pA, in (a): U = 1 V, in (b): U = -500 mV, in (c): U = 1 V, in (d): U = 300 mV, in I: U = 300 mV; STM images are the work of M. VOGT, M. SCHMITT, and M. BODE.[257] Reprinted with permission from M. Vogt, R. Buschmann, S. Toksabay, M. Schmitt, M. Schwab, M. Bode, A. Krueger, **2019**, *123*, 5469–5478. Copyright 2019 American Chemical Society.

In contrast to the TBTQ-A islands, where the molecules of **68** lie flat on the Ag(111) surface and a consistently bright triangle shape is observed, the "L-shaped" molecule orientations shown, with a bright spot in the middle.[257] Two possible orientations are shown in Figure 3.10 below.

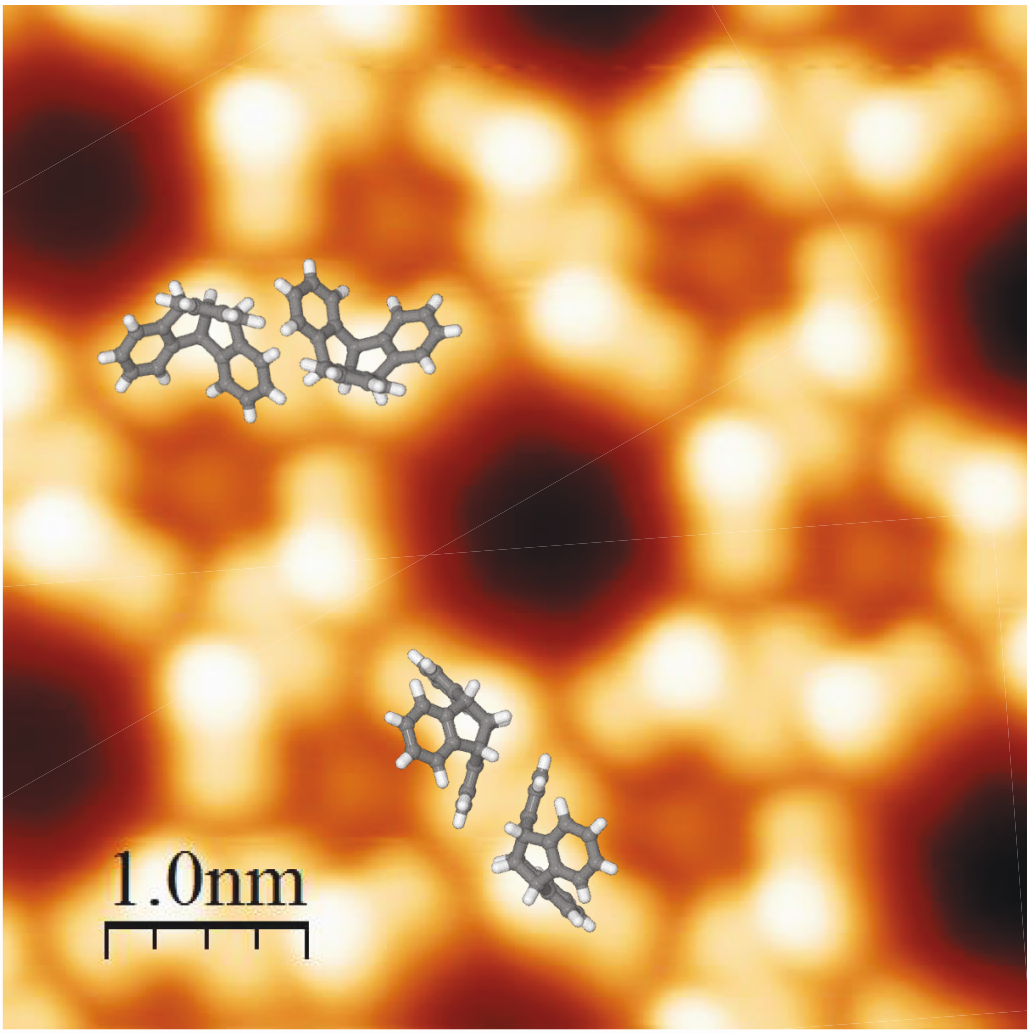

Figure 3.10 Windmill arrangement of H-TBTQ **68**, with two possible orientatons superimposed onto the STM image to indicate how a pair of molecules might interact with each other and the metal surface. STM image is the work of M. VOGT, M. SCHMITT, and M. BODE.[257] Adapted with permission from M. Vogt, R. Buschmann, S. Toksabay, M. Schmitt, M. Schwab, M. Bode, A. Krueger, **2019**, *123*, 5469–5478. Copyright 2019 American Chemical Society.

There are two possible orientations, which are visualised below in Figure 3.11: 1) TBTQ **68** stands on the rim of two benzene rings and a π–π interaction between two aromatic rings from neighbouring molecules dominates.[257] In contrast, 2) two of the benzene rings from TBTQ **68** interact strongly with the Ag(111) surface with the third perpendicular to the surface. For both configurations, the highest packing density can be achieved by rotating adjacent molecules by 180°. As shown in Figure 3.10 the TBTQ molecules form dimeric structures which constitute building blocks of the intertwined hexagonal lattice.[257] It seems reasonable to assume that these dimers have been formed prior to deposition on the substrate.[257] It is

thus obvious that such structures are only possible with higher TBTQ concentrations and are only observed for high coverages of the two dimensional TBTQ layers.[257]

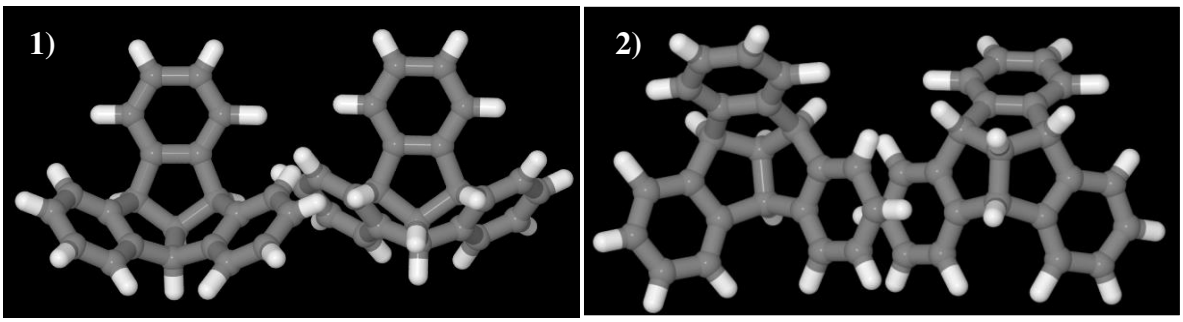

Figure 3.11 3D models of two alternative arrangements: 1) and 2) of the "windmill" H-TBTQ **68** dimer pair. These models are viewed from the side, whereas the same models are viewed from above in Figure 3.10. Adapted with permission from M. Vogt, R. Buschmann, S. Toksabay, M. Schmitt, M. Schwab, M. Bode, A. Krueger, **2019**, *123*, 5469–5478. Copyright 2019 American Chemical Society.

This exact alignment of TBTQ **68** to the surface cannot be explained when simply taking the height of the molecules into account.[257] The measured value of about 2.5 Å for the adlayer thickness does not correspond to the theoretical height of 5.7 Å for a TBTQ **68** molecule standing on its rim (1) or to 4.74 Å, which corresponds to TBTQ with two aromatic rings parallel to the surface (2).[257] Both of these values were which calculated from crystal structure data.[200] Worthy of note is that the "windmill" arrangement of TBTQs is not observed for Me-TBTQ **69** samples, which can be justified by the presence of the methyl group.[257] This group is larger than a hydrogen atom and therefore would prevents the molecules from packing close enough for (1), as well as the triquinacene core lying face down on the surface as is the case for (2).[257]

In the case of buckybowl corannulene, the hydrogen termination at its rim usually permits only weak adsorptive interactions with a surface, therefore a bowl-opening up configuration is favoured, because considerably higher electron density on the convex side causes strong electrostatic interactions with metallic surfaces.[44,257] Taking this into account, and the theory that TBTQ molecules Me-TBTQ **69** and H-TBTQ **68** in A-islands lie very close to the surface as a result of a strong dispersion or charge transfer interaction, this favours orientation (2).

However, for extended corannulene based systems it has been postulated that π–π interactions between buckybowls significant, to the extent that bowl opening-down configurations are favoured for maximise interactions between convex faces.[44,257] In addition, it was

hypothesised that C–H···π rim-to-convex face bonding contributed to the arragement of terphenylcorannulene on a Cu(111) surface. [252,257] In this light, orientation (1) is plausible, as a $C_{arom.}$-H···π interaction between a proton on one benezene ring with π-electrons from the ring of a neighbouring molecule.

The adsorption of $C_{80}H_{30}$ on a Cu(111) at a high coverage resulted in a hexagonal network, attributed to π–π interactions between neighbouring molecules, leading to the formation of dimers.[265] The conformational flexibility of $C_{80}H_{30}$, due to the prescence of multiple seven-membered rings near its periphery, allows the molecules to adapt their conformation to maximise enantioselective CH···π interactions between dimers.[265] Although the "windmilll" arrangement of TBTQ **68** also features hexagonal pores, the conformation of the molecules is determined by the rigid triquiacene core, therefore a direct comparison cannot be drawn.

Without calculations to predict which orientation is more probable or energetically favoured, a definite conclusion cannot be reached. When considering the STM images themselves, where the bright areas correspond to a higher local density of electrons, orientation (2) is most likely because the benzene ring points directly upwards in a perpendicular manner. For orientation (1), it would be expected that the bright area would extend further into the middle of one of the triangles of TBTQ molecules, six of which form the windmill pattern.

To conclude, the the two-dimensional self-assembly of TBTQs **68** and **69** on Ag(111) was studied by STM under ultrahigh vacuum conditions and highly ordered monolayers were observed for the first time.[257] At low to moderate coverage, both H-TBTQ **68** and Me-TBTQ **69** adsorb with the bowl opening faced downwards, appearing in two orientations that are rotated by 14° from the high symmetry axis of the Ag(111) surface.[257] At high TBTQ **68** coverage, extended islands with a self-assembled highly ordered windmill nanostructure and a regular distribution of nanometer-sized openings dominate the surface.[257] This windmill structure is not observed for Me-TBTQ **69**, which immediately forms double-layered regions at high coverage.[257] Investigations such as these into the self-assembly of curved aromatics provide a foundation for further work on the construction of multilayer nanostructures and the production of electronic devices.[257]

3.2 Functionalisation of the *ortho*-position – synthesis of fluorinated TBTQs

Fluorinated TBTQs are a desirable class of compounds to synthesise. Firstly, it is expected that fluorine substituents will reduce the HOMO-LUMO gap, as reported for other fluorinated PAHs,[164] which is interesting for potential electronic applications. Secondly, photocyclo-dehydrofluorination[152] or Al_2O_3 mediated hydrogen fluoride elimination reactions[155-159] could be used to extend the scaffold in a regioselective manner as a viable alternative to the SCHOLL reaction. The major advantage of these methods is the regioselectivity, which normally leads to high yields due to the formation of fewer side-products. As the the SCHOLL reaction frequently affords chlorinated side products, alternative aryl C-C coupling strategies are considered necessary.

No previous examples of fluorinated TBTQs were found and the selective introduction of fluorine atoms requires suitably functionalised starting materials. In order to start exploring the synthesis of *ortho*-fluorinated TBTQs, the triple cyclisation HOPF synthesis was chosen as a starting point, for which singly and triply *ortho*-brominated examples have been reported.[207] Synthetic aims TBTQ **100** and **101** as well as literature reported brominated TBTQs **110** and **111** are shown in Figure 3.12.

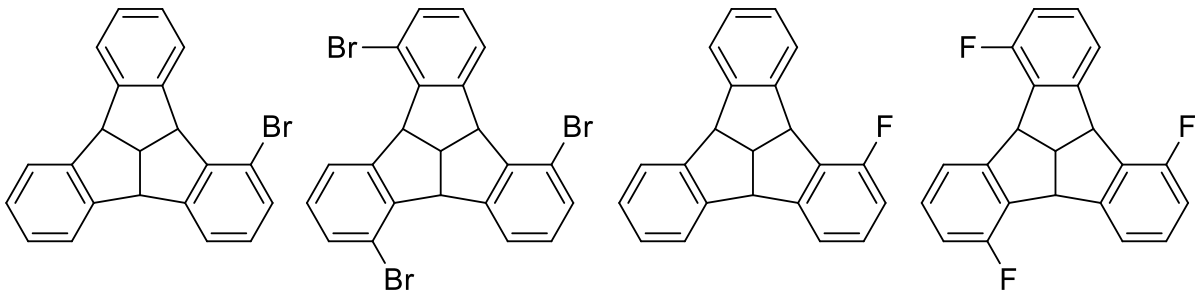

Figure 3.12 Literature known brominated TBTQs **110** and **111** and proposed fluorinated TBTQs **100** and **101**.

3.2.1 Monofluorinated TBTQs

For TBTQ **100**, the first step is the KNOEVENAGEL reaction between with 2-fluorobenz-aldehyde (**112**) and diketone **77** (shown in Figure 3.13). The first reaction attempt was carried out with 1 eq. of the aldehyde, as used by MARKOPOLOUS,[202,207] however 0.6 eq. of piperidine were added to catalyse the reaction instead of 0.1 eq. After 2 d the reaction was stopped, even though starting materials were still present. Traces of the product were isolated but many side products were formed and isolated fractions collected after column

chromatography were mixtures of products. Reverse phase (RP) HPLC separation was necessary to isolate single compounds and the desired product was isolated with a 21% yield.

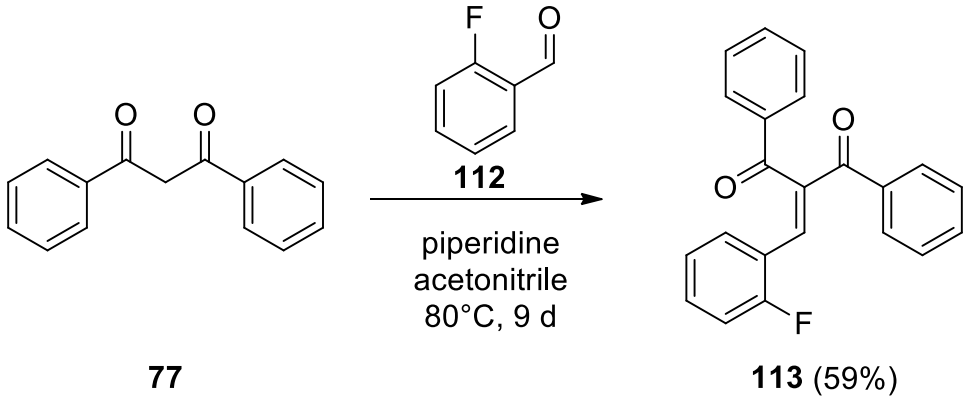

Figure 3.13 KNOEVENAGEL condensation to afford diketone **113**.

The next attempt at the KNOEVENAGEL reaction used 5 eq. of aldehyde **112**, in order to test if an excess of this reactant accelerates the reaction and reduces the number of side-products. The amount of piperidine was reduced to 0.2 eq. As the reaction was not complete, even after 9 d, HPLC reaction control was employed in addition to TLC at regular intervals. In this way, an end-point was determined, at which the amount of diketone **77** had fallen significantly. After 27 h, it was observed that the amount of 2-fluorobenzaldehyde **112** was very low, although 5 eq. were added at the start. The reason for this is unknown, as the boiling point of 2-fluorobenzaldehyde **112** is 90–91 C, which is higher than the reaction temperature of 80°C. Self-condensation under basic conditions is not possible, as aldehydes lack enolisable protons. To combat this problem, additional portions of 2-fluorobenzaldehyde **112** and piperidine were added, which did lead to an increased yield of 39%. After yield optimisation, which consisted of reducing the amount of aldehyde **112** to 2 eq. and taking 0.2 eq. piperidine, an increase to 59% after 9 d was achieved.

Following the triple cyclisation pathway employed by HOPF and MARKOPOLOUS for the synthesis of mono- and tribrominated TBTQs **110** and **111**,[202,207] the LUCHE reduction was carried out as the next step (depicted in Figure 3.14).

The conversion from diketone **113** to **114** afforded a mixture of two diastereomers **114a** and **114b**. $NaBH_4$ (2.1 eq.) and cerium(III) chloride heptahydrate (1.4 eq.) were employed, identical to the reagent proportions used by HOPF and MARKOPOLOUS.[202,207] TLC monitoring indicated complete conversion after 1 h 50 min and successful separation of the

diastereoisomers proceeded via column chromatograpy, affording the isomers **114a** and **114b** with a combined yield of 72%.

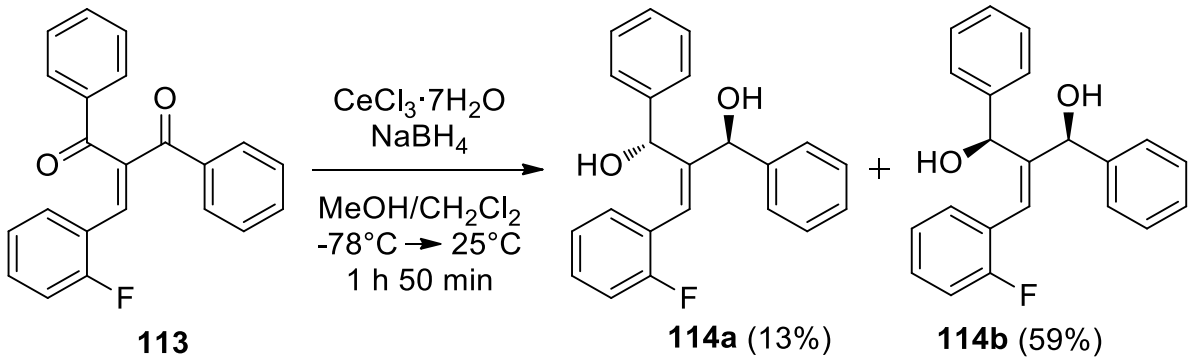

Figure 3.14 LUCHE reduction of diketone **113** to afford diastereoimers **114a** and **114b**.

MARKOPOULOS identified characteristic patterns in the ^{1}H NMR spectra of each of the diastereoisomers for brominated, methyl and methoxy functionalised analogues, based on a known configuration from the x-ray crystal structure.[202] For the R,S/S,R (*syn*) diastereomer, the O*H* protons are observed as either overlapping or closely lying resonances between 2.0 and 2.5 ppm, whereas the hydroxyl protons of the R,R/S,S (*anti*) diastereoisomer are separated by ~0.8–1.0 ppm and are found between 2.75 and 4.0 ppm. In addition, the olefinc proton is observed at approx. 7 ppm for the R,S/S,R (*syn*) isomer and at approx. 6 ppm for the R,R/S,S (*anti*) isomer. The ^{1}H spectra measured for the separated isomers of **114a** and **114b** also followed the pattern described by MARKOPOULOS, so the diastereomers were assigned accordingly.

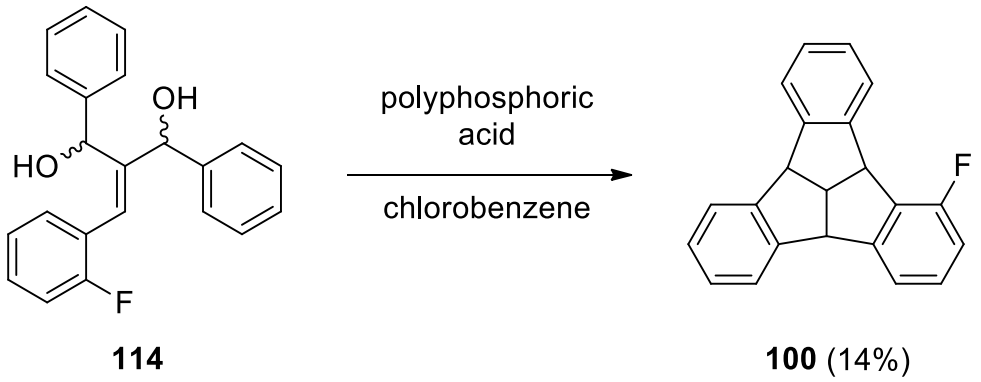

Figure 3.15 Cyclisaton of diol **114** to TBTQ **100**.

The final cyclisation step was carried out using HOPF's cyclisation conditions: polyphosphoric acid, chlorobenzene and reflux for 22 h.[207] After column chromatography and

recrystallisation from toluene, the colourless needles were confirmed to be the mono-fluorinated TBTQ, in a 14% yield.

To conclude, *ortho*-fluorinated TBTQ **100** was synthesised for the first time, adapting the conditions from HOPF's synthesis of *ortho*-brominated TBTQ derivatives.[207] This proves that fluorine atoms can be introduced into a TBTQ structure, which is a significant step forwards in exploring the surface-assisted extension of fluorinated TBTQs.

3.2.2 Trifluorinated TBTQs

The first molecule required for the synthesis of TBTQ **101** is a suitably fluorinated 1,3-diphenylpropane-1,3-dione **117**, as shown in Figure 3.16 below. An initial attempt using a base catalysed aldol reaction afforded only 4% of the desired product, and MARKOPOULOS reported a similar problem for the bromine analogues.[202] YI and ZHANG mention this exact transformation with NaH, but the yield and characterisation data are not provided.[266]

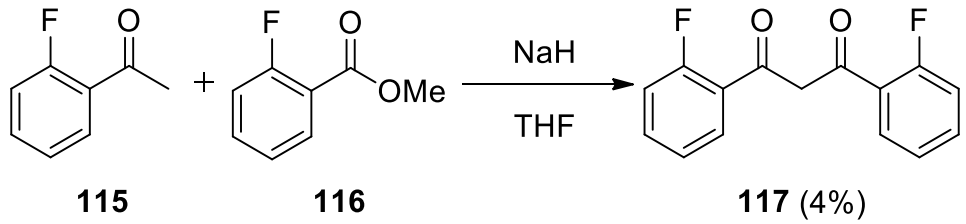

Figure 3.16 Initial synthesis attempt of diketone **117**.

An alterantive strategy based on the conditions of MARKOPOLOUS and HOPF was proposed,[207] as although ketone **117** is literature known, no yields were published by YI and ZHANG[266] or CHENG *et al*. who used several fluorinated diketones for further transformations.[267] Several other fluorinated diketones with a different subsitution pattern have however been reported by RAMAA *et al.*[268,269] which was also taken into consideration when planning the synthesis. The yields for the first two steps were very good (82 and 92%), but the bromine elimination only delivers a moderate yield of 49% (see Figure 3.17).

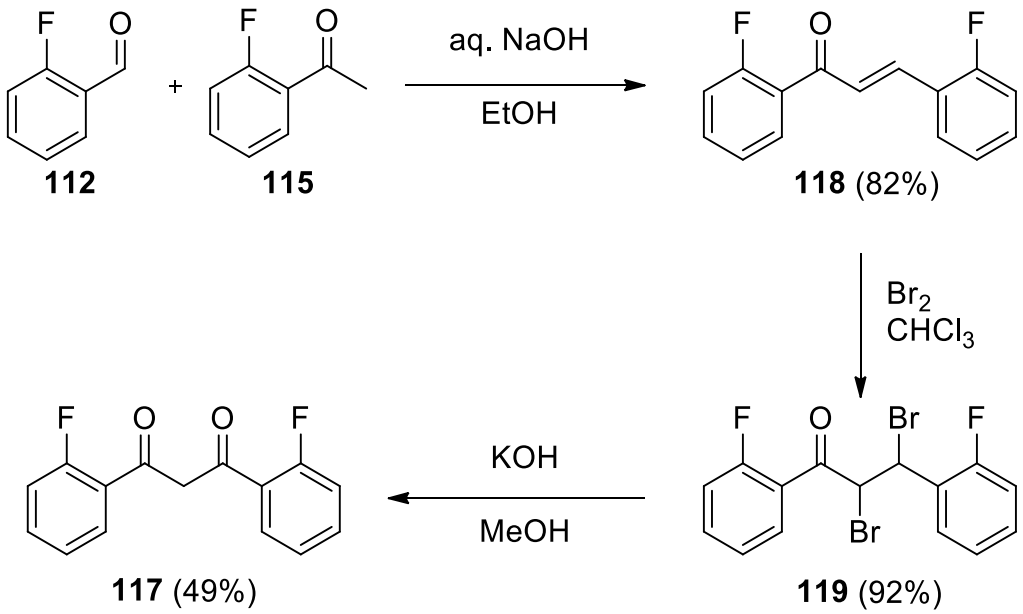

Figure 3.17 Synthesis of diketone **117**.

The KNOEVENAGEL reaction with diketone **117** did not succeed and instead the chromenone **121** was formed, as shown in Figure 3.18. Test experiments with benzaldehyde **78** and in the absence of aldehyde also led to the formation of **121** further substantiating that diketone **117** reacts with itself.

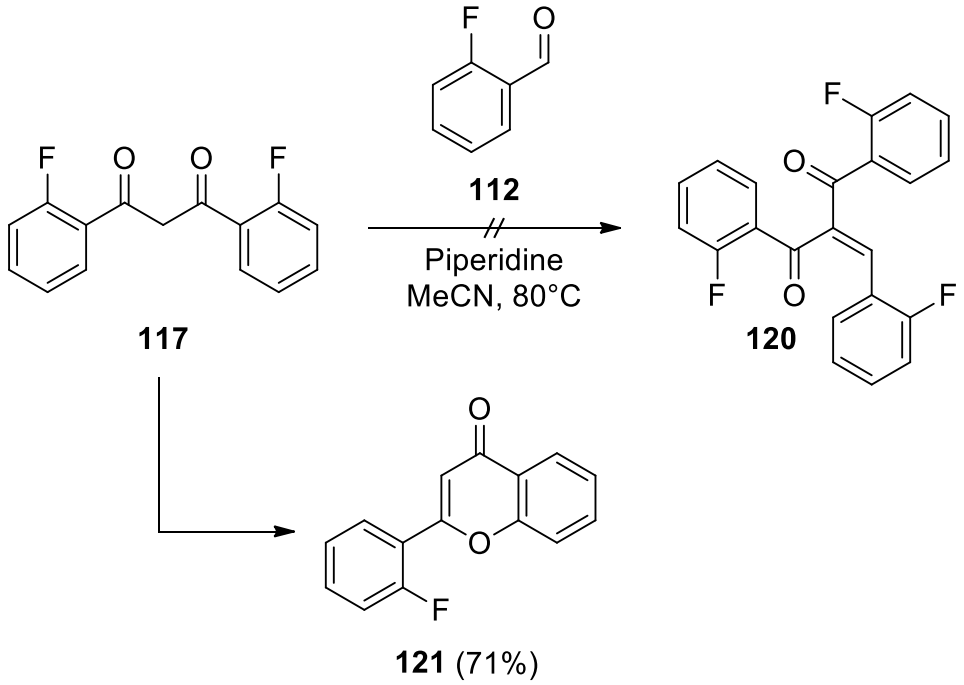

Figure 3.18 Unexpected formation of chromenone **121**.

It is most likely that this reaction proceeds via an S_NAr intramolecular ULLMANN-type *O*-arylation,[270] the mechanism of which is shown below in Figure 3.19. Enolisation of the

ketone group takes place under basic conditions, and the oyxgen atom is able to attack due to the the fluorine atom occupying the neighbouring 2-position and the ability of the molecule to rotate. In order to regain aromaticity, fluoride is eliminated.

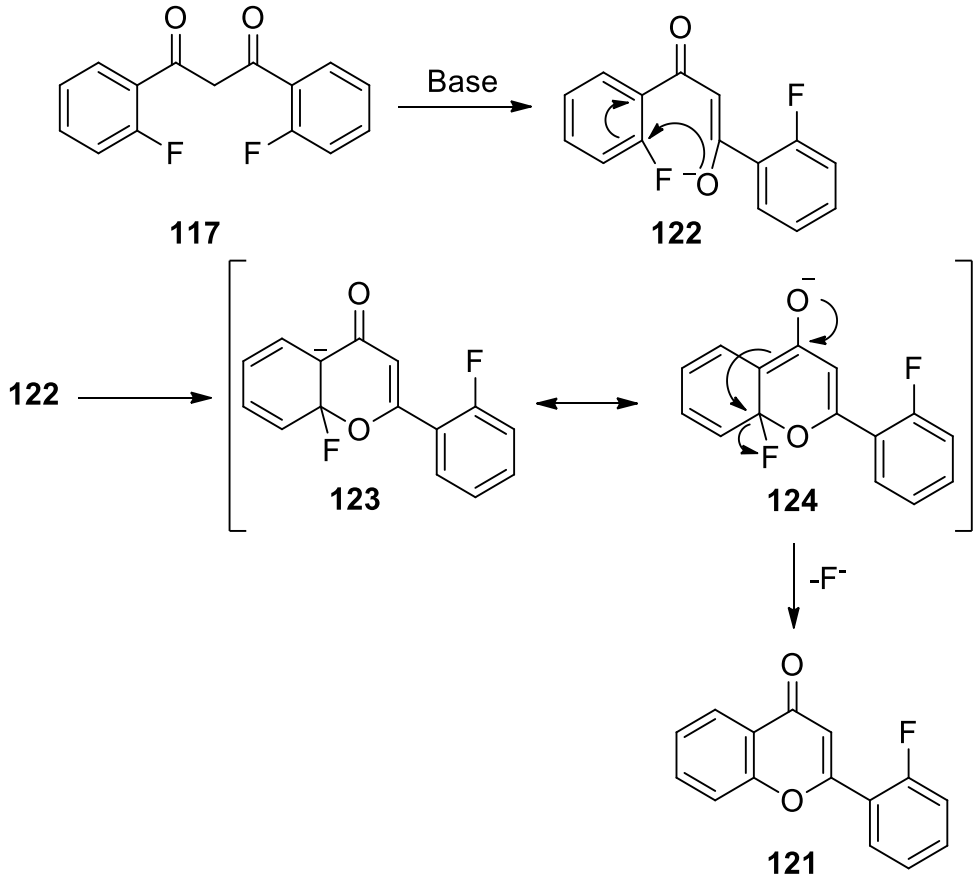

Figure 3.19 Mechanism of the S_NAr intramolecular ULLMAN-type *O*-arylation.

Earlier accounts of the direct formation of chomenones exist using a reaction of acyl chlorides with oxopropanoates[271] or oxobutanoates,[272] specific examples of which are shown in Figure 3.20 below. Furthermore, fluorine is not the only halogen to undergo this S_NAr intramolecular ULLMANN-type *O*-arylation, as examples of elimination of bromine and chlorine have also been reported.[270]

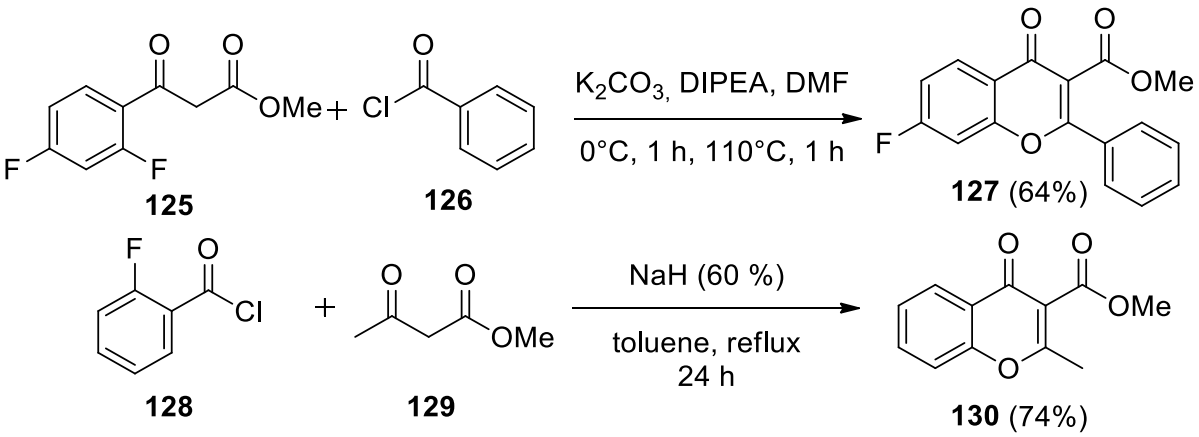

Figure 3.20 Literature-known examples of chromenone formation.[271,272]

In order to confirm the theory that the 2-position of the fluorine atom is required for the reaction to take place, several test reactions were carried out. Three different diketones were synthesised, which are shown below in Figure 3.21. Diketone **131** is singly fluorinated in the 2-position, in order to investigate whether one fluorine atom is sufficient for the reaction to take place. This is expected to be the case, as a single fluorine atom is eliminated in the S_NAr intramolecular ULLMANN-type *O*-arylation.

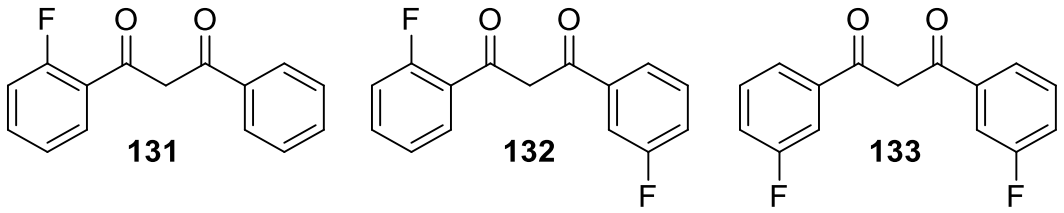

Figure 3.21 Diketones **131**–**133**.

Diketone **132** has fluorine atoms at the 2- and 3-positions of separate benzene rings, in order to investigate the reactivity of a fluorine atom at the 3-position. Finally, diketone **133** has both flurine atoms in the 3- and 3'-positions. This molecule is a viable alternative in synthesising a triple *ortho*-fluorinated TBTQ, as the ring closure at the 2' position leads to *ortho*-functionalised products from 3,3-functionalised diketones (see Figure 3.23).

The synthesis of diketone **131** proceeded using the conditions from diketone **117**. These reactions were tried both ways, once with a functionalised aldehyde and unfunctionalised ketone and *vice versa* (summarised in Table 1 and Figure 3.22). Moderate to good yields could be achieved for almost all substrates for the first two steps, whereas the third step was lower yielding in all cases. The final elimination step affords the same product from **136** and **139**, so that only one diketone was tested in the next step.

Diketone **132** was also synthesised using the same protocol, from 3-fluorobenzaldehyde (**137**) and 2-fluoroacetophenone (**140**), the yields for each step are also listed in **Table 1**.

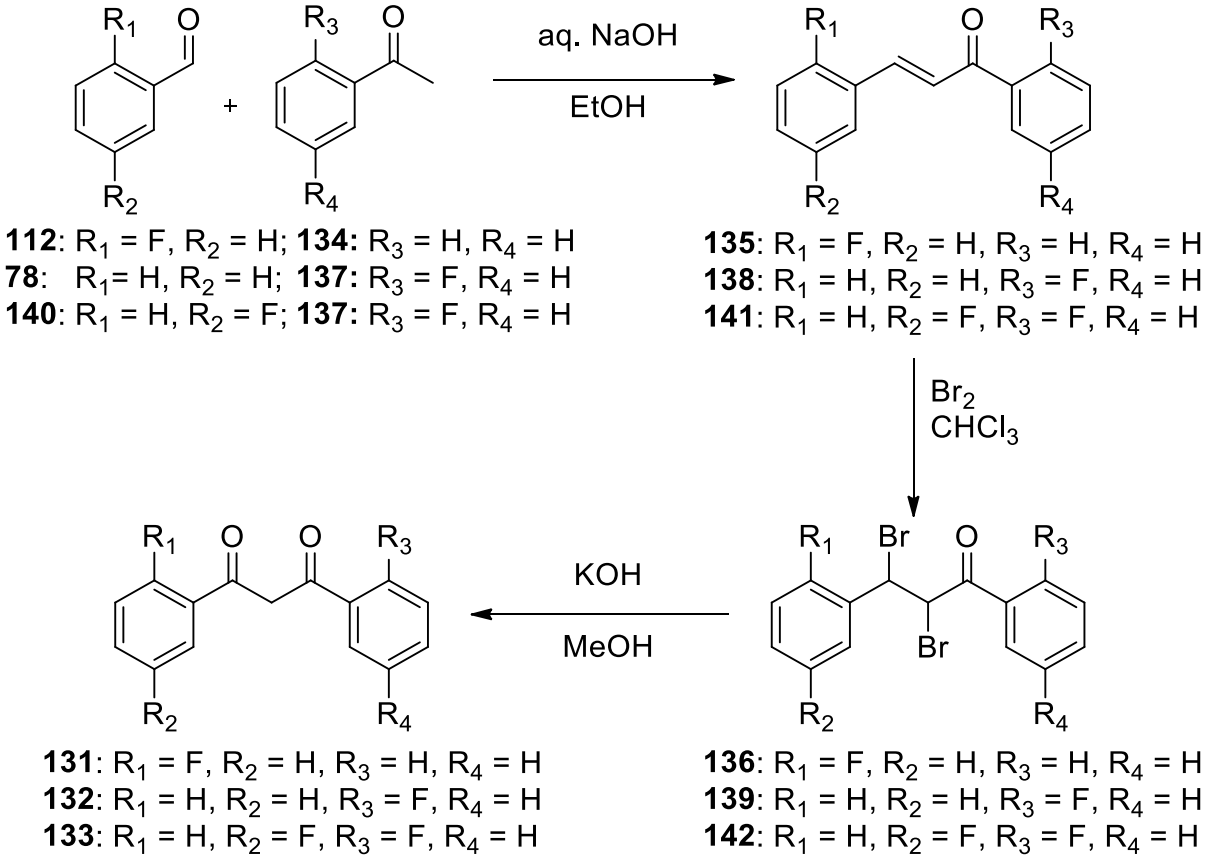

Figure 3.22 Synthesis of diketones **131-133**.

Table 1 Summary of yields for synthesised diketones **131–133**.

R_1	R_2	R_3	R_4	Step 1		Step 2		Step 3	
				Molecule	**Yield [%]**	**Molecule**	**Yield [%]**	**Molecule**	**Yield [%]**
F	H	H	H	**135**	64	**136**	51	**131**	43
H	H	F	H	**138**	51	**139**	53	**132**	59
H	F	F	H	**141**	75	**142**	75	**133**	51

Finally, the 3,3'-fluorophenyl diketone **133** was synthesised, as an alternative to ketone **117**, because the other *ortho*-positions are occupied with fluorine atoms. The synthesis of this diketone can be viewed below in Figure 3.24.

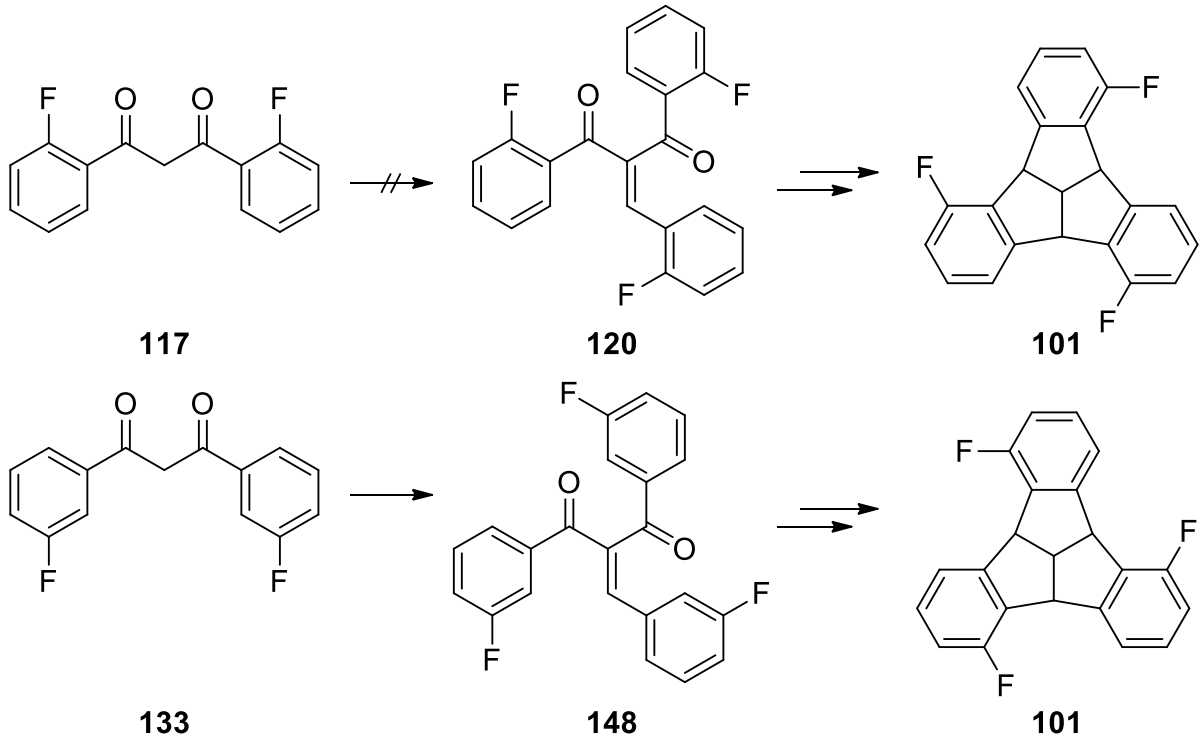

Figure 3.23 Two alternative diketone precursors: **117** and **133** for TBTQ **101**. Starting with diketone **117** theoretically leads to TBTQ **101** via diketone **120.** As the synthesis of diketone **120** cannot be realised, diketone **133**

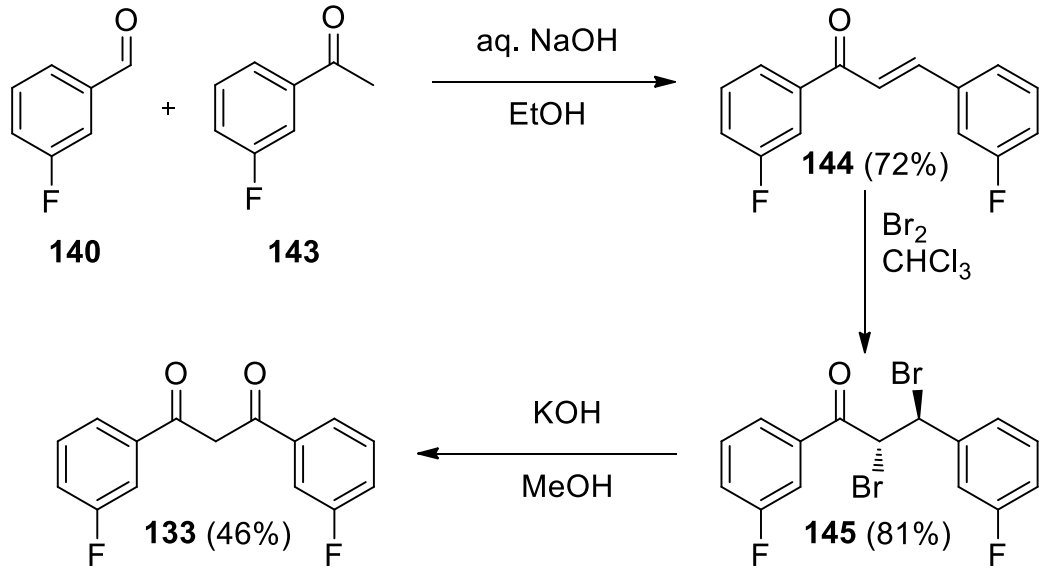

Figure 3.24 Synthesis of diketone **133**.

The test reactions are summarised below in Figure 3.25. All diketones were dissolved in MeCN with piperidine and heated to 80°C. For all starting materials except the 3,3'-difluorophenyl diketone **133**, chromenone product was isolated, as is shown in Figure 3.25. This proves the theory that only one *ortho*-positioned (2-position) fluorine atom is required

for the reaction to take place. Fluorine atoms at the 3-position are spatially too far removed from the enolised carbonyl group and not electronically favoured, which is why the reaction cannot take place. These test reactions provided valuable information, as diketone **133** does not lead to the formation of a chromenone product and can therefore be used as a precursor for the synthesis of trifluorinated TBTQ **101**.

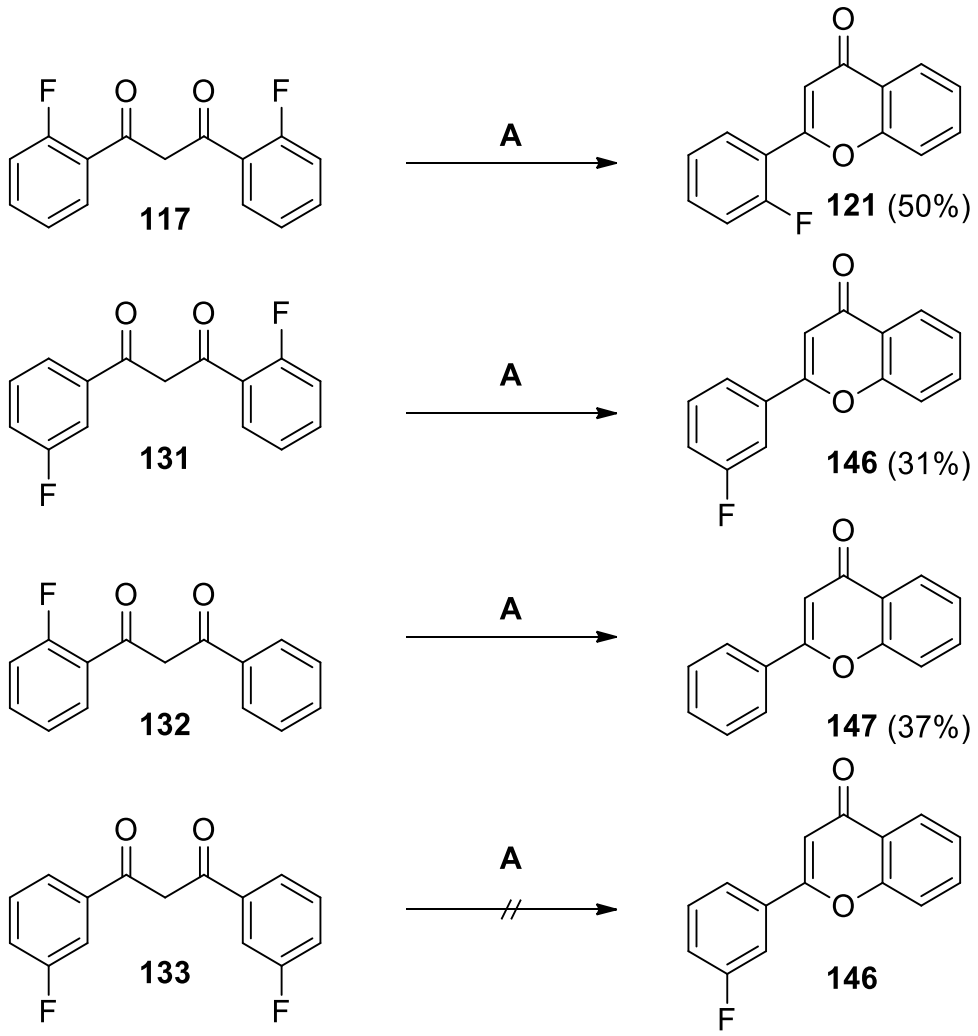

Figure 3.25 Test reactions with fluorinated diketones **117**, **131**, **132** and **133**.
A: acetonitrile, piperidine, 80°C.

The KNOEVENAGEL reaction of diketone **133** with 3-fluorobenzaldehyde (**137**) was successful (see Figure 3.26 below), but the product diketone **148** was difficult to isolate as many side-products were formed, with a 33% yield for the desired product.

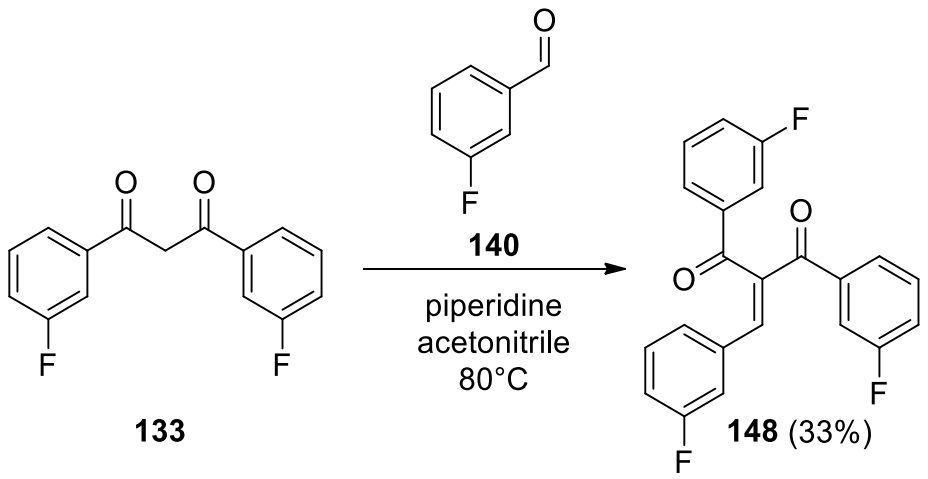

Figure 3.26 Synthesis of diketone **148**.

On increasing the amount of piperidine to 0.2 eq., the yield of the desired product decreased and diketone **144** was isolated with a 48% yield (see Figure 3.27). This result was unexpected, as a suitably fluorinated diketone is required for an aldol condensation to take place. Self-condensation of aldeyde **137** can also be excluded as there are no enolisable protons present.

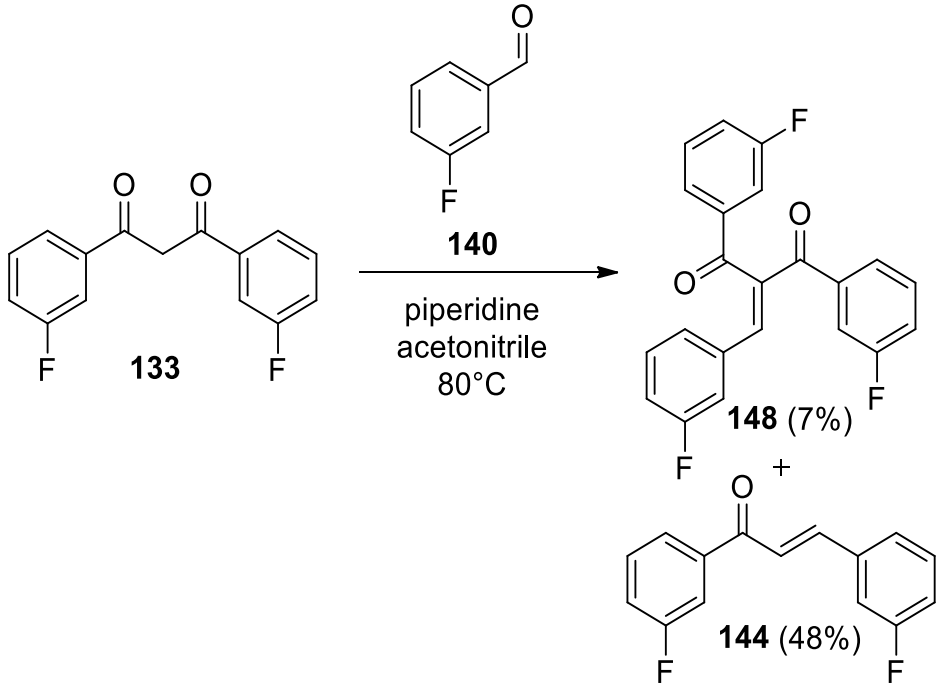

Figure 3.27 Formation of diketones **144** and **148**.

The mechanism of this reaction is likely to be similar to that reported by DYACHENKO *et al.*, who proposed that a hydrolysis product was responsible for an unexpected product.[273] The mechanism is detailed in Figure 3.28. Initial formation of enamino ketone intermediate **149** is followed by hydroylsis to intermediate **150**, instead of diketone **133** and piperidine. Acyl

cleavage of intermediate **150** results in ketone **143**, which readily undergoes condensation with 3-fluorobenzaldehyde (**137**), which is present in excess.

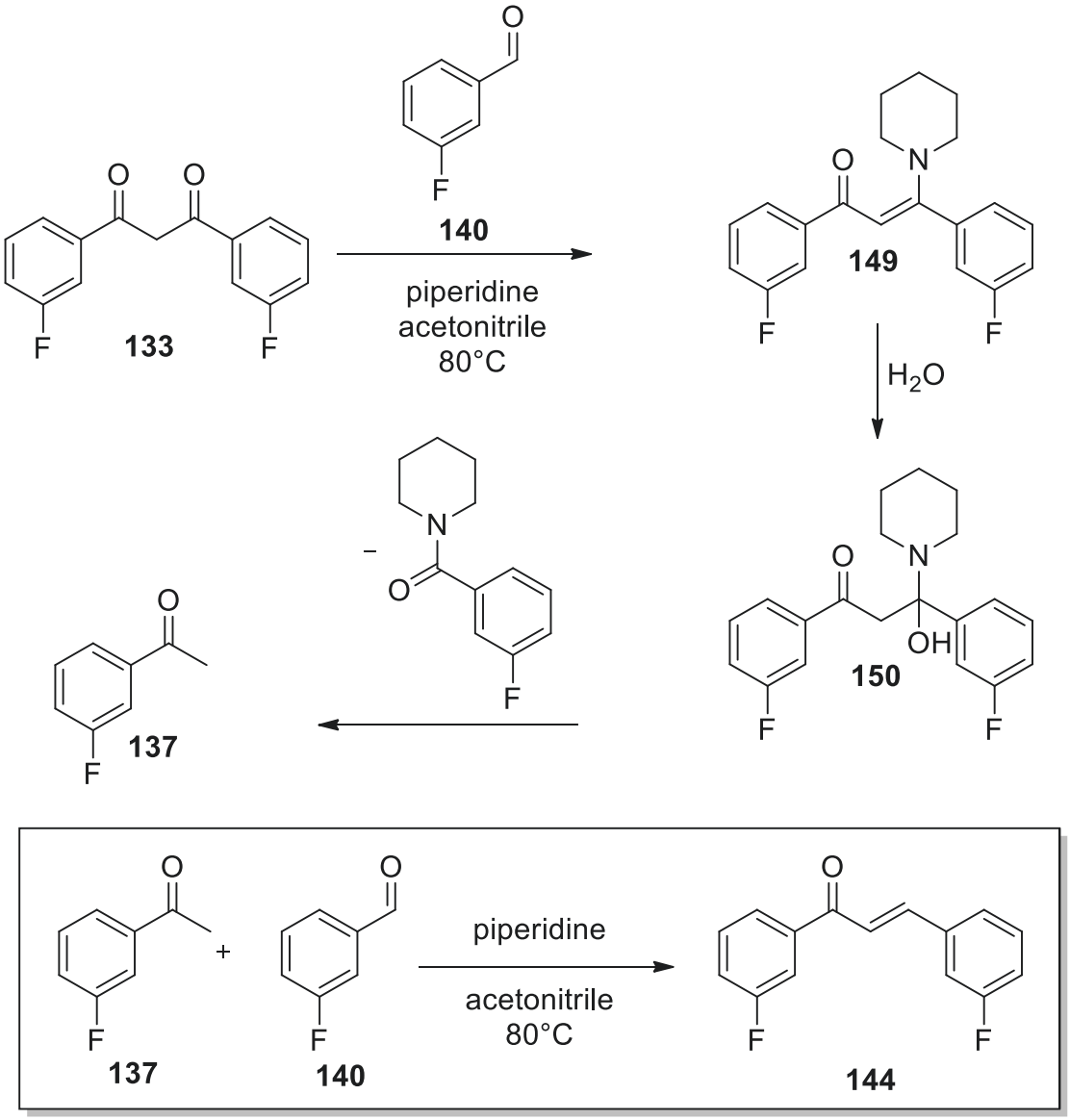

Figure 3.28 Mechanism of the hydrolysis of intermediate **149** and acyl cleavage of intermediate **150**.

The prescence of water is responsible for the hydrolysis and susbequent acyl cleavage reactions. Although a DEAN-STARK trap is commonly used for KNOEVANAGEL reactions in order to remove water, it was not used by MARKOPOULOS,[202,207] who heated the reaction in acetonitrile, as reported originally by TANIKAGA *et al.*[274] This approach was chosen for the fluorinated analogues, as examples of the Knoevenagel reaction with brominated[202,207,275] and chlorinated[275] aldehydes adapted TANIKAGA's method.[274] Although removal of water with a DEAN-STARK trap would be beneficial, the low boiling point of acetonitrile (81–82°C) does not facilitate efficient removal of water. Therefore, molecular sieve (4 Å) was added,

which gave an optimised yield of 41% after 5 d. After 4 h a solid precipitated out of the solution, which was a powdered debris of the molecular sieves. Although the reaction was not complete after 5 d, increasing amounts of the side-product were observed via TLC analysis and therefore the reaction was stopped at this point. It was possible to isolate 22% of the starting material. ·

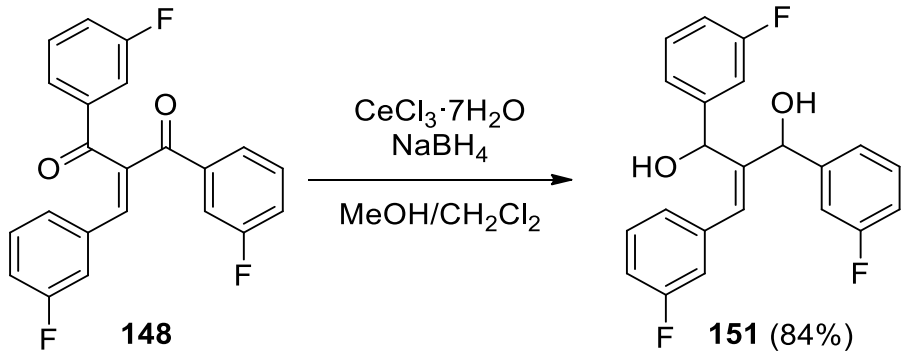

Figure 3.29 Synthesis of dialcohol **151**.

The LUCHE reduction proceeded smoothly, with full conversion after 1 h 30 min and 84% combined isolated yield of the diastereomers. For the final cyclisation step, diol **151** was heated to reflux at 130°C under nitrogen for 21 h.

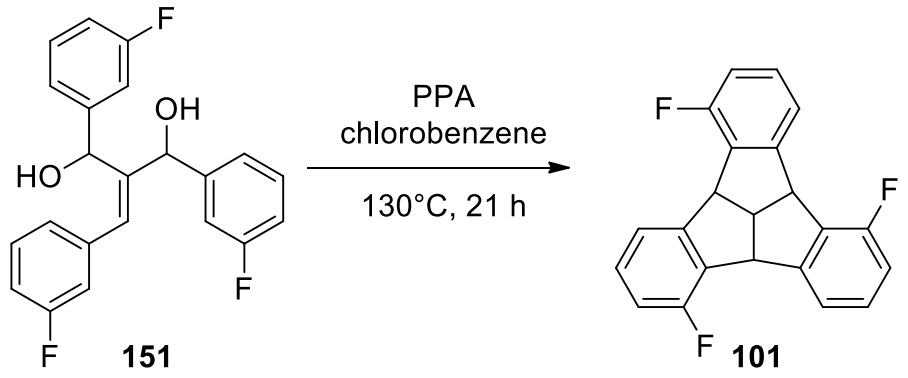

Figure 3.30 Reaction conditions for cyclisation of dialcohol **151**.

After column chromatography of the residue with 95:5 cyclohexane/CH_2Cl_2, several fractions were collected. Analysis of the ^{1}H NMR spectra of fraction B looked promising, as peaks between 5.0 and 4.5 ppm were present, which indicate the presence of bridgehead protons and therefore a completed cyclisation reaction. In addition, a second set of signals was visible, which suggests a mixture of TBTQs (Figure 3.31). Recrystalliation in toluene did not lead to the isolation of separate products. The main fraction (fraction A) collected appeared to comprise of a mixture of a side-product and fluorinated TBTQs.

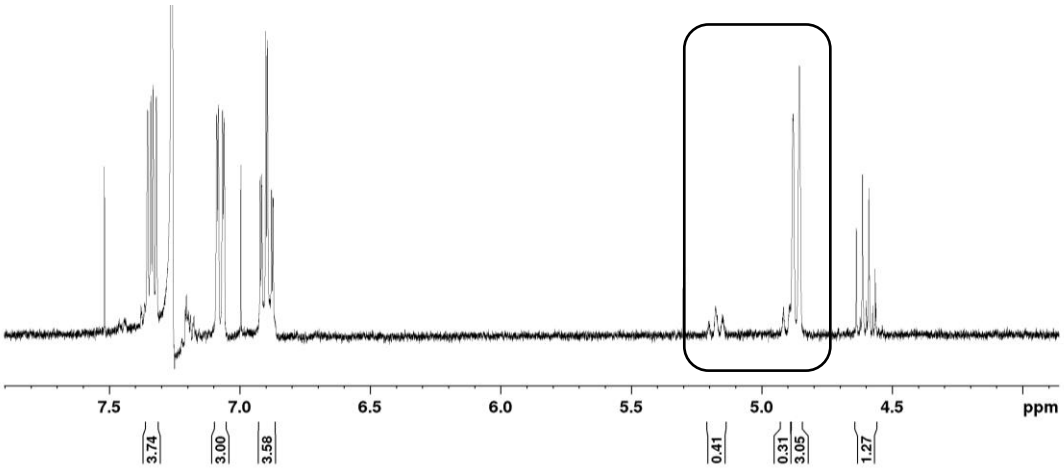

Figure 3.31 ^{1}H NMR spectrum of fraction B. The box indicates the bridghead protons, where signals from two molecules are visible.

A small sample of this fraction A was used for a test-run with HPLC and a chiral OD-H column (150 mm × 4.6 mm, 90:10 *n*-hexane:isopropanol). The solid did not fully dissolve and the solution was filtered (0.45 µm) before injection. Two peaks were observed on the chromatogram, but the ^{1}H NMR spectra were identical, implying that each peak belonged to an enantiomer of a racemic mixture. The solid which had not dissolved, whose ^{1}H NMR spectrum matched that of fraction B, appeared to be a mixture of isomers: C_3 and C_1-TBTQs which was unexpected, but several doublets were identified in the ^{1}H NMR spectrum, which indicates that the bridgehead positions are no longer equivalent. The side-product was separated by recrystallisation in hexane and hot filtration of the filtrate. As the TBTQs did not dissolve in hexane, they could be recystallised again in toluene.

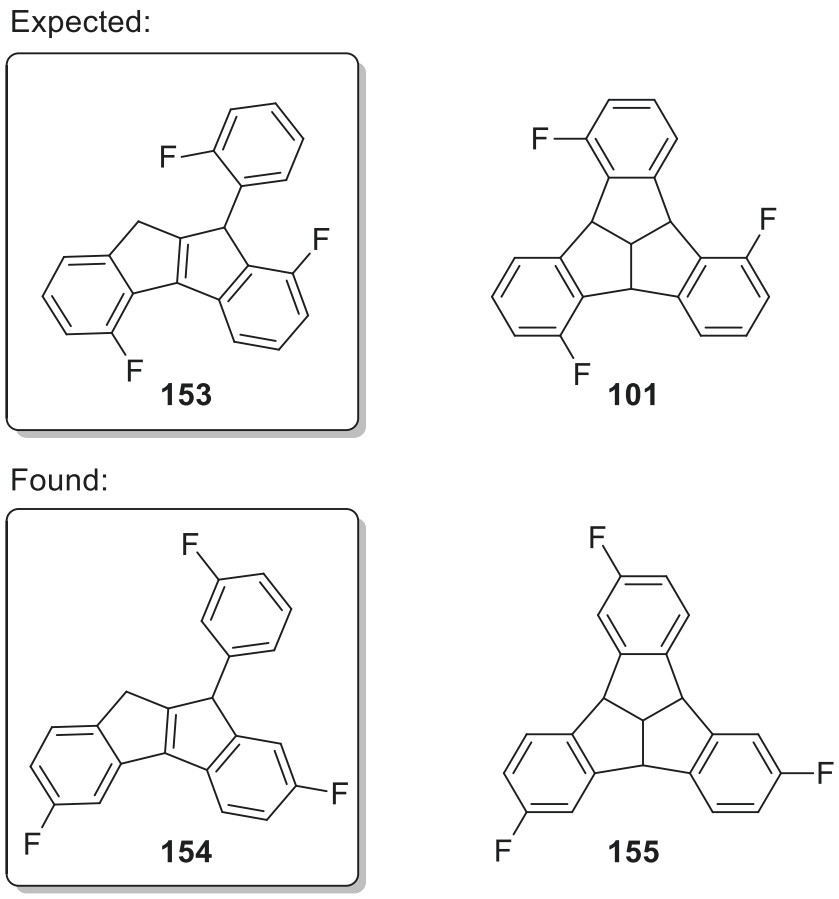

Figure 3.32 Dihydroindenoindene derivatives **153** and **154**.

The side product is of equal molecular weight to the desired product, with m/z = 334, so assuming that TBTQ **101** was formed, the logical consequence would be the formation of dihydroindenoindene derivative **153**. MARKOPOULOS' work is the basis of this assumption, as it describes the isolation and identification of dihydroindenoindene byproducts for bromo, methoxy and methyl C_1- and C_3-functionalised TBTQs and proposes a mechanism for their formation.[202,207] However, evaluation of the ^{13}C- and 2D-NMR spectra indicated that dihydroindenoindene **154** had been synthesised. Therefore, it can also be deduced that the C_3 fluorinated TBTQ is TBTQ **155** and not TBTQ **101**. In order to explain this further, the proposed mechnasim for the triple cylcisation pathway from MARKOPOULOS was adapted for the fluorinated derivatives, shown below in Figure 3.33.

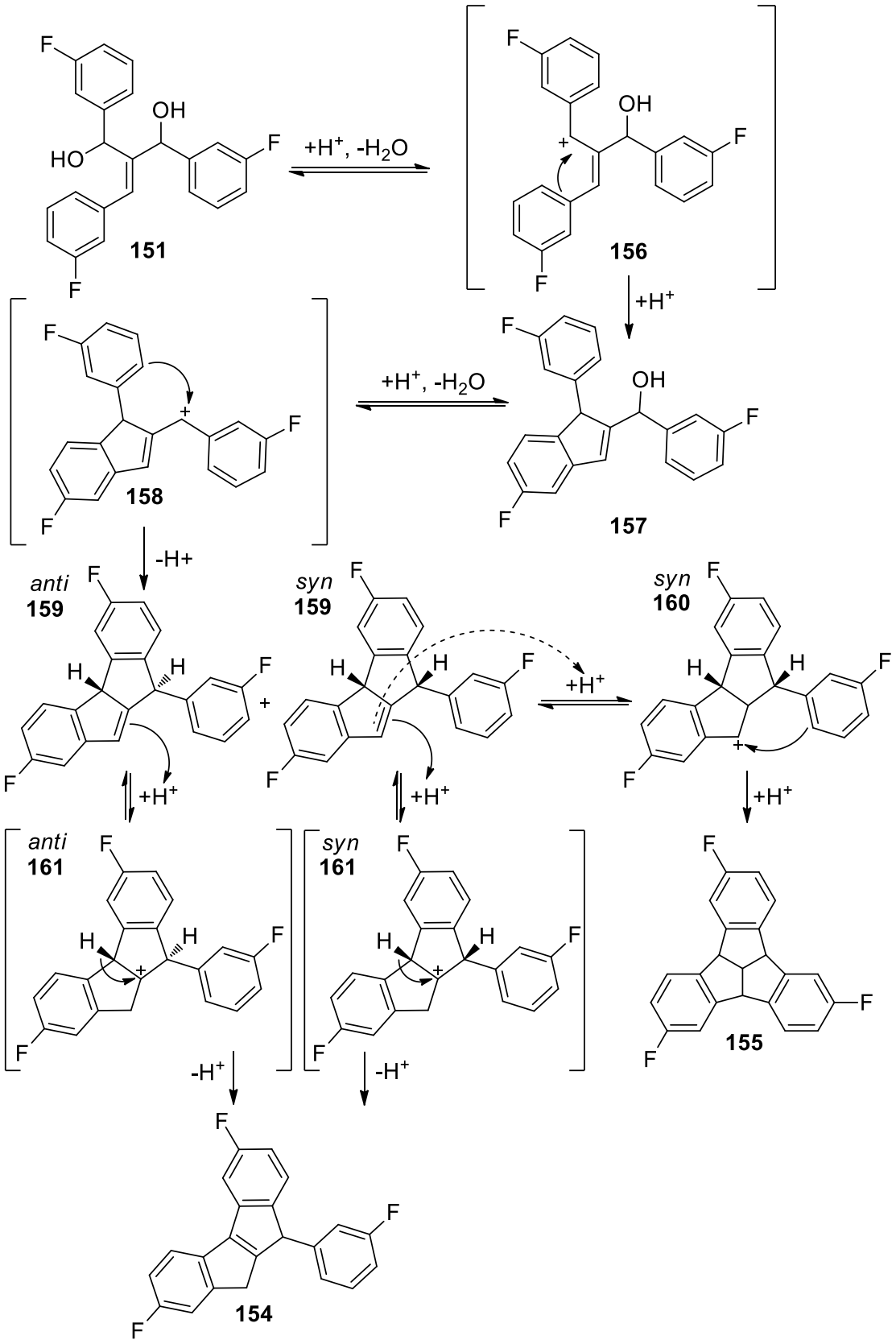

Figure 3.33 Proposed mechanism for tribenzotriquinacene **155** and dihydroindenoindene **154**, adapted from the mechanism from MARKOPOULOS.[202,207] *syn* and *anti* refer to the orientation of bridgehead hydrogen atoms.

After two cyclodehydrations, the intermediate **159** is formed, which consists of two five-membered rings. *syn*-**159** and *anti*-**159** are shown (Figure 3.33), as there are two diastereomers present, depending on the relative stereochemistry of the two bridgehead protons. Only *syn*-**159** proceeds with a FRIEDEL-CRAFTS type alkylation via *syn*-**160** to form TBTQ **155**, whereas both diastereoisomers of **159** can undergo an acid-catalysed double bond shift via *syn*-**161** and *anti*-**161** respectively to form side-product **154**. Therefore, the isolation of side-product **154** implies that TBTQ **155** has also been formed because they are both derived from cationic intermediate **158**.

The formation of TBTQ **155** instead of the desired product *ortho*-TBTQ **101** can be explained by rotation of each benzene ring around the C-C bond connecting them to the rest of the molecule (Figure 3.34). If all three benzene rings are rotated by 180°, the result would be TBTQ **155**, as the formation of five membered rings during cyclodehydrations prevents the benzene rings from rotating further. A possible reason for the preferred orientation of diol **152** is electrostatic repulsion between the fluorine atom attached to the aromatic ring and the side chain β-hydroxyl group, which is reduced as all fluorine atoms are oriented away from the hydroxyl groups. The dipole interaction of the strong C-F bond and other dipoles such as a hydroxyl group was proposed to be the cause of conformational bias in 2- and 6-fluoronorepinephrine by DEBERNARDIS *et al.*[276]

After identification of dihydroindenoindene **154**, separation of the TBTQ mixture, which appeared to be a mixture of C_3 and C_1 isomers, is required to confirm the formation of TBTQ **155**, as proposed in Figure 3.33.

A small fraction of the C_1 isomer had been isolated from the first column chromatography of the raw product. As the C_1 isomer is formed rotation of either one or two benzene rings, there are only two potential structures, as shown in Figure 3.35. Evaluating ^{13}C-, ^{19}F- and 2D-NMR spectra revealed that TBTQ **164** is the C_1 isomer.

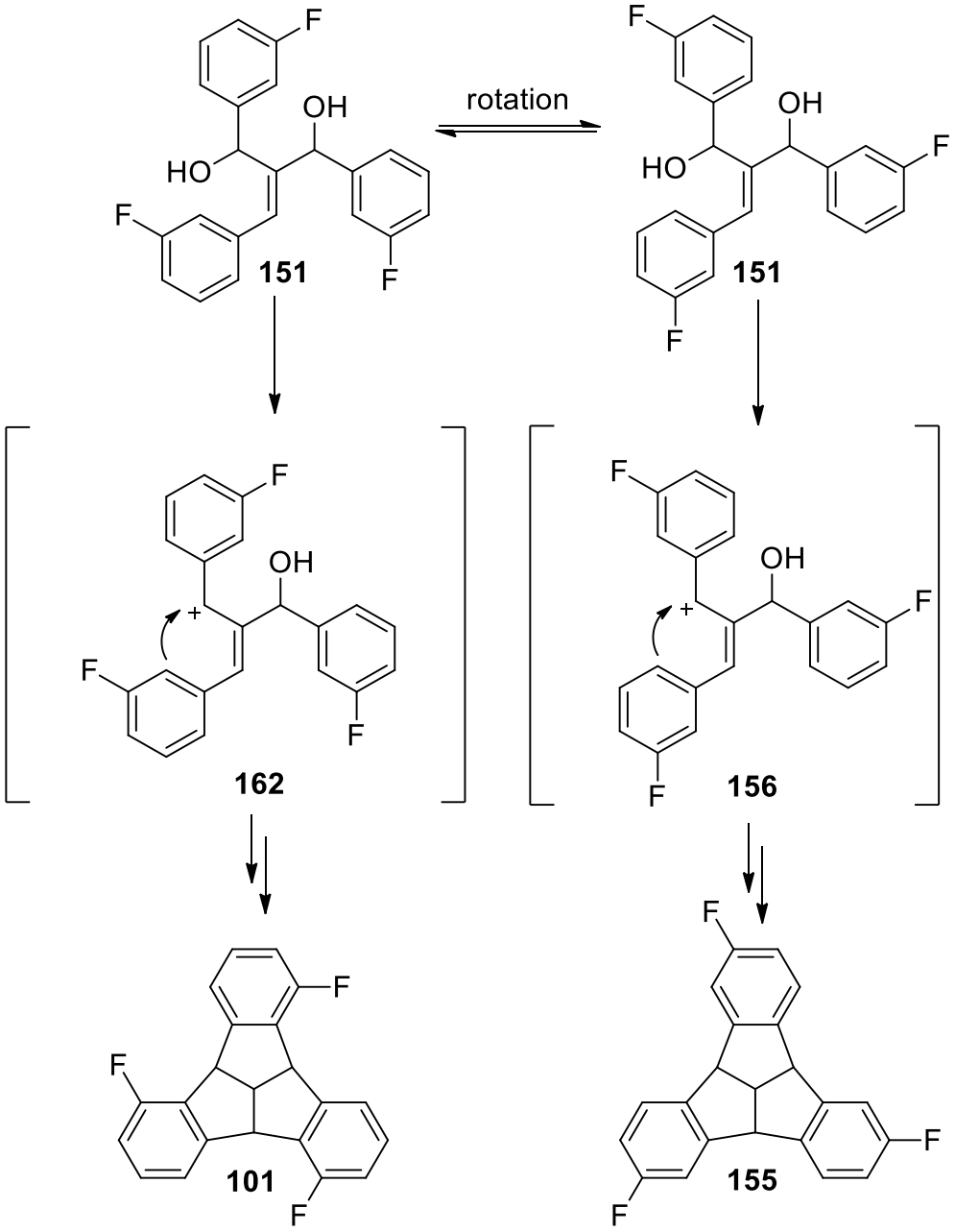

Figure 3.34 Proposed formation of TBTQ **155**, formed as a result of rotation of all three benzene rings in dialcohol **151** by 180°.

Recrystalliation of the C_3/C_1 TBTQ mixture from toluene, acetonitrile, ethanol, ethyl acetate, diethyl ether, methanol, chlroroform, xylene as well as mixtures thereof did not lead to the succesful isolsation of pure C_3 isomer. Column chromatography and HPLC separation were not possible, as once the side-product **154** was removed, the C_3/C_1 TBTQ mixture was no longer visible under UV light (254 nm). Visualisation of the TLC plate was achieved with the ceric ammonium molybdate stain, but poor solubility of the TBTQ mixture (0.08 mg/ml in CH_2Cl_2 and 0.09 mg/ml in $CHCl_3$) prevented successful separation.

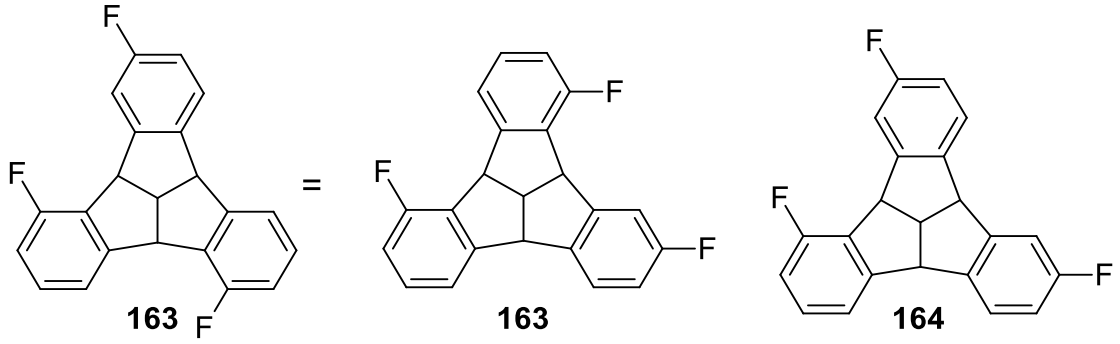

Figure 3.35 All potential C_1 isomers: TBTQ **163** is formed as a result of one benzene ring rotation during cyclisation; TBTQ **164** is formed as a results of two benzene ring rotations during cyclisation.

Melting points of the C_3/C_1 mixture and the C_1 TBTQ were measured: 306–307°C for the C_3/C_1 and 270–272°C for C_1 TBTQ. Based on these results, sublimation as a separation technique was also investigated, but despite increasing the temperature slowly and stopping the sublimation after first crystals were observed, the purified product on the cooled surface as well as the crude product left behind remained mixtures, with the ratio of C_3 and C_1 products not changing.

A small fraction (5.1 mg) of C_3/C_1, whose isomer ratio was 4:1 was analysed with ^{1}H-^{1}H-COSY (400 MHz). The data collected indicates that TBTQ **155** was synthesised, as the bridghead protons (b in Figure 3.36) couple with two aromatic protons (d and e) per aromatic ring. For TBTQ **101**, the fluorine atom would occupy one of the *ortho* positions, therefore the brideghead protons would be expected to only couple with one proton per aromatic ring.

When measuring the C_3/C_1 mixture with an 600 MHz NMR spectrometer, it was noted that a siginificant portion of the product did not dissolve. In addition, the C_3:C_1 ratio of the resulting ^{1}H spectrum was 1:2 (earlier measurements of the sample: C_3:C_1 3:1), indicating that the C_3 TBTQ is less soluble than C_1 TBTQ in $CDCl_3$. As all the proton signals for the C_3 isomer overlap with those of the C_1 isomer and the 2D measurements only providing information on the coupling of the more soluble C_1 isomer, it was not possible to confirm the identitity of TBTQ **155** as the C_3 isomer unoquivically. A comparison of the ^{1}H NMR spectra for the C_1 isomer and the C_3:C_1 isomer mixture is shown below in Figure 3.37. Washing the C_3:C_1 mixture with chloroform could lead to their separation, as the C_1 isomer dissolves more readily.

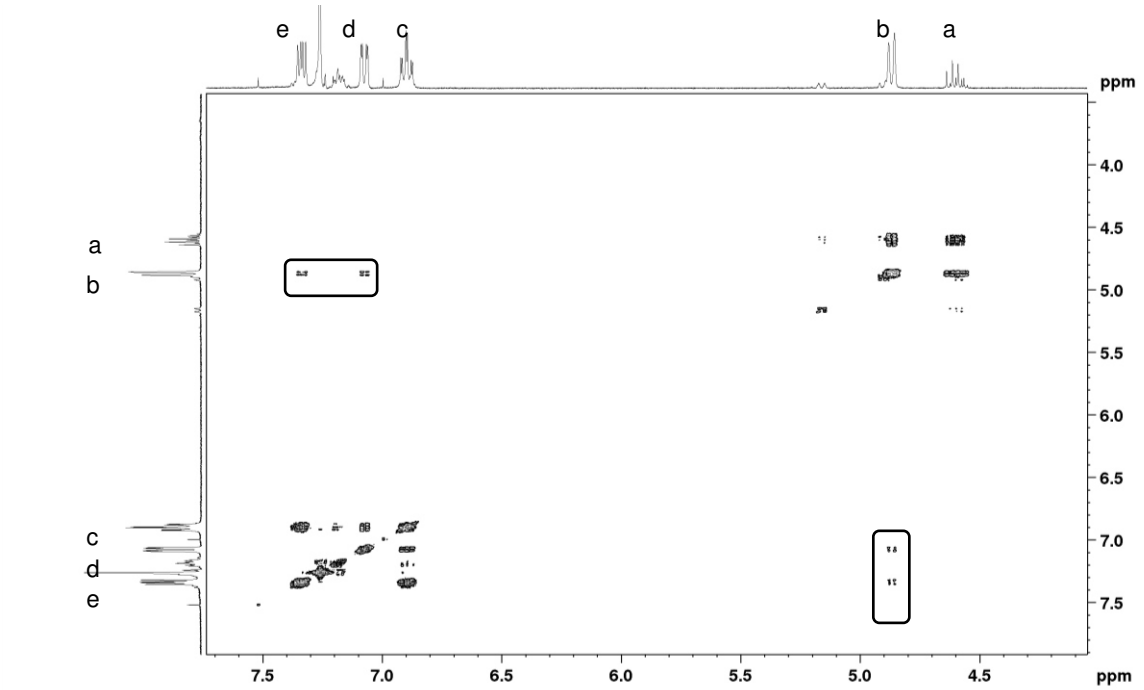

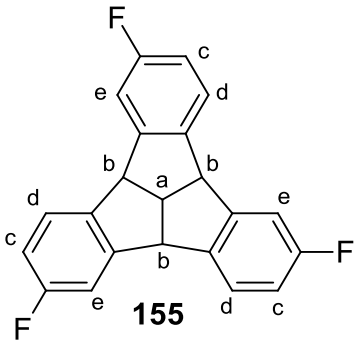

Figure 3.36 ^{1}H-^{1}H-COSY spectrum of C_3/C_1 mixture (ratio 1:0.3), annotated with protons a to e. The boxes indicate coupling between proton b and protons d and e.

The yield of side-product **154** is 8%, and taking the ratio of C_3:C_1 mixture to be 3:1, the yields are C_3: 3% and C_1 (TBTQ **164**): 2%. The synthesis of TBTQ **164**, although not expected, provides an interesting insight into the synthesis of multiply fluorinated TBTQs.

HOPF and GEORGIOS only isolated C_3-chiral brominated TBTQs, but the bromine atom occupied the 2-position on each ring.[202,207] Rotation of an aromatic ring would have not led to cyclodehydration in the first place, as the bromine atom would occupy the position where the a new C-C is formed, when creating the five-membered ring. A 2-substituted fluorinated analogue, diketone **119**, was synthesised, but using KNOEVENAGEL conditions a chromenone side-product was formed instead (chromenone **121** in Figure 3.18). Therefore a 3-substituted

diketone **133** was used for further synthesis steps. This raises the question if 2-substituted precursors are required for the formation of *ortho* C_3-chiral TBTQs, or if electrostatic repulsion between the aromatic fluorine atom and the side chain β-hydroxyl group is responsible for rotation of aromatic rings and the subsequent formation of C_1 TBTQ **164**. Further investigations are required to answer this question, as well as an alternative strategy to synthesise *ortho*-C_3 TBTQ **101**.

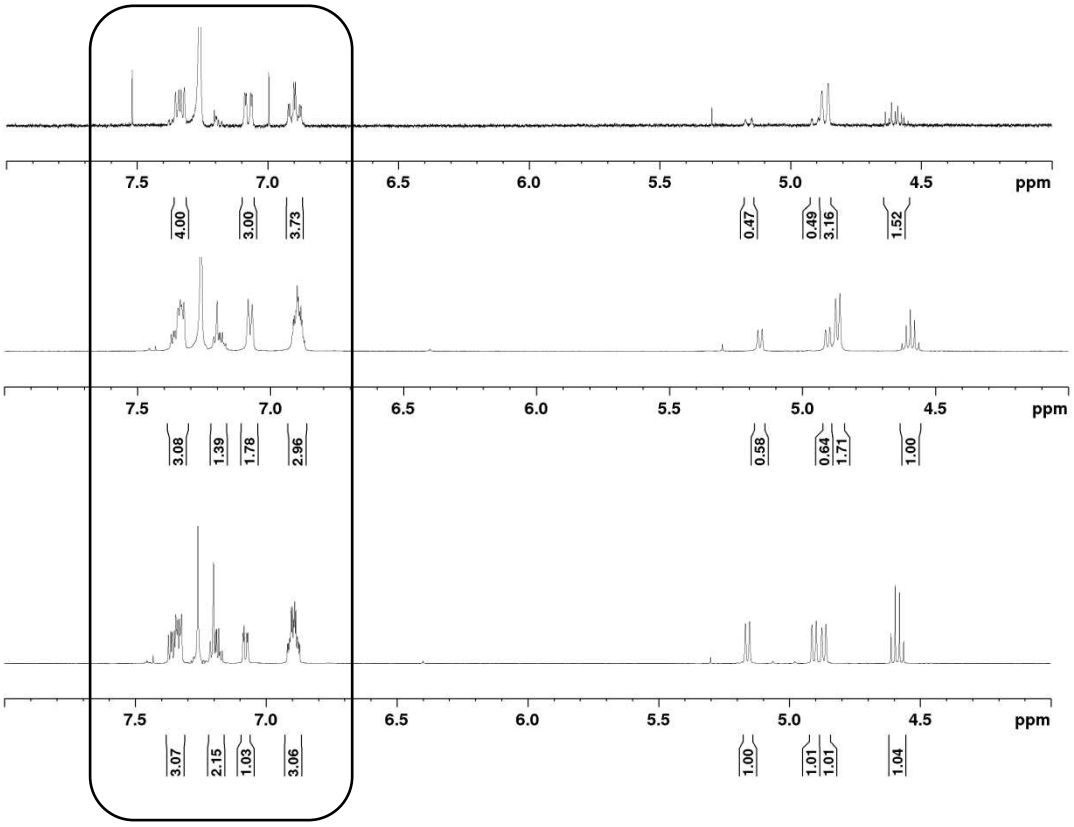

Figure 3.37 ^{1}H NMR spectra of the C_3:C_1 isomer mixture (top); the same C_3:C_1 isomer measured with an 600 MHz NMR spectrometer (middle) and the isolated C_1 isomer (bottom).The box indicates the aromatic signals of C_3 and C_1 isomers, which overlap.

To summarise, fluorinated TBTQs have been synthesised for the first time. Introducing fluorine into the TBTQ scaffold leads to side-reactions, as exemplified by the synthesis of chromenone **121** and the final cyclisation step, which affords a mixture of C_3 and C_1 isomers.

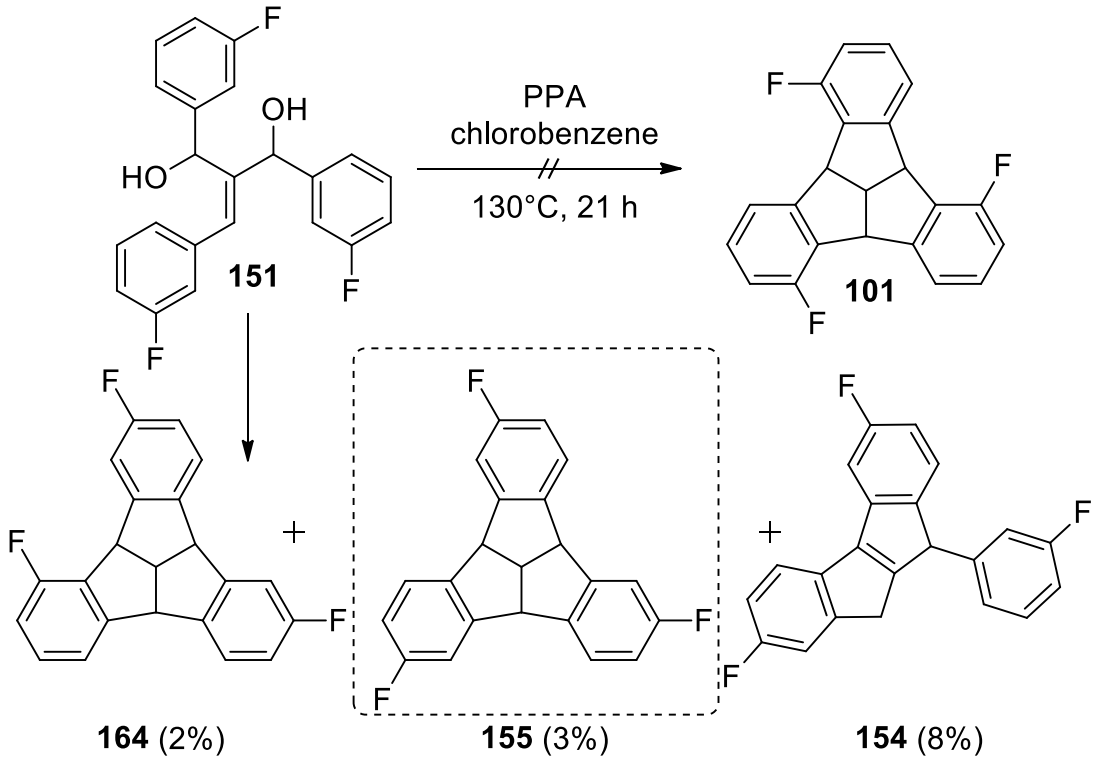

Figure 3.38 Isolated TBTQ **164** and side-product **154**. The dashed box indicates the TBTQ **155** as the proposed structure of the C_3 isomer, based on ^{1}H-^{1}H-COSY coupling data and the prescence of byproduct **154**.

3.3 Funtionalisation of the *ortho*-position – synthesis of phenanthreno-TBTQs and study of their stacking arrangements

3.3.1 Summary of previous work

In addition to tuning the electronic properties of TBTQs by functionalisation of the *ortho*-position, there is potential for enlarging the scaffold, thereby generating a defective nanographene with a TBTQ core. Such a model system would provide valuable insights into the properties and behaviour of defective nanographenes, as the TBTQ motif introduces significant curvature. KIRCHWEHM proposed that TBTQ **104** is a desirable synthetic aim for the extension of the carbon network (see Figure 3.39), as the SCHOLL reaction could be used to close the three bay regions, without further functionalisation.[242]

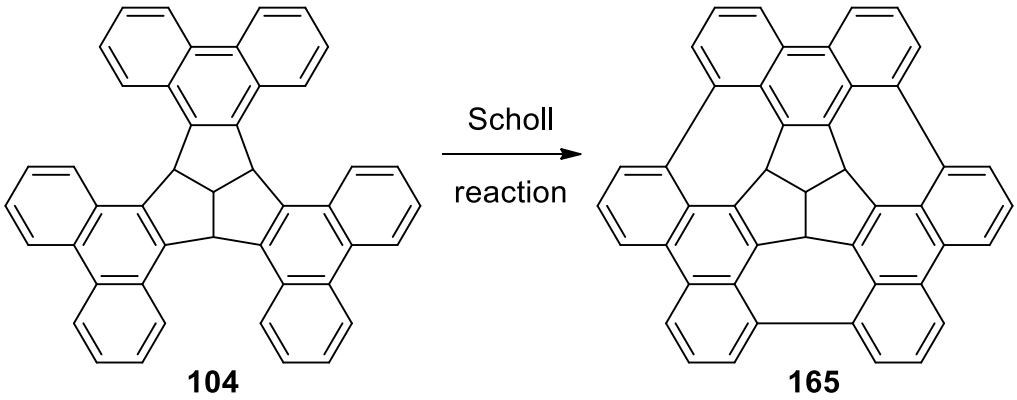

Figure 3.39 Proposed synthesis of TBTQ **165**.

A summary of the reactions presented in the thesis of Y. KIRCHWEHM, is found in Figure 3.40. The following paragraphs describe the outcome of these experiments.

KIRCHWEHM noted that whilst following the HOPF synthesis route with phenanthrene functionalised precursors, the KNOEVENAGEL condensation step between diphenanthreno diketone **166** and aldehyde **167** did not lead to the formation of product (see Figure 3.40).[250] This prevented the synthesis of desired product TBTQ **165**. Nevertheless, KIRCHWEHM described the succesful conversion of diketone **166** to diketone **169**, using benzaldehyde **78** instead of aldehyde **167** (see Figure 3.40).[250]

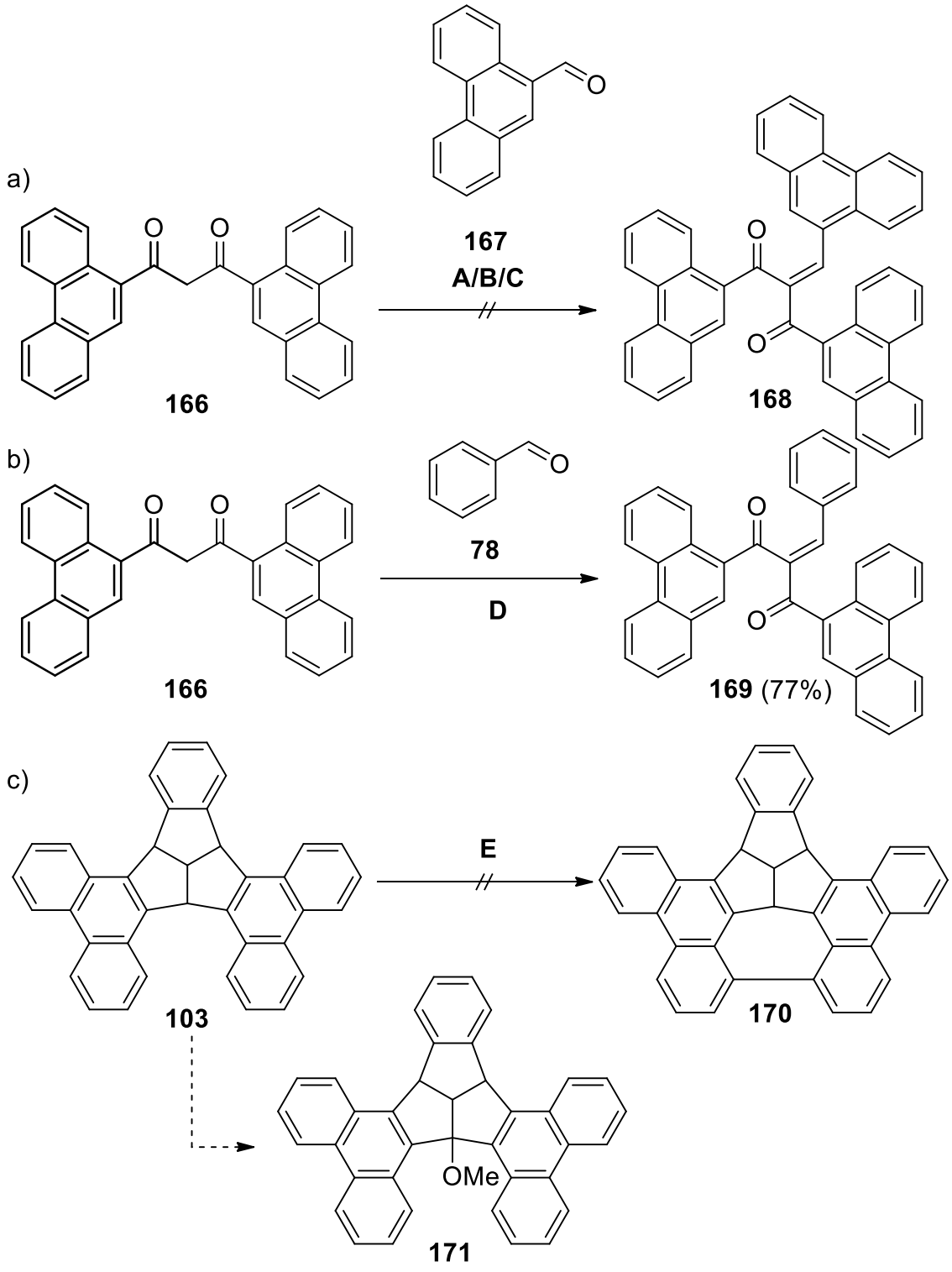

Figure 3.40 Summary of reactions reported by KIRCHWEHM.[250,277]

A: $NbCl_5$ (1.6 eq.), CH_2Cl_2, rt 1h, reflux 1 h 50 min; **B**: $NbCl_5$ (0.6 eq.), CH_2Cl_2, reflux, 69 h; **C:** Piperidine, butyric acid, toluene, 120°C, 25 h; **D**: butanoic acid, piperidine, toluene, reflux, 30 min; **E**: $FeCl_3$, CH_2Cl_2, 1.5 h.

After subsequent reduction and cyclisation reactions of diketone **169**, benzodiphenanthreno-triquinacene (BDPTQ, **103**) was isolated. Since this precursor only contains two phenanthrene groups, it would only be hypothetically possible to bridge one bay region. Several SCHOLL reaction attempts were carried out, the most promising of which afforded a mixture of starting material and another substance. KIRCHWEHM suggested that this molecule is TBTQ **171**, but full characterisation was not possible, as only 9.0 mg of starting material was used for the reaction.

Following on from KIRCHWEHM'S work, there remain several topics for further exploration:

1) Attempting to synthesise diketone **168** using different reaction conditions for the KNOEVENAGEL reaction, while also exploring an alternative strategy for synthesising TBTQ **104**.

2) Confirming the identity of TBTQ **171** formed during the SCHOLL reaction with benzodiphenanthrenotriquinacene (BDPTQ **103**) in order to choose alternative reagents for the synthesis of TBTQ **170.**

3) Exploring the introduction of methoxy or *tert*-butyl groups to exert control during the SCHOLL reaction of phenanthrene functionalised TBTQs.

3.3.2 Introduction of a third phenanthrene group via KNOEVENAGEL reaction

To complement the investigations of KIRCHWEHM, the KNOEVENAGEL reaction was attempted, using the reaction conditions used by HOPF *et al.*: catalytic amounts of piperidine and hexanoic acid in toluene[207] (see Figure 3.40, reaction a)). This reaction was however unsuccesful, as after 3 d at 120°C, only the starting materials were re-isolated.

A possible explaination for the failure of this reaction is that the phenanthrene aldehyde **167** is sterically hindered upon approaching diketone **166** during the reaction as a results of its size and the prescence of two other phenanthrene groups. In order to explore this reaction further, a test reaction between dibenzoylmethane (**77**) and phenanthrene aldehyde (**167**) was carried out, adapting the protocol from ANTONIOLETTI *et al.* (see Figure 3.41).[278]

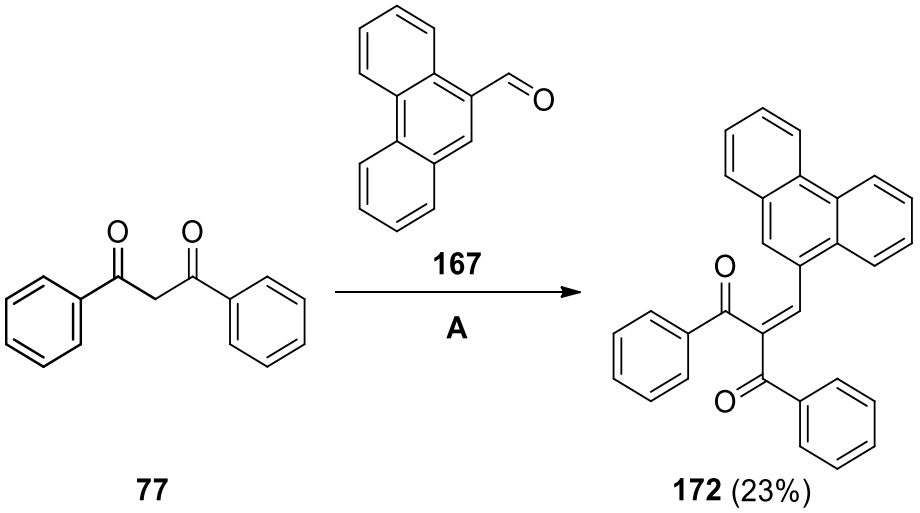

Figure 3.41 Synthesis of diketone **172**. **A**: butanoic acid, piperidine, toluene, reflux, 9 d.

Worthy of note is that this reaction did not run to completion, even after increasing the temperature to 130°C, extending the reaction time to 9 d and adding additional piperidine. The highest yield achieved was 23%, which spports the theory that steric hindrance influences this reaction. As a result an alternative approach is needed for the synthesis of TBTQ **104**.

Diketone **172** is a useful model system for exploring the introdution of a third phenanthrene group, as the final cyclisation reaction step with a phenanthrene group in this postion can be tested. Therefore, the synthesis of benzophenanthrenotriquinacene (**102**), from diketone **172** was explored, as detailed below.

3.3.3 Synthesis of dibenzophenanthrenotriquinacene (DBPTQ, 102)

Despite the low yield of the synthesis of diketone **172**, it was decided to explore whether dibenzophenanthrenotribenzotriquinacene (**102**) could be synthesied using this precursor, as shown below in Figure 3.42. The LUCHE reduction gave an excellent combined yield of 96% **173** (two isomers). The ^{1}H NMR spectra measured for the separated isomers of **173a** and **173b** also followed the ^{1}H NMR pattern described by MARKOPOULOS,[202] and therefore the diastereomers were assigned accordingly.

The cyclisation however was more challenging: three attempts were made to synthesise DBPTQ **102**, using the HOPF triple cyclisation conditions.[207] The raw product was analysed using column chromatography and RP-HPLC, and the most defined fraction which was isolated each time appeared to be a mixture of products, as 41 protons were observed in the spectrum, which is more than double the expected number for DBPTQ (**102**): $C_{30}H_{20}$.

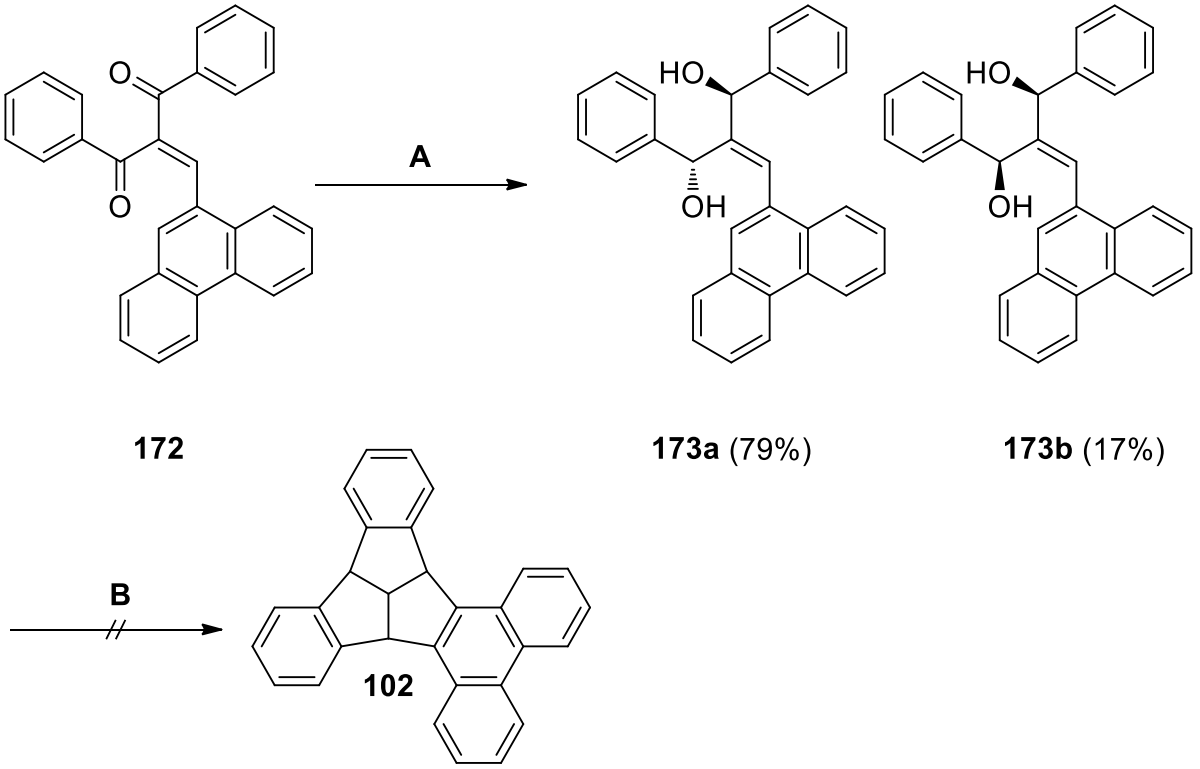

Figure 3.42 Attempted synthesis of DBPTQ **102**.

A: $CeCl_3 \cdot 7\ H_2O$, $NaBH_4$, CH_2Cl_2, MeOH, -78°C → rt

B: Polyphosphoric acid, chlorobenzene, 130°C, 22 h

On analysing the ^{1}H NMR spectrum, TBTQ molecules appear to be present, as several potential bridgehead protons are visible between 4.0–5.7 ppm. However the amount of this mixture was insufficient to determine the identity of this molecule, as the cyclisation step is low yielding. Owing to the low yielding first step, it was decided to synthesise this molecule by introducing the phenanthrene group at the start of the synthesis instead of via KNOEVENAGEL reaction.

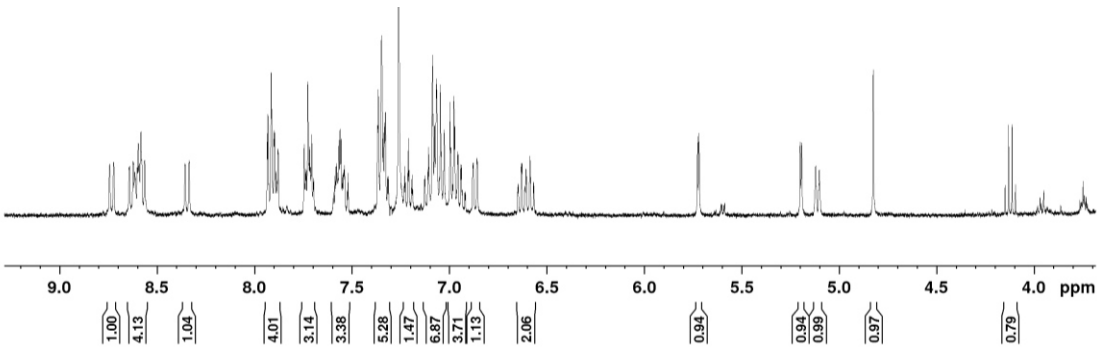

Figure 3.43 ^{1}H NMR spectrum of the cyclisation product of diol of **173.**

Using a literature known procedure,[279] diketone **176** was synthesised with a 66% yield (see Figure 3.44). The subsequent KNOEVENAGEL reaction step gave only a moderate yield of 49%, as after column chromatography the product fraction was a viscous oil, from which the product could only be isolated upon recrystallisation from cyclohexane.

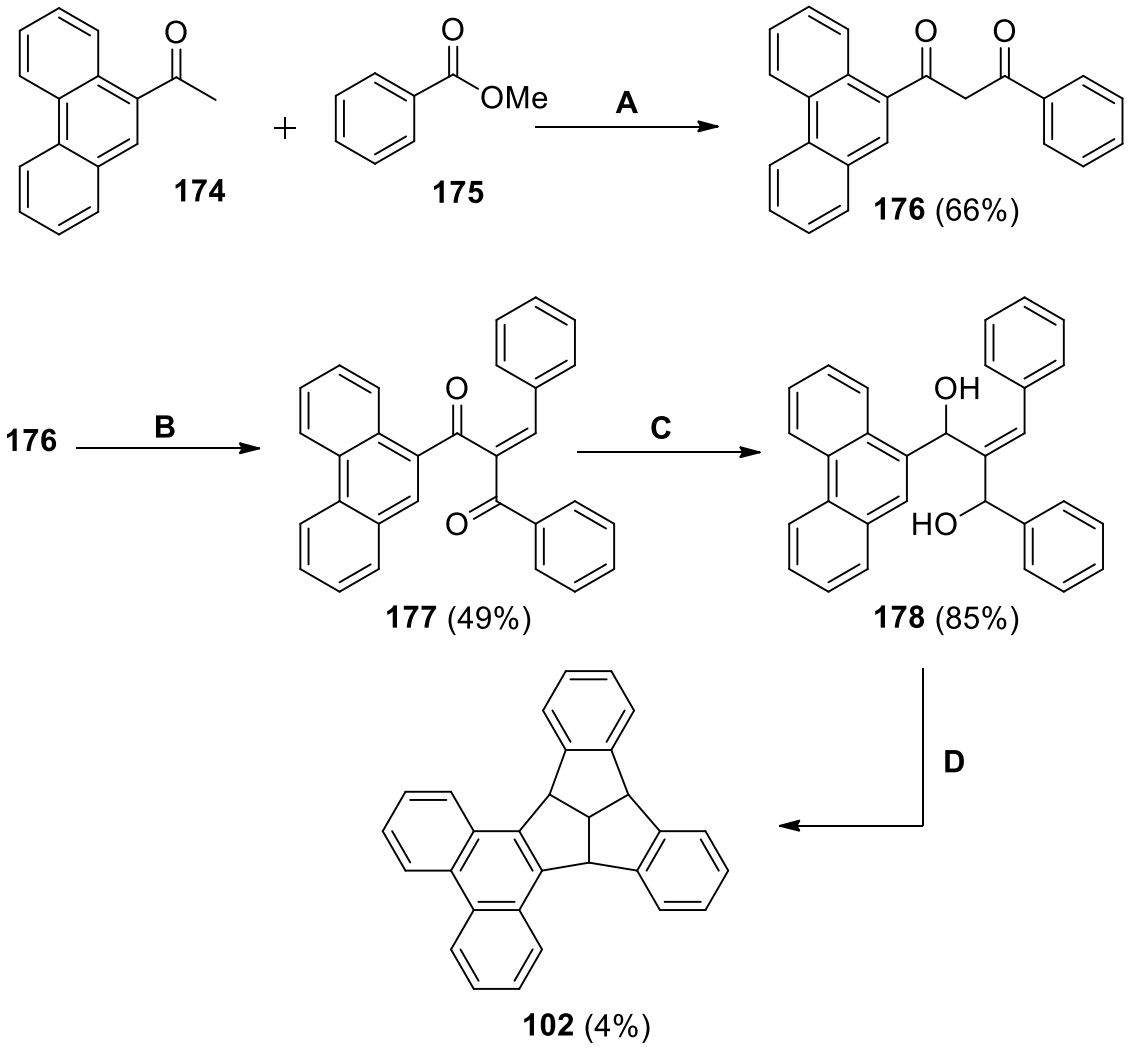

Figure 3.44 Synthesis of DBPTQ **102**.
A: NaH (60%), THF, 24 h; **B**: benzaldehyde, butanoic, acid, piperidine,toluene, 30 min; **C**: $CeCl_3 \cdot 7\ H_2O$, $NaBH_4$, CH_2Cl_2, MeOH, 3 h; **D**: polyphosphoric acid, chlorobenzene, 22 h.

In the next step, a more promising combined yield of 85% was achieved for the LUCHE reduction, which was followed by the cyclisation reaction with polyphosphoric acid. DBPTQ **102** was isolated in a yield of only 4%, despite a straightforward separation of the product from side-products via column chromatography. The reason for this poor yield is not known, but as no precursors were still present, a possible explanation is polymerisation reactions and potentially also influenced by poor solubilities of reaction intermediates and products.

Suitable crystals for x-ray crystallography were obtained after slow evaporation from toluene and CH_2Cl_2. The indane wings are roughly perpendicular to each other, as the three axes from the *centro* carbon atom C4b[1] to the midpoints of the C4c-C8a, C4a-C12c and C12a-C8c bonds (Figure 3.45 for atom numbering) are 86.1°, 90.1° and 89.9° (TBTQ **68**: 87.2°). The most significant bond angle deviation is for C4a-C4b-C4c: 116.75°, compared to 113.47° for TBTQ **68**. In addition, the bond angles C12c-C12b-C12a: 116.68°, C8a-C8b-C8c: 111.86° also deviate from this value. A comparison of bond lengths and angles of TBTQ **68** and TBTQ **102** can be found in Table 2.

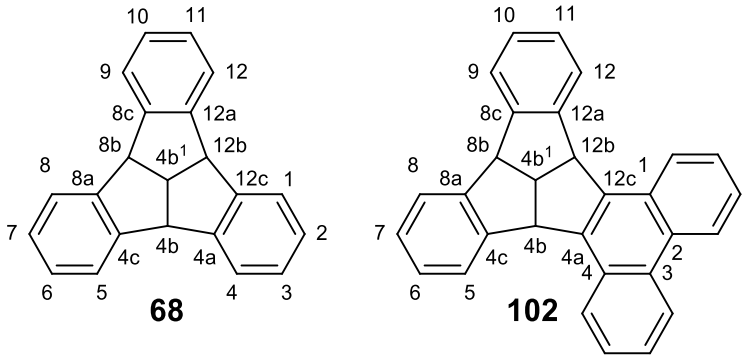

Figure 3.45 Atom numbering of TBTQ **68** and TBTQ **102**.

Despite this, the bond angles and bond lengths are broadly comparable, with exceptions due to the prescence of the phenanthrene moeity and the slight distortion caused as a result. This can for example be seen for the bond lengths C12c-C1: 1.439 Å and C4a-C4: 1.432 Å, which differ from the lengths for C4c-C5: 1.394 Å for DBPTQ **102** and 1.3956 Å for TBTQ **68**. The bowl depth of DBPTQ **102** is 3.0 Å, which is only marginally larger than the bowl depth of TBTQ **68**: 2.9 Å.

The stacking arrangement of DBPTQ **102** is unlike that of TBTQ **68,** where columnar stacks are formed, as showed in Figure 3.46. Neighbouring molecules of TBTQ **68** are alternately rotated by ±6° and all stacks point in the direction of the c axis. In contrast, DBPTQ **102** molecules align exactly one above the other in the stacks along the b axis, where the distance of the molecules in the stack corresponds to the b cell parameter. The molecular stacks are oriented to each other according to P21/n symmetry.

Table 2 Selected bond lengths, bond angles and torsional angles for DBPTQ **102** and TBTQ **68**. The values for TBTQ **68** are from data reported by KUCK *et al*.[200]

Bond	Bond length [Å]		Bond	Bond angle [°]	
	102	**68**		**102**	**68**
C4b^1-C4b	1.558	1.5593	C4b-C4b^1-C8b	107.82	107.30
C4b-C4c	1.528	1.5172	C4c-C4b-C4b^1	104.29	104.70
C4b-C4a	1.518	1.5140	C4b-C4c-C8a	113.13	111.52
C4c-C8a	1.392	1.3949	C4a-C4b-C4c	116.75	113.47
C4c-C5	1.394	1.3956	C4a-C4b-C4b^1	103.87	104.72
C5-C6	1.390	1.392	C6-C7-C8	119.97	120.29
C6-C7	1.388	1.391	C4c-C8a-C8b	111.98	111.72
C7-C8	1.390	1.3908	C4b-C4c-C5	129.34	128.30
C8-C8a	1.391	1.3958	C8-C8a-C8b	127.12	127.76
Bond	**Torsion angle [°]**		C4c-C5-C6	119.58	119.11
	102	**68**			
C4b-C4c-C5-C6	178.60	179.6	C7-C8-C8a	119.38	119.19
C4b^1-C4b-C4c-C5	177.52	179.5	C5-C6-C7	120.68	120.74
			C8a-C4c-C5	119.52	120.16
			C4c-C8a-C8	120.85	120.50

In Figure 3.46(b), viewing the stack along the c axis, it appears that the molecules are packed so that they overlap within a stack, but on changing the perspective to view along the b axis, it is clear that the TBTQ molecules coloured in red are shifted by one half of the unit cell along the c axis relative to the stacked TBTQ molecules coloured in grey.

SIEGEL and WU classified buckybowls according to their stacking arrangements: A) columnar convex-to-concave stacks with columns in a constant direction, B) columnar convex-to-concave stacks with neighbouring atoms in opposite directions and C) non-columnar structures.[280] Larger and deeper bowl-shaped aromatics favour stacking types A and B, due to strong π–π interactions, whereas smaller molecules more often belong to type C.[280]

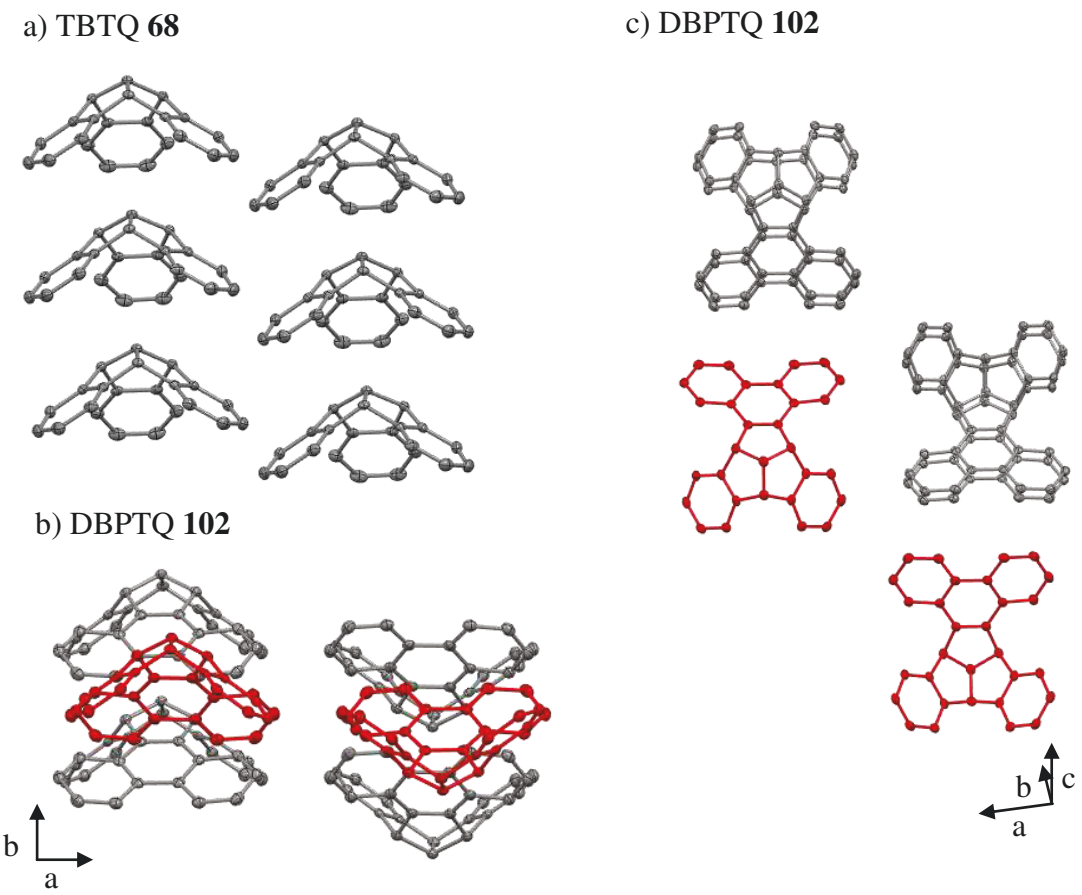

Figure 3.46 a) Molecular stacking of TBTQ **68** in the direction of the c axis, where neighbouring molecules are alternately rotated by ±6°. b) molecular stacking of DBPTQ **102** along the b axis; viewed along the c axis. c) the same stacking arrangement of DBPTQ **102** viewed almost paralell to the b axis. The molecules in grey are stacked directly underneath each other along b-axis, whereas the molecules in red are shifted by half a unit cell along the c-axis.

According to this classification, DBPTQ **102** belongs to type B, although this classification does not fully desribe the packing of this molecule. As seen in Figure 3.46c), the red TBTQ molecules in adjacent stacks to the grey molecules are oriented with the phenanthrene groups towards each other. A herringbone-like packing motif is observed (Figure 3.47), similar to a herringbone packing assigned to the arrangement of organic semi-conductors.[281] As the distance between phenanthrene groups within a stack is 4.5 Å (typical π–π interactions: 3.5–3.7 Å[282]) the packing arrangement is probably most similar to a herringbone packing without efficient face-to-face π–π overlap.[281]

Figure 3.47 Pictoral side-view representation of the herringbone-like arrangement of DBPTQ **102** molecules. The longer "arm" represents the phenanthrene group. The molecules in black are in the same row, whereas the grey molecules are in the row behind. This figure is not to scale.

As there is no direct overlap between phenenthrene groups of adjacent stacks, it is unlikely that π–π interactions dominate the stacking arrangement of DBPTQ **102**. C-H···π interactions could influence the relative arrangement of adjacent TBTQ stacks, as the distance between the nearest H atom of one phenanthrene group and the centre of an aromatic ring on an ajdacent phenanthrene group ranges from 3.34-3.85 Å. In conclusion, the packing of DBPTQ **102** is significantly altered to that of TBTQ **68**. A topic for further exploration is suitable functionalisation of TBTQ in order to control the crystal packing.

Once the identity of DBPTQ **102** was confirmed, the ^{1}H NMR spectrum was compared to those measured for cyclisation reaction with TBTQ **173** (see Figure 3.42). The comparison of these spectra can be seen below in Figure 3.48. Worthy of note is it that the peaks for DBPTQ **102** could not be found in the mixture of products isolated in the cyclistion of dialcohol **173**. Despite this, protons are visible between 4.5–6.0 ppm in the ^{1}H NMR spectrum of the unknown side-product, compared to bridgehead protons of DBPTQ **102**.

It can be concluded that the position of a bulky phenanthrene group is not trivial when planning the syntheses of phenanthrene-functionalised TBTQs. The KNOEVENAGEL reaction with the sterically hindered phenanthrene-9-carbaldehyde proceeded with a low yield: 23%, despite optimisation attempts. In contrast, the KNOEVENAGEL reaction with **166** and benzaldehyde proceeds with a 77% yield (Figure 3.40),[250] despite comprising of two phenanthrene groups. Multiple attempts to cyclise dialcohol **173** to afford DBPTQ **102** did not lead to the formation of the desired product, which suggests that the phenanthrene group hinders the cyclisation step. Further investigations are required to ascertain the exact influence of the position of the phenanthrene group in the cyclisation step.

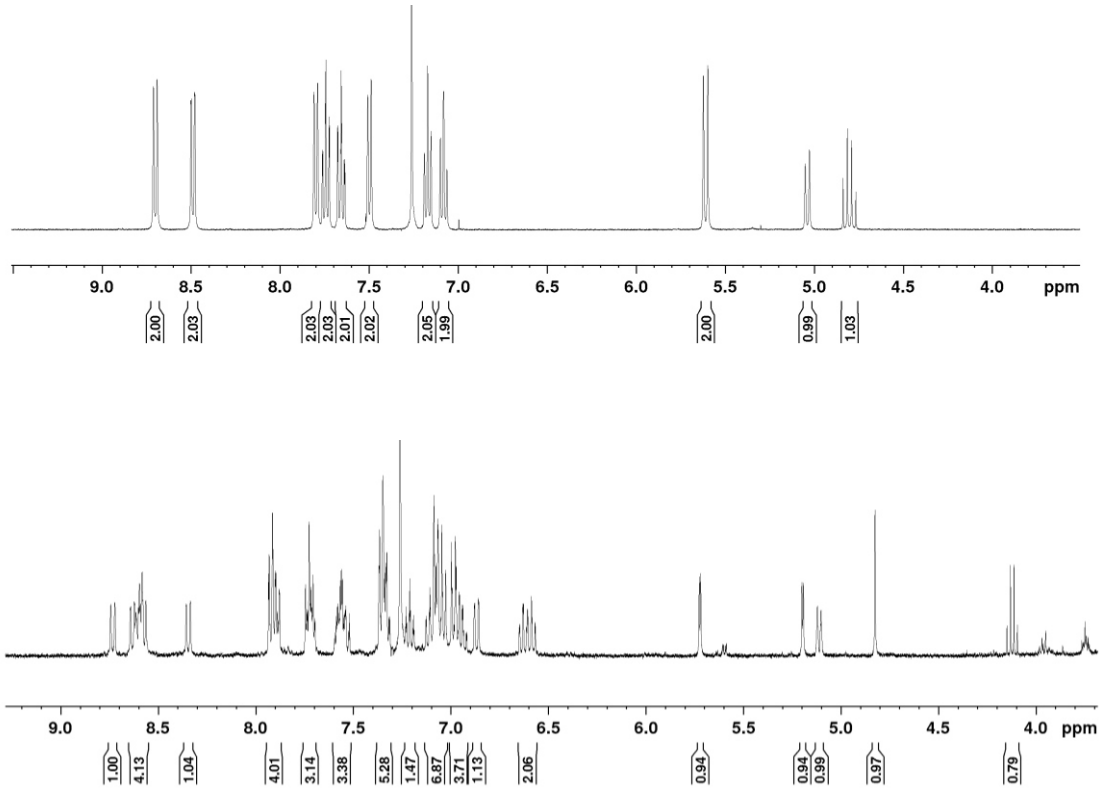

Figure 3.48 ^{1}H NMR spectra of DBPTQ **102** (above) and unknown reaction product of the reduction of dialcohol **173** (below).

As diol **173** did not yield DBPTQ **102** as the product, an alternative strategy is therefore required to achieve the synthesis of triphenanthrenotriquinacene **104**.

However, the synthsesis of DBPTQ **102** was achieved for the first time and is described above. In addition, the crystal structure of DBPTQ **102** reveals a significantly different packing arrangement to that of TBTQ **68**.

3.3.4 Alternative approach to phenanthrene group introduction: a simplified model system

A new strategy was devised, where a phenanthrene group would be introduced at the start of the synthesis, followed by the two phenanthrene groups introduced via a GRIGNARD reaction. In order to test this strategy, unsubstituted TBTQ **68** was chosen as a model system. An initial strategy is shown below in Figure 3.49. Aldehydes were chosen because they are reduced to alcohols during the GRIGNARD reaction, therefore an extra reduction step to attain a precursor suitable for triple cyclisation is not necessary. In addition, aldehydes react more readily with GRIGNARD reagents when compared to esters.

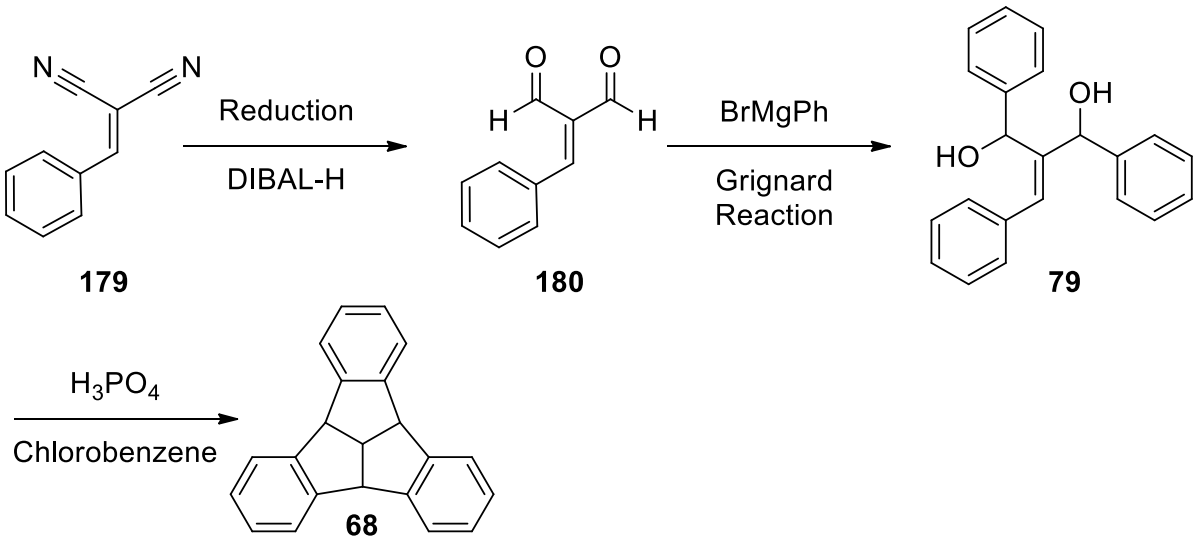

Figure 3.49 Proposed synthesis strategy for TBTQ **68**.

The reduction of nitriles to aldehydes with diisobutylaluminium hydride (DIBAL-H) to form imines is well known.[295] It was quickly decided that nitrile **179** was not a suitable precursor, as using more than one equivalent of DIBAL-H in the reaction, which would be necessary to reduce two nitrile groups, can lead to the formation of an amine instead of an aldehyde.[297] Several examples in the literature use 1.2 eq. of DIBAL-H for the reduction of one nitrile group.[296,298,299]

It is therefore difficult to choose an appropiate amount of DIBAL-H, as once partial reduction takes place (i.e. one nitrile group is reduced), the more reactive imine group would be reduced further, instead of the second nitrile group. In order to combat this problem, an alternative precursor was proposed, utilising an aldehyde protecting group so that only one nitrile group can be reduced. Subsequent deprotection would yield two aldehyde groups. As the literature protocol from DONG *et al.* indicates that 1.2 eq. DIBAL-H is sufficient for the conversion to the aldehyde,[296] this amount was chosen for the conversion. As the reported yields range between 23–67%, it is unknown whether this is due to purification issues or if the conversion was not complete.

The first two steps of this reaction are literature-known and were reported by ELLIOTT and coworkers.[304] After 5 d the conversion of benzaldehyde (**78**) to nitrile **181** was not complete according to TLC analysis but was worked up in order to determine if the desired product had been formed. In the publication, two protocols are described: either pure **181** was isolated via distillation before hydrolysis with hydrochloric acid or the raw product was directly reacted with the acid to afford nitrile **182**. On adding ethyl acetate to the raw product of nitrile **181** for

extraction, a solid precipitated out of solution, which was directly hydrolysed with hydrochloric acid. The achieved yield was 48% (based on **78**), which is due to the incomplete conversion of benzaldehyde (**78**) to methoxynitrile **181**. The protection procedure was an adaptation of the protocol from DANISHEFSKY and gave an excellent yield of 90%.[305]

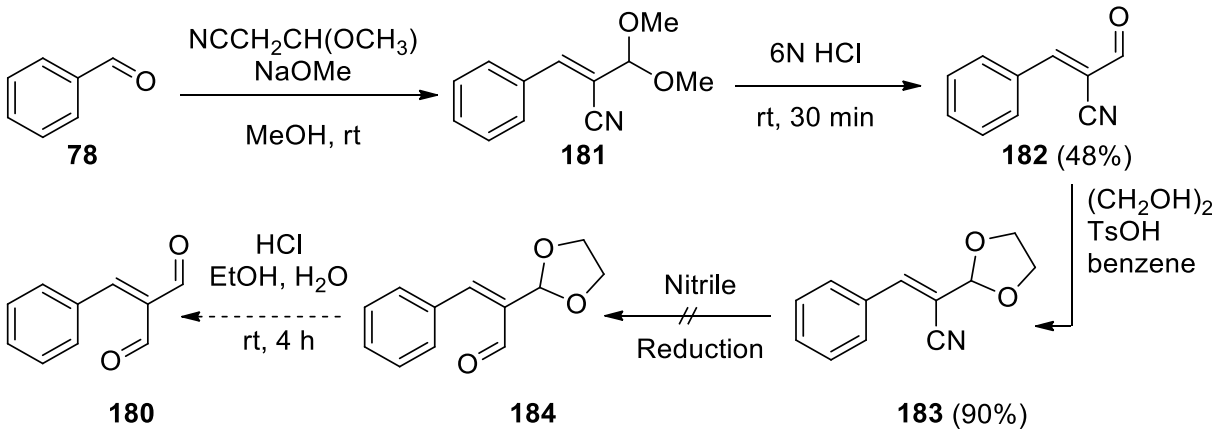

Figure 3.50 Synthesis strategy for aldehyde **180**.

The reduction with 1.2 eq. DIBAL-H was however not successful. The reaction was stopped after TLC reaction control confirmed that the starting material was no longer present, but the ^{1}H NMR spectrum showed no well-defined peaks, apart from solvent and other impurities.

In order to ascertain the quality and concentration of DIBAL-H, a volumetric analysis approach was used. The first method was titration with pyridine or isoquinoline.[300-302] Dialkylaluminium hydrides are able to form 2:1 and 1:1 complexes with certain nitrogen compounds. The 1:1 complex turns the solution yellow, which is visible until the red 2:1 complex is formed. On addition of further dialkyaluminum hydride, the red colour disappears again and the more stable 1:1 complex is formed. The second method from HOYE *et al.* involves reacting the DIBAL-H with *p*-methoxybenzaldehyde and quenching with acetic acid.[303] From the No-D NMR spectrum it is possible to deduce the concentration of the hydride species from the percentage conversion of aldehyde to alcohol, which can be found from the relative peak integrals. Both methods confirmed that the current commercial reagent was as reactive as the fresh commercial batch, which indicates that this is not responsible for the reaction not taking place.

There is potential to continue these investigations, for example by choosing an alternative nitrile reduction strategy such as STEPHEN aldehyde synthesis[306] with $SnCl_2$, however the yields for aliphatic nitriles are often moderate to poor.[307] FRY reported a milder protocol, in

which nitriles are alkylated to form electron-deficient *N*-alkylnitrilium ions, which can be reduced with triethylsilane.[308] A more recent method employs 1,1,3,3-tetramethyldisiloxane (TMDS) and triisopropoxyvanadium(V) oxide, as reported by LEMAIRE *et al.*[309] However, the results from Section 3.3.3, suggest that the positioning of the phenanthrene group could hinder a successful cyclisation reaction. Another possibility is exploring the formation of phenanthrene groups after cyclisation, based on the acid-catalysed bisannulation of 1,4-benzenediacetaldehyde from ITAMI and coworkers.[310] However, the bulky phenanthrene groups could hinder SCHOLL reactions due to their rigidity.

In the next section, the synthesis and subsequent SCHOLL reaction of benzodiphenanthrenotriquinacene are explored.

3.3.5 Synthesis of benzodiphenanthrenotriquinacene (BDPTQ, 103)

In order to continue investigations into the Scholl reaction of BDPTQ **103,** the synthesis pathway developed by KIRCHWEHM was used,[250] Suitably functionalised phenanthrenes were required in order to follow the HOPF triple cyclisation strategy for TBTQ **68** synthesis (see Figure 1.26 on page 24).[200] For both starting materials, 9-cyanophenanthrene (**186**) was required, which although commercially available, was synthesised on a larger scale from 9-bromophenanthrene (**185**) using two different methods for the ROSENMUND-VON BRAUN reaction.[283,284]

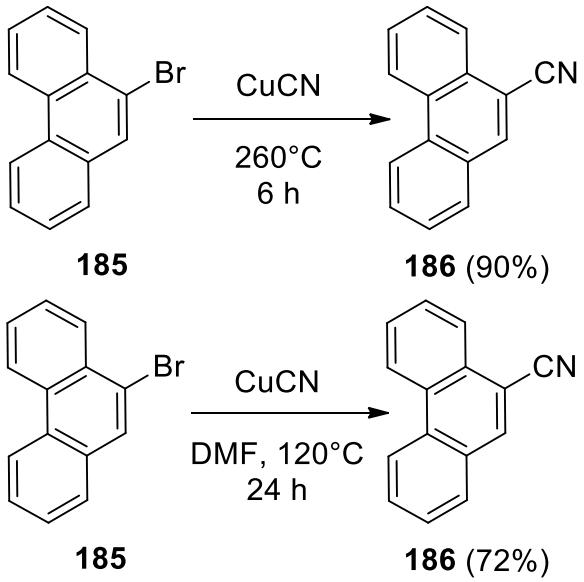

Figure 3.51 Synthesis of 9-cyanophenanthrene (**186**).[285,286]

The first protocol is a solvent free reaction, published by CALLEN *et al.*,[285] which is based on the protocol from VON BRAUN.[284] With 90%, a small improvement on the literature yield of

87% was achieved, although the purification procedure was time consuming due to the formation of a poorly soluble dark brown solid on reaching room temperature at the end of the reaction. This solid was a mixture of product and copper bromide, which was purified via extraction with CH_2Cl_2 in a SOXHLET apparatus, followed by column filtration and recrystallisation to remove discolouration.

An alternative protocol was tested, with a view to a more efficient work-up and isolation. This approach employed *N*,*N*-dimethylformamide (DMF) as the solvent and an excess of CuCN (2.06 eq.), which was adapted from the method of BOCK and coworkers.[286] Extraction of the reaction mixture and column chromatography yielded the desired product as a pale yellow solid. The yield of 72% is lower than that of the solvent free approach, but the isolation of the product is significantly less time-consuming. Overall, both protocols proved to be reproducible on a multigram scale.

The conversion of 9-cyanophenanthrene (**186**) to carboxylic acid **187** was achieved in 91% yield, which was an improvement on the 86% yield reported by NIKOLAITCHIK *et al.*[287] Column chromatography was used instead of recrystallisation to isolate the pure product, as reported by KIRCHWEHM.[250] The subsequent esterification, with a 85% yield was also satisfactory.

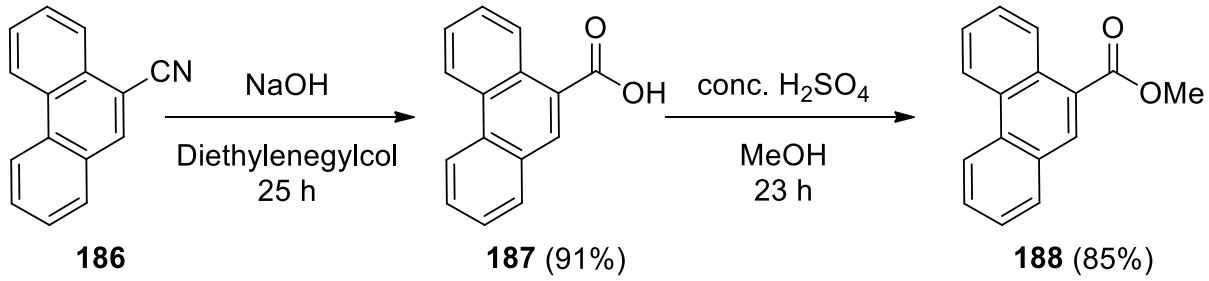

Figure 3.52 Synthesis of ester **188**.[250,287]

Ketone **189** was also required for the subsequent CLAISEN condensation, which was synthesised using a GRIGNARD reaction, using KIRCHWEHM's optimised conditions of the BACHMANN and BOATNER protocol.[250,288]

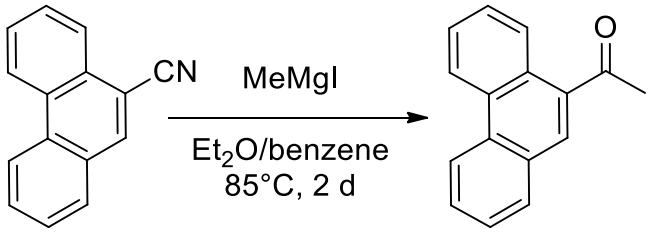

Figure 3.53 Synthesis of ketone **189**.[250]

The synthesis of BDPTQ **103** was achieved, following the pathway of KIRCHWEHM, of which the triple cyclisation is the key step (see Figure 3.54).[250] The first step is a CLAISEN condensation reaction, followed by a base catalysed KNOEVENAGEL condensation. Reduction with $LiAlH_4$ to give alcohol **190** is followed by cyclisation.

The final step was very low yielding, due to the presence of many side products, which were hardly separable using TLC. Achieving a good separation of the product was particularly challenging, as a substantial amount of a polar solvent such as CH_2Cl_2 was needed to dissolve the product, which in turn led to mixed fractions. Reverse phase separation was not possible, as the product did not dissolve in acetonitrile, methanol, tetrahydrofuran (THF) or water. Recrystallisation from hot toluene was possible, but the precipitate was formed of very fine needles, which formed a paper-like film. Many attempts to obtain suitable crystals for x-ray analysis were carried out without success.

KIRCHWEHM chose the SCHOLL reaction to bridge the bay region, using $FeCl_3$ as the LEWIS acid and oxidant, and isolated a mixture of the starting material and a side-product. Due to due the presence of a methyl group at 3.06 ppm in the ^1H NMR spectrum and a peak of the mixture at m/z = 510 (MALDI-TOF), TBTQ **171** was presumed to be the side-product (see Figure 3.40).[250]

In the literature, chlorination is a common side-reaction when using oxidants such as $FeCl_3$ for the SCHOLL reaction,[87,93,289,291] therefore it is possible to reason that the reactive bridgehead position between the phenanthrene groups of TBTQ **146** was chlorinated during the reaction, substituted for a methoxy group on addition of MeOH to end the reaction resulting in the product TBTQ **171**. The mass of TBTQ **103** m/z = 480, and by substituting a hydrogen atom for a methoxy group (m/z = 31), the mass of TBTQ **171** is reached (m/z = 510).

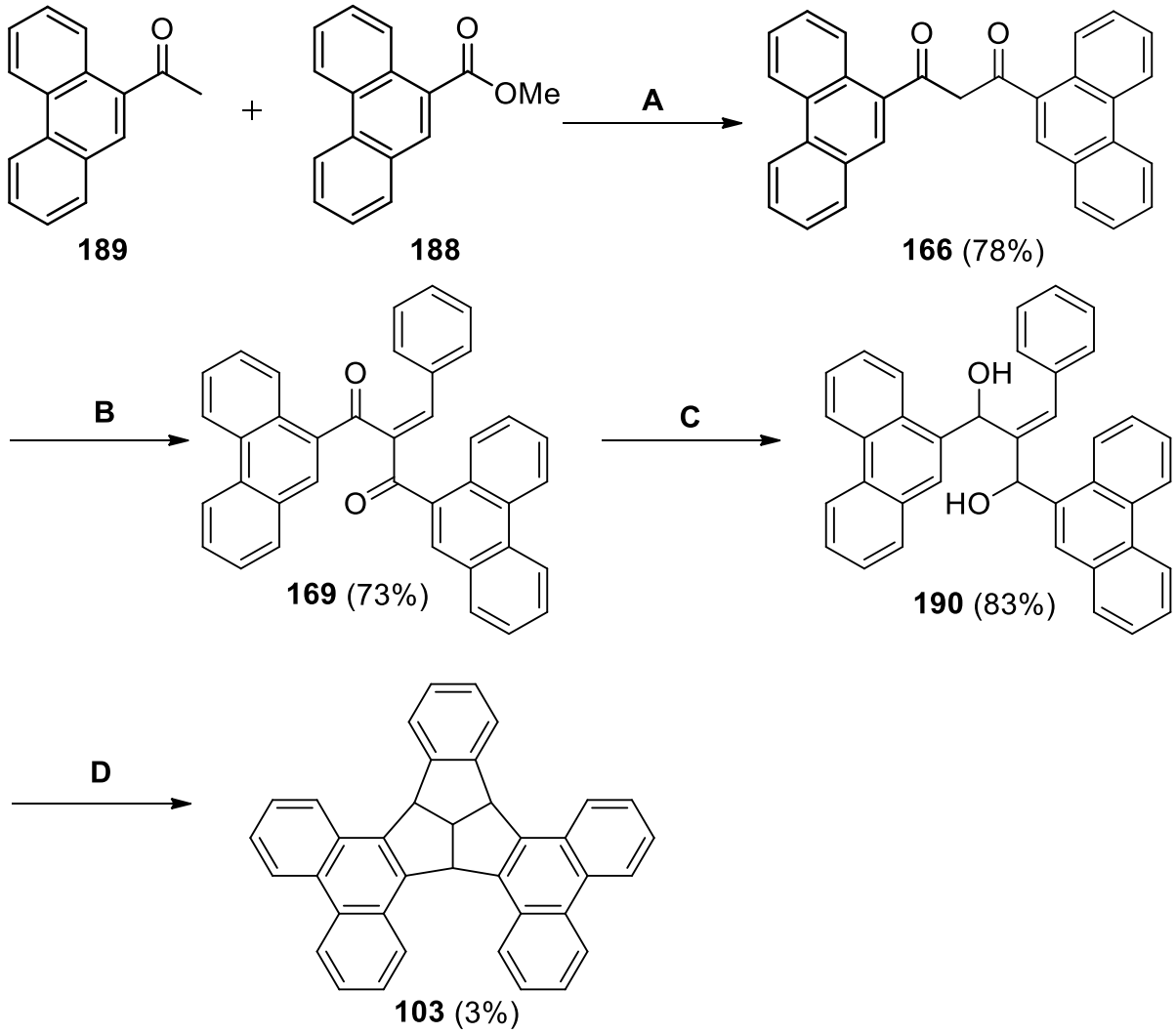

Figure 3.54 Synthesis of BDPTQ **103** according to the pathway of KIRCHWEHM.[250]
A: NaH (60%), THF, 24 h; **B**: 9-phenanthrenocarboxaldehyde, butanoic acid, piperidine, toluene, 30 min; **C**: $CeCl_3 \cdot 7\ H_2O$, $NaBH_4$, CH_2Cl_2, MeOH, 3 h; **D**: polyphosphoric acid, chlorobenzene, 24 h

KIRCHWEHM noted that a greater excess of the oxidant $FeCl_3$ than 4.4 eq. would be required for a complete transformation. Therefore 6 eq. were used and the disappearance of the starting material TBTQ **103** via TLC analysis was observed. After purification, the identity of TBTQ **171** was confirmed but could only be isolated in a yield of 14%. This experiment was repeated in the dark, in order to investigate if the exclusion of light prevents a radical chlorination taking place. After 2 h, starting material could no longer be detected and TBTQ **171** was the only isolated product. The large of excess of $FeCl_3$ is responsible for the initial chlorination, so a different oxidant was required, one which was not able to chlorinate molecules.

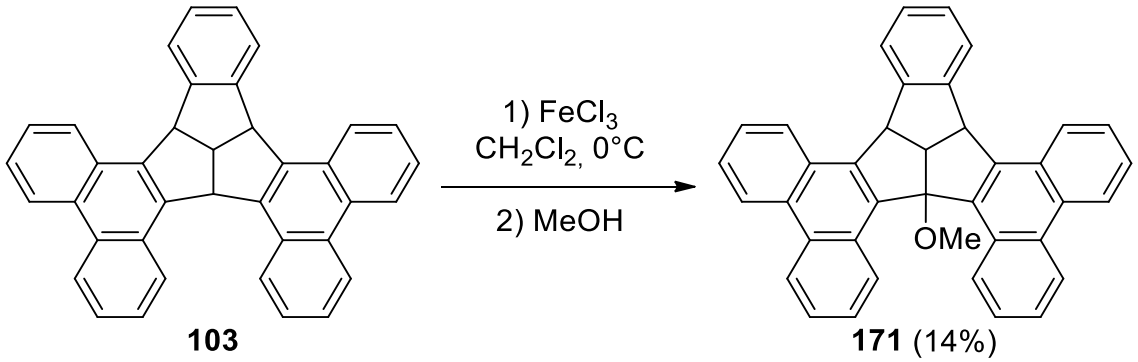

Figure 3.55 Formation of TBTQ **171**.

An alternative oxidant was also employed: with DDQ a large excess of oxidant is not necessary and chlorinated products are not observed. RATHORE *et al*. suggest that only 1 eq. of DDQ per C-C bond formation is required.[291] For the reaction of DDQ with TBTQ **103**, 1.46 eq. DDQ were used, as for more challenging transformations RATHORE increased the amount of DDQ to 1.5 eq.[291] After 30 min the reaction was complete and after analysis with normal phase (NP)-HPLC, the most defined fraction contained peaks in the aromatic region. However, the total number of protons did not match with the desired product, and although the sample also contained impurities, the amount (1 mg) prevented further purification.

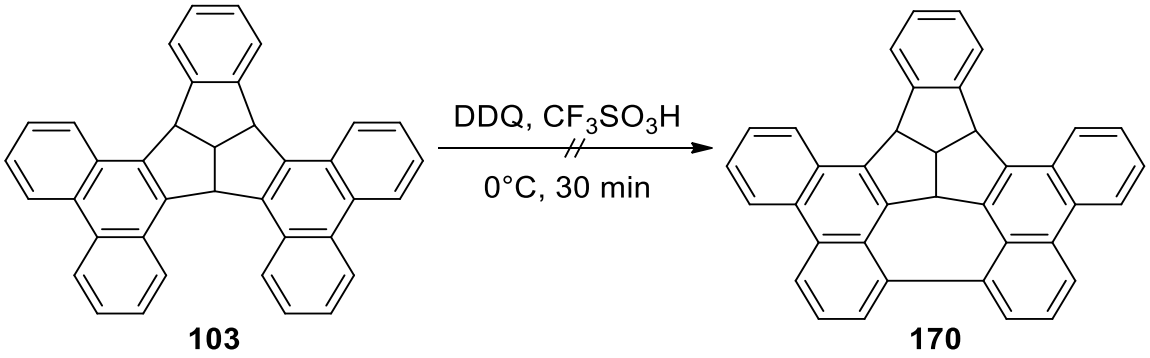

Figure 3.56 Attempted synthesis of TBTQ **170** with DDQ.

Finally, an alternative reaction to the SCHOLL reaction was tested, more specifically an oxidative coupling reaction featuring hypervalent iodine reagents from KITA *et al*.[293,294] Literature examples describe the successful oxidative coupling of phenol ether derivatives, for example the formation of a seven-membered ring in annulene derivative **192**,[293] in addition to the coupling of less electron rich and sterically hindered alkylarenes.[294]

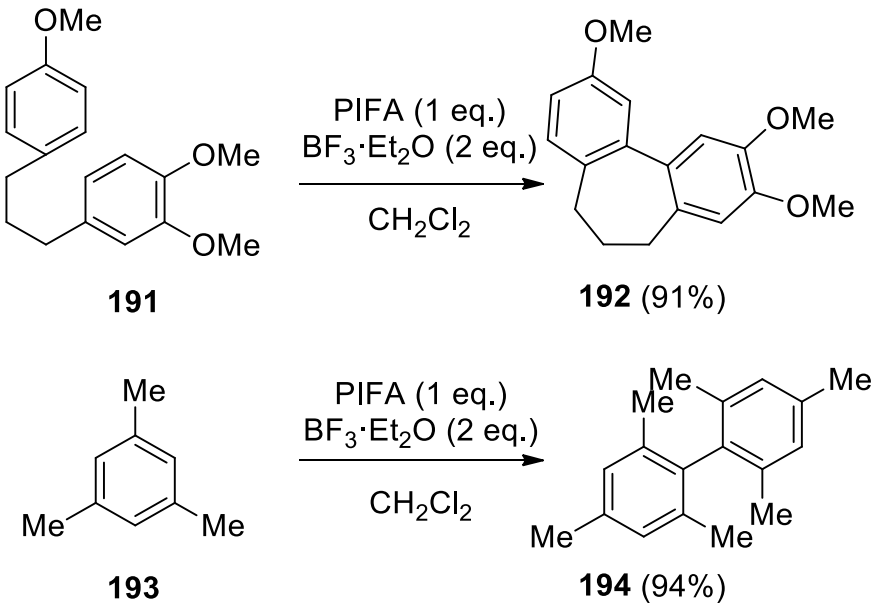

Figure 3.57 Literature examples of oxidative coupling from KITA *et al.*[293,294]

Using the protocol from KITA's oxidative coupling of phenol ether derivatives for the reaction with TBTQ **103**, no conversion could be detected after 3 h. A sample of the reaction (0.1 ml) was removed, extracted and dried. The ^{1}H NMR spectrum of this sample indicated that only the starting material TBTQ **103** was present. After a further 1 h, PIFA / $BF_3 \cdot Et_2O$ were added again. Reaction control at regular intervals could not detect a change and after 24 h the reaction was allowed to cool slowly to room temperature.

Additional peaks in the aromatic region of the ^{1}H NMR spectrum of the raw product were visible in the aromatic region, but they were numerous and overlapping that integration of individual peaks was not possible. After column chromatography, 37% of the starting material was re-isolated. The column was washed with CH_2Cl_2 and analysis of this fraction (a viscous yellow oil) was not promising, as the ^{1}H NMR spectrum showed many small, overlapping peaks in the aromatic region. As none of the product peaks were identified, this fraction was discarded. Comparing the retention time of this fraction to TBTQ **103** using NP-HPLC also confirmed that no starting material was present.

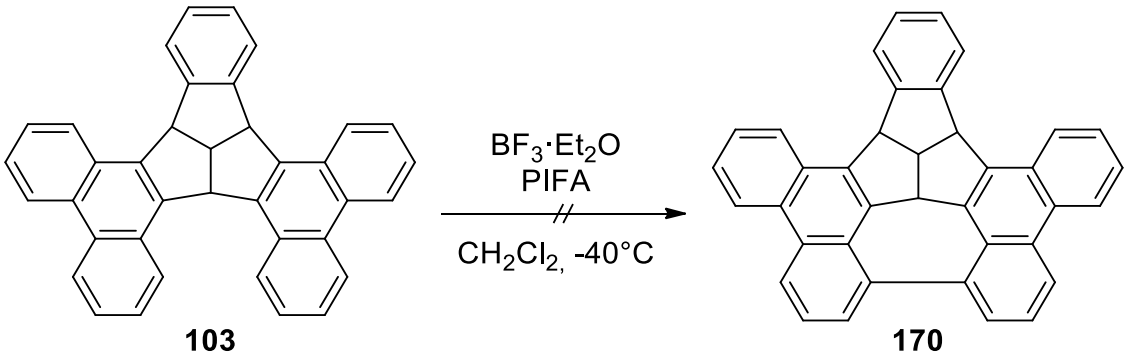

Figure 3.58 Attempted synthesis of TBTQ **170** with PIFA / $BF_3 \cdot Et_2O$.

Many other protocols for the SCHOLL reaction exist, which could be attempted with this system. The low yielding final step for the synthesis of TBTQ **103** restricts its large-scale synthesis. In addition, the formation of methoxy functionalised TBTQ **171** during the SCHOLL reaction with $FeCl_3$, as a result of chlorination at the bridgehead position, demonstrates that side-reactions compete with the desired transformation.

Without a crystal structure of TBTQ **103**, the exact distance between the phenanthrene groups is not known, as these moieties might be spatially too far away for the C-C coupling reaction to take place. Synthesis of methoxy functionalised or *tert*-butyl functionalised phenanthrenes would be useful, as these groups can be used to control the SCHOLL reaction.[83]

3.3.6 Methoxy functionalised phenanthrenes

In order to favour the SCHOLL reaction, functional groups can be introduced. KING and co-workers explored this topic for $MoCl_5$ and PIFA / $BF_3 \cdot Et_2O$, and reported that methoxy groups represent activating *ortho*/*para* directors and *tert*-butyl groups prevent oligomerisation.[83] *tert*-butyl groups are also known to increase the solubility, which is also advantageous.

More specifically, KING *et al*. demonstrated that the SCHOLL reaction is most effective in the terphenyl case when a new bond is formed *para* to two methoxy groups (see Figure 3.59 below), one on each side of the nascent bond.[74] This is the ideal case, but alternatively the methoxy groups can be positioned *para* and *ortho* to the site of the new C-C bond (Figure 3.59).

New bonds formed *ortho* to two methoxy groups led to the formation of a dimer of the starting compound, due to the ability of the molecules to rotate. Bonds are not formed *meta* to a methoxy group (Figure 3.60). MÜLLEN *et al.* also reported that the SCHOLL reaction methoxy groups *meta* to the coupling site led to a rearrangement and the formation of a

spirocyclic side-product.[94] For *tert*-butyl groups, the electronic effect on the formation of the new bond is negligible as the mildly *ortho*- and *para*-directing *tert*-butyl groups are placed *meta* to the new bonds.[83]

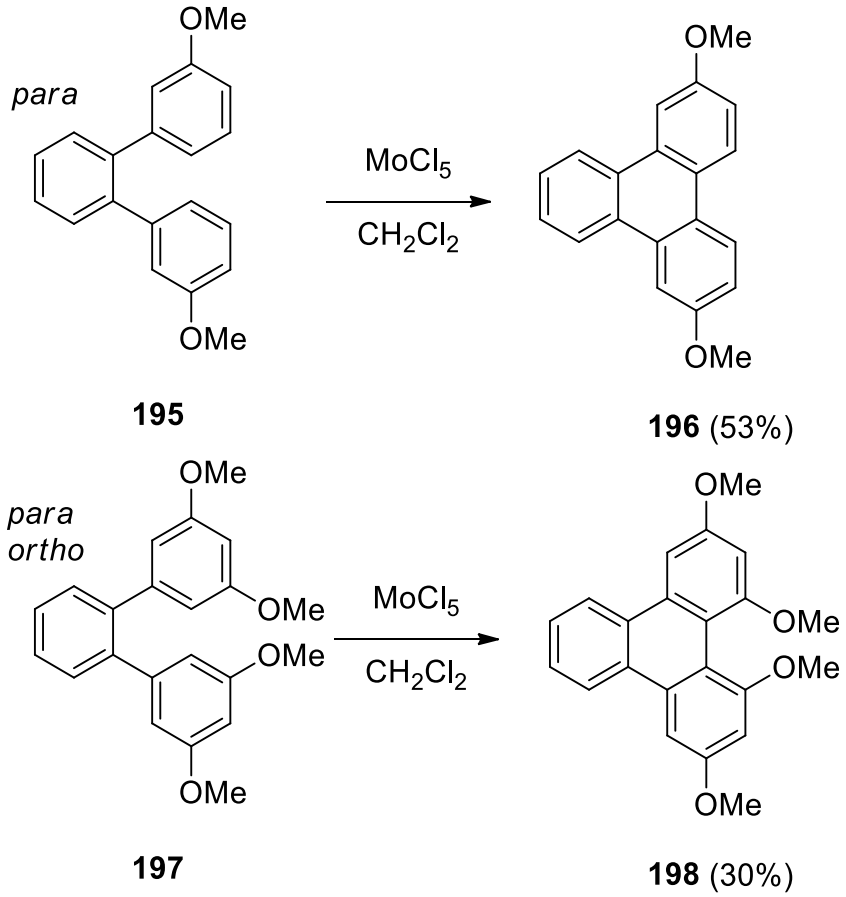

Figure 3.59 SCHOLL experiments from King *et al.*[83] Successful reactions take place in the case of methoxy groups positioned *para* (terphenylene **196**) and *ortho* and *para* (terphenylene **198**) to the nascent bond.

The success of the SCHOLL reaction also depends on the reagent system used, for example RATHORE and coworkers were able to achieve better yields than KING *et al*. with a DDQ / $MeSO_3H$ system for one *ortho* and one *para* methoxy group relative to the nascent bond (see Figure 3.61).[93] In addition, they also reported the successful aryl-aryl coupling between two *ortho*-positioned methoxy groups, with methyl groups in the *para* position and in the prescence of *meta*-methoxy groups, as shown below for the formation of biphenyl **205** in Figure 3.61.

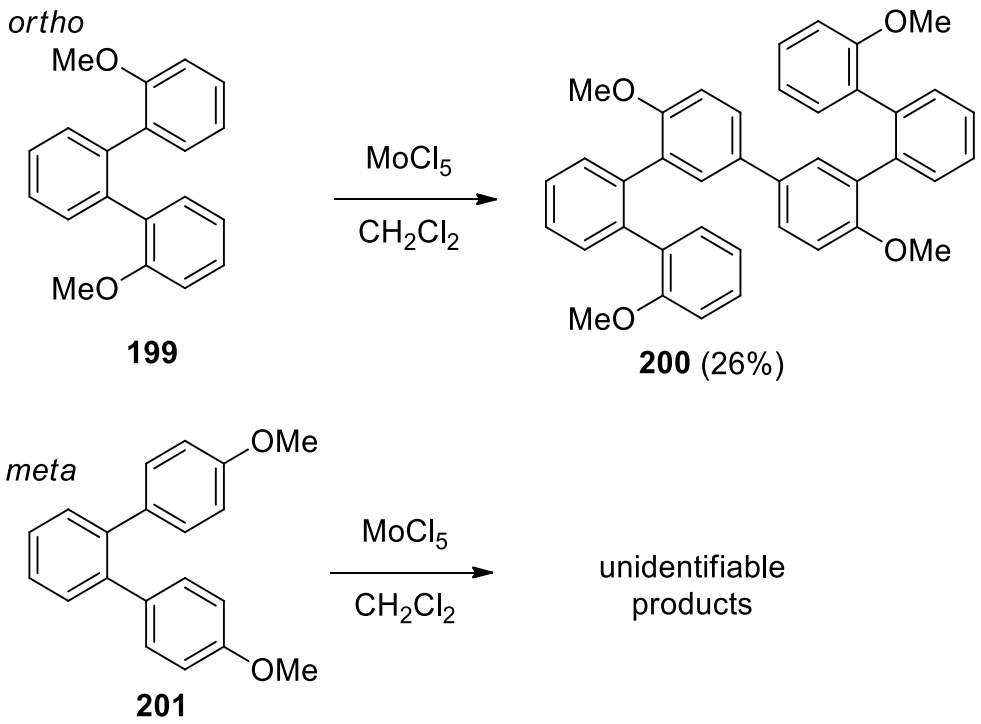

Figure 3.60 SCHOLL experiments from King *et al.*[83] Methoxy groups in the *ortho*-position led to dimer **200** and for the case of meta functionalised terphenyl **201**, no defined products could be isolated.

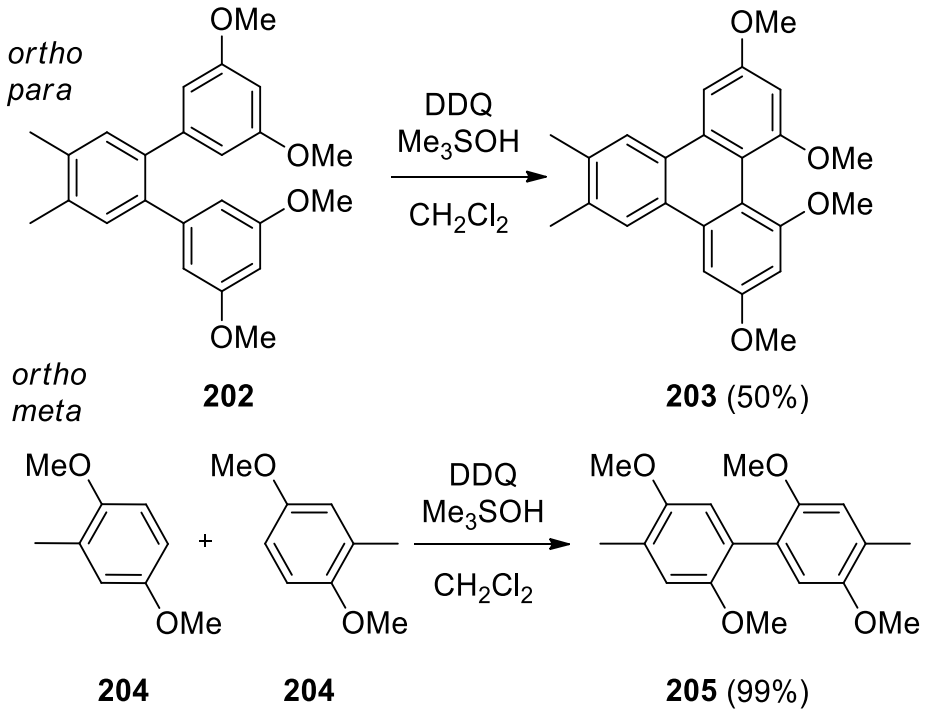

Figure 3.61 Literature examples of aryl coupling with DDQ by RATHORE *et al.*[93]

In the light of these findings, four TBTQ structures were proposed, which would favour the SCHOLL reaction, shown in in Figure 3.62 below.

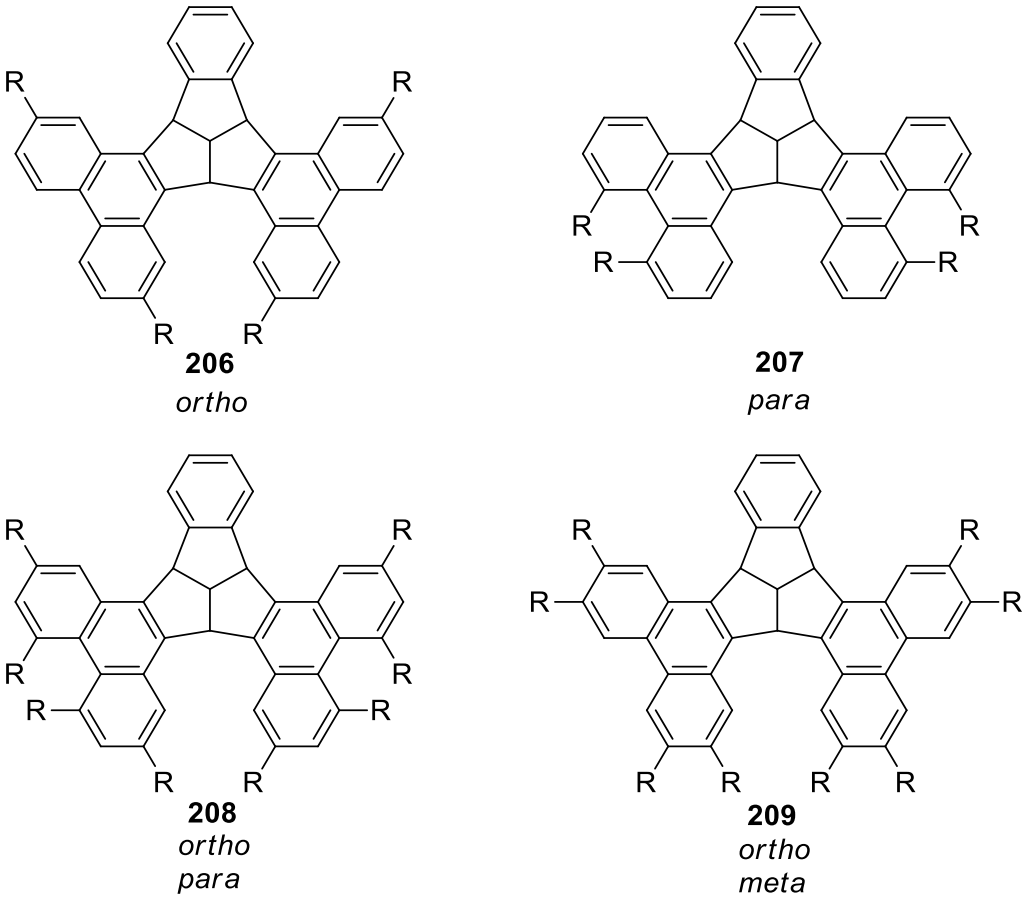

Figure 3.62 Proposed synthetic aims TBTQs **206**–**209**. R: OMe.

For TBTQs **206** and **207**, suitably functionalised phenanthrene precursors were required. Synthesising such phenanthrenes from stilbenes with either two *para* or two *ortho* methoxy groups to the nascent bond is however problematic, as the key step is a photoreaction, which according to the results of DYKER yields a mixture of three isomers (see Figure 3.63).[311] The lowest yield was reported for phenanthrene **211a**, due to the close proximity of the methoxy-groups to each other and induced steric strain.

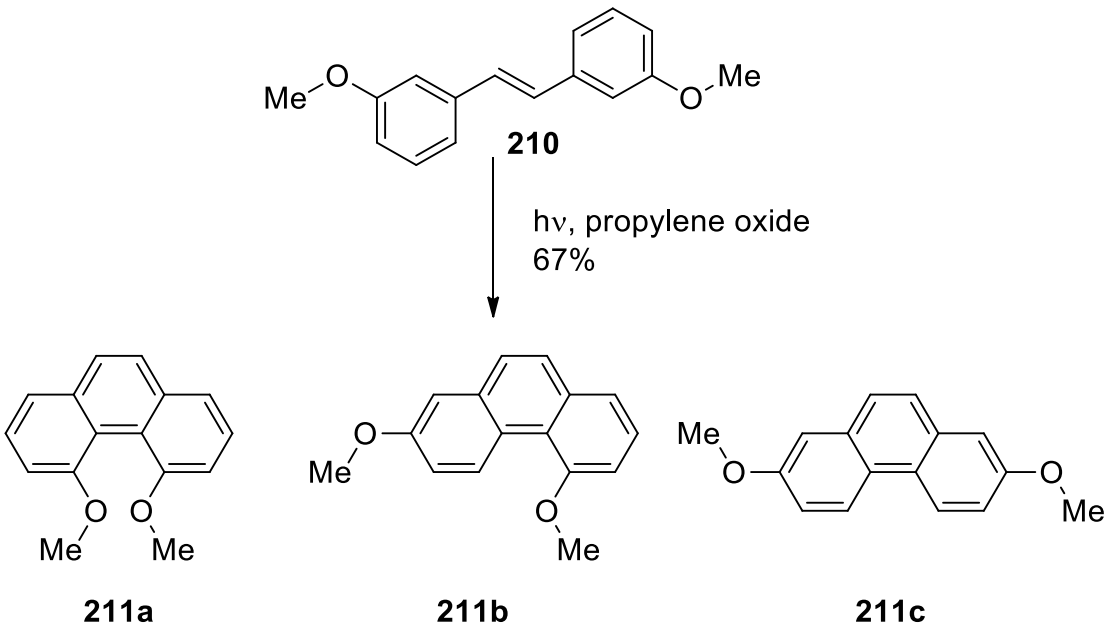

Figure 3.63 Literature known synthesis of phenanthrene isomers **211a-c**.[311] The predicted ratio of isomers is a:b:c = 1:2:1; observed isomer ratio: a:b:c = 1:4:2.

Preventing such a mixture of isomers can only be achieved by using a blocking group such as chlorine to prevent certain cyclisation pathways,[312] but this would add extra steps to the pathway, as the chlorine atom would need to be removed after the photoreaction by reduction with $LiAlH_4$ and $NiCl_2$.

Synthesis of the phenanthrenes with multiple methoxy groups can alternatively be achieved by a SCHOLL reaction from the stilbene precursors, however at least three methoxy groups are essential in order for the reaction to take place[313] (an example with LEWIS acid $FeCl_3$ and oxidant MCPBA is shown below in Figure 3.64). Therefore it is not possible to synthesise the phenanthrene precursors for TBTQs **206** and **207** via the SCHOLL reaction, as only two methoxy groups are present in the stilbene. The focus therefore shifted towards strategies for synthesising TBTQs **208** and **209**.

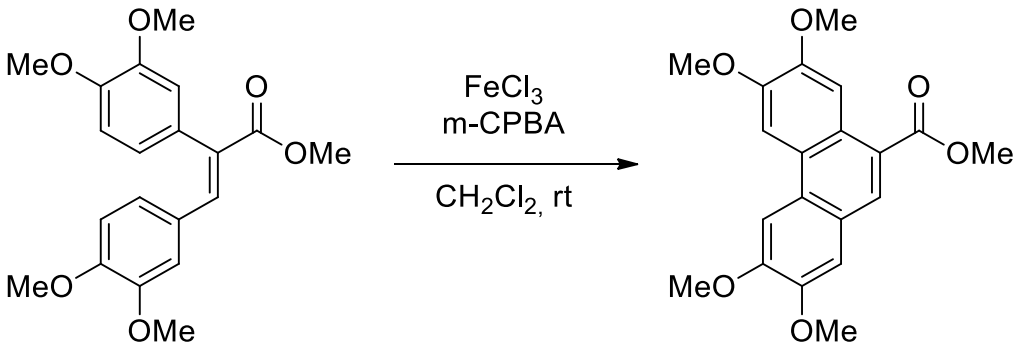

212 **213** (99%)

Figure 3.64 Synthesis of phenanthrene **213** by WANG *et al.*[313]

The desired phenanthrene starting materials **214** and **215** for the synthesis of TBTQ **209** are unknown, but similar molecules have been reported in the literature (see Figure 3.65 below). The first example is the ethoxy phenanthrene **216**, which was synthesised by WALDVOGEL and coworkers from an aryl-substituted phosphonoacetate and a substituted aldehyde in a base catalysed reaction.[314] This new stereoselective route offers 85–90:15–10 *E*:*Z* ratios for the stilbene precursors, whereas the more traditional PERKIN condensation leads to the formation of almost exclusively the *Z* stilbene isomer. The *E* isomer is required for bond formation to form the phenanthrene, which in this example is formed via an oxidative coupling with $MoCl_5$ and $TiCl_4$ in CH_2Cl_2. However, the phosphono acetate precursors can only be produced via a four step synthesis, so adapting this approach was disregarded, as it would increase the overall length of the pathway significantly.[315]

Phenanthrene **217** was synthesised using the PERKIN condensation, followed by an oxidative coupling with $FeCl_3$.[316] Although the methoxy groups are not positioned exactly in the desired positions in phenanthrene **217** (compare to phenanthenrene **213**), the synthesis could be adapted with suitably functionalised starting materials. The only uncertainty lies in the success of the SCHOLL reaction with such stilbene precursors to form the desired phenanthrenes.

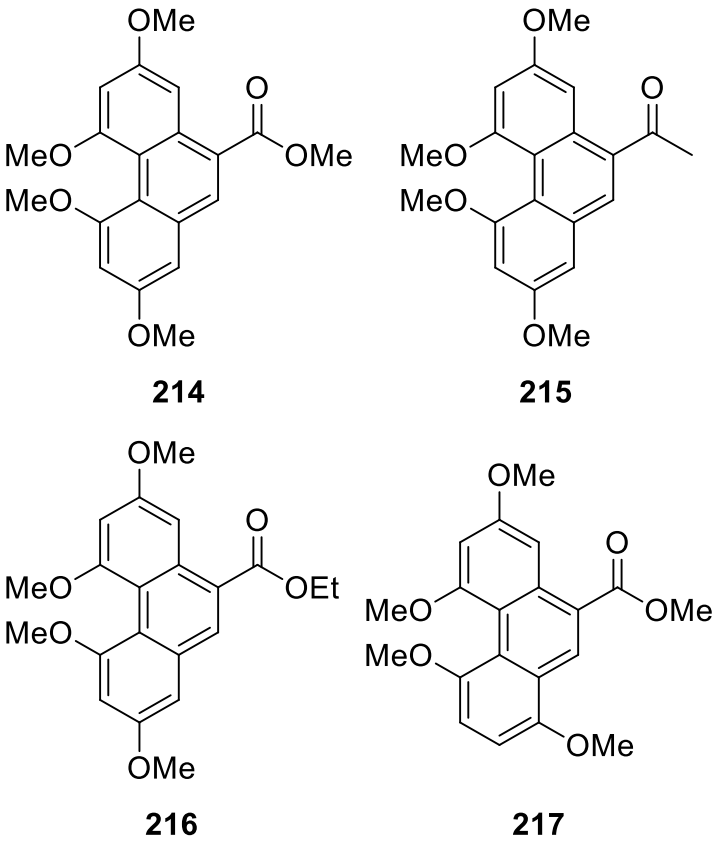

Figure 3.65 Desired phenanthrenes **214** and **215** and literature known phenanthrenes **216** and **217**.

To investigate the *ortho*-direction of methoxy groups, which is less well explored than for methoxy groups in the *para*-position, the synthetic aim TBTQ **209** was decided upon. KING and coworkers hypothesised that the formation of a dimer in the case of *ortho*-positioned methoxy groups, as shown in Figure 3.60, is due to rotation of the flexible starting materials. In TBTQ **209**, the phenanthrene groups are rigid and not able to rotate as the terphenyls could, therefore reducing the risk of dimer formation. *Meta* methoxy groups are also present in TBTQ **209**, which is dictated by the requirement of at least three methoxy groups in the stilbene precursors for the successful conversion via the SCHOLL reaction to form the desired phenanthrenes, from the stilbenes.[313] In addition, there are many examples in the literature for the synthesis of 2,3,6,7-tetramethoxyphenanthrenes.[313,317-319]

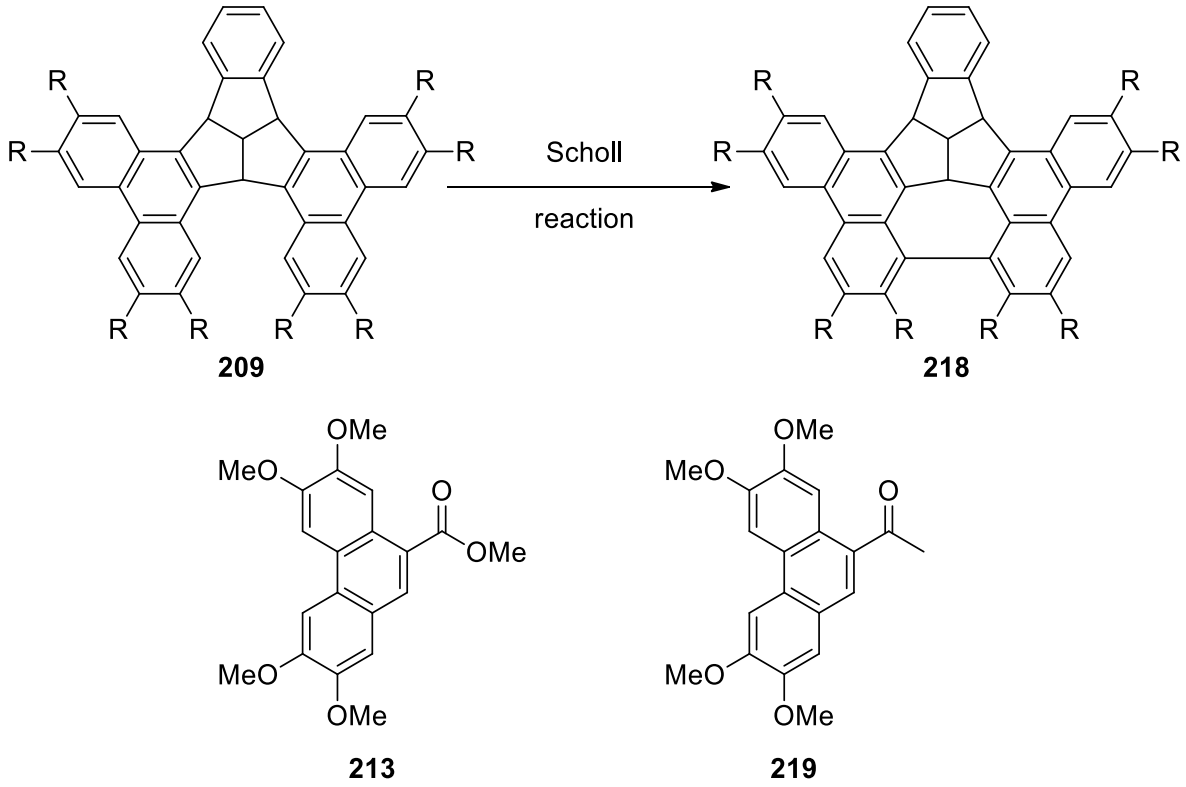

Figure 3.66 Proposed synthesis of TBTQ **218** and phenanthrene precursors **213** and **219**. R: OMe. The methoxy groups in TBTQ **209** are positioned *ortho* and *meta* to the nascent bond.

Syntheses of the phenanthrene starting materials were carried out successfully according to literature procedures. Starting with a PERKIN condensation, the formation of stilbene **222** was achieved with a 61% yield, which is comparable to the reported yield of 68%.[320] For the preparation of the methyl ketone **219**, acrylic acid **222** was treated with methyllithium (MeLi) in THF and the subsequent SCHOLL reaction with $FeCl_3$ led to the formation of the desired phenanthrene **219** (Figure 3.67).

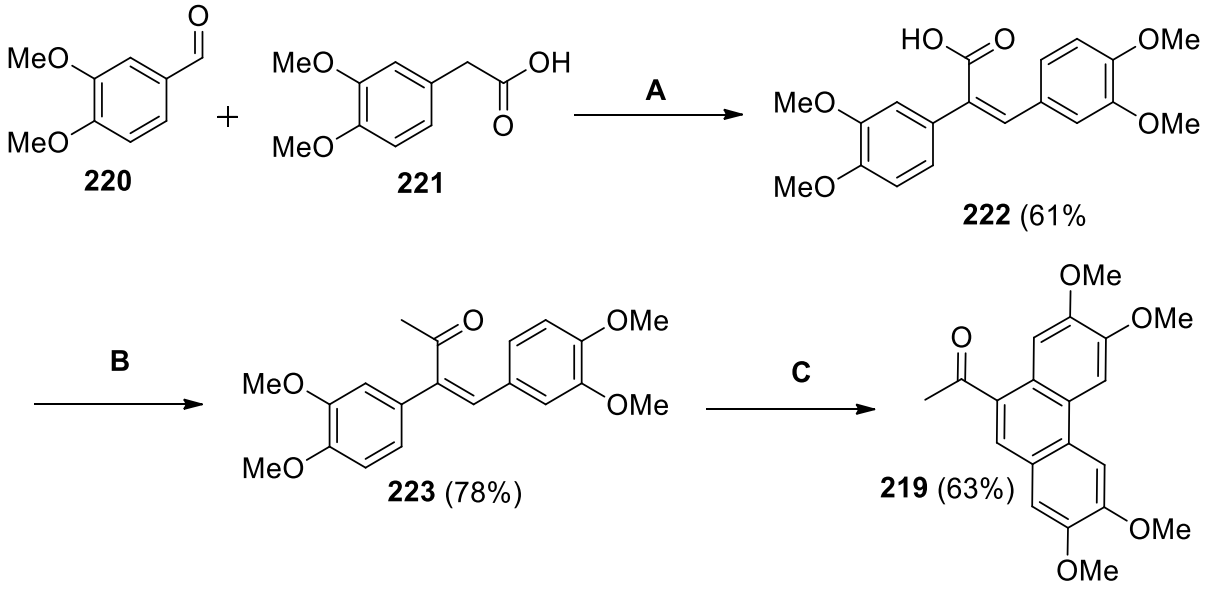

Figure 3.67 Synthesis of phenanthrene **219**.[317,320]
A: Et_3N/Ac_2O; **B**: MeLi, THF, 0°C; **C**: $FeCl_3$, CH_2Cl_2.

Esterification of stilbene **222** afforded the methyl ester **224** with 85% yield, which was followed by a ring closure via a $FeCl_3$ mediated SCHOLL reaction to give the desired phenanthrene **213** (see Figure 3.68).

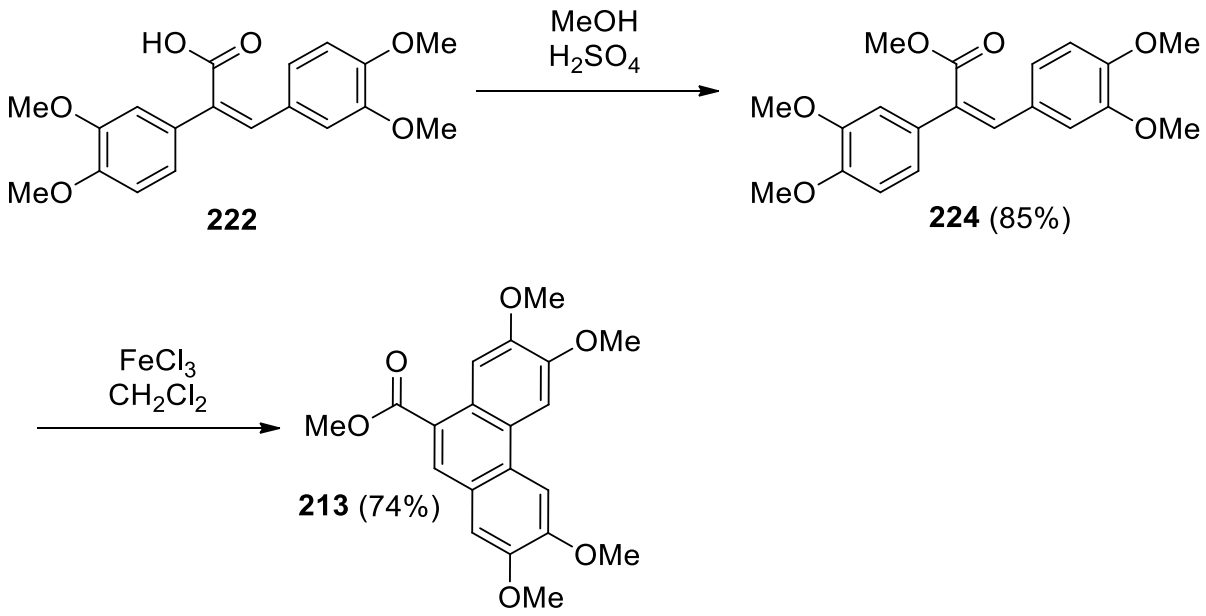

Figure 3.68 Synthesis of phenanthrene **213**.[318,320]

In order to follow the HOPF TBTQ synthesis pathway,[207] a diketone is required, synthesised from the phenanthrene precursors **213** and **219** via a base catalysed aldol reaction (see Figure 3.69). No conversion of starting materials to products could be detected, despite trials with several different bases, which are summarised below in Table 3. After the first few reactions

(reaction numbers: 1-3), the order of adding the reagents was altered, so that the base and ketone were combined first. The reason for this is to allow for the enol form to be generated before addition of the ester. However no conversion was observed, even after prolonged reaction times and heating to reflux. The starting materials were isolated again at the end of the reaction. This indicates that either the enolate was not formed or that methyl ester **213** was not reactive.

A colour change was observed on combining the ketone **219** and base for lithium diisopropyl-amide (LDA), *n*-butyllithium (*n*-BuLi) / potassium *tert*-butoxide (*t*-BuOK), *n*-BuLi / potassium *tert*-pentoxide and lithium bis(trimethylsilyl)amide (LiHMDS) (reaction numbers: 4,5,7-11), which indicates that a reaction took place. For reaction numbers 7 and 9, reaction control (TLC) was carried out after 30 min of combining the base and ketone **219**, at which point a shadow of the starting material spot was observed, under UV light at a wavelength of 365 nm. For both of these reactions, HPLC reaction control was also carried out, but only the two starting materials were visible. Increasing the excess of (*n*-BuLi) / (*t*-BuOK) and LDA from 1 eq. to 3 eq. also did not lead to formation of ketone **225**.

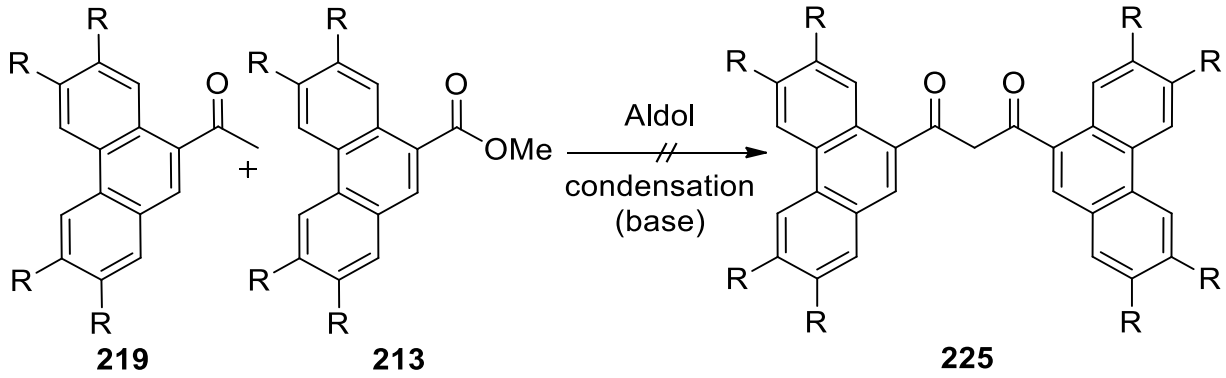

Figure 3.69 Attempted synthesis of diketone **225**. R: OMe

Table 3 Summary of reaction conditions for the aldol reaction.

Reaction No.	Conditions	Procedure and observations	Outcome
1	NaH (3.6 eq.) / THF, 80°C, 4 d	Ester + base; ketone added afterwards.	No conversion
2	NaH (3 eq.) / THF, 75°C, 2 d	Ester + base; ketone added afterwards.	No conversion
3	$NaNH_2$ (2 eq.), THF, 60°C, 5 d	Ketone + ester in THF; $NaNH_2$ added afterwards. After 1 d heated to 75°C, after 4 d more $NaNH_2$ added.	No conversion
4	$C_5H_{11}KO$ / *n*-BuLi THF, -78°C→rt, 24 h	Ketone + base, ester added after 30 min.	No conversion
5[a]	$C_5H_{11}KO$ (1 eq.) / *n*BuLi (1 eq.) THF, -78°C for 70 min, rt 3 d	Ketone + base, ester added after 30 min. Base added again after 39 h.	No conversion.
6[a]	NaH (2.3 eq.) THF, 75°C, 5 d	Ketone + base, ester added after 20 min. Base added again after 5 d. No change after 3 h.	No conversion.
7[a]	C_4H_9KO (1 eq.) / *n*-BuLi (1 eq.) THF, -78°C for 5 h, rt for 5 d, 75°C for 1.5 d	Ketone + base, ester added after 30 min. After 5 h HPLC reaction control: no product.	No conversion.
8	C_4H_9KO (3 eq.) / *n*-BuLi (3 eq.) THF, -78°C for 1 h, rt for 12 h, 75°C for 3 d	Ketone + base, ester added after 30 min.	No conversion.
9[a]	LDA (1.1 eq.) THF,-78°C for 3 h, rt for 4 d, 75°C for 1.5 d	Ketone + base, ester added after 30 min. After 3 h HPLC reaction control: no product.	No conversion.
10	LDA (3 eq.) THF, -78°C for 3 h, rt for 20 h, 75°C for 2 d	Ketone + base, ester added after 30 min.	No conversion.
11	LiHMDS (3 eq.) THF, -78°C for 1 h, rt for 14 h, 75°C for 2 d	Ketone + base, ester added after 2 h.	No conversion.
12	LDA (1.1 eq.), THF, 0°C for 1 h, rt 3 d	Ketone + base. Base added again after 19 h and 2 d (starting material less intense).	No conversion

[a]Experiments carried out by I. BODENSCHLÄGEL as part of her bachelor thesis.

Reaction number 9 in Table 3 was a test reaction, using ketone **219** as the only starting material, to see if self-condensation took place to afford diketone **226** (see Figure 3.70 below). After addition of a second portion of LDA after 17 h, a second substance was detected via TLC reaction control. After 2 d another portion of base was added and after a further 1 d the reaction was ended, as the intensity of the second substance had increased but starting

material was still present. The raw product was however only the ketone **219** mixed with impurities.

Titration of *n*-BuLi was carried out to determine the concentration before use using diphenylacetic acid until a permanent yellow colour was observed, which was the end–point.[321] LDA was freshly prepared from *n*-BuLi and freshly distilled diisopropylamine (DIPA)[322] and the concentration detemined by titration with *N*-benzylamide.[323]

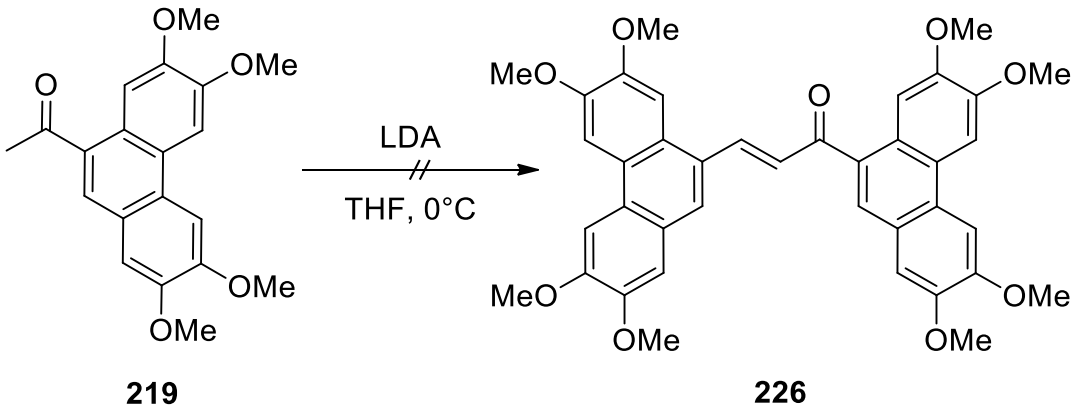

219 **226**

Figure 3.70 Test reaction for self-condensation of ketone **219**.

This result is unexpected, as the aldol reaction for phenanthrenes without methoxy functional groups takes place, as reported by KIRCHWEHM[250] and reproduced in section 3.3.5. In order to investigate the potential negative effect of the methoxy groups on the aldol reaction further, test reactions between methoxy substituted ketone **219** and unsubstituted ester **188** and *vice versa* with ketone **189** and ester **213** were carried out (see Figure 3.71).

For the attempted sysnthesis of ketone **227**, several bases were tested (detailed in Figure 3.71) but no conversion was detected in any of the reactions and the starting materials were re-isolated each time.

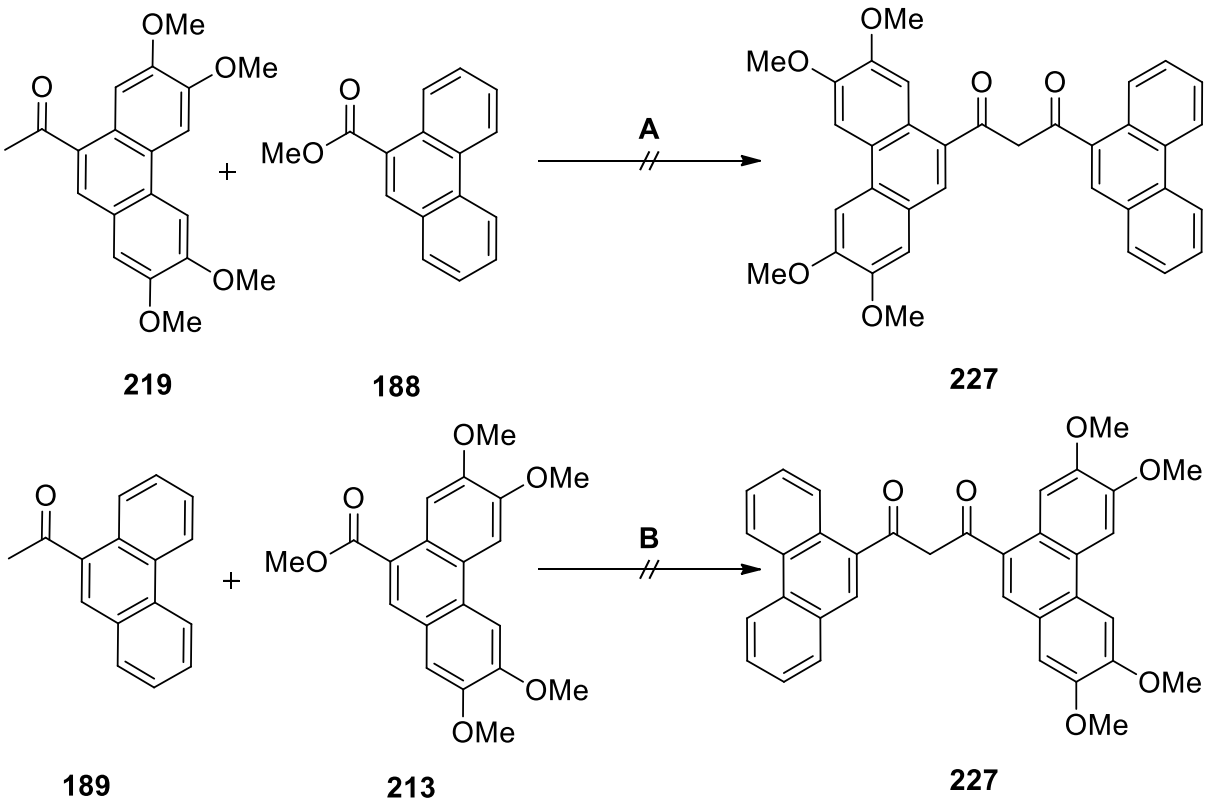

Figure 3.71 Attempted syntheses of diketone **227**. Bases tested for **Reaction A:** LDA, *n*-Buli / *t*-BuOK, *n*-Buli / potassium *tert*-pentoxide, NaH, LiHDMS; bases tested for **Reaction B:** NaH, LDA, *n*-Buli / *t*-BuOK and LiHDMS.

Another approach to ketone **225** was envisaged, for which a suitably substituted aldehyde **228** is required. A similar approach was used by HOPF *et al.* for the synthesis of brominated diketones.[207] To generate diketone **225**, bromination of the aldol condensation product **226** is followed by hydrolysis, as shown below in Figure 3.72.

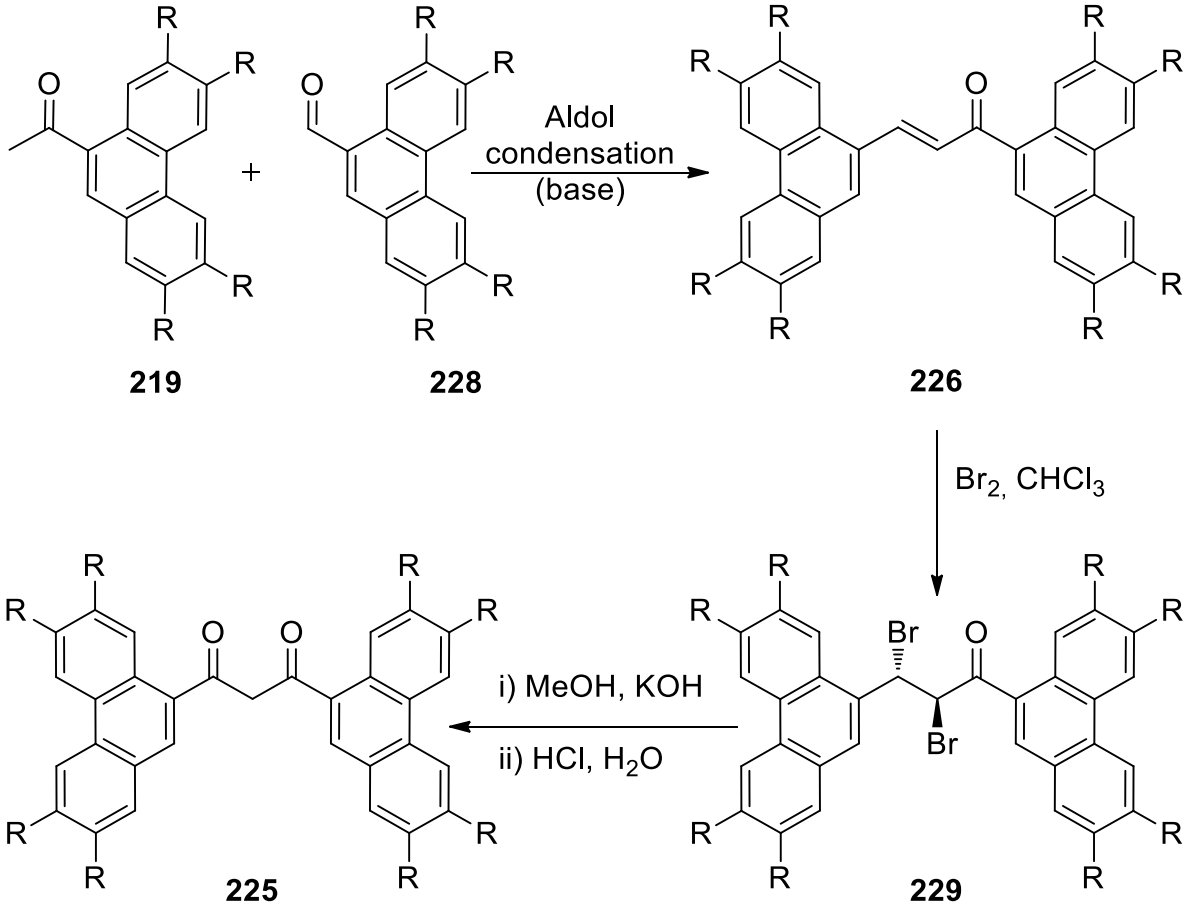

Figure 3.72 Proposed synthesis of ketone **225**. R: OMe.

Methoxy substituted aldehyde **228** was synthesised from stilbene **222** by I. BODENSCHLÄGEL as part of her bachelor thesis (see Figure 3.73). The first step is a SCHOLL reaction with TFA and $NaNO_2$, for which the literature yield of 95% could not be replicated. SU *et al*. described that a reaction time of 30 min was sufficient for a complete conversion,[317] but longer reaction times and additional $NaNO_2$ was required. After 2 d the reaction was stopped, as the ratio of product to starting material did not change, which was ascertained from the ^{1}H NMR spectrum. The following reduction step with $LiAlH_4$ gave an excellent yield of alcohol **231** (97%), which is comparable with the reported yield from WANG *et al*.[324] Oxidation to aldehyde **228** with pyridinium chlorochromate (PCC) led to formation of the desired product with 59% yield.

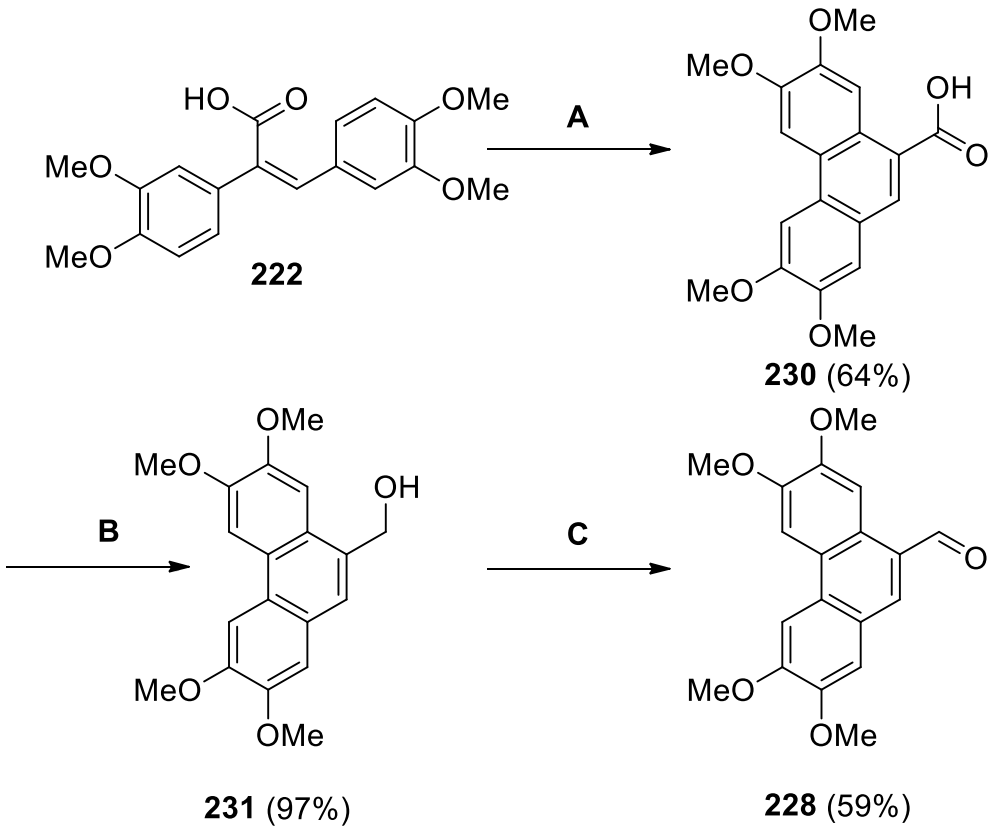

Figure 3.73 Synthesis of aldehyde **228**.[317,324]
A: 20% $NaNO_2$, MeCN/TFA (4:1), rt, 2 d; **B**: $LiAlH_4$, THF, 0°C→78°C, 2 h;
C: PCC, SiO_2, CH_2Cl_2, rt, 16 h

The aldol condensation was attempted with several bases (NaOH, KOH, LDA, *n*-BuLi / *t*-BuOK, LiHMDS), but enol **226** was not produced.

Theoretically, two conditions need to be met for a successful aldol cross condensation: 1) only one of the molecules is able to form an enolate and 2) the other molecule should be more electrophilic. In this case, both conditions are met, as the ketone would form the enolate and react with the more electrophilic aldehyde.

Both NaOH and KOH have relatively low pK_a values (approx. 16) when compared to the value of the α-H from the ketone (approx. 19–21).[325] The consequence is that the hydroxide ion is not basic enough to remove the proton, little or none of the nucleophilic enolate is formed and the keto-enol equilibrium remains on the side of ketone.

In order to shift the equilibrium to the enolate side, a stronger base and therefore a larger difference in pK_a value is required. The pK_a values for LDA (36) and *n*-Buli (50), which with *t*-BuOK forms the LOCHMANN-SCHLOSSER base, are sufficient for the enolate to be

formed[325,326] and a colour change on addition of the ketone to base was observed. Although this colour change suggests that a reaction took place, no conversion to ketone **225** was detected and the starting materials were re-isolated.

Methoxy groups directly adjacent to C=O lead to α-H with a higher pK_a, because the unpaired electrons on the alkoxy oxygen atom reduce the effectiveness of the carbonyl group to delocalise the negative charge. However, in the case of methoxy-functionalised phenanthrenes, there is no direct competition between the alkoxy group and the stabilisation of the enolate, due to the phenanthrene groups separating them. Therefore, it is unexpected that phenanthrene analogues without methoxy groups undergo the base catalysed aldol reaction, whereas the methoxy-functionalised phenanthrenes do not.

A test reaction with unsubstituted analogues was carried out (see Figure 3.74), adapting the protocol from ZHANG *et al.*[328] After 7 d, the reaction was not fully completed, but ketone **232** was isolated with a 41% yield. This result further reinforces the theory that the methoxy groups affect this reaction.

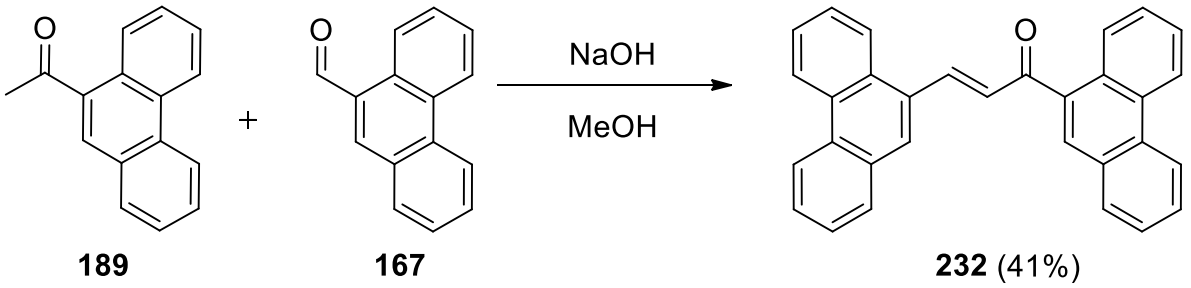

Figure 3.74 Test reaction to afford ketone **232**.

Synthesis of trimethoxy 1,3-propane-diones via base catalysed aldol reaction is however possible, the products of which are seen below in Figure 3.75. Ketone **233** was published in a patent from YASUO and colleagues,[329] using DMF as the solvent and NaH as the base. CHOSI and coworkers also employed NaH as the base and reported the synthesis of trimethoxy derivatives, using benzene as the solvent instead.[330]

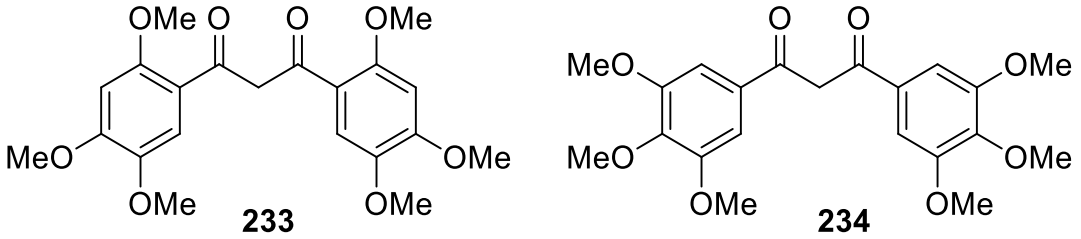

Figure 3.75 Literature known methoxy functionalised diketones **233** and **234**.[329,330]

Overall, it is surprising that the base catalysed aldol reaction between methoxy substituted phenanthrenes **213** and **219** does not take place. The methoxy groups clearly hinder the reaction, so that the goal of synthesising TBTQ **209** could not be realised.

In 2016, KUCK and coworkers bridged the bay regions of TBTQ, using electron rich dimethoxy groups in the *para*-position to achieve three-fold cycloheptatriene ring formation with a DDQ / TfOH system[249] (see Figure 1.34 on page 30). Thorough investigations of the electronic and steric effects of the position of the methoxy groups were published in 2017 and indicate that the addition of methoxy groups *ortho* to the nascent bond are detrimental to the success of the SCHOLL reaction, due to the incurred steric congestion.[331] However, this can be overcome if the aryl ring is electron rich enough, as demonstrated for TBTQ **235** in Figure 3.76.

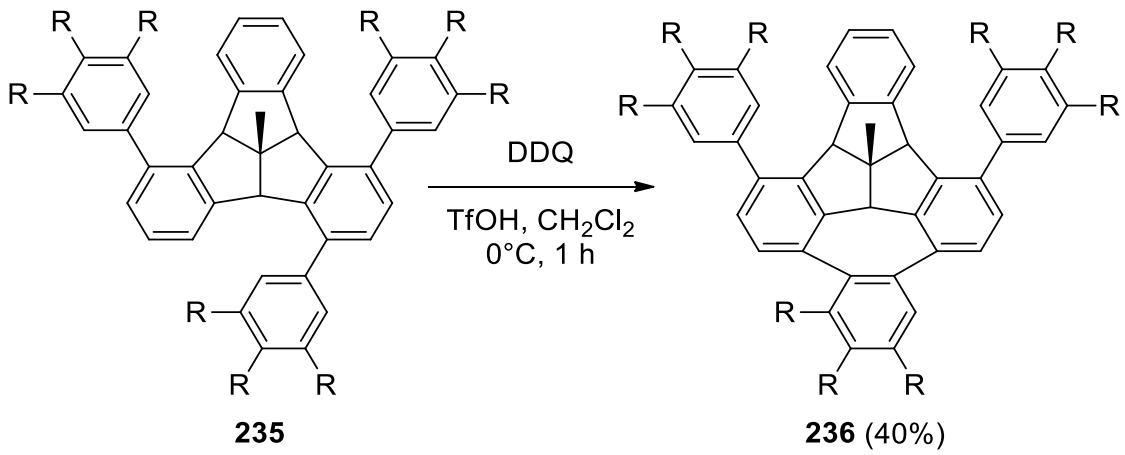

Figure 3.76 SCHOLL reaction example, where the methoxy groups are located in *ortho*-, *meta*- and *para*-positions in TBTQ **235**.[331] R: OMe.

This result demonstrates that cycloheptatriene formation in *ortho*-aryl-substituted TBTQs via the SCHOLL reaction is sensitive to electronic and steric factors and reinforces the importance of methoxy-substituted TBTQs for extending the carbon network.

In conclusion, this topic requires further investigation, for example the effect of different solvents in the aldol condensation, such as DMF or benzene. The synthesis of ketone **225** was attempted from literature known precursors via a base catalysed aldol condensation reaction. Six different different bases of varying strengths and in varying amounts were tested, but no conversion was detected and the starting materials were re-isolated. Test reactions between one methoxy functionalised reactant and one unsubstituted reactant were also carried out, without success. Methoxy functionalised TBTQ **209** could therefore not be realised. As

unsubstituted phenanthrene precursors lead to the formation of product, the presence of four electron rich methoxy groups obviously changes the reactivity of the phenanthrenes.

Computational modelling of diketone **225** and the precursors **213** and **219** would also provide valuable insight into the stability and electronic properties of the molecule. The synthesis of phenanthrenes **214** and **215,** which would lead to the *ortho-para* methoxy-functionalised TBTQ would provide the opportunity to explore if the positions of the methoxy groups on the phenanthrene moiety affect the outcome of the aldol condensation.

3.3.7 *tert*-butyl functionalised phenanthrenes

As already mentioned, *tert*-butyl groups can also be used as blocking groups to control the SCHOLL reaction, due to steric hindrance at adjacent positions.[74] This differs from the activating effect methoxy groups have on the SCHOLL reaction, but as *tert*-butyl groups increase the solubility of large PAHs,[103] their introduction is likely to be advantageous. Solubility is essential for characterisation and structure elucidation as NMR measurements are carried out in a particular solvent. Additionally, molecules which are soluble in a wide range of solvents offers a greater flexibility for subsequent reactions. KUCK often introduced methyl or propyl chains at the bridgehead positions, in order to increase the solubility of TBTQ derivatives[203] but long alkyl chains would not beneficial for bridging the bay regions, due to their close proximity to the nascent bond.

KING *et al.* reported that *tert*-butyl groups could be placed meta to the nascent bond, as the electronic effect of the mildly *ortho*- and *para*-directing *tert*-butyl groups is negligible.[83] Due to their steric bulk, positioning them in an *ortho*-position to the nascent bond would actively hinder the formation of a bond at this position. Therefore, TBTQ **237** is the synthetic aim of this project, in order to form a cycloheptatriene ring via the SCHOLL reaction and afford TBTQ **238** (see Figure 3.77 below).

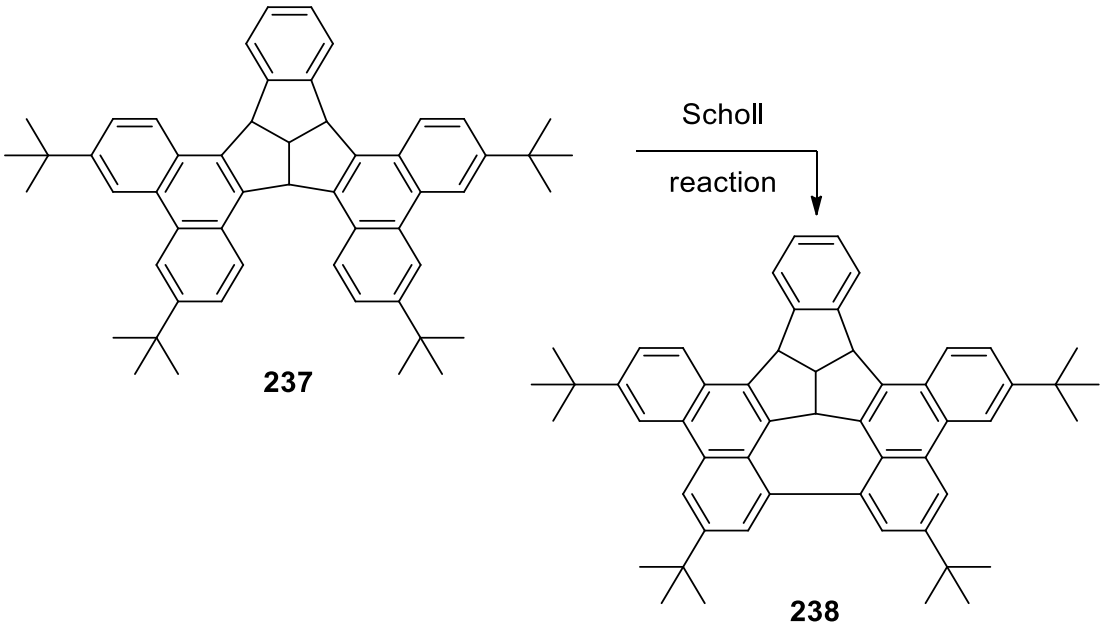

Figure 3.77 Proposed synthesis of TBTQ **238**.

As for the methoxy-functionalised TBTQ, pre-functionalised phenanthrenes are required for the HOPF synthesis pathway. *tert*-Butyl phenanthrenes cannot be synthesised from stilbenes via the SCHOLL reaction, so a photocylisation will be employed instead. The required phenanthrene starting materials **239** and **240** are shown below in Figure 3.78, which are not literature known.

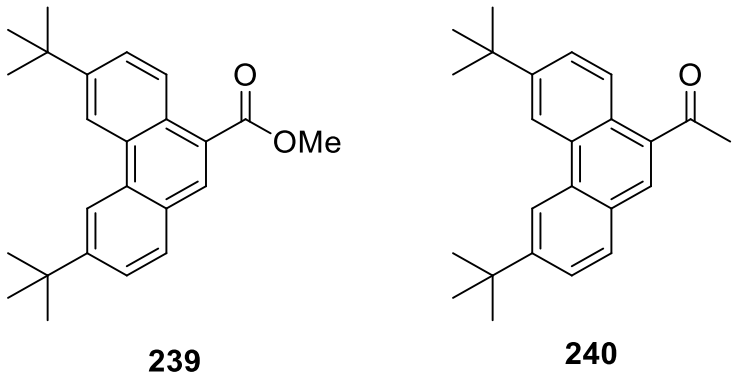

Figure 3.78 Phenanthrene precursors **239** and **240**.

The synthesis route for suitable stilbene precursors for phenanthrenes **239** and **240** was adapted from the protocol for methoxy functionalised stilbenes from YAMASHITA *et al.*[320] For the PERKIN condensation, a functionalised aldehyde and phenylacetic acid are required.

Synthesis of the phenylacetic acid **242** was carried out according to the protocol from CIRILLO *et al.*, which gave quantitative yields.[332] A yield for this transformation was not recorded in this publication.

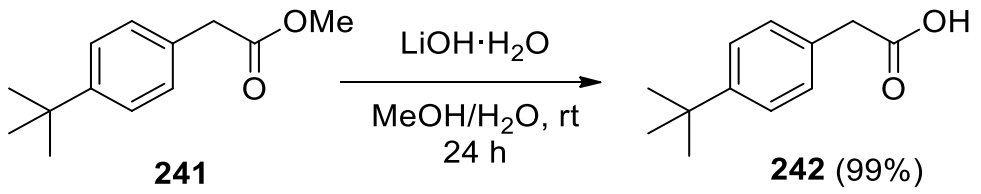

Figure 3.79 Synthesis of phenylacetic acid **242**.[332]

Aldehyde **243** is commercially available and was reacted with phenylacetic acid **242** via a PERKIN condensation to provide *trans*-stilbene **244** in 52% yield (see Figure 3.80 below), adapting the protocol from YAMASHITA *et al.*[320] Despite concerns that the concentrated sulfuric acid would cleave the *tert*-butyl groups in the esterification step, the stilbene **245** was synthesised with a good yield of 70%. For the photoreaction, the conditions were taken from literature known syntheses for 3,6-di-*tert*-butylphenanthrene, by WEI and KATZ.[146,333]

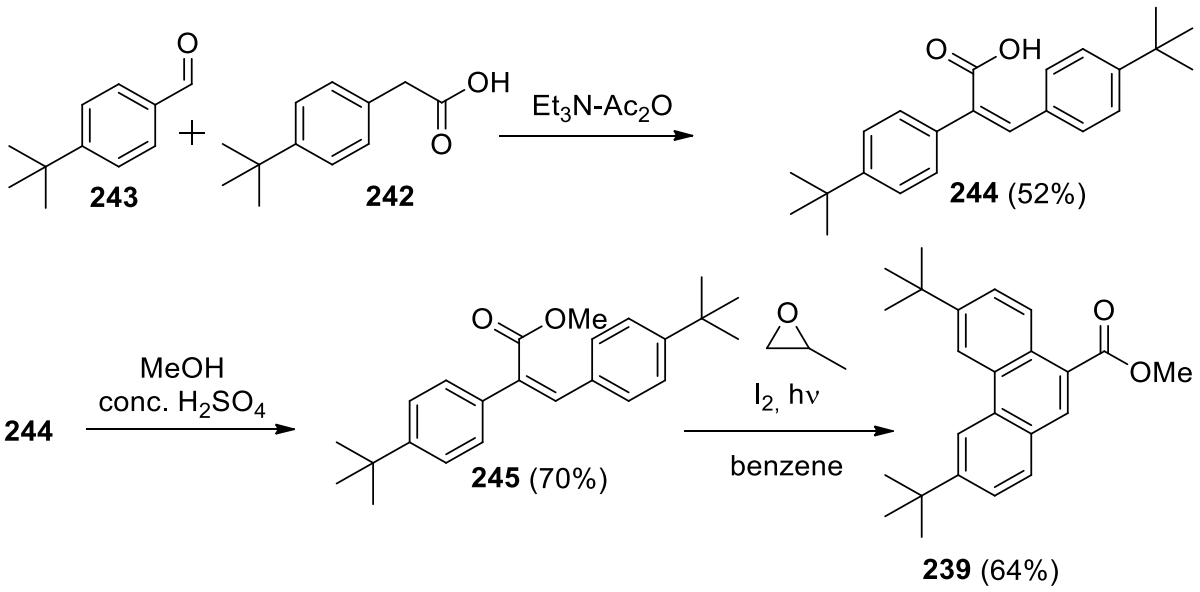

Figure 3.80 Synthesis of phenanthrene **239**.

For the synthesis of the ketone **240**, the method for the conversion from stilbene **244** to stilbene **246** with methyllithium (MeLi) was adapted from a literature known procedure for methoxy functionalised analogues (Figure 3.81).[317]

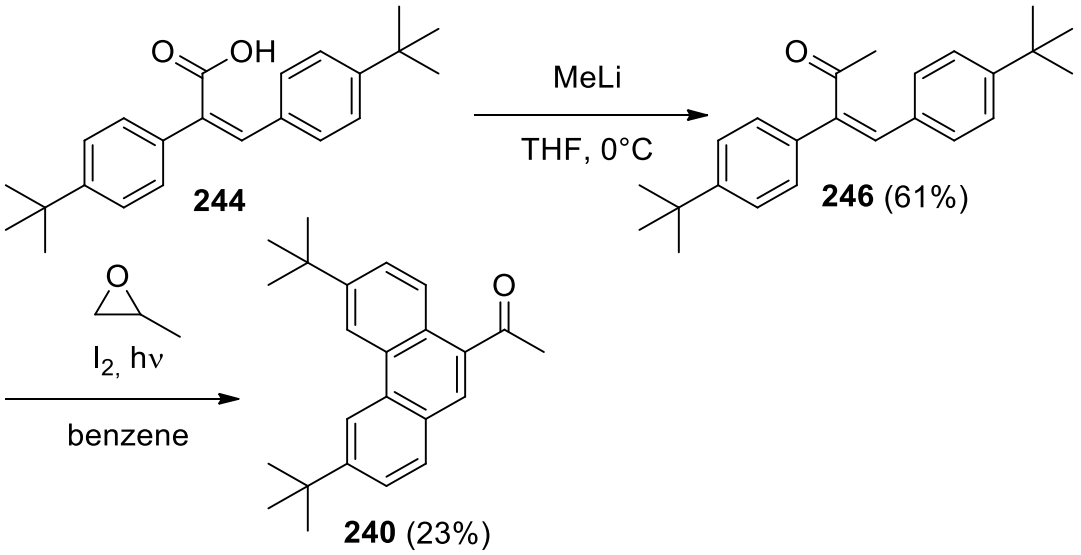

Figure 3.81 Synthesis of phenanthrene **240**.

The photocyclisation of stilbene **246** proved to be problematic, as indicated by the low yield of 23%. After 1 h the reaction was not complete and longer reaction times did however not lead to a complete conversion. A TLC reaction control after 1 h clearly indicated that starting material was still present but the iodine colour had disappeared from the solution. Stoichiometric amounts of iodine were used, so the disappearance of the characteristic pink iodine colour is an indication that the oxidant is consumed. At this point, the conversion should be complete. As several other substances were also detected, and the reaction was stopped at this point. After purification, 23% of the desired phenanthrene **240** was isolated, plus 27% of the reactant **246**. In addition, 19% of *cis*-stilbene **246** was recovered. Investigations by MALLORY *et al.* indicate that the conversion of the *trans*-stilbene to phenanthrene can only occur once a significant amount of the *cis*-isomer has accumulated via photoisomerisation.[142]

For this transformation, the conditions of KATZ were used, as hydrogen peroxide and hydrogen iodide are generated when using the MALLORY conditions: air/oxygen and catalytic amounts of iodine,[142,143] leading to poor yields as a result of side-reactions. An excess of propylene oxide was used by KATZ as a scavenger for hydrogen iodide, and the reaction is carried out under an inert atmosphere.[142,146]

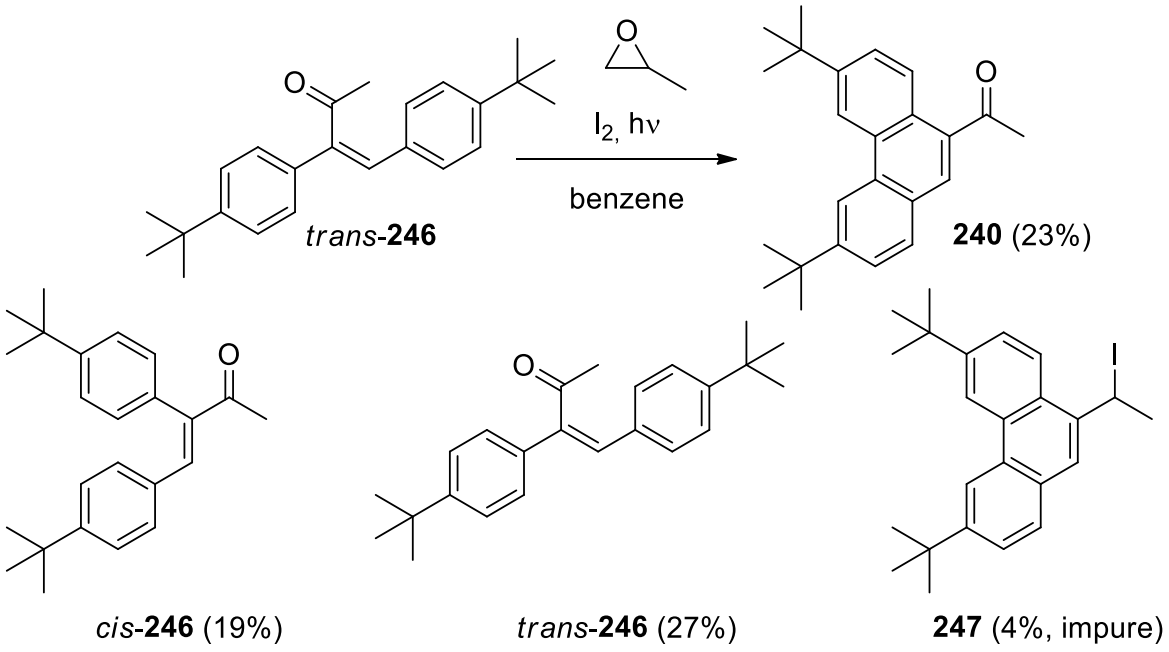

Figure 3.82 Isolation of stilbenes and proposed iodinated phenanthrene **247**.

Traces of another substance were also observed, which is believed to be iodinated phenanthrene **247**. On viewing the ^{1}H NMR spectrum, the absence of a singlet at 2.81 ppm for the methyl group was noted, which is present in the spectrum of phenanthrene **240** (see section 9). Secondly, a new doublet at 1.72 ppm (3H) for the methyl group and a quartet at 5.67 ppm (1H) are visible, which would fit the hypothesis that the molecule is phenanthrene **247**. The methyl group is shielded and therefore shifted, and an extra proton is visible, adjacent to the methyl group. In the area of the spectrum typical for aromatic protons, the signals pattern is different to that of phenanthrene **240**, but the number of aromatic protons is still seven, which supports the argument that the phenanthrene moiety is still present. The *tert*-butyl groups are also still present and the signals were slightly shifted when compared to the desired product.

When comparing the IR spectra of the desired product phenanthrene **240** and proposed side-product phenanthrene **247**, there is no C=O band visible for the side-product, as expected. A mass spectrum of this product was measured, using ASAP (+). The most intense peak was at m/z 317, with another peak at m/z 334, both of which are significantly lower than the expected molecular weight of iodinated phenanthrene **247** of m/z 444. However, the difference between m/z 444 and m/z 317 is 127, which suggests a loss of iodine. The mass of the remaining fragment: $C_{24}H_{29}^{+}$ also corresponds to m/z 317. ^{13}C NMR measurements also support the theory, as 24 C atoms are observed. An alternative mass spectrometry method ESI (+) indicated that m/z 410 is the most intense peak, which differs from the proposed mass by m/z 34. This difference cannot be accounted for by loss of a *tert*-butyl group (m/z 56) or a

methyl group (m/z 14). Therefore the identity of the side-product could not be confirmed unequivocally.

On extending the reaction time until the starting material was consumed did not lead to a higher yield of the desired product. The disappearance of the starting material led to the increased intensity of the side-product spot, and after a total reaction time of 2 h 30 min, it was observed that almost all substances disappeared, and on purification only 12% of the product phenanthrene **240** and 11% of the side-product (assuming the identity is phenanthrene **247**) were isolated.

This result indicates that despite a large excess of the propylene oxide, which is a HI scavenger (569 eq.), a reductive halogenation took place, initiated by the reduction of the ketone with hydroiodic acid to afford a secondary alcohol. This was followed by nucleophilic displacement by a halogen, as a result of a further reaction with hydroiodic acid again. Similar reactions have been reported in the literature for aromatic carbonyl compounds, albeit with $LiAlH_4$ as the reducing agent.[334] One possibility is that the propylene oxide degrades, reacts or polymerises, so that the large excess is no longer effective as a scavenger. Attempts to add iodine in portions to prevent side-reactions did not change the outcome. Optimisation of this photocyclisation is required in order to synthesise phenanthrene **240** on a larger scale, as there are four subsequent steps before TBTQ **237** can be reached (see Figure 3.83).

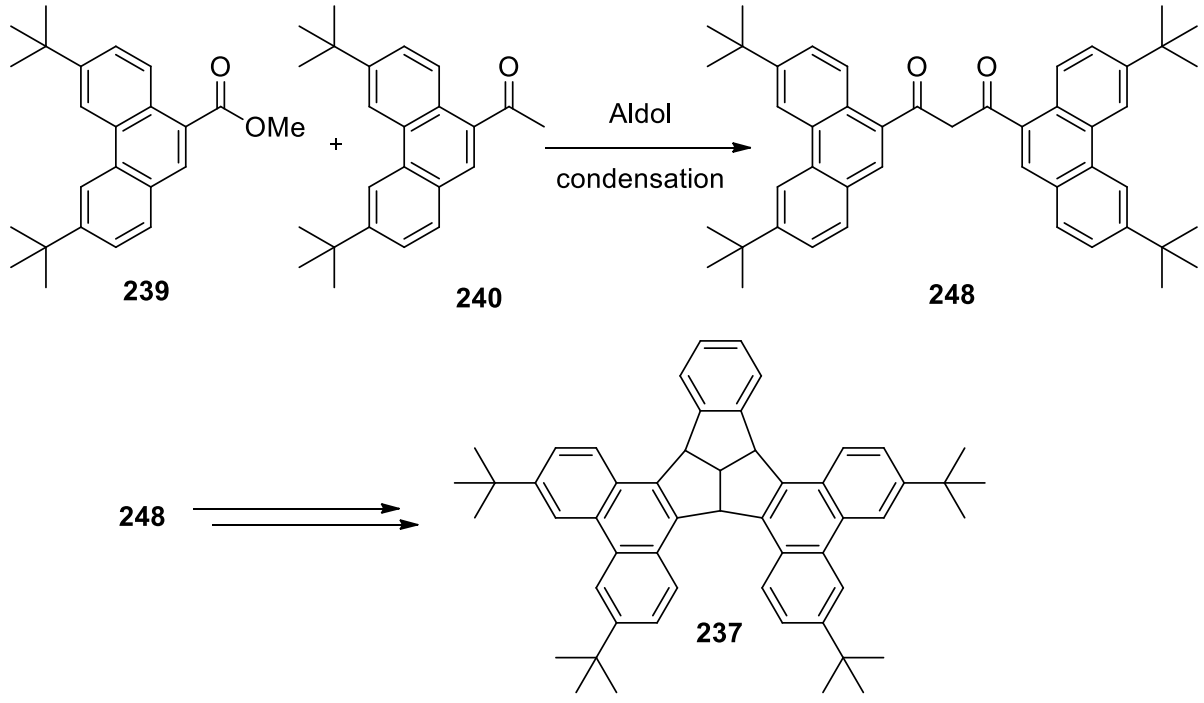

Figure 3.83 Proposed synthesis of TBTQ **237.**

One possibility is testing different reaction conditions, such as the efficient photoreaction with potassium iodide (KI) as the oxidant instead of iodine from WATANABE and coworkers. This reaction proceeds with a catalytic amount of potassium iodide in air, without the need for a scavenger.[335] The reaction times are also shorter than their iodine mediated equivalents. Alternatively, a different synthesis strategy could be explored, which prefers the *cis*-stilbene, or a reaction which selectively converts from *trans*- to *cis*-stilbenes before the photo-cyclisation step is carried out.

To conclude, phenanthrenes **239** and **240** were successfully synthesised, which are precursors for the envisaged HOPF synthesis pathway. The photocyclisation step to phenanthrene **240** requires further optimisation in order to accelerate the conversion to the desired product, improve the isolated yield and simultaneously prevent the formation of side-products.

3.4 Functionalisation of the meta position – Borylation and extension of TBTQ with pheanthrene moieties

Introducing functional groups at the *ortho*-positions of TBTQ in order to extend the carbon network, as was explored in section 3.3, has potential to bridge the bay region and thereby taking an important step forward to synthesising defective nanographenes with a TBTQ core. A major drawback of this strategy remains the necessity to introduce all required functional groups at the start of the synthesis, which often adds several extra steps to the reaction pathway.

A post-functionalisation method, i.e. functionalisation of an unsubstituted TBTQ would reduce the number of steps, however the individual *meta*-positions on the aromatic rings cannot be functionalised selectively, as all six positions will be functionalised. Introducing halogens is advantageous, as halogenated precursors are a prerequisite for such strategies as C-H arylation and cross-coupling reactions for the extension of PAHs, as detailed in section 1.4.1 on page 6. In the case of TBTQ, halogenation reactions carried out after the formation of the triquinacene core are not regioselective, and six-fold bromination or iodination was described by KUCK *et al.*[197,223] and shown in Figure 1.30. Therefore, an alternative strategy is needed for the post-functionalisation and extension of TBTQ.

Metal-catalysed C-H borylation is the conversion of a C-H to a C-B bond and results in the formation of boronic esters. Optimisation of the reaction conditions of iridium catalysed aryl C-H borylation was carried out by the groups of HARTWIG, ISHIYAMA, MARDER and MIYAURA.[336,339] The advantages of arene borylation are that halogenated arene precursors are not necessary for the conversion to an arylboron compound and the reaction is regioselective, determined by steric factors as the boronic ester functional group is sterically bulky.[338] In addition, high yields have been reported, even for multiple functionalisations in one step such as the five-fold borylation of corannulene.[132] In addition, borylation is a valuable technique for extending PAHs when followed by a SUZUKI-MIYAURA coupling.[133,134,187,340]

A new strategy was proposed for the post-functionalisation of TBTQ, with three-fold borylation as the key step. Borylated TBTQ **105** was chosen as a synthetic aim, as a potential precursor for TBTQ **106**, the structures of which are shown in Figure 3.84.

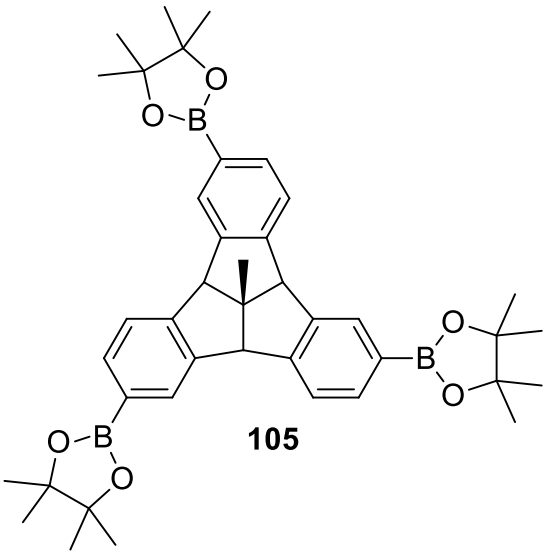

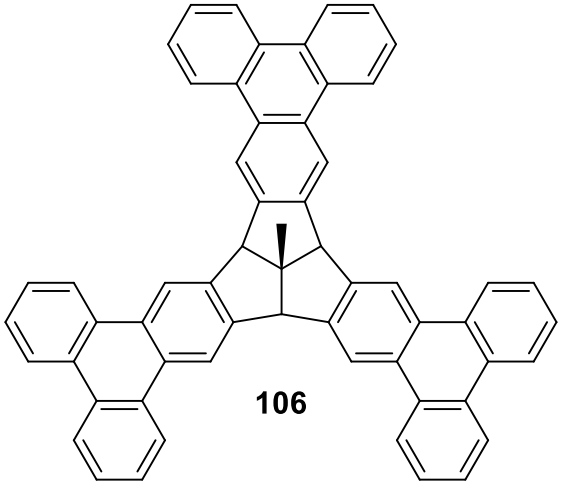

Figure 3.84 Borylated TBTQ **105** and extended TBTQ **106**.

ITAMI and SCOTT reported three different strategies for the extension of corannulene in 2013.[187] The borylation strategy was identified as being particularly promising, as the first two steps are high yielding and although a mixture of isomers is generated, this mixture can be used in the final SCHOLL reaction step to yield a single product. Worthy of note is that the aromatic coupling leads to the formation of five six-membered rings and five seven-membered rings in one step (see Figure 3.85). As corannulene (**107**) is also a bowl shaped molecule, it was decided that these reaction conditions would be a good starting point for the borylation of TBTQ.

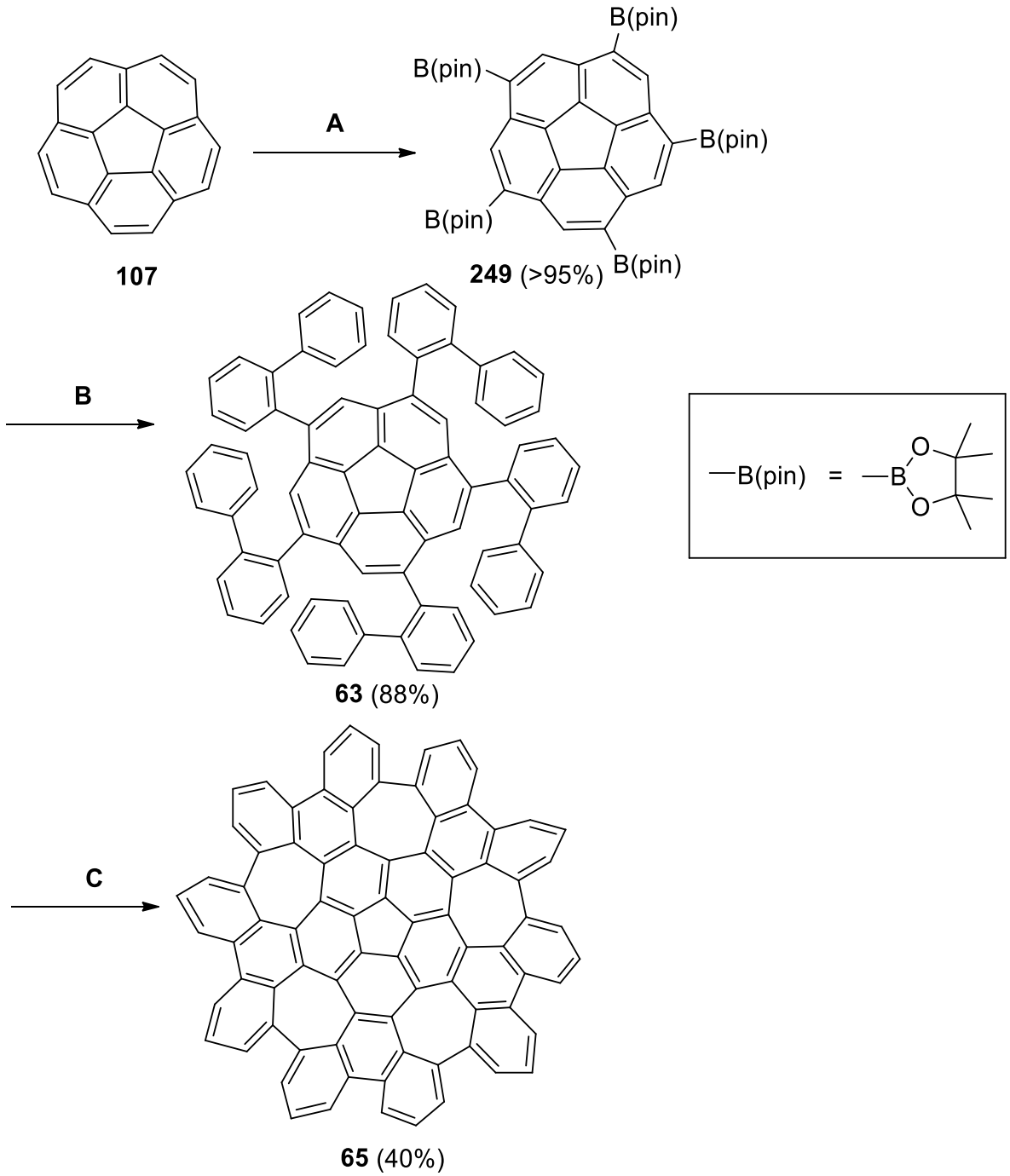

Figure 3.85 Synthesis of corannulene derivative **65**.[187]
A: $(Ir(OMe)(cod))_2$ (20 mol%), B_2pin_2 (5.2 eq.), 4,4'-dimethylbipyridyl (40 mol%), potassium *t*-butoxide (10 mol%), THF, 85°C, 4 d; **B**: 2-bromo-biphenyl (20 eq.), $Pd_2(dba)CHCl_3$ (10 mol%), 2-dicyclohexylphosphino-2',6'-dimethoxybiphenyl (SPhos, 20 mol%), Cs_2CO_3 (10 eq.) toluene/H_2O (2:1), 80°C, 24 h; **C**: DDQ (10 eq.), TfOH/CH_2Cl_2 (5:95), 0°C, 30 min.

TBTQ **106** is not literature known, but the synthesis of a similar molecule was described by TELLENBRÖKER and KUCK.[197,341] Six-fold iodination of TBTQ **83** is followed by a SUZUKI

coupling and an oxidative photocyclisation to afford TBTQ **251**, as shown in Figure 3.86.[197,341]

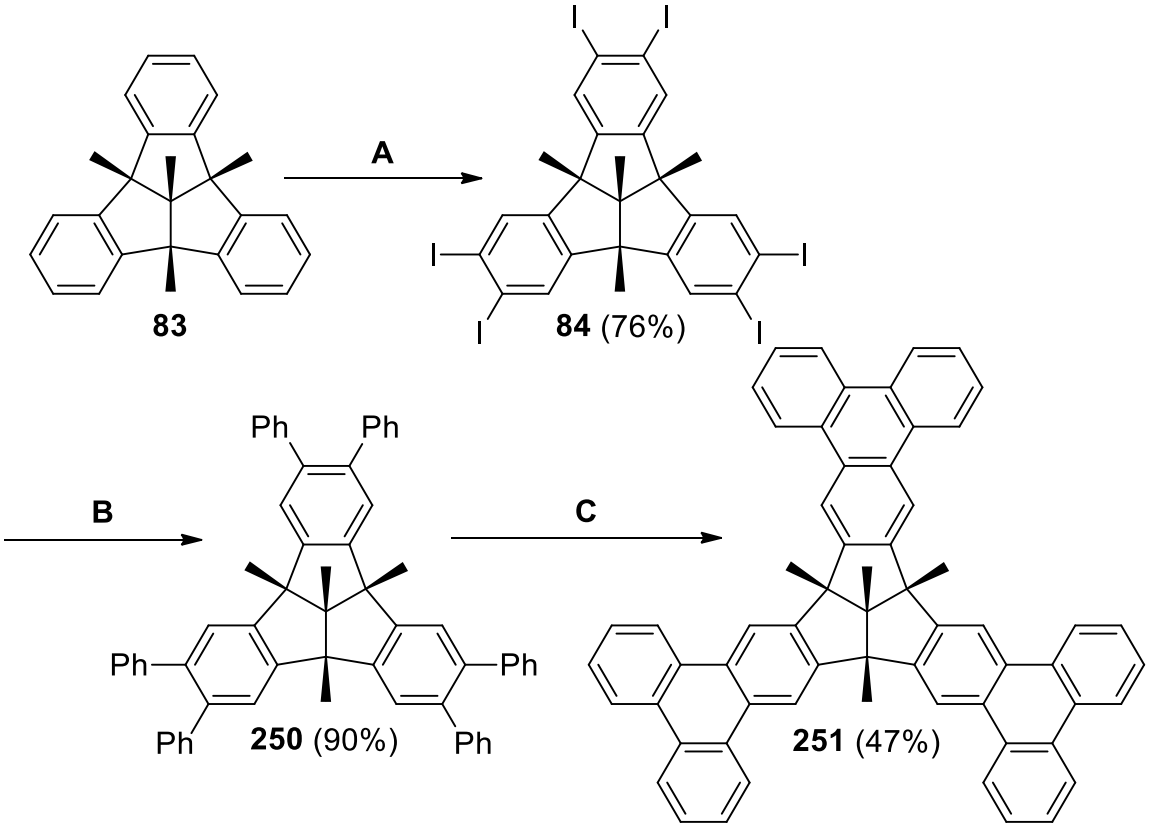

Figure 3.86 Synthesis of TBTQ **251** by TELLENBRÖKER.[197,341]
A: KI, H_5IO_6, conc. H_2SO_4, 0→20°C, 12 h; **B**: $PhB(OH)_2$, $[Pd(dba)_2]$, KOH, PPh_3, $PhNO_2/H_2O$, 100°C, 24 h; **C**: I_2, benzene, propylene oxide, hυ, 20°C, 18 h.

Taking the conditions from ITAMI and SCOTT,[187] the borylation and SUZUKI coupling steps were carried out with the expertise and assistance of J. MERZ from the research group of Prof. T.B. MARDER. A combined yield of 61% was achieved (Figure 3.87), comprising of a mixture of four isomers are formed, as the pinacol boronate ester (Bpin) group can attach to either one of the *meta*-positions at the aromatic periphery. Two C_3 enantiomers are formed and two C_1 enantiomers, as shown in Figure 3.87. This results from the size of the Bpin group and the bulky iridium catalyst, which cannot attack positions adjacent to the Bpin group, therefore it is not possible for more than one Bpin group to be positioned on each ring.

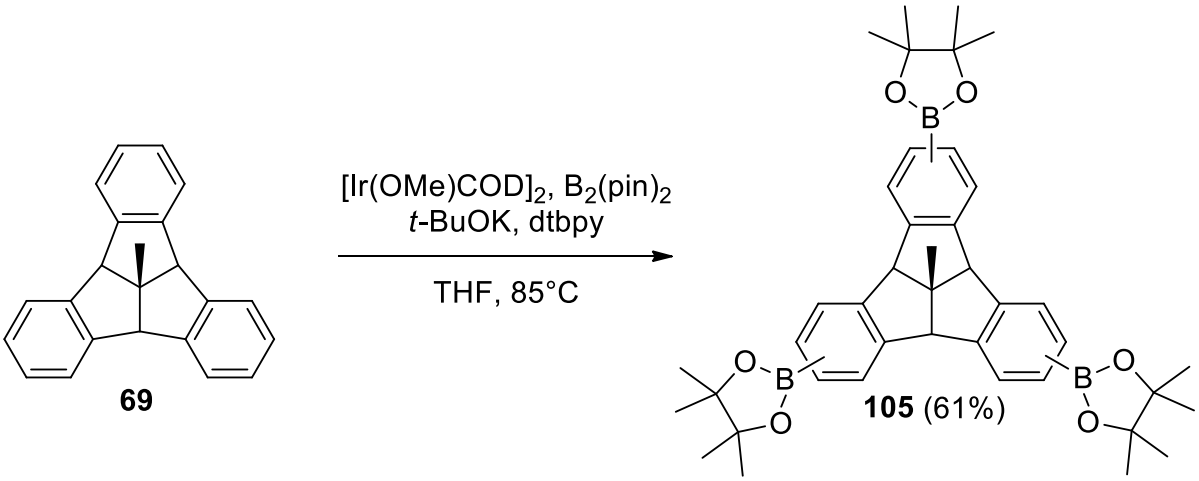

Figure 3.87 Synthesis of TBTQ **105** .

For the next step, the isomer mixture was sufficient, but for NMR characterisation, the isomer mixtures were separated with reverse phase high pressure liquid chromatography (RP-HPLC) with the solvent mixture 70:30 MeOH:MeCN. Two peaks were visible, which were assigned to the C_3 and C_1 enantiomer mixtures repectively.

The C_3:C_1 ratio after the borylation step is 1:1.08, as determined from comparing the % area of each peak on the HPLC chromatogram. Improving upon this ratio was not a priority, as an isomer mixture would lead to a single product in the final SCHOLL reaction step. A recent publication from MASTERLERZ *et al*. presented the borylation of 1,4,7-tripropyl-10-methyltribenzotriquinacene and reported a C_3:C_1 ratio of 2.6:1, by extending the reaction time to 6 d and reducing the temperature to room temperature.[342] This differs to the reaction conditions from ELISEEVA and SCOTT, who reported that the fivefold borylation of corannulene could be reversed at elevated temperatures,[132] so that after 4 d at 85°C yields of 50–70% for 1,3,5,7,9-pentakis(Bpin)corannulene were attained. In the case of corannulene however, there was only one possible structure of the five-fold borylated product. The first borylation reaction prevents a subsequent reaction at the *ortho*-position on the same ring and also in the *peri*-position on the adjacent ring.[132] For tribenzotriquinacene, borylation of one benzene ring does not dictate at which one of the *meta*-positions on the benzene ring, which is the reason for the presence of C_3 and C_1 isomers.

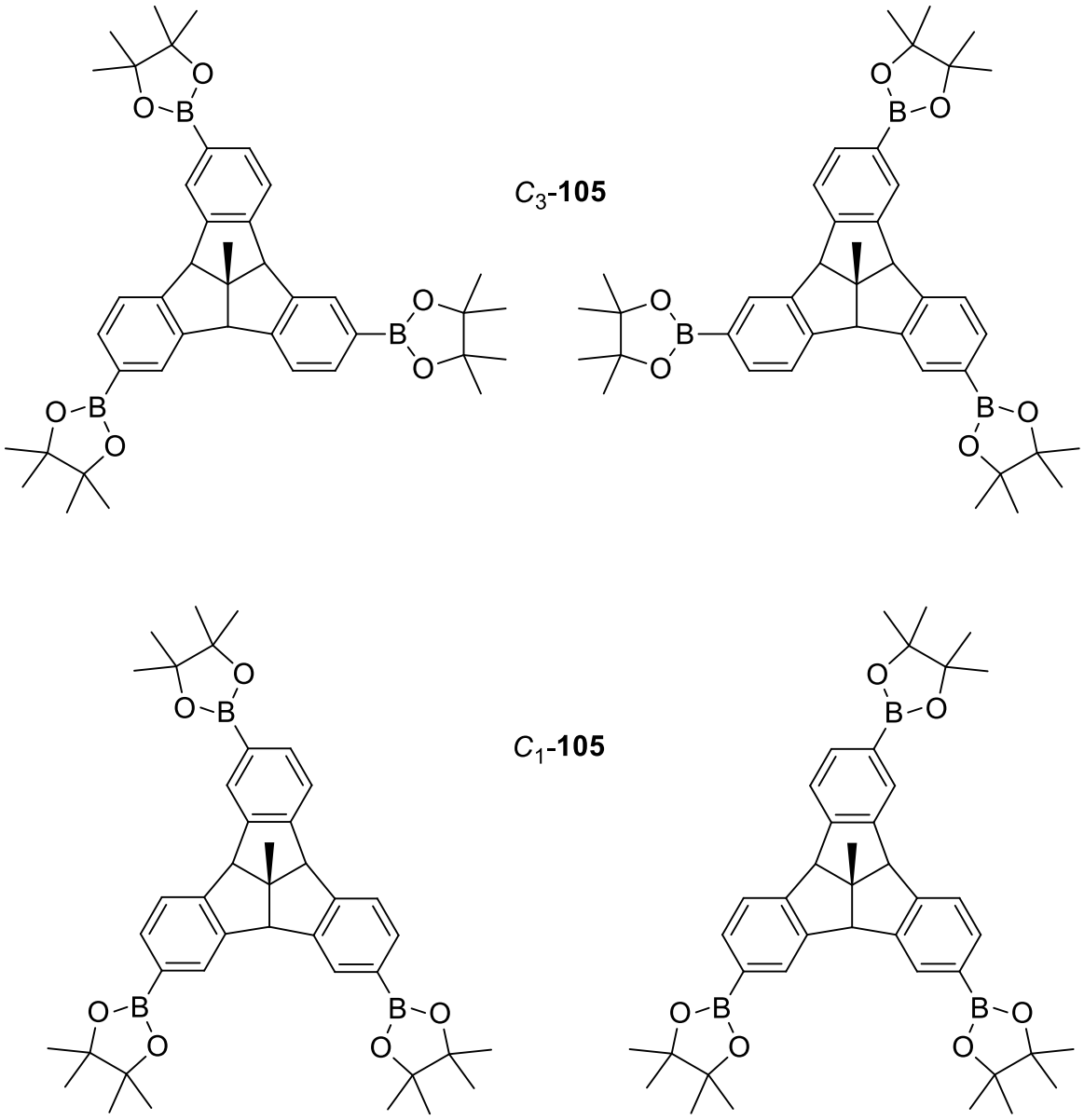

Figure 3.88 C_3 and C_1 isomers of TBTQ-**105**.

The SUZUKI coupling of TBTQ-**105** afforded TBTQ-**252** in a good yield of 84%, using the conditions of ITAMI and SCOTT.[187] A mixture of C_3/C_1 isomers of TBTQ **252** was isolated, as for TBTQ **105**, a sample of which was separated for NMR characterisation by RP-HPLC with acetonitrile as the mobile phase.

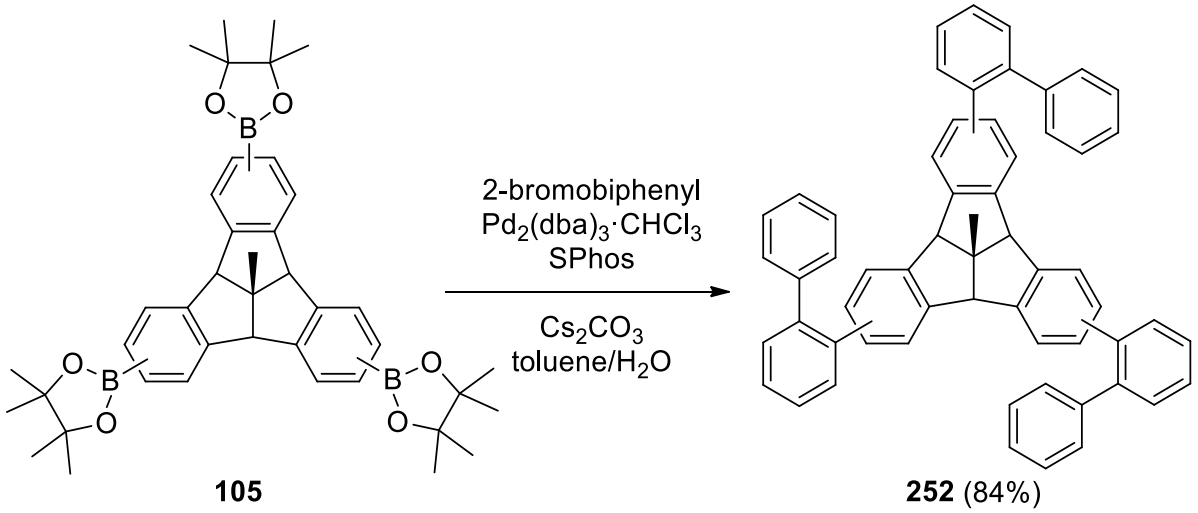

Figure 3.89 Synthesis of TBTQ **252**.

In following the pathway of ITAMI and SCOTT, the final step is the SCHOLL reaction. As already mentioned, a mixture of isomers can be employed, as the product from all three isomers is TBTQ **106**. For clarity, only one C_3 enantiomer is shown below in Figure 3.90.

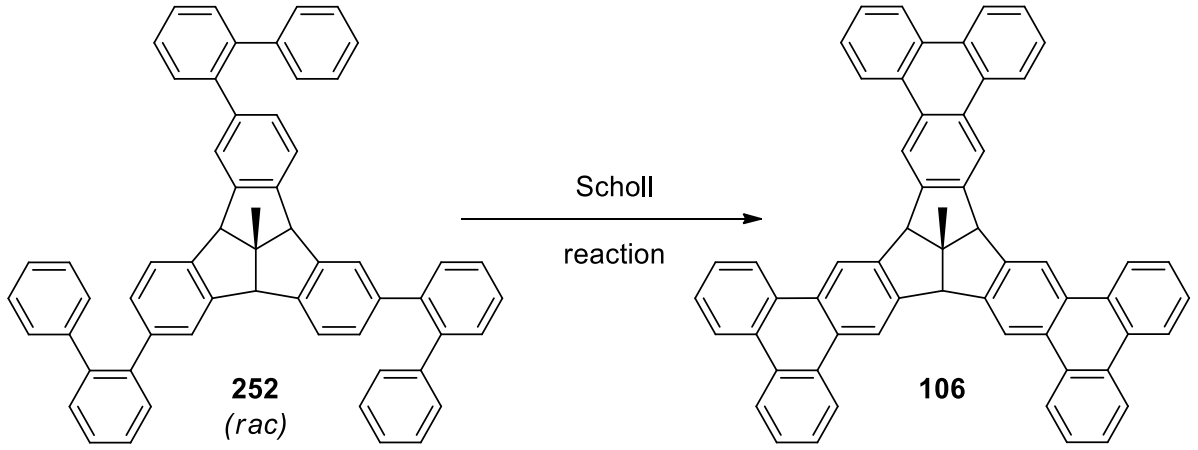

Figure 3.90 Proposed ring closure of isomer **252**. For clarity the C_3 isomer of TBTQ **252** is shown, but a C_1/C_3 mixture is used. The expected ^{1}H NMR spectrum for selected aromatic protons in TBTQ **106** is also shown.

Initial SCHOLL reaction attempts were carried out with DDQ, according to the protocols from ITAMI and SCOTT[187] and KUCK.[249] A summary of the reactions can be found below in Table 4. For reactions B and C, a mass spectrum using an atmospheric solids analysis probe (ASAP, +) was measured of the raw product, and a product peak at m/z 745 was observed, as well as peaks for partially closed products (m/z 747 corresponds to double ring closure; m/z 749 to single ring closure). Despite this observation, ^{1}H NMR of the isolated solids did not show any characteristic peaks for TBTQ **106**. Particular attention was paid to the presence of

peaks arising between 8–9 ppm of the ^{1}H NMR spectrum during the reaction, as TBTQ **251** reported by TELLENBRÖKER (Figure 3.86) shows the following peaks in the aromatic region: δ = 8.84 (6H, s), 8.78 (6H, d,^{3}J = 8.2 Hz), 8.55 (6H, d, ^{3}J = 8.1 Hz) ppm,[341] but no such peaks were observed. As extended reaction times and elevated temperatures relative to initial reaction conditions had been employed, it was decided to consider alternative reagents and protocols for this C-C bond formation.

Table 4 Summary of initial SCHOLL reaction attempts with DDQ.

Reaction	Amount of TBTQ 252	Conditions	Reaction control	Outcome
A	20.0 mg	DDQ (10 eq.), TfOH (250 µl), CH_2Cl_2, 5 min at 0°C, then 30 min at rt.[187]	TLC	TLC: starting material no longer present. After work-up only the starting material was isolated (confirmed by ^{1}H NMR and EI measurements).
B	184 mg	DDQ (10 eq.), TfOH (500 µl), CH_2Cl_2, 1 h at 0°C, then 3 h at rt[187]	TLC	TLC: starting material no longer present. ^{1}H NMR spectrum of the raw product is no longer starting material. Green solid filtered off (mass spectrometry (MS) indicates no product). Peaks at m/z 745, 747 and 749 are visible in ASAP (+) spectrum of solid from organic phase (15.3 mg)
C	100 mg	Recrystallised DDQ (3 eq.), TfOH (300 µl), CH_2Cl_2, 10 min at 0°C, 7 d at rt.[249]	TLC HPLC (NP)	Disappearance of starting material and UV-Vis of the main peak (HPLC) differs to that of starting material. ^{1}H NMR did not confirm presence of product. HPLC of residue after work up afforded 1.1 mg solid. Peaks at m/z 745, 747 and 749 visible in ASAP (+) of this solid.

Reaction	Amount of TBTQ 252	Conditions	Reaction control	Outcome
D	50.0 mg	Recrystallised DDQ (3 eq.), TfOH (200 µl) added slowly, CH_2Cl_2, 30 min at 0°C, 7 d at rt.[249].	TLC HPLC (RP) ASAP (+)	TLC: no starting material detected but ASAP (+) showed peaks only at m/z 747 and 749. After addition of DDQ and TfOH and heating to 45°C, no product was detected. No defined product could be isolated.

An alternative screening procedure was developed to test different reagent systems on a small scale, using ^{1}H NMR reaction control. Small tapered SCHLENK flasks were procured (ca. 5 ml volume) and reactions of a 5 mg batch size were carried out directly in 1 ml of a suitable deuterated solvent. All of the reactions were carried out under argon and a ^{1}H spectrum of the solvent was measured before addition of other reagents, to act as a baseline. The NMR tube was filled to the 40 mm level (ca. 0.6 ml) of the solvent under argon and 32 scans were measured with a Bruker Avance III HD 600. The solvent was removed from the NMR tube again and transferred back to the flask, where starting material was then added. 0.6 ml of sample (40 mm fill volume in a 5 mm NMR tube) was taken and ^{1}H NMR measured. The sample was transferred back to the SCHLENK flask afterwards. The reagents were added and ^{1}H spectra were measured at regular intervals, for at least 24 h.

Many literature protocols exist for the SCHOLL reaction, which were categorised first of all by the choice of LEWIS acid and oxidant, commonly used reagents include: $FeCl_3$,[75-77] $AlCl_3$,[78-80] (bis(trifluoroacetoxy)iodo)benzene (PIFA) / $BF_3 \cdot Et_2O$,[83] $MoCl_5$,[81,82] and DDQ.[86-88]

As the SCHOLL reaction is often unpredictable, trialling several different reagent systems using a ^{1}H NMR screening procedure is a good method to select a suitable oxidant/LEWIS base combination to repeat the experiment on a larger scale. Five methods were chosen for the first round of trials, which are summarised in Table 4 below. $FeCl_3$ was excluded, as initial tests using the protocol from MURATA *et al.*[75] showed very broad peaks in the ^{1}H NMR spectrum, which can be attributed to the paramagnetic nature of Fe^{3+}. Therefore $FeCl_3$ is not a suitable reagent for this ^{1}H NMR screening procedure.

During initial trials with the oxidant DDQ, a peak corresponding the molecular weight of the desired product was observed in the mass spectrum, therefore two protocols which utilise this

reagent were chosen for further investigation. ITAMI's DDQ / TfOH system in 1,2-dichloroethane was chosen because of the similarity of the molecules involved: C-C bond formation to convert terphenyls to triphenylenes.[85] In contrast, the protocol from TOBE *et al.* employs a DDQ / $Sc(OTf)_3$ reagent system,[88] for which there are several examples of nanographene synthesis.[343-345] A method employing *p*-chloranil, another oxidising quinone capable of oxidising aromatic hydrocarbons in the presence of acid,[93] was also selected.[84]

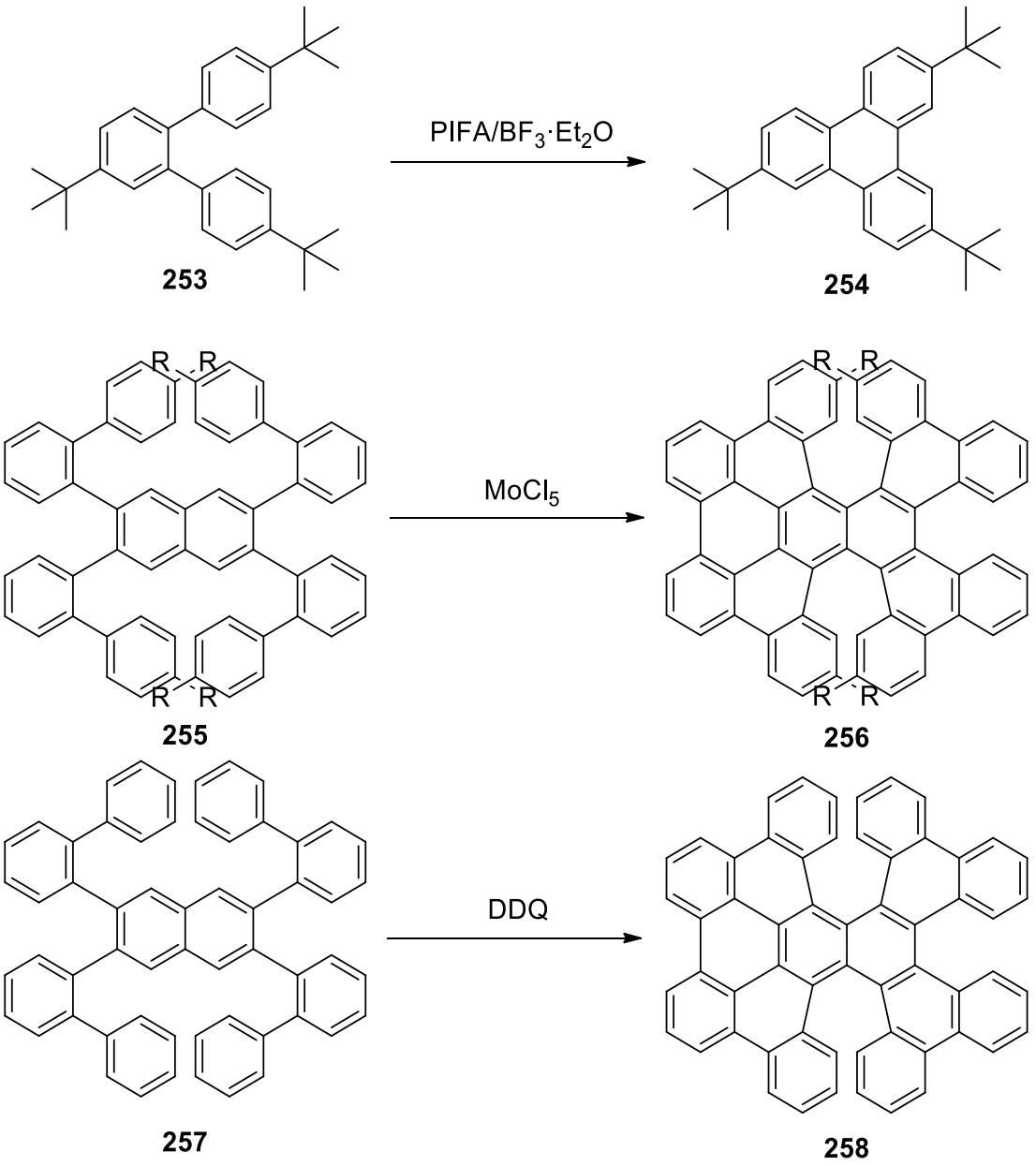

Figure 3.91. Literature examples of SCHOLL reaction protocols.[81,83,85] R = *n*-Bu.

Other reagent systems were chosen based upon similar structural motifs compared to TBTQ **252**. For example, PIFA / BF_3 . Et_2O was selected, as KING *et al*. investigated the

oxidation of terphenyls.[83] $MoCl_5$ is another commonly used reagent, for which a protocol from ITAMI was found.[81]

As already mentioned, particular attention was paid to the presence of peaks arising between 8–9 ppm of the ^1H NMR spectrum during the reaction. Of the five experiments, the only reaction with defined peaks in this region was using the PIFA / $BF_3 \cdot Et_2O$ reagent system. Repeating the reaction with a 80 mg batch led to the isolation of a solid (1 mg), which could be identified as the desired product by NMR characterisation. The reaction was however not complete, as starting material was detected via TLC reaction control and test reactions displayed that allowing the reaction to warm up to above -5°C resulted in the precipitation of an insoluble solid and the decomposition of product, presumably due to polymerisation reactions. The repeated addition of additional PIFA / $BF_3 \cdot Et_2O$ also led to the same result.

Table 5 SCHOLL reaction conditions chosen for NMR experiments.

LEWIS acid; oxidant	**Solvent**	**Time and conditions**	**Yield, no. of newly formed C-C bonds**	**Source**
DDQ (7 eq., 0.86 eq. per C-C)	1,2-dichloro-ethane / TfOH (100:1)	1 h, 0°C	64%, 6 C-C	ITAMI *et al.*[85]
DDQ (4.8 eq., 2.4 eq. per C-C), $Sc(OTf)_3$	chlorobenzene	5 h, 120°C, N_2	49%, 2 C-C (rearrangement)	TOBE *et al.*[88]
p-chloranil (2 eq., 1 eq. per C-C), TfOH	CH_2Cl_2	10 min, 0°C, Argon	57%, 2 C-C	MURATA *et al.*[84]
PIFA / $BF_3 \cdot Et_2O$ (1.5−2.5 eq. per C-C)	CH_2Cl_2	2 h -40°C, 1.5 h -10°C, N_2	86%, 1 C-C	KING *et al.*[83]
$MoCl_5$ (20 eq., 3.3 eq. per C-C)	CH_2Cl_2 (5 mmol l^{-1})	40 min, rt, N_2	26%, 6 C-C	ITAMI *et al.*[81]

In order to optimise the reaction conditions, the ratio of PIFA to $BF_3 \cdot Et_2O$ was altered. The procotol from KING *et al.* was consulted in preparation for the NMR screening procedure,[83] but the use of this hypervalent iodine reagent for mild, metal-free oxidative biaryl coupling reactions has been thoroughly investigated by KITA and coworkers.[346-351] For example, for

the mesitylene cross-coupling (Figure 3.92), a concentration of 0.1 mmol l^{-1} of the starting material in CH_2Cl_2 was employed, and a PIFA / $BF_3 \cdot Et_2O$ ratio of 1:2,[348] in contrast to the 1:1 ratio from KING and coworkers. Different conditions were applied for the synthesis of binapthalene **260** (Figure 3.92) by KITA *et al.*, where the highest yields were achieved with 0.50–0.55 eq. of PIFA. Increasing the excess of the oxidant or increasing the temperature above 0°C caused over-oxidations of the products such as oligiomers and quinone derivatives.[352]

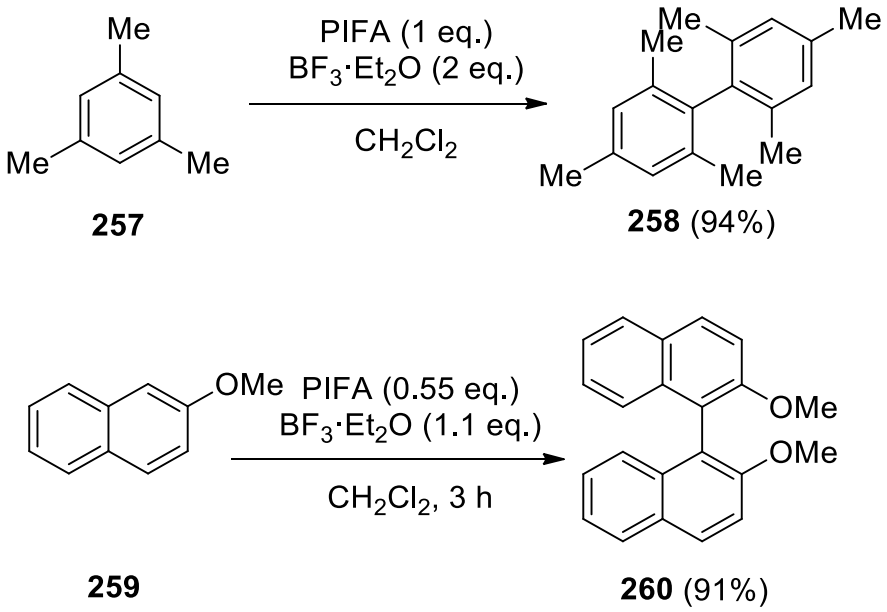

Figure 3.92 Literature examples of varying ratios of PIFA to $BF_3 \cdot Et_2O$ from KITA *et al.*[348,352]

In light of these findings, different conditions were tested, which are summarised in Table 6. For batch C, a syringe pump was employed, so that the PIFA / $BF_3 \cdot Et_2O$ solution in CH_2Cl_2 was added over the course of 5 h. The highest yield (6%) was achieved with a 1:2 PIFA / $BF_3 \cdot Et_2O$ ratio and a concentration of 0.02 M in CH_2Cl_2 for **252**. It was not possible to replicate the literature reported concentration of 0.1 mmol l^{-1} in CH_2Cl_2, as although the starting material itself dissolved readily, it was observed that PIFA did not dissolve fully in early attempts of the reaction and therefore the concentration was adjusted accordingly.

Table 6 Optimisation of reaction conditions for the cyclisation of TBTQ **252**.

Batch	Mass TBTQ 252	Reagents	Amounts per C-C bond	Yield
A	80.0 mg	PIFA (6 eq.) $BF_3 \cdot Et_2O$ (6 eq.)	PIFA (2 eq.) $BF_3 \cdot Et_2O$ (2 eq.)	2%
B	80.0 mg	PIFA (1.65 eq.) $BF_3 \cdot Et_2O$ (3.3 eq.)	PIFA (0.55 eq.) $BF_3 \cdot Et_2O$ (1.1 eq.)	4%
C	80.0 mg	PIFA (5.6 eq.) $BF_3 \cdot Et_2O$ (11.2 eq.)	PIFA (1.9 eq.) $BF_3 \cdot Et_2O$ (3.7 eq.)	6%
D	803.0 mg	PIFA (5.2 eq.) $BF_3 \cdot Et_2O$ (10.2 eq.)	PIFA (1.7 eq.) $BF_3 \cdot Et_2O$ (3.4 eq.)	1%

For batch D, 1 ml of the 12 ml PIFA / $BF_3 \cdot Et_2O$ (3.6 eq./7.2 eq.) in CH_2Cl_2 solution was added initially, with the remaining 11 ml added slowly over the course of 6 h. The progress of the reaction was monitored via TLC and NP-HPLC. After 30 min, a small peak corresponding to the retention time of the desired product (10.77 min) was observed in addition to the starting material (R_t = 3.44 min), likewise a spot was detected on the TLC plate. However, after 1 h, this peak at R_t = 10.77 min was no longer observed, and further chromatograms taken at regular intervals highlighted a general broadening of the most intense peak, which occupied the chromatogram between R_t = 4–11 min. This observation mirrors the TLC reaction control, which displays several spots between the starting material and product during the reaction. It is assumed that these spots correspond to partly cyclised products. As a result, it was not possible to determine an end point for the reaction with HPLC, but regular chromatograms were measured nonetheless.

A decrease in starting material via TLC was observed and after 7 h it was no longer detected. After no visible change after a further two hours, PIFA / $BF_3 \cdot Et_2O$ (0.25 eq./0.5 eq.) was added. No significant increase in product was observed, and after 1 h a further portion of PIFA / $BF_3 \cdot Et_2O$ (0.55 eq./1.0 eq.) was added to the reaction. After 30 min, the product spot appeared more intense than the other spots on the TLC plate, but after a further 30 min these other spots became more intense. PIFA / $BF_3 \cdot Et_2O$ (0.25 eq./0.5 eq.) was added once more, and after a further 35 min the reaction was stopped, as the product spot was once again more intense. After isolation and purification of the product, which consisted of column

chromatography (silica, 90:10 cyclohexane/ethyl acetate) and a preparative LC-MS column (70:30 cyclohexane/CH_2Cl_2).

Crystals suitable for x-ray analysis were obtained from reaction D upon slow evaporation from CD_2Cl_2. The crystal structure belongs to the triclinic space group $P\ \bar{1}$ and is shown below in Figure 3.93(a). In contrast to the molecular stacking arrangement of TBTQ 69, where molecules are arranged in columnar stacks parallel to the c axis and all pointing in one direction, the crystal packing of TBTQ 106 shows neighbouring molecules packed in opposite directions: one facing up and one facing down (Figure 3.93(b)).

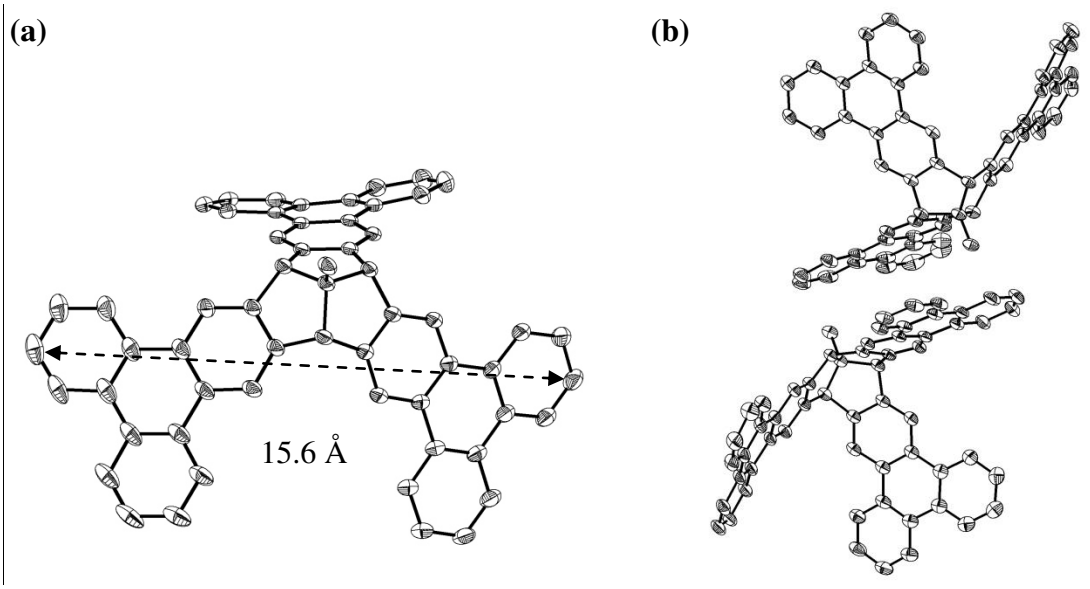

Figure 3.93 Crystal structure of TBTQ **106**: (a) as a single molecule (width: 15.6 Å) and (b) the arrangement with a neighbouring TBTQ molecule. For clarity, the solvent molecules and hydrogen atoms are omitted. These ORTEP style depictions are produced by A. FRIEDRICH and are reproduced with permission.

As one of the phenanthrene groups from one TBTQ arranged itself in an almost parallel fashion to phenanthrene group on a neighbouring group, there is likely to be π-π stacking between these groups. The intermolecular π–π distance of closest rings on convex faces is 3.7 Å (Figure 3.94), which is in agreement with the value reported by KUCK *et al*. for convex–convex π–π stacking of extended TBTQ **99**,[249] and the concave-concave packing distance for neighbouring molecules of TBTQ macrocycle **88**.[243]

Worthy of note is that the indane wings are no longer perpendicular to each other, as the three axes from the *centro* carbon atom C4b[1] to the midpoints of C4c-C8a, C4a-12c and C12a-8c bonds (Figure 3.95 for atom numbering) are 92.2°, 87.7° and 82.7° (TBTQ **69**: 87.2°). This

asymmetry is likely a result of the strong π-π interaction of the phenanthrene groups which slightly distorts the triquinacene core.

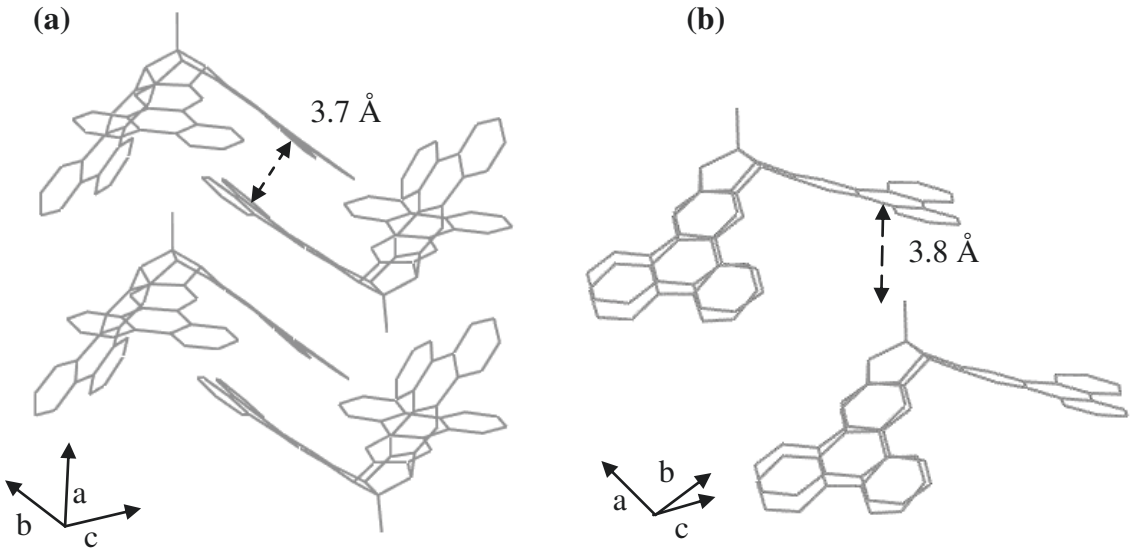

Figure 3.94 Stacking of TBTQ **106**, demonstrating (a) the distance between phenanthrene group (π–π stacking) and (b) C-H$^{Me\cdots}$π interaction between the *centro*-methyl group and a phenanthrene group of another molecule. Hydrogen atoms and solvent molecules (deuterated dichloromethane) were omitted for clarity, and the molecules are aligned relative to the a, b and c axes as indicated.

A C-H$^{Me\cdots}$π interaction between the *centro*-methyl group of one TBTQ molecule and the phenanthrene group of a molecule above it in a stack could also contribute to the distortion of the triquinacene core, as shown in Figure 3.94(b) below. The distance between the carbon atom of the *centro*-methyl group on one molecule and the centre of the triphenylene group of a TBTQ molecule above it is 3.8 Å.

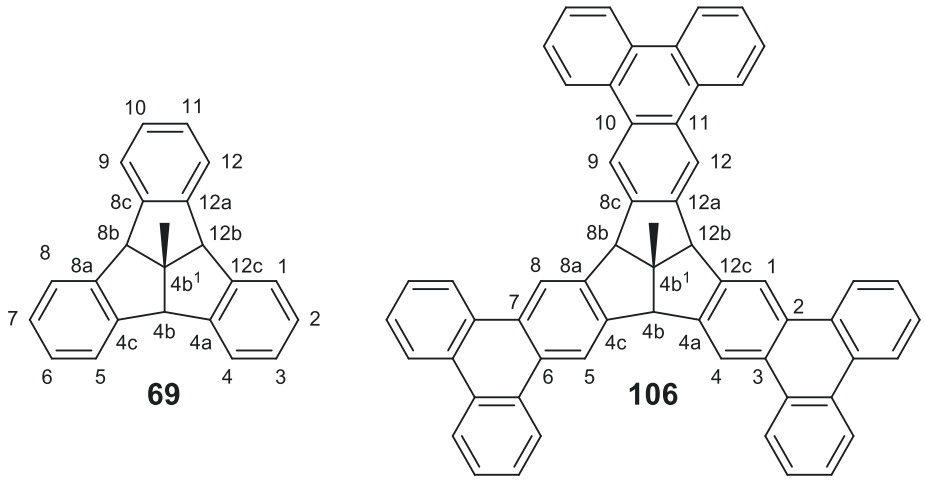

Figure 3.95 Atom numbering of TBTQs **69** and **106**.

A summary of selected bond lengths, bond angles and torsional angles is presented in **Table 7**. The distortion of the triquinacene core is seen clearly in the deviation in the bond angle C4a-C4b-C4c, which is 117.82° for TBTQ **106** and 113.53° for TBTQ **69**. In addition, the torsional angles C^{Me}-C4b^1-C4b-C4c, C^{Me}-C4b^1-C8b-C8c and C^{Me}-C4b^1-C12b-C12c in TBTQ **106** deviate between 1.8° and 11.4° from their counterpart angles in TBTQ **69**.

As the orientation of the indane wings is not symmetric, the bowl depth can either be expressed by measuring the distance between C4b^1 and a plane of all phenanthrene groups (4.8 Å) or between the two aligning phenanthrenes (6.2 Å) which stretch furthest away from the core in a vertical downwards direction (Figure 3.96).

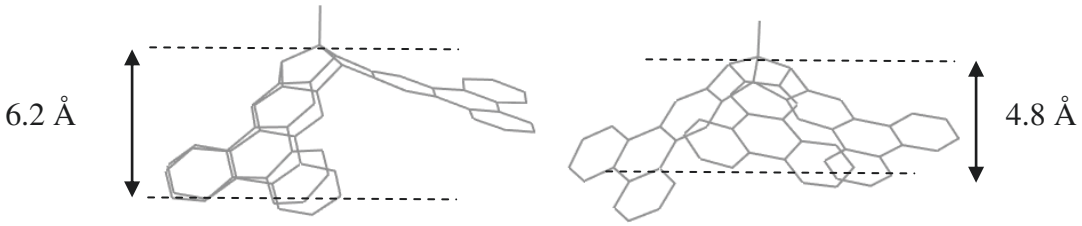

Figure 3.96 TBTQ **106**, showing two possible methods to determine the bowl depth. Hydrogen atoms and solvent molecules are omitted for clarity.

Table 7 Selected bond lengths, bond angles and torsional angles for TBTQ **106** and TBTQ **69**. The values for TBTQ **69** are from data reported by KUCK *et al.*[200]

Bond	**Bond length [Å]**		**Bond**	**Bond angle [°]**	
	106	**69**		**106**	**69**
Cb^1-C4b	1.569	1.5658	C4b-$C4b^1$-C8b	106.01	106.61
Cb^1-C12b	1.561	1.566	C4c-C4b-$C4b^1$	105.63	105.12
Cb^1-C8b	1.571	1.565	C4b-C4c-C8a	111.62	111.52
C4b-C4c	1.504	1.5142	C4a-C4b-C4c	117.82	113.53
C4c-C8a	1.397	1.3949	C12a-C12b-C12c	113.89	113.53
C4c-C5	1.380	1.3956	C8a-C8b-C8c	111.20	113.53
C5-C6	1.4109	1.392	C4c-C8a-C8b	113.34	111.52
C6-C7	1.415	1.391	C4b-C4c-C5	127.97	128.00
$C4b^1$-C^{Me}	1.522	1.524	C8-C8a-C8b	128.60	127.76
Bond	**Torsional angle [°]**		C4c-C5-C6	120.78	119.04
	106	**69**			
C4b-C4c-C5-C6	178.85	176.53	C7-C8-C8a	120.87	119.04
C4b1-C4b-C4c-C5	178.86	179.23	C5-C6-C7	118.77	120.29
C^{Me}-$C4b^1$-C4b-C4c	121.78	119.97	C8a-C4c-C5	120.40	120.42
C^{Me}-$C4b^1$-C8b-C8c	125.52	119.95	C4c-C8a-C8	119.92	120.42
C^{Me}-$C4b^1$-C12b-C12c	108.55	119.95			

To conclude, the goal to synthesise TBTQ **106** via a post-functionalisation method was achieved. Triple borylation, followed by SUZUKI coupling and finally a C-C coupling with PIFA / $BF_3 \cdot Et_2O$ lead to the formation of TBTQ **106**, for which an x-ray crystal structure was obtained. The final step is low yielding (6%) and requires further optimisation; STM investigations into the arrangement of TBTQ **106** on a Ag(111) surface would also provide a valuable insight.

4 Summary and Outlook

Synthesising curved π-systems offers the potential to tune electronic properties, through targeted functionalisation. Non-planar π-systems experience increased reactivity due to the poorer overlap of the π-orbitals and the subsequent lowering of the LUMO energy.

TBTQ can be employed as a rigid motif due to the three five-membered rings at its centre, making it an ideal candidate to simulate a defect centre in a nanographene. In addition, the four different sites: *centro*, bridgehead, *ortho* and *meta* offer selective functionalisation, provided that precursors and blocking groups are carefully selected.

The aims of the four chapters of this dissertation encompass a general objective to alter the physical and electronic properties of TBTQ by targeted functionalisation or manipulation.

4.1 Influence of the functionalisation of the *centro*-position: STM investigation of TBTQs

Starting with apical functionalisation, the first self-assembly of highly ordered monolayers of TBTQ **68** and TBTQ **69** on Ag(111) was studied by scanning tunnelling microscopy (STM) under ultrahigh vacuum conditions. The interaction between organic molecule and a metal substrate influences the orientation and arrangement of molecules relative to each other, which cannot be predicted from the crystal structures alone, providing valuable insights into the behaviour of bowl shaped molecules.

At low to moderate coverage, both TBTQ **68** and TBTQ **69** adsorb with the bowl opening faced downwards, appearing in two orientations that are rotated by 14° from the high symmetry axis of the Ag(111) surface. At high TBTQ coverage of **68**, extended islands of a self-assembled highly ordered windmill nanostructure dominate the surface, interspaced with nanometre-sized openings. This windmill structure is absent for Me-TBTQ **69**, which immediately forms double-layered regions at high coverage. Investigating the factors influencing the formation and packing of the windmill nanostructure for TBTQ **68**, such as the balance between molecule-substrate interactions and molecule-molecule interactions would help pave the way to the construction of multilayer nanostructures.

4.2 Functionalisation of the *ortho*-position: synthesis of fluorinated TBTQs

Fluorination of aromatic hydrocarbons is also favourable for tuning the electronic properties, for example with the aim of synthesising electron acceptor materials for organic semiconductors. As a proof of concept, the aim to synthesise the first *ortho* fluorinated TBTQs was achieved. Following the triple cyclisation pathway by HOPF *et al.*[202,207] mono-fluorinated TBTQ **101** was synthesised in three steps from commercially available starting materials. The final cyclisation step is low yielding (14%), but the fluorinated TBTQ was successfully synthesised for the first time (Figure 4.1).

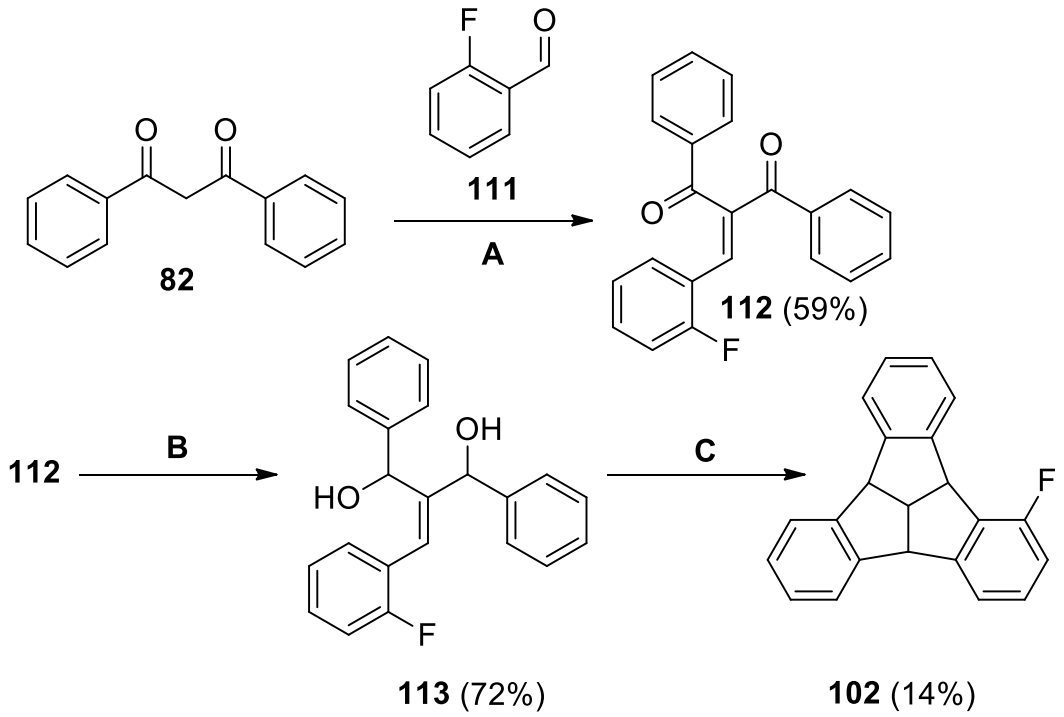

Figure 4.1 Formation of TBTQ **102**.
A: piperidine, acetonitrile, 80°C; **B**: $CeCl_3 \cdot 7\ H_2O$, $NaBH_4$, $MeOH/CH_2Cl_2$, -78°C → rt; **C**: polyphosphoric acid, chlorobenzene, 120°C.

Fluorine atoms significantly alter the reactivity of TBTQ precursors, as highlighted by the formation of a chromenone side-product during the KNOEVENAGEL condensation step of the C_3-chiral fluorinated TBTQ synthesis pathway. Therefore, an alternative precursor (diketone **133**) was used for further reaction steps.

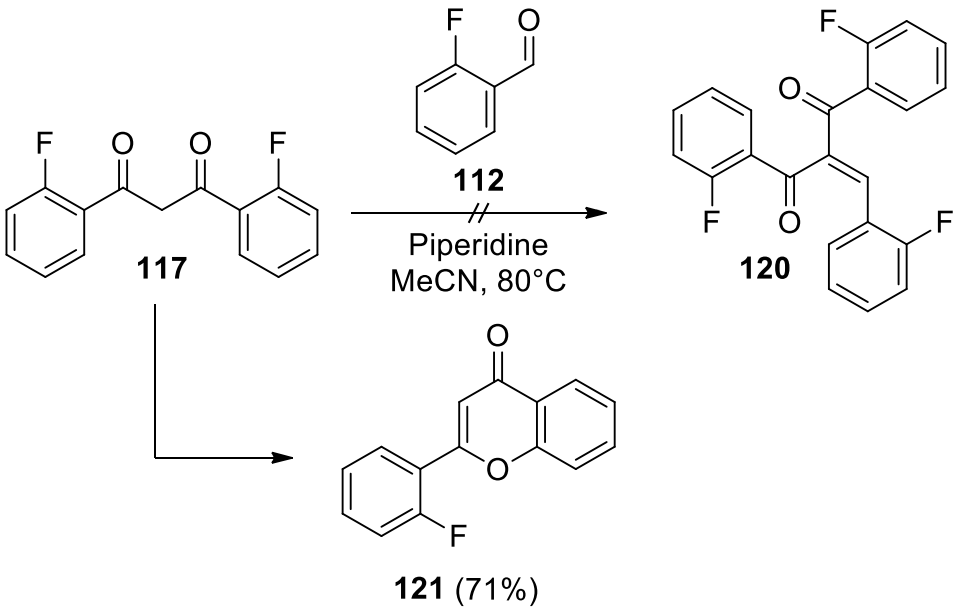

Figure 4.2 Formation of chromenone **121**.

The final reaction step also yielded several products: the C_1 TBTQ **164**, side-product **154** and a C_3-TBTQ isomer, which is believed to be TBTQ **155** (Figure 4.3). This assumption is based on ^{1}H-^{1}H COSY data and the presence of side-product **154**, which is formed from the same cationic intermediate that would afford TBTQ **155**. Rotation of the aromatic rings during cyclisation leads to the formation of a C_1-TBTQ **164**, the reason for which could be electrostatic repulsion between the fluorine atom and a nearby β-hydroxyl group. Optimising the separation of the C_3:C_1 isomers is an important first step, so that the identity of the C_3 isomer can be confirmed. *ortho*-C_3 threefold fluorinated TBTQs are promising candidates for further coupling reactions, whereas *meta*-C_3 threefold fluorinated TBTQs could be used for the construction of supramolecular assemblies.

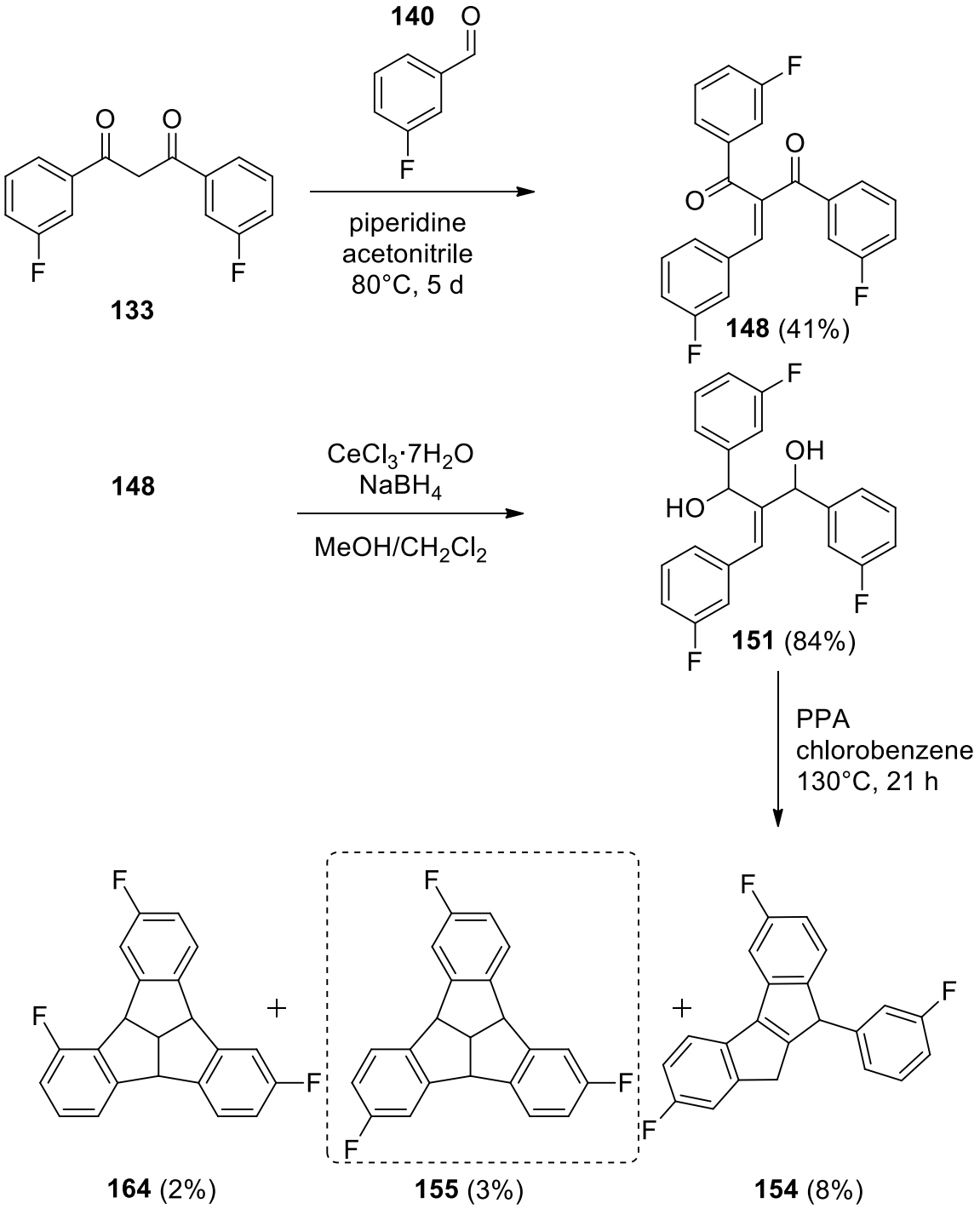

Figure 4.3 Synthesis of fluorinated TBTQs.

4.3 Functionalisation of the *ortho*-position: synthesis of phenanthreno-TBTQs and study of their stacking arrangements

The formation of TBTQ **171** was confirmed (Figure 4.4), which indicates that the reactivity of the bridgehead positions is critical in late stage functionalisation, although blocking groups at these positions would also hinder coupling reactions at the *ortho*-positions.

As methoxy and *tert*-butyl functionalised phenanthrenes have been explored in the literature to steer the SCHOLL reaction and prevent side-reactions such as dimerisation, suitable functionalised phenanthrene starting materials were synthesised. For the methoxy functionalised phenanthrenes **213** and **219** (Figure 4.4), despite exhaustive testing with different bases, the base catalysed CLAISEN condensation could not be realised, although this reaction succeeded with non-methoxy functionalised analogues.

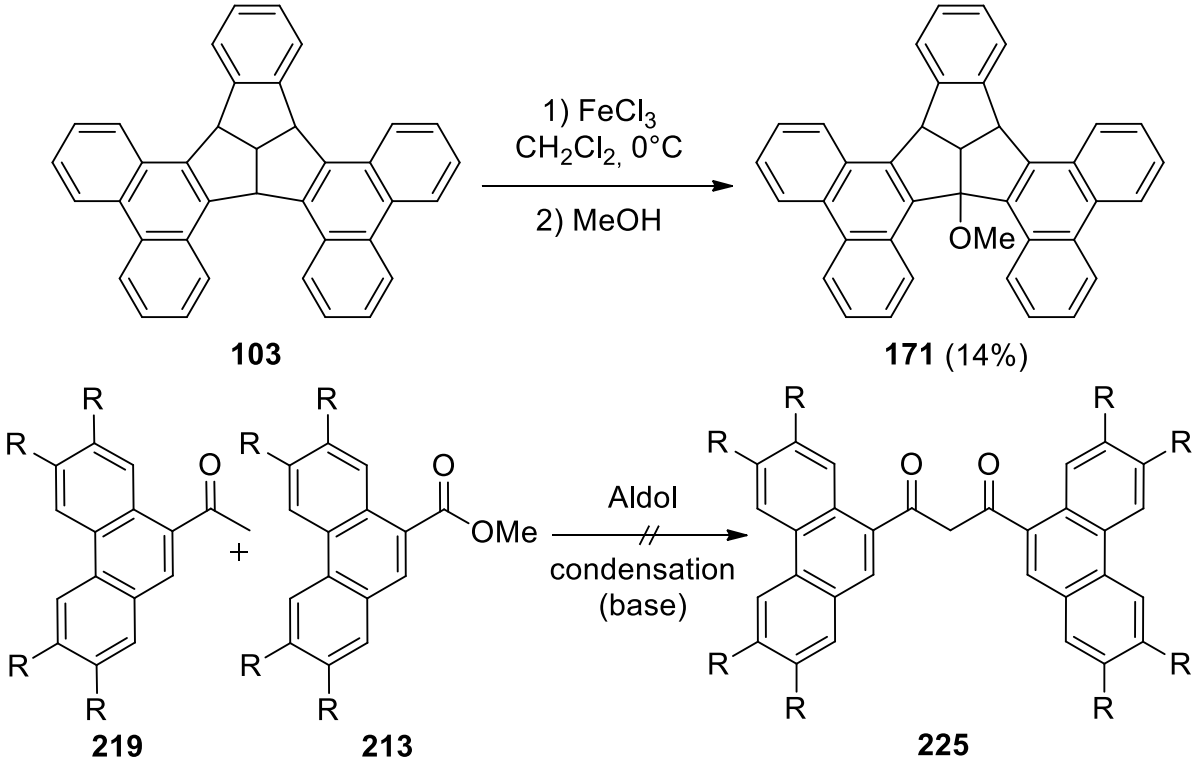

Figure 4.4 Synthesis of TBTQ **171**.

tert-butyl functionalised phenanthrenes **239** and **240** were synthesised for the first time (Figure 4.5) so that TBTQ **227** could be achieved in future work (Figure 4.5).

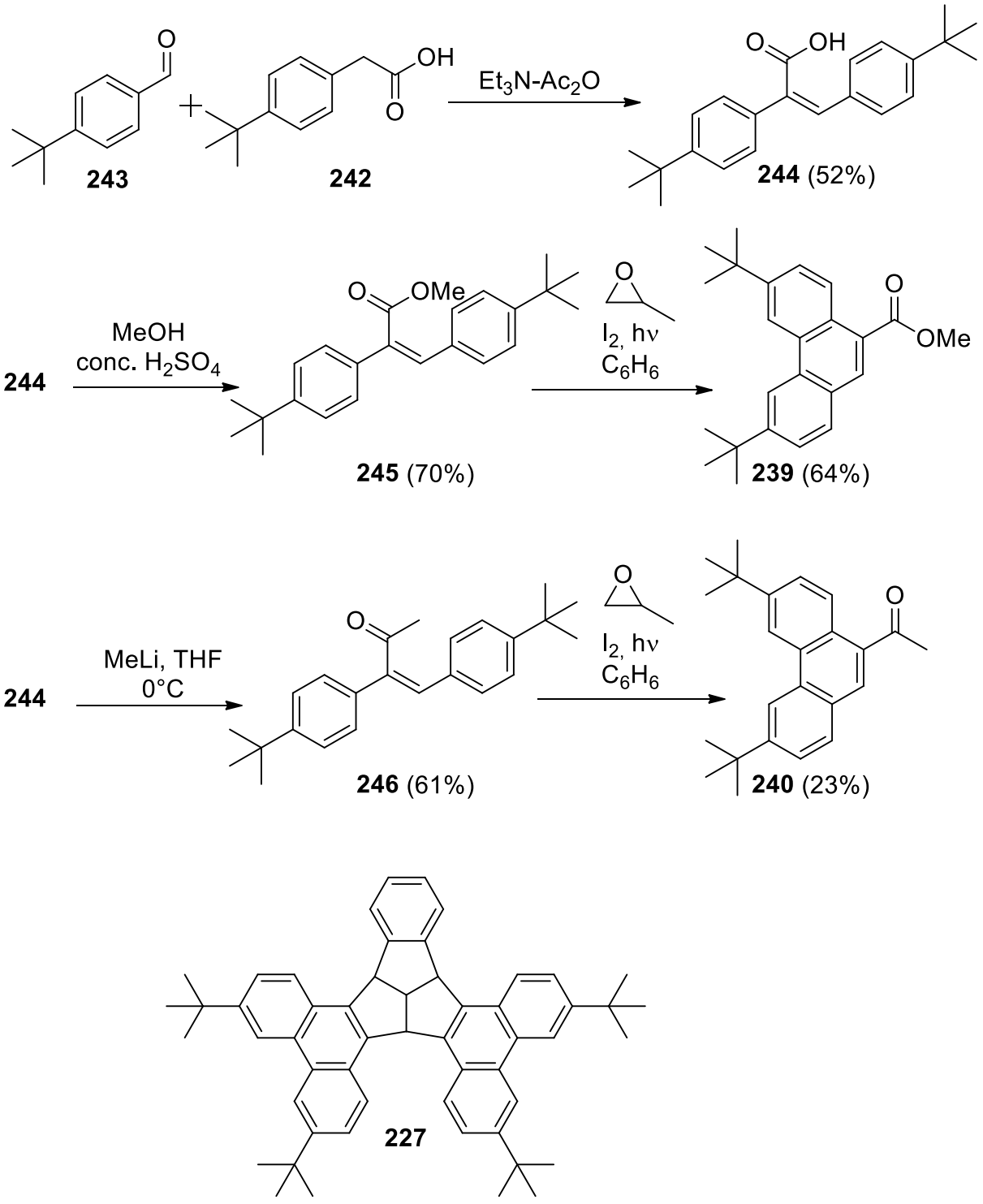

Figure 4.5 Summary of synthesis pathway for **239** and **240**, plus synthetic aim TBTQ **227**.

In addition, TBTQ **102** was isolated (Figure 4.6) and an x-ray crystal structure was obtained of this molecule. The packing arrangement of TBTQ **102** is comprised of stacks, where molecules are aligned exactly one above the other within a stack, but neighbouring stacks are orientated with the bowl opening in opposite directions. In contrast, the unsubstituted

TBTQ **68** forms columnar stacks in which neighbouring molecules within the stack are alternately rotated by ±6 and all stack align to the c-axis.

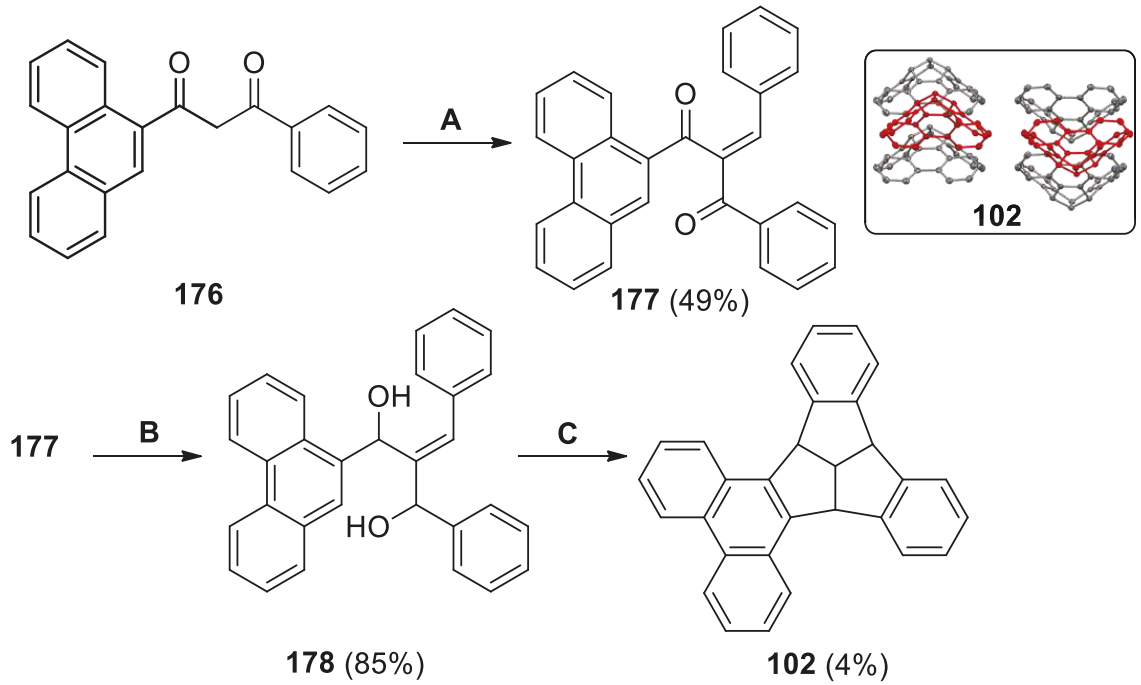

Figure 4.6 Synthesis of TBTQ **102** and molecular stacking of TBTQ **102**.
A: benzaldehyde, butanoic acid, piperidine, toluene, 30 min; **B**: $CeCl_3 \cdot 7\ H_2O$, $NaBH_4$, CH_2Cl_2, MeOH, 3 h; **C**: polyphosphoric acid, chlorobenzene, 22 h.

4.4 Functionalisation of the *meta*-position: Borylation and extension of TBTQ with phenanthrene moieties

Functionalisation of the *meta*-positions can be used for extension of the carbon network. Borylation offers the advantage of partial regioselectivity, due to its steric bulk hindering further reactions at directly adjacent positions, as well as the advantage of late-stage functionalisation. The goal to synthesise TBTQ **106** (Figure 4.7) via a post-functionalisation method was achieved, via triple borylation, followed by SUZUKI coupling and finally a C-C coupling with PIFA / $BF_3 \cdot Et_2O$. The final coupling step is low yielding (6%) but suitable crystals for x-ray analysis were obtained from the slow evaporation of CD_2Cl_2.

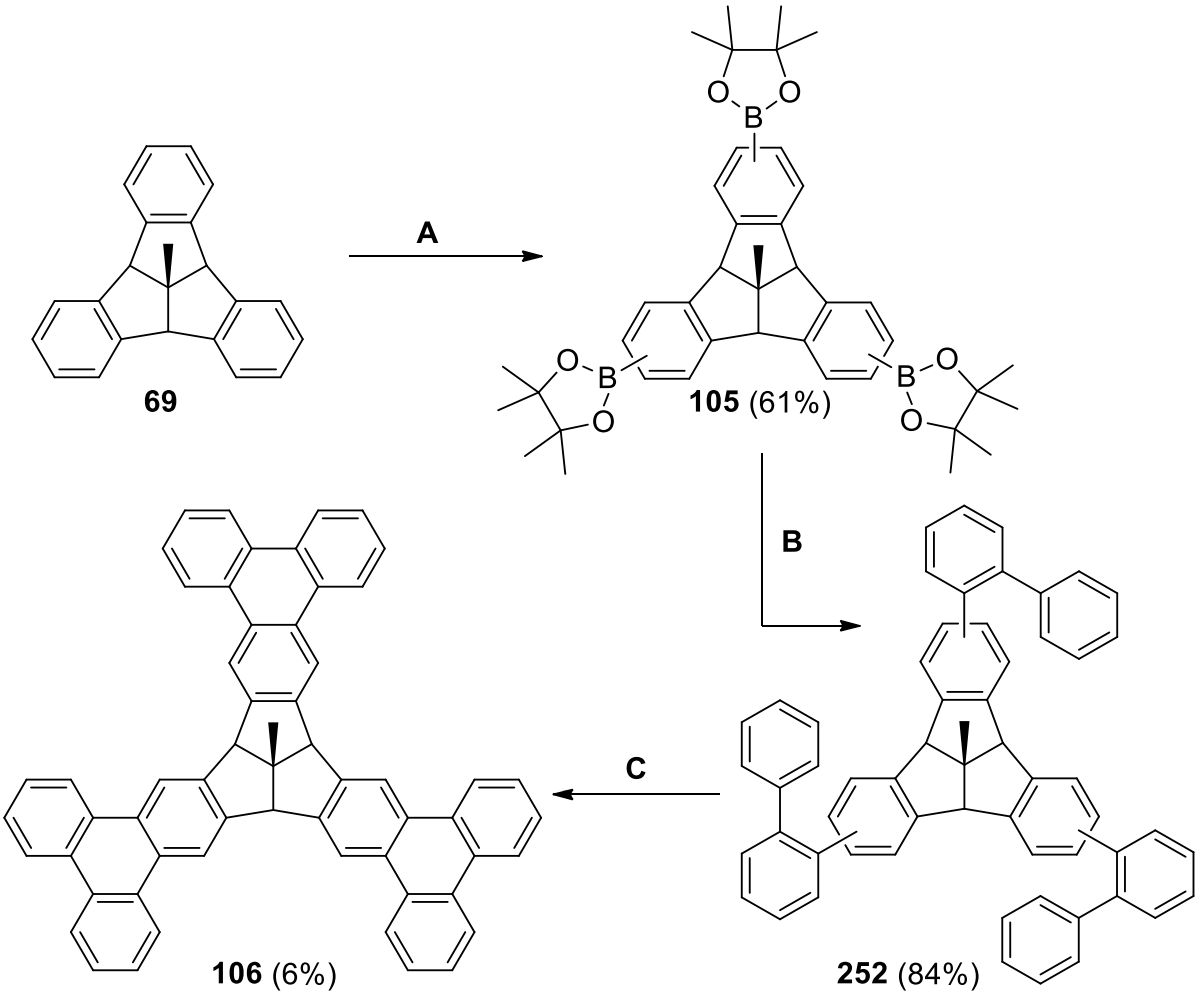

Figure 4.7 Synthesis of TBTQ **106**.
A: $[Ir(OMe)COD]_2$, $B_2(pin)_2$, *t*-BuOK, dtbpy, THF, 85°C; **B**: 2-bromobiphenyl, $Pd_2(dba)_3 \cdot CHCl_3$, SPhos, Cs_2CO_3, toluene/H_2O; **C**: PIFA/$BF_3 \cdot Et_2O$, CH_2Cl_2, -78°C.

Worthy of note is the asymmetry of the crystal structure, resulting from convex–convex π–π stacking of phenanthrene groups in neighbouring TBTQ molecules. The intermolecular π–π distance of closest rings on convex faces is 3.7 Å. A consequence of this interaction is that the triquinacene core is distorted and the bond angle between a pair of quinacene rings, which deviates from the value 113.53° for TBTQ **69**: 117.82°, 111.20° and 113.89° for TBTQ **106**. As a result, the indane wings of TBTQ **106**. are no longer aligned perpendicularly to each other, unlike the parent system TBTQ **69**.

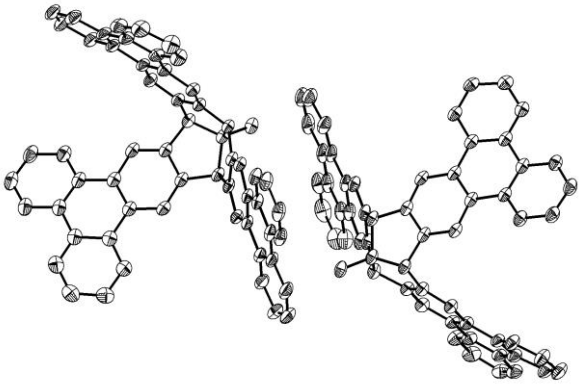

Figure 4.8 π–π stacking interaction of TBTQ **106**.

A valuable extension to this work would be to investigate the arrangement of TBTQ **106** on a Ag(111) surface, as interaction with the metal surface is expected to lead to a different arrangement compared to the measured x-ray crystal structure. In order to synthesise adequate material, either the PIFA / $BF_3 \cdot Et_2O$ reaction needs further optimisation, or a more efficient synthesis is required.

One alternative reaction worth pursuing is the one-step annulative π-extension (APEX) as demonstrated for introducing one phenanthrene group to corannulene by ITAMI and SEGAWA.[111] This palladium catalysed reaction would offer the advantage of achieving TBTQ **106** in one step (Figure 4.9), although examples of multiple APEX annulative extensions are currently restricted to pryrene derivatives as the starting point.[110,112] A second possibility is the SUZUKI coupling of borylated TBTQ **105** with chlorinated biphenyls to give TBTQ **261**, followed by Pd-catalysed C-H arylation (Figure 4.9). Such a method has been employed by SEGAWA and ITAMI *et al.* for suitably functionalised corannulene derivatives.[117,353]

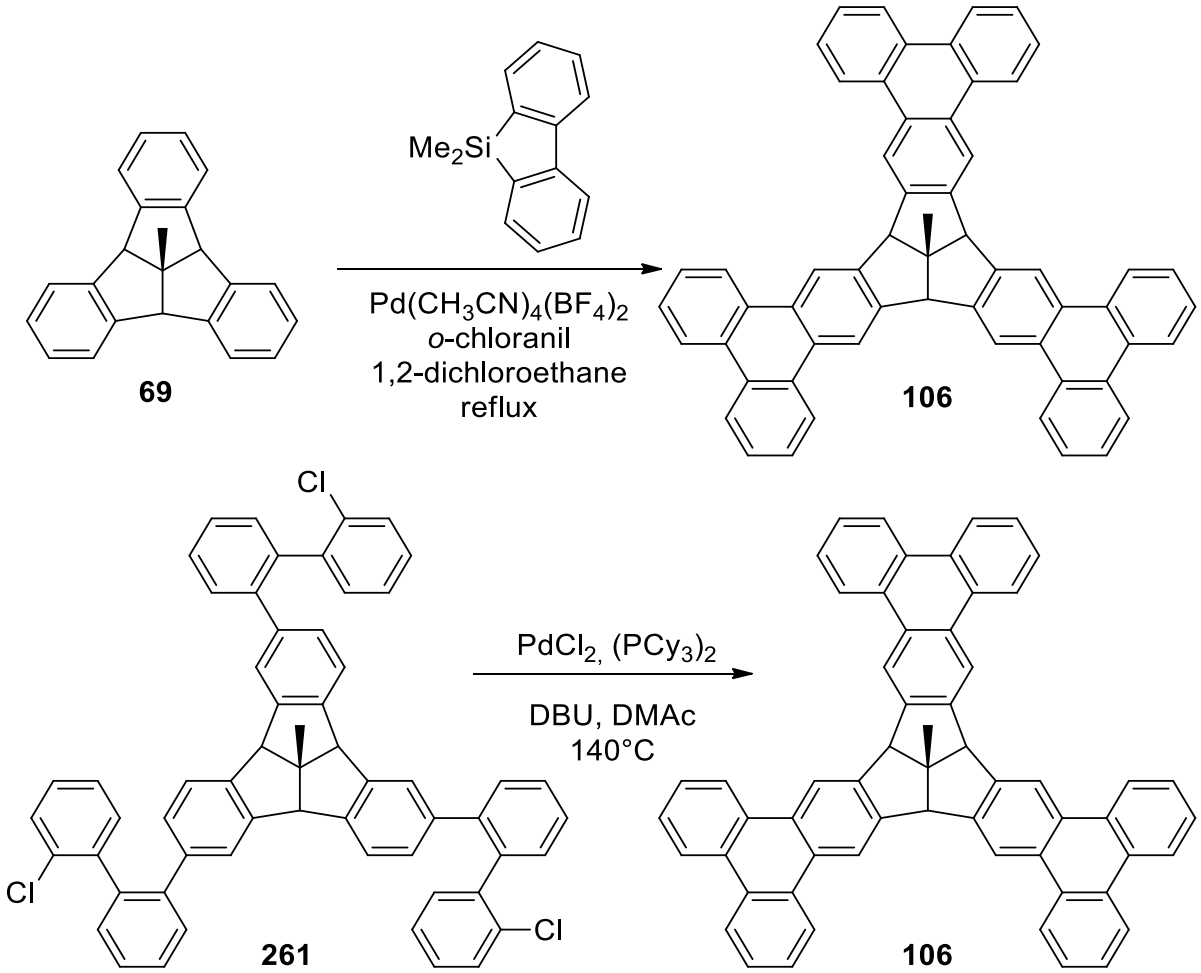

Figure 4.9 Proposed APEX and Pd-Arylation strategies to synthesise TBTQ **106**.

In summary, this work explored *centro*, *ortho* and *meta* functionalised TBTQs. The first STM images of H-TBTQ **68** and Me-TBTQ **69** with low surface coverage and a windmill-like arrangement of H-TBTQ **68** at high coverage both on a Ag(111) substrate were presented. Such an packing was not observed for Me-TBTQ **69**, highlighting that *centro*-functionalisation directly affects the relative orientation and arrangement of molecules on a metal substrate.

Additionally, the first fluorinated TBTQs were synthesised. The *ortho*-monofluorinated TBTQ **100** was achieved from suitable precursors. The synthesis of *ortho*-trifluorinated TBTQs proved to be more challenging, as the presence of multiple fluorine atoms alters the reactivity significantly, leading to several side-reactions which need to be taken into account for future projects. This work provides the foundation for a promising class of fluorinated TBTQ derivatives.

Moreover, further progress was made in the area of phenanthrene functionalised TBTQs: DBPTQ **102** was synthesised and the crystal structure analysis provided a valuable insight into the effect of phenanthrene groups on the stacking arrangements of the molecules. *tert*-Butyl phenanthrenes were also synthesised for the first time, in preparation for further work on *tert*-butyl functionalised phenanthrenes and their influence on the SCHOLL reaction when incorporated into a TBTQ scaffold.

Finally, borylation of TBTQ **69** led to its successful extension of the conjugated π system with three phenanthrene groups. The crystal structure of TBTQ **106** showed an arrangement of molecules, probably to maximise π–π and C-$H^{Me\cdots}$π interactions, which led to a distortion of the triquinacene core. STM investigations would provide a valuable insight into the extension of TBTQs with phenanthene groups.

5 Zusammenfassung und Ausblick

Der Synthese gekrümmter Aromaten bietet Potential, durch selektive Funktionalisierung die elektronischen Eigenschaften gezielt zu optimieren. Die Reaktivität der nicht-planaren Aromaten steigt aufgrund einer verschlechterten Überlappung der π-Orbitale und die dadurch energetisch niedrigeren LUMOs.

TBTQ verfügt über drei zentrale fünfgliedrige Ringe, wodurch sich dieses Molekül sehr gut zur Simulation als Defektzentrums einer Nanographen eignet. Außerdem ermöglichen die verschiedene Positionen *centro*, Brückenkopf, *ortho* und *meta* eine selektive Funktionalisierung, unter der Voraussetzung dass eine geeignete Auswahl von Ausgangsmolekülen und Schutzgruppen getroffen wird.

In der vorliegenden Arbeit wurden Beiträge zu dieser selektiven Funktionalisierung geliefert, um die physikalischen und elektronischen Eigenschaften von TBTQ zu ändern.

5.1 Einfluss der Funktionalisierung der *centro*-Position: STM Untersuchungen von TBTQs

Das erste Kapital beschreibt die Arbeiten an der *centro*-Position. Hochgeordnete Einzelschichten des TBTQ **68** und TBTQ **69** wurden im Ultrahochvakuum auf ein Ag(111)-Substrat gebracht und mittels Rastertunnelmikroskopie (STM) untersucht. Es konnte gezeigt werden, dass die Wechselwirkungen zwischen den organischen Verbindungen und der Metalloberfläche die Orientierung und die Anordnung benachbarter Moleküle beeinflusst. Dies konnte mit Kristallstrukturdaten allein nicht festgestellt werden, was zeigt, dass mit mikroskopischen Verfahren ein wertvoller Einblick in das Verhalten schalenförmiger Moleküle gewonnen werden kann.

Von niedriger bis moderater Flächenabdeckung werden beide schalenförmigen Moleküle mit der Schalenöffnung in Richtung Substrat gerichtet, adsorbiert. Zwei Orientierungen sind zu beobachten, die jeweils um 14° von der Hochsymmetrieachse weggedreht sind. Bei hoher Flächenabdeckung beherrschen erweiterte Inseln einer selbstangeordneten windmühlenartigen Struktur mit nanometergroßen Öffnungen in regelmäßigen Abständen. Diese windmühlenartige Nanostrukutr wurde nicht für Me-TBTQ **69** beobachtet, das bei hoher Flächenabdeckung stattdessen sofort Doppelschichten bildet. Weitere Untersuchungen, um die Bildung und Anordnung der windmühlenartigen Nanostruktur zu erkunden, und ein

besseres Verständnis der intermolekularen und Molekül-Substrat-Wechselwirkungen könnte die Konstruktion mehrlagigen Nanostrukturen ermöglichen.

5.2 Funktionalisierung der *ortho*-Position: Synthese fluorierter TBTQs

Die Fluorierung der Aromaten ist für die Beeinflussung elektronischer Eigenschaften vorteilhaft, beispielsweise im Hinblick auf die Herstellung von Elektronenakzeptoren für organische Halbleiter. Als Konzeptnachweis wurde die erste Synthese *ortho*-fluorierter TBTQs entwickelt. In Anlehnung an die Dreifach-Zyklisierung von HOPF *et al.*,[202,207] wurde das einfach fluorierte TBTQ **101** in drei Schritten aus kommerziell erhältlichen Ausgangsmaterialen hergestellt (Abb. **5.1**). Die Ausbeute des letzten Zyklisierungschritts betrug zwar nur 14%, aber eine vollständige Charakterisierung konnte dennoch erfolgreich durchgeführt werden.

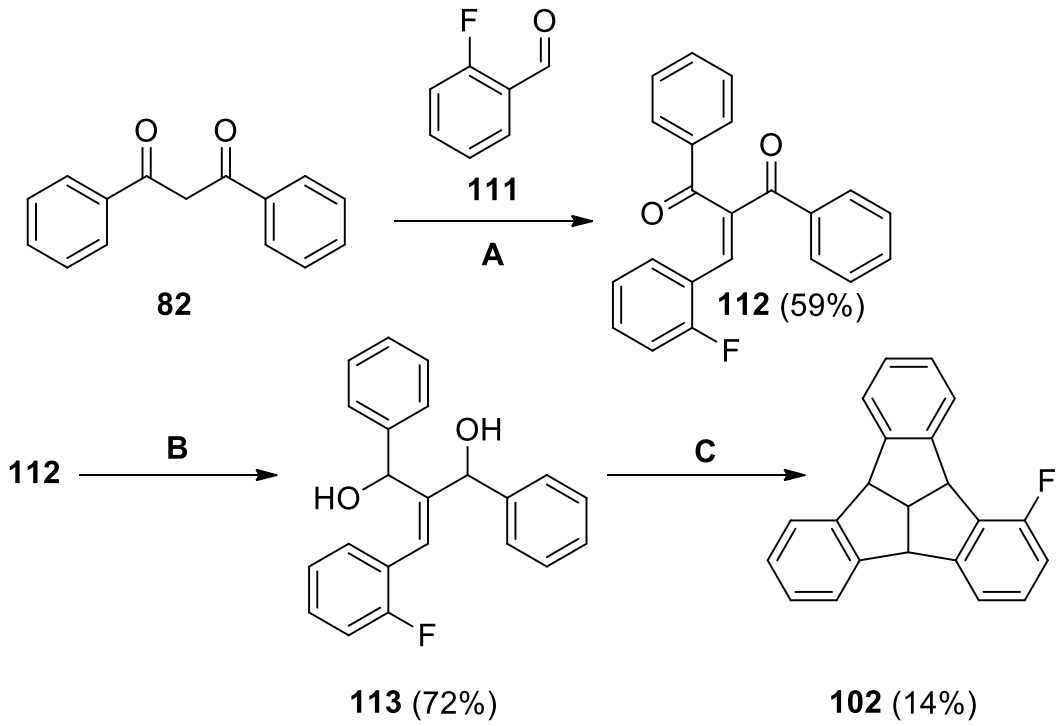

Abb. 5.1 Synthese von TBTQ **101**.
A: Piperidin, Acetonitril, 80°C; **B**: $CeCl_3 \cdot 7\ H_2O$, $NaBH_4$, $MeOH/CH_2Cl_2$;
C: Polyphosphorsäure, Chlorbenzol.

Die Fluoratome ändern die Reaktivität der TBTQ-Vorstufen signifikant, was durch die Entstehung des Nebenprodukts Chromenon (**121**) während der KNOEVENAGEL-Kondensation hervorgehoben wird (Abb. **5.2**). Deshalb wurde ein alternativer Ausgangsstoff (Diketon **133**; Abb. **5.3**) für weitere Reaktionen benutzt.

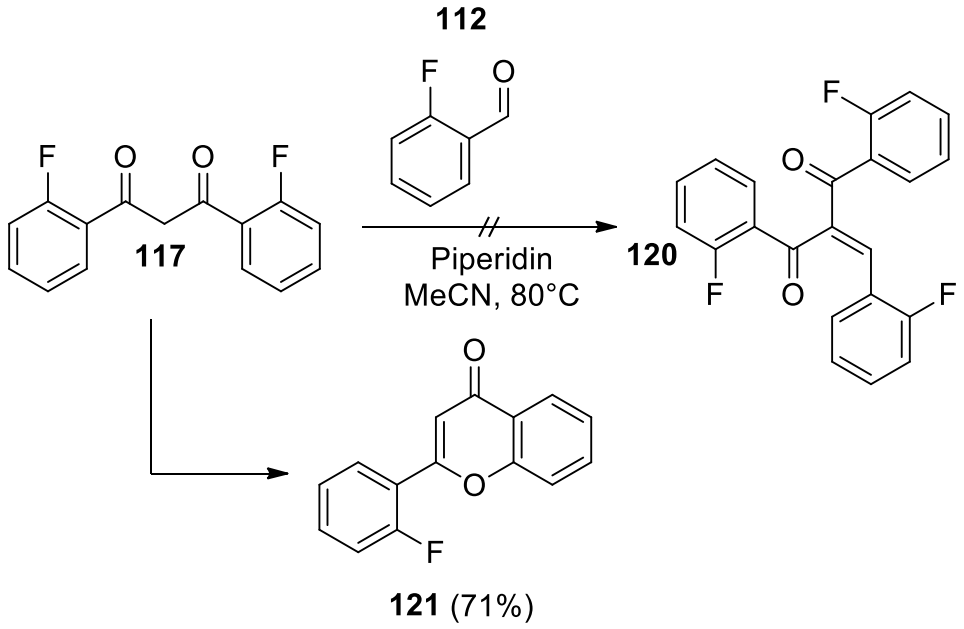

Abb. 5.2 Synthese von Chromenon (**121**).

Der letzte Reaktionsschritt ergab verschiedene Produkte: Das C_1-symmetrische TBTQ **164**, das Nebenprodukt **154** und ein TBTQ-Isomer mit C_3-Symmetrie, bei welchem es sich vermutlich um TBTQ **155** handelt. Diese Schlussfolgerung basiert auf der Auswertung von ^{1}H-^{1}H-COSY-Daten und der Anwesenheit von Nebenprodukt **154**, welches sich aus derselben kationischen Zwischenstufe wie **155** bildet. Die Rotation der aromatischen Ringe während der Zyklisierung führt zur Bildung des C_1-symmetrischen TBTQ **164**, welches aufgrund der elektrostatischen Abstoßung zwischen den Fluoratomen und den benachbarten β-Hydroxylgruppen gebildet werden könnte. Die Optimierung der Trennung der C_3- und C_1-Isomere war ein wichtiger erster Schritt, so dass die Identität des C_3-Isomers bestätigt werden konnte. *ortho*-C_3-dreifachfluoriertes TBTQs sind vielversprechende Kandidaten für weitere Kupplungsreaktion, wohingegen *meta*-C_3-dreifachfluorierte TBTQs zum Aufbau supramolekularer Gerüste verwendet werden könnten.

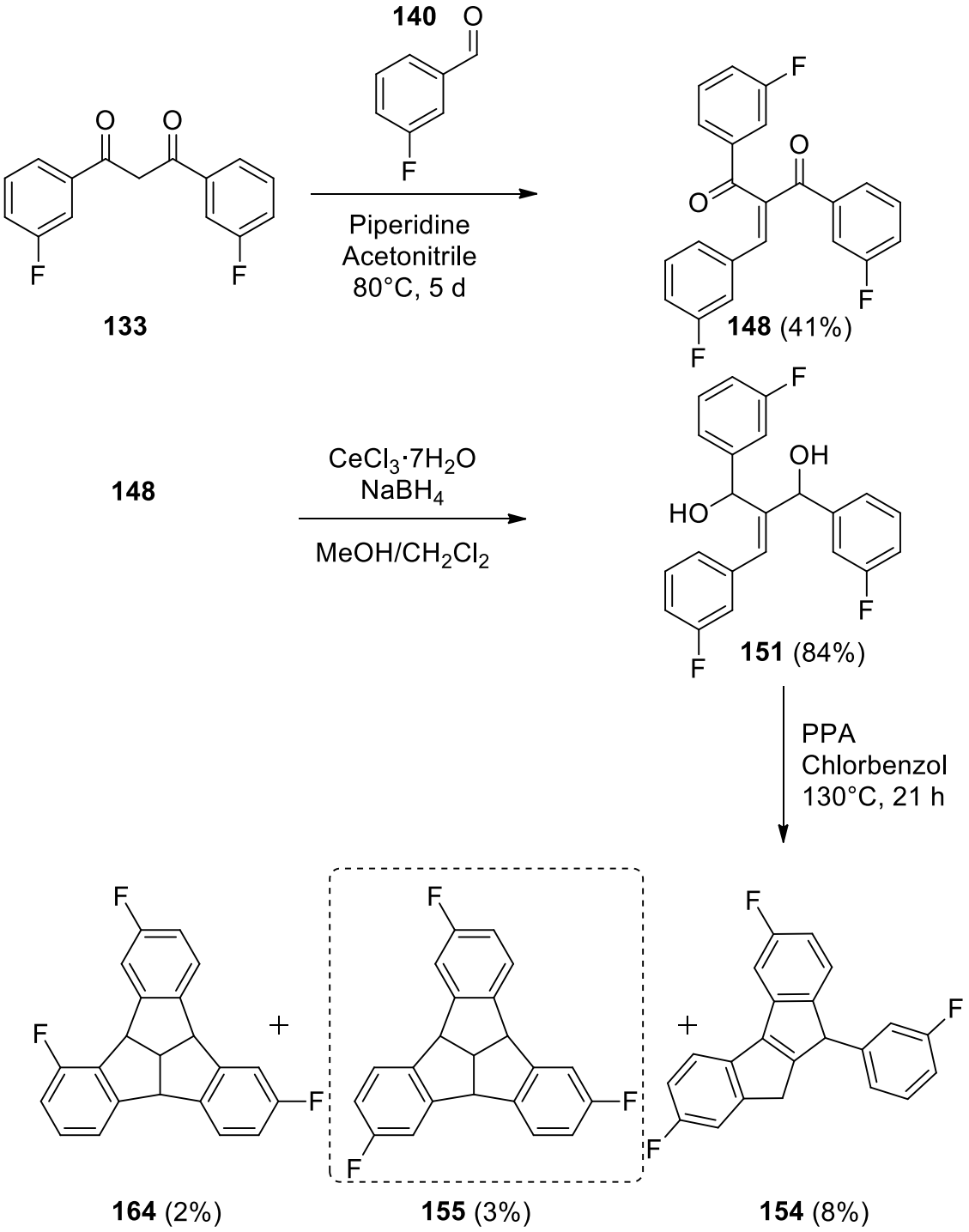

Abb. 5.3 Synthese von fluorierten Verbindungen.

5.3 Funktionalisierung der *ortho*-Position: Synthese von Phenanthreno-TBTQs und Untersuchung ihrer Stapelordnung

In Kapitel 3.3 wurde die Identität des TBTQ **171** bestätigt (Abb. **5.4**). Diese Information weist darauf hin, dass die Reaktivität der Brückenkopfpositionen während der Syntheseplanung beachtet werden muss. Trotzdem würde die Einführung von Schutzgruppen an dieser Stellen geplante Kupplungsreaktionen an den *ortho*-Positionen hindern.

Mehrere Veröffentlichungen beschreiben den Einfluss der Methoxy- und *tert*-Butyl-Gruppen während der SCHOLL Kupplungsreaktion, beispielsweise um die Kupplung zu ermöglichen und unerwünschte Nebenreaktionen zu verhindern. Trotz gründlicher Prüfung mit mehreren Basen fand die basenkatalysierten CLAISEN-Kondensation nicht statt, obwohl die Reaktion erfolgreich mit Phenanthren ohne Methoxygruppen durchgeführt worden ist.

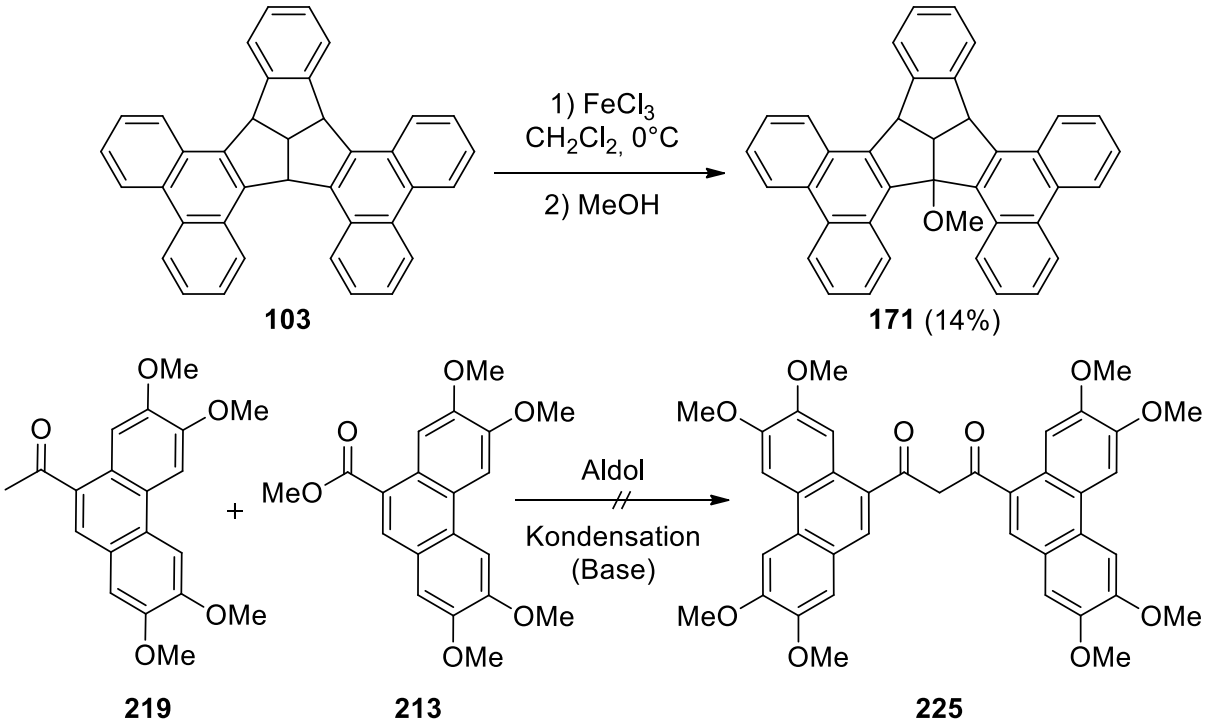

Abb. 5.4 Synthese von TBTQ **171**.

tert-Butylfunktionalisierte Phenanthrene **239** und **240** wurde erfolgreich hergestellt (Abb. **5.4**), sodass die Synthese des TBTQs **227** in weiteren Arbeiten erreicht werden könnte.

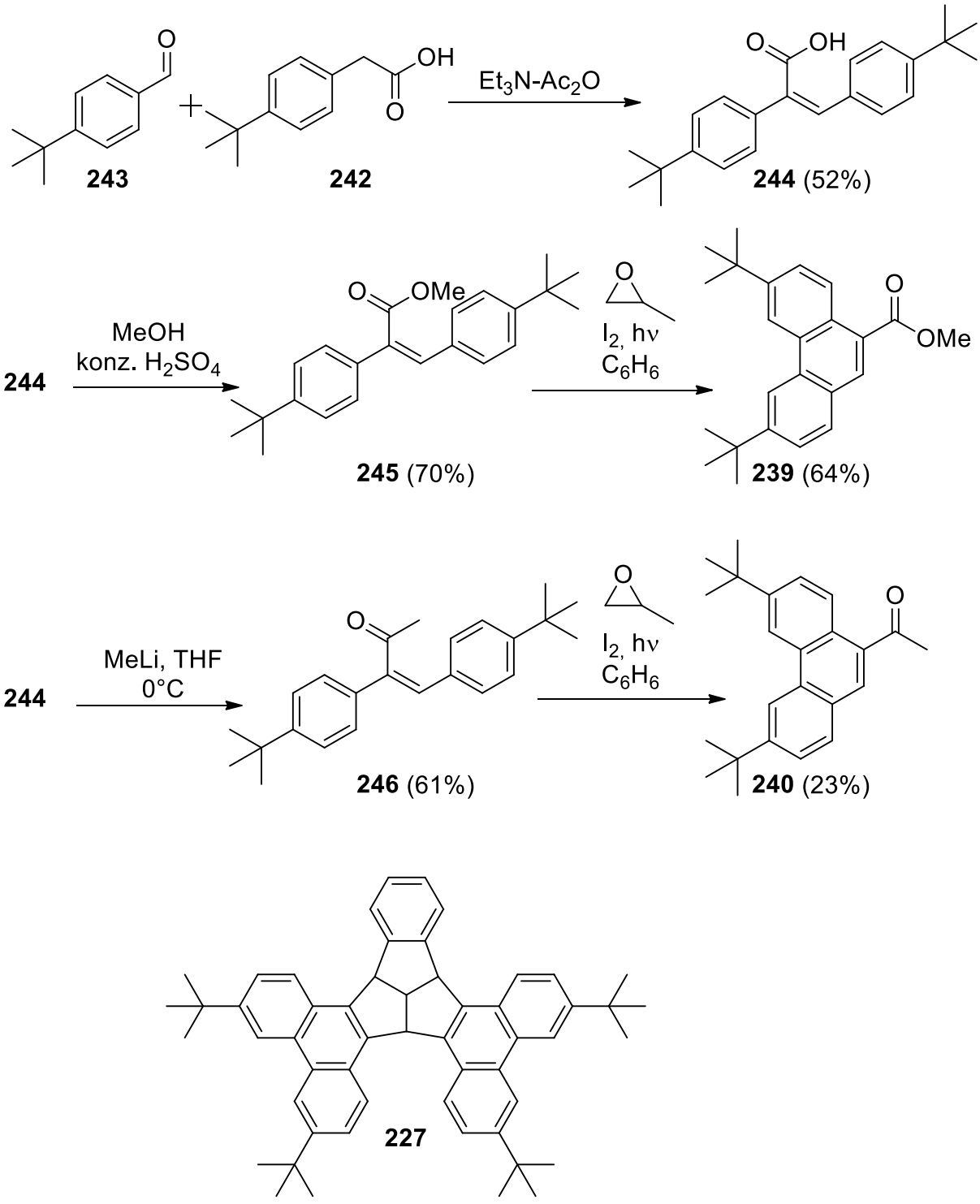

Abb. 5.5 Synthese von **239** und **240**. Das Syntheseziel TBTQ **227** ist unten dargestellt.

Zusätzlich wurde TBTQ **102** isoliert (Abb. **5.6**) und eine Kristallstruktur wurde mittels Röntgenstrukturanalyse für dieses Molekül erhalten. Die räumliche Anordnung erfolgt stapelförmig, wobei die Moleküle innerhalb eines Stapels exakt übereinander angeordnet sind und sich die schalenförmigen Öffnungen der Moleküle benachbarter Stapel in entgegengesetzte Richtungen orientieren. Im Gegensatz dazu formt das unsubstituierte TBTQ **68** säulenförmige

Stapel, in welchen benachbarte Moleküle innerhalb eines Stapels abwechselnd um ±6° gedreht sind und sich jeweils genau an der C-Achse anordnen.

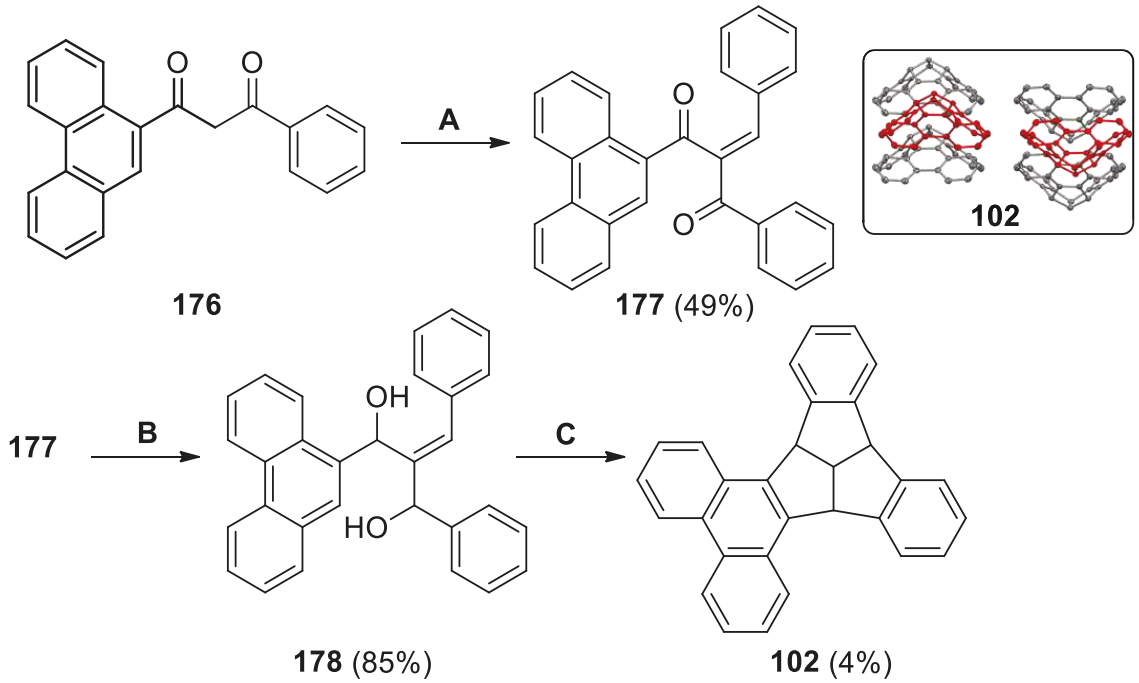

Abb. 5.6 Synthese und Anordnung molekularer Stapel von TBTQ **102**.
A: Benzaldehyd, Buttersäure, Piperidin, Toluol, 30 min; **B**: $CeCl_3 \cdot 7\ H_2O$, $NaBH_4$, CH_2Cl_2, MeOH, 3 h; **C**: Polyphosphorsäure, Chlorbenzol, 22 h.

5.4 Funktionalisierung der *meta*-Position: Borylierung und Erweiterung von TBTQ mit Phenanthrengruppen

Schließlich wurde durch Funktionalisierung der *meta*-Positionen das Kohlenstoffgerüst erweitert. Die Borylierung bietet den Vorteil eines gewissen Maßes an Regioselektivität, weil die benachbarten Positionen sterische Hinderung ausüben und darüber hinaus eine Funktionalisierung in einem späteren Syntheseschritt ermöglichen. Das Ziel, TBTQ **106** darzustellen, wurde erreicht. Als erstes wurde eine dreifache Borylierung durchgeführt, danach eine SUZUKI-Kupplung und als letztes eine C-C Kupplung mit PIFA / $BF_3 \cdot Et_2O$. Im letzten Schritt betrug die Ausbeute 6%, ergab aber nachdem langsamen Verdampfen von CD_2Cl_2 geeignete Kristalle für eine Einkristall-Röntgenstrukturanalyse.

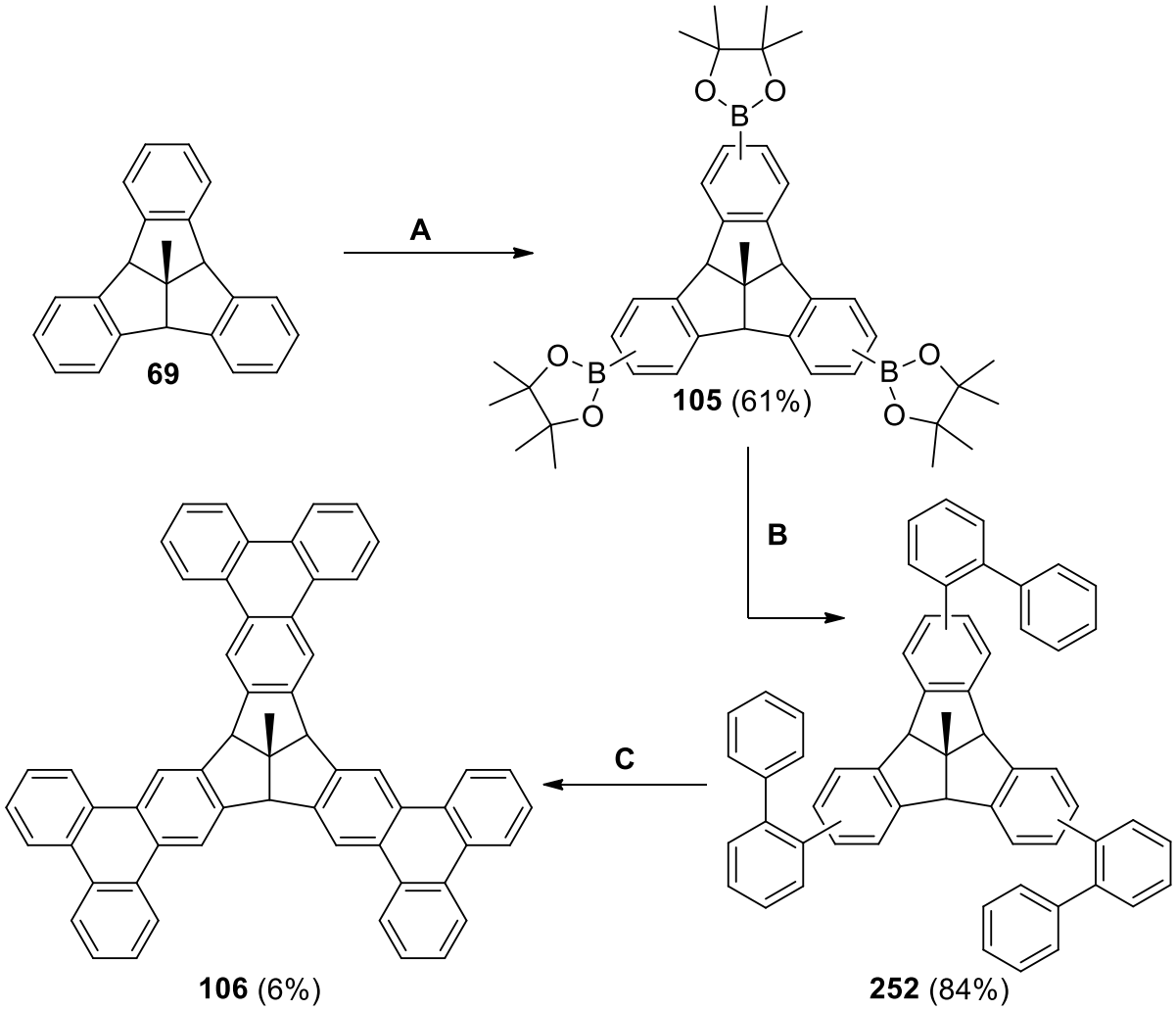

Abb. 5.7 Synthese von TBTQ **106**.
A: $[Ir(OMe)COD]_2$, $B_2(pin)_2$, *t*-BuOK, dtbpy, THF, 85°C; **B**: 2-Brombiphenyl, $Pd_2(dba)_3 \cdot CHCl_3$, SPhos, Cs_2CO_3, Toluol/H_2O; **C**: PIFA/$BF_3 \cdot Et_2O$, CH_2Cl_2, -78°C.

Beachtenswert ist die Ungleichmäßigkeit der Kristallstruktur als Folge von konvex-konvexen π–π-Stapeln des Phenanthrens zwischen benachbarten TBTQ-Molekülen. Der Abstand zwischen den Phenanthren Einheiten ist 3.7 Å. Demzufolge verzerrt sich der Triquinacen-Kern, was zur Folge hat Abweichungen der Bindungswinkel zwischen je zwei fünfgliedrigen Ringen für TBTQ **106**. Diese betragen 117.82°, 111.20° und 113.89° im Vergleich zum Wert von 113.53° für TBTQ **69**. Entprechend ordneten sich die Indan-Einheiten des TBTQ **106** nicht mehr senkrecht zu einander und wichen so ebenfalls von TBTQ **69** ab.

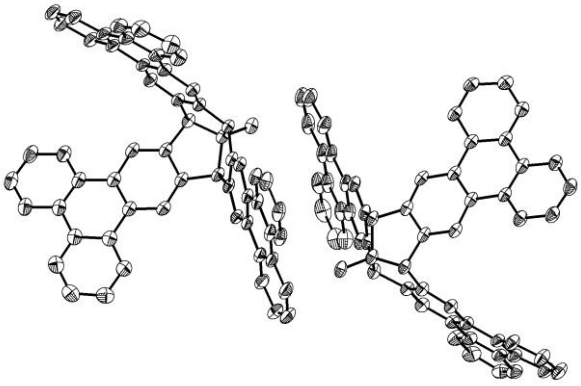

Abb. 5.8 π–π Stapel von TBTQ **106**.

Eine wertvolle Fortführung dieser Arbeit wäre die Untersuchung der Anordnung von TBTQ **106** auf einer Ag(111)-Oberfläche, weil die Wechselwirkung zwischen diesem Molekül und der Oberfläche wahrscheinlich zu einer anderen Anordnung als im Kristallführen würde. Um ausreichende Mengen an TBTQ **106** herzustellen, muss entweder die Reaktion mit PIFA / $BF_3 \cdot Et_2O$ optimiert werden oder eine effiziente anderweitigen Synthese entwickelt werden.

Eine sinnvolle Möglichkeit wird von der „one-step annulative π-extension“ (APEX) geboten, mit der ITAMI and SEGAWA das Hinzüfugen einer einzelnen Phenanthren-Gruppe zu Corannulen (**107**) demonstrierten.[111] Diese Pd-katalysierte Reaktion ist vorteilhaft, weil TBTQ **106** in einem Schritt synthetisiert werden könnte (Abb. **5.9**), obwohl sich die Beispiele von mehrfachen APEX-Schritten bisher auf Pyrenderivate beschränken.[110,112] Eine zweite Alternative präsentiert sich in Form einer SUZUKI-Kupplung des bereits borylierten TBTQs **105** mit chlorierten Biphenylen. Als Produkt entsteht TBTQ **261**, das nach einer Pd-katalysierten C-H Arylierung das TBTQ **106** ergibt (Abb. **5.9**). SEGAWA and ITAMI *et al.* haben bereits diese Strategie für verschiedene Corannulen-Derivate benutzt.[117,353]

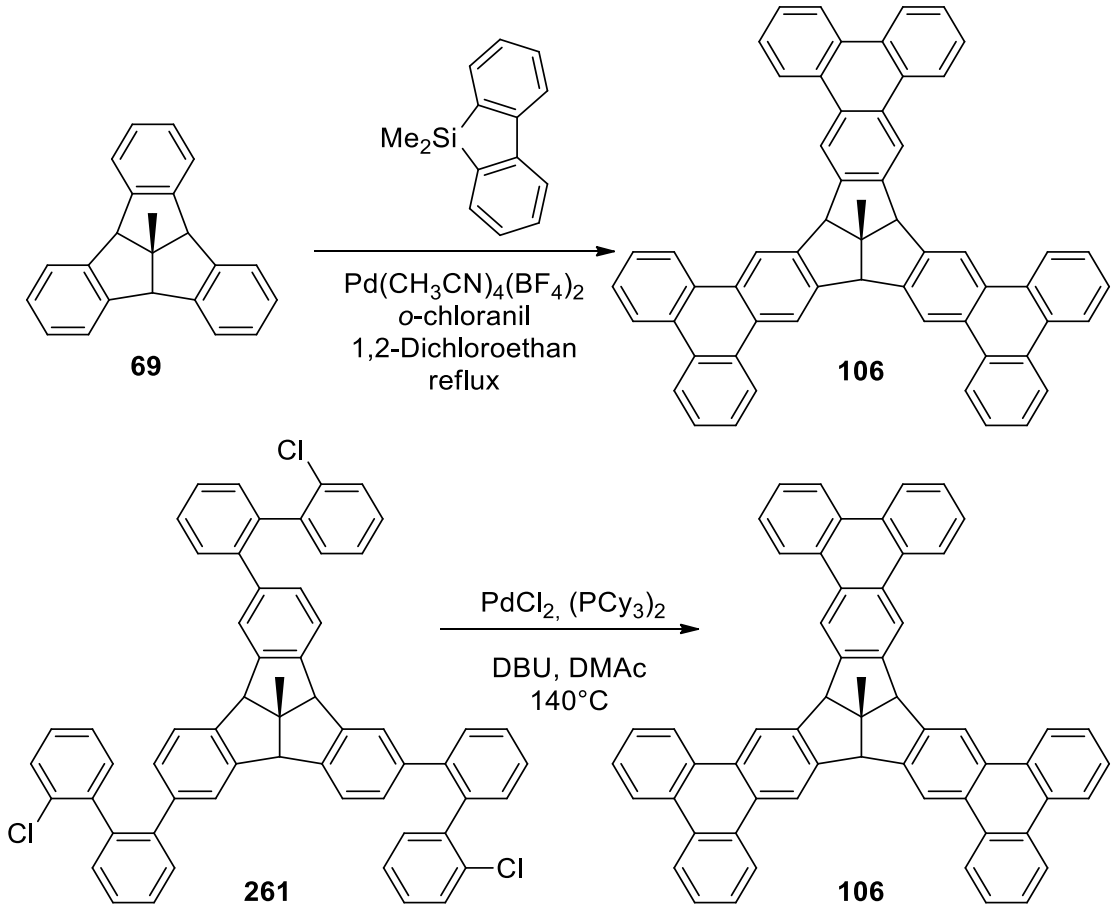

Abb. 5.9 Vorschlag für APEX und Pd-Arylierungstrategien, um TBTQ **106** herzustellen.

Zusammenfassend wurden in dieser Arbeit *centro*-, *ortho*- und *meta*-funktionalisierte TBTQs untersucht. Die ersten STM-Bilder von H-TBTQ **68** und Me-TBTQ **69** mit niedriger Oberflächenbelegung und eine windmühlenartige Anordnung von H-TBTQ **68** mit hoher Oberflächenbelegung jeweils auf einem Ag(111)-Substrat wurden vorgestellt. Eine ähnliche Anordnung wurde für Me-TBTQ **69** nicht beobachtet, was zeigt, dass die *centro*-Funktionalisierung direkt die relative Orientierung und Ausrichtung der Moleküle auf Metallsubstraten beeinflusst.

Zusätzlich wurden die ersten fluorierten TBTQs synthetisiert. Das *ortho*-monofluorierte TBTQ **100** wurde durch geeignete Vorstufen erreicht. Die Synthese von *ortho*-trifluorierten TBTQs war herausfordernder, da die Anwesenheit mehrerer Fluoratome die Reaktivität signifikant beeinflusst, was zu verschiedenen Nebenreaktionen führt, die für zukünftige Projekte berücksichtigt werden müssen. Diese Arbeit legt den Grundstein für eine vielversprechende Klasse fluorierter TBTQ-Derivate.

Zudem wurde weiterer Fortschritt im Bereich der phenanthrenfunktionalisierten TBTQs gemacht: DBPTQ **102** wurde synthetisiert und dessen Kristallstrukturanalyse lieferte wertvolle

Erkenntnisse über den Einfluss von Phenanthrengruppen auf die Stapelanordnung der Moleküle. *tert*-Butylphenanthrene wurden ebenfalls erstmals dargestellt, was den Grundstein für weitere Arbeiten an *tert*-butylfunktionalisierten Phenanthrenen und ihren Einfluss auf die SCHOLL-Reaktion innerhalb von TBTQ-Gerüsten legt.

Schließlich führte die die Borylierung von TBTQ **69** zu dessen erfolgreicher Erweiterung des konjugierten π-Systems mit drei Phenanthrengruppen. Die Kristallstruktur von TBTQ **106** zeigte eine Anordnung der Moleküle, die wahrscheinlich die π-π- sowie C-$H^{Me\cdots}$π-Wechselwirkungen maximierte, was zu einer Verzerrung des Triquinacenkerns führte.

6 Experimental Section

6.1 General methods

Chemicals: Commercial chemicals from Acros Organics, Alfa Aesar, Fluka, Merck or Sigma Aldrich were used without further purification, unless stated otherwise. Solvents were distilled or dried before use, using standard procedures. Dried solvents were used immediately after distillation. Nitrogen and argon (purity: 99.99990%) were used from Linde, which were dried using calcium chloride and silica gel.

Vacuum pumps: Vacuubrand diaphragm pumps and Leybold oil pumps of different kinds were used.

Melting points: Melting points were measured using a Reichert Austria Kofler Heizbank or an Optimelt MPA 100 (>350°C) and are un-corrected.

NMR spectroscopy: ^{1}H and ^{13}C spectra were measured using a Bruker AVANCE 400 FT-NMR-Spectrometer (^{1}H: 400 MHz, ^{13}C: 100 MHz) and a Bruker DMX 600 FT-NMR-Spectrometer (^{1}H: 600 MHz, ^{13}C: 150 MHz). Chemical shifts (δ) are listed in parts per million (ppm) and are reported relative to internal standards. The internal standard came from the deuterated solvents used:

^{1}H: $CDCl_3$ δ = 7.26, $(CD_3)_2CO$ δ = 2.05, CD_2Cl_2 δ = 5.32.

^{13}C: $CDCl_3$ δ = 77.16, $(CD_3)_2CO$ δ = 29.84. ^{13}C: $CDCl_3$ δ = 77.16, $(CD_3)_2CO$ δ = 29.84, CD_2Cl_2 δ = 53.84.

Coupling constants (*J*) are quoted in Hertz (Hz). The following abbreviations are used to describe nuclear spin coupling: s: singlet, br s: broad singlet, d: doublet, br d: broad doublet, t: triplet, q: quartet, and m: multiplet. ^{13}C NMR, DEPT and standard two-dimensional techniques (COSY, HSQC, HMBC, NOESY) were used to assign the spectra. Deuterated chloroform was filtered through neutral aluminium oxide before sample preparation.

TLC: Thin layer chromatography was carried out using Merck TLC-aluminium coated silica 60 F254 plates (thickness: 0.2 mm) and suitable TLC stains were used when necessary.[354] Column chromatography was carried out using compressed air, Merck Geduran Si 60 silica gel (40–63 µm) using columns of different sizes and lengths. Solvent mixtures are given in volume percent (v/v).

Column chromatography: Silica gel from Merck was used (particle size 0.04-0.063 mm) was used and columns of varying sizes and widths were used. Solvent mixtures are given in volume percent (v/v).

MPLC: The following instruments were used: Büchi Pump Module C-605, Büchi Pump Manager C-615, Büchi UV Photometer C-635 and the Büchi Fraction Collector C-660. Flash cartridges were also used: Interchim SI-HP, 30 µm, F0040, Interchim PF-C18AQ, 30 µm, F0040. A LC-Preparative column was also used: Interchim Uptisphere US5SI, 5 µm, 250 mm × 21.2 mm.

HPLC: The following instruments were used: Jasco MD-2010 Plus Multiwavelength Detector, Jasco DG-2080-53 3-Line Degasser, Jasco LC-Net II/ADC, Jasco PU-2080 Plus Intelligent HPLC Pump. The following columns were used: Reprosil C-18-PQ-JASCO, 5 µm, 250 mm × 4 mm, Reprosil C-18-PQ-JASCO column, 5 µm, 250 mm × 10 mm and an Interchim Uptisphere US5SI silica column, 5 µm, 250 mm × 4.6 mm. HPLC solvents were used and given in volume percent (v/v). A rate of 3 ml/min was used for semi-preparative columns, and a rate of 1 ml/min was used for analytical columns.

UV/Vis spectroscopy: UV/Vis measurements were carried out using a Jasco V-630 spectrometer or Jasco V-770 spectrometer in 1 cm quarz cuvettes, using the solvents listed.

Mass spectromety: The following mass spectrometers were used:

Electronspray Ionisation (ESI): Bruker Daltonics micrOTOF Focus II.

Electron Ionisation (EI): Finnigan MAT Incos 500, MAT 90 Varian MS 320.

Atmospheric-pressure chemical ionization (APCI) Bruker Daltonics micrOTOF Focus II.

All mass spectra were measured in the Institute for Organic Chemistry (Würzburg) and high resolution measurements are accurate to < 2 ppm (EI) and < 3 ppm (ESI, APCI).

FT-IR spectroscopy: FT-IR spectra were recorded with a Jasco FT-IR equipped with an ATR unit. The intensity of the adsorption bands is denoted: vs: very strong, s: strong, m: medium, and w: weak.

Elemental Analysis: Measurements for the determination of the chemical composition were carried out using an Elementar Vario Micro in the Institute for Inorganic Chemistry (Würzburg). V_2O_5 was added when necessary to aid combustion.

6.2 Synthesised molecules

6.2.1 Synthesis of H-TBTQ 68 and Me-TBTQ 69.

2-Benzylidene-1,3-diphenylpropane-1,3-dione (79)

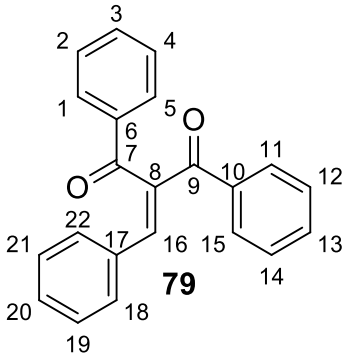

Dibenzoylmethane (**77,** 3.00 g, 13.4 mmol) and freshly distilled benzaldehyde **78** (2.84 g, 2.7 ml, 26.8 mmol) were dissolved in toluene (100 ml). Hexanoic acid (400 µl) and piperidine (170 µl) were added and the reaction mixture was heated to 125°C for 3 d using a DEAN-STARK trap. After cooling to room temperature the solution was washed with a saturated $NaHCO_3$ solution (100 ml), 5% AcOH (100 ml) and brine (100 ml). The aqueous phase was extracted with ethyl acetate (2 × 30 ml) and the combined organic phases were dried over Na_2SO_4. The solvent was removed *in vacuo* to afford orange oil, which was purified using column chromatography (silica, pentane/ethyl acetate 90:10) to afford the product as a viscous yellow oil. Traces of solvent were removed using Kugelrohrdestillation.

Yield: 2.74 g (8.78 mmol, 65%, lit.[207] 66%).

$\mathbf{R_f}$ = 0.18 (pentane/ethyl acetate 90:10).

^{1}H NMR (400 MHz, $CDCl_3$): δ = 7.96–7.99 (2H, m, 1,5-H), 7.86–7.89 (2H, m, 11,15-H), 7.59 (1H, t, ^3J = 7.4 Hz), 7.55–7.47 (4H, m, 3,12,14,16-H), 7.43–7.39 (2H, m, 2,4-H), 7.35–7.33 (2H, m, 18,22-H), 7.31–7.22 (3H, m, 19,20,21-H) ppm.

^{13}C NMR (100 MHz, $CDCl_3$): δ = 197.1 (C_q, C-7), 195.1 (C_q, C-9), 144.1 (C_t, C-16), 139.6 (C_q, C-8), 137.5 (C_q, C-10), 136.4 (C_q, C-6), 134.0 (C_t, C-3), 133.2 (C_q, C-17), 132.7 (C_t, C-13), 130.6 (C_t, *C*H), 130.2 (C_t, C-18,22), 129.7 (C_t, C-11,15), 129.5 (C_t, C-1,5), 129.0 (C_t, C-2,4), 128.9 (C_t, *C*H), 128.7 (C_t, C-12,14) ppm.

FT-IR (ATR): ϑ = 3060 (w, *ν*(C-H_{arom})), 1733 (w), 1671 (m, *ν*(C=O)), 1635 (m, *ν*(C=O)), 1597 (m, ν(C=C_{arom})), 1576 (w), 1493 (w), 1446 (w). 1373 (w), 1319 (w), 1259 (s), 1228 (vs),

1174 (w), 1115 (w), 1074 (w), 1026 (w), 978 (m), 933 (w), 872 (w), 758 (m), 733 (m), 688 (vs), 644 (w) cm^{-1}.

UV/Vis (CH_2Cl_2, lg ε): λ_{max} = 300 (4.06), 259 (4.15) nm.

MS (EI, 70 eV): m/z = 312 (M^+, 15%), 294 (36), 279 (20), 207 (23), 178 (15), 138 (3), 105 (100), 77 (54).

The spectroscopic data corresponded to the data reported in the literature.[202,207]

2-Benzylidene-1,3-diphenylpropane-1,3-diol (80)

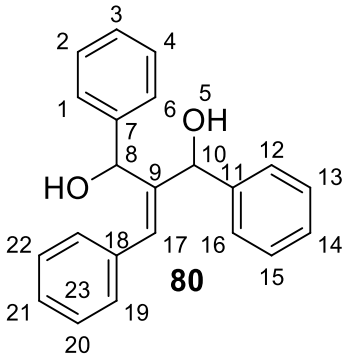

Diketone **79** (897 mg, 2.87 mmol) was dissolved in anhydrous CH_2Cl_2 (15 ml) and cooled to -78°C. $CeCl_3 \cdot 7\ H_2O$ (1.49 g, 4.02 mmol, 1.4 eq.) was dissolved in anhydrous MeOH (10 ml) and the resulting 0.4 M solution was added to the reaction mixture. After 15 min, $NaBH_4$ (228 mg, 6.03 mmol, 2.1 eq.) was added and the reaction stirred at -78°C for 30 min. The reaction was allowed to reach room temperature over the course of 1 h. TLC reaction control confirmed that the reaction was complete and Et_2O (30 ml) and 2 M HCl (15 ml) were added. The phases were separated and the aqueous phase was extracted with Et_2O (3 × 20 ml). The combined organic phases were washed with brine (20 ml), dried over $MgSO_4$ and the solvent was removed *in vacuo*. The resulting yellow oil was purified using column chromatography (silica, $CHCl_3$/ethyl acetate 98:2,) to afford the two isomers with a combined yield of 82% (lit.[207] 92%; *syn*:*anti*: 37%:55%): *syn*-**80** isomer as a colourless solid and the *anti*-**80** isomer as a colourless oil. The *anti*-isomer contained traces of solvent, which were removed using Kugelrohrdestillation.

2-Benzylidene-1,3-diphenylpropane-cis-1,3-diol (syn-80)

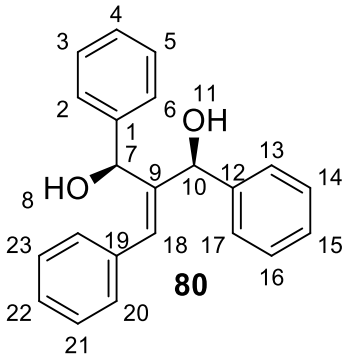

Yield: 109 mg (344 µmol, 12%).

m.p.: 110–111°C (lit.[207] 108–109°C).

R_f = 0.36 ($CHCl_3$/ethyl acetate 98:2).

^{1}H NMR (400 MHz, $CDCl_3$): δ = 7.40–7.23 (15H, m, C*H*), 7.07 (1H, s, 18-H), 5.96 (1H, d, ^3J = 6.2 Hz, 7-H), 5.37 (1H, d, ^3J = 3.6 Hz, 10-H), 2.05 (1H, d, ^3J = 6.2 Hz, 11-H), 2.03 (1H, d, ^3J = 3.8 Hz, 8-H) ppm.

^{13}C NMR (100 MHz, $CDCl_3$): δ = 143.7 (C_q), 143.0 (C_q), 142.3 (C_q, C-9), 136.4 (C_q), 130.4 (C_t), 128.9 (C_t), 128.8 (C_t), 128.6 (C_t), 128.5 (C_t), 128.2 (C_t), 127.5 (C_t), 127.3 (C_t), 127.3 (C_t), 125.0 (C_t), 74.2 (C_t, C-10), 71.3 (C_t, C-7) ppm.

FT-IR (ATR): $\tilde{\upsilon}$ = 3301 (m, *ν*(O-H)), 3024 (w, *ν*(C-H_{arom})), 1599 (w), 1492 (w), 1448 (w), 1255 (w), 1209 (w), 1130 (w), 1076 (w), 1043 (m), 1007 (s), 920 (w), 863 (w), 766 (m), 742 (w), 696 (vs), 629 (w) cm^{-1}.

UV/Vis (CH_2Cl_2, lg ε): λ_{max} = 249 (4.08) nm.

MS (EI, 70 eV): m/z = 298 (M^+-H_2O, 69%), 297 (24), 280 (M^+ - 2 H_2O, 2), 209 (100), 207 (19), 193 (26), 191 (38), 189 (10), 178 (13), 165 (13), 131 (29), 105 (70), 79 (26).

HRMS (ESI): calc. for [$C_{22}H_{20}O_2$ + Na^+] m/z 339.13555, found m/z 339.13483.

The spectroscopic data corresponded to the data reported in the literature.[202,207]

2-Benzylidene-1,3-diphenylpropane-anti-1,3-diol (anti-80)

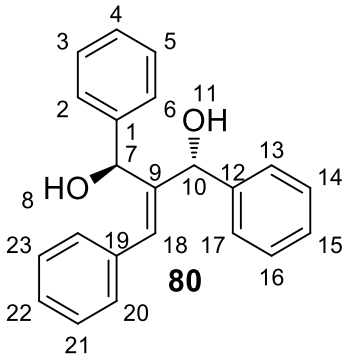

Yield: 642 mg (2.03 mmol, 70%).

R_f = 0.28 ($CHCl_3$/ethyl acetate 98:2).

^{1}H NMR (400 MHz, $CDCl_3$): δ = 7.44–7.22 (15H, m), 6.23 (1H, s, 18-H), 5.98 (1H, d, ^3J = 6.9 Hz, 7-H), 5.34 (1H, s, 10-H), 3.77 (1H, d, ^3J = 7.4 Hz, 8-H), 2.77 (1H, d, ^3J = 3.5 Hz, 11-H) ppm.

^{13}C NMR (100 MHz, $CDCl_3$): δ = 143.6 (C_q), 142.8 (C_q), 141.5 (C_q), 136.3 (C_q), 133.2 (C_t, C-18), 128.9 (C_t), 128.5 (C_t), 128.5 (C_t), 128.4 (Ct), 127.9 (C_t), 127.6 (C_t), 127.2 (C_t), 127.2 (C_t), 125.7 (C_t), 74.9 (C_t, C-10), 72.2 (C_t, C-7) ppm.

FT-IR (ATR): $\tilde{\upsilon}$ = 3487 (w, *ν*(O-H)), 2360 (w), 1599 (w), 1495 (w), 1450 (w), 1383 (w), 1325 (w), 1178 (w), 1018 (s), 951 (w), 920 (w), 858 (w), 758 (m), 739 (m), 700 (vs) cm^{-1}.

UV/Vis (CH_2Cl_2, lg ε): λ_{max} = 248 (3.92) nm.

MS (EI, 70 eV): m/z = 298 (M^+-H_2O, 84%), 297 (27), 280 (M^+ - 2 H_2O, 3), 209 (100), 207 (23), 193 (37), 191 (50), 189 (13), 178 (17), 165 (16), 131 (33), 105 (89), 79 (32).

HRMS (ESI): calc. for [$C_{22}H_{20}O_2$ + Na^+] m/z 339.13555, found m/z 339.13592.

The spectroscopic data corresponded to the data reported in the literature.[202,207]

4b,4b1,8b,12b-Tetrahydrodibenzo[2,3:4,5]pentaleno[1,6-ab]indene (TBTQ, 68)

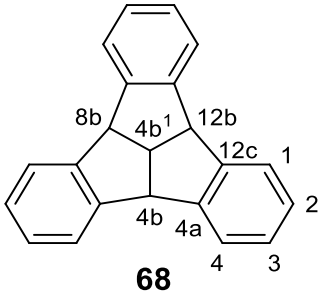

68

The alcohol **80** (2.40 g, 7.58 mmol) was dissolved in chlorobenzene (18 ml) and poly-phosphoric acid (1.22 g) was added The reaction mixture was refluxed at 130°C under nitrogen and stirred rigorously for 24 h. Upon cooling, a colourless crystals precipitated out of solution, which were washed with acetone and dried. Graduation sublimation was carried out to purify the product (Ts = 80–95°C, rate = 0.2–0.8 nm/min, pressure = $2.5 \cdot 10^{-6}$ mbar, d = 30 nm).

Yield: 374 mg (1.34 mmol, 18%, lit.[207] 32%).

m.p.: 321°C (lit.[207] 322°C, decomposition), 360°C (lit.[207] 362°C, melting).

R_f = 0.44 (cyclohexane/CH_2Cl_2 95:5).

^{1}H NMR (400 MHz, $CDCl_3$): δ = 7.48–7.43 (6H, m, 1,4-H), 7.20–7.15 (6H, m, 2,3-H), 4.97 (3H, d, ^3J = 9.7 Hz, 4b,8b,12b-H), 4.49 (1H, q, ^3J = 9.7 Hz, 4b^1-H) ppm.

^{13}C NMR (100 MHz, $CDCl_3$): δ = 145.9 (C_q, C-4a, 12c), 127.5 (C_t, C-2,3), 124.4 (C_t, C-1,4), 56.0 (C_t, C-4b,8b,12b), 51.2 (C-4b^1) ppm.

FT-IR (ATR): ῡ = 3068 (w, *ν*(C-H_{arom})), 3020 (w, *ν*(C-H_{arom})), 2974 (w, *ν*(C-H)), 2900 (w, *ν*(C-H)), 1683 (w), 1603 (w), 1480 (m, *ν*(C=C_{arom})), 1474 (m, *ν*(C=C)$_{arom}$), 1456 (m, δ(C-H)), 1315 (w), 1295 (w), 1274 (w), 1255 (w), 1199 (w), 1172 (w), 1157 (w), 1083 (w), 1033 (w), 1025 (w), 1012 (w), 975 (w), 959 (w), 935 (w), 888 (w), 877 (w), 866 (w), 832 (w), 750 (s, δ(C-H_{arom})), 741 (s, δ(C-H_{arom})), 711(s, δ(C-H_{arom})), 662 (w), 647 (w), 630 (w), 617 (w), 603 (m) cm^{-1}.

UV/Vis (CH_2Cl_2, lg ε): λ_{max} = 277 (3.56), 269 (3.47), 233 (2.91) nm.

MS (EI, 70 eV): m/z = 280 (M^+, 100%), 276 (18), 252 (6), 203 (22), 138 (9).

The spectroscopic data corresponded to the data reported in the literature.[202,207]

2-Methyl-1H-indene-1,3-(2H)-dione (71)

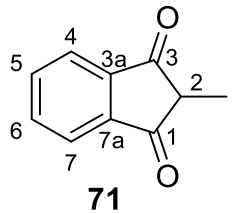

71

60% NaH in paraffin oil (3.93 g, 98.5 mmol) was suspended in benzene (80 ml) under a flow of N_2. Dimethylpthalate (19.5 g, 100 mmol) and 3-pentanone (8.00 g, 92.9 mmol) were added dropwise and the reaction mixture was heated to 100°C for 3 d. The red precipitate was washed with benzene and dried for 6 h *in vacuo*, before dissolving in water and acidifying with 10 ml conc. hydrochloric acid. Pale yellow crystals precipitated out of solution, which were washed with H_2O and dried.

Yield: 8.48 g (53.0 mmol, 57%, lit.[355] 68%).

m.p.: 80–82°C (lit.[355] 83–84°C).

R_f = 0.18 (cyclohexane/ethyl acetate 5:1).

^{1}H NMR (400 MHz, $CDCl_3$): δ = 7.98–7.96 (2H, m, 4,7-H), 7.84–7.82 (2H, m, 5,6-H), 3.05 (1H, q, $^3J_{2,Me}$ =7.6 Hz, 2-H), 1.41 (3H, d, $^3J_{Me,2}$ =7.6 Hz, CH_3) ppm.

^{13}C NMR (100 MHz, $CDCl_3$): δ = 201.2 (C_q, C=O), 142.1 (C_q, C-3a,7a), 135.8 (C_t, C-5,6), 123.4 (C_t, C-4,7), 48.9 (C_t, C-2), 10.6 (C_p, *C*H_3) ppm.

FT-IR (ATR): $\tilde{\upsilon}$ = 3392 (w), 3087 (w, ν(C-H_{arom})), 2976 (w, ν(C-H)), 2933 (w, ν(C-H)), 2877 (w, ν(C-H)), 1743 (s, ν(C=O), 1700 (vs, ν(C=O)), 1589 (m, ν(C=C_{arom})), 1446 (w), 1371 (w), 1352 (w), 1288 (s), 1230 (m), 1201 (s), 1155 (m), 1103 (w), 1083 (w), 1016 (w), 978 (w), 930 (m), 854 (w), 802 (m), 737 (s), 688 (w) cm^{-1}.

UV/Vis (CH_2Cl_2, lg ε): λ_{max} = 301 (2.58), 284 (2.68), 247 (3.97), 232 (3.99) nm.

MS (EI, 70 eV): m/z = 160 (M^+, 100%), 132 (12), 104 (92), 76 (37).

The spectroscopic data corresponded to the data reported in the literature.[355]

2-Benzhydryl-2-methyl-1H-indene-1,3(2H)-dione (74)

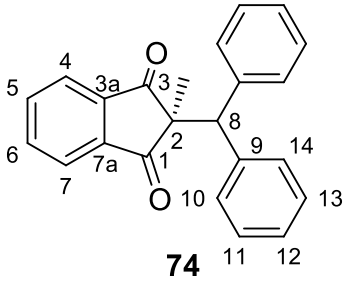

74

2-Methyl-1,3-indanedione **71** (7.50 g, 46.8 mmol), diphenylmethanol (8.62 g, 46.8 mmol) and *p*-toluenesulfonic acid (PTSA) monohydrate (445 mg, 2.34 mmol, 0.05 eq.) were dissolved in benzene (100 ml). The reaction mixture was heated to 110 C for 6 h using a DEAN-STARK trap, and after reaching room temperature the solvent was removed *in vacuo*. The resulting oil was dissolved in $CHCl_3$ (55 ml) and was washed with 5% $NaHCO_3$ solution (2 × 50 ml) and H_2O (2 × 50 ml). The organic phase was dried with Na_2SO_4 and the solvent was removed *in vacuo*. The remaining orange oil was suspended in MeOH (25 ml) and cooled to 5°C overnight. The resulting beige crystals were filtered and washed with MeOH, before drying.

Yield: 11.6 g (35.4 mmol, 76%, lit.[205] 90%).

m.p.: 121–122°C (lit.[205] 122°C).

R_f = 0.30 (cyclohexane/ethyl acetate 5:1).

^{1}H NMR (400 MHz, $CDCl_3$): δ = 7.84–7.80 (2H, m, 4,7-H), 7.72–7.67 (2H, m, 5,6-H), 7.45 (4H, d, ^3J = 7.9 Hz, 10,14-H), 7.16 (4H, t, ^3J = 7.7 Hz, 11,13-H), 7.07 (2H, t, ^3J = 7.3 Hz, 12-H), 4.58 (1H, s, 8-H), 1.30 (s, 3H, CH_3) ppm.

^{13}C NMR (100 MHz, $CDCl_3$): δ = 204.5 (C_q, C-1,3), 141.6 (C_q, C-3a,7a), 140.0 (C_q, C-9), 135.7 (C_t, C-5,6), 129.8 (C_t, C-10,14), 128.4 (C_t, C-11,13), 126.9 (C_t, C-12), 123.2 (C_t, C-4,7), 58.3 (C_q, C-2), 58.0 (C_t, C-8), 20.1 (C_p, CH_3) ppm.

FT-IR (ATR): $\tilde{\upsilon}$ = 3064 (w, ν(C-H_{arom})), 3030 (w, ν(C-H_{arom})), 1738 (w), 1697 (s, ν(C=O)), 1592 (w, ν(C=C_{arom})), 1495 (w, ν(C=C_{arom})), 1450 (w), 1371 (w), 1348 (w), 1271 (m), 1244 (m), 1031 (w), 987 (w), 766 (m), 731 (w), 701 (vs, δ(C-H_{arom})), 617 (w) cm^{-1}.

UV/Vis (CH_2Cl_2, lg ε): λ_{max} = 304 (2.53), 247sh (4.11), 234 (4.27) nm.

MS (EI, 70 eV): m/z = 167 ($CHPh_2^+$, 100%), 165 (16), 152 (9), 115 (3).

HRMS (ASAP, -): calc. for $[C_{23}H_{18}O_2 - H]^-$ m/z 325.1234, found m/z 325.1233.

The spectroscopic data corresponded to the data reported in the literature.[205]

2-Benzhydryl-2-methyl-2,3-dihydro-1H-indene-1,3-diol (76)

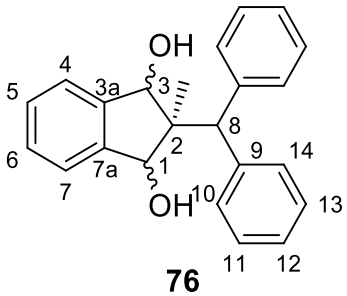

76

$LiAlH_4$ (340 mg, 8.96 mmol, 1.02 eq.) was suspended in abs THF (10 ml). Diketone **74** (2.90 g, 8.80 mmol) was dissolved in abs THF (20 ml) and this solution was added slowly to the reaction mixture and stirred rigorously. The reaction mixture was refluxed at 80°C for 4 h. After cooling to room temperature and addition of Et_2O (80 ml), the mixture is carefully hydrolysed by the addition ice until no further reaction was visible. The phases were separated and the aqueous phase was washed with Et_2O (6 × 20 ml). The combined organic phases were washed with brine (20 ml), dried over $MgSO_4$ and the solvent was removed *in vacuo*. The resulting oily yellow residue was purified using fractional recrystallisation from MeOH, to afford first the all-*cis* isomer as a colourless solid and then the *cis*,*trans* isomer as a colourless solid.

Yield: 1.32 g (3.98 mmol, 45%, lit.[205] 82%).

all cis-76:

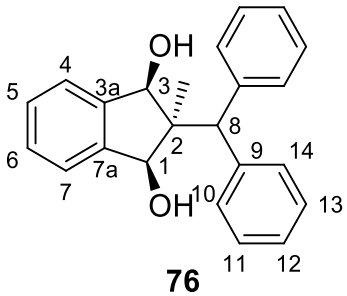

76

Yield: 304 mg (920 µmol, 10%).

m.p.: 193–194°C (lit.[205] 191–192°C).

R_f = 0.34 (cyclohexane/ethyl acetate 5:1).

^{1}H NMR (400 MHz, $CDCl_3$): δ = 7.58 (4H, d, ^3J = 8.4 Hz, 10,14-H), 7.46–7.42 (2H, m, 5,6-H), 7.38–7.33 (6H, m, 3a,7a,11,13-H), 7.28–7.24 (2H, m, 12-H), 5.26 (1H, s, 8-H), 4.57 (2H, d, ^3J = 7.2 Hz, 1,3-H), 2.23 (2H, d, ^3J = 7.3 Hz, O*H*), 0.84 (3H, s, C*H*$_3$) ppm.

^{13}C NMR (100 MHz, $CDCl_3$): δ = 144.9 (C_q, C-3a,7a), 142.0 (C_q, C-9), 130.1 (C_t, C-10,14), 129.3(C_t, C-4,7), 128.7 (C_t, C-11, 13-H), 126.7 (C_t, C-12), 126.3 (C_t, C-5,6), 81.9 (C_t, C-1,3), 53.6 (C_q, C-2), 49.0 (C_t, C-8), 20.6 (C_t, *C*H$_3$) ppm.

FT-IR (ATR): $\tilde{\upsilon}$ = 3425 (w, *ν*(O-H)), 3246 (m, br, ν(O-H)), 3056 (w, *ν*(C-H)$_{arom}$), 3024 (w, *ν*(C-H)$_{arom}$), 2960 (w), 2913 (w), 1596 (w), 1493 (w), 1448 (w), 1411 (w), 1250 (w), 1209 (w), 1155 (w), 1072 (w), 1007 (s), 949 (w), 922 (w), 847 (w), 794 (w), 759 (m), 741 (m), 698 (vs), 623 (w) cm^{-1}.

UV/Vis (CH_2Cl_2, lg ε): λ_{max} = 271 (2.76), 264 (2.90), 259 (2.86), 230 (2.64) nm.

MS (EI, 70 eV): m/z = 326 (M^+, 0.3%), 312 (M^+-H_2O, 3%), 294 (M^+ - 2 H_2O, 11), 279 (4), 167 (100), 165 (18), 145 (44), 115 (44), 91 (8), 77 (5).

HRMS (ASAP -): calc. for $[C_{23}H_{22}O_2\text{-}H]^-$ m/z 329.1547, found m/z 329.1548.

cis,trans-76:

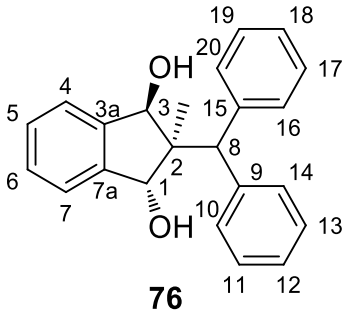

76

Yield: 1.01 g (3.07 mmol, 35%).

m.p.: 71–72°C (lit.[205] 70–73°C).

R_f = 0.36 (cyclohexane/ethyl acetate 5:1).

^{1}H NMR (400 MHz, $CDCl_3$): δ = 7.67–7.65 (2H, m, 16,20/10,14-H), 7.60–7.58 (2H, m, 16,20/10,14-H), 7.41–7.22 (10H, m, 4,5,6,7,11,12,13,17,18,19-H), 5.50 (1H, d, ^3J = 4.3 Hz, 3-H), 4.90 (1H, s, 8-H), 4.76 (1H, d, ^3J = 4.4 Hz, 1-H), 1.76 (1H, d, ^3J = 4.5 Hz, C1-O*H*), 1.10 (3H, s, C3-O*H*), 1.00 (1H, d, J = 4.4 Hz, C*H*$_3$) ppm.

^{13}C NMR (100 MHz, $CDCl_3$): δ = 144.3 (C_q, C-3a/7a), 142.7 (C_q, C-9/15), 142.2 (C_q, C-9/15), 141.2 (C_q, C-3a/7a), 130.2 (C_t, C-16,20/10,14), 129.8 (C_t, C-16,20/10,14), 129.4 (C_t, *C*H), 128.7 (C_t, *C*H), 128.4 (C_t, *C*H), 127.2 (C_t, *C*H), 126.7 (C_t, *C*H), 125.3 (C_t, *C*H), 124.8 (C_t, *C*H), 81.3(C_t,C-3), 81.1(C_t,C-1), 55.8 (C_q, C-2), 55.4 (C_t, C-8), 15.4 (C_t,*C*H_3) ppm.

FT-IR (ATR): $\tilde{\upsilon}$ = 3579 (w, *ν*(O-H)), 3487 (w, *ν*(O-H)), 3026 (w, *ν*(C-H)$_{arom}$), 2910 (w), 2360 (w), 1599 (w), 1495 (w), 1450 (w), 1383 (w), 1325 (w), 1178 (m), 1018 (s), 951 (w), 920 (w), 858 (w), 758 (s), 739 (w), 700 (vs) cm^{-1}.

UV/Vis (CH_2Cl_2, lg ε): λ_{max} = 271 (2.88), 265 (2.99), 259 (2.93), 232 (2.95) nm.

MS (EI, 70 eV): m/z = 312 (M^+-H_2O, 2%), 294 (3), 279 (3), 167 ($CHPh_2^+$, 100), 165 (17), 145 (21), 117 (7), 115 (9), 91 (8), 77 (5).

HRMS (ASAP -): calc. for $[C_{23}H_{22}O_2\text{-}H]^-$ m/z 329.1547, found m/z 329.1548.

The spectroscopic data corresponded to the data reported in the literature.[205]

4b¹-Methyl-4b,4b¹,8b,12b-tetrahydrodibenzo[2,3:4,5]pentaleno[1,6-ab]indene (69)

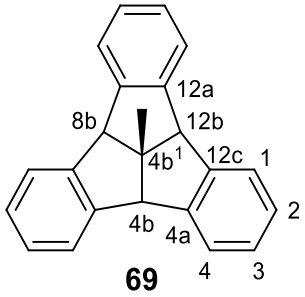

69

Diol **76** (8.23 g, 24.9 mmol) was dissolved in xylene (80 ml) and *ortho*-phosphoric acid (2.27 g, 0.93 eq.) was added. The reaction was heated to 180°C for 5 h using a DEAN-STARK trap. The warm solution was filtered over $CaCO_3$ and the solvent partially removed *in vacuo*. Colourless crystals precipitated out on cooling the mixture. These crystals were washed with xylene and the filtrate recrystallised. The product was purified using sublimation (T = 180°C, pressure = $2.6 \cdot 10^{-1}$ mbar).

Yield: 864 mg (2.93 mmol, 12%, lit.[205] 33%).

m.p.: 242°C (lit.[205] 244°C).

R_f = 0.47 (cyclohexane/CH_2Cl_2 95:5).

^{1}H NMR (400 MHz, $CDCl_3$): δ = 7.46–7.43 (6H, m, 1;4-H), 7.22–7.18 (6H, m, 2,3-H), 4.49 (3H, s, 4b,8b,12b-H), 1.70 (3H, s, C(4b^{1})CH_3) ppm.

^{13}C NMR (100 MHz, $CDCl_3$): δ = 145.6 (C_q, C-4a,12c), 127.6 (C_t, C-2,3), 124.5 (C_t, C-1,4-H), 63.7 (C_t, C-4b,8b,12b), 60.8 (C_q, C-4b^{1}), 27.7 (C_t, C(4b^{1})CH$_3$) ppm.

FT-IR (ATR): $\tilde{\upsilon}$ = 3064 (w, *ν*(C-H_{arom})), 3019 (w, *ν*(C-H_{arom})), 2894 (w, ν(C-H)), 1479 (m, ν(C=C_{arom})), 1309 (w), 1207 (w), 1155 (w), 1083 (w), 1027 (w), 974 (w), 952 (w), 821 (w), 748 (w), 748 (s), 731 (vs), 660 (w), 613 (w) cm^{-1}.

UV/Vis (n-C_7H_{16}, lg ε): λ_{max} = 276 (2.11), 269 (2.83), 262 (2.94), 232 (2.90) nm.

MS (EI, 70 eV): m/z = 294 (M^+,100 %), 279 (52), 276 (17), 265 (6), 217 (14), 178 (18), 138 (8).

The spectroscopic data corresponded to the data reported in the literature.[205]

Experimental conditions for STM Analysis (M. VOGT, M. SCHMIDT, M. BODE):

Monolayer formation was carried out after degassing the compounds TBTQs **68** and **69** for about 30 min under ultrahigh vacuum (UHV) conditions. Measurements were performed in a UHV system with a base pressure $p \leq 1 \cdot 10^{-10}$ mbar in each of the two chambers. The Ag(111) single crystal was prepared in the preparation chamber by cycles of 15 min Ar^+ sputtering with an ion energy of 1.0 keV and subsequent annealing up to a temperature of 700 K for 15 min. Upon cooling the substrate down to room temperature, TBTQ **68** or Me-TBTQ **69** molecules are deposited onto the surface by thermal evaporation from a resistively heated quartz crucible. During the deposition, the pressure remained below $p \leq 3 \cdot 10^{-10}$ mbar. Upon molecule deposition, the sample was moved to a home-built low-temperature STM, operating at a temperature of T ≈ 5.5 K. In this microscope the bias voltage is applied to the sample, thus occupied sample states are probed at negative bias voltages whereas unoccupied states are probed at positive bias voltage. For measurements of the differential conductance dI/dU, the bias was modulated at typical amplitudes U_{mod} = 10 mV at a frequency f_{mod} = 5777 Hz.

6.2.2 Synthesis of fluorinated TBTQs 104 and TBTQ 164

2-(2-fluorobenzylidene)-1,3-diphenylpropane-1,3-dione (113)

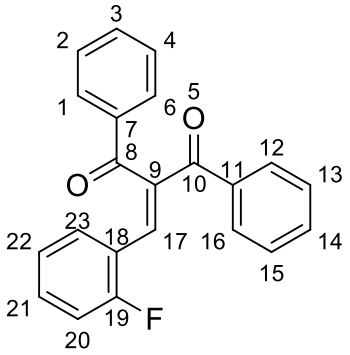

113

Dibenzoylmethane **77** (5.00 g, 22.3 mmol) and 2-fluorobenzaldehyde **112** (5.54 g, 44.6 mmol) were dissolved in acetonitrile (80 ml) and piperidine (0.44 ml, 4.46 mmol, 0.2 eq.) was added. The reaction mixture was refluxed at 80°C for 9 d. The reaction was allowed to cool to room temperature and ethyl acetate (300 ml) and H_2O (100 ml) were added. The aqueous phase was extracted with ethyl acetate (3 × 50 ml) and the combined organic phases were washed with H_2O (40 ml) and dried over $MgSO_4$. The solvent was removed *in vacuo* and the resulting brown oil was purified using column chromatography (silica, pentane/ethyl acetate, 9:1) to afford the product as a yellow oil which solidified upon prolonged drying under vacuum.

Yield: 4.32 g (13.1 mmol, 59%).

m.p.: 72–73°C.

$\mathbf{R_f}$ = 0.14 (pentane/ethyl acetate, 90:10).

^{1}H NMR (400 MHz, $CDCl_3$): δ = 7.96–7.94 (2H, m, 1,6-H), 7.91–7.69 (2H, m, 12,16-H), 7.71 (1H, s, 17-H), 7.62–7.57 (1H, m, 14-H), 7.54–7.47 (3H, m, 3,13,15-H), 7.42–7.38 (2H, m, 2,4-H), 7.32 (1H, dd, ^3J = 7.6 Hz, ^4J = 1.6 Hz, 23-H), 7.28–7.24 (1H, 20-H), 7.04–6.99 (1H, m, 21-H), 6.98–6.94 (1H, m, 22-H) ppm.

^{13}C NMR (100 MHz, $CDCl_3$): δ = 195.5 (C_q, d, J = 166 Hz, C-8,10), 160.8 (C_q, d, J = 252.4 Hz, C-19), 141.1 (C_q, C-9), 137.1 (C_q, C-11), 136.3 (C_q, C-7), 135.9 (C_t, d, J = 5.7 Hz, C-17), 134.0 (C_t, C-3,13,15), 133.0 (C_t, C-14), 132.3 (C_t, d, J = 8.9 Hz, C-20), 130.4 (C_t, d, J = 2.1 Hz, C-22), 129.8 (C_t, C-12,16), 129.5 (C_t, C-1,6), 128.9 (Ct, C-2,4), 128.8 (C_t, C-3,13,15), 124.5 (C_t, d, J = 3.7 Hz, C-22), 121.6 (C_q, d, J = 12.3 Hz, C-18), 115.9 (C_t, d, J = 21.7 Hz, C-21) ppm.

^{19}F NMR (376 MHz, $CDCl_3$): δ = -112.7 ppm.

FT-IR (ATR): $\tilde{\upsilon}$ = 3062 (w, *ν*(C-H_{arom})), 1672 (m, *ν*(C=O)), 1641 (m, *ν*(C=O)), 1612 (m, ν(C=C_{arom})), 1577 (w, ν(C=C_{arom})), 1483 (w), 1448 (m), 1367 (w), 1301 (w), 1255 (s), 1224 (vs), 1176 (w), 1116 (w), 1093 (w), 1074 (w), 1028 (w), 982 (m), 933 (w), 874 (w), 804 (w), 757 (vs), 737 (s), 715 (s), 688 (vs), 646 (w) cm^{-1}.

UV/Vis (acetonitrile, lg ε): λ_{max} = 257 (4.29), 287sh (4.19) nm.

MS (EI, 70 eV): m/z = 312 ($C_{22}H_{16}O_2^+$, 100%), 311 (76), 297 (29), 235 (13), 208 (13), 207 (75), 178 (19), 152 (5), 129 (13).

HRMS (ASAP, +): calc. for $[C_{22}H_{15}FO_2+H]^+$: m/z 331.1129, found m/z 331.1128.

EA: calc.: C 79.99, H 4.58, found: C 79.92, H 4.65.

2-(2-Fluorobenzylidene)-1,3-diphenylpropane-1,3-diol (114)

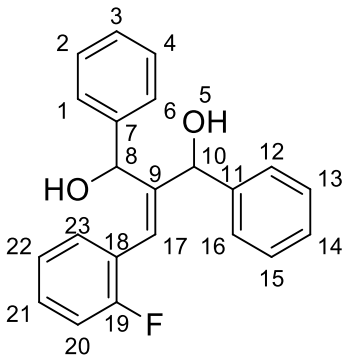

114

Diketone **113** (3.70 g, 11.2 mmol) was dissolved in anhydrous CH_2Cl_2 (45 ml) and cooled to -78°C. To this mixture was added a 0.4 M solution of $CeCl_3 \cdot 7\,H_2O$ (5.84 g, 15.7 mmol, 1.4 eq.) in MeOH (39 ml). The resulting suspension was stirred for 20 min, after which $NaBH_4$ (464 mg, 12.3 mmol, 2.1 eq.) was added. The reaction mixture was stirred at -78°C for 50 min and then allowed to reach room temperature for 1 h, after which the reaction was complete. Et_2O (70 ml) and 2 M HCl (50 ml) were added and the phases separated. The aqueous phase was extracted with Et_2O (3 × 40 ml) and the organic phases were washed with H_2O (40 ml) and dried over $MgSO_4$. The solvent was removed *in vacuo* to afford an yellow oil, which was purified using column chromatography (silica, $CHCl_3$/ethyl acetate 95:5) to afford two isomers as beige solids, which were recrystallised from EtOH/pentane to afford colourless solids.

Yield: 2.69 g, 8.05 mmol, 72%.

R,R/S,S-diastereoisomer-**114**

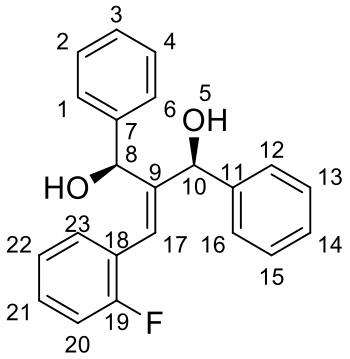

114

Yield: 478 mg (1.43 mmol, 13%).

m.p.: 108–110°C.

$\mathbf{R_f}$ = 0.28 ($CHCl_3$/ethyl acetate, 95:5).

^{1}H NMR (400 MHz, $CDCl_3$): δ = 7.40–7.22 (12H, m, C*H*), 7.11–7.06 (2H, m, 21,23-H), 7.02 (1H, s, 17-H), 5.78 (1H, d, *J* = 5.7 Hz, C*H*), 5.35 (1H, d, *J* = 3.5 Hz, C*H*), 2.13 (1H, d, *J* = 3.7 Hz, O*H*), 2.09 (1H, d, *J* = 5.7 Hz, O*H*) ppm.

^{13}C NMR (100 MHz, $CDCl_3$): δ = 160.3 (C_q, d, *J* = 246.1 Hz, C-19), 146.3 (C_q, C-9), 142.3 (C_q, d, *J* = 97.0 Hz), 130.7 (C_t, d, *J* = 3.1 Hz, *C*H), 129.4 (C_t, d, *J* = 8.2 Hz, *C*H), 128.8 (C_t, *C*H), 128.4 (C_t, *C*H), 128.1 (C_t, *C*H), 127.3 (C_t, *C*H), 127.2 (C_t, *C*H), 125.8 (C_t, *C*H), 124.3 (C_q, d, *J* = 15.0 Hz, *C*H), 124.2 (C_t, d, *J* = 3.6 Hz, *C*H), 123.1 (C_t, d, *J* = 2.7 Hz, *C*H), 115.6 (C_t, d, *J* = 22.0 Hz, *C*H), 74.0 (C_t, *C*-OH), 71.6 (C_t, *C*-OH) ppm.

FT-IR (ATR): ϑ = 3529 (m, *ν*(O-H)), 3424 (m, *ν*(O-H)), 1486 (m, ν(C=C_{arom})), 1448 (m), 1234 (m), 1186 (m), 1093 (w), 1026 (m), 849 (w), 812 (w), 760 (vs), 696 (vs), 667 (s) cm^{-1}.

UV/Vis (acetonitrile, lg ε): λ_{max} = 193 (4.73), 244 (3.94).

MS (EI, 70 eV): m/z = 316 ($C_{22}H_{20}O_2^+$, 37%), 227 ($C_{15}H_{15}O_2^+$, 100), 209 (32), 105 (68), 77 (44).

HRMS (ESI, +): calc. for $[C_{22}H_{19}FO_2+Na]^+$: m/z 357.12613, found m/z 357.12637.

EA: calc.: C 79.02, H 5.73, found: C 79.28, H 5.73.

*R,S/S,R-diastereoisomer -**114***

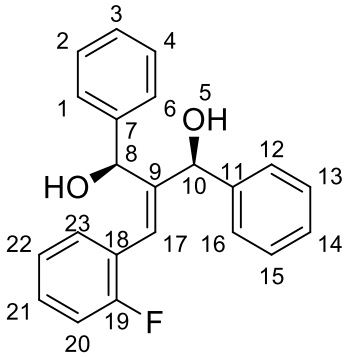

114

Yield: 2.22 g (6.62 mmol, 59%).

m.p.: 93–94°C.

$\mathbf{R_f}$ = 0.1 ($CHCl_3$/ethyl acetate, 95:5).

^{1}H NMR (400 MHz, $CDCl_3$): δ = 7.40–7.20 (12H, m, C*H*),7.08 (1H, t, *J* = 7.5 Hz, 23-H), 7.02 (1H, t, J = 8.5 Hz, 21-H), 6.17 (1H, s, 17-H), 5.80 (1H, d, J = 6.1 Hz, C*H*), 5.30 (1H, s, C*H*), 4.04 (1H, d, *J* = 6.9Hz, O*H*), 3.25 (1H, s, O*H*) ppm.

^{13}C NMR (100 MHz, $CDCl_3$): δ = 160.2 (C_q, d, *J* = 247 Hz, C-18), 145.8 (C_q, C-9), 142.2 (C_q), 141.2 (C_q), 130.8 (C_t, d, *J* = 3.1 Hz, *C*H), 129.5 (C_t, d, *J* = 8.1 Hz, *C*H), 128.4 (C_t, d, *J* = 8.0 Hz, *C*H), 127.8 (C_t, *C*H), 127.2 (C_t, d, *J* = 1.3 Hz, *C*H), 126.0 (C_t, d, *J* = 2.5 Hz, *C*H), 125.6 (C_t, *C*H), 124.2 (C_t, *C*H), 124.1 (C_t, d, *J* = 3.7 Hz, C-23), 124.0 (C_t, *C*H), 115.5 (C_t, d, *J* = 21.8 Hz, C-21), 74.6 (C_t, *C*-OH), 72.5 (C_t, *C*-OH) ppm.

FT-IR (ATR): $\tilde{\upsilon}$ = 3320 (w, *ν*(O-H)), 3029 (w, *ν*(C-H_{arom})), 1484 (w, ν(C=C_{arom})), 1452 (m), 1325 (w), 1288 (w), 1230 (w), 1188 (w), 1095 (w), 1039 (m), 1007 (m), 948 (w), 918 (w), 877 (w), 814 (w), 789 (w), 758 (vs), 742 (s), 717 (w), 698 (vs), 611 (w) cm^{-1}.

UV/Vis (acetonitrile, lg ε): λmax = 193 (4.82), 243 (4.03).

MS (EI, 70 eV): m/z = 316 ($C_{22}H_{20}O_2^+$, 68%), 287 (14), 227 ($C_{15}H_{15}O_2^+$, 100), 210 (42), 105 (87), 77 (53).

HRMS (ESI, +): calc. for $[C_{22}H_{19}FO_2+Na]^+$: m/z 357.12613, found m/z 357.126786.

EA: calc.: C 79.02, H 5.73, found: C 79.27, H 5.76.

1-fluoro-4b,4b1,8b,12b-tetrahydrodibenzo[2,3:4,5]pentaleno[1,6-ab]indene (100)

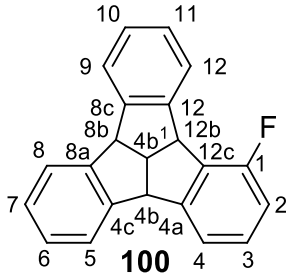

Dialcohol **114** (905 mg, 2.71 mmol) was dissolved in chlorobenzene (6 ml) and poly-phosphoric acid was added (500 mg), upon which the solution turned red. This reaction mixture was heated to reflux at 130°C for 22 h. After allowing to cool to room temperature, CH_2Cl_2 (10 ml) and H_2O (10 ml) were added and the phases separated. The aqeous phase was extracted with CH_2Cl_2 (2 × 10 ml) and the combined organic phases were washed with H_2O (2 × 10 ml), dried over $MgSO_4$ and the solvent was removed *in vacuo*. The resulting brown solid was combined with silica and purified using column chromatography (silica, cyclohexane/CH_2Cl_2, 85:15). Recrystallisation with toluene afforded the desired product as colourless needles.

Yield: 110 mg (367 µmol, 14%).

m.p.: 260°C (sublimation), 297–298°C (melting).

$\mathbf{R_f}$ = 0.36 (Cyclohexane/CH_2Cl_2, 85:15).

^{1}H NMR (600 MHz, CD_2Cl_2): δ = 7.63–7.62 (1H, m, 12-H), 7.49–7.44 (3H, m, 5,8,9-H), 7.27 (1H, d, *J* = 7.6 Hz, 4-H), 7.20–7.16 (5H, m, 3,6,7,10,11-H), 6.90–6.86 (1H, m, 2-H), 5.21 (1H, d, *J* = 9.7 H, 12b-H), 4.97 (2H, d, *J* = 9.6 Hz, 4b,8b-H), 4.52 (3H, q, J = 9.7 Hz, 4b^1-H) ppm.

^{13}C NMR (150 MHz, $CDCl_3$): δ = 159.8 (C_q, d, *J* = 246 Hz, C-1), 150.0 (C_q, d, *J* = 5.4 Hz, C-4a), 146.3 (C_q, d, *J* = 26.3 Hz), 145.2 (C_q, d, *J* = 55.1 Hz), 132.4 (C_t, d, *J* = 17.5 Hz, C-12c), 129.8 (C_t, d, *J* = 7.4 Hz, *C*H), 128.0 (C_t, d, *J* = 9.0 Hz, *C*H), 127.8 (C_t, *C*H), 127.8 (C_t, *C*H), 127.8 (C_t, *C*H), 126.2 (C_t, d, *J* = 8.6 Hz, C-12), 124.6 (C_t, d, *J* = 4.9 Hz, C-5 or C-8 or C-9), 124.5 (C_t, C-5 or C-8 or C-9), 120.5 (C_t, d, *J* = 3.2 Hz, C-4), 114.1 (C_t, d, *J* = 21.2 Hz, C-2), 56.5 (C_t, d, *J* = 1.5 Hz, C-4b or C-8b), 56.0 (C_t, C-4b or C-8b), 53.8 (C_t, d, *J* = 2.2 Hz, C-12b), 51.9 (C_t, C-4b^1) ppm.

^{19}F NMR (376 Hz, CD_2Cl_2): δ = -116.2 ppm.

FT-IR (ATR): $\tilde{\upsilon}$ = 3019 (w, *ν*(C-H_{arom})), 2900 (w, *ν*(C-H)), 2360 (w), 1616 (w), 1585 (w), 1456 (m), 1288 (w), 1240 (m), 1155 (w), 1057 (w), 1026 (w), 984 (m), 876 (w), 841 (w), 812 (w), 773 (m), 744 (vs), 692 (w) cm^{-1}.

UV/Vis (acetonitrile, lg ε): λ_{max} = 200 (4.94), 222 (4.52), 268 (3.30), 275 (3.35).

MS (EI, 70 eV): m/z = 298 (M^+, 100%), 294 (14), 276 (9), 270 (6), 221 (22), 203 (5), 196 (5), 138 (6).

HRMS (ASAP, +): calc. for $[C_{22}H_{15}+H]^+$: m/z 299.1231, found m/z 331.1221.

EA: calc.: C 88.56, H 5.07, found: C 88.51, H 5.06.

(E)-1,3-Bis(2-fluorophenyl)prop-2-en-1-one (118)

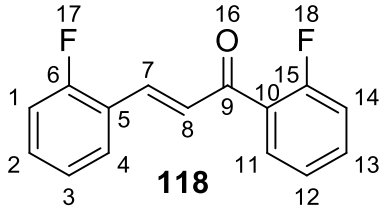

2-Fluorobenzaldehyde **112** (2.25 g, 18.3 mmol) and 2-fluoroacteophenone **115** (2.52 g, 18.2 mmol) were dissolved in a solution of NaOH (907 mg, 22.7 mmol, 1.25 eq.) in EtOH (15 ml), which was cooled to 10°C. After addition, the reaction mixture was allowed to reach room temperature and after 24 h the reaction was cooled to 0°C. CH_2Cl_2 (50 ml) and distilled H_2O (50 ml) were added and the phases were separated. The aqueous phase was extracted with CH_2Cl_2 (10 ml) and the organic phase was washed with 3 × 10 ml and 4 × 20 ml distilled H_2O, at which point the solution was neutral. The combined organic phases were dried over $MgSO_4$ and the solvent was removed *in vacuo*. The resulting solid was recrystallised using EtOH (5 ml) and a yellow solid precipitated out at -29°C, which liquefies on warming to room temperature.

Yield: 3.64 g (14.9 mmol, 82%).

^{1}H NMR (400 MHz, $CDCl_3$): δ = 7.88 (1H, dd, ^3J = 16.0 Hz, ^4J = 1.8 Hz; 7-H), 7.83 (1H, td, ^3J = 7.5 Hz, ^4J = 1.9 Hz, 11-H), 7.65 (1H, td, ^3J = 7.6 Hz, ^4J = 1.7 Hz, 4-H), 7.57–7.52 (1H, m, 13-H), 7.49 (1H, dd, ^3J = 16.0 Hz, ^4J = 2.8 Hz, 8-H), 7.42–7.35 (1H, m, 2-H), 7.27 (1H, td, ^3J = 7.6 Hz, ^4J = 1.0 Hz, 12-H), 7.21–7.10 (3H, m, 1,3,14-H) ppm.

^{13}C NMR (100 MHz, $CDCl_3$): δ = 189.2 (C_q, d, J = 2.7 Hz, C-9), 137.4 (C_q, d, J = 1.1 Hz, C-6 or C-15), 137.4 (C_q, d, J = 1.3 Hz, C-6 or C-15), 134.2 (C_t, d, J = 8.9 Hz, C-7), 132.2 (C_t,

d, *J* = 8.8 Hz, C-13), 131.2 (C_t, d, *J* = 2.7 Hz, C-11), 130.0 (C_t , d, *J* = 2.8 Hz, C-2), 128.0 (C_t , t, *J* = 6.6 Hz, C-8), 127.1 (C_q, C-10), 124.7 (C_t , d, *J* = 3.5 Hz, C-12), 124.6 (C_t, d, *J* = 3.7 Hz, C-1 or C-3 or C-14), 123.0 (C_q, d, *J* = 11.6 Hz, C-5), 116.7 (C_t, d, *J* = 22.9 Hz, C-1 or C-3 or C-14), 116.4 (C_t, d, *J* = 22.0 Hz, C-1 or C-3 or C-14) ppm.

^{19}F NMR (376 MHz, $CDCl_3$): δ = -110.7, -114.6 ppm.

FT-IR (ATR): $\tilde{\upsilon}$ = 3064 (w, ν(C-H_{arom})), 2360 (w), 1928 (w), 1670 (w), 1637 (w), 1604 (s, ν(C=C)), 1575 (m), 1481 (m), 1452 (s), 1332 (m), 1309 (w), 1284 (m), 1224 (m), 1203 (m), 1153 (w), 1095 (m), 1049 (w), 1018 (m), 982 (m), 945 (w), 872 (w), 833 (w), 798 (w), 748 (vs), 671 (w), 644 (w) cm^{-1}.

UV/Vis (acetonitrile, lg ε): λ_{max} = 223 (3.92), 297 (4.27) nm.

MS (EI, 70 eV): m/z = 244 (M^+, 100%), 243 (66), 225 (28), 215 (16), 196 (13), 123 (54), 101 (37), 95 (33), 75 (26).

EA: calc.: C 73.77, H 4.13, F: 15.56, O: 6.55, found: C 73.79, H 4.05.

anti-2,3-Bromo-1,3-bis(2-fluorophenyl)-2-methylpropan-1-one (119)

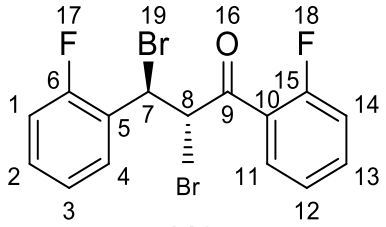

119

Ketone **118** (3.63 g, 14.8 mmol) was dissolved in $CHCl_3$ (15 ml) and the resulting solution was refluxed at 65°C. Br_2 (380 µl, 1.19 g, 14.9 mmol, 1 eq.) was added dropwise, on which the solution turned red/brown before returning to yellow. After 3.5 h $Na_2S_2O_3$ solution was added and the phases were separated. The organic phase was washed with distilled H_2O (2 × 10 ml) and dried over $MgSO_4$. The solvent was removed *in vacuo* to afford a yellow solid.

Yield: 5.50 g (13.6 mmol, 92%).

m.p.: 105–106 C.

R_f = 0.58 (cyclohexane/CH_2Cl_2 1:1).

^{1}H NMR (400 MHz, $CDCl_3$): δ = 8.06 (1H, td, ^{3}J = 7.7 Hz, ^{4}J = 1.8, 11-H), 7.66–7.60 (1H, m, 13-H), 7.50 (1H, td, *J* = 7.5 Hz, *J* = 1.7 Hz, 3-H), 7.41–7.36 (1H, m, 2-H), 7.35–7.31 (1H, m, 14-H), 7.24–7.20 (2H, m, 4,12-H), 7.16–7.11 (1H, m, 1-H), 6.03 (1H, dd, ^{3}J = 11.4, ^{4}J = 2.5 Hz, 8-H), 5.88 (1H, d, *J* = 11.4, 7-H) ppm.

^{13}C NMR (100 MHz, $CDCl_3$): δ = 189.2 (C_q, d, *J* = 4.1 Hz, C-9), 162.4 (C_q, d, *J* = 115 Hz, C-6 or C-15), 159.9 (C_q, d, *J* = 110 Hz, C-6 or C-15), 136.1 (C_t, d, *J* = 9.4 Hz, C-13), 132.1 (C_t,d, *J* = 1.9 Hz, C-11), 131.2 (C_t, d, *J* = 8.7 Hz, C-2), 130.1 (C_t, d, *J* = 2.7 Hz, C-3), 125.9 (C_q, d, *J* = 12.2 Hz, C-5), 125.1 (C_t, d, *J* = 3.5 Hz, C-14), 124.8 (C_t, d, *J* = 3.6 Hz, C-12 or C-4), 123.2 (C_q, d, *J* = 11.3 Hz, C-10), 117.2 (C_t, d, *J* = 23.9 Hz, C-12 or C-4), 116.4 (C_t, d, *J* = 21.7 Hz, C-1), 49.6 (C_t, dd, ^{3}J = 11 Hz, ^{4}J = 3 Hz, C-8), 43.0 (C_t, C-7) ppm.

^{19}F NMR (376 MHz, $CDCl_3$): δ = -108.8 ppm.

FT-IR (ATR): $\tilde{\upsilon}$ =3101 (w, *ν*(C-H_{arom})), 1681 (s, *ν*(C=O)), 1608 (s, *ν*(C=O)), 1479 (m), 1450 (s), 1375 (w), 1315 (w), 1275 (m), 1244 (m), 1205 (s), 1147 (s), 1105 (s), 1031 (w), 984 (w), 893 (w), 862 (w), 835 (m), 793 (s), 754 (s), 634 (w) cm^{-1}.

UV/Vis (acetonitrile, lg ε): λ_{max} = 252 (3.34), 297 (3.92) nm.

HRMS (ASAP, +): calc. for $[C_{15}H_{10}Br_2F_2O + H]^+$: m/z 402.9139, found m/z 402.9138.

EA: calc.: C, 44.66; H, 2.34, for $C_{15}H_{10}Br_2F_2O$, found: C, 44.59; H, 2.49%.

(Z)-1,3-Bis(2-fluorophenyl)-3-hydroxyprop-2-en-1-one (117)

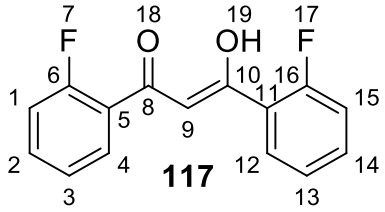

117

Ketone **119** (5.46 g, 13.5 mmol) was suspended in MeOH (80 ml) and refluxed at 80°C. KOH (3.42 g, 61.0 mmol, 4.5 eq.) was dissolved in MeOH (40 ml) and this solution was added dropwise to the reaction mixture. The reaction mixture changed in colour from yellow to orange and a yellow precipitate was observed. After 5.5 h a solution of conc. HCl (5 ml) in distilled H_2O (45 ml) was added slowly and the precipitate dissolves. After a further 15 h a pale yellow solid had precipitated out of solution and was filtered off after cooling to room temperature. CH_2Cl_2 (50 ml) was added to the filtrate and the phases were separated. The aqueous phase was extracted with CH_2Cl_2 (2 × 50 ml) and the combined organic phases were

dried over $MgSO_4$.The solvent was removed *in vacuo* to afford a red oil and the raw product recrystallised in EtOH to afford yellow crystals.

Yield: 1.74 g (6.67 mmol, 49%).

m.p.: 102–103 C (EtOH, lit.[359] 101.6–102.6°C).

R_f = 0.56 (pentane/CH_2Cl_2: 1:1).

^{1}H NMR (400 MHz, $CDCl_3$): δ = 16.6 (1H, s, OH), 8.00 (2H, td, ^3J = 7.8 Hz, ^4J = 1.8 Hz), 7.54–7.51 (1H, m), 7.51–7.47 (1H, m), 7.30 (1H, d, ^3J = 1.3 Hz), 7.28 (1H, m), 7.18 (1H, dd, ^3J = 8.3 Hz, ^4J = 0.9 Hz). 7.15 (1H, dd, ^3J = 8.3 Hz, ^4J = 0.9 Hz), 7.07 (1H, t, ^3J = 0.9 Hz) ppm.

^{13}C NMR (100 MHz, CDCl3): δ = 182.4 (C_q, d, J = 2.3 Hz), 161.4 (C_q, d, J = 255.9 Hz), 133.9 (C_t, d, J = 9.4 Hz), 130.4 (C_t, d, J = 1.9 Hz), 124.7 (C_t, d, J = 3.7 Hz), 123.9 (C_q, d, J = 10.4 Hz), 116.8 (C_t, d, J = 23.4 Hz), 102.6 (C_t , t, J = 13.2 Hz) ppm.

^{19}F NMR (376 MHz, $CDCl_3$): δ = -109.9 ppm.

FT-IR (ATR): $\tilde{\upsilon}$ = 3082 (w, ν(C-H_{arom})), 1828 (w), 1611 (m, ν(C=O)), 1588 (m), 1514 (m), 1487 (m), 1273 (m), 1252 (m), 1217 (m), 1152 (m, ν(C-F)), 1109 (w), 1089 (w), 1061 (w), 1033 (w), 955 (m), 869 (w), 840 (w), 819 (m), 777 (w), 747 (vs, δ(=C-H)$_{1,3\text{-subst}}$), 695 (w), 667 (w), 651 (w) cm^{-1}.

UV/Vis (acetonitrile, lg ε): λ_{max} = 227(3.97), 245 (3.96), 337 (4.29) nm.

MS (EI, 70 eV): m/z = 260 (M^+, 57), 241 (55), 212 (5), 165 (50), 123 (100), 95 (40), 69 (30).

The spectroscopic data corresponded to the data reported in the literature.[359]

2-(2-Fluorophenyl)-4H-chromen-4-one (121)

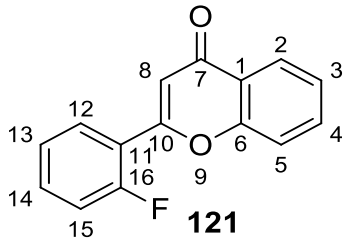

121

Diketone **117** (200 mg, 768 µmol) and aldehyde (99.0 mg, 798 µmol, 1.04 eq.) were dissolved in acetontrile (15 ml) and piperidine (0.05 ml) was added. The reaction mixture was refluxed at 80°C for 48 h. The solvent was removed *in vacuo* and the residue was purified using column chromatography (silica, pentane/ethyl acetate, 85:15) and recrystallised from cyclohexane to afford the product as pale yellow crystals.

Yield: 132 mg, 547 µmol, 71%.

m.p.: 97–99°C (cyclohexane, lit.[360] 99–100°C).

$\mathbf{R_f}$ = 0.16 (pentane/ethyl acetate; 85:15).

^{1}H NMR (400 MHz, $CDCl_3$): δ = 8.24 (1H, dd, ^3J = 8.0 Hz, ^4J = 1.7 Hz, 2-H), 7.92 (1H, td,^3J = 7.7 Hz, ^4J = 1.8 Hz), 7.71 (1H, ddd, ^3J = 8.5 Hz, ^4J = 7.2 Hz, ^4J = 1.7 Hz, 4-H), 7.55 (1H, d, ^3J = 8.5 Hz, 3-H), 7.53–4.49 (1H, m, 14-H), 7.44 (1H, ddd, ^3J = 8.1 Hz, ^4J = 7.1 Hz, ^4J = 1.1 Hz, 5-H), 7.33 (1H, td, ^3J = 7.6 Hz, ^4J = 1.2 Hz, 13-H), 7.25–7.21 (1H, m, 15-H), 6.95 (1H, s, 8-H) ppm.

^{13}C NMR (100 MHz, $CDCl_3$): δ = 178.6 (C_q, C-7), 160.7 (C_q, d, J = 255.9 Hz, C-16), 159.0 (C_q, d, J = 3.8 Hz, C-6), 156.5 (C_q, C-10), 134.0 (C_t, C-4), 133.0 (C_t, d, J = 9.1 Hz, C-14), 129.2 (C_t, d, J = 1.5 Hz, C-12), 125.9 (C_t, C-2), 125.4 (C_t, C-5), 124.8 (C_t, d, J = 3.9 Hz, C-13), 124.0 (C_q, C-1), 120.5 (C_q, d, J = 10.0 Hz, C-11), 118.2 (C_t), 117.1 (d, J = 22.5 Hz), 112.6 (d, J = 11.3 Hz) ppm.

^{19}F NMR (376 MHz, $CDCl_3$): δ = -110.8 ppm.

FT-IR (ATR): $\tilde{\upsilon}$ = 3066 (w, ν(C-H_{arom})), 1657 (s, ν(C=O)), 1606 (s, ν(C=O)), 1574 (m, ν(C=C_{arom})), 1491 (m), 1456 (s), 1371 (vs, ν(C-O)), 1308 (w), 1277 (w), 1236 (w), 1215 (m), 1126 (m), 1108 (w), 1041 (m), 1012 (w), 941 (w), 910 (w), 858 (m), 809 (w), 779 (m), 748 (vs), 675 (w), 660 (w) cm^{-1}.

UV/Vis (acetonitrile, lg ε): λ_{max} = 198 (3.40), 340 (3.01) nm.

MS (EI, 70 eV): m/z = 240 (M^+, 100), 212 (54), 183 (15), 120 (76), 92 (47), 64 (13).

HRMS (ESI+): calc. for $[C_{15}H_{10}FO_2]^+$ m/z 241.0659, found m/z 241.0662.

EA: calc.: C 75.00, H 3.78, F: 7.91, O: 13.32, found: C 75.26, H 3.77.

I-3-(2-Fluorophenyl)-1-phenylprop-2-en-1-one (135)

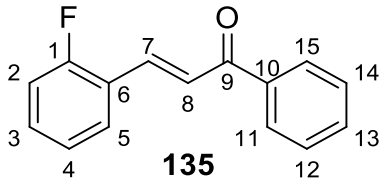

135

To a solution of acetophenone **134** (200 mg, 1.66 mmol) and 2-fluorobenzaldehyde **112** (206 mg, 1.66 mmol) in EtOH (2.5 ml) was added a solution of KOH (186 mg, 3.32 mmol, 2 eq.) in H_2O (5 ml), turning the clear mixture cloudy. After 24 h stirring at room temperature, CH_2Cl_2 (10 ml) and H_2O (10 ml) were added and the phases separated. The aqueous phase was extracted with CH_2Cl_2 (2 × 10 ml) and the combined organic phases were washed with H_2O (2 × 10 ml) and dried over $MgSO_4$. The solvent was removed *in vacuo* to afford a yellow oil. This raw product was purified using column chromatography (silica, CH_2Cl_2/petane 2:1) to give a pale yellow oil which became solid on standing.

Yield: 230 mg (1.02 mmol, 70%).

m.p.: 34–36°C (lit.[366] 36°C).

R_f = 0.48 (CH_2Cl_2/pentane, 2:1).

^{1}H NMR (400 MHz, $CDCl_3$): δ = 8.05–8.01 (2H, m, 11,15-H), 7.91 (1H, d, *J* = 16.0 Hz, 7-H), 7.68–7.63 (2H, m, 5,8-H), 7.60 (1H, t, *J* = 7.2 Hz, 13-H), 7.52 (2H, t, *J* = 7.4 Hz, 12,14-H), 7.42–7.36 (1H, m, 3-H), 7.21 (1H, td, *J* = 7.6 Hz, *J* = 1.0 Hz, 4-H), 7.14 (1H, dd, *J* = 10.8 Hz, *J* = 2.6 Hz, 2-H) ppm.

^{13}C NMR (100 MHz, $CDCl_3$): δ = 190.7 (C_q, C-9), 161.9 (C_q, d, *J* = 254.4 Hz, C-1), 138.2 (C_q, C-10), 137.7 (C_t, d, *J* = 2.1 Hz, C-7), 133.1 (C_t, C-13), 132.0 (C_t, d, *J* = 8.7 Hz, C-3), 130.0 (C_t, d, *J* = 3.1 Hz, C-5), 128.8 (C_t, C-12,14), 128.7 (C_t, C-11,15), 124.8 (C_t, d, *J* = 7.3 Hz, C-8), 124.7 (C_t, d, *J* = 3.6 Hz, C-4, 123.2 (C_q, d, *J* = 11.6 Hz, C-6), 116.5 Hz (C_t, d, *J* = 22.0 Hz, C-2) ppm.

^{19}F NMR (376 MHz, $CDCl_3$): δ = -113.3 ppm.

FT-IR (ATR): $\tilde{\upsilon}$ = 3056 (w, *ν*(C-H_{arom})), 1660 (s, *ν*(C=O)), 1604 (vs, ν(C=C_{arom})), 1573 (m, ν(C=C_{arom})), 1481 (m), 1452 (m), 1336 (m), 1317 (m), 1280 (s), 1213 (vs), 1184 (w), 1151 (w), 1093 (w), 1036 (w), 1012 (s), 974 (m), 893 (w), 864 (w), 831 (w), 783 (w), 754 (vs), 721 (s), 684 (vs), 663 (m) cm^{-1}.

UV/Vis (acetonitrile, lg ε): λ_{max} = 224 (3.79), 294 (4.05) nm.

MS (EI, 70 eV): m/z = 226 (M^+, 100), 207 (25), 197 (19), 121 (21), 105 (44), 101 (33), 77 (47).

The spectroscopic data corresponded to the data reported in the literature.[367]

anti-2,3-Dibromo-3-(2-fluorophenyl)-1-phenylpropan-1-one (136)

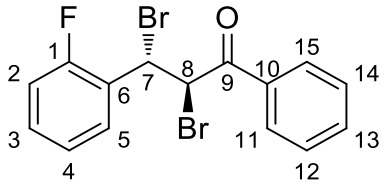

136

Ketone **135** (2.94 g, 13.0 mmol) was dissolved in $CHCl_3$ (15 ml) and the resulting solution was refluxed at 65°C. Br_2 (330 µl, 1.04 g, 13.0 mmol, 1 eq.) was added dropwise, on which the solution turned red/brown before returning to yellow. After 1.5 h $Na_2S_2O_3$ solution (20 ml) was added and the phases were separated. The organic phase was washed with $Na_2S_2O_3$ solution (2 × 10 ml) and distilled H_2O (4 × 20 ml) and dried over $MgSO_4$. The solvent was removed *in vacuo* to afford a yellow solid.

Yield: 256 mg (6.63 mmol, 51%, lit.[366] 51%).

m.p.:151–152°C; (lit.[366] 146°C).

^{1}H NMR (400 MHz, $CDCl_3$): δ = 8.12–8.09 (2H, m, 11,15-H), 7.69–7.64 (1H, m, 13-H), 7.58–7.53 (2H, m, 12,14-H), 7.50 (1H, t, ^3J = 7.5 Hz, 3-H), 7.42–7.37 (1H, m, 2-H), 7.22 (1H, t, ^3J = 7.6 Hz, 4-H), 7.15 (1H, dd, ^3J = 10.8 Hz,^{4} J = 8.3 Hz, 5-H), 6.03 (1H, d, ^3J = 11.3 Hz, 8-H), 5.87 (1H, d, ^3J = 11.2 Hz, 7-H) ppm.

^{13}C NMR (100 MHz, $CDCl_3$): δ = 191.0 (C_q, C-9), 160.8 (C_q, d, J = 250.4 Hz, C-1), 134.4 (C_q, C-10), 134.4 (C_t, C-13), 131.3 (C_t, C-2), 130.3 (C_t, C-3), 129.2 (C_t, C-11,15), 129.1 (C_t, C-12,14), 125.9 (C_q, d, J = 12.1 Hz, C-6), 124.8 (C_t, d, J = 4.1 Hz, C-4), 116.5 (C_t, d, J = 21.8 Hz, C-5), 45.4 (C_t, C-8), 43.4 (C_t, C-7) ppm.

^{19}F NMR (376 MHz, $CDCl_3$): δ = -114.3 (br) ppm.

FT-IR (ATR): $\tilde{\upsilon}$ = 3023 (w, *ν*(C-H_{arom})), 1677 (s, *ν*(C=O)), 1591 (m, ν(C=C_{arom})), 1491 (m), 1450 (m), 1382 (w), 1315 (w), 1272 (s), 1230 (vs), 1184 (w), 1149 (m), 1099 (w), 1074 (w), 1031 (w), 983 (m), 825 (m), 807 (w), 760 (vs), 736 (s), 721 (s), 683 (s), 660 (w) cm^{-1}.

UV/Vis (acetonitrile, lg ε): λ_{max} = 257 (4.15) nm.

HRMS (ASAP, +): calc. for $[C_{15}H_{11}Br_2FO + H]^+$ m/z 384.9233, found m/z 384.9226.

The spectroscopic data corresponded to the data reported in the literature.[366]

(E)-1-(2-Fluorophenyl)-3-phenylprop-2-en-1-one (138)

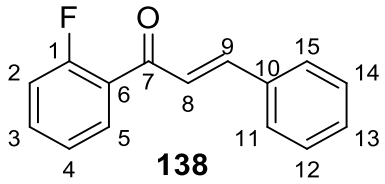

138

To a solution of 2-fluoroacetophenone **137** (200 mg, 1.45 mmol) and benzaldehyde **78** (154 mg, 1.45 mmol) in EtOH (2.5 ml) was added a solution of KOH (163 mg, 2.90 mmol, 2 eq.) in H_2O (5 ml), turning the clear mixture cloudy. After 24 h stirring at room temperature, CH_2Cl_2 (10 ml) and H_2O (10 ml) were added and the phases separated. The aqueous phase was extracted with CH_2Cl_2 (2 × 10 ml) and the combined organic phases were washed with H_2O (2 × 10 ml) and dried over $MgSO_4$. The solvent was removed *in vacuo* to afford a yellow oil. This raw product was purified using column chromatography (silica, CH_2Cl_2/ pentane 2:1) to give a pale yellow oil which became solid on standing.

Yield: 194 mg (857 mmol, 59%).

m.p.: 34–35°C.

^{1}H NMR (400 MHz, $CDCl_3$): δ = 7.82 (1H, td, *J* = 7.4 Hz, *J* = 1.8 Hz, 5-H), 7.75 (1H, dd, *J* = 15.8 Hz, *J* = 1.7 Hz, 9-H), 7.64–7.62 (2H, m, 11,15-H), 7.56–7.50 (1H, m, 3-H), 7.43–7.41 (3H, m, 12,13,14-H), 7.41–7.38 (1H, m, 8-H), 7.27 (1H, td, *J* = 7.4 Hz, *J* = 1.1 Hz, 4-H), 7.17 (1H, dd, *J* = 10.8 Hz, *J* = 2.5 Hz, 2-H) ppm.

^{13}C NMR (100 MHz, $CDCl_3$): δ = 189.3 (C_q, d, *J* = 2.6 Hz, C-7), 161.4 (C_q, d, *J* = 253.1 Hz, C-1), 145.0 (C_t, d, *J* = 1.4 Hz, C-9), 134.8 (C_q, C-10), 134.1 (C_t, d, *J* = 8.7 Hz, C-3), 131.1 (C_t, d, *J* = 2.8 Hz, C-5), 130.8 (C_t, C-12 or C-13 or C-14), 129.1 (C_t, C-12 or C-13 or C-14),

128.8 (C_t, C-11,15), 127.3 (C_q, d, J = 13.3 Hz, C-6), 125.8 (C_t, d, J = 6.6 Hz, C-8) 124.7 (C_t, d, J = 3.5 Hz, C-4), 116.7 (C_t, d, J = 23.1 Hz, C-2) ppm.

^{19}F NMR (376 MHz, $CDCl_3$): δ = -110.8 ppm.

FT-IR (ATR): $\tilde{\upsilon}$ = 3064 (w, ν(C-H_{arom})), 1664 (s, ν(C=O)), 1592 (vs), 1573 (s), 1484 (m), 1448 (m), 1334 (m), 1305 (w), 1224 (m), 1207 (s), 1159 (w), 1120 (w), 1020 (s), 978 (s), 949 (w), 893 (w), 870 (w), 839 (w), 758 (vs), 735 (s), 694 (m), 679 (m), 652 (m), 619 (w) cm^{-1}.

UV/Vis (acetonitrile, lg ε): λ_{max} = 226 (3.99), 303 (4.30) nm.

MS (EI, 70 eV): m/z = 226 (M^+, 74%), 225 (100), 197 (13), 131 (26), 123 (27), 103 (26), 77 (22).

anti-2,3-Dibromo-1-(2-fluorophenyl)-3-phenylpropan-1-one (139)

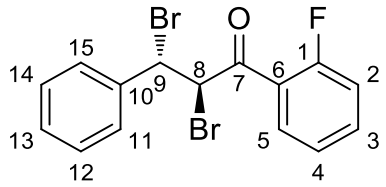

139

Ketone **138** (750 mg, 3.31 mmol) was dissolved in $CHCl_3$ (15 ml) and the resulting solution was refluxed at 65°C. Br_2 (90.0 µl, 264 mg, 3.31 mmol, 1 eq.) was added dropwise, on which the solution turned red/brown before returning to yellow. After 1.5 h $Na_2S_2O_3$ solution (15 ml) was added and the phases were separated. The organic phase was washed with distilled H_2O (4 × 20 ml) and dried over $MgSO_4$. The solvent was removed *in vacuo* to afford a yellow solid.

Yield: 682 mg (1.77 mmol, 53%).

m.p.: 108–109°C.

^{1}H NMR (400 MHz, $CDCl_3$): δ = 8.05 (1H, td, ^3J = 7.7 Hz, ^4J = 1.85 Hz, 5-H), 7.66–7.60 (1H, m, 3-H), 7.51–7.49 (2H, m, 11,15-H), 7.44–7.38 (3H, m, 12,13,14-H), 7.34–7.31 (1H, m, 4-H), 7.23 (1H, dd, ^3J = 11.6 Hz, ^4J = 8.3 Hz, 2-H), 5.86 (1H, dd, ^3J = 5.9 Hz, ^4J = 2.6 Hz, 8-H), 5.63 (1H, dd, ^3J = 11.2 Hz, ^4J = 2.7 Hz, 9-H) ppm.

^{13}C NMR (100 MHz, $CDCl_3$): δ = 189.6 (C_q, d, J = 4.0 Hz, C-7), 161.7 (C_q, d, J = 255.4 Hz, C-1), 138.3 (C_q, C-10), 136.0 (C_t, d, J = 9.4 Hz, C-3), 132.2 (C_t, d, J = 1.7 Hz, C-5), 129.4 (C_t, C-12,13,14), 129.0 (C_t, C-12,13,14), 128.5 (C_t, C-11,15), 125.1 (C_t, d, J = 3.3 Hz, C-4),

123.3 (C_q, d, J = 11.4 Hz, C-6), 117.2 (C_t, d, J = 23.1 Hz, C-2), 51.1 (C_t, d, J = 10.4 Hz, C-8), 49.9 (C_t, C-9) ppm.

^{19}F NMR (376 MHz, $CDCl_3$): δ = -108.8 ppm.

FT-IR (ATR): ῡ = 1685 (vs, ν(C=O)), 1606 (s), 1577 (w), 1487 (m), 1452 (m), 1373 (w), 1267 (m), 1230 (m), 1217 (m), 1141 (w), 1122 (w), 1062 (w), 1028 (w), 968 (m), 865 (w), 825 (w), 794 (w), 754 (vs), 692 (vs), 656 (w), 617 (w) cm^{-1}.

UV/Vis (acetonitrile, lg ε): λ_{max} = 251 (4.12), 296sh (3.40) nm.

HRMS (ASAP, +): calc. for $[C_{15}H_{11}Br_2FO+H]^+$ m/z 384.9233, found m/z 384.9228.

1-(2-fluorophenyl)-3-phenylpropane-1,3-dione (131)

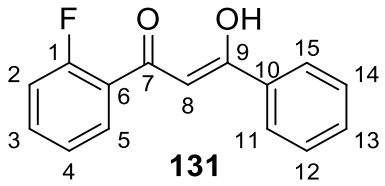

131

Ketone **139** (2.40 g, 6.22 mmol) was suspended in MeOH (40 ml) and refluxed at 80°C. KOH (1.57 g, 28.0 mmol, 4.5 eq.) was dissolved in MeOH (30 ml) and this solution was added dropwise to the reaction mixture. The reaction mixture changed in colour from yellow to orange and a yellow precipitate was observed. After 5 h a solution of conc. HCl (2 ml) in distilled H_2O (25 ml) was added slowly and the precipitate dissolves. After a further 15 h a colourless solid had precipitated out of solution and was filtered off after cooling to room temperature.

Yield: 652 mg (2.69 mmol, 43%).

m.p.: 58–60°C (MeOH/H_2O, lit.[361] 59.8–61.2°C)

^{1}H NMR (400 MHz, $CDCl_3$): δ = 16.8 (1H, s, O*H*), 8.03–7.99 (2H, m, 11,14-H), 7.98–7.97 (1H, m, 3-H) 7.58–7.56 (1H, m, 5-H), 7.52–7.47 (3H, m, 11,15,13-H), 7.29 (1H, dd, ^3J = 8.2 Hz, ^4J = 7.1 Hz, 4-H), 6.98 (1H, dd, ^3J = 11.6, ^4J = 8.3 Hz, 8-H) ppm.

^{13}C NMR (100 MHz, $CDCl_3$): δ = 186.6 (C_q, C-7), 181.5 (C_q, d, J = 3.8 Hz, C-9), 161.4 (C_q, C-1), 135.5 (C_q, C-10), 133.8 (C_t, d, J = 9.2 Hz, C-11 or C-13 or C-15), 132.8 (C_t, C-5), 130.3 (C_t, d, J = 2.1 Hz, C-12,14), 128.9 (C_t, C-11 or C-13 or C-15), 127.5 (C_t, C-3), 124.7 (C_t, d, J = 3.7 Hz, C-4), 124.0 (C_q, d, J = 10.6 Hz, C-6), 116.7 (C_t, d, J = 23.5 Hz, C-2), 98.1 (C_t, d, J = 13.3 Hz, C-8) ppm.

^{19}F NMR (376 MHz, $CDCl_3$): δ = -110.1 ppm.

FT-IR (ATR): ϑ̃ = 1592 (m, ν(C=C_{arom})), 1525 (m), 1484 (m, ν(C=C_{arom})), 1284 (w), 1259 (w), 1213 (w), 1118 (w), 1089 (w), 1060 (w), 1025 (w), 952 (w), 831 (w), 752 (vs), 684 (s), 621 (w) cm^{-1}.

UV/Vis (acetonitrile, lg ε): λ_{max} = 246 (3.97), 339 (4.31) nm.

MS (EI, 70 eV): m/z = 242 (M^+, 100), 223 (41), 165 (51), 123 (50), 105 (66), 95 (21), 77 (41).

2-phenyl-4H-chromen-4-one (147)

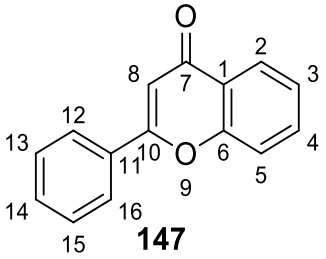

147

Fluorinated diketone **134** (107 mg, 442 µmol) was dissolved in acetonitrile (15 ml), to which piperidine (50 µl) was added. The reaction mixture was stirred at 80°C for 28 h. After allowing to cool to room temperature, ethyl acetate (10 ml) and H_2O (10 ml) were added and the phases separated. The aqueous phase was extracted with ethyl acetate (3 × 10 ml) and the combined organic phases were washed with H_2O (10 ml) and dried over $MgSO_4$. The solvent was removed *in vacuo* and the resulting orange oil was recrystallised in ethyl acetate to afford the product as a yellow solid. The filtrate was further purified, after distillation of the solvent with column chromatography (silica, pentane/ethyl acetate 9:1) to afford another portion of the product.

Yield: 35.9 mg (162 µmol, 37%).

m.p.: 94–96°C (lit.[364] 95–96°C).

R_f = 0.11 (9:1, pentane/ethyl acetate).

^{1}H NMR (400 MHz, $CDCl_3$): δ = 8.25 (1H, d, ^3J = 8.0 Hz, 2-H), 7.96–7.93 (2H, m, 12,16-H), 7.74–7.69 (1H, m, 4-H),7.59 (1H, d, ^3J = 8.4 Hz, 5-H), 7.57–7.51 (3H, m, 13,14,15-H), 7.45–7.41 (1H, m, 3-H), 6.85 (1H, s, 8-H) ppm.

^{13}C NMR (100 MHz, $CDCl_3$): δ = 178.6 (C_q, C-7), 163.6 (C_q, C-10), 156.4 (C_q, C-6), 133.9 (C_t, C-4), 132.0 (C_q, C-11), 131.8 (C_t, C-13,14,15), 129.2 (C_t, C-13,14,15), 126.5 (C_t, C-12), 125.9 (C_t, C-2), 125.4 (C_t, C-3), 124.1 (C_q, C-1), 118.3 (C_t, C-5), 107.8 (C_t, C-8) ppm.

FT-IR (ATR): $\tilde{\upsilon}$ = 3072 (w, *ν*(C-H_{arom})), 1639 (vs, ν(C=O)), 1603 (s, *ν*(C=O)), 1568 (m, ν(C=C_{arom})), 1494 (w), 1465 (s), 1373 (vs, ν(C-O)), 1311 (w), 1284 (w), 1261 (w), 1227 (w), 1128 (m), 1101 (w), 1078 (w), 1043 (w), 1028 (w), 1010 (w), 906 (m), 850 (m), 756 (vs), 686 (s), 671 (vs), 603 (m) cm^{-1}.

UV/Vis (acetonitrile, lg ε): λ_{max} = 193 (3.36), 250 (2.43), 256 (2.50), 290 (2.84), 309sh (2.97) nm.

MS (EI, 70 eV): m/z = 222 (M^+, 100%), 221 (29), 194 (42), 165 (14), 120 (56).

The spectroscopic data corresponded to the data reported in the literature.[364]

I-1-(2-Fluorophenyl)-3-(3-fluorophenyl)prop-2-en-1-one (141)

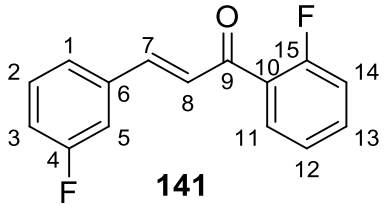

141

To a solution of 2-fluoroacetophenone **137** (459 mg, 3.70 mmol) and 3-fluorobenzaldehyde **140** (507 mg, 3.67 mmol) in EtOH (5 ml) was added a solution of NaOH (198 mg, 4.95 mmol, 1.35 eq.) in H_2O (10 ml), turning the clear mixture cloudy. After 24 h stirring at room temperature, CH_2Cl_2 (10 ml) and H_2O (10 ml) were added and the phases separated. The aqueous phase was extracted with CH_2Cl_2 (1 × 10 ml) and the combined organic phases were washed with H_2O (3 × 10 ml) and dried over $MgSO_4$. The solvent was removed *in vacuo* to afford a yellow oil. This raw product was purified using column chromatography (silica, pentane/CH_2Cl_2 2:1) to give a pale yellow oil which solidified upon standing.

Yield: 500 mg (2.05 mmol, 55%).

m.p.: 50–51°C.

R_f = 0.10 (pentane/CH_2Cl_2, 2:1).

^{1}H NMR (400 MHz, $CDCl_3$): δ = 7.83 (1H, td, *J* = 7.5 Hz, 11-H), 7.70 (1H, d, ^3J = 15.7 Hz, 7-H), 7.58–7.52 (1H, m, 13-H), 7.41–7.37 (3H, m, H-1,2,3), 7.32 (1H, d, *J* = 10.0 Hz, 8-H),

7.28 (1H, td, ^3J = 7.4 Hz, ^4J = 1.0 Hz, 12-H), 7.18 (1H, dd, ^3J = 10.8 Hz, ^4J = 8.3 Hz, 14-H), 7.14–7.09 (1H, m, 5-H) ppm.

^{13}C NMR (100 MHz, $CDCl_3$): δ = 188.9 (C_q, d, J = 2.7 Hz, C-9), 163.1 (C_q, d, J = 246.9 Hz, C-4), 162.5 (C_q, d, J = 253.3 Hz, C-15), 143.3 (C_t, dd, J = 2.7 Hz, J = 1.3 Hz, C-7), 137.1 (C_q, d, J = 7.7 Hz, C-6), 134.4 (C_t, d, J = 8.9 Hz, C-13), 131.2 (C_t, d, J = 2.7 Hz, C-11), 130.6 (C_t, d, J = 8.3 Hz, C-2), 127.0 (C_q, d, J = 13.1 Hz, C-10), 126.8 (C_t, d, J = 6.7 Hz, C-1), 124.8 (C_t, d, J = 2.9 Hz, C-3), 124.8 (C_t, d, J = 3.5 Hz, C-12), 117.6 (C_t, d, J = 21.4 Hz, C-5), 116.7 (C_t, d, J = 23.1 Hz, C-14), 114.8 (C_t, d, J = 21.8 Hz, C-8) ppm.

^{19}F NMR (376 MHz, $CDCl_3$): δ = -110.6, -112.5 ppm.

FT-IR (ATR): $\tilde{\upsilon}$ = 3064 (w, ν(C-H_{arom})), 1658 (s, ν(C=O)), 1603 (vs, ν(C=C)), 1576 (vs, ν(C=C_{arom})), 1477 (m), 1452 (s), 1328 (m), 1303 (m), 1267 (s), 1234 (s), 1203 (vs), 1147 (m), 1104 (m), 1051 (w), 1018 (s), 995 (vs), 941 (w), 899 (w), 870 (w), 854 (w), 816 (w), 783 (s), 760 (vs), 740 (vs), 690 (w), 665 (s), 646 (s) cm^{-1}.

UV/Vis (acetonitrile, lg ε): λ_{max} = 223 (3.91), 297 (4.33) nm.

MS (EI, 70 eV): m/z = 244 (M^+, 100), 215 (23), 196 (12), 123 (52), 101 (30), 95 (40), 75 (26).

EA: calc.: C 73.77, H 4.13, found: C 74.08, H 4.14.

***anti*-2,3-Dibromo-1-(2-fluorophenyl)-3-(3-fluorophenyl)propan-1-one (*142*)**

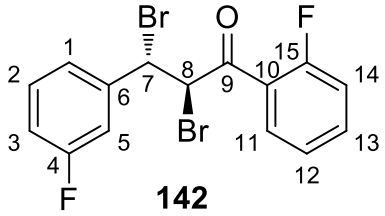

142

Ketone **141** (4.14 g, 17.0 mmol) was dissolved in $CHCl_3$ (130 ml) and heated to 65°C. Br_2 (0.9 ml, 2.8 g, 18 mmol) was added dropwise within 15 min and the reaction was stirred for a further 90 min. The reaction was allowed to cool to room temperature and saturated $Na_2S_2O_3$ solution (45 ml) was added and the resulting mixture was stirred for 10 min. The phases were separated and the organic phase was washed with distilled H_2O (3 × 55 ml) until neutral. The organic phase was dried over $MgSO_4$ and the solvent removed *in vacuo*. The raw product was recrystallised using EtOH to afford the product as colourless crystals.

Yield: 5.19 g (12.8 mmol, 75%).

m.p.: 92–94°C (EtOH).

$\mathbf{R_f}$ = 0.6 (cyclohexane/CH_2Cl_2 1:1).

^{1}H NMR (400 MHz, $CDCl_3$): δ = 8.05 (1H, dt, ^3J = 7.6 Hz, ^4J = 1.6 Hz, 11-H), 7.67–7.61 (1H, m, 13-H), 7.42–7.36 (1H, m, 2-H), 7.33 (1H, dd, ^3J = 8.1 Hz, ^4J = 7.1 Hz, 12-H), 7.28 (1H, d, ^3J = 7.7 Hz, H-1) 7.24–7.18 (2H, m, H-4,14), 7.08 (1H, ddt, ^3J = 8.3 Hz, ^4J = 2.5 Hz, ^4J = 1.0 Hz, 3-H), 5.78 (1H, dd, ^3J = 11.3 Hz, ^4J = 2.8 Hz, 8-H), 5.59 (1H, dd, ^3J = 11.3 Hz, ^4J = 2.7 Hz, 7-H) ppm.

^{13}C NMR (100 MHz, $CDCl_3$): δ = 189.2 (C_q, d, J = 4.0 Hz, C-9), 163.5 (C_q, d, J = 109 Hz, C-4 or C-15), 161.0 (C_q, d, J = 116.9 Hz, C-4 or C-15), 140.7 (C_q, d, J = 7.3 Hz, C-6), 136.1 (C_t, d, J = 9.2 Hz, C-13), 132.2 (C_t, d, J = 1.8 Hz, C-11), 130.5 (C_t, d, J = 8.3 Hz, C-2), 125.2 (C_t, d, J = 3.3 Hz, C-12), 124.3 (C_t, d, J = 3.1 Hz, C-1), 123.1 (C_q, d, J =11.4 Hz, C-10) 117.2 (C_t, d, J = 23.9 Hz, C-14), 116.5 (C_t, d, J = 21.2 Hz, C-3), 115.5 (C_t, d, J = 22.5 Hz, C-5), 50.8 (C_t, d, J = 10.6 Hz, C-8), 48.6 (C_t, d, J = 2.1 Hz, C-7) ppm.

^{19}F NMR (376 MHz, $CDCl_3$): δ = -108.7, -111.8 ppm.

FT-IR (ATR): $\tilde{\upsilon}$ = 1680 (vs, ν(C=O)), 1608 (s), 1592 (s, ν(C=C_{arom})), 1479 (s), 1450 (vs), 1371 (w), 1303 (m), 1263 (vs), 1240 (m), 1205 (m), 1143 (s), 1105 (m), 985 (m), 960 (w), 847 (w), 788 (vs), 756 (vs), 729 (w), 690 (vs), 658 (w), 638 (w) cm^{-1}.

UV/Vis (acetonitrile, lg ε): λ_{max} = 251 (4.04), 297sh (3.34) nm.

HRMS (ASAP, +): calc. for $[C_{15}H_{10}Br_2F_2O+H]^+$: m/z 402.9139, found m/z 402.9134.

EA: calc.: C 44.59, H 2.49, Br: 39.55 F: 9.40, O: 3.96, found: C 44.71, H 2.37.

1-(2-Fluorophenyl)-3-(3-fluorophenyl)propane-1,3-dione (132)

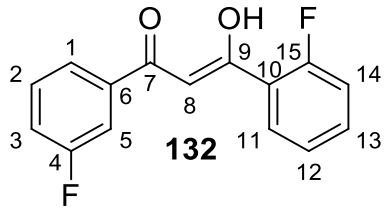

Ketone **142** (5.19 g, 12.8 mmol) was suspended in MeOH (190 ml) and heated to 80°C. KOH (3.25 g, 57.9 mmol) was dissolved in MeOH (60 ml) and added over the course 15 min to the reaction, upon which the solution turned brown. The reaction mixture was stirred for 4.5 h at 80°C, after which conc. HCl (6 ml) in H_2O (60 ml) was added dropwise within 15 min. The

reaction mixture turned yellow and after 18 h was allowed to cool to room temperature. A precipitate was observed and the solution was cooled to 0°C before filtration and washing with cooled H_2O to afford the product as a yellow solid.

Yield: 1.69 g (6.49 mmol, 51%).

m.p: 67–71 C.

R_f = 0.5 (cyclohexane/CH_2Cl_2, 1:1).

^{1}H NMR (400 MHz, $CDCl_3$): δ = 16.6 (1H, s, O*H*), 8.02 (1H, dt, ^3J = 7.7 Hz, ^4J = 1.7 Hz, 11-H), 7.76 (1H, ddd, ^3J = 7.7 Hz, ^4J = 1.5 Hz, ^4J = 0.9 Hz, 3-H), 7.68 (1H, ddd, ^3J = 9.5 Hz, ^4J = 2.6 Hz, ^4J = 1.7 Hz. 5-H), 7.55–7.50 (1H, m, 13-H), 7.49–7.44 (1H, m, 2-H), 7.29 (1H, dd, ^3J = 8.2 Hz, ^4J = 7.1 Hz, 12-H), 7.28–7.25 (1H, m, 1-H), 7.18 (1H, dd, ^3J = 11.7 Hz, ^4J = 8.2 Hz, 14-H), 6.95 (1H, d, *J* = 0.8 Hz, 8-H) ppm.

^{13}C NMR (100 MHz, $CDCl_3$): δ = 185.0 (C_q, C-7), 181.9 (C_q, d, J = 3.6 Hz, C-9), 163.5 (C_q, d, *J* = 161.4 Hz, C-4 or C-15), 161.0 (Cq, d, *J* = 169.4 Hz, C-4 or C-15), 137.8 (C_q, d, *J* = 7.1 Hz, C-6), 134.1 (C_t, d, *J* = 9.3 Hz, C-13), 130.5 (C_t, d, *J* = 7.8 Hz, C-2), 130.4 (C_t, d, *J* = 1.9 Hz, C-11), 124.8 (C_t, d, *J* = 4.0 Hz, C-12), 123.7 (C_q, d, J = 10.3 Hz, C-10), 123.1 (C_t, d, *J* = 3.0 Hz, C-3), 119.6 (C_t, d, *J* = 21.4 Hz, C-1), 116.8 (C_t, d, *J* = 23.3 Hz, C-14), 114.4 (C_t, d, *J* = 22.9 Hz, C-5), 98.2 (C_t, d, *J* = 13.7 Hz, C-8) ppm.

^{19}F NMR (376 MHz, $CDCl_3$): δ = -110.0, -111.9 ppm.

FT-IR (ATR): $\tilde{\upsilon}$ = 1610 (m, ν(C=O)), 1527 (s, ν(C=C_{arom})), 1483 (s), 1309 (m), 1263 (s), 1217 (m), 1186 (m), 1155 (m), 1115 (m), 1080 (m), 1057 (m), 999 (w), 941 (m), 887 (m), 868 (w), 823 (m), 787 (m), 756 (vs), 660 (m), 606 (m) cm^{-1}.

UV/Vis (acetonitrile, lg ε): λ_{max} = 245 (3.91), 340 (4.31) nm.

HRMS (ASAP, +): calc. for $[C_{15}H_{10}F_2O_2 + H]^+$: m/z 261.0716, found m/z 261.0722.

EA: calc.: C 69.23, H 3.87, F: 14.60, O: 12.30, found: C 68.93, H 3.87.

2-(3-Fluorophenyl)-4H-chromen-4-one (146)

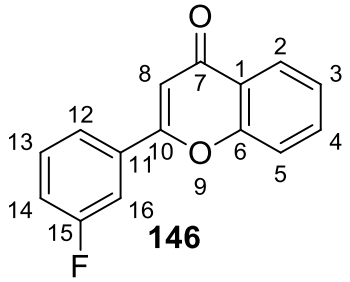

146

To a solution of fluorinated diketone **131** (102 mg, 392 µmol) in acetonitrile (15 ml) was added piperidine (50 µl). The resulting reaction mixture was stirred at 80°C for 5 h. After allowing to cool to room temperature, ethyl acetate (10 ml) and H_2O (10 ml) were added and the phases separated. The aqueous phase was extracted with ethyl acetate (2 × 10 ml) and the combined organic phases were washed with H_2O (10 ml) and dried over $MgSO_4$. The solvent was removed *in vacuo* and the precipitate was recrystallised from cyclohexane (2 ml) to afford 11.4 mg of the desired product. The filtrate was purified, after removal of the solvent, with column chromatography (silica, pentane/ethyl acetate, 9:1) to afford 20.8 mg product as a yellow solid and 10.3 mg (10%) of the starting material as an orange solid.

Yield: 32.2 mg (134 µmol, 34%).

m.p.: 98–100°C (lit.[365] 97–99°C).

$\mathbf{R_f}$ = 0.14 (pentane/ethyl acetate 9:1).

^{1}H NMR (400 MHz, $CDCl_3$): δ = 8.24 (1H, d, ^3J = 8.0 Hz, 2-H), 7.75–7.70 (2H, m, 4,13-H), 7.65 (1H, d, ^3J = 9.7 Hz, 12-H), 7.59 (1H, d, ^3J = 8.4 Hz, 5-H), 7.54–7.49 (1H, m, 14-H), 7.47–7.43 (1H, m, 3-H), 7.28–7.22 (1H, m, 12-H), 6.83 (1H, s, 8-H) ppm.

^{13}C NMR (100 MHz, $CDCl_3$): δ = 178.5 (C_q, C-7), 163.2 (C_q, d, J = 237 Hz, C-15), 161.2 (C_q, d, J = 7.2 Hz, C-10), 156.3 (C_q, C-10), 134.2 (C_t, C-4), 134.1 (C_q, C-11), 130.9 (C_t, d, J = 8.2 Hz, 14), 125.9 (C_t C-2), 125.6 (C_t, C-3) 124.1 (C_q, C-1), 122.1 (C_t, d, J = 3.1 Hz, C-13), 118.7 (C_t, d, J = 21.4 Hz, C-16), 118.3 (C_t, C-5), 113.5 (C_t, d, J = 23.9 Hz, C-12), 108.3 (C_t, C-8) ppm.

^{19}F NMR (376 MHz, $CDCl_3$): δ = -111.3 ppm.

FT-IR (ATR): ϑ = 3075 (w, ν(C-H_{arom})), 1643 (vs, ν(C=O)), 1602 (s, ν(C=O)), 1567 (m, ν(C=C_{arom})), 1468 (m), 1448 (m), 1373 (s, ν(C-O)), 1270 (m), 1248 (w), 1224 (w), 1174 (w),

1126 (m), 1078 (w), 1045 (w), 1016 (w), 947 (m), 897 (w), 874 (m), 816 (w), 777 (s), 756 (s), 696 (m), 657 (w), 607 (w) cm^{-1}.

UV/Vis (acetonitrile, lg ε): λ_{max} = 193 (4.44), 250 (4.06), 256 (4.06) 287 (4.06), 309sh (3.88) nm.

MS (EI, 70 eV): m/z = 240 (M^+, 100%), 212 (54), 183 (14), 120 (65).

The spectroscopic data corresponded to the data reported in the literature.[365]

(E)-1,3-Bis(3-fluorophenyl)prop-2-en-1-one (144)

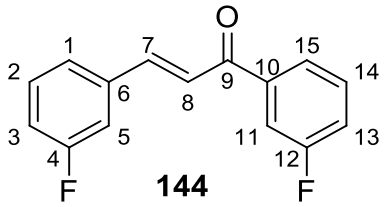

144

To a solution of ketone **140** (507 mg, 3.67 mmol) and aldehyde **137** (459 mg, 3.70 mmol) in EtOH (5 ml) was added a solution of NaOH (198 mg, 4.95 mmol, 1.35 eq.) in H_2O (10 ml), turning the clear mixture cloudy. After 24 h stirring at room temperature, CH_2Cl_2 (10 ml) and H_2O (10 ml) were added and the phases separated. The aqueous phase was extracted with CH_2Cl_2 (1 × 10 ml) and the combined organic phases were washed with H_2O (3 × 10 ml) and dried over $MgSO_4$. The solvent was removed *in vacuo* to afford a yellow oil. This raw product was purified using column chromatography (silica, pentane/CH_2Cl_2 2:1) to give a pale yellow solid.

Yield: 573 mg (2.34 mmol, 63%).

m.p.: 63–64°C.

^{1}H NMR (400 MHz, $CDCl_3$): δ = 7.81–7.76 (2H, m, 7,15-H), 7.71 (1H, d, ^3J = 9.4 Hz, 13-H), 7.53–7.48 (2H, m, 8,14-H), 7.44–7.38 (2H, m, 1,2-H), 7.35 (1H, d,^{3} J = 9.7 Hz, 5-H), 7.30 (1H, td, ^3J = 8.2 Hz, ^4J = 2.6 Hz, 11-H), 7.16–7.11 (1H, m, 3-H) ppm.

^{13}C NMR (100 MHz, $CDCl_3$): δ = 189.0 (C_q, d, J = 2.2 Hz, C-9), 163.1 (C_q, d, J = 247 Hz, C-4,12), 144.2 (C_t, d, J = 2.9 Hz, C-7), 140.2 (C_q, d, J = 6.4 Hz, C-10), 137.0 (C_q, d, J = 7.7 Hz, C-6), 130.7 (C_t, d, J = 8.3 Hz, C-2), 130.5 (C_t, d, J = 7.7 Hz, C-14), 124.8 (C_t, d, J = 2.9 Hz, C-1), 124.3 (C_t, d, J = 3.0 Hz, C-15), 122.8 (C_t, C-8), 120.1 (C_t, d, J = 21.4 Hz, C-11), 117.8 (C_t, d, J = 21.4 Hz, C-3), 115.5 (C_t, d, J = 22.3 Hz, C-13), 114.7 (C_t, d, J = 21.9 Hz, C-5) ppm.

^{19}F NMR (376 MHz, $CDCl_3$): δ = -111.6, -112.3 ppm.

FT-IR (ATR): ϑ̃ = 1670 (m, *ν*(C=O)), 1610 (s, ν(C=C)), 1581 (vs, ν(C=C_{arom})), 1484 (s, ν(C=C_{arom})), 1442 (s), 1336 (s), 1313 (m), 1274 (s), 1244 (vs), 1217 (s), 1176 (m), 1151 (s), 1072 (w), 1024 (s), 999 (w), 972 (vs), 920 (w), 874 (w), 845 (m), 816 (s), 777 (vs), 729 (m), 671 (vs). cm^{-1}.

UV/Vis (acetonitrile, lg ε): λ_{max} = 225 (4.04), 299 (4.35) nm.

MS (EI, 70 eV): m/z = 244 (100, M^+), 243 (78), 215 (20), 123 (35), 101 (30), 95 (46), 75 (23).

The spectroscopic data (^{1}H, ^{13}C, ^{19}F NMR) corresponded to the data reported in the literature.[363]

(E)E-2,3-Dibromo-1,3-bis(3-fluorophenyl)prop-2-en-1-one (145)

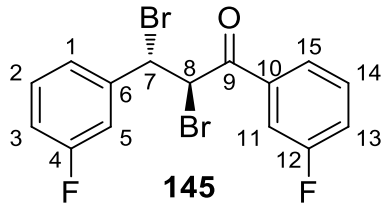

145

Ketone **144** (4.40 g, 18.0 mmol) was dissolved in $CHCl_3$ (140 ml) and refluxed at 65°C. Br_2 (1.0 ml, 3.1 g, 19 mmol) was added dropwise within 15 min and the solution was refluxed for a further 75 min. After allowing to cool to room termperature, saturated $Na_2S_2O_3$ solution (50 ml) was added and the resulting mixture was stirred for 10 min. The phases were separated and the organic phase was washed with distilled H_2O (3 × 60 ml) until neutral. The organic phase was dried over $MgSO_4$ and the solvent removed *in vacuo*. The raw product was recrystallised using EtOH to afford the product as a colourless solid.

Yield: 5.84 g (14.5 mmol, 81%).

m.p.: 112–115 C (EtOH).

R_f = 0.3 (cyclohexane/CH_2Cl_2, 1:1).

^{1}H NMR (400 MHz, $CDCl_3$): δ = 7.87 (1H, qd, ^3J = 7.8 Hz, J = 0.9 Hz, 13-H), 7.78 (1H, qd, ^3J = 9.2 Hz, ^4J = 1.3 Hz, 15-H), 7.57–7.52 (1H, m, 14-H), 7.43–7.35 (2H, m, 11,3-H), 7.30 (1H, td, ^3J = 7.7 Hz, ^4J = 1.2 Hz, 1-H), 7.24 (1H, td, ^3J = 9.4 Hz, ^4J = 2.1 Hz, 5-H), 7.09 (2H, ddt, ^3J = 8.3 Hz, ^4J = 2.5 Hz, ^4J = 1.0 Hz, 8-H), 5.63 Hz (2H, dd, ^3J = 39.6 Hz, ^4J = 11.3 Hz, 7-H) ppm.

^{13}C NMR (100 MHz, $CDCl_3$): δ = 190.1 (C_q, C-9), 164.4 (C_q, d, *J* = 26.3 Hz, C-4 or C-12), 162.0 (C_q, d, *J* = 24.9 Hz, C-4 or C-12), 140.7 (C_q, d, *J* = 7.5 Hz, C-6), 136.6 (C_q, d, *J* = 6.5 Hz, C-10), 131.1 (C_t, d, *J* = 7.7 Hz, C-14), 130.8 (C_t, d, *J* = 8.3 Hz, C-3), 124.9 (C_t, d, *J* = 3.1 Hz, C-13), 124.5 (C_t, d, *J* = 3.0 Hz, C-1), 116.6 (C_t, d, J = 21.1 Hz, C-2), 116.1 (C_t, d, *J* = 22.9 Hz, C-15), 115.7 (C_t, d, *J* = 22.6 Hz, C-5), 48.6 (C_t, d, *J* = 2.1 Hz, C-7), 46.9 (C_t, C-8) ppm.

^{19}F NMR (376 MHz, $CDCl_3$): δ = -110.7 , -111.6 ppm.

UV/Vis (acetonitrile, lg ε): λ_{max} = 253 (4.03), 300sh (3.11) nm.

FT-IR (ATR): $\tilde{\upsilon}$ = 1680 (s, ν(C=O)), 1589 (s, ν(C=C_{arom})), 1489 (w),1446 (s), 1373 (w), 1298 (w), 1281 (w), 1254 (vs), 1140 (s), 1078 (s), 1024 (s), 937 (w), 895 (s), 796 (s), 758 (s), 729 (s), 700 (s), 671 (s) cm^{-1}.

HRMS (ASAP, +): calc. for $[C_{15}H_{10}Br_2F_2O + H]^+$m/z 402.9139, found m/z 402.9133.

EA: calc.: C 44.59, H 2.49, found: C 44.91, H 2.41

1,3-bis(3-fluorophenyl)propane-1,3-dione (133)

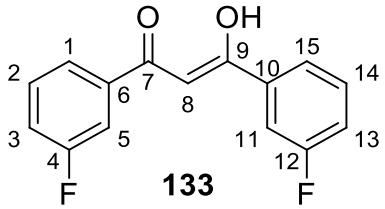

133

Ketone **145** (5.84 g, 14.5 mmol) was suspended MeOH (200 ml) and heated to 80°C. KOH (3.72 g, 66.3 mmol) was dissolved in MeOH (60 ml) and added over the course 15 min to the reaction, upon which the solution turned brown. The reaction mixture was stirred for 4.5 h at 80°C, after which conc. HCl (7 ml) in H_2O (60 ml) was added dropwise within 15 min. The reaction mixture turned yellow and after 17 h was allowed to cool to room temperature. A precipitate was observed and the solution was cooled to 0°C before filtration and washing with cooled H_2O to afford the product as a yellow solid.

Yield: 1.68 (6.46 mmol, 46%).

m.p.: 124–125°C (MeOH/H_2O, lit.[362] 127°C).

R_f = 0.50 (cyclohexane/CH_2Cl_2 1:1).

^{1}H NMR (400 MHz, $CDCl_3$): δ = 16.63 (1H, O*H*), 7.77 (2H, qd, ^{3}J = 7.9 Hz, ^{4}J = 0.9 Hz, 5,11-H), 7.68 (2H, ddd, ^{3}J = 9.67 Hz, ^{4}J = 2.3 Hz, ^{4}J = 1.7 Hz, 1,15-H), 7.52–7.45 (2H, m, 3,13-H), 7.29–7.24 (2H, m, 2,14-H), 7.29 (1H, s, 8-H) ppm.

^{13}C NMR (100 MHz, $CDCl_3$): δ = 184.7 (C_q, d, *J* = 2.5 Hz, C-7,9), 164.3 (C_q, C-4 or C-12), 161.9 (C_q, C-4 or C-12), 137.7 (C_q, d, *J* = 7.1 Hz, C-6,10), 130.5 (C_t, d, *J* = 7.9 Hz, C-3,13), 123.0 (C_t, d, *J* = 3.1 Hz, C-5,11), 119.7 (C_t, d, *J* = 21.4 Hz, C-2,14), 114.31 (C_t, d, *J* = 22.9 Hz, C-1,15), 93.6 (C_t, s, C-8) ppm.

^{19}F NMR (376 MHz, $CDCl_3$): δ = -111.7 ppm.

FT-IR (ATR): $\tilde{\upsilon}$ = 1539 (m, ν(C=C_{arom})), 1468 (m), 1306 (w), 1252 (s), 1184 (m), 1078 (w), 999 (w), 926 (m), 883 (w), 854 (m), 766 (vs), 737 (s), 665 (s), 614 (w) cm^{-1}.

UV/Vis (acetonitrile, lg ε): λ_{max} = 226sh (3.80), 246 (3.88), 294sh (3.81), 343 (4.27) nm.

MS (EI, 70 eV): m/z = 260 (M^+, 100), 165 (70), 123 (78), 95 (47).

EA: calc.: C 69.23, H 3.87, F: 14.60, O: 12.30, found: C 69.52, H 3.93.

2-(4-fluorobenzylidene)-1,3-bis(3-fluorophenyl)propane-1,3-dione (148)

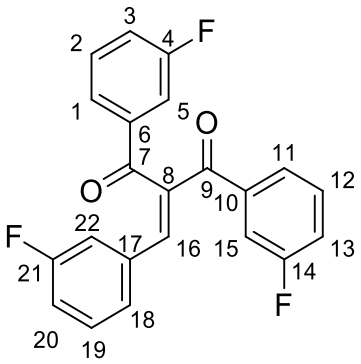

148

Diketone **133** (3.7 g, 14.2 mmol) and 3-fluorobenzaldehyde (5.29 g, 42.6 mmol, 3 eq.) were dissolved in acetontrile (100 ml) and piperidine (140 µl, 121 mg, 1.42 mmol, 0.1 eq.) was added. Molecular sieve (4 Å, 10 g) was added and the resulting solution was heated to reflux at 80°C for 4 h. It was observed that a solid precipiated out of solution. Acetonitrile was added (50 ml), but the solid did not dissolve. After refluxing for a further 15 h, TLC reaction control inidcated that starting material was still present. A sample (0.2 ml) of the reaction mixture was taken after a further 5 h and after ^{1}H NMR analysis the ratio of product: starting material was determined to be 1:1.7. 3-fluorobenzaldehyde (1.80 g, 14.5 mmol, 1.02 eq.) was added. After a further 42 h at 80°C, 3-fluorobenzaldehyde (900 mg) and piperidine (20 µl)

were added, as the ratio of product: starting material had decreased from 1:1.45 to 1:1.39. A final TLC reaction control after a further 23 h indicated that the side-product was present and ^{1}H NMR reaction control indicated that the ratio of starting material: product was 1:1.14. After allowing to cool to room temperature, ethyl acetate (150 ml) and H_2O (150 ml) were added and the phases separated. The solid remains in the aqeous phase, which was extracted with ethyl acetate (3 × 50 ml). The combined organic phases were washed with brine (50 ml) and dried over MgSO4. The solvent was removed *in vacuo* and the oily residue was combined with silica and was purified using column chromatography (pentane/ethyl acetate, 95:5) to afford the product as a yellow solid. Starting material was collected in a separate fraction (819 mg) and a further mixture fraction of starting material and side-product (743 mg).

Yield: 2.14 g (5.84 mmol, 41%) + 819 mg **133** (3.15 mmol, 22%).

m.p.: 36–37°C.

$\mathbf{R_f}$ = 0.2 (pentane/ethyl acetate, 9:1).

^{1}H NMR (400 MHz, $CDCl_3$): δ = 7.69 (1H, d, *J* = 7.7 Hz, 1-H), 7.66–7.61 (2H, m, 5,15-H), 7.55 (1H, d, *J* = 9.0 Hz, 11-H), 7.51–7.46 (2H, m, 16,13-H), 7.42–7.37 (1H, m, 2-H), 7.31 (1H, td, *J* = 8.3 Hz, *J* = 2.6 Hz, 13-H), 7.28–7.21 (2H, m, 3,19-H), 7.11 (1H, d, *J* = 7.5 Hz, 22-H), 7.05–6.99 (1H, m, 18,20-H) ppm.

^{13}C NMR (100 MHz, $CDCl_3$): δ = 195.1 (d, J = 2.4 Hz, C_q, C-7), 193.2 (d, *J* = 2.1 Hz, C_q, C-9), 163.1 (C_q, d, *J* = 248.9 Hz, C-4), 162.7 (C_q, d, *J* = 249.1 Hz, C-21), 162.7 (C_q, d, *J* = 247.9 Hz, C-14), 142.9 (C_t, d, *J* = 2.5 Hz, C-16), 139.8 (C_q, C-8), 139.0 (d, *J* = 6.4 Hz, C_q, C-10), 138.1 (C_q, d, *J* = 6.3 Hz, C-6), 134.8 (d, *J* = 7.9 Hz, C_q, C-17), 130.8 (C_t, d, *J* = 7.7 Hz, C-3), 130.7 (C_t, d, *J* = 8.3 Hz, C-2 or C-19), 130.6 (C_t, d, *J* = 7.8 Hz, C-12), 125.9 (C_q, d, *J* = 3.1 Hz, C-22), 125.4 (C_t, t, *J* = 3.2 Hz, C-15 or C-5), 121.5 (C_t, d, *J* = 21.6 Hz, C-2 or C-19), 120.2 (d, *J* = 21.4 Hz, C_t, C-13), 117.9 (d, *J* = 21.2 Hz, C_t, C-18 or C-20), 116.7 (C_t, d, *J* = 21.4 Hz, C-18 or C-20), 116.5 (C_t, d, *J* = 21.6 Hz, C-11), 115.9 (C_t, d, *J* = 22.5 Hz, C-15 or C-5) ppm.

^{19}F NMR (376 Hz, $CDCl_3$): δ = -111.0, -111.1, -111.4 ppm.

FT-IR (ATR): $\tilde{\upsilon}$ = 3074 (w, *ν*(C-H_{arom})), 2923 (w, *ν*(C-H_{arom})), 1675 (m, *ν*(C=O)), 1643 (m, *ν*(C=O)), 1610 (w), 1581 (s, ν(C=C_{arom})), 1483 (w), 1439 (s), 1367 (w), 1250 (vs), 1194 (m), 1173 (m), 1149 (m), 1097 (w), 1074 (w), 1001 (w), 966 (w), 937 (w), 872 (m), 825 (m), 781 (s), 756 (m), 679 (s), 654 (w), 617 (w) cm^{-1}.

UV/Vis (acetonitrile, lg ε): λ_{max} = 253 (4.43), 292 (4.40) nm.

MS (EI, 70 eV): m/z = 366 (M^+, 17%), 338 (18), 227 (13), 123 (100), 95 (53).

HRMS (ESI, +): calc. for $[C_{22}H_{13}F_3O_2 + Na]^+$ m/z 389.07599 found m/z 389.07542.

EA: calc.: C 72.13, H 3.58 for $C_{22}H_{13}F_3O_2$, found: C 72.48, H 3.55.

2-(3-Fluorobenzylidene)-1,3-bis(3-fluorophenyl)propane-1,3-diol (151)

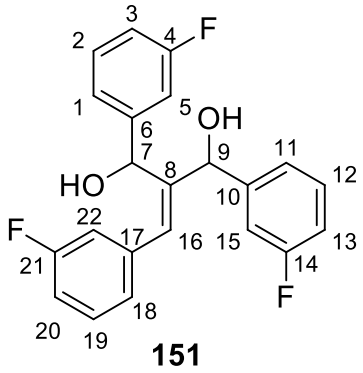

151

Diketone **148** (2.14 g, 5.84 µmol, 1 eq.) was dissolved in anhydrous CH_2Cl_2 (25 ml) and cooled to -78°C. To this mixture was added a 0.4 M solution of $CeCl_3 \cdot 7\ H_2O$ (3.05 g, 8.18 mmol) in MeOH (20 ml). The resulting suspension was stirred for 20 min, after which $NaBH_4$ (464 mg, 12.3 mmol, 2.1 eq.) was added. The reaction mixture was stirred at -78°C for 30 min and then allowed to reach room temperature for 1 h, after which the reaction was complete. Et_2O (40 ml) and 2 M HCl (25 ml) were added and the phases separated. The aqueous phase was extracted with Et_2O (3 × 30 ml) and the organic phases were washed with H_2O (30 ml) and dried over $MgSO_4$. The solvent was removed *in vacuo* to afford an orange oil, which was purified using column chromatography (silica, $CHCl_3$/ethyl acetate 95:5) to afford two isomers as colourless solids.

Yield: 1.82 g (4.90 mmol, 84%).

*R,R/S,S-diasteroisomer-**151***

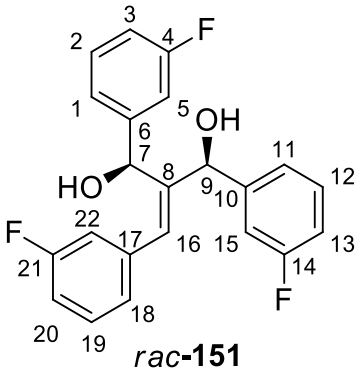

rac-**151**

Yield: 387 mg (1.04 mmol, 18%).

m.p.: 110–111°C.

$\mathbf{R_f}$ = 0.24 ($CHCl_3$/ethyl acetate, 95:5).

^{1}H NMR (400 MHz, $CDCl_3$): δ = 7.33–7.20 (3H, m, 2,19,12-H), 7.11–7.08 (2H, m, C*H*), 7.06–6.88 (6H, m), 5.88 (1H, d, *J* = 5.1 Hz), 5.38 (1H, s), 2.45 (1H, d, *J* = 5.8 Hz), 2.39 (1H, d, *J* = 3.3 Hz) ppm.

^{13}C NMR (100 MHz, $CDCl_3$): δ = 163.1 (C_q, d, *J* = 246 Hz), 163.0 (C_q, d, *J* = 247 Hz), 162.9 (C_q, d, *J* = 247 Hz), 145.3 (C_q, d, *J* = 6.7 Hz), 144.5 (C_q, d, *J* = 6.8 Hz), 143.9 (Cq), 138.1 (C_q, d, *J* = 7.7 Hz), 130.4 (C_t, d, *J* = 2.1 Hz), 130.2 (C_t, d, *J* = 5.2 Hz), 130.2 (C_t, d, *J* = 4.9 Hz), 130.0 (C_t, d, *J* = 8.2 Hz), 124.5 (C_t, d, *J* = 2.9 Hz), 122.4 (C_t, d, *J* = 2.9 Hz), 121.5 (C_t, d, *J* = 2.9 Hz), 115.7 (C_t, d, *J* = 21.8 Hz), 114.9 (C_t, d, *J* = 13.2 Hz), 114.7 (C_t, d, *J* = 13.1 Hz), 114.3 (C_t, d, *J* = 21.2 Hz), 113.7 (C_t, d, *J* = 22.2 Hz), 113.1 (C_t, d, *J* = 22.7 Hz), 74.4 (C_t, d, *J* = 1.9 Hz), 70.7 (C_t, d, *J* = 1.9 Hz) ppm.

^{19}F NMR (376 Hz, $CDCl_3$): δ = -112.7, -112.6, -112.4 ppm.

FT-IR (ATR):ϑ̃ = 3318 (m, *ν*(O-H)), 2919 (w), 1612 (w), 1581 (m), 1485 (m, ν(C=C_{arom})), 1439 (m), 1244 (vs), 1142 (m), 1117 (w), 1024 (m), 962 (w), 933 (w), 881 (s), 833 (w), 806 (m), 773 (s), 698 (vs) cm^{-1}.

UV/Vis (acetonitrile, lg ε): λ_{max} = 248 (5.53) nm.

HRMS (ESI, +): calc. for $[C_{22}H_{17}F_3O_2+Na]^+$ m/z 393.10729, found m/z 393.10790.

EA: calc.: C 71.35, H 4.63 for $C_{22}H_{17}F_3O_2$, found: C 71.67, H 4.62.

*R,S/S,R-diasteroisomer-**151***

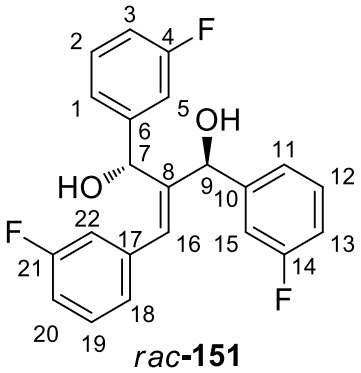

rac-**151**

Yield: 1.43 g (3.86 mmol, 66%).

m.p.: 114–115°C.

$\mathbf{R_f}$ = 0.12 ($CHCl_3$/ethyl acetate, 95:5).

^{1}H NMR (400 MHz, $CDCl_3$): δ = 7.35–7.27 (3H, m, 2,12,19-H), 7.16–7.12 (1H, m, 15-H), 7.11–7.07 (2H, m, 5,22-H), 7.00–6.95 (6H, m, 1,3,11,13,18,20-H) 6.20 (1H, s, 16-H), 5.88 (1H, d, *J* = 7.4 Hz, 9-H), 5.28 (1H, d, *J* = 3.0 Hz, 7-H), 3.80 (1H, d, *J* = 7.4 Hz, C9-O*H*), 2.89 (1H, d, *J* = 3.4 Hz, C7-O*H*) ppm.

^{13}C NMR (100 MHz, $CDCl_3$): δ = 163.3 (C_q, d, *J* = 246 Hz, C-4 or C-14 or C-21), 163.0 (C_q, d, *J* = 247 Hz, C-4 or C-14 or C-21), 162.8 (C_q, d, *J* = 247 Hz, C-4 or C-14 or C-21), 145.2 (C_q, d, *J* = 6.7 Hz, C-8), 143.8 (C_q, C-6), 143.7 (C_q, d, *J* = 6.9 Hz, C-10), 138.0 (C_q, d, *J* = 7.7 Hz, C-17), 132.3 (C_t, d, *J* = 2.1 Hz, C-16), 130.2 (C_t, d, *J* = 2.1 Hz, C-2 or C-12 or C-19), 130.1 (C_t, d, *J* = 1.9 Hz, C-2 or C-12 or C-19), 130.1 (C_t, d, *J* = 8.2 Hz, C-2 or C-12 or C-19), 124.5 (C_t, d, *J* = 2.9 Hz, C-5 or C-22), 122.8 (C_t, d, *J* = 2.9 Hz, C-1 or C-3 or C-11 or C-13 or C-18 or C-20), 121.2 (C_t, d, *J* = 2.7 Hz, C-5 or C-22) 115.7 (C_t, d, *J* =21.7 Hz, C-1 or C-3 or C-11 or C-13 or C-18 or C-20), 115.0 (C_t, d, *J* = 20.7 Hz, C-1 or C-3 or C-11 or C-13 or C-18 or C-20), 114.8 (C_t, d, *J* = 20.7 Hz, C-1 or C-3 or C-11 or C-13 or C-18 or C-20), 114.3 (C_t, d, *J* = 12.6 Hz, C-1 or C-3 or C-11 or C-13 or C-18 or C-20), 114.1 (C_t, d, *J* = 13.5 Hz, C-1 or C-3 or C-11 or C-13 or C-18 or C-20), 112.8 (Ct, d, *J* = 22.5 Hz), 74.1 (C_t, d, *J* = 2.1 Hz, C-7), 71.6 (C_t, d, *J* = 1.9 Hz, C-9) ppm.

^{19}F NMR (376 Hz, $CDCl_3$): δ = -112.7, -112.5, -112.4 ppm.

FT-IR (ATR): ῡ = 3484 (w, *v*(O-H)), 3315 (w, *v*(O-H)), 1739 (w), 1610 (w), 1585 (m), 1485 (m, ν(C=C_{arom})), 1437 (m), 1240 (vs), 1143 (m), 1039 (s), 1018 (s), 941 (m), 876 (m), 837 (w), 791 (vs), 754 (s), 702 (s), 687 (m), 638 (w) cm^{-1}.

UV/Vis (acetonitrile, ε / l mol^{-1} cm^{-1}): λ_{max} = 247 (4.04) nm.

HRMS (ESI, +): calc.for $[C_{22}H_{17}F_3O_2 + Na]^+$ m/z 393.10729, found m/z 393.10786.

EA: calc.: C 71.35, H 4.63 for $C_{22}H_{17}F_3O_2$, found: C 71.73, H 4.70.

2,6-difluoro-9-(3-fluorophenyl)-9,10-dihydroindeno[1,2-a]indene (154)

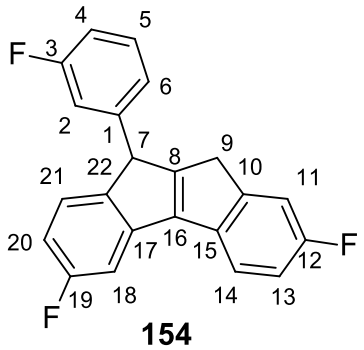

154

Dialcohol **151** (900 mg, 2.43 mmol) was dissolved in chlorobenzene (6 ml) and polyphosphoric acid (480 mg) was added, upon which the solution turned red. The reaction mixture was heated to 130°C under nitrogen for 21 h. After allowing to cool to room temperature, H_2O (50 ml) and CH_2Cl_2 (25 ml) were added and the phases separated. The aqueous phase was extracted with CH_2Cl_2 (3 × 25 ml) and the combined organic phases were dried over $MgSO_4$ and the solvent removed *in vacuo*. The resulting oily brown residue was purified via column chromatography (silica, 95:5, cyclohexane, CH_2Cl_2) and **154** was separated from the C_3/C_1 TBTQ mixture by recrystallisation in hexane, before recrystallisation in toluene to afford colourless crystals.

Yield: 68.6 mg (205 µmol, 8%).

m.p.: 122–123°C (toluene).

$\mathbf{R_f}$ = 0.24 (Cyclohexane/CH_2Cl_2, 95:5).

^{1}H NMR (400 MHz, $CDCl_3$): δ = 7.63 (1H, dd, *J* = 8.3 Hz, *J* = 5.1 Hz, 14-H), 7.38 (1H, d, *J* = 8.7 Hz, 18-H), 7.28–7.24 (1H, m, 2-H), 7.22–7.18 (2H, m, 11,21-H), 7.13–7.10 (1H, m. 13-H), 6.95–6.87 (3H, m, 4,6,20-H), 6.75 (1H, d, ^3J = 9.72 Hz, 5-H), 4.74 (1H, s, 7-H), 3.54 (1H, ^3J = 23.3 Hz, 9-H), 3.42 (1H, d, ^3J = 23.4 Hz 9-H) ppm.

^{13}C NMR (100 MHz, $CDCl_3$): δ = 163.2 (C_q, d, *J* = 246.6 Hz, C-3 or C-12 or C-19), 163.0 (C_q, d, *J* = 178.8 Hz, C-3 or C-12 or C-19), 161.34 (C_q, d, *J* = 178.9 Hz, C-3 or C-12 or C-19), 158.6 (C_q, d, *J* = 3.5 Hz, C-8), 150.0 (C_q, d, *J* = 8.4 Hz, C-10), 147.5 (C_q, d, *J* = 2.5 Hz, C-22),

146.5 (C_q, d, J = 2.7 Hz, C-16), 142.1 (C_q, d, J = 7.0 Hz, C-1), 140.2 (C_q, d, J = 9.5 Hz, C-17), 134.8 (C_q, d, J = 2.2 Hz, C-15), 130.5 (C_t, d, J = 8.4 Hz, C-2), 125.7 (C_t, d, J = 9.2 Hz, C-21), 123.7 (C_t, d, J = 2.8 Hz, C-6), 120.4 (C_t, d, J = 8.8 Hz, C-14), 114.7 (C_t, d, J = 21.6 Hz, C-5), 114.2 (C_t, d, J = 21.1 Hz, C-21), 113.6 (C_t, d, J = 22.8 Hz, C-13), 113.0 (C_t, d, J = 23.4 Hz, C-11), 111.8 (C_t, d, J = 22.9 Hz, C-20), 107.4 (C_t, d, J = 23.8 Hz, C-18), 52.3 (C_t, d, J = 1.7 Hz, C-7), 38.9 (C_t, d, J = 2.26, C-9) ppm.

^{19}F NMR (376 Hz, $CDCl_3$): δ = -112.5, -115.5, -117.3 ppm.

FT-IR (ATR): $\tilde{\upsilon}$ = 1612 (m), 1587 (s), 1483 (m, ν(C=C_{arom})), 1462 (s), 1444 (s), 1382 (w), 1289 (w), 1270 (m), 1247 (m), 1197 (m), 1150 (w), 1130 (s), 1072 (w), 990 (w), 975 (m), 931 (w), 902 (m), 855 (s), 828 (w), 813 (m), 801 (m), 777 (vs, δ(=C-H)), 748 (w), 714 (w), 684 (m), 654 (w), 626 (m), 613 (w) cm^{-1}.

UV/Vis (CH_2Cl_2, lg ε): λ_{max} = 234sh (4.72), 239 (4.73), 247sh (4.66), 262 (4.37), 269 (4.30), 289 (3.19), 301 (3.02) nm.

MS (EI, 70 eV): m/z = 334 (M+, 100%), 330 (10), 312 (14), 239 (51), 214 (5).

HRMS (APCI, +): calc. for $[C_{22}H_{13}F_3 + H]^+$ m/z 335.10421, found m/z 335.10498.

EA: calc.: C 79.03, H 3.92 for $C_{22}H_{13}F_3$, found: C 79.02, H 3.90.

2,8,10-trifluoro-4b,4b1,8b,12b-tetrahydrodibenzo[2,3:4,5]pentaleno[1,6-ab]indene (164)

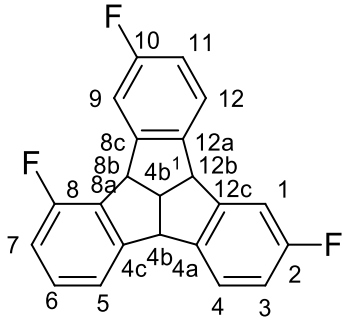

164

Dialcohol **151** (900 mg, 2.43 mmol) was dissolved in chlorobenzene (6 ml) and poly-phosphoric acid (480 mg) was added, upon which the solution turned red. The reaction mixture was heated to 130°C under nitrogen for 21 h. After allowing to cool to room temperature, H_2O (50 ml) and CH_2Cl_2 (25 ml) were added and the phases separated. The aqueous phase was extracted with CH_2Cl_2 (3 × 25 ml) and the combined organic phases were

dried over $MgSO_4$ and the solvent removed *in vacuo*. The resulting oily brown residue was purified via column chromatography (silica, 95:5, cyclohexane, CH_2Cl_2) to afford **164** as colourless crystals.

Yield: 12.7 mg (38.0 µmol, 2%).

m.p.: 270–272°C.

$\mathbf{R_f}$ = 0.23 (cyclohexane/ $CHCl_3$, 98:2).

^{1}H NMR (600 MHz, $CDCl_3$): δ = 7.37–7.32 (3H, m, 1,5,9-H), 7.22–7.16 (2H, m, 4,5-H) 7.08 (1H, d, *J* = 8.9 Hz, 12-H), 6.92–6.87 (3H, m, 3,7,11-H), 5.16 (1H, d, *J* = 9.8 Hz, 8b-H), 4.90 (1H, d, *J* = 9.7 Hz, 4b-H), 4.87 (1H, d, *J* = 9.5 Hz, 12b-H), 4.59 (1H, q, *J* = 9.6 Hz, 4b^1-H) ppm.

^{13}C NMR (100 MHz, $CDCl_3$): δ = 163.0 (C_q, d, *J* = 244.9 Hz, C-2 or C-8 or C-10), 159.5 (C_q, d, *J* = 247.0 Hz, C-2 or C-8), 149.3 (C_q, d, *J* = 5.3 Hz, C-4c), 147.9 (C_q, d, *J* = 6.9 Hz, C-8a), 146.8 (C_q, d, *J* = 8.0 Hz, C-8c), 140.7 (C_q, d, *J* = 2.4 Hz, C-4a), 140.4 (C_q, d, *J* = 2.5 Hz, C 12a), 131.1 (C_q, d, *J* = 17.4 Hz, C-12c), 129.9 (C_t, d, *J* = 7.4 Hz, C-6), 125.4 (C_t, d, *J* = 8.9 Hz, C-5), 125.0 (C_t, d, *J* = 9.0 Hz, C-1), 120.1 (C_t, d, *J* = 3.3 Hz, C-4), 115.0 (C_t, d, *J* = 22.9 Hz, C-3 or C-11), 114.9 (C_t, d, *J* = 22.8 Hz, C-3 or C-11), 114.2 (C_t, d, *J* = 21.0 Hz, C-7), 113.0 (C_t, d, *J* = 9.0 Hz, C-9), 112.9 (C_t, d, *J* = 9.0 Hz, C-9), 111.1 (C_t, d, *J* = 21.9 Hz, C-12), 55.5 (C_t, d, *J* = 1.4 Hz, C-4b), 54.9 (C_t, d, *J* = 2.0 Hz, C-12b), 53.5 (C_t, t, *J* = 2.0 Hz, C-8b), 53.1 (C_t,C-4b^1) ppm.

^{19}F NMR (376 Hz, $CDCl_3$): δ = -115.4, -115.5, -115.6 ppm.

FT-IR (ATR): $\tilde{\upsilon}$ = 2919 (w, *v*(C-H)), 2851 (w, *v*(C-H)), 1738 (w), 1611 (w), 1582 (s), 1482 (vs), 1466 (vs), 1307 (w), 1286 (m), 1268 (m), 1238 (vs), 1183 (m), 1156 (w), 1128 (m), 1093 (w) 1018 (w), 986 (w), 939 (s), 880 (w), 848 (m), 825 (w), 802 (s), 792 (s), 766 (vs), 720 (w), 710 (m) 691 (m), 634 (w), 613 (w) cm^{-1}.

UV/Vis (CH_2Cl_2, lg ε): λ_{max} = 272 (3.79), 279 (3.81) nm.

MS (EI, 70 eV): m/z = 334 (M^+, 100%), 312 (15), 239 (27), 214 (6).

HRMS (APCI, +): calc. for $[C_{22}H_{13}F_3 + H]^+$ m/z 335.10421, found m/z 335.10475.

EA: calc.: C 79.03, H 3.92 for $C_{22}H_{13}F_3$, found: C 78.11, H 3.90.

6.2.3 Phenanthrene functionalised TBTQs

2-(Phenanthren-9-ylmethylene)-1,3-diphenylpropane-1,3-dione (172)

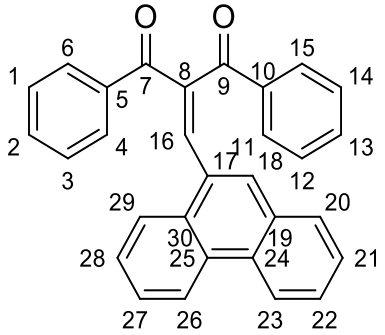

172

Dibenzoylmethane **77** (3.00 g, 13.4 mmol) and 9-Phenanthrenecarboxaldehyde **167** (2.77 g, 13.5 mmol) were dissolved in acetic acid (100 ml). piperidine (100 µl) was added and the solution was refluxed using a DEAN-STARK trap for 5 d. Piperidine (50 µl) was added and the reaction continued for a further 2 d. After cooling to room temperature, ethyl acetate (80 ml) and brine (50 ml) were added and the phases separated. $NaHCO_3$ (30 ml) was added to the aqueous phase, which was extracted with ethyl acetate (3 × 50 ml). The organic phases were washed with $NaHCO_3$ (3 × 50 ml) and dried over $MgSO_4$. The solvent was removed *in vacuo* to afford a dark orange oil. The desired diketone **172** was obtained after flash chromatography (silica, ethyl acetate/pentane 10:90) as a yellow solid, which was recyrstallised from ethyl acetate to give canary yellow crystals.

Yield: 1.23 g, 2.98 mmol, 22%.

m.p.:173–175°C.

$\mathbf{R_f}$ = 0.36 (pentane/ethyl acetate 90:10).

^{1}H NMR (400 MHz, $CDCl_3$): δ = 8.66–8.63 (1H, m, 26-H), 8.56 (1H, d, *J* = 8.0 Hz, 23-H), 8.27 (1H, d, *J* =1.0 Hz, 16-H), 8.03–7.97 (3H, m, 6-H, 4-H and 29-H), 7.89–7.86 (2H, m, 11-H and 15-H), 7.78 (1H, s, 18-H), 7.72 (1H, dd, 20-H) 7.70–7.59 (4H, m)7.55–7.49 (3H, m), 7.31 (1H, tt, *J* = 7.4 Hz, *J* = 1.3 Hz, 13-H), 7.20–7.15 (2H, m, 13-H) ppm.

^{13}C NMR (100 MHz,$CDCl_3$): δ = 196.4 (C_q, C-9), 194.6 (C_q, C-7), 141.9 (C_q, C-8), 141.9 (C_t, C-16). 137.4 (C_q), 136.7 (C_q), 133.6 (C_t, C-13), 133.1(C_t), 130.9 (C_q), 130.9 (C_q), 130.4 (C_q), 129.9 (C_q), 129.9(C_t, C-6 and C-4), 129.9(C_t, C-18), 129.8(C_q), 129.5 (C_t, C-20), 129.2 (C_t,

C-11 and C-15), 128.8 (C_t), 128.6 (C_t, C-12 and C-14), 128.0 (C_t), 127.3 (C_t), 127.2 (C_t), 127.2 (C_t), 124.9 (C_t, C-29), 123.4 (C_t, C-26), 122.5 (C_t, C-23) ppm.

FT-IR (ATR): $\tilde{\upsilon}$ = 3029 (w, ν(C-H_{arom})), 1672 (m, ν(C=O)), 1633 (s, ν(C=C)), 1602 (m, ν(C=C_{arom})), 1590 (m, ν(C=C_{arom}), 1528 (w), 1494 (w), 1445 (m), 1389 (w), 1352 (m), 1315 (w), 1285 (w), 1257 (m), 1248 (m), 1226 (s, ν(C-H)), 1173 (m), 1146 (w), 1116 (w), 1079 (w), 1038 (w), 1023 (w), 1002 (w), 980 (m), 936 (m), 929 (m), 901 (s), 886 (w), 863 (w), 850 (w), 807 (w), 795 (w), 775 (w), 763 (w), 747 (m), 737 (s, δ(=C-H)), 717 (vs, δ(=C-H)), 711 (vs, δ(=C-H)), 702 (m), 692 (m), 682 (s), 637 (m), 623 (m), 616 (m) cm^{-1}.

UV/Vis (acetonitrile, lg ε): λ_{max} = 252 (4.57), 332 (3.84) nm.

MS (EI, 70 eV): m/z = 412 (M+, 45%), 394 (7), 308 (19), 307 (M^+-$C_5H_7O^+$, 69), 279 (14), 202 (22), 105 (M+ - $C_{23}H_{13}O^+$, 100), 77 (63).

HRMS (EI): calc.for $C_{30}H_{20}O_2$ + H, m/z 414.1536, found m/z 414.1533.

EA: calc.: C 87.36, H 4.89 for $C_{30}H_{20}O_2$, found: C 87.12, H 5.13.

2-(Phenanthren-9-ylmethylene)-1,3-diphenylpropane-1,3-diol (173)

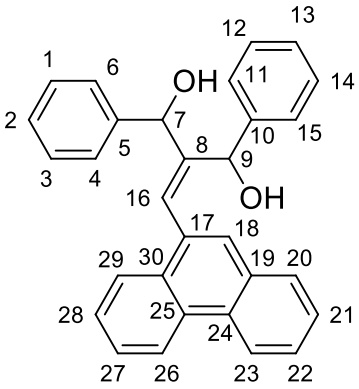

173

Diketone **172** (100 mg, 0.242 mmol) was dissolved in anhydrous CH_2Cl_2 (10 ml) and the mixture was cooled to -78°C in a dry-ice/acetone bath under nitrogen. To this solution was added a 0.4 M solution of $CeCl_3 \cdot 7\ H_2O$ in MeOH (188 mg $CeCl_3$ 7 H_2O in 2.53 ml MeOH, 0.506 mmol, 2.09 eq.). After additional stirring and continued cooling, $NaBH_4$ (0.51 g, 13.6 mmol, 2.1 eq.) was added and effervescence observed. After 1h stirring at -78°C, the cooling bath was removed and the reaction mixture slowly reached room temperature. Complete conversion using a TLC analysis was observed after 17 h. Two isomers were observed. The reaction was diluted with ether (20 ml) and quenched by the addition of 0.5 M

HCl (20 ml). The aqueous layer was extracted with ether (2 × 15 ml) and the combined organic layers were washed with brine, dried ($MgSO_4$) and concentrated under reduced pressure. The diastereomers were separated by flash chromatography (silica, ethyl acetate/ $CHCl_3$ 10:90) to give pale yellow crystals

Yield: 96.7 mg, 232 µmol, 96%.

R,S/S,R-Diastereomer-173

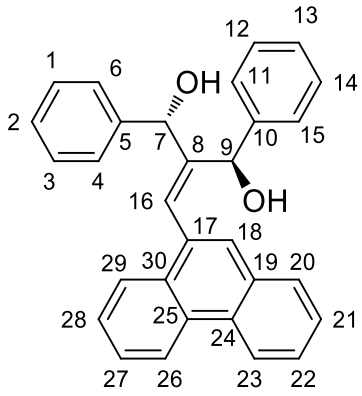

rac-**173**

Yield: 79.8 mg, 192 µmol, 79%.

m.p.: 164–166°C.

$\mathbf{R_f}$ = 0.42 (ethyl acetate/$CHCl_3$ 10:90).

^{1}H NMR (400 MHz, $CDCl_3$): δ = 8.86 (1H, dt, *J* = 8.2 Hz, *J* = 0.6 Hz, 23-H or 26-H), 8.80 (1H, d, *J* = 8.0 Hz, 23-H or 26-H), 7.95 (1H, dd, *J* = 7.7 Hz, 1.6 Hz, 20-H), 7.90 (1H, s, 18-H), 7.86 (1H, dd, *J* = 8.0 Hz, 1.0 Hz, 29-H), 7.74–7.61 (4H, m, 21,22,27,28-H), 7.39–7.32 (6H, m, C*H*), 7.29–7.23 (3H, m, C*H*), 7.21–7.16 (1H, m,C*H*), 6.65 (1H, s, 16-H), 5.94–5.91 (1H, m, 7-H or 9-H), 5.51–5.48 (1H, m, 7-H or 9-H), 5.29 (1H, dd, *J* = 5.9 Hz, 1.4 Hz, O*H*), 4.98 (1H, dd, *J* = 3.2 Hz, 0.88 Hz, O*H*) ppm.

^{13}C NMR (100 MHz, $CDCl_3$): δ = 148.9 (C_q, C-5 or C-8 or C-10), 144.0 (C_q, C-5 or C-8 or C-10), 143.8 (C_q, C-5 or C-8 or C-10), 133.5 (C_q), 132.4 (C_q), 132.1 (C_q), 131.3 (C_q), 130.9 (C_q), 130.0 (C_t), 129.6 (C_t, C-20), 128.9 (C_t, C-16), 128.8 (C_t), 127.9 (C_t), 127.8 (C_t, C-21,22,26,27), 127.8 (C_t), 127.7 (C_t), 127.6 (C_t, C-18), 127.5 (C_t), 126.6 (C_t), 126.4 (C_t, C-29), 124.0 (C_t, C-23 or C-26), 123.5 (C_t, C-23 or C-26), 73.7 (C_t, C-7 or C-9), 72.6 (C_t, C-7 or C-9) ppm.

FT-IR (ATR): $\tilde{\upsilon}$ = 3558 (w, ν(O-H)), 3444 (w, ν(O-H)), 3058 (w, ν(C-H_{arom})), 3025 (w, ν(C-H_{arom})), 2962 (w), 1600 (w), 1492 (w, ν(C=C_{arom})), 1447 (m), 1423 (w), 1372 (w), 1322 (w), 1258 (w), 1190 (w), 1150 (w), 1136 (w), 1080 (w), 1027 (s), 1007 (s), 954 (w), 915 (m), 895 (w), 797 (w), 766 (w), 748 (s, δ(=C-H)), 725 (s), 694 (vs, δ(=C-H)), 666 (m), 629 (w), 617 (w) cm^{-1}.

UV/Vis (acetonitrile, lg ε) λ_{max} = 255 (4.49), 290sh (3.78), 300 (3.87) nm.

MS (EI, 70 eV): m/z = 416 (M^+, 1%), 398 (100, M^+-H_2O), 380 (6), 321 (16), 307 (44), 292 (71), 215 (38), 202 (37), 178 (16), 105 (71), 77 (40).

HRMS (ESI): calc.for $C_{30}H_{24}O_2$ + Na, m/z 439.16685, found m/z 439.16636.

EA: calc.: C 86.51, H 5.81 for $C_{30}H_{24}O_2$, found C 86.15, H 6.00.

R,R/S,S-Diastereomer-173

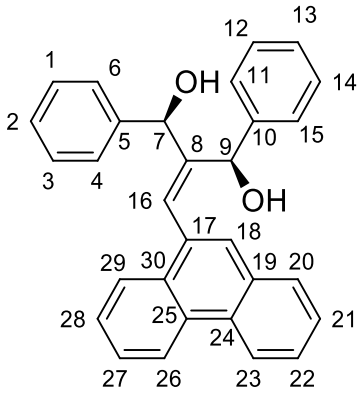

rac-**173**

Yield:16.9 mg, 40.6 µmol, 17%.

m.p.: 167–169°C.

$\mathbf{R_f}$ = 0.60 (10:90 Ethyl acetate/$CHCl_3$).

^{1}H NMR (400 MHz, $CDCl_3$): δ = 8.86 (1H, d, ^3J = 8.2 Hz, 23-H or 26-H), 8.80 (1H, d, ^3J = 8.1 Hz, 23-H or 26-H), 8.14 (1H, d, ^3J = 7.9 Hz, 20-H), 7.90 (1H, s, 18-H), 7.86 (2H, dd, ^3J = 7.8 Hz, ^4J = 1.6 Hz, 29-H), 7.76–7.70 (1H, m, C*H*), 7.70–7.58 (5H, m, C*H*), 7.46 (1H, s, 18-H), 7.39–7.32 (4H, m, C*H*), 7.25 (1H, tt, ^3J = 7.5 Hz, ^4J = 1.5 Hz, 13-H), 7.22–7.17 (2H, m, C*H*), 7.16–7.11 (1H, m, 2-H), 5.90 (1H, d, *J* = 4.7 Hz, 7-H), 5.49 (1H, d, J = 4.6, 9-H), 4.48 (1H, d, ^3J = 2.1 Hz, O*H*), 4.47 (1H, d, ^3J = 2.4 Hz, O*H*) ppm.

^{13}C NMR (100 MHz, $CDCl_3$): δ = 148.9 (C_q, C-8), 145.3 (C_q, C-5,10), 143.3 (C_q), 132.9 (C_q), 131.5 (C_q), 131.4 (C_q), 130.3 (C_q), 129.9 (C_q),128.4 (C_t) 127.7 (C_t), 127.6 (C_t), 127.1 (C_t), 126.9 (C_t, C-16), 126.7 (C_t, C-18), 126.7 (C_t), 126.6 (C_t), 126.6 (C_t), 126.6 (C_t), 126.5 (C_t , C-13), 126.3 (C_t, C-2), 126.0 (C_t), 125.8 (C_t),122.9 (C_t, C-23 or C-26), 122.4 (C_t, C-23 or C-26), 72.0 (C_t, C-9), 70.6 (C_t, C-7) ppm.

FT-IR (ATR): $\tilde{\upsilon}$ = 3335 (w, ν(O-H)), 3060 (w, ν(C-H_{arom})), 2963 (w, ν(C-H_{arom})), 1600 (w), 1492 (w, ν(C=C_{arom})), 1448 (w), 1424 (w), 1258 (m), 1194 (w), 1148 (w), 1064 (m), 1014 (s), 954 (w), 915 (w), 901 (w), 849 (w), 798 (s), 754 (s, δ(=C-H)), 727 (s), 699 (s, δ(=C-H)), 675 (m), 614 (m) cm^{-1}.

UV/Vis (acetonitrile, lg ε): λmax = 255 (4.55), 290sh (3.85), 300 (3.93) nm.

MS (EI, 70 eV): m/z = 416 (M^+, 2%), 398 (100, M^+-H_2O), 380 (8), 321 (16), 307 (46), 292 (73), 215 (40), 202 (37), 178 (16), 105 (72), 77 (41).

HRMS (ESI): calc. for $C_{30}H_{24}O_2$ + Na, m/z 439.16685, found m/z 439.16534.

(Z)-3-Hydroxy-3-(phenanthren-9-yl)-1-phenylprop-2-en-1-one (176)

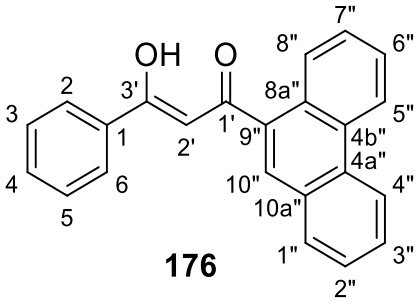

176

Ketone **174** (2.41 g, 10.9 mmol) was dissolved in abs. THF (50 ml) and NaH (3.48 g, 87.2 mmol, 8 eq.) was added. The reaction mixture was stirred at room temperature for 5 min, after which a solution of ester **175** (1.74 g, 12.8 mmol, 1.17 eq.) in abs. THF (45 ml) was added dropwise. The resulting mixrure was stirred at 75°C for 22 h, after which another portion of NaH (1.3 g, 3 eq.) was added. The reaction mixture was stirred for a further 6 h, after which methyl benzoate (791 mg) was added. After a further 18 h the reaction was allowed to cool to room temperature and CH_2Cl_2 (100 ml) and H_2O (50 ml) were added. The mixture was acidified with conc. HCl (50 ml) and cooled to 0°C and the phases separated. The aqueous phase was extracted with CH_2Cl_2 (2 × 50 ml) and the combined organic phases were washed with H_2O (50 ml) and dried over $MgSO_4$. The solvent was removed *in vacuo* and the resulting orange solid was recrystallised in ethyl acetate (35 ml) to afford a portion of the product as a pale yellow solid (1.64 g). The filtrate, after removal of the solvent, was

purified using column chromatography (silica, pentane/CH_2Cl_2 2:1–1:1) to afford another portion of the product.

Yield: 2.32 g (7.15 mmol, 66%; lit.[279] 82%).

m.p.: 141–142°C (Ethyl acetate, lit.[279] 172–174°C).

R_f = 0.22 (pentane/CH_2Cl_2, 2:1).

^{1}H NMR (400 MHz, $CDCl_3$): δ = 16.8 (1H, s, O*H*), 8.77 (1H, d, ^3J = 8.1 Hz, 5”-H), 8.72 (1H, d, ^3J = 8.4 Hz, 4”-H), 8.53 (1H, d, ^3J = 8.1 Hz, 8”-H), 8.10 (1H, s, 10”-H), 8.02–8.00 (2H, m, 2,6-H), 7.97 (1H, d, ^3J = 7.9 Hz, 1”-H), 7.78–7.64 (4H, m, 2”,3”,6”,7”-H), 7.59–7.55 (1H, m, 4-H), 7.52–7.48 (2H, m, 3,5-H), 6.80 (1H, s, 2’-H) ppm.

^{13}C NMR (100 MHz, $CDCl_3$): δ = 191.0 (C_q, C-1’), 184.6 (C_q, C-3’), 135.1 (C_q, C-1), 134.3 (C_q, C-8a”), 132.8 (C_t, C-4), 131.6 (C_q, C-4a”), 130.9 (C_q, C-10a”), 130.6 (C_q, C-4b”), 129.8 (C_t, C-1”), 128.9 (C_t, C-3,5), 128.8 (C_t, C-10”), 128.6 (C_q, C-9”), 128.5 (C_t, C-2”,3” or C-6”,7”), 127.4 (C_t, C-2,6), 127.3 (C_t, C-2”,3” or C-6”,7”), 126.6 (C_t, C-8”), 123.2 (C_t, C-5”), 122.9 (C_t, C-4”), 98.4 (C_t, C-2’) ppm.

FT-IR (ATR): $\tilde{\upsilon}$ = 3046 (w, ν(C-H_{arom})), 1596 (m, ν(C=C_{arom})), 1523 (s), 1448 (s), 1380 (m), 1303 (w), 1265 (w), 1246 (w), 1209 (w), 1186 (w), 1139 (m), 1079 (w), 1041 (w), 980 (w), 898 (w), 864 (w), 804 (w), 767 (s), 744 (m), 727 (s), 688 (vs), 642 (w), 617 (w) cm^{-1}.

UV/Vis (acetonitrile, lg ε): λ_{max} = 204 (4.46), 250 (4.60) 291 (4.09), 347 (4.28) nm.

MS (EI, 70 eV): m/z = 324 (M^+, 100%), 323 (20), 307 (30), 306 (64), 305 (45), 278 (11), 247 (14), 229 (19), 220 (16), 219 (92), 202 (21), 191 (19), 190 (10), 189 (29), 178 (55), 177 (70), 176 (60), 151 (18), 77 (50).

Despite the descrepancy in the melting point value compared the the literatue value, the spectroscopic data indicates that the molecule was isolated. Repeated rerystallisations and drying at $1 \cdot 10^{-3}$ mbar also gave the same result.

(E)-2-Benzylidene-1-(phenanthren-9-yl)-3-phenylpropane-1,3-dione (177)

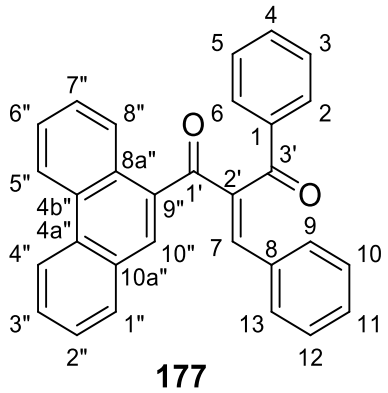

177

Diketone **176** (1.71 g, 5.27 mmol) was dissolved in toluene (220 ml) and benzaldehyde (2.94 g, 27.7 mmol), Piperidine (1 ml), butyric acid (1 ml) und Molecular sieves 4 Å (1.13 g) were added. The reaction mixture was heated to reflux for 1 h and after allwoing to cool to room temperature, H_2O (180 ml) and CH_2Cl_2 (180 ml) were added and the phases separated. The aqueous phase was extracted with CH_2Cl_2 (60 ml) and the organic phases were combined. The solvent was removed *in vacuo* to give a yellow oil, which was further purified using column chromatography (1:1, Cyclohexane/CH_2Cl_2). This sticky solid was recrystallised from an acetonitrile/H_2O mixture, purified again with column chromatography (silica, cyclohexane/ CH_2Cl_2 1:1) and finally recrystallised from cyclohexane to afford the desired product as a yellow solid.

Yield: 551 mg, 1.33 mmol, 25%.

m.p.: 144–145°C.

$\mathbf{R_f}$ = 0.13 (cyclohexane/CH_2Cl_2, 1:2).

^{1}H NMR (400 MHz, $CDCl_3$): δ = 8.77 (1H, d, ^3J = 8.3 Hz, 5”-H), 8.74 (1H, d, ^3J = 8.3 Hz, 4”-H), 8.21 (1H, d, ^3J = 8.2 Hz, 8”-H), 8.08–8.05 (3H, m, 2,6,10”-H), 7.96 (1H, d, ^3J = 7.8 Hz, 1”-H), 7.78 (1H, td, ^3J = 7.0 Hz, ^4J = 1.4 Hz, 3”-H), 7.73 (1H, td, ^3J = 7.0 Hz, ^4J = 1.4 Hz, 6”-H), 7.69–7.63 (1H, m, 2”,7”-H), 7.50–7.56 (2H, m, 4,7-H), 7.49–7.45 (2H, m, 3,5-H), 7.30–7.27 (3H, m, 10,11,12-H), 7.23–7.18 (2H, m, 9,13-H) ppm.

^{13}C NMR (100 MHz, $CDCl_3$): δ = 197.7 (C_q, C-3’), 197.2 (C_q, C-1’), 145.8 (C_t, C-7), 141.5 (C_q, C-2’), 136.5 (C_q, C-1), 134.7 (C_q, C-9”), 134.2 (C_t, C-4), 132.9 (C_q C-8), 131.5 (C_q, C-4a”), 131.0 (C_t, C-10,12 or C-11), 130.8 (C_q, C-4b”), 130.6 (C_t, C-10,12 or C-11), 130.1 (C_q, C-10a”), 129.8 (C_t, C-1”), 129.4 (C_t, C-2,6), 129.2 (C_q, C-8a”), 129.1 (C_t, C-3,5), 129.0

(C_t, C-9,13), 128.9 (C_t, C-10"), 128.6 (C_t, C-3"), 127.6 (C_t, C-7"), 127.5 (C_t, C-6"), 127.4 (C_t, C-2"), 126.5 (C_t, C-8"), 123.1 (C_t, C-5"), 122.9 (C_t, C-4") ppm.

FT-IR (ATR): $\tilde{\upsilon}$ = 3060 (w, ν(C-H_{arom})), 1660 (s, ν(C=O)), 1641 (vs, ν(C=O)), 1614 (s, ν(C=C_{arom})), 1527 (w, ν(C=C_{arom})) 1492 (w), 1448 (m), 1373 (w), 1313 (w), 1232 (vs), 1178 (s), 1101 (w), 1076 (w), 1026 (w), 1000 (w), 958 (m), 933 (m), 904 (m), 862 (w), 837 (m), 756 (vs), 725 (vs), 688 (vs), 525 (w) cm^{-1}.

UV/Vis (acetonitrile, lg ε): λ_{max} = 203 (4.66), 252 (4.76), 294 (4.40) nm.

MS (EI, 70 eV): m/z = 412 (64%, M^+), 307 (M^+-$C_{14}H_9CO$, 100), 279 (53), 205 ($C_{14}H_9CO^+$, 94), 191 (40), 177 ($C_{14}H_8^+$, 100), 151 (18).

EA: calc.: C 87.36, H 4.89 for $C_{30}H_{20}O_2$, found C 87.49, H 5.07.

HRMS (ESI): calc. for $C_{30}H_{20}O_2 + Na^+$ m/z 435.13555, found m/z 435.13546

(E)-2-Benzylidene-1-(phenanthren-9-yl)-3-phenylpropane-1,3-diol (178)

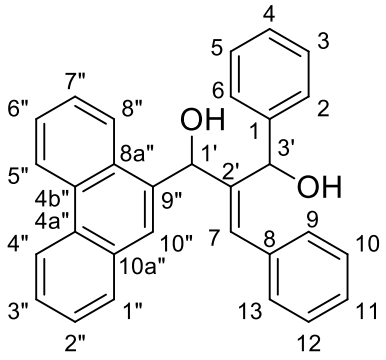

178

Diketone **177** (1.22 g, 2.98 mmol) was dissolved in anhydrous CH_2Cl_2 (25 ml) and the mixture was cooled to -78°C in a dry-ice/acetone bath under nitrogen. To this solution was added a 0.2 M solution of $CeCl_3$ 7 H_2O in MeOH (2.32 g, 6.23 mmol, 2.09 eq. $CeCl_3$ 7 H_2O in 31 ml MeOH). After additional stirring and continued cooling, $NaBH_4$ (340 mg, 8.97 mmol, 3.01 eq.) was added and effervescence observed. After 1 h stirring at -78°C, the cooling bath was removed and the reaction mixture slowly reached room temperature. Complete conversion using a TLC analysis was observed after a total reaction time of 4 h. Two isomers were observed. After addition of 5 ml H_2O and 25 ml 0.5 M HCl, 100 ml CH_2Cl_2 and 20 ml Et_2O were added and the phases separated. The aqueous layer was extracted with CH_2Cl_2 (3 × 30 ml) and the combined organic layers were washed with H_2O (30 ml), dried

over $MgSO_4$ and concentrated under reduced pressure. The diastereomers were separated by flash chromatography (silica, ethyl acetate/$CHCl_3$ 10:90) to give colourless crystals.

Yield: 1.06 g, 2.55 mmol, 85%.

R,S/S,R-Diastereomer 178

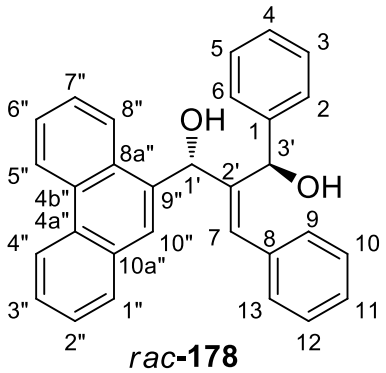

rac-**178**

Yield: 478 mg, 1.15 mmol, 38%.

m.p.: 56–58°C

$\mathbf{R_f}$ = 0.24 (CH_2Cl_2/pentane, 80:20).

^{1}H NMR (400 MHz, $CDCl_3$): δ = 8.72 (1H, d, ^3J = 8.1 Hz, 5”-H), 8.66 (1H, d, ^3J = 8.1 Hz, 4”-H), 8.29 (1H, d, ^3J = 8.1 Hz, 8”-H), 7.98 (1H, s, 10”-H), 7.88 (1H, dd, ^3J = 7.8 Hz, ^3J = 1.5 Hz, 1”-H), 7.68–7.63 (2H, m, 3”,6”-H), 7.62–7.57 (2H, m, 2”,7”-H), 7.43–7.41 (2H, m, 9,13-H), 7.32–7.21 (8H, m, 2,3,4,5,6,10,11,12-H), 6.90 (1H, s, 7-H), 6.27 (1H, d, ^3J = 4.1 Hz, 3’-H), 6.11 (1H, d,^3J = 5.4 Hz, 1’-H), 2.38 (1H, d, ^3J = 5.4 Hz, (C1’)O*H*), 2.09 (1H,d, ^3J = 4.1 Hz, (C3’)O*H*) ppm.

^{13}C NMR (100 MHz, $CDCl_3$): δ = 143.1 (C_q, C-1), 142.5 (C_q, C-9”), 136.5 (C_q, C-2’), 136.1 (C_q), 132.4 (C_t, C-7), 131.4 (C_q, C-4b”), 130.9 (C_q), 130.5 (C_q), 130.0 (C_q, C-4a”), 129.1 (C_t, C-1”), 128.8 (C_t, *C*H), 128.7 (C_t, *C*H), 128.5 (C_t, *C*H), 127.6 (C_t, *C*H), 127.5 (C_t, *C*H), 127.0 (C_t, C-3” or C-6”), 126.9 (C_t, C-3” or C-6”), 126.8 (C_t, *C*H), 126.5 (C_t, *C*H), 126.1 (C_t, C-10”), 125.9 (C_t, C-9,13), 124.9 (C_t, C-8”), 123.3 (C_t, C-4”), 122.6 (C_t, C-5”), 71.4 (C_t, C-3’), 70.9 (C_t, C-1’) ppm.

FT-IR (ATR): $\tilde{\upsilon}$ = 3396 (w, ν(O-H)), 3058 (w, ν(C-H_{arom})), 1600 (w), 1492 (w, ν(C=C_{arom})), 1448 (w), 1246 (w), 1024 (m), 906 (m), 796 (s), 727 (vs), 698 (vs), 615 (w) cm^{-1}.

UV/Vis (acetonitrile, lg ε): λ_{max} = 207 (4.88), 252 (4.95), 296 (4.17) nm.

MS (EI, 70 eV): m/z = 416 (M^+, 4%), 398 (67,M^+-H_2O), 307 (32), 291 (46), 289 (32), 238 (12), 215 (18), 207 (11), 205 (22), 191 (38), 179 (52), 178 (100, $C_{14}H_{10}^+$), 131 (17).

HRMS (ESI,+) calc. for $C_{30}H_{24}O_2 + Na^+$ m/z 439.16685, found m/z 439.16618.

EA: calc.: C 86.51, H 5.81 for $C_{30}H_{24}O_2$, found: C 86.40, H 5.78.

R,R/S,S-Diastereomer 178

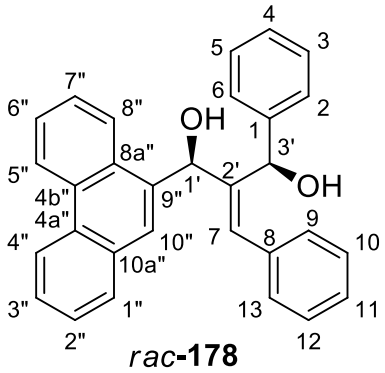

rac-**178**

Yield: 582 mg, 1.40 mmol, 47%.

m.p.: 80–82°C.

$\mathbf{R_f}$ = 0.1 (CH_2Cl_2/pentane, 80:20).

^{1}H NMR (400 MHz, CDCl3): δ = 8.68 (1H, d, ^3J = 8.4 Hz, 5”-H), 8.65 (1H, d, ^3J = 8.1 Hz, 4”-H), 8.06 (1H, s, 10”-H), 7.90 (1H, d, ^3J = 7.7 Hz, 1”-H), 7.65 (1H, td, ^3J = 7.0 Hz, ^4J = 1.5 Hz, 3”-H), 7.60 (1H, m, 2”-H), 7.57–7.53 (3H, m, 2,6,6”-H), 7.49–7.45 (2H, m, 3,5-H), 7.40–7.36 (1H, m, 4-H), 7.33–7.28 (1H, m, 7”-H), 7.29–7.25 (2H, m, 9,13-H), 7.23–7.19 (3H, m, 10,11,12-H), 7.14 (1H, d, ^3J = 8.2 Hz, 8”-H), 6.18 (1H, s, 7-H), 6.15 (1H, d, ^3J = 6.9 Hz, 3’-H), 5.94 (1H, d, ^3J = 3.0 Hz, 1’-H), 4.09 (1H, d, ^3J = 7.0 Hz, (C3’)O*H*), 3.24 (1H, d, ^3J = 3.0 Hz, (C1’)O*H*) ppm.

^{13}C NMR (100 MHz, $CDCl_3$): δ = 142.8 (C_q, C-1), 141.8 (C_q, C-2’), 136.3 (C_q, C-8), 135.2 (C_q, C-9”), 133.3 (C_t, C-7), 131.4 (C_q, C-10a”), 130.5 (C_q, C-4b”), 130.3 (C_q, C-4a”), 129.8 (C_q, C-8a”), 129.0 (C_t, C-1”), 128.8 (C_t, C-11), 128.6 (C_t, C-3,5), 128.5 (C_t, C-9,13), 127.6 (C_t, C-10,12), 127.6 (C_t, C-4), 126.9 (C_t, C-3”), 126.9 (C_t, C-2”), 126.4 (C_t, C-7”), 126.3 (C_t, C-6”), 126.1 (C_t, 10”), 125.7 (C_t, C-2,6), 124.5 (C_t, C-8”), 123.1 (C_t, C-5”), 122.6 (C_t, C-4”), 72.7 (C_t, C-3’), 72.1 (C_t, C-1’) ppm.

FT-IR (ATR, cm^{-1}): $\tilde{\upsilon}$ = 3291 (w, ν(O-H)), 3058 (w, ν(C-H_{arom})), 2078 (w), 1892 (w), 1600 (w), 1492 (w, ν(C=C_{arom})), 1448 (w), 1328 (w), 1245 (w), 1066 (w), 1016 (m), 948 (w), 921 (w), 889 (w), 796 (w), 746 (s), 721 (s), 698 (vs), 652 (w) cm^{-1}.

UV/Vis (acetonitrile, lg ε): λ_{max} = 205 (4.73), 253 (4.82), 286sh (4.05), 297 (4.08) nm.

MS (EI, 70 eV): m/z = 400 (5%), 398 (M^+-H_2O, 100), 321 (11), 309 (15), 308 (11), 307 (39), 293 (43), 292 (55), 289 (20), 238 (10), 215 (21), 205 (28), 192 (25), 191 (21), 179 (42), 178 (54), 177 (22), 131 (16).

HRMS (ESI,+) calc. for $C_{30}H_{24}O_2 + Na^+$ m/z 439.16685, found m/z 439.16605.

4c,4c1,8b,12b,-tetrahydrobenzo[5,6]indeno[1',2',3':3,4]pentaleno[1,2-yl] phenanthrene (102)

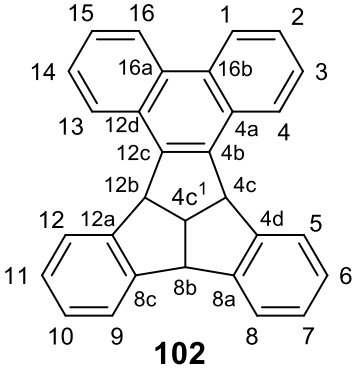

102

To a solution of dialcohol **178** (500 mg, 1.20 mmol) in chlorobenzene (20 ml) was added polyphosphoric acid (953 mg). The reaction mixture was heated to reflux at 130°C for 21 h. After allowing to cool to room temperature, H_2O (30 ml) and CH_2Cl_2 (100 ml) were added and the phases separated. The aqueous phase was extracted with CH_2Cl_2 (3 × 30 ml) and the combined organic phases were washed with H_2O (50 ml) and dried with $MgSO_4$. The solvent was removed *in vacuo* and the brown residue was purified using column chromatography (silica, pentane/CH_2Cl_2 4:1) to afford the product as fine colourless crystals.

Yield: 22.1 mg, 58.1 µmol, 5%.

m.p.: 302–303°C.

R_f = 0.4 (CH_2Cl_2/pentane, 4:1).

^{1}H NMR (400 MHz, $CDCl_3$): δ = 8.70 (2H, d, ^3J = 8.2 Hz), 8.49 (2H, d, ^3J = 8.1 Hz), 7.80 (2H, d, ^3J = 7.72 Hz), 7.76–7.72 (2H, m), 7.68–7.64 (2H, m), 7.50 (2H, d, ^3J = 7.6 Hz), 5.61 (2H, d, ^3J = 9.8 Hz), 5.04 (1H, d, ^3J = 9.2 Hz), 4.80 (3H, q, ^3J = 9.7 Hz) ppm.

^{13}C NMR (100 MHz, $CDCl_3$): δ = 148.1 (C_q, C-8a, 8c), 144.4 (C_q, C-4b,12c), 140.0 (C_q, C-4b,12c), 131.4 (C_q, C-16a, 16b), 129.8 (C_q, C-4a,12d), 127.8 (C_t, C-7,10), 127.1 (C_t, C-6,11), 126.5 (C_t, C-4,13), 126.5 (C_t, C-3,14), 126.2 (C_t, C-2,15), 125.9 (C_t, C-5,12), 124.6 (C_t, C-8,9), 123.5 (C_t, C-1,16), 56.1 (C_t, C-4c,12b), 54.8 (C_t, C-8b), 52.2 (C_t, C-4c[1]) ppm.

FT-IR (ATR): ῡ = 3068 (w, ν(C-H_{arom})), 3020 (w, ν(C-H_{arom})), 2879 (w), 1608 (w), 1475 (w, ν(C=C_{arom})), 1450 (w), 1325 (w), 1263 (w), 1236 (w), 1153 (w), 1081 (w), 1038 (w), 947 (w), 874 (w), 791 (w), 728 (vs), 698 (w), 615 (w) cm^{-1}.

UV/Vis (acetonitrile, lg ε) λ_{max} = 207 (4.33), 222 (4.11), 257 (4.32), 270sh (3.97), 293 (3.70), 305 (3.73), 339 (3.34), 354 (3.23) nm.

MS (EI, 70 eV): m/z = 380 (M^+, 100%), 379 (32), 377 (13), 376 (13), 303 (11), 302 (13), 188 (6), 151 (9).

HRMS (ESI,+) calc. for $C_{30}H_{20}$ m/z 380.15595, found m/z 380.15538.

EA: calc.: C 94.70, H 5.30 for $C_{30}H_{20}$, found: C 94.38, H 5.47.

I-2-Formyl-3-phenylacrylonitrile (182)

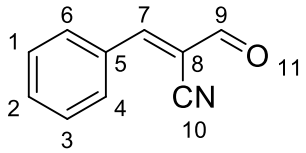

182

A sodium methoxide solution was prepared from anhydrous MeOH (20 ml) and Na (350 mg, 15.2 mmol) at 0°C. Benzaldehyde **78** (1.00 g, 9.42 mmol) and 3,3-dimethoxypropionitrile (1.40 g, 12.2 mmol) were added at room temperature and the reaction mixture was stirred for 5 d. The solvent was removed in vacuo and ethyl acetate (25 ml) was added to the residue, affording a solid. 6 M HCl (20 ml) was added to this solid and the resulting mixture was stirred at room temperature for 4 h. The pale yellow solid was filtered off, washed with H_2O and dried. Further portions of product were isolated upon removing the solvent from the filtrate.

Yield: 704 mg (4.48 mmol, 48%; lit.[304] 74%).

m.p.: 95–97°C; (lit.[304] 96–97°C).

^{1}H NMR (400 MHz, $CDCl_3$): δ = 9.61 (1H, s, 9-H), 8.06–8.04 (2H, m, 4,6-H), 7.91 (1H, s. 7-H), 7.64 (tt, 1H, ^3J= 7.4 Hz, ^4J = 2.3 Hz, 2-H), 7.59–7.54 (2H, m, 1,3-H) ppm.

^{13}C NMR (100 MHz, $CDCl_3$): δ = 186.9 (C_t, C-9), 159.0 (C_q, C-7), 134.5 (C_t, C-2), 131.6 (C_t, C-4,6), 131.4 (C_q, C-5), 129.7 (C_t, C-1,3), 114.3 (C_q, C-10), 112.6 (C_q, C-8) ppm.

FT-IR (ATR): $\tilde{\upsilon}$ = 3357 (w), 3068 (w, ν(C-H_{arom})), 2870 (w), 2220 (w), 1984 (w), 1685 (s, ν(C=O)), 1591 (s, ν(C=O)), 1452 (m), 1406 (w), 1323 (m), 1300 (m), 1220 (m), 1194 (m), 1155 (s), 1101 (m), 1074 (m), 1001 (m), 943 (m), 883 (w), 852 (w), 754 (s), 675 (s) cm^{-1}.

UV/Vis (acetonitrile, lg ε): λ_{max} = 203sh (3.97), 224 (3.91), 228 (3.91), 305 (4.38) nm.

MS (EI, 70 eV): m/z = 157 (M^+, 100), 129 (41), 102 (46), 91 (11), 78 (93), 51 (32).

The spectroscopic data corresponded to the data reported in the literature.[304]

I-2-(1,3-Dioxolan-2-yl)-3-phenylacrylonitrile (183)

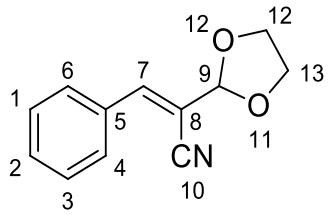

183

Nitrile **182** (540 mg, 3.44 mmol), ethylenglycol (890 µl, 990 mg, 15.9 mmol) and TsOH · H_2O (10 mg) were dissolved in toluene (20 ml) and the resulting mixture was refluxed at 120°C for 4 h. Upon cooling, cyclohexane (50 ml) and saturated $NaHCO_3$ solution (15 ml) were added and the phases separated. The organic phase was washed with H_2O (3 × 15 ml) and brine (15 ml) and dried over $MgSO_4$. The solvent was removed *in vacuo* to afford the product as a colourless oil.

Yield: 621 mg, 3.08 mmol, 90%.

^{1}H NMR (400 MHz, $CDCl_3$): δ = 7.81–7.79 (2H, m, 4,6-H), 7.46–7.42 (3H, m, 1,2,3-H), 7.23 (1H, s, 7-H), 5.54 (1H, d, ^3J = 0.64 Hz, 9-H), 4.23–4.17 (2H, m, 12-H or 13-H), 4.08–4.02 (2H, m, 12-H or 13-H) ppm.

^{13}C NMR (100 MHz, $CDCl_3$): δ = 145.9 (C_t, C-7), 132.5 (C_t, C-5), 131.4 (C_t, C-1,3), 129.6 (C_t, C-4,6), 129.1 (C_t, C-2), 116.5 (C_q, C-10), 110.3 (C_q, C-8), 103.8 (C_t, C-9), 66.0 (C_s, C-12,13) ppm.

FT-IR (ATR): $\tilde{\upsilon}$ = 2961 (w, ν(C-H)), 2893 (w, ν(C-H)), 2218 (w), 1697 (w), 1632 (w), 1492 (w), 1450 (w), 1450 (w), 1397 (w) 1325 (w), 1293 (w), 1174 (m), 1092 (s), 1026 (m), 1000 (w), 964 (w), 942 (s), 930 (s), 890 (m), 840 (w), 754 (m), 688 (s), 606 (w) cm^{-1}.

UV/Vis (acetonitrile, lg ε): λ_{max} = 216 (4.13), 274 (4.25) nm.

MS (EI, 70 eV): m/z = 201 (M^+, 48), 156 (17), 129 (24), 73 (100), 45 (27).

HRMS (ESI, +): calc. for $[C_{12}H_{11}NO_2 + Na]^+$ m/z 224.06820, found m/z 224.06779.

9-Cyanophenanthrene (186)

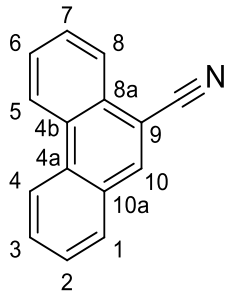

186

Method A: Bromophenanthrene **185** (66.3 g, 257.9 mmol) was heated to 260°C and CuCN (26.4 g, 294.8 mmol, 1.14 eq.) were added over the course of 20 min. After 6 h 20 min the reaction was allowed to cool, upon which the brown solution solidified. This residue was purified using SOXHLET extraction with CH_2Cl_2, followed by column chromatography (silica, CH_2Cl_2, 100%) and recrystallization from EtOH to afford the product as a yellow solid.

Yield: 47.2 g, (232.2 mmol, 90%; lit.[285] 87%).

Method B: To a solution of 9-bromophenanthrene **185** (5.00 g, 19.5 mmol) in DMF (100 ml) was added copper(I)cyanide (3.60 g, 40.2 mmol, 2.06 eq.) and refluxed at 140° C for 24 h. Saturated ammonium chloride solution (100 ml) and CH_2Cl_2 (100 ml) were added and the phases separated. A pale yellow solid was observed in the organic phase. The aqueous phase was washed with CH_2Cl_2 (2 × 100 ml) and the combined organic phases were dried over $MgSO_4$. The solvent was removed *in vacuo* and the residue was purified using column chromatography (silica, pentane/CH_2Cl_2 1:1) to give **186** as a pale yellow solid.

Yield: 2.84 g, 14.0 mmol, 72%.

m.p.: 111–113°C (lit.[356] 111°C).

R_f = 0.36 (cyclohexane/CH_2Cl_2 1:1).

^{1}H NMR (400 MHz, $CDCl_3$): δ = 8.75–8.70 (2H, m, 4,5-H), 8.35–8.30 (1H, m, 8-H), 8.28 (1H, s, 9-H), 7.96 (1H, d, ^3J = 8.0 Hz, 1-H), 7.84–7.74 (3H, m, C*H*), 7.72–7.67 (1H, m, C*H*) ppm.

^{13}C NMR (100 MHz, $CDCl_3$): δ = 135.8 (C_t, C-10), 132.0 (C_q), 130.2 (C_q, *C*H), 130.0 (C_t, *C*H), 129.7 (C_t, C-6), 129.1 (C_q), 128.4 (C_t, *C*H), 128.3 (C_t, *C*H), 127.8 (C_t), 126.3 (C_t, C-8), 123.3 (C_t), 123.1 (C_t), 118.1 (C_q, *C*≡N), 109.6 (C_q, C-9) ppm.

FT-IR (ATR): ϑ = 3073 (w, *ν*(C-H_{arom})), 2219 (m, *ν*(CN)), 1956 (w), 1833 (w), 1708 (w), 1613 (w), 1593 (w), 1573 (w), 1526 (w), 1495 (w), 1448 (m), 1395 (w), 1350 (w), 1308 (w), 1247 (w), 1219 (w), 1208 (w), 1160 (w), 1147 (w), 1035 (w), 984 (w), 916 (m), 861 (w), 760 (s), 742 (vs), 717 (vs), 620 (m) cm^{-1}.

MS (EI, 70 eV): m/z = 203 (M^+, 100%), 176 (8), 102 (4), 88 (6).

9-Acetylphenanthrene (189)

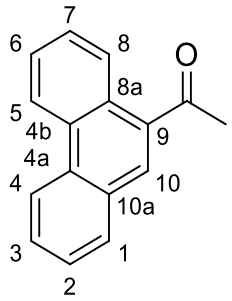

189

A Grignard reagent was freshly prepared from Mg (4.32 g, 178 mmol) and methyliodide (9.12 ml, 146 mmol, 20.7 g) in Et_2O (100 ml). To this reagent was added 9-cyanophenanthrene **186** (16.4 g, 80.7 mmol) in benzene (180 ml) and the reaction mixture was heated to 85°C for 20 h. Freshly prepared Grignard reagent, consisting of Mg (4.52 g 178 mmol), Et_2O (60 ml) and methyliodide (9.12 ml, 146 mmol, 20.7 g), was added. After a further 20 h the reaction was allowed to cool to 0°C and a cooled solution of saturated NH_4Cl was added. A yellow solid precipitates out. 2 M HCl (150 ml) and Et_2O (500 ml) were added and the phases separated. The organic phase and the yellow solid were dissolved in CH_2Cl_2 (90 ml) and washed with 2 M HCl (3 × 50 ml). The aqueous phase was extracted with CH_2Cl_2 (4 × 60 ml)

and the organic phases were combined and the solvent removed in vacuo to afford a dark orange oil. This residue was purified using column chromatography (1:1, cyclohexane/ CH_2Cl_2) to afford the product as a pale yellow solid.

Yield: 12.2 g (55.4 mmol, 69%; lit.[250] 73%).

m.p.:73°C (lit.[288] 73–74°C).

R_f = 0.19 (cyclohexane/CH_2Cl_2 1:1).

^{1}H NMR (400 MHz, $CDCl_3$): δ = 8.74–8.68 (3H, m, C*H*), 8.21 (1H, s, 10-H), 7.98–7.96 (1H, m, 1-H), 7.76 (1H, ddd, $^3J_{3,2}$ = 7.0 Hz, $^3J_{3,4}$ = 7.0 Hz, $^4J_{3,1}$ = 1.4 Hz, 3-H), 7.72–7.63 (3H, m, CH), 2.83 (3H, m, CH_3) ppm.

^{13}C NMR (100 MHz, CDCl3): δ = 202.0 (C_q, C=O), 135.0 (C_q, C-9), 132.2 (C_q, C-4a), 131.0 (C_q), 130.7 (C_t, C-10), 130.1 (C_q), 129.9 (C_t, C-1), 129.1 (C_t, C-3), 128.5 (C_q, C-8a), 127.7 (C_t, CH), 127.3 (C_t, CH), 127.0 (C_t, CH), 123.0 (C_t, CH), 122.9 (C_t, CH), 30.2 (C_p, CH_3) ppm.

FT-IR (ATR): $\tilde{\upsilon}$ = 3062 (w, *ν*(C-H_{arom})), 1666 (s, *ν*(C=O)), 1613 (w), 1573 (w), 1526 (w), 1493 (w), 1444 (m), 1389 (m), 1351 (m), 1293 (m), 1248(m), 1230 (m), 1212 (m), 1167 (m), 1156 (m), 1141 (m), 1005 (w), 958 (w), 914 (m), 893 (m), 860 (w), 791 (w), 770 (vs), 749 (s), 722 (vs), 644 (m), 618 (w) cm^{-1}.

MS (EI, 70 eV): m/z = 220 (M^+, 62%), 205 (M^+-Me, 100), 177 (M^+-COMe, 66), 151 (12), 88 (11).

The spectroscopic data corresponded to the data reported in the literature.[250]

Phenanthrene-9-carboxylic acid (187)

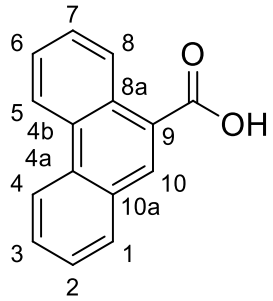

187

Cyanophenanthrene **186** (13.3 g, 65.4 mmol) and NaOH (8.98 g, 224.5 mmol) were suspended in diethyleneglycol (215 ml) for 25 h. H_2O (100 ml) and conc. HCl (15 ml) were added upon allowing to cool to room temperature. A colourless precipitate was observed,

which was filtered off, washed with H_2O and dried over P_4O_{10}. This sticky residue was purified using column chromatography (silica, cyclohexane/ethyl acetate 1:1 + 1% TFA) to afford the product as pale yellow crystals.

Yield: 13.2 g (59.4 mmol, 91%; lit.[287] 86%).

m.p.: 251°C (MeOH; lit.[287] 252°C).

R_f = 0.30 (cyclohexane/ethyl acetate, 1:1 + 1% TFA).

^{1}H NMR (400 MHz, $(CD_3)_2CO$)): δ = 11.48 (br s, 1H, COOH), 9.07–9.04 (1H, m, C*H*), 8.92–8.90 (1H, m, C*H*), 8.87 (1H, d, ^3J = 8.4 Hz, C*H*), 8.64 (1H, s, 10-H), 8.15–8.13 (1H, m, C*H*), 7.86–7.81 (1H, m, C*H*), 7.78–7.70 (3H, m, C*H*) ppm.

^{13}C NMR (100 MHz, $(CD_3)_2CO$)): δ = 168.9 (C_q, COOH), 133.4 (C_t, C-10), 133.1 (C_q), 131.8 (C_q), 131.3 (C_q), 131.0 (C_t, *C*H), 130.3 (C_q), 130.2 (C_t, *C*H), 128.3 (C_t, *C*H), 128.3 (C_t, CH), 128.0 (C_t, *C*H), 127.8 (C_t, *C*H), 127.3 (C_q), 124.1 (C_t, *C*H), 123.8 (C_t,*C*H) ppm.

FT-IR (ATR): $\tilde{\upsilon}$ = 3051 (w, *ν*(C-H_{arom})), 2919 (w, *ν*(C-H)), 2798 (w), 2593 (w, *ν*(O-H)), 1680 (s, ν(C=O)), 1617 (m), 1574 (w), 1529 (w), 1496 (w), 1443 (m), 1416 (m), 1291 (m), 1255 (s), 1213 (m), 1193 (m), 1170 (w), 1157 (m), 986 (w), 954 (w), 886 (m), 857 (m), 791 (s), 737 (s), 716 (s), 620 (w) cm^{-1}.

MS (EI, 70 eV): m/z = 222 (M^+, 100%), 205 (M^+-OH, 26), 177 (M^+-COOH, 32), 165 (7), 151 (7), 88 (11).

The spectroscopic data corresponded to the data reported in the literature.[250]

Methyl phenanthrene-9-carboxylate (188)

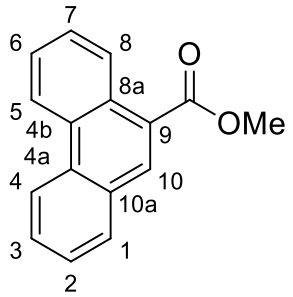

188

Acid **187** (12.0 g, 54.0 mmol) was suspended in MeOH (180 ml). conc. H_2SO_4 (3.5 ml) was added and the reaction mixture was heated to reflux at 80°C for 23 h. After allowing to cool to room temperature, a colourless solid precipited out of solution (10.1 g), which was filtered off and washed with MeOH. CH_2Cl_2 (100 ml) and H_2O (100 ml) were added to the filtrate and the phases separated. The aqueous phase was extracted with CH_2Cl_2 (3 × 50 ml) and the

combined organic phases were washed with $NaHCO_3$ solution (3 × 50 ml). The organic phases were dried over $MgSO_4$ and the solvent removed *in vacuo* to afford the second portion of product (778 mg).

Yield: 10.9 g (46.0 mmol, 85%, lit.[287] 91%).

m.p.: 118°C (MeOH; Lit.[287] 115°C).

R_f = 0.67 (cyclohexane/ethyl acetate, 1:1).

^{1}H NMR (400 MHz, $CDCl_3$): δ = 8.94–8.91 (1H, m, 6-H), 8.75–8.73 (1H, m, 5-H), 8.70 (1H, d, $^3J_{4,3}$ = 8.2 Hz, 4-H), 8.48 (1H, s, 10-H), 7.98–7.96 (1H, m, 1-H), 7.76 (1H, ddd, $^3J_{3,2}$ = 7.0 Hz, $^3J_{3,4}$ = 7.0 Hz, $^4J_{3,1}$ = 1.4 Hz, 3-H), 7.74–7.68 (2H, m, 7,8-H), 7.64 (1H, ddd, $^3J_{2,1}$ = 7.0 Hz, $^3J_{2,3}$ = 7.0 Hz, $^4J_{2,4}$ = 1.1 Hz, 2-H), 4.05 (3H, s, CH_3) ppm.

^{13}C NMR (100 MHz, $CDCl_3$): δ = 168.2 (C_q, *C*OOMe), 132.6 (C_t, C-10), 132.3 (C_q, C-4a), 130.8 (C_q, C-4b), 130.2 (C_q, C-10a), 130.1 (C_t, C-1), 129.2 (C_q, C-8a), 129.1 (C_t,C-3), 127.6 (C_t, C-7), 127.2 (C_t, C-8), 127.1 (C_t, C-2), 126.8 (C_t, C-6), 126.4 (C_q, C-9), 123.0 (Ct, C-5), 122.8 (Ct, C-4), 52.4 (Cp, *C*H3) ppm.

FT-IR (ATR): $\tilde{\upsilon}$ = 3004 (w, *ν*(C-H_{arom})), 2951 (w, *ν*(C-H)), 1705 (s,*ν*(C=O)), 1614 (w), 1571 (w), 1526 (w), 1495 (w), 1444 (s), 1432 (m), 1397 (w), 1350 (w), 1292 (m), 1252 (s), 1234 (s), 1210 (s), 1194 (s), 1157 (s), 1143 (s), 1103 (m), 1029 (s), 958 (w), 912 (m), 870 (w), 785 (s), 734 (s), 718 (s), 618 (w) cm^{-1}.

MS (EI, 70 eV): m/z = 236 (M^+, 100%), 205 (M^+-Ome, 80), 177 (M^+-COOMe, 58), 151 (10), 88 (20).

The spectroscopic data corresponded to the data reported in the literature.[250]

1,3-Di(phenanthren-9-yl)propane-1,3-dione (166)

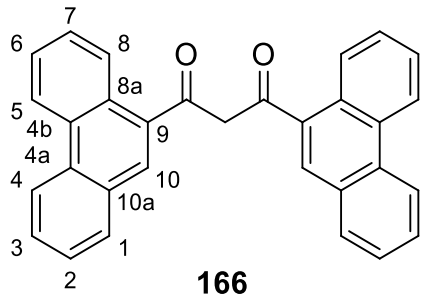

166

To a solution of ester **188** (10.0 g, 42.3 mmol) in anhydrous THF (90 ml) was added NaH (4.81 g, 121.1 mmol, 60% suspension in oil) to give a yellow suspension. A solution of

ketone **189** (7.43 g, 33.7 mmol) in anhydrous THF (80 ml) was added dropwise to the mixture and refluxed at 75° C for 20 h. Another portion of NaH (870 mg) was added and the mixture refluxed for a further 5 h. After reaching room temperature, CH_2Cl_2 (160 ml), H_2O (150 ml) and conc. HCl (20 ml) were added and the phases separated. The aqueous phase was extracted with CH_2Cl_2 (3 × 50 ml) and the organic phases were washed with H_2O (100 ml) and dried over $MgSO_4$. After removal of the solvent *in vacuo*, a yellow solid was isolated and recrystallized from ethyl acetate (10.5 g). The filtrate was purified using column chromatography (1:1 pentane/CH_2Cl_2) and recrystallised from ethyl acetate to afford a second portion of the product (687 mg).

Yield: 11.2 g (26.4 mmol, 78%; lit.[250] 87%).

m.p.: 194–195°C (lit.[250] 194–196°C, ethyl acetate).

R_f = 0.4 (pentane/CH_2Cl_2 1:1).

^{1}H NMR (400 MHz, $CDCl_3$): δ = 16.76 (1H, s, O*H*), 8.79–8.76 (2H, m, C*H*), 8.72 (2H, d, *J* = 8.2 Hz), 8.66–8.63 (2H, m, C*H*), 8.15 (2H, s, 10-H), 7.97(2H, d, *J* = 7.9 Hz), 7.78–7.70 (6H, m, C*H*), 7.69–7.63 (2H, m, C*H*), 6.76 (1H, s, C*H*) ppm.

^{13}C NMR (100 MHz, CDCl3): δ = 189.6 (C_q, *C*=O), 133.6 (C_q, C-9), 131.7 (C_q), 131.0 (C_q), 130.6 (C_q), 129.8 (C_t, *C*H), 129.3 (C_t, C-10), 128.7 (C_t, *C*H), 128.7 (C_q), 127.4 (C_t, *C*H), 127.4 (C_t, *C*H), 127.3 (C_t, *C*H), 126.7 (C_t, *C*H), 123.2 (C_t, *C*H), 122.9 (C_t, *C*H), 103.3 (C_t, *C*H) ppm.

FT-IR (ATR): ῡ = 3082 (w, *ν*(C-H_{arom})), 3058 (w, *ν*(C-H_{arom})),1946 (w), 1808 (m), 1598 (m), 1526 (s), 1504 (s), 1446 (s), 1379 (m), 1315 (w), 1250 (w), 1208 (m), 1180 (w), 1164 (w), 1147 (w), 1134 (m), 1047 (w), 1038 (w), 972 (w), 954 (w), 943 (w), 904 (m), 872 (m), 851 (w), 809 (m), 769 (s), 741 (vs), 722 (vs), 687 (m), 624 (m), 615 (m) cm^{-1}.

MS (EI, 70 eV): m/z = 424 (M^+, 35%), 405 (9), 219 (18), 205 ($C_{15}H_9^+$, 100), 177 ($C_{14}H_9^+$, 41).

The spectroscopic data corresponded to the data reported in the literature.[250]

2-Benzylidene-1,3-di(phenanthren-9-yl)propane-1,3-dione (169)

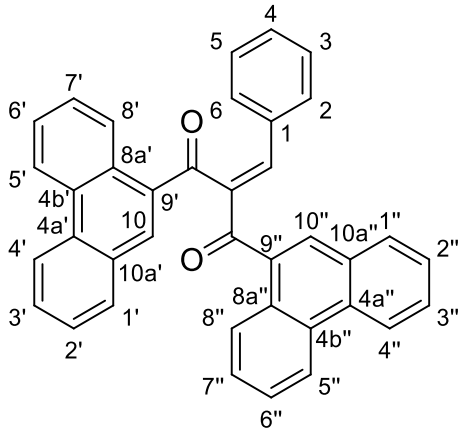

169

Diketone **166** (4.11 g, 9.68 mmol) was dissolved in toluene (350 ml) and benzaldehyde (5.14 g, 48.4 mmol, 5 eq.), butyric acid (2.2 ml), 4 Å molecular sieves (2 g) and piperidine (2.2 ml) were added. The reaction mixture was heated to 120°C for 2 h. After cooling to room temperature, CH_2Cl_2 (200 ml) and H_2O (60 ml) were added and the phases separated. The aqueous phase was extracted with CH_2Cl_2 (2 × 50 ml) and the organic phase was washed with H_2O (200 ml).The organic phases were dried over Na_2SO_4 and the solvent was removed in vacuo. The resulting brown oil was purified using column chromatography (silica, cyclohexane/CH_2Cl_2 1:3) to afford the product as a pale yellow solid.

Yield: 3.60 g (7.02 mmol, 73%; lit [250] 77%).

m.p.: 198–200°C (lit.[250] 199–201°C).

R_f = 0.18 (cyclohexane/CH_2Cl_2, 2:3).

^{1}H NMR (400 MHz, $CDCl_3$): δ = 9.09 (1H, dd, ^3J = 8.1 Hz, J = 1.1 Hz, C*H*), 8.67- 8.62 (4H, m, C*H*), 8.42 (1H, s, 10'-H), 8.15 (1H, dd, ^3J = 8.2 Hz, J = 0.9 Hz, C*H*), 8.06 (1H, s, 10''-H), 7.95 (1H, dd, ^3J = 7.9 Hz, J = 1.4 Hz, C*H*), 7.89 (1H, dd, ^3J =7.9 Hz, J = 1.4 Hz, C*H*), 7.77–7.72 (2H, m, C*H*), 7.72 (1H, s, C*H*=C), 7.68–7.59 (5H, m, C*H*), 7.53–7.48 (3H, m, C*H*), 7.28–7.18 (3H, m, C*H*) ppm.

^{13}C NMR (100 MHz, CDCl3): δ = 198.7 (C_q, C(9')*C*=O), 197.2 (C_q, C(9'')*C*=O), 145.5 (C_t, *C*H=C), 142.6 (C_q, *C*=CH), 135.2 (C_q), 134.6 (C_t, C-10'), 133.1 (C_q), 133.0(C_q), 131.4 (C_q), 131.1 (C_t, *C*H), 131.0 (C_q), 130.8 (C_t, *C*H), 130.7 (C_q), 130.4 (C_t, *C*H), 130.1 (C_q), 130.0 (C_q), 129.8 (C_t, *C*H), 129.7 (C_t, *C*H), 129.0 (C_t, *C*H), 129.0 (C_q), 128.7 (C_t, C-10''), 128.6 (C_q), 128.5 (C_t, *C*H), 128.1 (C_t, *C*H), 127.5 (C_t, *C*H), 127.4 (C_t, *C*H), 127.4 (C_t, *C*H), 127.2 (C_t,

*C*H), 127.0 (C_t, *C*H), 126.3 (C_t, *C*H), 123.0 (C_t, *C*H), 122.9 (C_t, *C*H), 122.8 (C_t, *C*H), 122.7 (C_t, *C*H) ppm.

FT-IR (ATR): $\tilde{\upsilon}$ = 3056 (w, ν(C-H_{arom})), 1662 (s, ν(C=O)), 1635 (m, ν(C=O)), 1604 (m, ν(C=C_{arom})), 1573 (w, ν(C=C_{arom})), 1527 (w), 1493 (w), 1445 (m), 1401 (w), 1371 (w), 1320 (w), 1247 (m), 1230 (m), 1206 (m), 1184 (m), 1164 (m), 1147 (m), 1125 (m), 1097 (w), 1080 (w), 1042 (w), 1003 (w), 948 (w), 897 (m), 876 (w), 850 (w), 826 (s), 791 (w), 739 (vs), 722 (vs), 691 (vs), 651 (w), 616 (w) cm^{-1}.

MS (EI, 70 eV): m/z = 512 (M^+, 28%), 494 (3), 307 (M^+-$C_{14}H_9CO$, 14), 291 (24), 276 (5), 205 ($C_{14}H_9CO^+$, 100), 176 ($C_{14}H_8^+$, 15), 151 (6).

The spectroscopic data corresponded to the data reported in the literature.[250]

2-Benzylidene-1,3-di(phenanthren-9-yl)propane-1,3-diol (190)

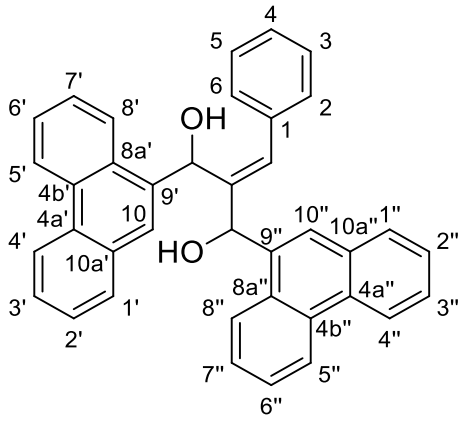

190

Diketone **169** (1.65 g, 3.21 mmol) was dissolved in CH_2Cl_2 (28 ml) and cooled to -78°C. To this mixture was added a 0.2 M solution of $CeCl_3 \cdot 7\ H_2O$ (2.51 g, 6.74 mmol) in MeOH (34 ml). The resulting suspension was stirred for 10 min, after which $NaBH_4$ (364 mg, 9.63 mmol, 3 eq.) was added. The reaction mixture was stirred at -78°C for 1 h and then allowed to reach room temperature. After 3 h the reaction was complete and Et_2O (20 ml), CH_2Cl_2 (150 ml), H_2O (5 ml) and 2 M HCl (25 ml) were added. A colourless precipitate was observed in the organic phase, which dissolved upon addition of CH_2Cl_2 (150 ml). The aqueous phase was extracted with CH_2Cl_2 (3 × 50 ml) and the organic phases were washed with brine (100 ml) and dried over $MgSO_4$. The solvent was removed *in vacuo* to afford a yellow solid, which was purified using column chromatography (silica, Pentane/CH_2Cl_2 1:7) to afford two isomers as colourless solids.

Yield: 1.38 g (2.67 mmol, 83%, lit.[250] 92%).

R,S/S,R-diastereomer 190

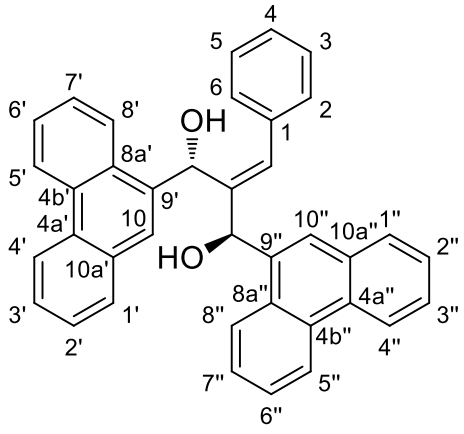

***rac*-190**

Yield: 257 mg (497 µmol, 16%).

m.p.: 152–154°C (lit.[250] 153–155°C).

R_f = 0.28 (pentane/CH_2Cl_2 1:7).

^{1}H NMR (400 MHz, $CDCl_3$): δ = 8.72–8.70 (2H, m, C*H*), 8.66–8.63 (2H, m, C*H*), 8.23 (1H, d, ^3J = 8.4 Hz, C*H*), 7.93 (1H, s, 10'-H), 7.87 (1H, s, 10''-H), 7.76 (1H, dd, ^3J = 7.9 Hz, J = 1.3 Hz, C*H*), 7.68–7.53 (10H, m, C*H*), 7.50–7.46 (1H, m, C*H*), 7.45–7.39 (3H, m, C*H*), 7.33–7.30 (1H, m, C*H*), 7.16 (1H, s, C*H*=C), 6.54 (1H, br d, J = 4.8 Hz, (C9')C*H*OH), 6.03 (1H, br d, J = 3.8 Hz, (C9'')C*H*OH), 2.38 (1H, br d, J = 5.0 Hz, (C9')CHO*H*), 1.78 (1H, br d, J = 4.2 Hz, (C9'')CHO*H*) ppm.

^{13}C NMR (100 MHz, $CDCl_3$): δ = 142.4 (C_q, *C*=CH), 136.5 (C_q), 136.1 (C_q),135.9 (C_q), 132.8 (C_t, *C*H=C), 131.4 (C_q), 131.3 (C_q), 130.9 (C_q), 130.7 (C_q), 130.5 (C_q),130.4 (C_q), 129.9 (C_q), 129.6 (C_q), 129.2 (C_t, *C*H), 129.1 (C_t, *C*H), 129.1 (C_t, *C*H),128.7 (C_t, *C*H), 127.9 (C_t, *C*H), 127.0 (C_t, *C*H), 127.0 (C_t, *C*H), 126.9 (C_t, *C*H), 126.9(C_t, *C*H), 126.8 (C_t, *C*H), 126.7 (C_t, *C*H), 126.7 (C_t, *C*H), 126.6 (C_t, *C*H), 126.5 (C_t,*C*H), 125.0 (C_t, *C*H), 124.9 (C_t, *C*H), 124.1 (C_t, *C*H), 123.4 (C_t, *C*H), 123.2 (C_t, *C*H), 122.6 (C_t, *C*H), 122.6 (C_t, *C*H), 70.8 (C_t, *C*HOH), 69.7 (C_t, *C*HOH) ppm.

FT-IR (ATR): ϑ̃ = 3557 (w, *v*(O-H)), 3264 (w, *v*(O-H)), 3046 (w, *v*(C-H_{arom})), 1606 (w), 1530 (w), 1494 (m, *v*(C=C_{arom})), 1447 (m), 1304 (w), 1244 (m), 1160 (w), 1102 (w), 1065 (s), 1037 (w), 950 (w), 920 (w), 903 (w), 886 (w), 821 (w), 789 (w), 748 (vs), 725 (vs), 700 (vs), 628 (w), 614 (s) cm^{-1}.

MS (EI, 70 eV): m/z = 516 (M^+, 30%), 498 (28, M^+-H_2O), 407 (39), 291 (51), 215 (27) 205 (53), 178 ($C_{14}H_{10}^+$, 100).

The spectroscopic data corresponded to the data reported in the literature.[250]

R,R/S,S-diastereomer 190

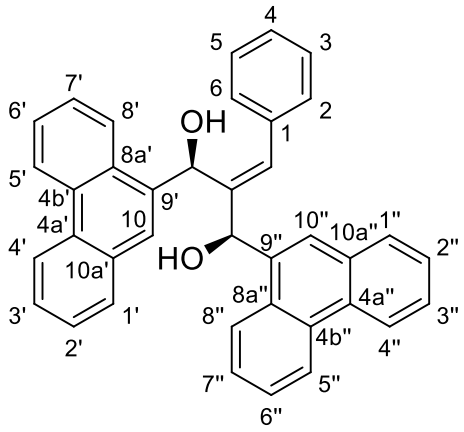

rac-**190**

Yield: 1.12 g (2.17 mmol, 68%).

m.p.: 217–219°C (lit.[250] 218–220°C).

R_f = 0.1 (pentane/CH_2Cl_2 1:7).

^{1}H NMR (400 MHz, $CDCl_3$): δ = 8.82 (1H, d, ^3J = 8.5 Hz, C*H*), 8.72 (1H, d, ^3J = 8.0 Hz, C*H*), 8.58–8.53 (2H, m, C*H*), 8.44 (1H, s, 10'-H), 8.03–8.02 (1H, m, C*H*), 8.00 (1H, s, 10''-H), 7.85 (1H, dd, ^3J = 7.8 Hz, J = 1.5 Hz, C*H*), 7.73–7.52 (5H, m, C*H*), 7.46–7.29 (8H, m, C*H*), 6.74–6.70 (1H, m, C*H*), 6.56 (1H, s, (C9')C*H*OH), 6.46 (1H, d, ^3J = 8.4 Hz, C*H*), 6.24 (1H, s, C*H*=C), 5.68 (1H, s, (C9'')C*H*OH), 4.34 (1H, s, (C9')CHO*H*), 2.76 (1H, s, (C9'')CHO*H*) ppm.

^{13}C NMR (100 MHz, $CDCl_3$): δ = 141.4 (C_q, *C*=CH), 136.7 (C_q), 136.1 (C_q), 135.3 (C_q), 134.6 (Ct, *C*H=C), 131.6 (C_q), 131.4 (C_q), 130.9 (C_q), 130.4 (C_q), 130.2 (C_q), 130.1 (C_q), 129.6 (C_q), 129.5 (C_q), 129.2 (C_t, *C*H), 129.0 (C_t, *C*H), 128.7 (C_t, *C*H), 128.2 (C_t, *C*H), 127.1 (C_t, *C*H), 126.9 (C_t, *C*H), 126.8 (C_t, *C*H), 126.6 (C_t, *C*H), 126.6 (C_t, *C*H), 126.1 (C_t, *C*H), 126.1 (C_t, *C*H), 125.7 (C_t, *C*H), 124.6 (C_t, *C*H), 124.4 (C_t, *C*H), 124.2(C_t, *C*H), 123.5 (C_t, *C*H), 122.9 (C_t, *C*H), 122.7 (C_t, *C*H), 122.5 (C_t, *C*H), 72.2 (C_t, (C9'')*C*HOH), 71.0 (C_t, (C9')*C*HOH) ppm.

FT-IR (ATR): ῡ = 3284 (m, *ν*(O-H)), 3060 (w, *ν*(C-H_{arom})), 1603 (w), 1495 (w, ν(C=C_{arom})), 1420 (w), 1308 (w), 1278 (w), 1247 (m), 1105 (w), 1064 (m), 1038 (w), 1003 (m), 948 (w),

928 (w), 900 (m), 859 (w), 822 (w), 797 (w), 786 (w), 746 (vs), 723 (vs), 706 (s), 696 (s), 646 (w), 617 (w) cm^{-1}.

MS (EI, 70 eV): m/z = 516 (M^+, 11%), 498 (M^+-H_2O, 88), 407 (63), 292 (78), 291 (75), 215 (53) 205 (100), 178 ($C_{14}H_{10}^+$, 85).

The spectroscopic data corresponded to the data reported in the literature.[250]

4c,4c1,12c,16b-Tetrahydroindeno[1',2',3':3,4]pentaleno[1,2-l:5,6-l']diphenanthrene (103)

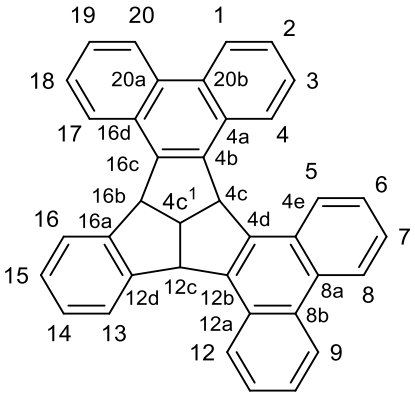

103

Diol **190** (767 mg) was suspended in chlorobenzene (20 ml) and polyphosphoric acid (454 mg) was added. The reaction mixture was heated to 130°C for 2 d. The reaction mixture, which had turned a red/brown colour was allowed to cool to room temperature. CH_2Cl_2 (50 ml) and H_2O (50 ml) were added and the phases separated. The aqueous phases was extracted with CH_2Cl_2 (4 × 15ml) and the combined organic phases were washed with H_2O (15 ml) and dried over $MgSO_4$. The solvent was removed in vacuo and the resulting brown residue was purified using column chromatography (silica, pentane/CH_2Cl_2, 3:1) and recrystallization from toluene to afford the product as very fine colourless crystals.s

Yield: 20.2 mg (42.0 µmol, 3%; lit.[250] 4%).

m.p.: 315–316°C (lit.[250]: 316–317°C).

R_f = 0.30 (pentane/CH_2Cl_2, 3:1).

^{1}H NMR (400 MHz, $CDCl_3$): δ = 8.73 (2H, d, ^3J = 8.2 Hz, 9,20-H), 8.71 (2H, d, ^3J = 8.2 Hz, 1,8-H), 8.54 (2H, d, ^3J = 8.2 Hz, 12,17-H), 8.44 (2H, dd, ^3J = 8.3 Hz, J = 1.0 Hz, 4,5-H), 7.81–7.78 (2H, m, 11,18-H), 7.74–7.68 (4H, m, 10,13,16,19-H), 7.61–7.57 (2H, m, 2,7-H),

7.46–7.42 (2H, m, 3,6-H), 7.02–6.99 (2H, m, 14,15-H), 5.77 (1H,d, ^3J = 9.9 Hz, 4c-H), 5.64 (2H, d, ^3J = 9.1 Hz, 12c,16b-H), 5.04 (1H, dt, ^3J = 9.2 Hz, ^3J = 9.2 Hz, 4c^1-H) ppm.

^{13}C NMR (100 MHz, $CDCl_3$): δ = 146.6 (C_q, C-12d,16a), 143.7 (C_q, C-12b,16c), 138.4 (C_q, C-4b,4d), 131.7 (C_q, C-8b,20a), 131.1 (C_q, C-8a,20b), 130.6 (C_q, C-4a,4e), 129.8 (C_q, C-12a,16d), 127.5 (C_t, C-4,5), 127.1 (C_t, C-14,15), 126.7 (C_t, C-11,18), 126.4 (C_t, C-10,19), 126.3 (C_t, C-12,17), 125.9 (C_t, C-2,7), 125.8 (C_t, C-3,6), 125.6 (C_t, C-13,16), 123.5 (C_t, C-1,8), 123.5 (C_t, C-9,20), 58.2 (C_t, C-4c), 54.2 (C_t, C-4c^1), 53.9 (C_t, C-12c,16b) ppm.

FT-IR (ATR): $\tilde{\upsilon}$ = 3059 (w, ν(C-H_{arom})), 2923 (w, ν(C-H)), 2871 (w, ν(C-H)), 1587 (w), 1587 (w), 1498 (w), 1474 (w), 1446 (w), 1423 (w), 1326 (w), 1236 (w), 1155 (w), 1041 (w), 974 (w), 951 (w), 868 (w), 822 (w), 791 (w), 748 (vs), 723 (vs), 708 (m), 613 (w) cm^{-1}.

MS (EI, 70 eV): m/z = 480 (M^+, 100%), 302 (20), 278 (9), 201 (3).

The spectroscopic data corresponded to the data reported in the literature.[250]

4c-methoxy-4c,4c1,12c,16b-tetrahydroindeno[1',2',3':3,4]pentaleno[1,2-l:5,6-l']di-phenanthrene (171)

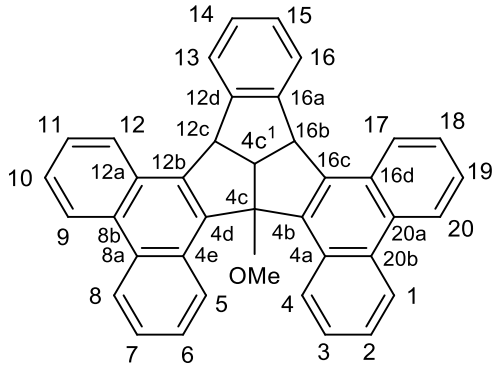

171

TBTQ **103** (12.0 mg, 25.0 µmol) was dissolved in anhydrous CH_2Cl_2 (10 ml) and cooled to 0°C in a nitrogen atmosphere. Anhydrous $FeCl_3$ (24.3 mg, 150 µmol, 6 eq.) was added and stirred for 2.5 h. MeOH (10 ml) and H_2O (10 ml) were added. The phases were separated and the organic phase was washed with H_2O (2 × 10 ml) and dried over $MgSO_4$. The solvent was removed to afford TBTQ **171** as a brown solid, which was purified with column chromatography (silica, CH_2Cl_2/pentane, 40:60) to afford the product as a yellow solid.

Yield: 1.80 mg, 3.52 µmol, 14%.

m.p.: 251–252°C (decomp.).

R_f = 0.3 (pentane/CH_2Cl_2, 1:1).

^{1}H NMR (400 MHz, $CDCl_3$): δ = 8.92 (2H, d, *J* = 9.2 Hz, 4,5-H), 8.75 (2H, d, *J* = 7.8 Hz, 9,20-H), 8.71 (2H, d, *J* = 8.7 Hz, 1,8-H), 8.57 (2H, d, *J* = 8.0 Hz, 12,17-H), 7.83–7.78 (2H, m, 10,19-H), 7.77–7.72 (2H, m, 13,16-H), 7.68–7.66 (2H, m, 2,7-H), 7.62–7.58 (2H, td, *J* = 7.0 Hz, *J* = 1.3 Hz, 3,6-H), 7.01–6.98 (2H, m, 14,15-H), 5.67 (2H, d, *J* = 9.0 Hz, 12c,16b-H), 4.81 (1H, t, *J* = 9 Hz, 4c^1-H), 3.07 (3H, s, OC*H*$_3$) ppm.

^{13}C NMR (100 MHz, $CDCl_3$): δ = 145.7 (C_q, C-12d,16a), 144.8 (C_q, C-12b,16c), 136.3 (C_q, C-4b,4d), 132.6 (C_q, C-8b,20a), 131.4 (C_q, C-8a,20b), 129.9 (C_q, C-4a,4e), 129.1 (C_q, C-12a,16d), 128.3 (C_t, C-4,5), 127.4 (C_t, C-14,15), 127.2 (C_t, C-10,19), 126.7 (C_t, C-11,12,17,18), 126.1 (C_t, C-2,7), 125.9 (C_t, C-3,6), 125.7 (C_t, C-13,16), 123.5 (C_t, C-9,20), 123.3 (C_t, C-1,8), 107.2 (C_q, C-4c), 58.3 (C_t, C-4c^1), 51.5 (C_t, C-12c,16b), 50.6 (C_t, O*C*H$_3$) ppm.

FT-IR (ATR): $\tilde{\upsilon}$ = 2960 (w, *v*(C-H)), 2922 (w, *v*(C-H)), 2360 (w), 1591 (w), 1496 (w), 1446 (w), 1259 (m), 1018 (s, *v*(C-O)), 906 (w), 796 (s), 750 (s), 725 (vs), 646 (w), 617 (w) cm^{-1}.

UV/Vis (acetonitrile, lg ε): λ_{max} = 193 (4.68), 210 (4.51), 228 (4.23), 254 (4.65), 259 (4.66), 270sh (4.38), 297 (4.01), 309 (3.96) nm.

MS (EI): m/z = 480 ($C_{38}H_{23}^+$, 100%), 477 (21), 463 (7), 302 (22), 278 (11), 240 (8), 237 (23), 201 (18).

HRMS (ASAP, +): calc. for $[C_{39}H_{26}O+H]^+$ m/z 511.2056, found m/z 511.2054.

(Z)-2,3-Bis(3,4-dimethoxyphenyl)acrylic acid (222)

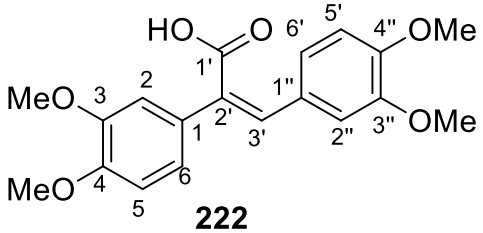

222

3,4-Methoxybenzaldehyde **220** (7.84 g, 47.7 mmol) and 3,4-dimethoxyphenylacetic acid **221** (10.0 g, 51.0 mmol, 1.07 eq.) were dissolved in a mixture of dry Et_3N (10 ml) and acetic anhydride (20 ml) and the resulting solution was refluxed under N_2 for 23 h. Upon reaching room temperature, H_2O (5 ml) was added and the mixture was stirred for 1 h. A K_2CO_3 solution (75 g in 500 ml H_2O) was added and the mixture was refluxed at 120°C until the

brown oil dissolved completely. At room temperature conc. HCl (110 ml) was added and the precipitate was filtered and recrystallised from MeOH.

Yield: 10.5 g (30.4 mmol, 64%; lit.[320] 69%).

m.p.: 215–217°C (lit.[320] 216–217 C).

^{1}H NMR (400 MHz, DMSO): δ = 12.4 (1H, br s, O*H*), 6.65 (1H, s, 3'-H), 6.99 (1H, d, ^{3}J = 8.3 Hz, C*H*), 6.85 (1H, d, ^{3}J = 8.3 Hz, C*H*), 6.81 (1H, d, ^{3}J= 8.4 Hz, C*H*), 6.76 (1H, s), 6.69 (1H, dd, ^{3}J = 8.2 Hz, ^{4}J = 1.9H z, C*H*), 6.56 (1H, s, OCH_3), 3.77 (3H, s, OCH_3), 3.71 (3H, s, OCH_3), 3.68 (3H, s, OCH_3), 3.37 (3H, s, OCH_3) ppm.

^{13}C NMR (100 MHz, DMSO): δ = 168.7 (C_q), 149.6 (C_q), 149.0 (C_q), 148.3 (C_q), 147.9 (C_q), 138.9 (C_t), 130.6 (C_q), 129.2 (C_q), 127.1 (C_q), 124.6 (C_t), 121.8 (C_t), 113.3 (C_t), 112.8 (C_t), 112.2 (C_t), 111.2 (C_t), 55.6 (C_p, O*C*H_3), 55.6 (C_p, O*C*H_3), 55.4 (C_p, O*C*H_3), 54.6 (C_p, O*C*H_3) ppm.

FT-IR (ATR): ϑ̃ = 2938 (w, *ν*(C-H)), 2835 (w), 2609 (w), 2050 (w), 1666 (m, *ν*(C=O)), 1591 (m), 1506 (s), 1458 (m), 1417 (m), 1321 (w), 1292 (w), 1252 (vs), 1233 (vs), 1160 (m), 1133 (s, *ν*(C-O)), 1014 (s), 928 (w), 895 (w), 866 (w), 802 (m), 764 (w), 744 (w), 717 (w), 604 (w) cm^{-1}.

UV/Vis (acetonitrile, lg ε): λ_{max} = 199 (4.61), 289 (4.10), 321 (4.17) nm.

MS (EI, 70 eV): m/z = 344 (M^+, 100%), 269 (6), 255 (4), 167 (9).

The spectroscopic data corresponded to the data reported in the literature.[320]

2,3,6,7-tetramethoxyphenanthrene-9-carboxylic acid (230)

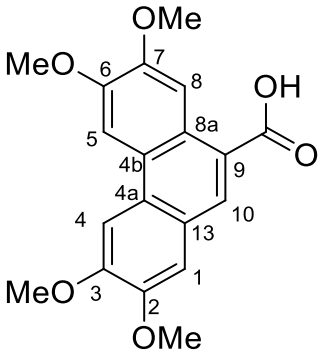

230

To a solution of acid **222** 1.00 g (2.90 mmol, 1 eq.) in acetonitrile (46 ml) were added TFA (11.6 ml) and NaN_3 (80.0 mg, 1.16 mmol, 0.4 eq.) and the resulting mixture was stirred at room temperature for 2 d. After TLC reaction control, H_2O (60 ml) was added and the precipitate was filtered off and washed with ethyl acetate. The solid was purified via a continuous extraction with refluxing MeOH (250 ml) to afford the desired product as an orange solid.

Yield: 632 mg, (1.85 mmol, 64 %; lit.[317] 95 %).

m.p.: 288–291°C (MeOH; lit.[317] 285–287°C).

$\mathbf{R_f}$ = 0.11 (ethyl acetate/ cyclohexane 2:1).

^{1}H NMR (400 MHz, DMSO): δ = 12.9 (1H, br s, O*H*), 8.55 (1H, s, C*H*), 8.42 (1H, s, C*H*), 8.05 (1H, s, C*H*), 8.01 (1H, s, C*H*), 7.57 (1H, s, C*H*), 4.06 (3H, s, OC*H*$_3$), 4.05 (3H, s, OC*H*$_3$), 3.92 (3H, s, OC*H*$_3$), 3.89 (3H, s, OC*H*$_3$) ppm.

^{13}C NMR (100 MHz, $CDCl_3$): δ = 169.1 (C_q, *C*OOH), 151.1 (C_q), 148.9 (C_q), 148.8 (C_q), 129.8 (C_t), 126.5 (C_q), 125.0 (C_q), 124.2 (Cq), 123.5 (C_q), 122.7 (C_q), 109.6 (C_t), 106.7 (C_t), 103.9 (C_t), 103.4 (C_t), 56.0 (C_p, O*C*H$_3$), 55.9 (C_p, O*C*H$_3$), 55.6 (C_p, O*C*H$_3$), 55.2 (C_p, O*C*H$_3$) ppm.

FT-IR (ATR): ϑ = 2918 (w, *v*(C-H)), 2360 (w), 1664 (m, *v*(C=O)), 1620 (w, *v*(C=C$_{arom}$)), 1510 (m, *v*(C=C$_{arom}$)), 1467 (m, δ(CH$_3$)), 1423 (m, δ(CH$_3$)), 1265 (m, *v*(C-O-C)), 1236 (vs, *v*(C-O-C)), 1188 (s, *v*(C-O-C)), 1163 (m, *v*(C-O-C)), 1132 (vs, *v*(C-O-C)), 1038 (m, *v*(C-O-C)), 1011 (m, *v*(C=O)), 991 (m), 901 (m), 868 (m), 827 (m, δ(=C-H)), 798 (w), 773 (m), 735 (w), 701 (w), 658 (w), 615 (w) cm^{-1}.

UV/Vis (acetonitrile, lg ε): λ_{max} = 207 (3.86), 225 (3.92), 250sh (4.15), 262 (4.29), 288 (4.10), 323 (3.61) nm.

MS (EI, 70 eV): m/z = 342 (M^+, 100 %), 299 (M – COOH, 13), 284 (5), 171 ($C_{11}H_7O_2^+$, 5).

The spectroscopic data corresponded to the data reported in the literature.[317]

(2,3,6,7-Tetramethoxyphenanthrene-9-yl)methanol (231)

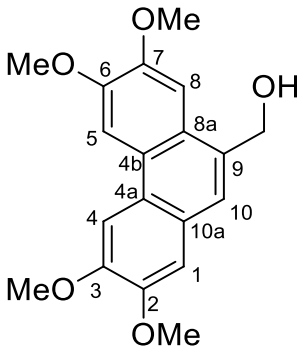

231

To a suspension of $LiAlH_4$ (125 mg, 1.5 eq.) in abs. THF (18 ml) at 0°C was added gradually acid **236** (750 mg, 2.19 mmol, 1 eq.). The reaction mixture was stirred at 78°C for 2 h and cooled to 0°C, after which ethyl acetate (1.1 ml) and 2 M HCl (1.1 ml) were added. After stirring for 5 min, the solution was filtered to afford the product as a beige solid.

Yield: 695 mg (2.12 mmol, 97%; lit.[324] 95%).

m.p.: 181–184°C (THF; lit.[324] 183–185°C).

R_f = 0.18 (cyclohexane/ethyl acetate 1:1).

^{1}H NMR (400 MHz, $CDCl_3$): δ = 7.82 (1H, s, 4-H or 5-H), 7.77 (1H, s, 4-H or 5-H), 7.58 (1H, s, 10-H), 7.55 (1H, s, C*H*), 7.20 (1H, s, C*H*), 5.12 (2H, s, CH_2OH), 4.13 (OCH_3), 4.12 (3H, s, OCH_3), 4.06 (3H, s, OCH_3), 4.02 (3H, s, OCH_3), 1.77 (1H, br s 11-H) ppm.

^{13}C NMR (100 MHz, $CDCl_3$): δ = 149.6 (C_q), 149.2 (C_q), 149.0 (C_q), 149.0 (C_q), 132.2 (C_q), 126.0 (C_q), 125.2 (C_q), 124.8 (C_q), 124.8 (C_q), 124.3 (C_t, C-10), 108.5 (C_t), 105.0 (C_t), 103.4 (C_t, C-4 or C-5), 102.9 (C_t, C-4 or C-15), 64.9 (C_s, CH_2OH), 56.2 (C_p, OCH_3), 56.2 (C_p, OCH_3), 56.1 (C_p, OCH_3), 56.1 (C_p, OCH_3) ppm.

FT-IR (ATR): $\tilde{\upsilon}$ = 3502 (w, ν(O-H)), 2910 (w, ν(C-H)), 1616 (w, ν(C=C_{arom})), 1508 (m), 1468 (m, δ(CH3)), 1427 (m, δ(CH3)), 1250 (s, ν(C-O-C)), 1196 (m, ν(C-O-C)), 1147 (s,

v(C-O-C)), 1065 (m, v(C-O-C)), 1037 (m, v(C-O-C)), 1014 (m, v(C-O)), 997 (m), 968 (w), 885 (w), 846 (m), 795 (w), 769 (m, δ(=C-H)), 674 (s), 617 (w) cm^{-1}.

UV/Vis (acetonitrile, lg ε): λ_{max} = 207 (3.84), 225 (3.91), 249sh (4.11), 263 (4.27), 288 (4.07), 323 (3.59) nm.

MS (EI, 70 eV): m/z = 328 (M^+, 100%), 313 (7), 267 ($C_{17}H_{15}O_3^+$, 4), 150 (4).

The spectroscopic data corresponded to the data reported in the literature.[324]

2,3,6,7-Tetramethoxyphenanthrene-9-aldehyde (228)

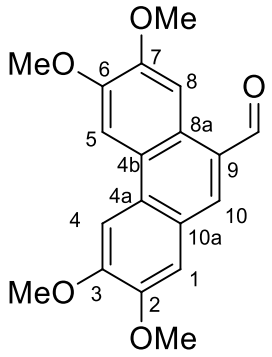

228

Alcohol **231** (200 mg, 609 µmol, 1 eq.),PCC (394 mg (1.83 mmol, 3 eq.) and silica gel (400 mg, 6.66 mmol, 11.1 eq.) were dissolved in abs. CH_2Cl_2 (6 ml) and the reaction mixture was stirred at room temperature for 16 h. Once the reaction was complete, the mixture was filtered and the solvent was removed *in vacuo*. The resulting precipitate was purified using column chromatography (silica, cyclohexane/ethyl acetate 1:1) to afford the desired product as a yellow solid.

Yield: 118 mg, (362 µmol, 59%; lit.[324] 80%).

m.p.: 223–226°C (ethyl acetate; lit.[324] 227–228°C).

R_f = 0.44 (cyclohexane/ethyl acetate 1:1).

^{1}H NMR (400 MHz, $CDCl_3$): δ = 10.3 (1H, s, C*H*O), 8.98 (1H, s, C*H*), 8.08 (1H, s, 10-H), 7.81 (1H, s, C*H*), 7.79 (1H, s, C*H*), 7.35 (1H, s, C*H*), 4.17 (3H, s, OCH_3), 4.14 (3H, s, OC$H_3$4.11 (3H, s, OCH_3), 4.07 (3H, s, OCH_3) ppm.

^{13}C NMR (100 MHz, $CDCl_3$): δ = 194.1 (C_p, *C*HO), 152.4 (C_q), 150.3 (C_q), 149.7 (C_q), 149.3 (C_q), 139.5 (C_t, C-9), 128.2 (C_q), 128.2 (C_q), 125.3 (C_q), 124.9 (C_q), 123.2 (C_q), 109.6 (C_t),

106.4 (C_t), 102.8 (C_t), 102.8 (C_t), 56.3 (C_p, O*C*H$_3$), 56.2 (C_p, O*C*H$_3$), 56.2 (C_p, O*C*H$_3$), 56.1 (C_p, O*C*H$_3$) ppm.

FT-IR (ATR): $\tilde{\upsilon}$ = 3103 (w, *v*(C=H$_{arom}$)), 3006 (w, *v*(C=H$_{arom}$)), 2958 (w, *v*(C-H)), 2924 (w, *v*(C-H)), 2833 (w, *v*(C-H)), 2715 (w), 2360 (w), 1739 (w), 1685 (m, *v*(C=O)), 1614 (m, *v*(C=O)), 1511 (m), 1473 (s, δ(CH$_3$)), 1429 (m, δ(CH$_3$)), 1414 (m, δ(CH$_3$)), 1369 (w), 1257 (vs, *v*(C-O-C)), 1213 (s, *v*(C-O-C)), 1196 (s, *v*(C-O-C)), 1163 (m, *v*(C-O-C)), 1066 (s, *v*(C-O-C)), 1028 (vs, *v*(C-O-C)), 995 (m), 945 (w), 881 (m), 831 (s, δ(=C-H)), 800 (m, δ(=C-H)), 777 (m, δ(=C-H)), 739 (m, δ(=C-H)), 671 (w), 642 (w), 619 (w) cm^{-1}.

UV/Vis (acetonitrile, lg ε): λ_{max} = 211 (4.33), 234 (4.28), 257sh (4.55), 268 (4.67), 283 (4.45), 292 (4.41), 342 (4.15) nm.

MS (EI, 70 eV): m/z = 326 (M$^+$, 100 %), 283 (11), 240 (6), 163 (5).

The spectroscopic data corresponded to the data reported in the literature.[324]

Methyl (Z)-2,3-bis(3,4-dimethoxyphenyl)acrylate (224)

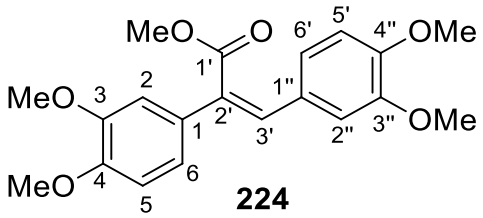

224

Stilbene **222** (5.02 g, 14.5 mmol) was dissolved in MeOH (240 ml) and conc. H_2SO_4 (2 ml) was added. The reaction mixture was heated to 80°C for 24 h. After cooling to room temperature, CH_2Cl_2 (100 ml), H_2O (50 ml) and brine (5 ml) were added and the phases were separated. The aqueous phase was extracted with CH_2Cl_2(3 × 30 ml) and the combined organic phases were washed with saturated $NaHCO_3$ solution (30 ml). The salt was filtered off and the organic phase was dried over $MgSO_4$. The solvent was dried *in vacuo* to afford a yellow solid.

Yield: 3.62 g (10.1 mmol, 70%; lit.[320] 92%).

m.p.: 126–128 C (lit.[320] 127–128 C).

R$_f$ = 0.40 (cyclohexane/ethyl acetate 1:1).

^{1}H NMR (400 MHz, $CDCl_3$): δ = 7.77 (1H, s, 3'-H), 6.92 (1H, d, ^3J = 8.2 Hz, C*H*), 6.81 (2H, dd, ^3J = 8.2 Hz,^4J = 2.0 Hz, C*H*), 6.77 (1H, d, ^3J = 1.9 Hz, C*H*), 6.72 (1H, d, ^3J = 8.4 Hz,

C*H*), 6.52 (1H, d, ^3J = 2.0 Hz, C*H*), 3.90 (3H, s, OCH_3), 3.84 (3H, s, OCH_3), 3.82 (3H, s, OCH_3), 3.80 (3H, s, OCH_3), 3.48 (3H, s, COOCH_3) ppm.

^{13}C NMR (100 MHz, $CDCl_3$): δ = 168.8 (C_q, C-1'), 150.1 (C_q), 149.4 (C_q), 148.7 (C_q), 148.3(C_q), 140.6 (C_t, C-3'), 129.8 (C_q), 128.9 (C_q), 127.6 (C_q), 125.5 (C_t, *C*H), 122.4 (C_t, *C*H), 113.0 (C_t, *C*H), 112.6 (C_t, *C*H), 111.6 (C_t, *C*H), 110.6 (C_t, *C*H), 56.1 (C_p, O*C*H_3), 56.1 (C_p, O*C*H_3), 55.9 (C_p, O*C*H_3), 55.4 (C_p, O*C*H_3), 52.5 (C_p, COO*C*H_3) ppm.

FT-IR (ATR): $\tilde{\upsilon}$ = 3089 (w), 2945 (w, *v*(C-H)), 2834 (w), 1698 (m, *v*(C=O)), 1594 (m), 1511 (s), 1469 (m), 1417 (m), 1319 (w), 1292 (w), 1250 (s), 1223 (vs), 1180 (m), 1163 (m), 1134 (vs, *v*(C-O)), 1049 (w), 1020 (vs), 938 (w), 889 (w), 858 (w), 815 (m), 771 (m), 723 (w), 609 (w) cm^{-1}.

UV/Vis (acetonitrile, lg ε): λ_{max} = 199 (4.65), 291 (4.14), 325 (4.25) nm.

MS (EI, 70 eV): m/z = 358 (M^+, 100%), 311 (3), 299 (7), 269 (4), 241 (3), 181 (45).

The spectroscopic data corresponded to the data reported in the literature.[320]

(Z)-3,4-Bis(3,4-dimethoxyphenyl)but-3-en-2-one (223)

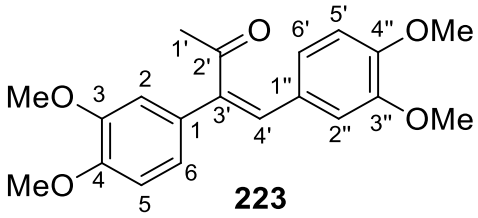

223

Acid **222** (4.00 g, 12.0 mmol) was suspended in anhydrous THF (45 ml) and cooled to 0°C. MeLi (16.5 ml, 1.6 M, 580 mg, 26.4 mmol) was added dropwise and the solution was stirred at 0°C for 10 min and 1 h at room temperature. 2 M HCl (15 ml) and ethyl acetate (80 ml) were added and the phases were separated. The aqueous phases were washed with ethyl acetate (2 × 50 ml) and the combined organic phases were dried over $MgSO_4$.The solvent was removed in vacuo and the raw product was purified using column chromatography (silica, cyclohexane/ethyl acetate 1:1) to afford the desired product as a yellow solid.

Yield: 2.14 g (6.25 mmol, 52%; lit.[317] 88%).

m.p.: 108–110 C (lit.[317] 108–109°C).

R_f = 0.37 (cyclohexane/ethyl acetate: 1:1).

^{1}H NMR (400 MHz, $CDCl_3$): δ = 7.58 (1H, s, 4'-H), 6.95 (1H, d, ^3J = 8.2 Hz, *C*H), 6.83 (1H, dd, ^3J = 8.4 Hz, ^3J = 2.0 Hz, *C*H), 6.77 (1H, dd, ^3J = 8.1 Hz, ^4J = 2.0 Hz, *C*H), 6.74–6.71 (2H, m, *C*H), 6.52 (1H, d, *J* = 2.0 Hz, *C*H), 3.91 (3H, s, OC*H*$_3$), 3.85 (3H, s, OC*H*$_3$), 3.83 (3H, s, OC*H*$_3$), 3.49 (3H, s, OC*H*$_3$), 2.34 (3H, s, 1'-H) ppm.

^{13}C NMR (100 MHz, $CDCl_3$): δ = 199.6 (C_q, C-2'), 150.3 (C_q), 149.8 (C_q), 148.8 (C_q), 148.4 (C_q), 139.2 (C_t, *C*H) , 138.6 (C_q), 130.0 (C_q), 127.6 (C_q), 125.9 (C_t, *C*H), 122.1 (C_t, *C*H), 112.8 (C_t, *C*H), 112.8 (C_t, *C*H), 112.0 (C_t, *C*H), 110.7 (C_t, *C*H), 56.1 (C_p, O*C*H$_3$), 56.1 (C_p, O*C*H$_3$), 56.0 (C_p, O*C*H$_3$), 55.4 (C_p, O*C*H$_3$), 27.9 (C_p, C-1') ppm.

FT-IR (ATR): $\tilde{\upsilon}$ = 2991 (w), 2935 (w, *ν*(C-H)), 2835 (w), 1678 (m, *ν*(C=O)), 1581 (m, *ν*(C=C$_{arom}$)), 1504 (s), 1460 (m), 1415 (m), 1356 (w), 1317 (w), 1236 (vs), 1207 (vs), 1159 (m), 1136 (vs), 1020 (vs), 978 (m), 949 (w), 918 (w), 879 (w), 863 (w), 817 (m), 766 (m), 640 (w) cm^{-1}.

UV/Vis (acetonitrile, lg ε): λ_{max} = 199 (4.69), 236 (4.26), 288 (4.09), 333 (4.31) nm.

MS (EI, 70 eV): m/z = 342 (M^+, 100%), 299 (52), 268 (9), 253 (5), 165 (3).

The spectroscopic data corresponded to the data reported in the literature.[317]

Methyl 2,3,6,7-tetramethoxyphenanthrene-9-carboxylate (213)

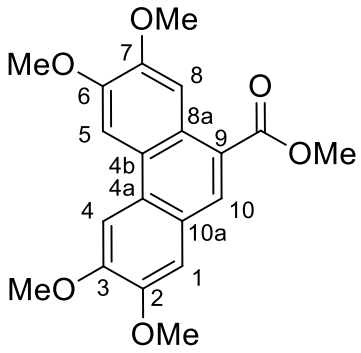

213

Ester **224** (6.50 g, 18.1 mmol) was dissolved in dry CH_2Cl_2 (120 ml) and anhydrous $FeCl_3$ (10.0 g, 63.4 mmol, 3.5 eq.) was added. The resulting black solution was stirred at room temperature for 21 h, after which H_2O (120 ml) and CH_2Cl_2 (100 ml) was added and the phases separated. The aqueous phase was extracted with CH_2Cl_2 (3 × 100 ml) and the combined organic phases were dried over $MgSO_4$. The solvent was removed *in vacuo* to

afford the product as a light brown solid, which was purified with column chromatography (silica, cyclohexane/ethyl acetate 1:1) to give the desired product as a beige solid.

Yield: 4.77 g, (13.4 mmol, 74%; lit.[318] 96%).

m.p.: 201–203°C (lit.[318] 202–204°C).

$\mathbf{R_f}$ = 0.36 (cyclohexane/ethyl acetate 1:1).

^{1}H NMR (400 MHz, $CDCl_3$): δ = 8.66 (1H, s, C*H*), 8.44 (1H, s, C*H*), 7.82 (1H, s, C*H*), 7.78 (1H, s, C*H*), 7.28 (1H, s, C*H*), 4.15 (3H, s, OCH_3), 4.14 (3H, s, OCH_3), 4.08 (3H, sOCH_3), 4.04 (3H, s, OCH_3), 4.02 (3H, s, COOCH_3) ppm.

^{13}C NMR (100 MHz, $CDCl_3$): δ = 168.4 (C_q, CO_2Me), 151.4 (C_q), 149.5 (C_q), 149.2 (C_q), 130.5 (C_t), 127.3, (C_q),127.3 (C_q), 125.3 (C_q), 124.7 (C_q), 124.4 (C_q), 122.4 (C_q), 109.4 (C_t), 107.0 (C_t), 102.8 (C_t), 102.6 (C_t), 56.2 (C_p, OCH_3), 56.1 (C_p, OCH_3), 56.1 (C_p, OCH_3), 56.0 (C_p, OCH_3), 52.2 (C_p, COOCH_3) ppm.

FT-IR (ATR): $\tilde{\upsilon}$ = 2947 (w, ν(C-H)), 2833 (w), 1711 (m, ν(C=O)), 1619 (m), 1508 (s), 1471 (s), 1429 (s), 1365 (w), 1261 (vs), 1236 (vs), 1188 (vs), 1126 (vs), 1041 (m), 997 (s), 908 (w), 876 (w), 833 (m), 779 (m), 748 (w), 700 (w), 660 (w), 619 (w) cm^{-1}.

UV/Vis (acetonitrile, lg ε): λ_{max} = 203 (4.39), 225 (4.35), 264 (4.75), 279sh (4.56), 289 (4.51), 326 (4.07) nm.

MS: (EI, 70 eV): m/z = 356 (M^+, 100%), 313 (12), 283 (5), 178 (5).

The spectroscopic data corresponded to the data reported in the literature.[318]

1-(2,3,6,7-Tetramethoxyphenanthren-9-yl)ethan–1-one (219)

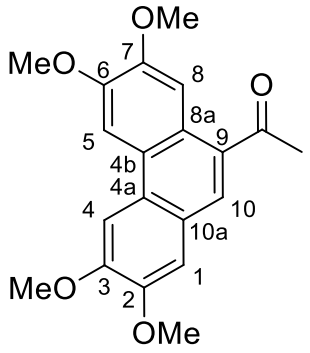

219

Ketone **223** (171 mg, 500 µmol) was dissolved in TFA/MeCN (10 ml, 1:4) and $NaNO_2$ (6.90 mg, 100 µmol) was added. The solution was stirred for 15 min at room temperature, after which saturated $NaHCO_3$ solution was added until neutral (6 ml). CH_2Cl_2 (10 ml) and H_2O (10 ml) were added and the phases were separated. The aqueous phase was extracted with CH_2Cl_2 (2 × 10 ml) and the combined organic phases were washed with H_2O (10 ml) and brine (10 ml), after which they were dried over $MgSO_4$. The solvent was removed in vacuo to afford a brown raw product, which was purified using column chromatography (silica, cyclohexane/ethyl acetate 1:2) to afford the desired product as a yellow solid.

Yield: 103 mg (303 µmol, 61%; lit.[317] 95%).

m.p.: 199–201 C (lit.[317] 201–203°C).

R_f = 0.23 (cyclohexane/ethyl acetate 1:2).

^{1}H NMR (400 MHz, $CDCl_3$): δ = 8.57 (1H, s, C*H*), 8.19 (1H, s, C*H*), 7.80 (1H, s, C*H*), 7.78 (1H, s, C*H*), 7.29 (1H, s, C*H*), 4.15 (3H, s, OC*H*$_3$), 4.13 (3H, s, OC*H*$_3$), 4.06 (6H, s, OC*H*$_3$), 2.79 (3H, s, O=C-C*H*$_3$) ppm.

^{13}C NMR (100 MHz, $CDCl_3$): δ = 201.7 (C_q, *C*OCH_3), 151.6 (C_q), 149.7 (C_q), 149.3 (C_q), 149.3 (C_q), 130.7 (C_q), 130.1 (C_t), 127.3 (C_q), 125.5 (C_q), 124.5 (C_q), 123.5 (C_q), 109.4 (C_t), 107.4 (C_t), 102.7 (C_t), 102.7 (C_t), 56.3 (C_p, O*C*H_3), 56.2 (C_p, O*C*H_3), 56.1 (C_p, O*C*H_3), 56.0 (C_p, O*C*H_3) 29.8 (C_p, *C*OCH_3) ppm.

FT-IR (ATR): $\tilde{\upsilon}$ = 2939 (w, ν(C-H)), 2834 (w), 1666 (m, ν(C=O)), 1616 (m), 1506 (s), 1468 (s), 1423 (s), 1365 (w), 1261 (vs), 1240 (s), 1219 (vs), 1192 (s), 1167 (m), 1120 (vs), 1936 (m), 1014 (m), 945 (w), 908 (w), 883 (m), 831 (m), 787 (m), 764 (w), 687 (w), 619 (w) cm^{-1}.

UV/Vis (acetonitrile, lg ε): λ_{max} = 203 (4.22), 225 (4.35), 264 (4.58), 279sh (4.29), 289 (4.35), 325 (3.90) nm.

MS (EI, 70 eV): m/z = 340 (M^+, 100%), 325 (45), 297 (12), 267 (8), 239 (4), 196 (2), 170 (6).

The spectroscopic data corresponded to the data reported in the literature.[317]

(E)-1,3-Di(phenanthren-9-yl)prop-2-en-1-one (232)

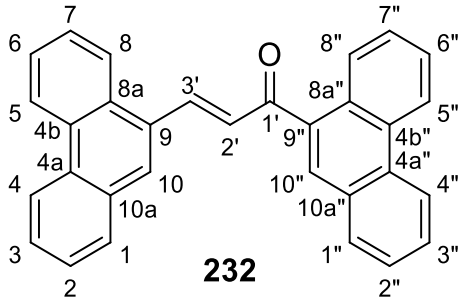

232

Ketone **189** (100 mg, 454 µmol) and aldehyde **167** (93.6 mg, 454 µmol) were dissolved in EtOH (10 ml). NaOH (36.3 mg) was dissolved in H_2O (10 ml) and this solution was added to the reaction mixture, turning the clear solution cloudy. After 15 min the solution had turned yellow and was continued to stir at room temperature. After 24 h CH_2Cl_2 (10 ml) and H_2O (10 ml) were added and the phases separated. The aqueous phase was extracted with CH_2Cl_2 (2 × 10 ml) and the combined organic phases were washed with H_2O (20 ml) and dried over $MgSO_4$. The solvent was removed *in vacuo* to afford a yellow solid, which was purified using column chromatography (silica, CH_2Cl_2/pentane 2:1) and recrystallised from EtOH.

Yield: 75.1 mg, (184 µmol, 41%; lit.[358] 81%).

m.p.: 189–190°C (lit.[358] 185–186°C).

$\mathbf{R_f}$ = 0.25 (pentane/CH_2Cl_2 1:1).

^{1}H NMR (400 MHz, $CDCl_3$): δ = 8.80 (1H, d, ^3J = 8.2 Hz, 5”-H), 8.76 (1H, d, ^3J = 4.0 Hz, 4”-H), 8.74 (1H, d, ^3J = 3.2 Hz, 4-H), 8.69 (1H, d, ^3J = 8.2 Hz, 5-H), 8.57 (1H, d, ^3J = 15.8 Hz, 3’-H), 8.47 (1H, d, ^3J = 8.0 Hz, 1”-H), 8.18 (1H, s, 10”-H), 8.15 (1H, s, 10-H) 8.12 (1H, d, ^3J = 8.2 Hz, 1-H), 8.00 (1H, d, ^3J = 7.9 Hz, 8”-H), 7.95 (1H, d, ^3J = 7.9 Hz, 8-H), 7.81–7.61 (8H, m, 2,3,6,7,2”,3”,6”,7”-H), 7.55 (1H, d, ^3J = 15.6 Hz, 2’-H) ppm.

^{13}C NMR (100 MHz, $CDCl_3$): δ = 195.6 (C_q, C-1’), 143.8 (C_t, C-3’), 136.2 (C_q, C-8a”), 131.7 (C_q, C-9”), 131.4 (C_q, C-9), 131.3 (C_q, C-8a), 131.2 (C_q, C-4b), 131.0 (C_q, C-10a”), 130.6 (C_q, C-10a), 130.4 (C_q, C-4b or C-4b”), 130.2 (C_q, C-4b or C-4b”), 130.2 (C_t, C-2’), 129.8 (C_t,

C-8”), 129.5 (C_t, C-8), 129.3 (C_t, C-1”), 129.1 (C_q, C-4a”), 128.7 (C_t, *C*H), 128.1 (C_t, *C*H), 127.6 (C_t, *C*H), 127.4 (C_t, *C*H), 127.4 (C_t, *C*H), 127.3 (C_t, *C*H), 127.3 (C_t, *C*H), 127.2 (C_t, C-10), 127.1 (C_t, *C*H), 126.8 (C_t, C-1”), 124.4 (C_t, C-1), 123.4 (C_t, C-4 or C-4”), 123.1 (C_t, C-5”), 122.9 (C_t, C-4 or C-4”), 122.8 (C_t, C-5) ppm.

FT-IR (ATR): $\tilde{\upsilon}$ = 3055 (w, ν(C-H_{arom})), 1655 (m, ν(C=O)), 1592 (m), 1527 (w), 1492 (w), 1444 (w), 1387 (w), 1304 (w), 1257 (w), 1209 (m), 1147 (w), 1120 (m), 1093 (w), 1052 (w), 980 (m), 951 (w), 889 (w), 863 (w), 843 (m), 743 (s), 717 (s), 658 (w), 617 (w) cm^{-1}.

UV/Vis (acetonitrile, lg ε): λ_{max} = 207 (4.72), 250 (4.91), 293sh (4.23), 344 (4.23) nm.

MS (EI, 70 eV): m/z =408 (M^+, 100%), 407 (41), 379 (13), 231 (27), 230 (27), 205 (38), 202 (52), 177 (32), 176 (24), 151 (8), 101 (2).

The spectroscopic data corresponded to the data reported in the literature.[358]

2-(4-(tert-Butyl)phenyl)acetic acid (242)

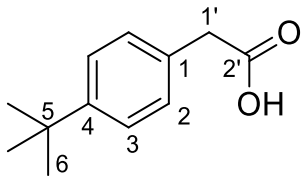

242

Methyl *p*-tert-phenylacetate **241** (200 mg, 970 µmol) and LiOH ·H_2O (122 mg, 2.91 mmol, 3 eq.) were dissolved in MeOH (5 ml) and H_2O (5 ml) and the resulting mixture was stirred at room temperature for 24 h. The mixture was acidified by adding 2 M HCl (10 ml) and CH_2Cl_2 (10 ml) was added and the phases separated. The aqueous phase was extracted with CH_2Cl_2 (3 × 10 ml) and the combined organic phases were washed with H_2O (10 ml) and dried over $MgSO_4$. The solvent was removed in vacuo to afford a colourless solid.

Yield: 186 mg (967 mmol, 99%).

m.p.:79–81 C (lit.[357] 80–81°C).

R_f = 0.22 (cyclohexane/ethyl acetate 3:1).

^{1}H NMR (400 MHz, $CDCl_3$): δ = 7.37–7.34 (2H, m, 3-H), 7.24–7.21 (2H, m, 2-H), 3.63 (2H,s, 1’-H), 1.31 (9H, s, 6-H) ppm.

^{13}C NMR (100 MHz,$CDCl_3$): δ = 176.4 (C_q, C-2’), 150.4 (C_q, C-4), 130.4 (C_q, C-1), 129.1 (C_t, C-2), 125.8 (C_t, C-3), 40.4 (C_s, C-11’), 34.6 (C_q, C-5), 31.5 (C_t, C-6) ppm.

FT-IR (ATR): $\tilde{\upsilon}$ = 3030 (w, ν(C-H_{arom})), 2959 (m), 2904 (w), 2868 (w), 2727 (w), 2642 (w), 1708 (vs, ν(C=O)), 1518 (w), 1462 (w), 1400 (m), 1365 (w), 1329 (w), 1259 (m), 1232 (s, δ(O-H)), 1200 (s), 1092 (m), 1018 (m), 926 (m), 862 (w), 810 (vs, δ(=C-H)$_{1,4\text{-subst}}$), 746 (w), 696 (m), 660 (s) cm^{-1}.

UV/Vis (acetonitrile, lg ε): λ_{max} = 210 (2.92), 263 (1.32), 269 (1.23) nm.

MS (EI, 70 eV): m/z =192 (M^+, 15%), 177 (100), 131 (25), 117 (8), 91 (10).

The spectroscopic data corresponded to the data reported in the literature.[357]

(Z)-2-(4-(tert-Butyl)cyclohexa-2,4-dien-1-yl)-3-(4-(tert-butyl)phenyl)acrylic acid (244)

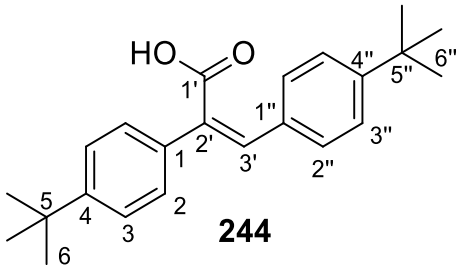

244

[4-(2-Methyl-2-propanyl)phenyl]acetic acid **242** (4.35 g, 22.6 mmol) and 4-*tert*-butylbenzaldehyde **243** (4.10 ml, 3.98 g, 22.6 mmol) were dissolved in anydrous triethylamine (7 ml) and acetic anhydride (12 ml) and the resulting mixture was refluxed at 100°C for 24 h. After allowing to cool to room temperature, conc. HCl (5 ml) was added, upon which a brown solid precipitated out. After filtration the orange product was isolated.

Yield: 3.91 g, 11.6 mmol, 52 %.

m.p: 228–233 C.

^{1}H NMR (400 MHz, $CDCl_3$): δ =7.89 (1H, s, 3'-H), 7.41 (2H, d, ^3J = 8.6 Hz, 2-H), 7.18 (4H, d, ^3J = 8.6 Hz, 3,3''-H), 7.01 (2H, d, ^3J = 8.4 Hz, 2''-H), 1.36 (9H, s, 6-H), 1.25 (9H, s, 6''-H) ppm.

^{13}C NMR (100 MHz,$CDCl_3$): δ = 171.9 (C_q, C-1'), 153.2 (C_q, C-4''), 151.1 (C_q, C-4), 142.2(C_t, C-3'), 132.6 (C_q, C-2'), 131.7 (C_q, *C*H), 131.0 (C_t, C-2''), 130.3 (C_q, *C*H), 129.4 (C_t, C-3''), 125.9 (C_t, C-2), 125.4 (C_t, C-3), 34.9 (C_q, C-5), 34.8 (C_q, C-5''), 31.5 (C_t, C-6), 31.2 (C_t, C-6'') ppm.

FT-IR (ATR): $\tilde{\upsilon}$ = 2960 (m, ν(C-H_{arom})), 2500 (w), 2360 (w), 1674 (s, ν(C=O)), 1604 (m), 1508 (w), 1460 (w), 1415 (m), 1361 (w), 1319 (w), 1265 (vs, δ(O-H)), 1218 (m), 1192 (m),

1108 (w), 997 (w), 922 (w), 833 (s, δ(=C-H)$_{1,4\text{-subst}}$), 758 (w), 717 (w), 678 (m), 630 (w), 611 (w) cm^{-1}.

UV/Vis (acetonitrile, lg ε): λ_{max} = 222 (4.24), 290 (4.25) nm.

MS (EI, 70 eV): m/z = 335 (M^+, 54%), 321 (100), 219 (4), 153 (9), 125 (9), 57 (14).

HRMS (EI): calc. for $C_{23}H_{28}O_2$ m/z 336.20838, found m/z 336.20804.

EA: calc.: C 82.10, H 8.39 for $C_{23}H_{28}O_2$, found C 81.91, H 8.65.

Methyl (Z)-2,3-bis(4-(tert-butyl)phenyl)acrylate (245)

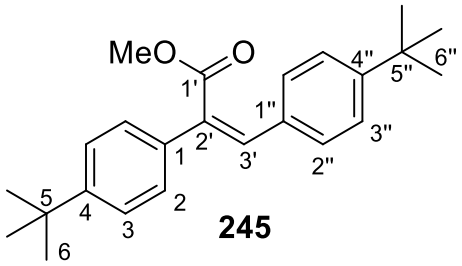

245

To a solution of acid **244** (1.00 g, 2.97 mmol) in MeOH (25 ml) was added conc. H_2SO_4 (0.5 ml) and the resulting solution was refluxed at 80°C for 24 h. Upon cooling, pale yellow crystals precipitated out of the solution, which were filtered off and dried.

Yield: 734 mg, 2.09 mmol, 70%.

m.p.: 93–95°C.

R_f = 0.21 (cyclohexane/CH_2Cl_2 1:1).

^{1}H NMR (400 MHz, $CDCl_3$): δ = 7.79 (1H, s, 3'-H), 7.40 (2H, d, ^3J = 8.6 Hz, 3-H), 7.17 (2H, d, ^3J = 5.0 Hz, 3''-H), 7.15 (2H, d, ^3J = 5.0 Hz, 2-H), 6.98 (2H, d, ^3J = 8.3 Hz, 2''-H), 3.78 (3H, s, CH_3), 1.37 (9H, s, 6-H), 1.25 (9H, s, 6''-H) ppm.

^{13}C NMR (100 MHz, $CDCl_3$): δ = 168.9 (C_q, C-1'), 152.6 (C_q, C-4''), 150.8 (C_q, C-4), 140.3 (C_t, C-3'), 133.2 (C_q, C-1), 132.0 (C_q, C-2'), 131.4 (C_q, C-1''), 130.7 (C_t, C-2''), 129.3 (C_t, C-2), 125.7 (C_t, C-3), 125.3 (C_t, C-3''), 52.5 (C_t, *C*H$_3$), 34.8 (C_q, C-5''), 34.8 (C_q, C-5), 31.5 (C_t, C-6), 31.2 (C_t, C-6'') ppm.

FT-IR (ATR): $\tilde{\upsilon}$ = 3085 (w, ν(C-H$_{arom}$)), 3035 (w, ν(C-H$_{arom}$)), 2960 (m, ν(C-H)), 2902 (w, ν(C-H)), 2865 (w, ν(C-H)), 1708 (s, ν(C=O)), 1621 (m, ν(C=C$_{arom}$)), 1604 (m), 1509 (w), 1459 (w), 1432 (m), 1409 (w), 1394 (w), 1363 (m), 1319 (w), 1247 (s), 1213 (m), 1186 (m),

1166 (m), 1105 (m), 1016 (m), 956 (w), 935 (w), 831 (s), 800 (m), 777 (m), 671 (w), 626 (w) cm^{-1}.

UV/Vis (acetonitrile, lg ε): λ_{max} = 222 (4.22), 292 (4.26) nm.

MS (EI, 70 eV): m/z (%) = 350 (M^+, 61%), 335 (M^+- CH_3, 100), 177 (15), 160 (10), 57 (15).

HRMS (EI): calc. for $C_{24}H_{30}O_2$ m/z 350.22403, found m/z 350.22374.

EA: calc.: C 82.24, H 8.63 for $C_{24}H_{30}O_2$, found: C 82.05, H 8.98.

Methyl 3,6-di-tert-butylphenanthrene-9-carboxylate (239)

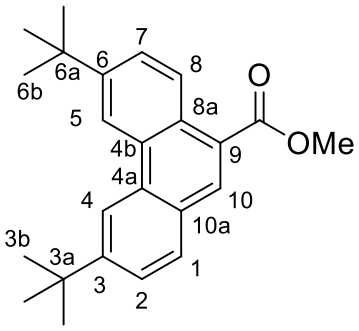

239

Stilbene **245** (100 mg, 285 µmol) was dissolved in Cyclohexane (430 ml) in a Quartz photoreaction vessel. I_2 (73.8 mg, 290 µmol, 1.02 eq.) was added and the solution was degassed with nitrogen for 30 min, after which propylene oxide (11 ml, 9.27 g, 160 mmol) was added. After photoirradiation for 30 min, a $Na_2S_2O_3$ solution (250 ml) was added and the phases separated. The organic phase was washed with H_2O (200 ml) and brine (200 ml), before drying over Na_2SO_4. The solvent was removed *in vacuo* and the resulting yellow oil was purified using column chromatography (silica, petroleum ether/CH_2Cl_2 2:1) to afford the desired product as pale yellow crystals.

Yield: 63.6 mg, 183 µmol, 64%.

m.p.: 116–118°C.

$\mathbf{R_f}$ = 0.20 (petroleum ether/CH_2Cl_2 2:1).

^{1}H NMR (400 MHz, $CDCl_3$): δ = 8.86 (1H, d, ^3J = 8.8 Hz, 8-H), 8.72 (1H, s, 5-H), 8.68 (1H, s, 4-H), 8.42 (1H, s, 10-H), 7.90 (1H, d, ^3J = 8.4 Hz, 1-H), 7.75 (1H, d, J = 8.9 Hz, 7-H), 7.71 (1H, d, ^3J = 8.4 Hz, 2-H), 4.04 (3H, s, OCH_3), 1.52 (9H, s, 3b-H), 1.51 (9H, s, 6b-H) ppm.

^{13}C NMR (100 MHz, $CDCl_3$): δ = 168.4 (C_q, *C*OOMe), 151.9 (C_q, C-3), 149.4 (C_q, C-6), 132.2 (C_q, C-4a), 131.7 (C_t, C-10), 130.7 (C_q, C-4b), 129.9 (C_t, C-1), 128.3 (C_q, C-10a), 127.3 (C_q, C-8a), 126.5 (C_t, C-8), 125.8 (C_t, C-7), 125.4 (C_t, C-2), 125.2 (C_q, C-9), 118.2 (C_t, C-5), 118.1 (C_t, C-4), 52.3 (C_t, *C*H_3), 35.6 (C_q, C-3a), 35.2 (C_q, C-6a), 31.5 (C_t, C-3b), 31.5 (C_t, C-6b) ppm.

UV/Vis (acetonitrile, lg ε): λ_{max} = 198 (4.41), 216 (4.41), 239 (4.50), 259 (4.65), 308 (4.12) nm.

FT-IR (ATR): $\tilde{\upsilon}$ = 2951 (m, ν(C-H_{arom})), 2902 (w, ν(C-H)), 2868 (w, ν(C-H)), 2360 (w), 1712 (vs, ν(C=O)), 1619 (w), 1562 (w), 1514 (w), 1460 (w), 1434 (w), 1415 (w), 1392 (w), 1360 (w), 1296 (w), 1265 (m), 1236 (s), 1182 (s), 1157 (s), 1099 (w), 1045 (w), 1028 (m), 928 (w), 906 (w), 875 (w), 833 (m), 781 (w), 685 (w), 634 (w) cm^{-1}.

MS (EI, 70 eV): m/z = 348 (M^+, 63%), 333 (M^+ - CH_3, 100), 317 (8), 245 (4), 217 (4), 215 (5), 202 (7), 159 (6), 131 (8).

EA: calc.: C 82.72, H 8.10 for $C_{24}H_{28}O_2$, found: C 82.63, H 8.35.

(Z)-3,4-Bis(4-(tert-butyl)phenyl)but-3-en-2-one (246)

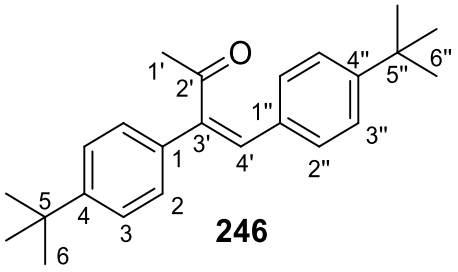

246

To a solution of acid **244** (1.00 g, 2.97 mmol) in anhydrous THF (20 ml) was added MeLi (4.1 ml, 1.6 M in diethylether, 6.54 mmol) dropwise for 5 min 0°C under nitrogen. The reaction mixture was stirred at room temperature for 2 h, after which 2 M HCl (20 ml) and ethyl acetate (10 ml) was added. The phases were separated and the aqueous phase was extracted with ethyl acetate (3 × 25 ml). The organic phases were combined and washed with brine (25 ml) and dried over $MgSO_4$. The solvent was removed in vacuo and the brown residue was purified using MPLC (pentane/CH_2Cl_2 50:50–30:70) to afford the product as a beige solid.

Yield: 604 mg, 1.81 mmol, 61%.

m.p.: 55–57° C.

R_f = 0.37 (pentane/CH_2Cl_2, 50:50).

^{1}H NMR (400 MHz, $CDCl_3$): δ = 7.61 (1H, s, 4'-H), 7.43 (2H,d, ^3J = 8.7 Hz, 2'-H), 7.17 (2H, d, ^3J = 8.5 Hz, 2-H), 7.11 (2H,d, ^3J = 8.5 Hz, 3''-H), 6.98 (2H,d, ^3J = 8.3 Hz, 3-H), 2.29 (3H, s, 1'-H), 1.37 (9H, s, 6''-H), 1.25 (9H, s, 6-H) ppm.

^{13}C NMR (100 MHz, $CDCl_3$): δ = 199.9 (C_q, C-2'), 152.8 (C_q, C-4), 150.9 (C_q, C-4''), 140.0 (C_q, C-1''), 138.7 (C_t, C-4'), 134.3 (C_q, C-3'), 132.0 (C_q, C-3), 131.0 (C_t, C-1), 129.2 (C_t, C-3''), 126.1 (C_t, C-2''), 125.4 (C_t, C-2), 31.6 (C_t, C-6''), 31.3 (C_t, C-6), 28.2 (C_q, C-1') ppm.

FT-IR (ATR): $\tilde{\upsilon}$ =2960 (m, ν(C-H_{arom})), 2902 (w, ν(C-H)), 2867 (w, ν(C-H)), 1668 (s, ν(C=O)), 1595 (m), 1506 (m), 1461 (w), 1414 (w), 1394 (w), 1356 (m), 1319 (w), 1294 (m), 1267 (w), 1234 (s), 1196 (m), 1159 (w), 1107 (m), 1009 (w), 982 (m), 912 (m), 831 (vs), 769 (w), 739 (w), 663 (w), 625 (w) cm^{-1}.

UV/Vis (acetonitrile, lg ε): λ_{max} = 225 (4.26), 300 (4.32) nm.

MS (EI, 70 eV): m/z = 334 (M^+, 73%), 319 (100), 291 (27), 277 (50), 261 (9), 202 (5), 115 (6), 91 (3), 57 (28), 43 (18).

EA: calc.: C 86.18, H 9.04, O 4.78, found: C 86.27, H 9.11, O 4.62.

1-(3,6-Di-tert-butylphenanthren-9-yl)ethan-1-one (240)

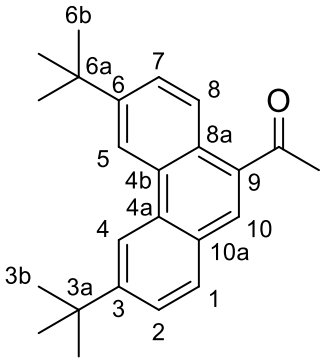

240

To a solution of stilbene **246** (100 mg, 299 µmol) in cyclohexane (380 ml) was added I_2 (38.7 mg, 152 µmol) and degassed with N_2 for 30 min in an ultrasonic bath. Propylene oxide (11.9 ml, 9.90 g, 170 µmol) was added and the reaction mixture was irradiated with light. After 30 min photoirridation, a solution of I_2 (38.7 mg, 152 µmol) in cyclohexane (70 ml) and degassed and added to the reaction mixture over 15 min. After a further 1 h 15 min, a degassed solution of I_2 (15 mg) in cyclohexane (10 ml) was added. After 10 min the iodine colour was no longer observed and the reaction mixture was washed with $Na_2S_2O_3$ (250 ml),

H_2O (250 ml) and brine (250 ml). The organic phase was dried over $MgSO_4$ and the solvent was removed *in vacuo*. The resulting yellow oil was purified using column chromatography (silica, cyclohexane/CH_2Cl_2, 60:40–40:60) to give the desired product as a pale yellow solid. Recrystallisation from EtOH gave yielded colourless crystals.

Yield: 20.3 mg, 612 µmol, 20%.

m.p.: 145–147 C (EtOH).

R_f = 0.12 (cyclohexane/CH_2Cl_2, 60:40)

^{1}H NMR (400 MHz, $CDCl_3$): δ = 8.70 (1H, d, ^3J = 8.7 Hz, 8-H), 8.70 (1H, s, 4-H), 8.67 (1H, s, 5-H), 8.16 (1H, s, 10-H), 7.89 (1H, d, ^3J = 8.4 Hz, 1-H), 7.75–7.70 (2H, t, ^3J = 8.8 Hz, 2,7-H), 2.97 (3H, s, COCH_3), 1.52 (9H, s, 3b-H), 1.51 (9H, s, 6b-H) ppm.

^{13}C NMR (100 MHz, $CDCl_3$): δ = 202.0 (C_q, *C*OCH_3), 152.0 (C_q, C-3), 149.7(C_q, C-6), 133.7(C_q, C-9), 132.1(C_q, C-4a), 130.8 (C_q, C-4b), 130.2 (C_t, C-10), 129.7 (C_t, C-1), 128.2 (C_q, C-10a), 126.7 (C_t, C-8), 126.5 (C_q, C-8a), 126.0 (C_t, C-2 or C-7), 125.4 (C_t, C-2 or C-7), 118.2 (C_t, C-4), 118.2 (C_t, C-5), 35.6 (C_q, C-3a), 35.2 (C_q, C-6a), 31.5 (C_t, *C*H_3), 31.5 (C_t, C-6b), 30.0 (C_t, C-3b) ppm.

FT-IR (ATR): $\tilde{\upsilon}$ = 2956 (m, ν(C-H_{arom})), 2866 (w, ν(C-H)), 1675 (vs, ν(C=O)), 1617 (w), 1516 (w), 1464 (w), 1414 (w), 1360 (w), 1292 (w), 1259 (s), 1238 (m), 1201 (w), 1182 (w), 1162 (w), 1095 (m), 1020 (s), 926 (m), 904 (m), 877 (m), 825 (vs), 800 (vs), 742 (w), 669 (w), 634 (w), 611 (w) cm^{-1}.

UV/Vis (acetonitrile, lg ε): λmax = 195 (4.47), 217 (4.30), 252 (4.52), 312 (3.96) nm.

MS (EI, 70 eV): m/z = 332 (M^+, 53), 317 (100), 301 (3), 274 (4), 259 (3), 215 (4), 202 (6), 151 (5), 123 (5).

EA: calc.: C 86.70, H 8.49 for $C_{24}H_{28}O$, found: C 86.57, H 8.52.

I-3,4-Bis(4-(tert-butyl)phenyl)but-3-en-2-one (cis-246)

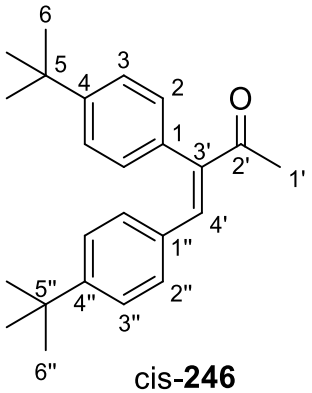

cis-**246**

Yield: 31.3 mg (936 µmol, 31%).

m.p.: 55–57°C.

$\mathbf{R_f}$ = 0.38 (Cyclohexane/CH_2Cl_2, 60:40).

^{1}H NMR (400 MHz, $CDCl_3$): δ = 7.41–7.33 (6H, m, C*H*), 7.29–7.27°(2H, m, C*H*), 6.93 (1H, s, 4'-H), 2.28 (3H, s, 1'-H), 1.33 (9H, s, 6-H or 6''-H), 1.32 (9H, s, 6-H or 6''-H) ppm.

^{13}C NMR (100 MHz, $CDCl_3$): δ = 208.0 (C_q, C-2'), 151.6 (C_q, C-4 or C-4'), 151.5 (C_q, C-4 or C-4''), 142.9 (C_q, C-1), 134.5 (C_q,), 133.0 (C_q,), 128.7 (C_t, C-4'), 128.6 (C_t, *C*H), 126.4 (C_t, *C*H), 125.9 (C_t, *C*H), 125.7 (C_t, *C*H), 34.8 (C_q, C-5 or C-5''), 34.8 (C_q, C-5 or C-5''), 31.8 (C_t, C-1'), 31.4 (C_t, , C-6 or C-6''), 31.4 (Ct, , C-6 or C-6'') ppm.

FT-IR (ATR): $\tilde{\upsilon}$ = 2954 (m, ν(C-H_{arom})), 2904 (w, ν(C-H)), 2867 (w, ν(C-H)), 1698°(s, ν(C=O)), 1509 (w), 1461 (w), 1411 (w), 1363 (m), 1268 (w), 1201 (w), 1161 (m), 1110 (w), 1018 (w), 979 (w), 951 (w), 925 (w), 887 (w), 838 (vs), 734 (w), 676 (w) cm^{-1}.

UV/Vis (acetonitrile, lg ε): λ_{max} = 202 (4.37), 227 (4.02), 298 (4.35) nm.

MS (EI, 70 eV): m/z = 334 (M^+, 75%), 319 (100), 291 (27), 277 (59), 261 (9), 203 (7), 115 (8), 57 (50).

EA: calc. for C 86.18, H 9.04 for $C_{24}H_{30}O$, found: C 86.29, H 9.21.

6.2.4 Synthesis of extended TBTQ 106

Tris-boronic esters of 4b1-methyltribenzotriquinacene (105)

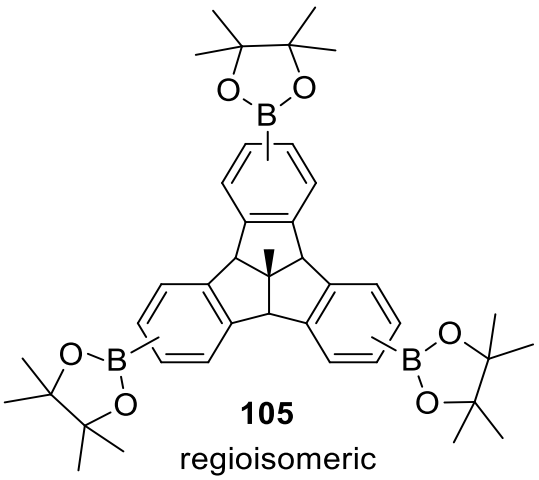

TBTQ **69** (1.00 g, 3.40 mmol), bis(1,5-cyclooctadien)-μ-methoxyiridium(I) ([Ir(OMe)COD]$_2$, 113 mg, 170 μmol, 5 mol-%), bis(pinacolato)diboron (B_2pin_2) (2.84 g, 11.2 mmol, 3.3 eq.), 4,4'-di-*tert*-butyl-2,2'-bipyridine (91.3 mg, 340 μmol, 10 mol-%) and potassium *tert*-butoxide (19.1 mg, 170 μmol) were suspended in anhydrous THF (3 ml) in a Schlenk bomb flask in a glovebox. The resulting reaction mixture was refluxed at 85°C. GC-MS confirmed after 24 h that no starting material was present, but mass measurement (ASAP, +) of the reaction mixture after 4 d showed a mixture of di- and tri-borylated products. B_2pin_2 (3.40 mmol, 860 mg, 1 eq.), [Ir(OMe)COD]$_2$ (3.40 μmol, 22.6 mg, 1 mol-%), 4-*tert*-butyl-2-(4-*tert*-butyl-pyridin-2-yl)pyridine (6.80 μmol, 18.3 mg, 2 mol-%) were added with a few drops of THF. After a further 24 h there were traces of starting material still visible and B_2pin_2, [Ir(OMe)COD]$_2$ and 4-*tert*-butyl-2-(4-*tert*-butylpyridin-2-yl)pyridine were added again. After 24 h, the reaction was allowed to cool and washed with toluene, CH_2Cl_2 and methanol through a pad of silica gel. The solvent was removed *in vacuo* and a colourless solid was precipated out of methanol upon cooling to -29°C. This regioisomeric mixture was characterised and a 20 mg sample was separated using RP-HPLC (Reprosil C-18-PQ-JASCO column, 5 μm, 250 mm × 10 mm; acetonitrile/MeOH 30:70) to isolate the C_3 (3.8 mg) and C_1 (4.9 mg) isomers respectively.

Yield: 1.40 g, 2.08 mmol, 61%.

m.p.: 205–207°C.

FT-IR (ATR): $\tilde{\upsilon}$ = 2976 (w, *ν*(C-H)), 2360 (w, *ν*(C-H)), 1610 (w), 1411 (m), 1354 (s), 1323 (m), 1267 (m), 1213 (w), 1143 (s), 1099 (w), 1074 (w), 966 (w), 904 (w), 856 (m), 812 (w), 733 (w), 692 (w), 669 (m), 632 (w) cm^{-1}.

UV/Vis (acetonitrile, lg ε): λ_{max} = 203 (4.87), 232 (4.59), 275 (3.72), 283 (3.74) nm.

MS (EI, 70 eV): m/z = 672 (M^+, 100), 671 (62), 670 (15), 487 (16), 101 (39), 83 (31).

HRMS (ESI): calc. for $C_{41}H_{51}B_3O_6$+Na^+ m/z 695.38570, found m/z 695.38670.

EA: calc.: C 73.25, H 7.65 for $C_{41}H_{51}B_3O_6$, found: C 73.23, H 7.97.

2,2',2''-(4b1-Methyl-4b,4b1,8b,12b-tetrahydrodibenzo[2,3:4,5]pentaleno[1,6-ab]-indene-2,6,10-triyl)tris(4,4,5,5-tetramethyl-1,3,2-dioxaborolane) (C_3-105)

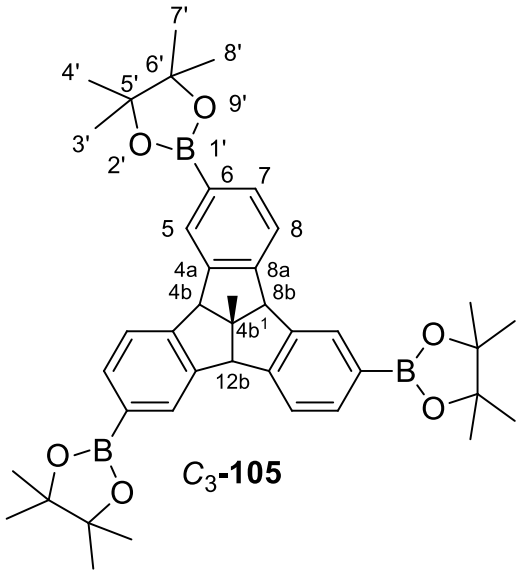

C_3-105

^{1}H NMR (400 MHz, CD_2Cl_2): δ = 7.83 (3H, s, 5-H), 7.61 (3H, d, ^3J = 7.6 Hz, 7-H), 7.53 (3H, d, ^3J = 7.6 Hz, 8-H), 4.48 (1H, s, 3H, 4b,8b,12b-H), 1.65 (3H, s, 4b^1-H), 1.31 (18H; s, 3',4'-H or 7',8'-H), 1.30 (18H, s, 3',4'-H or 7',8'-H) ppm.

^{13}C NMR (100 MHz, CD_2Cl_2): δ = 149.3 (C_q, C-8a), 145.0 (C_q, C-4a), 134.4 (C_t, C-7), 131.1 (C_t, C-5), 128.7 (C_q, C-6), 124.3 (C_t, C-8), 84.1 (C_q, C-5',6'), 63.8 (C_t C-4b,8b,12b), 60.8 (C_q, C-4b^1), 27.7 (C_t, C(4b^1)*C*H$_3$), 25.1 (C_s, C-3',4' or C-7',8'), 24.9 (C_s, C-3',4' or C-7',8') ppm.

4b¹-Methyl-4b,4b1,8b,12b-tetrahydrodibenzo[2,3:4,5]pentaleno[1,6-ab]indene-2,6,11-triyl)tris(4,4,5,5-tetramethyl-1,3,2-dioxaborolane) (C_1-105)

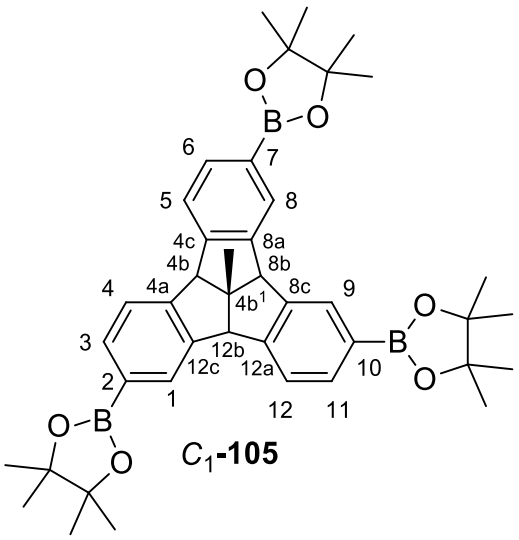

^{1}H NMR (400 MHz, $CDCl_3$): δ = 7.99 (1H, s, 1-H or 9-H), 7,98 (1H, s, 1-H or 9-H), 7.86 (1H, s, 8-H), 7.68–7.62 (3H, m, 3,6,11-H), 7.55 (1H, d, ^3J = 7.6 Hz, 5-H), 7.44 (2H, d, ^3J = 7.6 Hz, 4,12-H), 4.46 (3H, s, 4b,8b,12b-H), 1.64 (3H, s, C(4b^1)CH_3), 1.32 (36 H, s, -O-C$(CH_3)_2$-C$(CH_3)_2$-O-) ppm.

^{13}C NMR (100 MHz, $CDCl_3$): δ = 148.9 (C_q, *C*H), 148.7 (C_q, *C*H), 148.7 (C_q, *C*H), 145.0 (C_q *C*H), 144.9 (C_q, *C*H), 144.8 (C_q,*C*H), 134.3 (C_t, *C*H), 134.3 (C_t, *C*H), 131.4 (C_t, C-1 or C-9), 131.2 (C_t, C-1 or C-9), 131.9 (C_t, C-8), 128.1 (C_q, C-2,7,10), 124.2 (C_t, C-5), 124.0 (C_t, C-4 or C-12), 124.0 (C_t, C-4 or C-12), 83.8 (C_q, *C*$(CH_3)_2$), 83.8 (C_q, *C*$(CH_3)_2$), 83.7 (C_q, *C*$(CH_3)_2$), 63.9 (C_t, C-4b or C-8b or C-12b), 63.6 (C_t, C-4b or C-8b or C-12b), 63.4 (C_t, C-4b or C-8b or C-12b), 60.6 (C_q, C-4b^1), 27.7 (C_t, C(4b1)*C*H_3), 25.0 (C_t, C(*C*$H_3)_2$), 24.9 (C_t, C(*C*$H_3)_2$) ppm.

C_3/C_1 Isomer mixture (252)

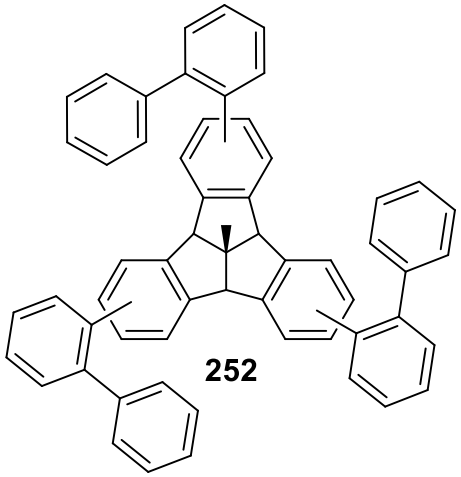

TBTQ **105** (500 mg, 744 µmol), $Pd_2(dba)_3 \cdot CHCl_3$ (38.5 mg, 5 mol %), 2-dicyclohexyl-phosphino-2',6'-dimethoxybiphenyl (Sphos) (30.5 mg, 10 mol %), $CsCO_3$ (1.45 g, 6 eq.) were suspended in anhydrous toluene (10 ml) in a SCHLENK bomb flask. 2-Bromobiphenyl (770 µl, 1.04 g, 4.46 mmol, 6 eq.) and a few drops of H_2O were added and the solution degassed. The Schlenk bomb flask was heated at 80°C for 24 h, after which no starting material could be observed on the mass spectrum. A green solid was filtered off and washed with H_2O. The filtrate was extracted with CH_2Cl_2 (2 × 25 ml) and the organic phases were dried over $MgSO_4$. The solvent was removed in vacuo and the residue was purified using column chromatography (silica, cyclohexane/CH_2Cl_2 80:20). After recrystallisation in cyclo-hexane a colourless powder was isolated. This regioisomeric mixture was characterised and a 20 mg sample was separated using RP-HPLC (Reprosil C-18-PQ-JASCO column, 5 µm, 250 mm × 10 mm; acetonitrile) to isolate the C_3 (5.8 mg) and C_1 (8.6 mg) isomers respectively.

Yield: 468 mg, 623 µmol, 84%.

m.p.: 139–141°C (cyclohexane).

$\mathbf{R_f}$ = 0.1 (cyclohexane/CH_2Cl_2, 80:20).

FT-IR (ATR): $\tilde{\upsilon}$ = 3021 (w, ν(C-H_{arom})), 2923 (w, ν(C-H)), 2850 (w, ν(C-H)), 2058 (w), 1596 (w), 1471 (m, ν(C=C_{arom})), 1448 (w), 1157 (w), 1072 (w), 1009 (w), 897 (w), 819 (w), 802 (w), 742 (s), 698 (w), 615 (w) cm^{-1}.

UV/Vis (acetonitrile, lg ε): λ_{max} = 235sh (4.82), 276sh (4.37) nm.

MS (EI, 70 eV): m/z = 750 (M^+, 100%), 735 (10), 521 (4), 482 (6), 375 (4), 165 (2).

HRMS (ESI): calc. for $C_{59}H_{42}+Na^+$ m/z 773.31787, found m/z 773.31829.

2,6,10-Tri([1,1'-biphenyl]-2-yl)-4b1-methyl-4b,4b1,8b,12b-tetrahydrodibenzo-[2,3:4,5]pentaleno[1,6-ab]indene (C_3-252)

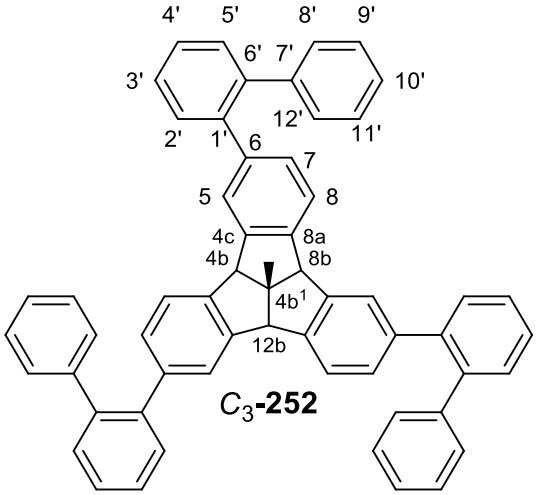

C_3-252

^{1}H NMR (400 MHz, $CDCl_3$): δ = 7.40–7.36 (12H, m, 2',3',4',5'-H), 7.19–7.14 (15H, m, 8',9',10',11',12'-H), 7.12 (3H, s, 5-H), 6.99 (1H, d, ^3J = 7.9 Hz, 7-H), 6.85 (1H, d, ^3J = 7.9 Hz, 8-H), 4.21 (3H, s, 4b,8b,12b-H), 1.56 (3H, s, C(4b^1)CH_3) ppm.

^{13}C NMR (100 MHz, $CDCl_3$): δ = 145.2 (C_q, C-4c), 144.0 (C_q, C-8a), 142.2 (C_q, C-7'), 141.0 (C_q, C-6), 140.9 (C_q, C-6'), 140.8 (C_q, C-1'), 131.2 (C_t, C-2' or C-3' or C-4' or C-5'), 131.2 (C_t, C-2' or C-3' or C-4' or C-5'), 130.2 (C_t, C-8' or C-9' or C-10' or C-11' or C-12'), 129.6 (C_t, C-7), 128.4 (C_t, C-8' or C-9' or C-10' or C-11' or C-12'), 127.9 (C_t, C-2' or C-3' or C-4' or C-5'), 127.7 (C_t, C-8' or C-9' or C-10' or C-11' or C-12'), 127.0 (C_t, C-8' or C-9' or C-10' or C-11' or C-12'), 126.3 (C_t, C-5), 124.4 (C_t, C-8), 63.3 (C_t, C-4b,8b,12b), 61.6 (C_q, C-4b^1), 27.6 (C_t, C(4b^1)CH_3) ppm.

(4b1S)-2,6,11-tri([1,1'-biphenyl]-2-yl)-4b1-methyl-4b,4b1,8b,12b tetrahydro-dibenzo[2,3:4,5]pentaleno[1,6-ab]indene (C_1-252)

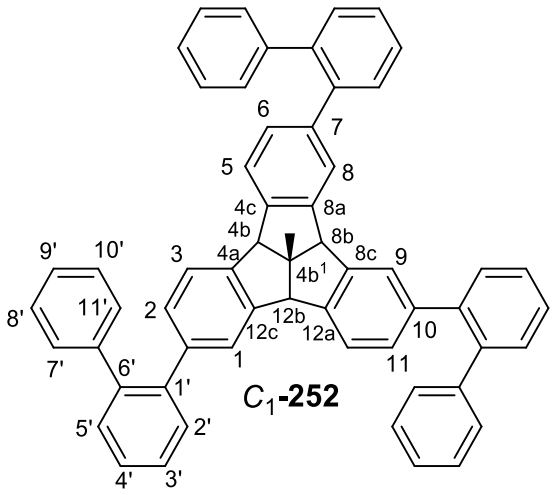

^{1}H NMR (400 MHz, CD_2Cl_2): δ = 7.43–7.32 (12H, m, 2',3',4',5'-H), 7.27 (2H, t, *J* = 8.1 Hz, 2,6-H), 7.20–7.11 (15H, m, C*H*), 7.06 (1H, d, *J* = 7.9 Hz, 3-H), 7.01–6.96 (3H, m, 1,5-H and C*H*), 6.95 (1H, s, 8-H), 6.92–6.90 (2H, m, 9,11-H), 6.80 (1H, d, *J* = 8.4 Hz, 12a-H), 4.34 (1H, s, 4b-H), 4.21 (1H, s, 12b-H), 4.11 (1H, s, 8b-H), 1.56 (3H, s, C(4b^1)*C*H$_3$) ppm.

^{13}C NMR (100 MHz, CD_2Cl_2): δ = 145.6 (C_q), 145.6 (C_q), 145.2 (C_q),144.0 (C_q), 143.9 (C_q), 142.2 (C_q), 142.1 (C_q), 142.0 (C_q), 141.2 (C_q), 141.1 (C_q), 141.1 (C_q), 140.9 (C_q), 140.9 (C_q), 140.9 (C_q), 140.8 (C_q), 140.6 (C_q), 131.4 (C_t, *C*H), 131.4 (C_t, *C*H), 131.3 (C_t, *C*H), 131.2 (C_t, *C*H), 131.1 (C_t, *C*H), 131.1 (C_t, *C*H), 130.1 (C_t, *C*H), 130.1 (C_t, *C*H), 129.8 (C_t, *C*H), 129.7 (C_t, C-9 or C-11), 129.5 (C_t, C-3), 128.4 (C_t, *C*H), 128.2 (C_t, *C*H), 127.9 (C_t, *C*H), 127.9 (C_t, *C*H), 127.7 (C_t, *C*H), 127.7 (C_t, *C*H), 126.9 (C_t, *C*H), 126.9 (C_t, *C*H), 126.8 (C_t, *C*H), 126.6 (C_t, *C*H), 126.3 (C_t, C-8), 126.0 (C_t, C-9 or C-11), 124.29 (C_t, *C*H), 124.2 (C_t, *C*H), 124.1 (C_t, *C*H), 63.6 (C_t, C-8b), 63.2 (C_t, C-4b,12b), 61.7 (C_q, C-4b^1), 27.7 (C_t, C(4b^1)*C*H$_3$) ppm.

10b1-methyl-10b,10b1,20b,30b-tetrahydrodibenzo[l]benzo[9',10']phenanthro-[2',3':5,6]phenanthro[9'',10'':5',6']indeno[1',2',3':3,4]pentalo[1,2-b]phenanthrene (106)

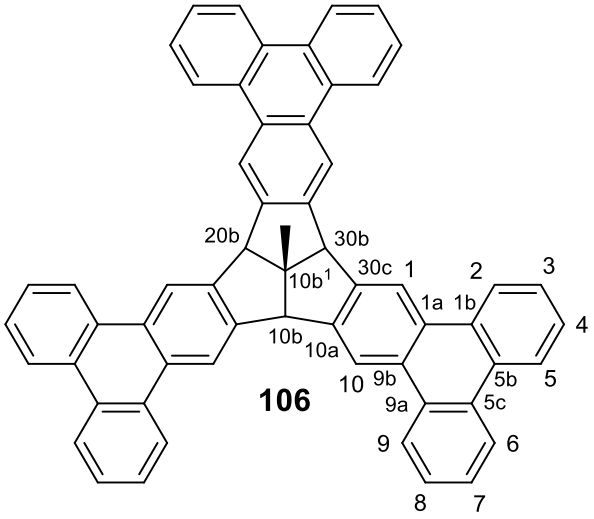

TBTQ **252** (80.0 mg, 107 µmol) was dissolved in anhydrous CH_2Cl_2 (2 ml) and cooled to -78°C. PIFA (207 mg, 482 µmol, 4.5 eq.) was dissolved in anhydrous CH_2Cl_2 (3 ml) and $BF_3{\cdot}Et_2O$ (120 µl, 137 mg, 963 µmol, 9 eq.) was added. This solution was added dropwise to the reaction with a syringe pump for 5 h. On dropwise addition of this solution, the colour of the reaction solution, changes from colourless to purple. TLC reaction control after 6 h confirmed that starting material was still present. A solution of PIFA (25.3 mg) and $BF_3{\cdot}Et_2O$ (14.9 µl) in anhydrous CH_2Cl_2 (0.5 ml) was prepared and added to the reaction. TLC reaction control after 1 h 30 min indicated that starting material was still present. PIFA (25.3 mg) and $BF_3 \cdot Et_2O$ (14.9 µl) in anhydrous CH_2Cl_2 (0.5 ml) was prepared and added to the reaction. After 15 min, TLC reaction control confirmed that no starting material was present. MeOH (26 ml) and Na_2SO_3 solution (10 ml) were added and the reaction allowed to warm to room temperature. The aqueous phase was extracted with CH_2Cl_2 (3 × 6 ml) and the combined organic phases were washed with H_2O (15 ml) and dried over $MgSO_4$. The solvent was removed *in vacuo* and the the green resisude was purified by filtration over silica (cyclo-hexane/CH_2Cl_2 1:1), followed by column chromatography (MPLC, column: Interchim PF-30SiHP-F0040, cyclohexane/ethyl acetate 90:10) and (MPLC, silica, cyclohexane/ethyl acetate 90:10). The pale yellow solid was further purified with NP-HPLC (cyclohexane/ CH_2Cl_2 1:1) to yield the product as an amorphous colourless solid.

Yield: 4.8 mg, 6.44 µmol, 6%.

m.p.: 344–345°C (decomp.).

R_f = 0.25 (Cyclohexane/Ethyl acetate, 90:10).

^{1}H NMR (600 MHz, CD_2Cl_2): δ = 9.00 (6H, s, 1,10-H), 8.85 (6H, d, *J* = 7.7 Hz, 2,9-H), 8.62 (6H, d, *J* = 8.0 Hz, 5,6-H), 7.77–7.74 (6H, m, 3,8-H), 7.67–7.64 (6H, m, 4,7-H), 5.10 (3H, s, 10b,20b,30b-H), 1.99 (3H, s, C(10b^1)CH_3) ppm.

^{13}C NMR (100 MHz, CD_2Cl_2): δ = 145.9 (C_q, C-10a,30c), 130.3 (C_q, C-1a,9b), 130.2 (C_q, C-1b,9a), 129.9 (C_q, C-5b,5c), 127.7 (C_t, C-3,8), 127.5 (C_t, C-4,7), 123.7 (C_t, C-5,6), 123.6 (C_t, C-2,9), 119.3 (C_t, C-1,10), 64.1 (C_t, C-10b,20b,30b), 63.0 (C_q, C-10b^1), 28.1 (C_t, C(10b^1)*C*H$_3$) ppm.

FT-IR (ATR): ῡ = 3080 (w, ν(C-H_{arom})), 2920 (w, ν(C-H)), 2360 (w), 2079 (w), 1490 (w), 1437 (w), 1408 (w), 1294 (w), 1227 (w), 1163 (w), 1049 (w), 941 (w), 897 (w), 860 (w), 810 (w), 748 (vs), 715 (w), 617 (w) cm^{-1}.

UV/Vis (acetonitrile, lg ε): λ_{max} = 252sh (4.16), 260 (4.25), 268 (4.18), 291sh (3.83), 312 (3.54) nm.

MS (EI, 70 eV): m/z = 744 (M^+, 100%), 729 (M^+-CH_3, 22), 516 (10), 478 (17), 267 (4.92), 276 (4.98), 314 (4.47), 372 (18), 364 (9), 361 (6), 349 (4).

HRMS (ASAP, +): calc. for $[C_{59}H_{36} + H]^+$ m/z 745.2890, found m/z 745.2865.

6.3 X-ray crystal structures

Crystallographic data deposited with the Cambridge Data Centre (as denoted by a CCDC number) can be accessed free of charge at www.ccdc.cam.ac.uk/data_request/cif.

6.3.1 Structure detemination of TBTQ 102

The measurements and structure determination of TBTQ **102** was carried out by Dr. Alexandra FRIEDRICH (Institute of Inorganic Chemistry, Universität Würzburg).

A crystal suitable for single-crystal X-ray diffraction was selected, coated in perfluoropolyether oil, and mounted on a MiTeGen sample holder. Diffraction data of TBTQ **102** were collected on a RIGAKU OXFORD DIFFRACTION XTALAB SYNERGY diffractometer with a semiconductor HPA-detector (HyPix-6000) and multi-layer mirror monochromated $Cu_{K\alpha}$ radiation. The crystal was cooled using an Oxford Cryostreams 800 low-temperature device. Data were collected at 100 K. The images were processed and corrected for Lorentz-polarization effects and absorption (empirical scaling) as implemented in the CrysAlis^{Pro} software. The structure was solved using the intrinsic phasing method

(SHELXT, G. SHELDRICK, *Acta Cryst.*, **2015**, *A71*, 3–8) and FOURIER expansion technique. All non-hydrogen atoms were refined in anisotropic approximation, with hydrogen atoms 'riding' on idealised positions by full-matrix least squares against F^2 of all data, using SHELXL software (G. SHELDRICK, *Acta Cryst.*, **2008**, *A64*, 112–122).

6.3.2 Structure determination of TBTQ 106

The analysis was carried out by Dr. Alexandra FRIEDRICH, Dr. Krzysztof RADACKI and Johannes KREBS (Institute of Inorganic Chemistry, Universität Würzburg) in cooperation with Carsten Paulmann (DESY). The crystal data of **RK106** were collected at the PETRA-III synchrotron at the chemical crystallography beamline P24 on a HUBER four-circle kappa diffractometer with a MAR CCD area detector and silicon double-crystal monochromated synchrotron X-ray radiation of 20 keV ($\lambda = 0.6199$ Å). Data reduction, including empirical absorption correction, was performed with the CrysAlis^{Pro} software (version 1.171.40.9a, Rigaku Oxford Diffraction, 2018). The structure was solved using intrinsic phasing method (SHELXT, G. SHELDRICK, *Acta Cryst.*, **2015**, *A71*, 3–8), refined with the SHELXL program (G. SHELDRICK, *Acta Cryst.*, **2008**, *A64*, 112–122) and expanded using FOURIER techniques. All non-hydrogen atoms were refined anisotropically. Hydrogen atoms were included in structure factors calculations. All hydrogen atoms were assigned to idealised geometric positions.

The displacement parameters of some atoms of some of the disordered dichloromethane solvent molecules (residues 2, 3, 4 and 10) were restrained to the same value with similarity restraint SIMU.

The Uii displacement parameters of some atoms of some of the disordered dichloromethane solvent molecules (both chlorine atoms of residue 4, the carbon atoms of residues 5 and 6, and all atoms of residue 9) were restrained with ISOR keyword to approximate isotropic behaviour.

The 1-2 and 1-3 distances in the disordered parts of the dichloromethane molecule in residue 10 were restrained to the same values with SAME.

The positions and anisotropic displacement parameters of atoms Cl1A and Cl1B of the disordered dichloromethane molecule of residue 10 were constrained to the same values with EXYZ and EADP, respectively.

6.3.3 Crystal structure data and parameters

Data	**TBTQ 102**
Empirical formula	$C_{30}H_{20}$
Formula weight ($g \cdot mol^{-1}$)	380.46
Temperature (K)	100.0(1)
Radiation, λ (Å)	$Cu_{K\alpha}$ 1.54184
Crystal colour, habit	Colorless needle
Crystal size (mm^3)	0.030×0.039×0.676
Crystal system	Orthorhombic
Space group	$P2_1/n$
Unit cell dimensions	
a (Å)	19.7313(5)
b (Å)	4.52972(11)
c (Å)	21.3125(5)
α (°)	90
β (°)	100.976(2)
γ (°)	90
Volume ($Å^3$)	1870.01(8)
Z	4
Calculated density ($Mg \cdot m^{-3}$)	1.351
Absorption coefficient (mm^{-1})	0.580
F(000)	800
Theta range for collection	2.798 to 67.048°
Reflections collected	9932
Independent reflections	3291
Minimum/maximum transmission	0.695/0.983
Refinement method	Full-matrix least-squares on F^2
Data / parameters / restraints	3291 / 271 / 0
Goodness-of-fit on F^2	1.041
Final R indices [I>2σ(I)]	R_1 = 0.0417, wR^2 = 0.0505
R indices (all data)	R_1 = 0.1000, wR^2 = 0.1045
Maximum/minimum residual electron density ($e \cdot Å^{-3}$)	0.204 / –0.200

Data	**TBTQ 106**
Empirical formula	$C_{59}H_{36}$, 1.9(CH_2Cl_2)
Formula weight ($g \cdot mol^{-1}$)	905.68
Temperature (K)	100(2)
Radiation, λ (Å)	Synchrotron, 0.6199
Crystal system	Triclinic
Space group	$P\ \bar{1}$
Unit cell dimensions	
a (Å)	9.47730(10)
b (Å)	17.9592(3)
c (Å)	26.9096(5)
α (°)	84.8540(10)
β (°)	80.9970(10)
γ (°)	87.1620(10)
Volume ($Å^3$)	4502.55(12)
Z	4
Calculated density ($Mg \cdot m^{-3}$)	1.336
Absorption coefficient (mm^{-1})	0.201
F(000)	1878
Theta range for collection	1.976 to 23.312°
Reflections collected	67707
Independent reflections	17395
Minimum/maximum transmission	0.9927/1.0000
Refinement method	Full-matrix least-squares on F^2
Data / parameters / restraints	17395 / 1334 / 90
Goodness-of-fit on F^2	1.021
Final R indices [I>2σ(I)]	R_1 = 0.0632, wR^2 = 0.1754
R indices (all data)	R_1 = 0.0742, wR^2 = 0.1876
Maximum/minimum residual electron density ($e \cdot Å^{-3}$)	0.600 / –0.851

7 List of abbreviations

Å	Angström
Abb.	*Abbildung*
APCI	atmospheric pressure chemical ionisation
APEX	annulative π-extension
aq.	aqueous solution
arom.	aromatic
ATR	attenuated total reflection
BDPTQ	benzodiphenanthreno-triquinacene
bpin	pinacol boronate ester
BPTQ	benzophenanthreno-triquinacene
BTPTQ	benzotriphenanthreno-triquinacene
n-BuLi	*n*-butyllithium
t-BuOK	potassium *tert*-butoxide
calc.	calculated
CCDC	Cambridge crystallographic data centre
CDFC	cyclodehdrogenofluorination
CDHC	cyclodehydrochlorination
conc.	concentrated
COSY	correlation spectroscopy
DBU	1,8-Diazabicyclo(5.4.0)undec-7-ene
DDQ	2,3-dichloro-5,6-dicyano-1,4-benzoquinone
DEPT	distortionless enhancement by polarisation transfer
DFT	density functional theory
DIBAL-H	diisobutylaluminium hydride
DIPA	diisopropylamine
DL	double layer
DMF	*N*,*N*-dimethylformamide
DMSO	dimethylsulfoxide
ε	extinction coefficient
EA	elemental analysis
EI	eletron ionisation
ESI	electrospray ionisation
eq.	equivalents
Et_2O	diethylether
EtOH	ethanol
fcc	face centered cubic
FVP	Flash vacuum pyrolysis
FT-IR	fourier transform infrared spectroscopy
IR	infrared
hcp	hexagonal close-packed
HMBC	heteronuclear multiple bond correlation
HPLC	high pressure liquid chromatography
HRMS	high resolution mass spectrometry
HSQC	heteronuclear single quantum coherence
LDA	lithium diisopropylamide
LiHMDS	lithium bis(trimethylsilyl)-amide
M	molar concentration

MALDI-TOF	matrix assisted laser desorption ionisation-time of flight
Me	methyl
MeLi	methyllithium
MeOH	methanol
m.p.	melting point
MPLC	medium pressure liquid chromatography
MS	mass spectrometry
NBS	*N*-bromosuccinimide
NIS	*N*-iodosuccinimide
NOESY	nuclear OVERHAUSER enhancement and exchange spectroscopy
NMR	nuclear magnetic resonance
Otf	trifluoromethanesulfonate
PAH	polycyclic aromatic hydrocarbon
PCC	pyridinium chlorochromate
PCDHF	photocyclodehydrofluorination
PIFA	(Bis(trifluoroacetoxy)-iodo)benzene
ppm	parts per million
quant.	quantitative yield
rac-	racemic mixture
R_f	retention factor
RP-HPLC	reverse phase high pressure liquid chromatography
rt	room temperature
sh	shoulder
SPhos	2-Dicyclohexylphosphino-2',6'-dimethoxybipheny
STM	scanning tunneling microscopy
TFA	trifluoroacetic acid
TBTQ	tribenzotriquinacene
TfOH	trifluoromethanesulfonic acid
THF	tetrahydrofuran
TLC	thin layer chromatography
UV/Vis	ultraviolet/visible
% v/v	volume percent
λ_{max}	wavelength of maximum absorption

Abbreviations in NMR spectroscopy:

s	singulet
d	doublet
t	triplet
q	quartet
m	multiplet
br s	broad singulet
br d	broad doublet
C_q	quaternary carbon
C_t	tertiary carbon
C_p	primary carbon
J	coupling constant
δ	chemical shift

Abbreviations in IR spectroscopy:

vs	very strong
s	strong
m	medium
w	weak

8 References

1 E. H. L Falcao, F. Wudl, *J. Chem. Technol. Biotechnol*. **2007**, *82*, 524–531.

2 S. Nasir, M. Z. Hussein, Z. Zainal, N. A. Yusof, *Materials* **2018**, *11*, 295.

3 A. Krüger, *Neue Kohlenstoffmaterialien*, Vieweg+Teubner, Wiesbaden, **2007**.

4 K. S. Novoselov, A. K. Geim, S. V. Morozov, D. Jiang, Y. Zhang, S. V. Dubonos, I. V. Grigorieva, A. A. Firsov, *Science* **2004**, *306*, 666–669.

5 R. E. Peierls, *Ann. I. H. Poincare* **1935**, *5*, 177–222.

6 L. D. Landau, *Phys. Z. Sowjetunion* **1937**, *11*, 26–35.

7 N. D. Mermin, *Phys. Rev.* **1968**, *176*, 250–254.

8 P. R. Wallace, *Phys. Rev.* **1947**, *71*, 622–634.

9 J. W. McClure, *Phys. Rev.* **1956**, *104*, 666–671.

10 J. C. Slonczewski, P.R. Weiss, *Phys. Rev.* **1958**, *109*, 272–279.

11 G. W. Semenoff, *Phys. Rev. Lett.* **1984**, *53*, 2449–2452.

12 B. C. Brodie, *Philos. Trans. R. Soc. London* **1859**, *149*, 249–259.

13 W. S. Hummers, R. E. Offeman, *J. Am. Chem. Soc.* **1958**, *80*, 1339–1339.

14 H. P. Boehm, A. Clauss, G. O. Fischer, U. Hofmann, *Z. anorg. allgem. Chem.* **1962**, *316*, 119–127.

15 M.S. Dresselhaus, G. Dresselhaus, *Adv. Phys*. **2002**, *51*, 1–186.

16 L. M. Viculis, J. J. Mack, R. B. Kaner, *Science* **2003**, *299*, 1361.

17 X. K. Lu., M. F. Yu, H. Huang, R. S. Ruoff, *Nanotechnology* **1999**, *10*, 269–272.

18 Y. B. Zhang, J. P. Small, W. V. Pontius, P. Kim, *Appl. Phys. Lett*. **2005**, *86*, 073104-1.

19 C. Lee, X. Wei, J. W. Kysar, J. Hone, *Science* **2008**, *321*, 385–388.

20 A. K. Geim, *Science* **2009**, *324*, 1530-1534.

21 F. Banhart, J. Kotakoski, A. V. Krasheninnikov, *ACS Nano* **2011**, *5*, 26–41.

22 F. Bonaccorso, L. Colombo, G. Yu, M. Stoller, V. Tozzini, A. C. Ferrari, R. S. Ruoff, V. Pellegrini, *Science* **2015**, *347*, 1246501.

23 K. S. Novoselov, V. I. Fal′ko, L. Colombo, P. R. Gellert, M. G. Schwab, K. Kim, *Nature* **2012**, *490*, 192–200.

24 S. Gilje, S. Han, M. Wang, K. L. Wang and R. B. Kaner, *Nano Lett.* **2007**, *7*, 3394.

25 D. Li, M. B. Muller, S. Gilje, R. B. Kaner, G. G. Wallace, *Nat. Nanotechnol*. **2008**, *3*, 101–105.

26 S. Stankovich, D. A. Dikin, G. H. B. Dommett, K. M. Kohlhaas, E. J. Zimney, E. A. Stach, R. D. Piner, S. T. Nguyen, R.S Ruoff, *Nature* **2006**, *442*, 282–286.

27 S. Stankovich, R. D. Piner, X. Q. Chen, N. Q. Wu, S. T. Nguyen, R. S. Ruoff, *J. Mater. Chem*. **2006**, *16*, 155–158.

28 S. Stankovich, D. A Dikin, R. D Piner, K. A. Kohlhaas, A. Kleinhammes, Y. Jia, Y. Wu, S. T. Nguyen, R. S. Ruoff, *Carbon* **2007**, *45*, 1558–1565.

29 S. Guoab and S. Dong, *Chem. Soc. Rev.* **2011**, *40*, 2644–2672.

30 X. Y. Yang, X. Dou, A. Rouhanipour, L. J. Zhi, H. J. Rader, K. Müllen, *J. Am. Chem. Soc*. **2008**, *130*, 4216–4217.

31 J. S. Wu, W. Pisula, K. Mullen, *Chem. Rev*. **2007**, *107*, 718–747.

32 C. Soldano, A. Mahmood, E. Dujardin, *Carbon* **2010**, *48*, 2127–2150.

33 C. Botas, P. Álvarez, P. Blanco, M. Granda, C. Blanco, R. Santamaría, L. J. Romasanta, R. Verdejo, M. A. López-Manchado, R. Menéndez, *Carbon* **2013**, *65*, 156–164.

34 D. Xiang, X. Wang, C. Jia, T. Lee, X. Guo, *Chem. Rev*. **2016**, *116*, 4318–4440.

35 M. Ratner, *Nat. Nanotechnol*. **2013**, *8*, 378–381.

36 J. Tersoff, D. R. Hamann, *Phys. Rev. B* **1985**, *31*, 805–813.

37 K. Müllen, J. P. Rabe, *Acc. Chem. Res.* **2008**, *41*, 511–520.

38 J. K. Gimzewski, C. Joachim, *Science* **1999**, *283*, 1683–1688.

39 D. M. Eigler, E. K. Schweizer, *Nature* **1990**, *344*, 524–526.

40 S. W. Hla, L. Bartels, G. Meyer, K.–H. Rieder, *Phys. Rev. Lett.* **2000**, *85*, 2777.

41 D. Umadevi, S. Panigrahi, G. N. Sastry, *Acc. Chem. Res.* **2014**, *47*, 2574–2581.

42 L. Kronik, N. Koch, *MRS Bull*. **2010**, *35*, 417–421.

43 A. Tkatchenko, L. Romaner, O. T. Hofmann, E. Zojer, C. Ambrosch-Draxl, M. Scheffler, *MRS Bull*. **2010**, 35, 435–442.

44 Q. S. Stöckl, Y.-C. Hsieh, A. Mairena, Y.–T. Wu, K.-H. Ernst, *J. Am. Chem. Soc*. **2016**, *138*, 6111–6114.

45 K. Nakada, M. Fujita, G. Dresselhaus, M. S. Dresselhaus, *Phys. Rev. B*. **1996**, *54*, 17954–17961.

46 M. Ezawa, *Phys. Rev. B.* **2006**, *73*, 045432.

47 V. Barone, O. Hod, G. E. Scuseria, *Nano Lett.* **2006**, *6*, 2748–2754.

48 C. Moreno, M. V.-Varela, B. Kretz, A. Garcia-Lekue, M. V. Costache, M. Paradinas, M. Panighel, G. Ceballos, S. O. Valenzuela, D. Peña, A. Mugarza, *Science* **2018**, *360*, 199–203.

49 L. Liu, M. Qing, Y. Wang, S. Chen, *J. Mater. Sci. Technol.* **2015**, *31*, 599–606.

50 H. Lu, H. Wang, W. E, D. Dai, H. Fan, Z. Ma, X. Yang, *J. Phys. Chem. C* **2019**, *123*, 14404–14407.

51 C. Moreno, M. Pamighel, M. Vilas-Varela, G. Suathier, M. Tenorio, G. Ceballos, D. Peña, A. Mugarza, *Chem. Mater.* **2019**, *31*, 331–341.

52 S. Xing, Z. Zhang, W. Zhao, R. Zhang, T. Lin, D. Zhao, H. Ju, H. Xu, J. Fan, J. Zhu, Y.-Q. Ma, Z. Shi, *Nat. Commun.* **2019**, *10*, 70.

53 K. Xu, J. I. Urgel, K. Eimre, M. D. Giovannantonia, A. Keerthi, H. Komber, S. Wang, A. Narita, R. Berger, P. Ruffieux, C. A. Pignedoli, J. Liu, K. Müllen, R. Fasel, *J. Am. Chem. Soc.* **2019**, *141*, 7726–7730.

54 S. Chair, D. G. de Oteyza, *Chem. Rev.* **2019**, *119*, 4717–4776.

55 J. Cai, P. Ruffieux, R. Jaafar, M. Bieri, T. Braun, S. Blankenburg, M. Muoth, A. P. Seitsonen, M. Saleh, X. Feng, K. Müllen, R. Fasel, *Nature* **2010**, *466*, 470–473.

56 Y.-C. Chen, D. G. de Oteyza, Z. Pedramrazi, C. Chen, F. R. Fischer, M. F. Crommie, *ACS Nano* **2013**, *7*, 76123–6128.

57 Q. Zhong, Y. Hu, K. Niu, H. Zhang, B. Yang, D. Ebeling, J. Tschakert, T. Cheng, A. Schirmeisen, A. Narita, K. Müllen, L. Chi, *J. Am. Chem. Soc*. **2019**, *141*, 7399–7406.

58 A. J. Stone, D. J. Wales, *Chem. Phys. Lett*. **1986**, *128*, 501–503.

59 J. Ma, D. Alfè, A. Michaelides, E.Wang, *Phys. Rev. B.* **2009**, *80*, 033407.

60 M. T. Lusk, L. D. Carr, *Phys. Rev. Lett.* **2008**, *100*, 175503.

61 J. Hieulle, E. Carbonell-Sanromà, M. Vilas-Varela, A. Garcia-Leuke, E. Guitán, D. Peña, *Nano Lett*. **2018**, *18*, 418–423.

62 J. Liu, S. Mishra, C. A. Pignedoli, D. Passerone, J. I. Urgel, A. Fabrizio, T. G. Lohr, J. Ma, H. Komber, M. Baumgarten, C. Corminboeuf, R. Berger, P. Raffieux, K. Müllen, R. Fasel, X. Feng, *J. Am. Chem. Soc.* **2019**, *141*, 12011–12020.

63 N. Gorjizadeh, A. A Farajian, Y. Kawazoe, *Nanotechnol*. **2009**, *20*, 015201.

64 F. Karlický, K. K. R. Datta, M. Otyepka, R. Zbořil, *ACS Nano* **2013**, 7, 6434–6464.

65 R. R. Nair, W. Ren, R. Jalil, I. Riaz, V. G. Kravets, L. Britnell, P. Blake, F. Schedin, A. S. Mayorov, S. Yuan, M. I. Katsnelson, H.-M. Cheng, W. Strupinski, L. G. Bulusheva, A. V. Okotrub, I. V. Grigorieva, A. N. Grigorenko, K. S. Novoselov, A. K. Geim, *Small* **2010**, *6*, 2877–2884.

66 F.-G. Zhao, G. Zhao, X.-H. Liu, C.-W. Ge, J.-T. Wang, B.-L. Li, Q.-G. Wang, W.-S. Li, Q.-Y. Chen, *J. Mater. Chem. A* **2014**, *2*, 8782–8789.

67 J. T. Robinson, J. S. Burgess, C. E. Junkermeier, S. C. Badescu, T. L. Reinecke, F. Keith Perkins, M. K. Zalalutdniov, J. W. Baldwin, J. C. Culbertson, P. E. Sheehan, E. S. Snow, *Nano Lett.* **2010**, *10*, 3001–3005.

68 K.-J. Jeon, Z. Lee, E. Pollak, L. Moreschini, A. Bostwick, C.-M. Park, R. Mendelsberg, V. Radmilovic, R. Kostecki, T. J. Richardson, E. Rotenberg, *ACS Nano*. **2011**, *5*, 1042–1046.

69 M. Leclerc, J.-F.Morin, *Synthetic Methods for Conjugated Polymers and Carbon Materials*, Wiley-VCH, Weinheim, **2017**.

70 J. Löwe, *Z. Chemie* **1868**, *4*, 603–604.

71 R. Scholl, J. Mansfeld, *Ber. Dtsch. Chem. Ges*. **1910**, *43*, 1734–1746.

72 M. Grzybowski, K. Skonieczny, H. Butenschön, D. T. Gryko, *Angew. Chem*. **2013**, *125*, 10084–10115; *Angew. Chem. Int. Ed*. **2013**, *52*, 9900–9930.

73 C. D. Nenitzescu, A. Balban, *Chem. Ber*. **1958**, *91*, 2109–2116.

74 J. J. Rooney, R. C. Pink, *Proc. Chem. Soc*. **1961**, 142–143.

75 Chaolumen, M. Murata, A. Wakamiya, Y. Murata, *Angew. Chem.* **2017**, *129*, 5164–5168; *Angew. Chem. Int. Ed*. **2017**, *56*, 5082–5086.

76 B. Alameddine, R Sobhana Anju, S. Shetty, N. Baig, F. Al-Sagheer, S. Al-Mousawi , T. A. Jenny, *New J. Chem*. **2017**, *41*, 6025–6032.

77 J. Zhao, Z. Xu, K. Oniwa, N. Asao, Y. Yamamoto, T. Jin, *Angew. Chem*. **2016**, *128*, 267–271; *Angew. Chem. Int. Ed*. **2016**, *55*, 259–263.

78 C. D. Simpson, J. D. Brand., A. J. Berresheim, L. Przybilla, H. J. Räder, K. Müllen, *Chem. Eur. J.* **2002**, *8*, 1424–1429.

79 Y. Avlasevich , C. Kohl, K. Müllen, *J. Mater. Chem*. **2006**, *16*, 1053–1057.

80 Y. Netanel Oded, S. Pogodin, I. Agranat, *J. Org. Chem*. **2016**, *81,* 11389–11393.

81 T. Fujikawa, N. Mitoma, A. Wakamiya, A.Saeki, Y. Segawa , K. Itami, *Org. Biomol. Chem*. **2017**, *15*, 4697–4703.

82 M. Schubert, P. Franzmann, A. Wünsche von Leupoldt, K. Koszinowski, K. Heinze, S. R. Waldvogel, *Angew. Chem*. **2016**, *128*, 1168–1172; *Angew. Chem. Int. Ed.* **2016**, *55*, 1156–1159.

83 B. T . King, J. Kroulík, C. R. Robertson, P. Rempala, C. L. Hilton, J. D. Korinek, L. M. Gortari, *J. Org. Chem.* **2007**, *72*, 2279–2288.

84 Chaolumen, M. Murata, A. Wakamiya, Y. Murata, *Org. Lett.* **2017**, *19*, 826–829.

85 T. Fujikawa, Y. Segawa, K. Itami, *J. Am. Chem. Soc*. **2015**, *137*, 7763–7768.

86 D. Reinhard, F. Rominger, M. Mastalerz, *J. Org. Chem*. **2015**, *80*, 9342–9348.

87 M. S. Little, S. G. Yeates, A. A. Alwattar, K. W. J. Heard, J. Raftery, A. C. Edwards, A. V. S. Parry, P. Quayle, *Eur. J. Org. Chem*. **2017**, 1694–1703.

88 S. Nobusue, K. Fujita, Y. Tobe, *Org. Lett.* **2017**, *19*, 3227–3230.

89 S. Yamaguchi, T. M. Swager, *J. Am. Chem. Soc.* **2001**, *123*, 12087–12088.

90 A. McKillop, A. G. Turrell, D. W. Young, E. C. Taylor, *J. Am. Chem. Soc.* **1980**, *102*, 6504–6512.

91 J.B. Aylward, *J. Chem. Soc. B* **1967**, 1268−1270.

92 M. Schubert, S. R. Waldvogel, *Eur. J. Org. Chem*. **2016**, *11*, 1921–1936.

93 L. Zhai, R. Shukla, S. H. Wadumethrige, R. Rathore, *J. Org. Chem.* **2010**, *75*, 4748–4760.

94 X. Dou, X. Yang, G. J. Bodwell, M. Wagner, V. Enkelmann, K. Müllen, *Org. Lett.* **2007**, *9*, 2485–2488.

95 A. Stabel, P. Herwig, K. Müllen, J. P. Rabe, *Angew. Chem*. **1995**, *107*, 1768–1770; *Angew. Chem. Int. Ed*. **1995**, *34*, 1609–1611.

96 C. D. Simpson, G. Mattersteig, K. Martin, L. Ghergl, R. E. Bauer, H. J. Räder, K. Müllen, *J. Am. Chem. Soc*. **2004**, *126*, 3139–3147.

97 C. Köbel, K. Eckhardt, V. Enkelmann, G. Wegner, K. Müllen, *J. Mater. Chem*. **2000**, *10*, 879–886.

98 J. Wu, M. D. Watson, L. Zhang, Z. Wang, K. Müllen, *J. Am. Chem. Soc*. **2004**, *126*, 177–186.

99 Z. Wang, F. Dötz, V. Enkelmann, K. Müllen, *Angew. Chem*. **2005**, *117*, 1273–1276; *Angew. Chem. Int. Ed*. **2005**, *44*, 1247–1250.

100 J. Wu, Ž. Tomović, V. Enkelmann, K. Müllen, *J. Org. Chem*. **2004**, *69*, 5179–5186.

101 Z. Wang, Ž. Tomović, M. Kastler, R. Pretsch, F. Negri, V. Enkelmann, K. Müllen, *J. Am. Chem. Soc*. **2004**, *126*, 7794–7795.

102 S. Ito, M. Wehmeier, J. Diedrich Brand, C. Kübel, R. Epsch, J. P. Rabe, K. Müllen, *Chem. Eur. J*. **2000**, *6*, 4327–4342.

103 P. T. Herwig, V. Enkelmann, O. Schmelz, K. Müllen, *Chem. Eur. J*. **2000**, *6*, 1834–1839.

104 F. Dötz, J. Diedrich Brand, S. Ito, L. Ghergl, K. Müllen, *J. Am. Chem. Soc*. **2000**, 122, 7707–7717.

105 A. J. Berresheim, M. Müller, K. Müllen, *Chem. Rev*. **1999**, *99*, 1747–1786.

106 S. Grätz, D. Beyer, V. Tkachova, S. Hellmann, R. Berger, X. Feng, L. Borchardt, *Chem. Comm*. **2018**, *54*, 5307–5310.

107 W. Yang, J. H. S. K. Monteiro, A. de Bettencourt-Dias, V. J. Catalano, W. A. Chalifoux, *Angew. Chem*. **2016**, *128*, 10583–10586; *Angew. Chem. Int. Ed*. **2016**, *55*, 10427–10430.

108 W. Yang, A. Lucotti, M. Tommasini, W. A. Chalifoux. *J. Am. Chem. Soc.* **2016**, *138*, 9137–9144.

109 X. Jia, J. Campos-Delgado, M. Terrones, V. Meunier, M. S. Dresselhaus, *Nanoscale* **2011**, *3*, 86–95.

110 K. Ozaki, K. Kawasumi, M. Shibata, H. Ito, K. Itami, *Nat. Commun.* **2015**, *6*, 6251.

111 K. Kato, Y. Segawa, K. Itami, *Can. J. Chem*. **2017**, *95*, 329–333.

112 Y. Yano, H. Ito, Y. Segawa, K. Itami, Synlett, **2016**, *27*, 2081–2084.

113 K. Ozaki, W. Matsuoka, H. Ito, K. Itami, *Org. Lett.* **2017**, *19*, 1930–1933.

114 K. Ozaki, K. Murai, W. Matsuoka, K. Kawasumi, H. Ito, K. Itami, *Angew. Chem*. **2017**, *129*, 1381–1384; *Angew. Chem. Int. Ed*. **2017**, *56*, 1361–1364.

115 M. Treier, C. A. Pignedoli, T. Laino, R. Rieger, K. Müllen, D. Passerone, R. Fasel, *Nat. Chem.* **2011**, *3*, 61–67.

116 A. M. Echavarren, B. Gómez-Lor, J. J. González, Ó.de Frutos, *Synlett* **2003**, *5*, 0585–0597.

117 E. A. Jackson, B. D. Steinberg, M. Bancu, A. Wakamiya, L. T. Scott, *J. Am. Chem. Soc.* **2007**, *129*, 484–485.

118 L. Wang, P. B. Shevlin, *Org. Lett.* **2000**, *2*, 3703–3705.

119 N.-H. Chang, X.-C. Chen, H. Nonobe, Y. Okuda, H. Mori, K. Nakajima, Y. Nishihara, *Org. Lett.* **2013**, *15*, 3558–3561.

120 N.-H. Chang, H. Mori, X.-C. Chen, Y. Okuda, T. Okamoto, Y. Nishihara, *Chem. Lett*. **2013**, *42*, 1257–1259.

121 K. Kamikawa, I. Takemoto, S. Takemoto, H. Matsuzaka, *J. Org. Chem*. **2007**, *72*, 7406–7408.

122 Y. Koga, T. Kaneda, Y. Saito, K. Murakami, K. Itami, *Science* **2018**, *359*, 435–439.

123 Y. Hatanaka, T. Hiyama, *J. Org. Chem*. **1988**, *53*, 918–920.

124 K. Tamao, K. Sumitani, M. Kumada, *J. Am. Chem. Soc*. **1972**, *94*, 4374–4376.

125 E. Negishi, A. O. King, N. Okikado, *J. Org. Chem.* **1977**, *42*, 1821–1823.

126 J.K. Stille, *Angew. Chem.* **1986**, *98*, 504–519; *Angew. Chem. Int. Ed*. **1986**, *25*, 508–524.

127 T. Y. Miyuara, A. Suzuki, *Synth. Comm*. **1981**, *11*, 513–519.

128 H. Ito, K. Ozaki, K. Itami, *Angew. Chem*. **2017**, *129*, 11296–11317; *Angew. Chem. Int. Ed*. **2017**, *56*, 11144–11164.

129 A. Suzuki, *Angew. Chem.* **2011**, *123*, 6854–6869; *Angew. Chem. Int. Ed.* **2011**, *50*, 6722–6737.

130 H. Shinokoubo, *Proc. Jpn. Acad. Ser. B Phys. Biol. Sci*. **2014**, *90*, 1–11.

131 D. N. Coventry, A. S. Batsanov, A. E. Goeta, J. A. K. Howard, T. B. Marder, R. N. Perutz, *Chem. Commun*. **2015**, *51*, 2172-2174.

132 M. N. Eliseeva, L. T. Scott, *J. Am. Chem. Soc.* **2012**, *134*, 15169–15172.

133 R. P. Kaiser, J. Ulč, I. Císařová, D. Nečas, *RSC Adv*. **2018**, *8*, 580–583.

134 D. Nečas, R. P. Kaiser, J. Ulč, *Eur. J. Org. Chem*. **2016**, *34*, 5647–5652.

135 J. M. Quimby, L. T. Scott, *Adv. Synth. Catal*. **2009**, *351*, 1009–1013.

136 H. A. Wegner, H. Reisch, K. Rauch, A. Demeter, K. A Zachariasse, A. de Meijere, L. T. Scott, *J. Org. Chem*. **2006**, *71*, 9080–9087.

137 H. A. Wegner, L. T. Scott, A. de Meijere, *J. Org. Chem*. **2003**, *68*, 883–887.

138 S. Seifert, D. Schmidt, F. Würthner, *Org. Chem. Front*. **2016**, *3*, 1435–1442.

139 S. Seifert, D. Schmidt, K. Shoyama, F. Würthner, *Angew. Chem*. **2017**, *129*, 7703–7708; *Angew. Chem. Int. Ed*. **2017**, *56*, 7595–7600.

140 S. Seifert, K. Shoyama, D. Schmidt, F. Würthner, *Angew. Chem*. **2016**, *128*, 6500–6505; *Angew. Chem. Int. Ed*. **2016**, *55*, 6390–6395.

141 M. Mahl, K. Shoyama, J. Rühe, V. Grande, F. Würthner, *Chem. Eur. J*. **2018**, *24*, 9409–9416.

142 F. B. Mallory, C. S. Wood, J. T. Gordon, *J. Am. Chem. Soc*. **1964**, 86, 3094–3102.

143 F. B. Mallory, C. S. Wood, J. T. Gordon, L. C. Lindquist, M. L. Savitz, *J. Am. Chem. Soc*. **1962**, *84*, 4361–4362.

144 Y. Shen, C.-F. Chen, *Chem. Rev.* **2012**, *112*, 1463–1535.

145 H. Saito, A. Uchida, S. Watanabe, *J. Org. Chem.* **2017**, *82*, 5663–5668.

146 L. Liu, B. Yang, T. Katz, M. Poindexter, *J. Org. Chem*. **1991**, *56*, 3769–3775.

147 K.B. Jørgensen, *Molecules* **2010**, *15*, 4334–4358.

148 T. Sato, S. Shimada, K. Hata, *J. Chem. Soc. Chem. Commun*. **1970**, 766–767.

149 T. Sato, S. Shimada, K. Hata, *Bull. Chem. Soc. Jpn*. **1971**, *44*, 2484–2490.

150 M. Daigle, A. Picard-Lafond, E. Soligo, J.-F. Morin, *Angew. Chem*. **2016**, *128*, 2082–2087; *Angew. Chem. Int. Ed*. **2016**, *55*, 2042–2047.

151 M. Daigle, D. Miao, A. Lucotti, M. Tommasini, J.-F. Morin, *Angew. Chem*. **2017**, *129*, 6309–6313; *Angew. Chem. Int. Ed*. **2017**, *56*, 6213–6217.

152 Z. Li, R. J. Twieg, *Chem. Eur. J*. **2015**, *21*, 15534–15539.

153 M. J. Plater, *J. Chem. Soc., Perkin Trans*. *1* **1997**, 2903–2909.

154 F. B. Mallory, C. W. Mallory, *J. Org. Chem.* **1983**, *48*, 526–532.

155 K. Y. Amsharov, P. Merz, *J. Org. Chem.* **2012**, *77*, 5445–5448.

156 K. Y. Amsharov, M. A. Kabdulov, M. Jansen, *Angew. Chem*. **2012**, *124*, 4672–4675; *Angew. Chem. Int. Ed*. **2012**, *51*, 4594–4597.

157 D. Sharapa, A.-K. Steiner, K. Amsharov, *Phys. Status Solidi B*, **2018**, 1800189.

158 N. Suzuki, T. Fujita, K. Y. Amsharov, J. Ichikawa, *Chem. Commun*. **2016**, *52*, 12948–12951.

159 K. Amsharov, *Phys. Status Soldi B* **2016**, *253*, 2473–2477.

160 O. Papaianina, V. A. Akhmetov, A. A. Goryunkov, F. Hampel, F. W. Heinemann, K. Y. Amsharov, *Angew. Chem*. **2017**, *129*, 4912–4916; *Angew. Chem. Int. Ed*. **2017**, *56*, 4834–4838.

161 V. Akhmetov, M. Feofanov, O. Papaianina, S. Troyanov, K. Amsharov, *Chem. Eur. J.* **2019**, *25*, 11609–11613.

162 V. Akhmetov, K. Amsharov, *Phys. Status Solidi B* **2019**, 1900254.

163 A.-K. Steiner, K. Y. Amsharov, *Angew. Chem*. **2017**, *129*, 14926–14931; *Angew. Chem. Int. Ed*. **2017**, *56*, 14732–14736.

164 K. Fuchibe, K. Shigeno, N. Zhao, H. Aihara, R. Akisaka, T. Morikawa, T. Fujita, K. Yamakawa, T.Shimada, J. Ichikawa, *J. Fluor. Chem*. **2017**, *203*, 173–184.

165 K.Fuchibe, T. Morikawa, K. Shigeno, T. Fujita, J. Ichikawa, *Org. Lett.* **2015**, *17*, 1126–1129.

166 K. Fuchibe, T. Morikawa, R. Ueda, T. Okauchi, J. Ichikawa, *J. Fluor. Chem*. **2015**, *179*, 106–115.

167 S. Banerjee, S. Sinha, P. Pradhan, A. Caruso, D. Liebowitz, D. Parrish, M. Rossi, B. Zajc, *J. Org. Chem.* **2016**, *81*, 3983–3993.

168 F. B. Mallory, C. W. Mallory, W.M. Ricker, *J. Am. Chem. Soc.* **1975**, *97*, 4770–4771.

169 D. J. Sardella, E. Boger, *Magn. Reson. Chem*. **1989**, *27*, 13–20.

170 V. M. Tsefrikas, L. T. Scott, *Chem. Rev.* **2006**, *106*, 4868–4884.

171 C. Doll, PhD Thesis, Braunschweig, **1999**.

172 J. Liu, A. Narita, S. Osella, W. Zhang, D. Schollmeyer, D. Beljonne, X. Feng, K. Müllen, *J. Am. Chem. Soc.* **2016**, *138*, 2602–2608.

173 M. S. Markoulides, C. Venturini, D. Neumeyer, A. Gourdon, *New J. Chem*. **2015**, *39*, 6498–6503.

174 S. Nagarajan, C. Barthes, N. K.Girdhar, T. T. Dang, A. Gourdon, *Tetrahedron* **2012**, *68*, 9371–9375.

175 K. Ota, T. Tanaka, A. Osuka, *Org. Lett.* **2014**, *16*, 2974–2977.

176 S. Kumar, M.-T. Ho, Y.-T. Tao, *Org. Lett.* **2016**, *18*, 200–203.

177 C. L. Eversloh, Y. Avlasevich, C. Li, K. Müllen, *Chem. Eur. J.* **2011**, *17*, 12756–12762.

178 S. R. Bheemireddy, P. C. Ubaldo, A. D. Finke, L. Wang, K. N. Plunkett, *J. Mater. Chem. C* **2016**, *4*, 3963–3969.

179 E.-C. Liu, M.-K. Chen, J.-Y. Li, Y.-T. Wu, *Chem. Eur. J*. **2015**, *21*, 4755–4761.

180 G. Dai, J. Chang, W. Zhang, S. Bai, K.-W.Huang, J. Xu, C. Chi, *Chem. Commun.* **2015**, *51*, 503–506.

181 G. Dai, J. Chang, J. Luo, S. Dong, N. Aratani, B. Zheng, K.-W. Huang, H. Yamada, C. Chi, *Angew. Chem*. **2016**, *128*, 2743–2746; *Angew. Chem. Int. Ed*. **2016**, *55*, 2693–2696.

182 C. K. Frederickson, L. N. Zakharov, M. M. Haley, *J. Am. Chem. Soc.* **2016**, *138*, 16827–16838.

183 J. J. Dressler, Z. Zhou, J. L. Marshall, R. Kishi, S. Takamuku, Z. Wei, S. N. Spisak, M. Nakano, M. A. Petrukhina, M. M. Haley, *Angew. Chem*. 2917, 129, 15565–15569; *Angew. Chem. Int. Ed.* **2017**, *56*, 15363–15367.

184 D. T. Chase, A. G. Fix, S. J. Kang, B. D. Rose, C. D. Weber, Y. Zhong, L. N. Zakharov, M. C. Lonergan, C. Nuckolls, M. M. Haley, *J. Am. Chem. Soc.* **2012**, *134*, 10349–10352.

185 A. Pradhan, P. Dechambenoit, H. Bock, F. Durola, *J. Org. Chem.* **2013**, *78*, 2266–2274.

186 K. Kawai, K. Kato, L. Peng, Y. Segawa, L. T. Scott, K. Itami, *Org. Lett.* **2018**, *20*, 1932–1935.

187 K. Kawasumi, Q. Zhang, Y. Segawa, L. T. Scott, K. Itami, *Nat. Chem*. **2013**, *5*, 739–744.

188 K. Yamamoto, T. Harada, M. Nakazaki, T. Naka, Y. Kai, S. Harada, N. Kasai, *J. Am. Chem. Soc.* **1983**, *105*, 7171–7172.

189 K. Yamamoto, H. Sonobe, H. Matsubara, M. Sato, S. Okamoto, K. Kitaura, *Angew. Chem.* **1996**, *108*, 69–70; *Angew. Chem. Int. Ed. Engl.* **1996**, *35*, 69–70.

190 S. H. Pun, Y. Wang, M. Chu, C. K. Chan, Y. Li, Z. Liu, Q. Miao, *J. Am. Chem. Soc*. **2019**, *141*, 9680–9686.

191 C. M. Cruz, S. Castro-Fernández, E. Maçôas, A. Millán, A. G. Campaña, *Synlett* **2019**, *30*, 997–1002.

192 X. Yang, D. Liu, Q. Miao, *Angew. Chem*. **2014**, *126*, 6904–6908; *Angew. Chem. Int. Ed*. **2014**, *53*, 6786–6790.

193 J. Luo, X. Xu, R. Mao, Q. Miao*, J. Am. Chem. Soc*. **2012**, *134*, 13796–13803.

194 K. Y. Cheung, X. Xu, Q. Miao, *J. Am. Chem. Soc.* **2015**, *137*, 3910–3914.

195 C. M. Cruz, I. R. Márquez, I. F. A. Mariz, V. Blanco, C. Sánchez-Sánchez, J. M. Sobrado J. A. Martín-Gago, J. M. Cuerva, E. Maçôas, A. G. Campaña, *Chem. Sci*. **2018**, *9*, 3917–3924.

196 S. H. Pun, Q. Miao, *Acc. Chem. Res.* **2018**, *51*, 1630–1642.

197 J. Tellenbröker, D. Kuck, *Angew. Chem.* **1999**, *111*, 1000–1004; *Angew. Chem. Int. Ed*. **1999**, *38*, 919–922.

198 R. B. Woodward, T. Fukunaga, R. C. Kelly, *J. Am. Chem. Soc*. **1964**, *86*, 3162–3164.

199 A. Schuster, D. Kuck, *Angew. Chem.* **1991**, *103*, 1717–1720; *Angew. Chem. Int. Ed.* **1991**, *30*, 1699–1702.

200 J. G. Brandenburg, S. Grimme, P. G. Jones, G. Markopoulos, H. Hopf, M. K. Cyranski, D. Kuck, *Chem. Eur. J*. **2013**, *19*, 9930–9938.

201 D. Kuck, A. Schuster, R. A. Krause, J. Tellenbröker, C. P. Exner, M. Penk, H. Bögge, A. Müller, *Tetrahedron* **2001**, 3587–3613.

202 G. Markopoulos, PhD Thesis, TU Braunschweig, **2013**.

203 D. Kuck, *Pure Appl. Chem*. **2006**, *78*, 749–775.

204 D. Kuck, *Angew. Chem.* **1984**, *96*, 515–516; *Angew. Chem. Int. Ed. Engl.* **1984**, *23*, 508–509.

205 D. Kuck, T. Lindenthal, A. Schuster, *Chem. Ber*. **1992**, *125*, 1449–1460.

206 D. Kuck, E. Neumann, A. Schuster, *Chem. Ber*. **1994**, *127*, 151–164.

207 G. Markopoulos, L. Henneicke, J. Shen, Y. Okamoto, P. G. Jones, H. Hopf, *Angew. Chem.* **2012**, *124*, 13057–13060; *Angew. Chem. Int. Ed*. **2012**, *51*, 12884–12887.

208 S. Klotzbach, T. Scherpf, F. Beuerle, *Chem. Commun.* **2014**, *50*, 12454–12457.

209 J. Vile, M. Carta, C. G. Bezzu, N. B. McKeown, *Polym. Chem.* **2011**, *2*, 2257–2260.

210 D. Kuck, T. Lindenthal, A. Schuster, *Chem. Ber. Recl.* **1992**, *125*, 1449–1460.

211 A. Dhara, J. Weinmann, A.-M. Krause, F. Beuerle, *Chem. Eur. J.* **2016**, *22*, 12473–12478.

212 A. Dhara, F. Beuerle, *Synthesis* **2018**, *50*, 2867–5877.

213 E. U. Mughal, D.Kuck, *Org. Biomol. Chem*. **2010**, *8*, 5383–5389.

214 M. Mastalerz, D. Beaudoin, F. Rominger, *Synthesis* **2015**, *47*, 3846–3848.

215 D. Kuck, *Top. Curr. Chem.* **1998**, *196*, 167–220.

216 J. Tellenbroker, D. Kuck, *Beilstein J. Org. Chem.* **2011**, *7*, 329–337.

217 D. Kuck, *Chem. Rev.* **2006**, *106*, 4885–4925.

218 R. Haag, B. Ohlhorst, M. Noltemeyer, R. Fleischer, D. Stalke, A. Schuster, D. Kuck, A.de Meijere, *J. Am. Chem. Soc.* **1995**, *117*, 10474–1048.

219 J. Klett, *Chem.Commun*. **2014**, *50*, 7929–7932.

220 X.-P. Cao, D. Barth, D. Kuck, *Eur. J. Org. Chem.* **2005**, 3482–3488.

221 L. Zhou, X.-P. Cao, B. Neumann, H.-G. Stammler, D. Kuck, *Synlett* **2005**, *18*, 2771–2775.

222 T. Wang, Z.-Y. Li, A.-L. Xie, X.-J. Yao, X.-P. Cao, D. Kuck, *J. Org. Chem.* **2011**, *76*, 3231–3238.

223 J. Linke, N. Bader, J. Tellenbröker, D. Kuck, *Synthesis* **2018**, 50, 175–183.

224 J. Tomaschautzky, B.Neumann, H-G. Stammler, N. W. Mitzel, *Dalton Trans*. **2017**, *46*, 1112–1123.

225 M. Harig, B. Neumann, H.-G. Stammler, D. Kuck, *Eur. J. Org. Chem*. **2004**, 2381–2397.

226 R. Saravanakumar, G. Markopoulos, L. G. Bahrin, P. G. Jones, H. Hopf, *Synlett* **2013**, *24*, 453–456.

227 L. Zhou, T. X. Zhang, B. R. Li, X. P. Cao, D. Kuck, *J. Org. Chem.* **2007**, *72*, 6382–6389.

228 W.-X. Niu, E.-Q. Yang, Z.-F. Shi, X.-P. Cao, D. Kuck, *J. Org. Chem.* **2012**, 77, 1422–1434.

229 F. Lucchesini, M. Grasse, B. Neumann, H. G. Stammler, J. Tellenbröker, D. Kuck, *Eur. J. Org. Chem.* **2016**, *16*, 2828–2841.

230 E. U. Mughal, J. Eberhard, D. Kuck, *Chem. Eur. J*. **2013**, *19,* 16029–16035.

231 A. Dhara, F. Beuerle, *Chem. Eur. J*. **2015**, *21*, 17391–17396.

232 S. Klotzbach , T. Scherpf, F. Beuerle, *Chem. Commun*. **2014**, *50*, 12454–12457.

233 T.Wang, Y.-F. Zhang, Q.-Q. Hou, W.-R. Xu, X.-P. Cao, H.-F. Chow, D. Kuck, *J. Org. Chem.* **2013**, *78*, 1062–1069.

234 C.-F. Ng, H.-F. Chow, D. Kuck, T. C. W. Mak, *Cryst. Growth Des.* **2017**, *17*, 2822–2827.

235 B. Bredenkotter, S. Henne, D. Volkmer, *Chem. Eur. J.* **2007**, *13*, 9931–9938.

236 P. E. Georghiou, L. N. Dawe, H.-A. Tran, J. Strube, B. Neumann, H.-G. Stammler, D. Kuck, *J. Org. Chem.* **2008**, *73*, 9040–9047.

237 Z.-M. Li, D. Hu, J. Wei, Q. Qi, X.-P. Cao, H.-F. Chow, D. Kuck, *Synthesis* **2018**, *50*, 1457–1461.

238 W.-R. Xu, G.-Jie Xia, H.-F. Chow, X.-Ping Cao, D. Kuck, *Chem. Eur. J*. **2015**, *21*, 12011–12017.

239 W.-R. Xu, X.-R. Wang, H.-F. Chow, D. Kuck, *Synthesis* **2019**, *51*, 2116–2121.

240 J. Wie, Z.-M. Li, X.-J. Jin, X.-J. Yao, X.-P. Cao, H.-F. Chow, D. Kuck, *Chem. Asian J*. **2015**, *10*, 1150–1158.

241 W. Greschner, B. Neumann, H.-G. Stammler, H. Gröger, D. Kuck, *Angew. Chem*. **2015**, *127*, 13968–13972; *Angew. Chem. Int. Ed.* **2015**, *54*, 13764–13768.

242 W.-X. Niu, T. Wang, Q.-Q. Hou, Z.-Y. Li, X.-P. Cao, D. Kuck, *J. Org. Chem.* **2010**, *75*, 6704–6707.

243 L. He, C.-F. Ng, Y. Li, Z. Liu, D. Kuck, H.-F. Chow, *Angew. Chem*. **2018**, *130*, 13823–13827; *Angew. Chem. Int. Ed.* **2018**, *57*, 13635–13639.

244 Y. Kirchwehm, A. Damme, T. Kupfer, H. Braunschweig, A. Krueger, *Chem. Commun.* **2012**, *48*, 1502–1504.

245 C. A. Dullaghan, G. B. Carpenter, D. A. Sweigart, *Organometallics* **2000**, *19*, 2233–2236.

246 Y.-F. Zhang, W.-F. Tian, X.-P. Cao, D. Kuck, H.-F. Chow, *J. Org. Chem.* **2016**, *81,* 2308–2319.

247 E. U. Mughal, D. Kuck, *Chem. Commun.* **2012**, *48*, 8880–8882.

248 E. U. Mughal, B. Neumann, H.-G. Stammler, D. Kuck, *Eur. J. Org. Chem*. **2014**, *33*, 7469–7480.

249 H.-W. Ip, C.-F. Ng, H.-F. Chow, D. Kuck, *J. Am. Chem. Soc.* **2016**, *138*, 13778–13781.

250 Y. Kirchwehm, PhD Thesis, Universität Würzburg, **2013**.

251 S. Henne, B. Bredenkötter, D. Volkmer, *Appl. Surf. Sci*. **2015**, *356*, 645–650.

252 Q. S. Stöckl, T.-C. Wu, A. Mairena, Y.-T. Wu, K.-H. Ernst, *Faraday Discuss*. **2017**, *204*, 429–437.

253 M. Parschau, R. Fasel, K.-H. Ernst, O. Gröning, L. Brandenburger, R. Schillinger, T. Greber, A. P. Seitsonen, Y.-T. Wu, J. S. Siegel, *Angew. Chem*. **2007**, *119*, 8406–8409; *Angew. Chem. Int. Ed*. **2007**, *46*, 8258–8261.

254 L. Zoppi, Q. Stöckl, A. Mairena, O. Allemann, J. S. Siegel, K. K. Baldridge, K.-H. Ernst, *J. Phys. Chem. B*. **2018**, *122*, 871–877.

255 Q. S. Stöckl, Y.-C. Hsieh, A. Mairena, Y.-T. Wu, K.-H Ernst, *J. Am. Chem. Soc*. **2016**, *138*, 6111–6114.

256 J. Callbo. J. Aragó, R. A. Boto, J. Sánches-Marín, E. Ortí, J. Conteras-García, *J. Phys. Chem. A* **2018**, *122*, 1124–1137.

257 M. Vogt, R. Buschmann, S. Toksabay, M. Schmitt, M. Schwab, M. Bode, A. Krueger, *J. Phys. Chem. C* **2019**, *123*, 5469–5478.

258 J.-P. Jalkanen, F. Zerbetto, *J. Phys. Chem. B* **2006**, *110*, 5595–5601.

259 A. B.Anderson, M. R.McDevitt, F. L.Urbach, *Surf. Sci*. **1984**, *146*, 80–92.

260 D. P. Miller, S. Simpson, N. Tymińska, E. Zurek, *J. Chem. Phys*. **2015**, *142*, 101924.

261 C. F. Macrae, P. R. Edgington, P. McCabe, E. Pidcock, G. P. Shields, R. Taylor, M. Towler, J. van de Streek, *J. Appl. Cryst*. **2006**, *39*, 453–457.

262 C. F. Macrae, I. J. Bruno, J. A. Chisholm, P. R. Edgington, P. McCabe, E. Pidcock, L. Rodriguez-Monge, R. Taylor, J. van de Streekand, P. A. Wood, *J. Appl. Cryst*. **2008**, *41*, 466–470.

263 L. Zoppi, A. Garcia, K. K. Baldridge, *J Phys Chem A*. **2010**, *114*, 8864–8872.

264 T. Bauert, L. Zoppi, G. Koller, A. Garcia, K. K. Baldridge, K.-H. Ernst, *J. Phys. Chem. Lett.* **2011**, *2*, 2805–2809.

265 J. I. Urgel, M. Di Giovannantonio, Y. Segawa, P. Ruffieux, L. T. Scott, C. A. Pignedoli, K. Itami, R. Fasel, *J. Am. Chem. Soc*. **2019**, *141*, 13158–13164.

266 J. Qian, Wenbin Yi, X. Huang, J. P. Jasinski, W. Zhang, *Adv. Synth. Catal*. **2016**, *358*, 2811–2816.

267 X.-D. Li, L.-J. Xie, D.-L.Kong, L. Liu, L. Cheng, *Tetrahedron* **2016**, *72*, 1873–1880.

268 A. H. More, C. S. Ramaa*, Ind. J. Chem*. **2010**, *49B*, 364–367.

269 D. H Jadhav, C. S. Ramaa, *Ind. J. Chem*. **2007**, *46B*, 2064–2067.

270 J. Zhao, Y. Zhao, H. Fu, *Angew. Chem. Int. Ed.* **2011**, *50*, 3769–3773.

271 J.-P. Lin, Y.-Q. Long, *Chem. Commun*. **2013**, *49*, 5313–5315.

272 G. M. Coppola, R. W. Dodsworth, *Synthesis* **1981**, *7*, 523–524.

273 V. D. Dyachenko, A. N. Chernega, *Russ. J. Org. Chem*. **2007**, *43*, 60–63.

274 R. Tanikaga, N. Konya, K. Hamamura, A. Kaji, *Bull. Chem. Soc. Jpn.* **1988**, *61*, 3211–3216.

275 T.-T. Kao, S.-e. Syu, Y.-W. Jhang, W. Lin, *Org. Lett.* **2010***, 12*, 3066–3069.

276 J. F. DeBernardis, D. J. Kerkman, M. Winn, E. N. Bush, D. L. Arendsen, W. J. McClellan, J. J. Kyncl, F. Z. Bash, *J. Med.Chem*. **1985**, *28*, 1398–1404.

277 Y. Kirchwehm, unpublished results.

278 R. Antonioletti, P. Bovicelli, S. Malancona, *Tetrahedron* **2002***, 58*, 589–596.

279 M. Mamiya,Y. Suwa, H. Okamoto, M. Yamaji, *Photochem. Photobiol. Sci*. **2016**, *15*, 278–286.

280 Y.-T. Wu, J. S. Siegel, *Chem. Rev*. **2006**, *106*, 4843–4867.

281 H. Dong, C. Wang, W. Hu, *Chem. Comm*. **2010**, *46*, 5211–5222.

282 M. A. Petrukhina, K. A. Andreini, L. Peng, L. T. Scott, *Angew. Chem*. **2004**, *116*, 5593–5597; *Angew. Chem. Int. Ed*. **2004**, *43*, 5477–5481.

283 K. W. Rosenmund, E. Struck, *Ber. Dtsch. Chem. Ges.* **1919**, *52*, 1749–1756.

284 J. v. Braun, G. Manz, *Liebigs Ann.*, **1931**, *488*, 111–126.

285 J. E. Callen, C. A. Dornfeld, G. H. Coleman, *Org. Syn.* **1948**, 28, 34.

286 J. Kelber, M.-F. Achard, B. G. de Bonneval, H. Bock, *Chem. Eur. J*. **2011**, *17*, 8145–8155.

287 A. V. Nikolaitchik, M. A. J. Rodgers, D. C. Neckers, *J. Org. Chem*. **1996**, *61*, 1065–1072.

288 W. E. Bachmann, C. H. Boatner, *J. Am. Chem. Soc*. **1936**, *58*, 2097–2101.

289 F. Liu, X. Shen, Y. Wu, L. Bai, H. Zhao, X. Ba, *Tetrahedron Lett.* **2016**, *57*, 4157–4161.

290 S. Kumar, Y.-T. Tao, *J. Org. Chem*. **2015**, *80*, 5066–5076.

291 L. Zhai, R. Shukla, R. Rathore, *Org. Lett.* **2009**, *11*, 3474–3477.

292 J. M. Fernández-García, P. J. Evans, S. M. Rivero, I. Fernández, D. García-Fresnadillo, J. Perles, J. Casado, N. Martín, *J. Am. Chem. Soc.* **2018**, *140*, 17188–17196.

293 Y. Kita, M. Gyoten, M. Ohtsubo, H. Tohma, T. Takada, *Chem. Commun*. **1996**, 1481-1482.

294 H. Tohma, M. Iwata, T. Maegawa, Y. Kita, *Tetrahedron Lett*. **2002**, *43*, 9241–9244.

295 E. Winterfeldt, *Synthesis* **1975**, *9*, 617–630.

296 H. Dong, M. Shen, J. E. Redford, B. J. Stokes, A. L. Pumphrey and T. G. Driver, *Org. Lett.* **2007**, *9*, 5191–5194.

297 A. E. G. Miller, J. W. Biss, L. F. Schwartzman, *J. Org. Chem.* **1959**, *24*, 627–630.

298 A. J. M. Burrell, I. Coldham, L. Watson, N. Oram, C. D. Pilgram, N. G. Martin, *J. Org. Chem.* **2009**, *74*, 2290–2300.

299 A. B. Reitz, S. O. Nortey, B. E. Maryanoff, *J. Org. Chem.* **1987**, *52,* 4191–4202.

300 D. F. Hagen, W. D. Leslie, *Anal. Chem.* **1963**, *35*, 814–817.

301 J. H. Mitchen, *Anal. Chem*. **1961**, *33*, 1331–1334.

302 E. Bonitz, *Chem. Ber*. **1955**, *88*, 742–763.

303 T. R. Hoye, A. W. Aspaas, B. M. Eklov, T. D. Ryba, *Org. Lett.* **2005**, *7*, 2205–2208.

304 A. J. Elliott, P. E. Morris, S. L. Petty, C. H. Williams, *J. Org. Chem.* **1997**, *62*, 8071–8075.

305 S. Danishefsky, K. Vaughan, R. Gadwood, K. Tsuzuki, *J. Am. Chem. Soc*. **1981**, *103*, 4136–4141.

306 H. Stephen, *J. Chem. Soc. Trans*. **1925**, *127*, 1874–1877.

307 L. Turner, *J. Chem. Soc.* **1956**, 1686–1691.

308 J. L. Fry, R. A. Ott, *J. Org. Chem*. **1981**, *46*, 602–607.

309 S. Laval, W. Dayoub, L. Pehlivan, E. Métay, D. Delbrayelle, G. Mignani, M. Lemaire, *Tetrahedron Lett*. **2014**, *55*, 23–26.

310 Y. Li, A. Yagi, K. Itami, *Chem. Sci*. **2019**, *10*, 5470–5475.

311 G. Dyker, J. Körning, W. Stirner, *Eur. J. Org. Chem*. **1998**, 149–154.

312 J. T Zhang, W. Dai, R. G. Harvey, *J. Org. Chem*. **1998**, *63*, 8118–8124.

313 K. Wang, M. Lu, A. Yu, X. Zhu, Q. Wang, *J. Org. Chem.* **2009**, *74*, 935–938.

314 K. Wehming, M. Schubert, G. Schnakenburg, S. R. Waldvogel, *Chem. Eur. J*. **2014**, *20*, 12463–12469.

315 A. Ianni, S. R. Waldvogel, *Synthesis* **2006**, *13*, 2103–2112.

316 H.-Y. Lee, S. Kumar, T.-C. Lin, J.-P. Liou, *J. Nat. Prod*. **2016**, *79*, 1170−1173.

317 B. Su, L. Li, Y. Hu, Y. Liu, Q. Wang, *Adv. Synth. Catal*. **2012**, *354*, 383–387.

318 K. Wang, Y. Hu, M. Wu, Z. Li, Z. Liu, B. Su, A. Yu, Y. Liu, Q. Wang, *Tetrahedron* **2010**, *66*, 9135–9140.

319 M.-Y. Lü, K.-L. Wang, F. Cai, H.-Y. Wang, Q.-M. Wang, *Chin. J. Chem*. **2008**, *26*, 2241–2248.

320 S. Yamashita, N. Kurono, H. Senboku, M. Tokuda, K. Orito, *Eur. J. Org. Chem*. **2009**, 1173–1180.

321 W. G. Kofron, L. M. Baclawski, *J. Org. Chem.* **1976**, *41*, 1879–1880.

322 A. I. Meyers, D. Berney, *Org. Synth.* **1990**, *69*, 55.

323 A. F.Burchat, J. Michael, C. N. Nielsen, *J. Organomet. Chem*. **1997**, *542*, 281–283.

324 Z. Wang, P. Wei, Y. Liu, Q. Wang, *J. Agr. Food Chem.* **2014**, *62*, 10393–10404.

325 K. P. C. Vollhardt, N. E. Schore, *Organische Chemie, Vol. 5*, Wiley-VCH, Weinheim, **2011**.

326 J. Clayden, N. Greeves, S. Warren, *Organic Chemistry*, 2nd ed., Oxford University Press, Oxford, **2001**, 614–655.

327 M. Schlosser, *Pure Appl. Chem.* **1988**, *60*, 1627–1634.

328 X. Zhang, J. Kang, P. Niu, J. Wu, W. Yu, J. Chang, *J. Org. Chem.* **2014**, *79*, 10170–1017.

329 K. Yasuo, N. Kenji, Y. Shozo, A. Tetsuji, S. Takashi, K. Masayasu, WO9632384 (A1), 17.10.1996.

330 T. Chosi, S. Horimoto, C. Y. Wang, H. Nagase, M. Ichikawa, E. Sugino, S. Hibino, *Chem. Pharm. Bull.* **1992**, *40*, 1047–1049.

331 H.-W. Ip, H.-F. Chow, D. Kuck, *Org. Chem. Front*. **2017**, *4*, 817–822.

332 P. F. Cirillo, E. R. Hickey, N. Moss, S. Breitfelder, R. Betageri, T. Fadra, F. Gaenzler, T. Gilmore, D. R. Goldberg, V. Kamhi, T. Kirrane, R. R. Kroe, J. Madwed, M. Moriak, M. Netherton, C. A. Pargellis, U. R. Patel, K. C. Qian, R. Sharma, S. Suna, A. Swinamer, C. Torcellini, H. Takahashi, M. Tsang, Z. Xiong, *Bioorg. Med. Chem. Lett*. **2009**, *19*, 2386–2391.

333 Q. Zhang, H. Peng, G. Zhang, Q. Lu, J. Chang, Y. Dong, X. Shi, J. Wei, *J. Am. Chem. Soc.* **2014**, *136*, 5057–5064.

334 C. Bilger; R. Royer, P. Demerseman, *Synthesis* **1988**, *11*, 902–904.

335 T. Matsushima, S. Kobayashi, S. Watanabe, *J. Org. Chem*. **2016**, *81*, 7799−7806.

336 T. Ishiyama, J. Takagi, K. Ishida, N. Miyaura, *J. Am. Chem. Soc.* **2002**, *124*, 390–391.

337 J. F. Hartwig, *Acc. Chem. Res*. **2012**, *45*, 864–873.

338 I. A. I. Mkhalid, J. H. Barnard, T. B. Marder, J. M. Murphy, J. F. Hartwig, *Chem. Rev.* **2010**, *110*, 890931.

339 J. F. Hartwig, *Chem. Soc. Rev*. **2011**, *40*, 1992–2002.

340 G. Zhang, F. Rominger, M. Mastalerz, *Chem. Eur. J.* **2016**, *22*, 3084–3093.

341 J. Tellenbröker, PhD Thesis, Universität Bielefeld, **1999**.

342 P. Wagner, F. Rominger, M. Mastalerz, *Angew. Chem*. **2018**, *130*, 11491–11494; *Angew. Chem. Int. Ed*. **2018**, *57*, 11321–11324.

343 A. Matsumoto, M. Suzuki, D. Kuzuhara, H. Hayashi, N. Aratani, H. Yamada, *Angew. Chem.* **2015**, *127*, 15358-15361; *Angew. Chem. Int. Ed*. **2015**, *54*, 8175–8178.

344 A. Konishi, Y. Hirao, M. Nakano, A. Shimizu, E. Botek, B. Champagne, D. Shiomi, K. Sato, T.Takui, K. Matsumoto, H. Kurata, T. Kubo, *J. Am. Chem. Soc*. **2010**, 132, 11021–11023.

345 A. Konishi, Y. Hirao, K. Matsumoto, H. Kurata, T. Kubo, *Chem. Lett.* **2013**, *42*, 592–594.

346 T. Dohi, Y. Kita, *Curr. Org. Chem.* **2016**, *20*, 580–615.

347 Y. Kita, T. Dohi, *Chem. Rec*. **2015**, *15*, 886–906.

348 T. Dohi, M. Ito, K. Morimoto, M. Iwata, Y. Kita, *Angew. Chem*. **2008**, *120*, 1321–1324; *Angew. Chem. Int. Ed*. **2008**, *47*, 1301–1304.

349 T. Dohi, M. Ito, I. Itani, N. Yamaoka, K. Morimoto, H. Fujioka, Y. Kita, *Org. Lett*. **2011**, *13*, 6208–6211.

350 K. Morimoto, K. Sakamoto, Y. Ohnishi, T. Miyamoto, M. Ito, T. Dohi, Y. Kita, *Chem. Eur. J.* **2013**, *19*, 8726–8731.

351 E. Faggi, R. M. Sebastian, R. Pleixats, A. Vallribera, A. Shafir, A. Rodríguez-Gimeno, C. Ramírez de Arellanom, *J. Am. Chem. Soc*. **2010**, *51*, 17980–17982.

352 H.Tohma, H. Morioka, S. Takizawa, M. Arisawa, Y. Kita, *Tetrahedron* **2001**, *57*, 345–352.

353 K. Kato, Y. Segawa, L. T. Scott, K. Itami, *Angew. Chem*. **2018**, *130*, 1351–1355; *Angew. Chem. Int. Ed*. **2018**, *57*, 1337–1341.

354 M. C. Pirrung, *Handbook of Synthetic Organic Chemistry*, *Second Edition,* Academic Press, Cambridge, **2016**.

355 W. A. Mosher, R. W. Soeder, *J. Org. Chem.* **1971**, *36*, 1561–1563.

356 A. F. McKay, H. Brownell, *J. Org. Chem*. **1950**, *15*, 648–653.

357 G. S. Skinner, *J. Org. Chem.* **1960**, *25*, 1487–1491.

358 A. Lévai, *Die Pharmazie* **1981**, *36*, 449–450.

359 T. Yamada, T. Nagata, K. D. Sugi, K. Yorozu, T. Ikeno, Y. Ohtsuka, D. Miyazaki, T. Mukaiyama, *Chem. Eur. J*. **2003**, 9, 4485–4509.

360 F. C. Chen, T. S. Chen, T. J. Ueng, *J. Chi. Chem. Soc.* **1962**, *9*, 308–310.

361 J. Zawadiak, M. Mrzyczek, *Spectrochim Acta, Part A* **2012**, *96*, 815–819.

362 V. Cîrcu, T. J. K. Gibbs, L. Omnès, P. N. Horton, M. B. Hursthouse, D. W. Bruce, *J. Mater. Chem*. **2006**, *16*, 4316–4325.

363 K.Troshin, C. Schindele, H. Mayr, *J. Org. Chem.* **2011**, *76*, 9391–9408.

364 J. I. Lee, H. S. Son, M. G. Jung, *Bull. Korean Chem. Soc.* **2005**, *26*, 1461–1463.

365 Y. Yue, J. Peng, D. Wamg. Y. Bian, P. Sun, C. Chen, *J. Org. Chem*. **2017**, *82*, 5481–5486.

366 V. D. Orlov, N. P. Vorob'eva, A. Tishchenko, O. M. Pikalev, V. I. Popov, L. M. Yagupol'skii, *Chem. Heterocycl. Compd*. **1991**, *27*, 942–946.

367 V. A. Larionova, E. P. Markelova, A. F. Smol'yakova, T. F. Savel'yeva, V. I. Maleeva, Y. N. Belokon, *RSC Adv*. **2015**, *5*, 72764–72771.

9 Appendix

9.1 ^{1}H NMR Spectra

9.1.1 ^{1}H NMR spectrum of phenanthrene 247